THE ACTIVE CONTROL OF ACOUSTIC IMPEDANCE

by

Guy Charles Nicholson

Department of Applied Acoustics
University of Salford, UK

Thesis submitted for the degree of
Doctor of Philosophy

November 1994

ACKNOWLEDGEMENTS

I would like to thank my supervisor, Dr. Paul Darlington, for his help and advice, understanding and encouragement during the course of this research. I also thank Professor Peter Wheeler for supporting this research effort.

I have greatly appreciated the support and friendship of the other postgraduate students and staff at the Department of Applied Acoustics. I would particularly like to thank Dr. David Saunders and Mr. David O'Connor for their encouragement.

Knowles Electronics of Burgess Hill, West Sussex kindly supplied accelerometers and Mr. David Anderson generously provided microphones. These transducers were used to create results described in this thesis.

The financial support given by the Science and Engineering Research Council and the Research Fund at the University of Salford is gratefully acknowledged.

Finally, I thank my parents for their continuous encouragement and support.

GLOSSARY

A	sensitivity of velocity measurement (Vs/m), amplitude
A, B	filter transfer functions
Bl	force factor (NA^{-1})
c	speed of sound in air (343 ms^{-1})
C	forward-path
<C>	model of forward-path, filtered-X compensation filter
$\hat{C}$	estimate of C
C_{AB}	acoustic compliance of volume of air contained in sealed loudspeaker cabinet (m^5N^{-1})
C_{AD}	acoustic compliance of driver suspension (m^5N^{-1})
C_{AT}	total electrical equivalent compliance (m^5N^{-1})
C_m	driver mechanical compliance (mN^{-1})
C_{mbox}	mech. compliance from air in box (mN^{-1})
d	desired signal, distance (m), disturbance signal
e	error signal
E	expectation operator
f_s	sample frequency (=1/T =1/D) (Hz)
F	force (N), feedback path transfer function, acoustic delay
<F>	model of feedback path, feedback cancellation filter
F_s	force applied to source loudspeaker (N)
F_c	force applied to control loudspeaker (N)
G	control filter, plant
G_0	open loop gain
H	desired filter
i	time lag index, current (A)
I	identity matrix, acoustic delay
J	cost function
k	time index, wavenumber, scaling factor
K_m	mechanical stiffness (Nm)
L	length (m), pressure ratio
L_c	voice coil inductance (H)
M	sensitivity of pressure measurement (V/Pa)
M_{AD}	acoustic driver moving mass (kgm^{-4})

M_{AT}	total electrical-equivalent acoustic mass (kgm^{-4})
M_m	moving mass of loudspeaker cone (kg)
M_{mt}	total moving mass (kg)
n	integer
N	filter length
p	acoustic pressure (Pa)
p_c p_{cone}	acoustic pressure at loudspeaker cone (Pa)
p_d	desired pressure (Pa)
p_i	incident pressure (Pa)
p_r	reflected pressure (Pa)
p_{rad}	pressure generated by a vibrating surface, see Page 119
Q_{tc}	total quality factor of loudspeaker and box system
r	duct radius (m), autocorrelation function
R	complex acoustic reflection coefficient, adaptive filter
R_c	loudspeaker voice-coil resistance (Ω)
R_g	power amplifier output impedance (Ω)
R_{AD}	acoustic resistance of driver suspension (Ωm^{-4})
R_{AB}	acoustic resistance of air in sealed box (Ωm^{-4})
R_{AT}	total electrical equivalent acoustic resistance (Ωm^{-4})
R_m	mechanical resistance (mech. Ω)
R_{mt}	total mechanical resistance (mech. Ω)
R_{mbox}	box mechanical resistance (mech. Ω)
S	surface area (m^2)
S_d	effective surface area of loudspeaker cone (m^2)
t	time (s)
T, D	time periods (seconds)
u	velocity (ms^{-1}), emf (volts)
u_c u_{cone}	loudspeaker cone velocity (ms^{-1})
u_d	desired velocity (ms^{-1})
u_s	source loudspeaker surface velocity (ms^{-1})
U	volume velocity (m^3s^{-1})
V	electrical signal (volts)
W	adaptive digital filter
$\bar{W}_k$	impulse response vector of adaptive filter at time k
x	reference signal, displacement (m)

x(k)	digital filter discrete-time input value
$\bar{X}_k$	vector of input values at time k
X	displacement limit (m)
y(k)	digital filter discrete output value
z	specific acoustic impedance ($kgm^{-2}s^{-1}$) (Rayls)
z_d	desired specific acoustic impedance ($kgm^{-2}s^{-1}$) (Rayls)
z_{NAT}	un-driven loudspeaker cone z ($kgm^{-2}s^{-1}$) (Rayls)
Z	acoustic impedance ($kgm^{-4}s^{-1}$)
Z_m	mechanical impedance (kgs^{-1})
Z_{AF}	mechanical radiation impedance (kgs^{-1})
Z_{EB}	blocked electrical impedance (Ω)
Z_{RAD}	radiation impedance ($kgm^{-2}s^{-1}$) (Rayls)
α, β	adaptation rate parameters (= 2μ)
ϵ	error in adaptive filter estimation
μ	adaptive filter update gain constant
ξ	mean square error, displacement (m)
θ, Φ	phase angle (radians)
π	3.14...
ρ_0	density of air (1.21 kgm^{-3})
ω	angular frequency (radians / second)
ω_1	resonant angular frequency (radians / second)
∇	gradient
$\hat{\nabla}$	gradient estimate
$\Re(\ )$	real operator
λ	wavelength (m)
n η	efficiency
Δ	time delay
γ γ	Poisson's ratio
τ τ	time lag
Ψ	normalised cost function
$\rho(\tau)$	normalised autocorrelation coefficient at lag τ
σ	standard deviation

ABSTRACT

The application of an active control force on a thin-walled acoustic boundary can modify the motional dynamics, and so influence the impedance presented to incident waves. This impedance determines transmission of acoustic energy, reflection of acoustic waves from the boundary and absorption of incident energy.

This thesis studies control systems that generate control forces for the active control of surface acoustic impedance. The proposed systems rely on measurement of the acoustic pressure and surface velocity of the boundary. The systems can use adaptive digital signal processing, which offers significant advantages over non-adaptive techniques. The active control of the specific acoustic impedance of a loudspeaker that terminates a waveguide for axially propagating plane waves provides a motivating problem.

Theoretical analysis establishes the control of specific acoustic impedance of a simple compliantly-suspended piston by a control force. Operational constraints of a physical piston define theoretical operating limits for controlled specific acoustic impedances.

The control systems use either feedback or feed-forward techniques for which theoretical treatment reveals restrictions on the range of controlled specific acoustic impedance. A novel result is that conventional implementations of the control systems can be unstable for certain desired impedances unless feedback cancellation is used. Digital feedback techniques are less effective for broader frequency bandwidth where feed-forward techniques may work. Theoretical analysis produces solutions that confirm the feasibility of these control techniques for the active control of specific acoustic impedance. Potential errors in the implementation of the systems have predictable effects on the controlled specific acoustic impedance.

Experimental results support the theoretical work presented in this thesis, demonstrating active control of specific acoustic impedance for normally incident acoustic plane waves. An adaptive digital feed-forward control system creates desired specific acoustic impedances for band-limited noise and transient signals.

1 INTRODUCTION

1.1 PREFACE

The application of active methods to control acoustical problems is the subject of considerable recent research and development. One major area is in acoustic sound reduction by active methods. This has arisen from the scientific recognition of the phenomenum "sound interference" in acoustical space. At any position in an acoustical space, the sound pressure that arises with two or more coherent radiating sound sources depends on the interference between the different pressures generated by the sound sources. If the sources are suitably related then destructive interference can occur with a corresponding reduction in sound pressure. Conversely with constructive interference the sound pressure is increased. The possibility of controlling the sound pressure of an offending noise by destructive sound interference with an additional coherent sound source was first recognised by Paul Lueg in a patent filed in 1934 and granted later in 1936 (1). More recently, real systems that reduce acoustical noise by active methods have been demonstrated. The introduction of fast digital signal processors has prompted much growth in this area.

A newer area of research attention is in the control of the behaviour of sound at an acoustic boundary. Real acoustical problems often occur in acoustic spaces that are bounded by surfaces. Whether sound is reflected or absorbed at the surface boundaries dictates the sound field that occurs in the space. A reverberant sound field occurs in a space that is bounded by highly reflective surfaces. An anechoic sound field occurs when the boundaries are absorptive. The behaviour of sound at the surface can be described with *specific acoustic impedance* - this is defined in Section 1.2 on Page 3. The influence of the specific acoustic impedance of a boundary on the nature of the enclosed sound field motivates the control of specific acoustic impedance. This thesis studies the control of the specific acoustic impedance of surface boundaries by active methods. The analysis and implementation of a method for the direct control of specific acoustic impedance is presented. This work is original and experimental results demonstrate the active control of specific acoustic impedance.

A literature study on the field of active control of acoustical problems is presented in Chapter 2. This section reveals that active modification of specific acoustic impedance is not new - practical demonstration has already been made with a control system that was designed to control reflection coefficients. This thesis contributes to the field by presenting the first demonstration of direct modification of specific acoustic impedance by a new method. A review of contemporary techniques for active control is given in Chapter 3. This chapter, therefore, contains no original work. The description of adaptive algorithms used for the practical work is presented. Current techniques for treating feedback problems are also presented. The rest of the work reported in this thesis is original, except where otherwise credited.

The modification of the specific acoustic impedance of a simple surface by a control force is theoretically established in Chapter 4. Physical operating limits arise when the forced surface is implemented by a loudspeaker. These are illustrated with examples of controlled specific acoustic impedance.

The method for specific acoustic impedance control is presented in Chapter 5. Original theory is presented in Chapter 6 to describe the operation of the method. Controller solutions are presented that apply to any active method for the optimum control of impedance. The stability of feedback loop paths that occur are analyzed. The analysis reveals that the implementation of the control method by conventional techniques that contain inherent delay can not create certain specific acoustic impedances unless feedback paths are cancelled. The implementation of a suitable adaptive algorithm for impedance control is examined. Problems that affect the practical performance of the control method are also described.

The practical implementation of the system is described in Chapter 7. Observations are presented on instability and band-width constraints for the digital feedback implementation of the method. Results that demonstrate the control of specific acoustic impedance are presented in Chapter 8. The choice of test signal can affect adaptive system performance. In addition to sinusoidal

signals, this thesis uses noise and transient signals to test the modified specific acoustic impedance as this reflects generalized performance for real-world acoustical problems.

The findings of this thesis are discussed in Chapter 9 and concluded in Chapter 10 where recommendations for further work are offered.

1.2 SPECIFIC ACOUSTIC IMPEDANCE

This section defines specific acoustic impedance. The characteristic specific acoustic impedance of plane waves in air is also quantified.

The *specific acoustic impedance* ***z*** at a location in a fluid medium is the ratio of the acoustic pressure ***p*** to the particle velocity ***u***, Equation 1.1.

$$z = \frac{p}{u} \qquad \frac{kg}{m^2 s} \tag{1.1}$$

Note that as velocity is a vector, so ***z*** is a vector quantity. The unit of specific acoustic impedance is often given as the *Rayl*, in honour of Lord Rayleigh.

There is another definition of impedance called *acoustic impedance* ***Z***, Equation 1.2. This, for an acoustic wave acting on a surface of area ***S***, is the acoustic pressure divided by the volume velocity ***U*** of the surface.

$$Z = \frac{p}{U} \qquad \frac{kg}{m^4 s} \tag{1.2}$$

The specific acoustic impedance ***z*** at a surface of known area ***S*** is related to the acoustic impedance ***Z*** as shown in Equation 1.3.

$$z = Z.S \qquad \frac{kg}{m^2 s} \tag{1.3}$$

This thesis studies active methods that modify ***z*** at the surface of an acoustic boundary. Throughout the thesis this impedance is often called the *surface impedance*. Also the *specific acoustic impedance* is described simply as *impedance*. Other forms of impedance, such as mechanical and electrical, are expressed in full.

The impedance ***z*** for travelling plane waves in air is described in Equation 1.4 (a formal derivation is presented in (2)).

$$z = \pm \rho_0 c \qquad \frac{kg}{m^2 s} \qquad 1.4$$

This is often described as the *characteristic* impedance of air. The plus or minus sign indicates the direction of sound propagation. Although the impedance of the medium is a real quantity for progressive plane waves, this is not true for standing plane waves or for diverging waves - in these cases **z** will be complex (see pp20-21 and p25 in (2)). At a temperature of 20°C and at atmospheric pressure, the density of air is 1.21 kg/m^3 and the speed of sound is 343 m/s (3). The characteristic impedance of air is thus quantified in Equation 1.5.

$$(\rho_0 c)_{20} = 415 \qquad \frac{kg}{m^2 s} \qquad 1.5$$

If plane waves are propagating through a pipe in the direction assigned as positive, with frequency less than the plane wave cut-off frequency of that pipe, then the impedance at any position in the cross-section is described by Equation 1.6.

$$z = \rho_0 c \qquad \frac{kg}{m^2 s} \qquad 1.6$$

When the propagating wave arrives at the surface of an object, the impedance of the surface determines whether sound reflection or absorption occurs. If the surface impedance is much greater than the characteristic impedance of air then reflection will mainly occur. If there is little mismatch in impedance at the boundary, absorption mainly occurs. If the impedance of the surface can be controlled by active means, then sound reflection or absorption can be controlled. Of particular interest is the generation of a boundary impedance that matches the characteristic impedance of air and so absorbs normally-incident propagating waves. This surface is often described in this thesis as a "controlled characteristic termination".

1.3 THE ACTIVE CONTROL OF SPECIFIC ACOUSTIC IMPEDANCE

The previous sections in this chapter have identified that the desire to control impedance at an acoustic boundary is motivated by the relationship that impedance has with sound absorption and reflection. This thesis studies an active control method for the modification of impedance. An acoustic scenario that facilitates this study is the sound field that occurs in a waveguide with "axially" propagating plane waves. This acoustic environment has received much attention in active noise control research.

Sound energy in the waveguide is generated with an acoustic source at one end. The frequency band-width of the acoustic source is restricted so that acoustic plane waves propagate along the length. The waveguide is terminated at the other end with an acoustic boundary. The sound field in the waveguide thus depends on the impedance of this termination. The waveguide allows the use of a standard method to quantify the termination impedance - measurement of standing wave ratios. A control system is configured to modify the impedance of the termination. The analysis, design and demonstration of the control system is the subject of this thesis.

The use of the waveguide limits sound propagation to one spatial dimension. The thesis concentrates on impedance control for one-dimensional sound propagation to validate the control method. The control of impedance for three-dimensional sound is beyond the scope of this foundational work.

2 LITERATURE STUDY

2.1 INTRODUCTION

This chapter describes the literature study undertaken for this research project. The requirements of research originality demand that the efforts of other researchers are not repeated. The literature study reveals that the control of surface impedance has been considered by other researchers. However the method used in this thesis to perform surface impedance control has not been analyzed or implemented before.

The active control of acoustical noise problems encompasses different disciplines. Theoretical knowledge of acoustics and control theory and technical knowledge of signal processing and electronics are all necessary to design and implement active acoustic control systems. By 1992 there were more than 3500 references in the field of active noise and vibration control (4). A data base of most of these reference titles is available (5). The first monograph on the active control of sound was recently published by Nelson and Elliott (2). This book contains 420 pages concerning the theory and operation of active control in acoustics. This volume contains much theoretical work proving that sound can be reduced by active control implemented with radiating sources. The study of this quantity of literature is simplified by distinguishing two objectives that motivate the active control of sound: active reduction of noise by sound cancellation, and general modification of a sound field by the active control of impedance at a boundary. The distinction between these two objectives is discussed in Section 2.2. Separate discussions of the literature for each objective are presented in Section 2.3 and Section 2.4. Finally, publications on various aspects of active control that were educational for the author are referenced in Section 2.5.

2.2 PREAMBLE

This section discusses the distinction between the active reduction of noise by sound cancellation and the general modification of a sound field by the active control of the impedance of a boundary.

The active reduction of noise by sound cancellation attempts to minimise the acoustic pressure at a sensor (or multiple sensors) in an acoustic field. This is achieved by creating an acoustical "anti-noise" signal that destructively interferes with the offending noise at the sensors. The anti-noise signal is generated by modifying the motion of secondary pistons or vibrating surfaces. The modification of the surface vibration modifies the surface impedance presented to the surrounding medium. However the effect of this on the sound field is often not considered in the literature. Conversely, the active control of impedance is primarily concerned with creating a defined impedance at an acoustic boundary. The effect of boundary impedance on an enclosed sound field motivates this control objective. If a reverberant field is desired, then active control can increase sound reflection by increasing the impedance at a vibrating boundary surface. Or if an anechoic sound field is desired, then active control can reduce sound reflection by forcing the boundary to have characteristic impedance. This objective is fundamentally different to noise reduction by sound cancellation as the intention is to create a defined acoustic *load* rather than an anti-noise signal.

The active reduction of noise by sound cancellation is described in early works on active noise control, see Section 2.3.1. Researchers studying the active reduction of propagating noise in ducts by sound cancellation in the 1970's were aware that, whilst the sound pressure is minimised at downstream sound sensor locations, upstream radiation occurs from the anti-noise source. This interferes with the primary noise and complicates the controller design. Sound cancellation procedures were therefore designed to minimise these side effects with directional anti-noise sources, see Section 2.3.2. In the literature this is called sound absorption as the reflected wave from the anti-noise source back to the source of noise is minimised. However noise reduction still occurs at the sensor positions by the process of sound interference with an anti-noise signal - test results in these references show large levels of sound reduction. These systems therefore appear to combine two physical processes: sound cancellation and sound absorption. Conversely, the creation of sound absorption by the active control of impedance does not attempt to cause sound cancellation at a sound

sensor location. Reflected waves are minimised by matching the load impedance to the impedance of the acoustic medium. Both methods can absorb incident sound, but the objectives are different: the first method aims to reduce noise by sound interference, the second creates an acoustic load. The acoustic load can be used to reduce sound in an enclosed field. However this is not considered in the design of strategies for the active control of impedance.

The distinction between the two objectives is enhanced with the following discussion on a study of sound reduction by Curtis *et al* of a one-dimensional enclosed sound field by three different techniques (6). This paper does not concern itself with the design of control systems, choosing to concentrate on the physical mechanisms of active sound reduction. The three techniques are :

> "cancellation at a point (the acoustical virtual earth) and active absorption (the absorbing termination), both of which have been successfully used in ducts, and the strategy of minimization of energy that has been developed for the control of sound in enclosed spaces".

The first technique, the acoustic virtual earth, is the active reduction of noise by sound cancellation as described in early works on active noise control. The paper describes the results of experimental tests and concludes that this method is not recommended for enclosed sound fields as it can force new standing wave patterns which "result in new resonances and greatly increased sound levels at some frequencies". The second technique for sound reduction, the use of the absorbing termination, was set by applying an active control force on the termination so that reflections back to the source were minimised. The effect of this was to create a termination impedance that matched the characteristic impedance of the enclosed sound field. This was found to reduce sound levels in enclosed resonant sound fields. However increased sound levels were noted in enclosed anti-resonant sound fields (in the specific test described in this paper the increase in the total sound field at anti-resonance was 0.6dB). The results from these two techniques distinguish the behaviour of the active reduction of noise by sound cancellation and by absorption with the active control of acoustic impedance. However, neither of these techniques fully characterize the hybrid "sound absorber" systems described originally in the 1970's because, whilst sound absorption in these systems occurs in the sense that waves are not

reflected back to the source, the reduction of noise by sound cancellation also occurs at other locations in the sound field. The paper concludes that the third technique, the minimisation of acoustic energy, provides the best noise reduction for both on- and off-resonance sound fields. A separate successful research effort in energy based control of sound is described by Sommerfeldt, (7).

In summary, the active reduction of noise by sound cancellation and the active control of impedance are fundamentally different objectives. The first method is concerned with reducing sound pressure by wave interference whilst the second method concerns the creation of defined acoustic loads. Both methods can be used to reduce sound pressure with different degrees of success. Hybrid systems have been seen in the literature that attempt to reduce noise by sound cancellation but can also be termed "sound absorbers". The literature study is divided into the two parts: noise reduction by sound cancellation in Section 2.3 which includes discussion of hybrid systems in Section 2.3.2, and the active control of impedance in Section 2.4.

2.3 ACTIVE REDUCTION OF ACOUSTIC NOISE

This section discusses literature on the active reduction of acoustic noise by sound cancellation in Section 2.3.1. Section 2.3.2 discusses literature on systems that reduce noise by sound cancellation whilst preventing sound reflection back to the noise source. This literature is not discussed in great detail because this thesis is concerned with the active control of specific acoustic impedance. This section offers a brief historical perspective on the active control of sound.

2.3.1 The active reduction of acoustical noise by sound cancellation

The invention of active acoustic-noise cancellation is attributed to Paul Lueg, "a doctor of philosophy and medicine, who worked as a physicist for many years" (8). Early in 1934 he filed a US patent application (1) that described the principle of active noise cancellation by wave superposition. The cancellation of an offending sound is achieved by generating a negative replica, usually by installing an anti-phase compensation source next to the primary noise source.

This contribution was based on Lueg's ideas as opposed to any technical realization. The first successful laboratory demonstration of sound reduction by wave superposition occurred 20 years later by Olsen and May's "Electronic Sound Absorber" (9). The use of the phrase "sound absorber" to describe this system can be misleading. The system reduces sound pressure at a single microphone location in the acoustical field. However, it does not act to absorb *incident acoustic waves* and thereby prevent reflected sound. By reducing the pressure the system effectively reduces the impedance at the microphone location. However, the system does not attempt to create a *characteristic* impedance, that required for ideal sound absorption of incident plane waves. The first technical applications of active noise reduction appeared 50 years later with the emergence of stable digital signal processing electronics.

The number of references in this field precludes further discussion. Interested readers should refer to (5). A book by Nelson and Elliott (2) offers a unique contemporary study on the active control of sound and presents analysis on the physical principles behind noise reduction by sound cancellation for one-dimensional and three-dimensional sound fields

2.3.2 Directional Sound Cancellation

During the 1970's work was performed by Swinbanks (10) and Jessel (11) into cancelling sound in ducts by active acoustic side-branches. The secondary control sources developed in these separate research efforts prevent the reflection of sound back to the noise source. In this respect these sources are absorbers of sound. The contribution by Jessel (12) is seen as the earliest theoretical treatment of active noise control (4).

Jessel realized that it was possible to create a directional source of anti-noise that, whilst reducing downstream sound pressure level by wave cancellation, did not reflect sound back to the source. His theory was based on a reciprocal of Huygens' principle (13). By using an analogue control system he was able to demonstrate this for one-dimensional sound using a symmetrical secondary source configuration consisting of a monopole and a dipole source. Figure 4 of

(11) illustrates downstream attenuation in a duct with no modification of the upstream propagating wave. Mangiante (14) demonstrated this work in 3-dimensions by surrounding the primary noise source with arrays of both 12 and 20 secondary sources. The results presented show convincingly uniform reductions in the far field radiation for both pure tone and broad-band sound, page 303 of reference (2).

Swinbanks describes creating an unidirectional acoustic source in a duct with two rings of monopolar sources so that downstream waves in the duct are attenuated (10). The configuration of the sources produces no upstream radiation. Later work performs laboratory tests with Swinbanks method so demonstrating attenuation of sinusoidal propagating waves but concludes that the system was too expensive for common application (15). Swinbanks method is analyzed in Section 5.7 of (2). The use of two sources to create directional sound radiation is shown to have frequency bandwidth limitations. More complicated arrays can extend the operational bandwidth.

The complexity of the secondary sources used in Jessel and Swinbanks works has restricted the general development of these systems.

2.4 ACTIVE CONTROL OF SPECIFIC ACOUSTIC IMPEDANCE

This thesis distinguishes active noise reduction and active control of impedance as two separate areas for consideration: whilst active noise reduction addresses the treatment of a sound field, active impedance control is concerned with the dynamics of boundaries in response to excitation by acoustic waves. This section discusses literature on the active control of impedance. Section 2.4.1 describes the early published works on active control of acoustic impedance by Bobber and Beatty. Later work can be separated into two types of control strategy. The first strategy, realized with two pressure measurements, describes the work of Guicking *et al* on the active control of reflection coefficient in Section 2.4.2. The work of Orduña-Bustamente and Nelson on active absorption using adaptive techniques is also described. Literature on the second strategy, realized with velocity and pressure measurements, is described in Section 2.4.3.

This strategy is used in the active control work presented in this thesis and has been examined independently by Mazzola. Finally a patent on a variable reflection/absorption device is mentioned in Section 2.4.4.

2.4.1 Active acoustic load impedance

The earliest published work found during this literature study on acoustic impedance control is an abstract by Bobber and Beatty (16). They were interested in controlling the impedance at the termination at one end of a tube so that defined impedances could be presented to a source transducer at the other end for accurate calibration and evaluation measurements. The tube was terminated with an active transducer that could be made to have "any acoustical impedance". This work was for application in water-filled ducts at high static pressures where the ratio of feasible duct dimensions to the wavelength of the sound is too small to approximate the free-field conditions required for accurate evaluation of the source transducer. The work was, therefore, particularly motivated by the creation of a characteristic load impedance through active control techniques. Later publications by Bobber (17) and Beatty (18) analyze the active load impedance. This section discusses these publications.

Bobber presents an electro-mechanical-analog analysis of a tube terminated at both ends by independently driven transducers by assuming that waves are normally incident on the transducers, the duct is loss-less and all components are linear (17). He develops an equivalent circuit for the system where the transducers are simple electrical generators with defined impedances (these arise in the real system from the inherent electrical, mechanical and acoustical properties of the transducers) and the duct is a standard electrical network representation of an ideal transmission line. This is applicable as an ideal representation of either an air- of a water-filled duct. Therefore the conclusions of the analysis are equally valid for an air- or a water-filled duct. By adjusting the relative magnitude and phase of the generator voltages Bobber shows that the load impedance "seen" by the source generator can be adjusted to any value, even negative values when the termination acts as a source of energy. The load impedance is also dependent on the "length" of the transmission line,

the signal frequency, the speed of sound propagation, and the inherent impedances of the transducers. The paper then quantifies the load impedance arising from numerical values of these variables. The practical duct dimensions are small compared with the wavelength and Bobber studies the effect of varying these conditions in his model. The theoretical results indicate that the behaviour is subtle, for example the change in the load impedance caused by increasing the length varies with the ratio of generator voltages (or transducer surface velocities). For one example the change in load impedance is reduced with larger generator voltages. For another specific example the system is unstable. Simple deductions can not be drawn because of the large number of variables and coupling that occurs. The paper concludes that load impedance of any magnitude or phase can be obtained by varying the magnitude and phase of the two signals driving each transducer, but some combinations of the system variables may result in an unstable condition. The thesis author considers that it is not possible to make general recommendations on avoiding the instable conditions because of the number of variables and coupling in this idealised system.

Beatty provides a more rigorous treatment of the acoustics of the active impedance load (18). He omits any discussion on the generation of the control voltage signal and the active transducer electrical properties, choosing to analyze the load impedances presented to the acoustical waves by the source transducer, at one end of a water-filled rigid duct, and the termination transducer at the other end. The transducers are considered as pistons that are driven independently at a common frequency. Theoretical analysis shows that the actual values of the source and termination impedances are dependent on the velocities, or applied forces, and the surface areas of the pistons at either end and the complex speed of propagation in the medium as well as the dimensions of the duct. The control of a desired termination impedance is simply achieved by applying an appropriate force to the termination piston. This force is related to the driving force applied to the source piston. Beatty states that the termination transducer impedance can be made to assume any value of magnitude 0 to infinity and phase angle 0 to $\pm\pi$, as the velocities or forces were

considered in the analysis to be linearly independent and unrestricted with respect to magnitude and relative phase. However, Beatty acknowledges that the determination of an exact forcing function from the theoretical analysis is experimentally difficult to achieve because of the "elusive" parameters involved. The rest of the work is concerned with determining the load impedance, arising from the duct and termination, "seen" by the source. For a characteristic load impedance, Beatty identifies that the control forcing function can be correctly adjusted by observing defined pressure magnitude and phase relationships in the duct. Results are presented from pressure measurements on a water-filled steel tube with an active termination. A characteristic load impedance is successfully achieved as the results indicate that plane waves propagate from the source to the termination transducer without reflection. However, a direct control method for automatically adjusting the forcing function on the termination so that the load impedance seen by the source is set to an arbitrarily specified value was not established in this paper or in the paper by Bobber. This thesis presents an active control method that automatically controls the impedance at the termination of an air-filled duct to an arbitrary pre-specified value for incident plane waves.

2.4.2 The "2-mic" control system

Considerable research on the modification of the reflection coefficient at a surface for air-borne sound has been performed at the University of Göttingen, Germany (19)(20)(21). The reflection coefficient **R** is intimately related to impedance (see Appendix 5 on Page 344). Therefore the control of **R** is considered by the thesis author as equivalent to the control of impedance.

These works, initiated by Prof. M.R. Schroeder and supervised by Dr. D. Guicking, demonstrate experimental control of reflection coefficient using an analogue control system. The incident sound was plane and at normal incidence, experimentally achieved by constraining the sound to one dimension by use of a duct (or "waveguide"), see Figure 1 on Page 30 (taken from Figure 5 (20)). The source loudspeaker (*l/s*) generates a travelling plane wave that propagates down the pipe towards the controlled surface. Two microphones M1

and M2 are positioned in the duct with M1 at the surface of the controlled l/s and M2 at a distance of about 10cm along the duct. The control system uses the two microphone signals to separate the reflected and incident pressure waves in the duct. The ratio of the separated signals yields the complex reflection coefficient **R**. The direct extraction of **R** allows the control system to be adjusted so that desired values of **R** can be set. The use of two microphones to determine acoustic reflection coefficients is patented (22). The historical significance of this control system is such that the thesis author proposes an abbreviation that rests on the use of two microphones to separate incident and reflected pressure - the "2-mic" control system. This abbreviation will be used throughout the rest of this thesis.

The motivation behind this work arises because:

> "conventional, passive absorbers for low-frequency sound presents difficulties: Wedge-type absorbers have to be made quite long (approximately, 1/3 wavelength at the lowest frequency), and resonance absorbers are effective in narrow frequency bands only, aside from often becoming quite big". (21)

The application of active control offers practical solution to these problems for the acoustics described in this paper: spot frequencies between 180-500Hz, and defined band-pass noise operating in one-dimension with plane wave motion. Sound reflection coefficients of less than 0.1 are indicated. The sound absorber was able to function in sound pressure levels of 110-140 dB, this being limited by overload of the electronics.

The work described in (20) is concerned with providing arbitrary reflection coefficients "to find applications not only for noise abatement but more generally in room acoustics". This quotation reinforces the thesis author's desire to separate active noise reduction by sound cancellation with the more generalized applications of impedance control in acoustics. The abstract quotes

> "This system permits easy control of the reflection coefficient"..."Arbitrary reflection coefficients between almost 0 and about 1.5 have been realized in the frequency range from below 100Hz to more than 800Hz" for single frequency one-dimensional plane waves

The researchers were successfully able to hand adjust the system so that **R** was

less than 0.02 between 150 and 750Hz thus creating a termination of near-characteristic impedance over these frequencies. When the active termination has a reflection coefficient of greater than unity it is actually contributing additional energy to the sound field. This behaviour is consistent with Beatty's assertion that the phase of the termination impedance can be actively controlled to any value (18). It is interesting that the first control system described in (20), before the successful 2-mic implementation, used a single microphone: this was unstable at higher frequencies. Theory for the loop stability of an equivalent control system is presented in Section 6.4.4 of this thesis.

All of the references (19)(20)(21) use analogue electronic control systems. Whilst successfully achieving the desired impedances the use of analogue control limits practical implementation because manual adjustment is required for each spot frequency (20). Manual adjustment is unsatisfactory for practical implementation. Automatic analogue adjustment systems proposed in (19)(21) have long adjustment and settle time (such as 2 - 5 seconds (21)) compared with the latest digital control systems at the time of writing. One feature of the analogue control systems is that they do not need any "upstream" information from the source loudspeaker: control is achieved only with the information derived from the two microphones.

The work at Göttingen was continued in an experimental and theoretical PhD Thesis by Rollwage (23) and a JASA journal paper (24). The objective was to take the 2-mic control system from one-dimension to three-dimensional acoustics. "Free-field applications of active absorbers present several complications as compared to guided plane waves: arbitrary angles of incidence, spherical instead of plane waves, diffraction effects, discrete (matrix-type) structure of the active systems, and different transfer characteristics of the individual systems" (24); it is important to remember that the intention was to provide flexible impedance and not just active absorption. Experiments were made with a 3x3 loudspeaker array in an anechoic room situated 3m from a primary source. The research found that the 2-mic system could not calculate

the reflection coefficient because of distortions by evanescent and diffracted waves and the use of an intensity probe also failed. A system of scanning the complex pressure field between the controlled surface and the source, and then comparing the results with a model function of the acoustics allowed evaluation of the 3x3 loudspeaker array's acoustic reflection coefficient. The more specific case of providing a characteristic impedance (the case for ideal absorption) used a 2-mic setup with the distance between the microphones corresponding to a quarter-wavelength of the sound. As in the one-dimensional case R could be set at large (greater than 2) or small values (less than 0.1) at 500Hz.

> "Measurements at higher frequencies (eg: 750-1000Hz) have revealed that reflection coefficients below 10% can be realized as well"..."but certain spatial pressure fluctuations remain in the near field of the test box. This is caused by the discrete structure of the loudspeaker array and can only be avoided by applying more loudspeakers closer to one another"

The results presented in (23)(24) show three-dimensional control of impedance. However, as in previous references (19)(20)(21), practical limitations exist because of the non-adaptive analogue control system. The three-dimensional active absorber required re-spacing the two microphones for different frequencies therefore making broad-band control impossible.

Computer simulations in (24) reveal that active control of arrays of loudspeakers "can realize almost arbitrary reflection coefficients for sinusoidal waves at normal and oblique incidence". The research effort states that the control system needed further development so that it could work "with broad-band excitations and in real sound fields with waves incident from various directions simultaneously".

The first efforts to produce a more effective control strategy were published in 1986 by Guicking's team in (25). Digital adaptive filter techniques are adopted to eliminate the unsatisfactory manual control of the analogue system. The system presented no longer uses two microphones, but reverts to the use of a single microphone system as presented in (20). The limitations of the earlier

unstable analogue system are superseded by creating a digital control system with three compensation filters. The setup of these compensation filters requires pre-training of the system. The system concept limits itself to laboratory experimentation as the training of one of the filters (H_p) demands that the sound source is a loudspeaker set at the angle of incidence for the experiment. A generalised practical implementation for arbitrary angles of incidence is therefore not feasible. Another of the proposed fixed filters (H_s) is considered by the thesis author to be time-variant as a result of the active control's time-variance. Analysis of the stability of this single microphone system is not presented. The thesis author has not encountered any subsequent publication describing laboratory experimentation with this control setup.

An application for active impedance control of mechanical structures is described in (26). This is different from the active control of surface impedance described in this thesis so does not merit much further discussion. However, it is interesting that the control systems use similar concepts. In the mechanical impedance control example the actual force experienced by the structure is compared to a "desired" force, that which would occur if the structure has the "desired" impedance. If a control system acts to minimise the difference, or "error", between the actual and desired forces then the structure impedance assumes the desired value. The process of minimising an error signal is often used in modern adaptive control systems. This is employed in the impedance control systems described in this thesis, see Chapter 5.

The application of digital adaptive control to the 2-mic system is presented in (27). The 2-mic system is used to separate incident pressure to drive an adaptive filter. This prevents potentially unstable feedback loops as reflected pressure from the active source can not feedback into the active filter. An error signal is found by calculating the desired reflected pressure and comparing this with the measured reflected pressure. The adaptive filter is configured to adapt to a solution that reduces this error signal. The desired acoustic reflection coefficient is specified by setting a desired reflected pressure. This adaptive system is implemented on an AT&T DSP32C digital signal processor. However

an instability with a compensation filter is mentioned in the final paragraph of this paper. Active control results are not presented.

A personal communication with Dr. D. Guicking (28) mentions that no further work on the active control of impedance has been published partly because of funding difficulties.

A more recent publication by Orduña-Bustamente and Nelson (29) demonstrates one-dimensional broad-band active acoustic absorption by adaptive digital control using the 2-mic system. The reflected pressure is calculated as in (19) although the paper seems unaware of this despite references to Karcher's thesis. The paper describes a similar setup to that depicted in Figure 1 on Page 30 with a smaller duct and 20cm spacing between the two microphones. The adaptive control system is configured to minimise the reflected pressure thus maximising the acoustic absorption of the controlled surface - effectively this is a termination of characteristic impedance. Although reflection coefficients are not presented, absorption of a pulse propagating down the duct illustrates transient broad-band absorption with this system. However, the results indicate that the direct initial pulse from the source was also modified *before* arriving at the controlled surface - see Figure 10 in reference (29). This indicates that the controlled surface responded before the arrival of incident sound and therefore the controller did not implement an optimum solution for true acoustic absorption. The adaptive system is different from the analogue control system used in the work of Guicking *et al* in that it uses an electrical signal taken from the source to feed the input of the adaptive digital filter - see Figure 2 on Page 31 (adapted from Figure 6 of reference (29)). The behaviour of the adaptive system for input signals available in different acoustic scenarios, such as a pressure measurement at some point in the sound field, is not discussed. The paper theoretically demonstrates that the 2-mic system can be configured to achieve other acoustic termination impedances.

An aspect of the 2-mic system that has not yet been mentioned in this literature study is that the impedance is optimized at the centre of the two microphone

spacing (29). For the one-dimensional characteristic termination this is of no consequence: if the impedance between the 2-mic probe is characteristic then the impedance seen by the source will also be characteristic for propagating plane waves. If the 2-mic control system is configured as an active reflector, then the effective centre of reflection will be at the half distance between the microphones. This has the effect of reducing the acoustic length of the pipe compared with replacing the controlled surface with a highly-reflective physical surface. The three-dimensional control of oblique incident waves may be complicated by this "off-cone" controlled impedance. The thesis author feels that it is more relevant to implement a true surface impedance. This can be done by directly measuring the surface impedance with a microphone and an accelerometer. This is the subject of the next part of the literature study.

2.4.3 The "mic-accr" control method

The impedance of a vibrating surface is defined as the ratio of the total acoustic pressure at the surface to the surface velocity. A novel impedance control method is therefore based on instrumenting the surface with a microphone and accelerometer. With the application of conventional control techniques it is then possible to force the surface to have a desired surface impedance. A suitable abbreviation for this control technique is thus "mic-accr" and this will be used throughout this thesis.

Theoretical and practical publications on the mic-accr control method (30)(31)(32)(33) have resulted from this research effort. This thesis partly draws on work performed for these four publications. A schematic on the typical test-rig setup is shown in Figure 3, on Page 32.

A separate and independent publication by Mazzola (34) also demonstrates original research on the use of the mic-accr technique. This is the only other research effort seen by the thesis author on the use of the mic-accr method to control surface impedance. A discussion of this publication follows.

Mazzola's monograph "Active Sound Absorption" contains 106 pages of

theoretical work on a control method for the active absorption of sound. Active sound absorption in a fluid medium of incident waves by a surface is achieved when the surface has the same impedance as the contacting fluid medium - the "characteristic" impedance. Mazzola independently suggests that it is possible to achieve active sound absorption by the instrumentation of a surface with a pressure and a velocity measurement; by minimising an error signal with feedback control it is theoretically possible to force a characteristic surface impedance. Mazzola mainly describes the surface as a plate actuated by piezoelectric transducer material. A preliminary chapter in (34) (pp. 1-2) is reproduced here:

> "When an acoustic plane wave $P_{in}(x,t)$ is normally incident on an infinite, rigid, and fixed plate, the total pressure $P_t(x,t)$ at the surface, $x=0$ is given by:
>
> $$P_t(0,t) = 2P_{in}(0,t) \qquad \text{M.1}$$
>
> If the plate happens to be vibrating, then the total pressure at the plate surface is:
>
> $$P_t(0,t) = 2P_{in}(0,t) + P_p(0,t) \qquad \text{M.2}$$
>
> where $P_p(0,t)$ is the pressure corresponding to the vibration of the plate. If somehow we could set $P_p(0,t) = -P_{in}(0,t)$, then the total pressure at the plate surface would equal the incident pressure:
>
> $$P_t(0,t) = P_{in}(0,t) \qquad \text{M.3}$$
>
> Since $P_p(x,t) = \rho C v_p(x,t)$ it follows that,
>
> $$V_p(t) = -\frac{P_{in}(0,t)}{\rho c} \qquad \text{M.4}$$
>
> Equation M.4 implies that the plate velocity is equal to the particle velocity of the incident wave at the plate surface, consequently, the plate appears transparent, and there is no reflected wave. The minus sign in Equation M.4 accounts for the direction of the wave resulting from the plate vibration is opposite from the incident wave. If we could somehow construct a control system to implement Equation M.4, the plate would absorb all of the incident sound. As a pratical[sic] matter this relation is not useful because the incident pressure cannot be measured. However, under the stated condition, the total pressure equals the incident

pressure. Consequently, Equation M.4 becomes:

$$V_p(t) = -\frac{P_t(0,t)}{\rho c} \qquad \textbf{M.5}$$

Equation M.5 represents, from a control systems[sic] point of view, a useful relationship because both the plate velocity $\mathbf{V_p(t)}$, and the total pressure $\mathbf{P_t(0,t)}$ can be measured right on the plate surface. Using these measurements we wil[sic] show that a control system can be devised that will implement Equation M.5. This Equation is the genesis of the *theory of active absorption of sound* discussed in this book."

The thesis author considers the preliminary chapter to be an excellent introduction to Mazzola's book. The assertion that if the plate velocity is the same as the local velocity of the incident wave at the surface, then "the plate appears transparent, and there is no reflected wave" is later proved by the use of Euler's equation in Sections M1.1.1 and M1.1.2 (34). Section M1.1.3 also shows that all the incident intensity will be absorbed. By maximising instantaneous intensity, the same control law as Equation M.5 is derived (page 15), the same control law is also derived using the "Calculus of Variation" in Section M1.2.2. Mazzola thus proves that ideal acoustic absorption exists if the impedance is characteristic at the mic-accr measurement point. It is also stated that, with an assumption of uniform surface velocity caused by the transducer, the "external pressure does not have to be a travelling wave, plane or otherwise" for maximum intensity at the measurement point.

Chapter M2 describes a feedback control system in transform notation that appears to allow the control law of Equation M.5 to be implemented with a high loop gain for the plate with normal incidence plane waves. A schematic is reproduced in Figure 4 on Page 33. Section M2.3.2 extends this to show that if there is enough loop gain then, in addition to absorption of incident waves, any plate vibration from another noise mechanism will also be decoupled from the fluid medium by the controlled piezoelectric transducer. A conventional feed-forward control system as implemented later in this thesis will be able to do this for broad-band noise with a suitable "reference" signal for the control filter. However, no mention is made of the stability of a practical implementation of this feedback control system. This thesis shows that a potential unstable feedback

loop path exists around any feedback controlled active absorber. This loop can prevent the implementation of certain impedances with some control architectures - see Section 6.4 on Page 117. An analysis of Mazzola's system appears in Section 6.8.

Chapter M3 presents a calculation comparing the control system gain against the theoretical reflection coefficient at the surface of the plate. A worked example suggests that the required control system gain is 84dB for an underwater application with a desired reflection coefficient of -20dB. However, no account is offered on the feedback stability of the system with this gain in the loop. Section M3.2 takes a deviation from the fixed, rigid infinite plate to a simple compliantly suspended plate, but shows that the resonance is poorly controlled by the feedback structure.

Chapter M4 develop a similar feedback control law to Equation M.5 by differentiating the intensity at the plate to find the maximum power absorption. Mazzola then states the input impedance of an active absorber should equal the dual of its radiation load for maximum power absorption. This is demonstrated in the final chapter for several structures by showing that each can theoretically absorb incident waves. These structures are not constrained to one dimension. Unfortunately, in each case the analysis assumes that the incident wave has the same shape as the absorber's structure. Therefore, although the structures are multi-dimensional, these examples are limited in their application. Control strategies are designed for an absorbing infinite plate composed of thin active strips for oblique incidence waves and a baffled circular piston absorber for normal incident waves. The piston absorber is shown to have a larger absorption cross-section than the geometric cross-section (Section M5.5.3) for small ka. This result is independently mentioned in (29) for the free-field case.

Equation M.5 can be rearranged to give Equation 2.1. This represents the desired input impedance of the plate z_s.

$$z_s = -\rho c = \frac{P_t(0,t)}{V_p(0,t)} \qquad 2.1$$

The negative sign of Equation 2.1 arises because of the direction of positive sound propagation assigned by Mazzola. This direction is noted by the arrow symbol from the surface labelled as $V_p(t)$ in Figure 4 on Page 33. Mazzola chooses the unique case where the radiation load is ρc hence the desired input impedance of the plate is $z_s = -\rho c$ for sound absorption. In a practical implementation of this control strategy the actual radiation load impedance will have to be modelled in the filter shown in Figure 4. The thesis author, whilst impressed by the theoretical thoroughness of (34), feels that practical issues are generally overlooked. For example no consideration is made of the effect on the practical absorber performance of errors in the radiation load model and in the pressure and velocity measurements. Also the loop stability of the feedback control system is not discussed. This controller is examined in Section 6.8 of this thesis. Mazzola seems unaware of other research in this field as there is a complete absence of any reference to other pertinent and contemporary work on active sound absorption.

The systems described in this thesis for the control of impedance also measure the pressure and velocity at a surface. However, the systems allow the desired surface impedance to be arbitrarily assigned. The controlled surface can then, for example, be set to act as a sound reflector or a pressure release boundary. The control systems are analyzed and practical results are presented later on the general control of surface impedance.

2.4.4 Patent on a variable reflection/absorption system

The theoretical description of an "Electro-acoustics system having a variable reflection/absorption characteristic" is U.S. Patented (35). The patent theoretically refers to modifying the motion of the diaphragm of a loudspeaker with analogue active feedback circuitry to present a defined vibrational response to an acoustic excitation. The patent proposes using a multiplicity of such devices to influence the acoustics of an enclosed space.

2.5 GENERAL REFERENCES

Various papers on active control were educational for the thesis author. Reference is made to these and other works in this section.

The difference between feedback and feed-forward control structures is described in Chapters 6 and 7 of (2). The book "Adaptive Signal Processing" by Widrow and Stearns (36) is a fundamental text written by the creators of the Least Mean Squares (LMS) algorithm, and the LMS filtered-X variation. The filtered-X LMS algorithm is used by many researchers in the field of active control for acoustics and is described in this thesis in Section 3.6 on Page 45.

Papers on the stability and effects of the implementation of the filtered-X LMS algorithm include (37)(38)(39). The significant contribution of these works is this description of limits on the model of the control system's forward path: the LMS algorithm may still be able to converge even if the model has small errors.

The stability of the two basic control system forms used in active sound and vibration control, feedback and feed-forward (see Section 3.3 on Page 35), are examined in (40) with general conclusions of feed-forward being the more stable. This paper illustrates frequency domain theoretical analysis of control systems.

The filtered-X LMS algorithm conventionally adapts the weights of a non-recursive filter; the generation of poles in the control filter transfer function is not possible. Adaptive algorithms for recursive filters for control have also been described in the literature, allowing control transfer functions with poles. An important consideration of the use of such algorithms for acoustic control is whether real-time implementation is possible. Feintuch (41) describes a recursive filter based on feed-forward and feedback linear combiners. Larimore *et al* (42) describe the Simplified Hyperstable Adaptive Recursive Filtering (SHARF) algorithm for adapting recursive filters, this algorithm averages the error signal before calculating the updates for the filter taps. The LMS algorithm is shown to be a special case of the SHARF algorithm, by setting the weighted averaging to zero. Hsia (43) presents a "Simplified Adaptive Recursive Filter

Design" that is readily implementable with current real-time signal processing. Feintuch's recursive LMS filter was implemented and shown to have stable convergence (44). A significant contribution on recursive filtering for active acoustic control problems has been made with the development of the filtered-U RLMS algorithm (45). This allows compensated recursive control of a forward path.

The development of an active control strategy for a vibration problem is described by Sommerfeldt (46). A feature of this work is that the control system is designed not only to model solutions to the vibration problem with an LMS filter, but also to track real-time physical changes in the vibration path by "system-identification" techniques. Many laboratory examples of active control systems do not have the ability to monitor changes in the physics of the model environment, and are not able to cope with the changing environments of many real-world problems. Methods to model these changes are described in (47)(48)(49).

Research in the active control of noise generated by a vibrating panel generally concluded that the direct active structural control by forcing the vibration of the plate is more effective in reducing sound radiation than by using external acoustic sources (50).

On the subject of global control of enclosed sound fields Nelson and Elliott show that "large global reductions can be achieved, with secondary sources remotely placed from the primary source, provided the enclosure is excited at a frequency close to a lightly damped resonance" (p.356 (2)). Information on local control by cancelling the pressure at a microphone situated in the near field of a loudspeaker is discussed with observation of the small size of "zone of quiet" (pp.369-378 (2)) with useful observation of the size of the loudspeaker and the diameter of the loudspeaker.

The use of electrical equivalents for acoustic systems for active control is

commented on by Nelson and Elliott (2) :

> "We will not, however, attempt to interpret the physical behaviour of acoustic systems purely in terms of an electrical equivalent circuit. The physical behaviour of acoustic systems in active control applications is too subtle for this to be worthwhile. However, the obvious parallels between electrical and some acoustical systems will be pointed out."

Problems with the equivalent electrical representation of acoustical systems for active control applications are backed up by the thesis author's practical experience with real systems. This is often due to mechanisms that are not adequately described by simplified electrical equivalence such as non-linearity of the cone displacement against voltage input of a loudspeaker with different cone excursion levels. The thesis author acknowledges Nelson and Elliott's opinion that the physical behaviour of acoustic systems in active control applications is often too subtle for simplified representation by electrical equivalent circuits; this is in part because of incomplete understanding of acoustical systems. Electrical equivalents of acoustic systems are used in this thesis for illustrative purposes - comment is made of any additional factors, not described by the electrical circuits, that are properties of the acoustical system.

The ability of a single absorbing side-branch to reduce sound in a duct is discussed on pp.128-131 (2). A secondary source configured for maximum sound power absorption is mounted on the side of a duct. It is shown that the secondary source absorbs half of the incident sound energy, a quarter of the sound energy is transmitted down the duct and the remaining quarter is reflected back to the source. The spacing between the absorbing side-branch and the absorbing surface affects the radiated energy of the source. When the spacing corresponds to a quarter wavelength (or multiples of) the absorber will

> " 'suck' *more* sound power from the primary source than it would otherwise radiate into an infinite duct. When averaged over frequency however, the primary source power output remains unchanged".

It is necessary to mention that the maximum sound power absorption over a range of frequencies is not achieved with a single value of surface impedance. Instead the surface impedance must equal the dual of the radiation load presented to the controlled surface. The active control of surface impedance is, therefore, only appropriate as a means for maximising sound power absorption

if the radiation load is known. Alternatively, intensity measurement could be used with a suitable controller design to maximise the net energy flow into a controlled sound absorber.

The ability of a secondary source termination to absorb incident sound in ducts is theoretically examined on pp.157-158 (2). The pressure in the duct is described in terms of the travelling waves from a sound source, situated at one end of the duct, and a secondary source at the other end. Nelson and Elliott show that the reflected travelling wave can be cancelled if the strength of a secondary source is a delayed inverted version of the sound source strength. The termination is then seen to effectively absorb the incident radiation. This examination illustrates the opportunity to create sound absorbing terminations by active control of the secondary source radiation.

Anthony and Elliott discuss three methods of measuring volume velocity of a KEF B110B loudspeaker (51). The measurement of velocity at three discrete points over the loudspeaker cone using 'laser velocimetry' techniques reveals that the driven cone moves as a piston for frequencies up to approximately 500Hz. This research project uses KEF B200A loudspeakers. These use similar cone material to the B110B units but the B200A cone is nearly twice the radius. In the absence of laser measurement techniques, the thesis author assumes the B200A cone will have a lower frequency limit on piston-like motion than the 500Hz of the B110B cone.

The performance and robustness of feed-forward and feedback controllers that use feedback cancellation has been examined by Elliott and Sutton for the active reduction of noise (52). This recent work presents a method to quantify the effect of changes in the system under control on the maximum active noise reduction performance. The stability of adaptive algorithms in the feedback controller is examined - a simple modification to the LMS algorithm is shown to make the controller more stable. This paper is described in more detail on Page 55 in Section 3.8.

2.6 SUMMARY

The control of surface impedance has been theoretically and practically performed by other researchers for the active absorption of incident sound. The original contribution of this thesis is the analysis and implementation of a new method to achieve impedance control. A similar method for sound absorption has been examined independently in a theoretical work (34). However, the controller implementations presented in this thesis are different and the controlled impedance can be arbitrarily assigned (see Chapters 5 and 6 in this thesis). This thesis also presents practical results on the control of impedance that include the active reflection of sound (see Chapter 8).

2.7 CHAPTER FIGURES

The figures referred to in this chapter appear on following pages.

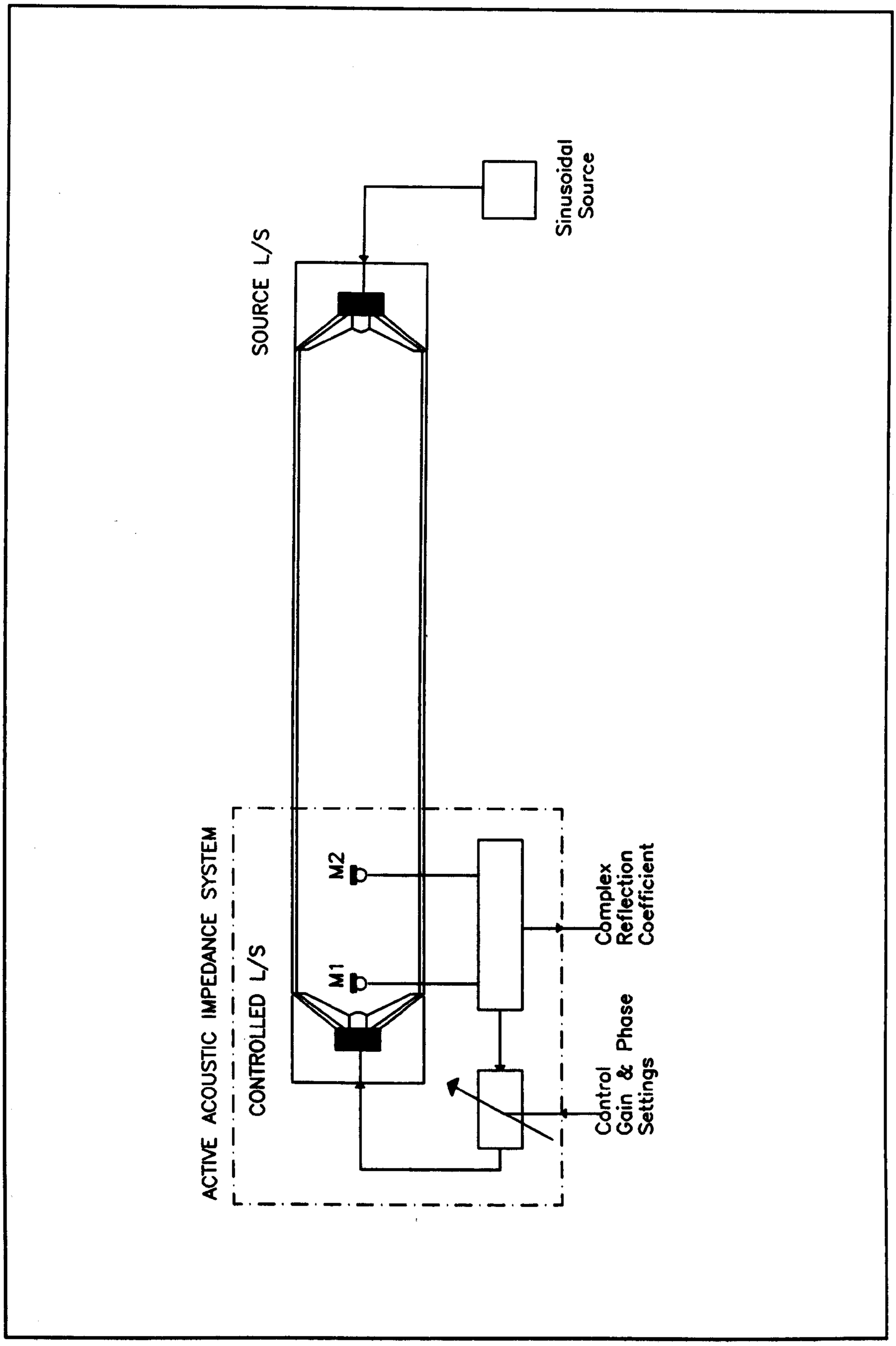

Figure 1. Laboratory test-rig for active acoustic impedance control: the "2-mic" analogue non-adaptive control system after Guicking et al.

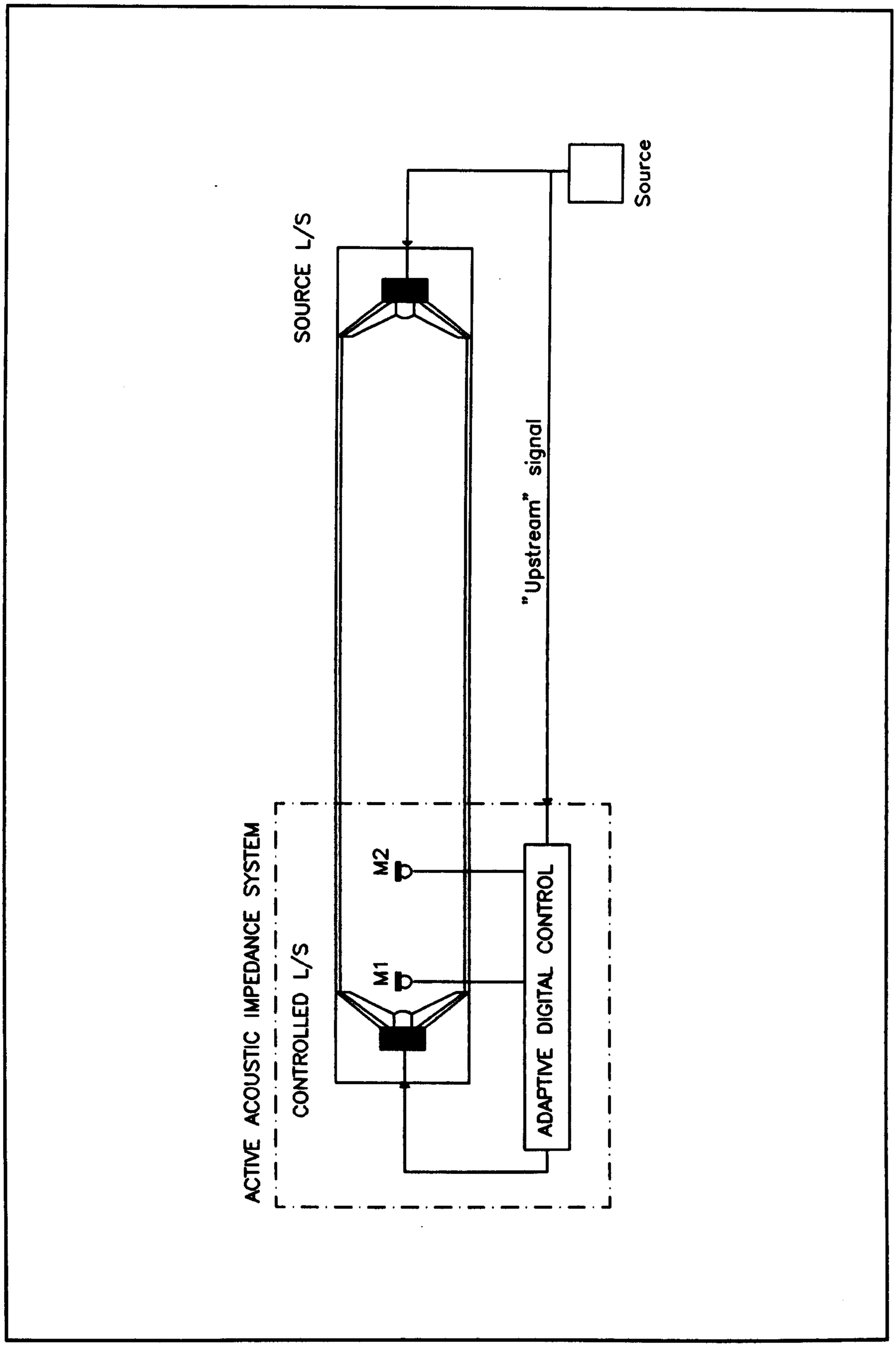

Figure 2. Laboratory test-rig for active acoustic absorption: the "2-mic" adaptive digital control system after Orduña-Bustamente and Nelson

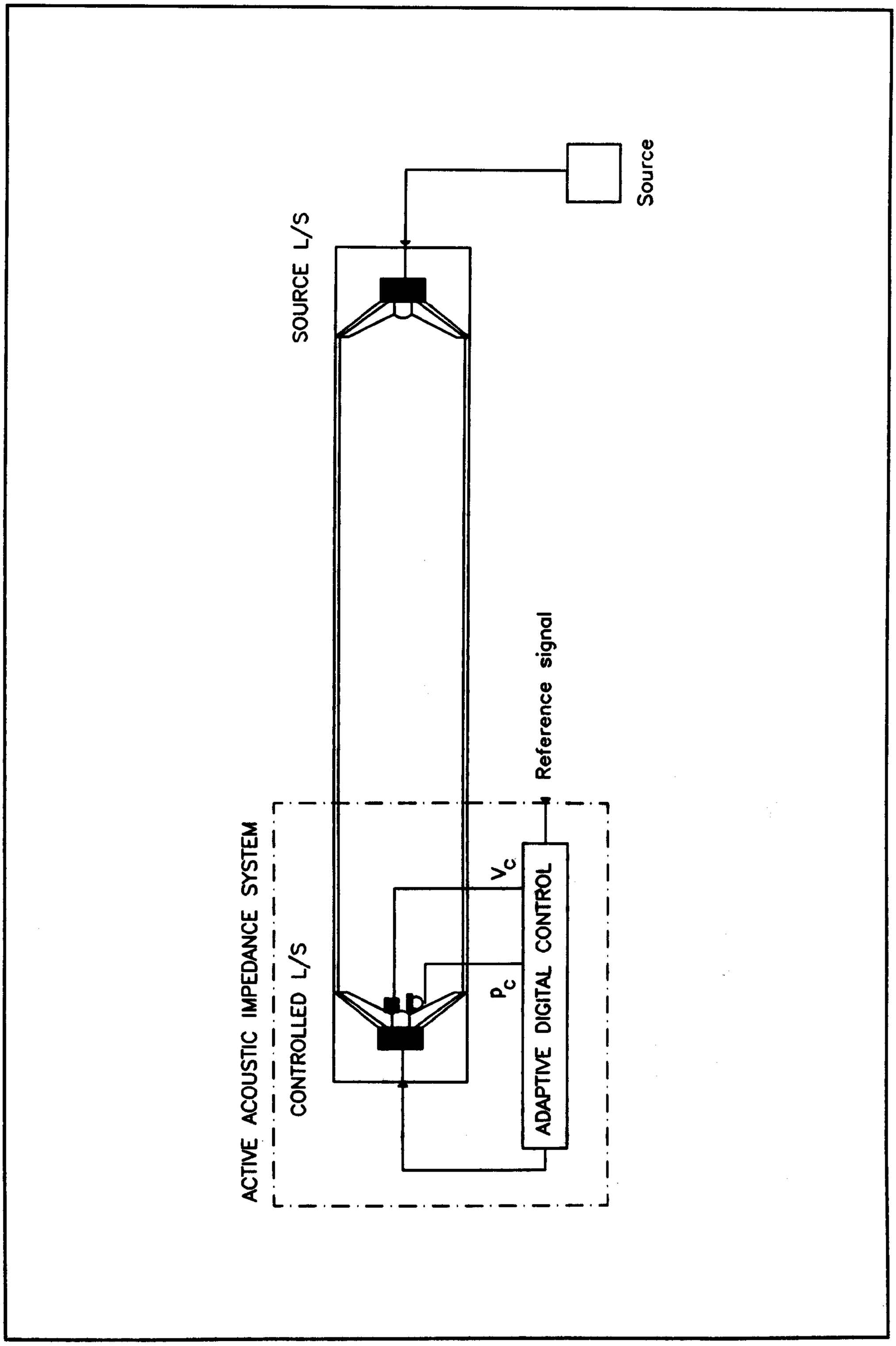

Figure 3. Laboratory test-rig for active acoustic impedance control: the "mic-accr" adaptive digital control system after Darlington and Nicholson

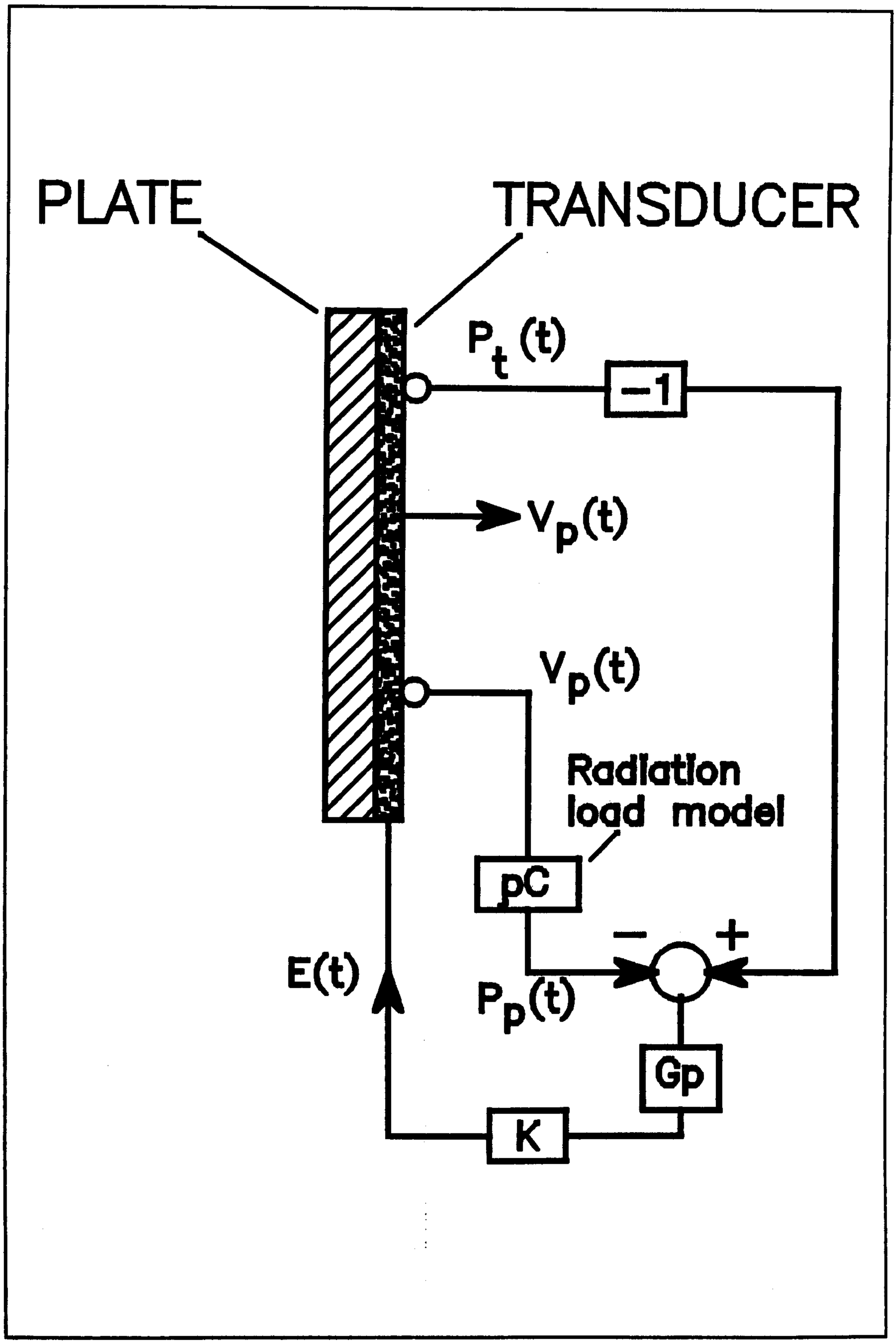

Figure 4. Theoretical control for active acoustic absorption with a plate: the "mic-accr" analogue non-adaptive feedback control system after Mazzola

3 A REVIEW OF CONTROL TECHNIQUES

3.1 INTRODUCTION

The research project uses active digital linear control techniques to modify surface impedance. This chapter provides a review of relevant contemporary control techniques. The differences between "feedback" and "feed-forward", fixed and adaptive control are explained. The adaptive "Least Mean Squares" algorithm and its' "filtered-X" variant are described. Limitations on the performance of the "filtered-X" algorithm are discussed, these include system modelling and unwanted feedback paths. Methods for overcoming these limitations are described, one of which is the "filtered-U" algorithm.

The aim of this chapter is to provide a description of the control techniques used for the work described in this thesis. The chapter contents are not original - all sources are cited.

3.2 MODIFICATION BY CONTROL

The application of control is motivated by a desire to modify an existing physical occurrence. The occurrence may be local pressure in a fluid medium, or motional vibration of a surface such as a plate. The introduction of a control-generated occurrence will modify the existing situation. If the operational environment allows linear addition of the occurrences then a simple illustration can be made with Figure 5, on Page 60. In Figure 5a there is a primary perturbation x_p that causes a physical result or output y_0. If a different output is preferred, say y_1, this can be achieved by the introduction of a suitable control perturbation x_c as in Figure 5b. The environment allows linear addition so y_1 can be defined by Eq. 3.1 as a combination of the two inputs.

$$y_1 = x_p + x_c \qquad 3.1$$

The control system task is to generate a suitable x_c. This ability to modify an existing occurrence is the essence of much recent work on the control of noise and vibration problems (2)(4)(5).

3.3 FEEDBACK AND FEED-FORWARD CONTROL

There are two principal arrangements used in the design of control systems. These forms are designated "feedback" and "feed-forward". A description of these follows.

The linear medium of Figure 5b shows the creation of a preferred output from the combination of a primary and a control perturbation. The control perturbation is generated by the action of a control system, represented as **W**, on an input. The sourcing of this input leads to the two different control arrangements known as feedback and feed-forward. If **W** is a linear system then the input must be coherent with the primary perturbation.

The feedback arrangement sources the control system input from the output y_1 - see Figure 6a on Page 61. The output is fed back into the environment by the control system W_1 hence the phrase *feedback*. For example, the output could be the pressure measured by a microphone at a point in a sound field.

The feed-forward arrangement sources the control system input from any signal that is time-advanced and related to the primary disturbance as shown in Figure 6b. For example, if the primary disturbance was generated by a loudspeaker then a time-advanced and related signal could be the electrical signal at the loudspeaker voice-coil input. It must be noted that x_p can not be used directly as the input because x_p and x_c can not be observed separately in the fluid medium. The extraction of a suitable input is a major consideration in the design of any feed-forward control system.

The practical implementation of the control system **W** may be unstable. A discussion of the stability of feedback and feed-forward systems for active noise control is given in (40), with the general conclusion that feed-forward systems offer greater stability for active noise cancellation.

3.4 FIXED AND ADAPTIVE CONTROL SYSTEMS

The relationship, or "transfer function", between the output and input of a real control system is definable mathematically and is implemented with a filter. The transfer functions of the feedback and feed-forward control system filters are not interchangeable; for either case the transfer function is unique. There are two principal schemes used to design control system filters: (i) "fixed" systems that use a filter of pre-designed transfer function; (ii) "adaptive" systems that are able to design the transfer function of the filter during control.

A principal book on adaptive digital systems by Widrow and Stearns (36) illustrates the importance of the use of adaptive systems in real life applications (p. 5):

> "The essential and principal property of the adaptive system is its time-varying, self-adjusting performance. The need for such performance may be readily seen by realizing that if a designer develops a system of *fixed design* which he or she considers optimal, the implications are that the designer has foreseen all possible input conditions, at least statistically, and knows what he or she would like the system to do under each of these conditions. The designer has then chosen a specific criterion whereby performance is to be judged, such as the amount of error between the output of the actual system and that of some selected model or "ideal" system. Finally, the designer has chosen the system that appears best according to the performance criterion selected, generally choosing this system from an a priori restricted class of designs (such as linear systems).
>
> In many instances, however, the complete range of input conditions may not be known exactly, or even statistically; or the conditions may change from time to time. In such circumstances, an adaptive system that continually seeks the optimum within an allowed class of possibilities, using an orderly search process, would give superior performance compared with a system of fixed design."

This illustrates the limitation of fixed control system design for many real life operating situations. Sections 3.5, 3.6 and 3.7 describe adaptive methods used in contemporary active control systems for noise and vibration.

3.5 THE LEAST MEAN SQUARES (LMS) ALGORITHM

The LMS algorithm is a well known and widely used adaptive filter design method, and has received considerable attention in the literature of active noise and vibration control. The LMS algorithm is formally described in (36), and reproduced here for completeness. A typical LMS implementation is based on the "Adaptive Linear Combiner", although it can be implemented for recursive structures (36)(41)(44)(45) as described later in this chapter on Page 50.

3.5.1 The Adaptive Linear Combiner

Widrow's introduction to the adaptive linear combiner (p.15 in reference (36)) is reproduced here:

> "The linear combiner, or non-recursive adaptive filter, is fundamental to adaptive signal processing. It appears, in one form or another, in most adaptive filters and systems, and it is the single most important element in "learning" systems and adaptive processes in general."
>
> "Because of its non-recursive structure, the adaptive linear combiner is relatively easy to understand and analyze. In essence it is a time-varying, non-recursive digital filter, and as such its performance is quite simple."

A diagram of the digital "transversal" form of the adaptive linear combiner is shown in Figure 7, on Page 62. The digital implementation involves discrete sampling of interval "k", the elements of any time sequence are sequential samples taken at points k, k-1,...., going back in time. There is a single time-domain input x_k that is fed to a "tapped delay line", the input propagates along the line with each delay D corresponding to the sample interval k ie: x_k , x_{k-1} , ... x_{k-L}. At each delay output, or tap, there is a corresponding set of adjustable weights, w_{0k} , w_{1k} , ... w_{Lk} , a summing unit, and a single output signal, y_k. A procedure for adjusting or adapting the weights is called "weight adjustment", "gain adjustment" or "adaptation". The mathematical description of the combiner in Figure 7 is:

$$y_k = \sum_{l=0}^{L} w_{lk} x_{k-l} \qquad 3.2$$

Note that for the discrete time instance k there is a unique set of weights

because of adaption. It is convenient to make vectors for the input and weight sequences:

$$\overline{X_k} = [\, x_k \; x_{k-1} \; \ldots \; x_{k-L} \,]^T \qquad 3.3$$

$$\overline{W_k} = [\, w_{0k} \; w_{1k} \; \ldots \; w_{Lk} \,]^T \qquad 3.4$$

In this notation T represents transpose, so $\overline{X_k}$ and $\overline{W_k}$ are actually column vectors. It is possible to express Eq. 3.2 in vector notation using Eq. 3.3 and Eq. 3.4 :

$$y_k = \overline{X_k}^T \overline{W_k} = \overline{W_k}^T \overline{X_k} \qquad 3.5$$

With this description of the adaptive linear combiner it is possible to proceed to a description of the adaption process.

The combiner is called "linear" because for a fixed setting of the weights its output is a linear combination of the input components. However, when the weights are in the process of being adjusted, the output of the combiner is not a linear function of the input. The nature of the adaption algorithm determines the function of the weight change and the input signal. It is possible to separate two distinct phases for successful adaptive processes: the "learning" phase where the adaptive combiner is not linear, and the "static" phase where the adaption has reached a steady solution for the weight coefficients, and the combiner is linear. Some implementations of the adaptive linear combiner may permanently operate in the "learning" phase, with a non-stationary relationship between the input and output of the adaptive filter. For example, Section 7.6.1 on Page 219 describes observation of non-stationary control of impedance with an adaptive linear combiner.

The transversal adaptive linear combiner or non-recursive filter is characterised by having an impulse response that is physically restricted to a maximum of L samples. This is often described as a finite impulse response (FIR) filter structure.

3.5.2 Desired Response and Error - the Error Estimation

The weights of the linear combiner are adjusted so that the output from the adaptive filter will agree with a desired response. This is achieved by "comparing the output with the desired response to obtain an "error" signal and then adjusting or optimizing the weight vector to minimize this signal. In most practical instances the adaptive process is oriented towards minimizing the mean-square value, or average power of the error signal" (p.18 in (36)). This method of design, by minimizing the difference between the output and the desired signal, is often referred to as "error estimation". This method is shown in Figure 8, on Page 63. The output signal, $\mathbf{y_k}$, is subtracted from the desired signal, $\mathbf{d_k}$, to produce the error signal Eq. 3.6.

$$e_k = d_k - y_k \qquad 3.6$$

Widrow states:

> "The source of the desired response signal, $\mathbf{d_k}$, depends on the application of the adaptive combiner. For the present assume the availability of such a signal." "We note, however, that considerable ingenuity is often required to find a suitable signal, since if the desired response were available one would generally not need the adaptive system."

Of particular interest to this thesis is the selection of $\mathbf{d_k}$ in the presence of coupling between $\mathbf{d_k}$ and $\mathbf{y_k}$. This is discussed for the mic-accr active control system in Section 6.6 on Page 139.

The error estimation Eq. 3.6 allows description of the "performance function" of the adaptive linear combiner. This is the subject of the next section.

3.5.3 The Performance Function

The performance of the adaptive linear combiner's error estimation can be considered by assuming statistical properties of the signals, this enables derivation of the mean-square-error. .The following section is taken from pp.19-20 in reference (36).

The error estimation Eq. 3.6 and the linear combiner output description Eq.

3.5 can be combined to yield:

$$\varepsilon_k = d_k - \overline{X_k}^T \overline{W} = d_k - \overline{W}^T \overline{X_k} \qquad 3.7$$

The subscript **k** has been dropped from weight vector $\overline{W}$ for convenience because in this discussion we do not wish to adjust the weights. Taking the square of Eq. 3.7 gives the instantaneous squared error:

$$\varepsilon_k^2 = d_k^2 + \overline{W}^T \overline{X_k} \overline{X_k}^T \overline{W} - 2 d_k \overline{X_k}^T \overline{W} \qquad 3.8$$

We assume that , ε_k d_k and $\overline{X_k}$ are statistically stationary and take the expected (or mean if the distribution is gaussian) value of Eq. 3.8 over k:

$$E[\varepsilon_k^2] = E[d_k^2] + \overline{W}^T E[\overline{X_k} \overline{X_k}^T] \overline{W} - 2E[d_k \overline{X_k}^T] \overline{W} \qquad 3.9$$

Note that the expected value of any sum is the sum of expected values, but that the expected value of a product is the product of the expected values when the variables are statistically independent. The signals $\mathbf{x}_k$ and $\mathbf{d}_k$ are *not* generally independent, so the last term in Eq. 3.9 cannot be separated.

The mean-square-error function can be expressed more conveniently as follows. Let $\overline{\overline{R}}$ be defined as the square matrix Eq. 3.10.

$$\overline{\overline{R}} = E\left[\overline{X_k}\,\overline{X_k}^T\right] = E \begin{bmatrix} x_k^2 & x_k x_{k-1} & x_k x_{k-2} & \cdots & x_k x_{k-L} \\ x_{k-1} x_k & x_{k-1}^2 & x_{k-1} x_{k-2} & \cdots & x_{k-1} x_{k-L} \\ \vdots & \vdots & \vdots & & \vdots \\ \vdots & \vdots & \vdots & & \vdots \\ x_{k-L} x_k & x_{k-L} x_{k-1} & x_{k-L} x_{k-2} & \cdots & x_{k-L}^2 \end{bmatrix} \qquad 3.10$$

This matrix is designated the "input correlation matrix". The main diagonal terms are the mean squares of the input components, and the cross terms are the cross correlations among the input components.

Let $\overline{P}$ be similarly defined as the column vector

$$\overline{P} = E[d_k \overline{X_k}] = E[\, d_k x_k \quad d_k x_{k-1} \quad \cdots \quad d_k x_{k-L} \,]^T \qquad 3.11$$

This vector is the set of cross correlations between the desired response and the input components. The elements of both $\overline{\overline{R}}$ and $\overline{P}$ are all constant second-order statistics when $\overline{X_k}$ and d_k are stationary.

We now let the mean-square-error in Eq. 3.9, on Page 40 be designated as ξ and re-express it in terms of Eq. 3.10 and Eq. 3.11 as

$$MSE = \xi = E[e_k^2] = E[d_k^2] + \overline{W}^T \overline{\overline{R}}\, \overline{W} - 2\overline{P}^T \overline{W} \qquad 3.12$$

It is clear from this expression that the mean-square error ξ is precisely a quadratic function of these components of the weight vector $\overline{W}$ when the input components and desired response input are stationary stochastic variables. That is, when Eq. 3.12 is expanded, the elements of $\overline{W}$ will appear in first and second degree only.

Widrow (36) plots a typical two-dimensional mean-square error function which is reproduced here in Figure 9, on Page 64. The vertical axis represents the mean-square error and the horizontal axes the values of the two weights. The bowl-shaped quadratic error function, or *performance surface*, formed in this manner is a paraboloid (a hyper-paraboloid if there are more than two weights). It must be concave upward; otherwise, there would be weight settings that would result in a negative mean-square error, an impossible result with real, physical signals. Contours of constant mean-square error are elliptical, as can be seen by setting ξ constant in Eq. 3.12. The point at the "bottom of the bowl" is projected onto the weight-vector plane as $\overline{W}^*$, the optimal weight vector or point of minimum mean-square error. With a quadratic performance function there is a single global optimum; no local minima exist.

3.5.4 Wiener-Hopf equation for minimum mean-square error

The last section has demonstrated the quadratic performance surface of the weight vector solution and mean-square error for the linear combiner with error estimation. Adaptive algorithms are designed to search the surface to find the single global minimum mean-square error. The rest of this section is taken from pp.21-22 in reference (36).

Many useful adaptive processes that cause the weight vector to seek the minimum of the performance surface do so by gradient methods. The

gradient of the mean-square error performance, designated $\nabla(\xi)$ or simply ∇ can be obtained by differentiating Eq. 3.12 to obtain the column vector

$$\nabla \doteq \frac{\partial \xi}{\partial \overline{W}} = \left[\frac{\partial \xi}{\partial w_0} \quad \frac{\partial \xi}{\partial w_1} \quad \cdots \quad \frac{\partial \xi}{\partial w_L} \right]^T \qquad 3.13$$

$$= 2\overline{\overline{R}}\,\overline{W} - 2\overline{P} \qquad 3.14$$

where $\overline{\overline{R}}$ and $\overline{P}$ are given by Eq. 3.10 and Eq. 3.11, respectively. This expression is obtained by expanding Eq. 3.12 and differentiating with respect to each component of the weight vector. Differentiation of the term $\overline{W}^T\overline{\overline{R}}\,\overline{W}$ can be treated as differentiation of the product $(\overline{W}^T)(\overline{\overline{R}}\,\overline{W})$.

To obtain the minimum mean-square error the weight vector $\overline{W}$ is set at its optimal value $\overline{W}^*$, where the gradient is zero:

$$\nabla = 0 = 2\overline{\overline{R}}\,\overline{W}^* - 2\overline{P} \qquad 3.15$$

Assuming that $\overline{\overline{R}}$ is non-singular, the optimal weight vector $\overline{W}^*$, sometimes called the Wiener weight vector, is found from Eq. 3.15 to be

$$\overline{W}^* = \overline{\overline{R}}^{-1}\overline{P} \qquad 3.16$$

This equation is an expression of the Wiener-Hopf equation in matrix form. The minimum mean-square error is now obtained by substituting $\overline{W}^*$ from Eq. 3.16 for $\overline{W}$ in Eq. 3.12:

$$\xi_{min} = E[d_k^2] + \overline{W}^{*T}\overline{\overline{R}}\,\overline{W}^* - 2\overline{P}^T\overline{W}^* \qquad 3.17$$

$$= E[d_K^2] + [\overline{\overline{R}}^{-1}\overline{P}]^T\overline{\overline{R}}\,\overline{\overline{R}}^{-1}\overline{P} - 2\overline{P}^T\overline{\overline{R}}^{-1}\overline{P} \qquad 3.18$$

We now simplify this result using three rules that are of general utility in discussions of the performance surface:

1. Identity rule for any square matrix $\overline{\overline{A}}\,\overline{\overline{A}}^{-1} = \overline{\overline{I}}$
2. Transpose of a matrix product $[\overline{\overline{A}}\,\overline{\overline{B}}]^T = \overline{\overline{B}}^T\overline{\overline{A}}^T$
3. Symmetry of the input correlation matrix: $\overline{\overline{R}}^T = \overline{\overline{R}}$; $[\overline{\overline{R}}^{-1}]^T = \overline{\overline{R}}^{-1}$ see Eq. 3.10.

Using these rules, Eq. 3.18 becomes

$$\xi_{min} = E[d_k^2] - \overline{P}^T\overline{\overline{R}}^{-1}\overline{P} = E[d_k^2] - \overline{P}^T\overline{W}^* \qquad 3.19$$

It is shown that the minimum mean-square error can be calculated from knowledge of the desired signal, the cross-correlation vector between desired

and input signal $\overline{P}$, and the optimum weight vector $\overline{W}^*$.

3.5.5 De-correlation of error and input components

A useful and important statistical condition exists between the error signal and the components of the input signal vector when $\overline{W} = \overline{W}^*$ (36). Recall from Eq. 3.7 that

$$\varepsilon_k = d_k - \overline{X}_k^T \overline{W} \qquad 3.20$$

We multiply both sides of this equation by $\overline{X}_k$. Since each term is a scalar, we can put $\overline{X}_k$ on either side of each term. Thus

$$\varepsilon_k \overline{X}_k = d_k \overline{X}_k - \overline{X}_k \overline{X}_k^T \overline{W} \qquad 3.21$$

Next, we take the expected value of Eq. 3.21 and obtain Eq. 3.22.

$$E[\varepsilon_k \overline{X}_k] = \overline{P} - \overline{\overline{R}}\,\overline{W} \qquad 3.22$$

Finally we let $\overline{W}$ take its optimum value, $\overline{W}^* = \overline{\overline{R}}^{-1}\,\overline{P}$ in Eq. 3.16, and get

$$E[\varepsilon_k \overline{X}_k]_{\overline{W}=\overline{W}^*} = \overline{P} - \overline{P} = 0 \qquad 3.23$$

This result is the same as the well-known result of Wiener filter theory: that when the impulse response of a filter is optimized, the error signal is un-correlated with (orthogonal to) the input signals to the weights.

3.5.6 Instantaneous Gradient Estimate - the LMS update

The linear adaptive combiner requires an adaptive algorithm to adjust the weight vector to give the minimum mean-square error (MSE). This is typically done by calculation of the gradient of the MSE. At the minimum MSE the gradient will be zero. If, when searching the performance surface, the gradient of the MSE is progressively reduced, then the adaptive algorithm is successfully training the weight vector towards the minimum MSE. The weights are adjusted in the direction of the negative gradient at each step or iteration:

$$\overline{W}_{k+1} = \overline{W}_k + \mu[-\hat{\nabla}_k] \qquad 3.24$$

This equation describes "gradient search by the method of steepest descent"

(36). In Eq. 3.24 $\overline{W}_{k+1}$ and $\overline{W}_k$ are the updated and current weight vectors, μ is a gain constant that regulates the speed and stability of adaption, and $\hat{\nabla}_k$ is the current estimate of the gradient. Since the weight vector change at each iteration is based on imperfect gradient estimates we would expect the adaptive process to be noisy; that is not to follow the true line of steepest descent on the performance surface. Reducing μ slows adaption and reduces the effects of gradient measurement noise.

The LMS algorithm uses an instantaneous gradient estimate of ε_k^2:

$$\hat{\nabla}_k = \frac{\partial [\varepsilon_k^2]}{\partial \overline{W}_k} = \left[\frac{\partial \varepsilon_k^2}{\partial W_0} \cdots \frac{\partial \varepsilon_k^2}{\partial W_L} \right]^T \qquad 3.25$$

instead of an estimate of the true gradient of the mean-square error $\nabla(\xi)$. This special estimate can be calculated at every sample and allows easy implementation of the LMS algorithm on current digital signal processing microprocessors. If we rewrite Eq. 3.25 as

$$\hat{\nabla}_k = 2\varepsilon_k \frac{\partial [\varepsilon_k]}{\partial \overline{W}_k} = 2\varepsilon_k \left[\frac{\partial \varepsilon_k}{\partial W_0} \cdots \frac{\partial \varepsilon_k}{\partial W_L} \right]^T \qquad 3.26$$

Recall from Eq. 3.7 that the adaptive linear combiner (Figure 8, on Page 63) is described by

$$\varepsilon_k = d_k - \overline{X}_k^T \overline{W}_k \qquad 3.27$$

By partially differentiating Eq. 3.27 with respect to $\overline{W}_k$

$$\frac{\partial [\varepsilon_k]}{\partial \overline{W}_k} = -\overline{X}_k \qquad 3.28$$

we can substitute Eq. 3.28 into Eq. 3.26 to give

$$\hat{\nabla}_k = -2\varepsilon_k \overline{X}_k \qquad 3.29$$

This is the instantaneous gradient estimate that is used as the basis for the LMS algorithm. Combining Eq. 3.24 and Eq. 3.29 yields the LMS algorithm :

$$\overline{W}_{k+1} = \overline{W}_k + 2\mu\varepsilon_k \overline{X}_k \qquad 3.30$$

As before μ is the gain constant that regulates the speed and stability of adaption.

The structure of the LMS algorithm applied to the adaption of an adaptive linear combiner is depicted in Figure 10, on Page 65, taken from Page 290 (36). Figure 10a shows the overall adaptive filter and signals. The adaptive linear combiner **W** is shown in Figure 7 on Page 62. Figure 10b shows the details of the LMS algorithm in the z-domain, as opposed to the discrete time domain equation Eq. 3.30. This representation shows smoothing of gradient estimate noise with integration of the update of the weights; the actual implementation in this thesis of the LMS algorithm is performed in the time domain as in Eq. 3.30. As the weight vector is adapted towards the optimum solution, the effects of gradient noise are reduced.

3.6 THE "FILTERED-X" LMS ALGORITHM

3.6.1 Introduction

"The use of an LMS algorithm for active control problems is complicated by a number of factors", page 195 of (2). The error estimation for the adaptive linear combiner of Figure 8 on Page 63 assumes that the output of the adaptive filter is directly compared with the desired signal. Active control problems for acoustics demand acoustic conversion of the adaptive output control signal, subsequently some acoustic quantity will be measured and converted to an electrical signal for error estimation. This implementation of control places an electrical-acoustic-electrical conversion in the output of the adaptive filter as in Figure 11, on Page 66. In general this transfer function will be complex. This transfer function was not present in the derivation of the LMS algorithm in the previous section. A variation of the LMS adaptive control system known as the "filtered-X" LMS algorithm has been designed for this control situation (36).

3.6.2 Development and Derivation of the Update Equation

The development of the filtered-X algorithm is based on the commutability of block transfer functions in linear systems. Consider Figure 12 on Page 67, adapted from p.291 of (36). For the sake of argument we commute the forward-path transfer function **C**, so that the LMS algorithm is directly

implemented as in Figure 12(a). The transfer function can be moved through the input node, to yield Figure 12(b). The change between Figure 12(b) and Figure 12(c) involves commuting the transfer function with the adaptive linear combiner, if both are linear then the same output will result for the same input. The validity of this interchangeability is argued on Page 290-291 of (36) as follows:

> "For the same input, the same output results when the positions of two cascaded filters are commuted provided that the filters are linear and time-invariant. The adaptive filter, however, is neither linear nor time invariant, as we see in Figure 11.24(b)" {reproduced in Figure 10b on Page 65}. "On the other hand, the adaptive filter and the plant would, to a good approximation, be commutable if the plant" {the plant is the forward-path **C** in Figure 11 on Page 66} "were linear and if the time variations of the impulse responses of both the plant and the adaptive filter took place with time constants long compared to the combined memory times of time constants of the adaptive filter and the plant. Thus, with slow adaption, the adaptive filter may be considered linear and commutable with ... (the plant)"

The adaptive linear combiner is non-stationary during training (see Page 38); the development of the filtered-X algorithm demands that the adaptive update speed is very small so that the adaptive filter is approximately linear. This argument allows justification of the filtered-X algorithm as displayed in Figure 12(c) on Page 67. Comparing the systems of Figure 12(a) and Figure 12(c), the input signals to the LMS algorithms are then identical. Providing the adaptive filter has slow adaption then the error signals will be similar. The derivation of the update equation is performed in a similar fashion to that of the LMS algorithm. Recall Eq. 3.26 reproduced here as Eq. 3.31.

$$\hat{\nabla}_k = 2e_k \frac{\partial [e_k]}{\partial \overline{W}_k} = 2e_k \left[\frac{\partial e_k}{\partial W_0} \cdots \frac{\partial e_k}{\partial W_L} \right]^T \qquad 3.31$$

The presence of the forward-path transfer function **C** modifies the error estimation equation as shown in Figure 12(c) on Page 67. The error estimation equation is expressed in vector notation as Eq. 3.32.

$$e_k = d_k - \overline{C_k}^T \overline{\overline{X}_k} \overline{W_k} \qquad 3.32$$

where $\overline{C_k}$ in Eq. 3.32 represents the discrete time-domain impulse response column vector of **C**. $\overline{\overline{X}_k}$ is a symmetric square matrix containing elements of the input signal, see Eq. 3.33.

$$\overline{\overline{X_k}} = \begin{bmatrix} x_k & x_{k-1} & x_{k-2} & \cdots & x_{k-L} \\ x_{k-1} & x_{k-2} & x_{k-3} & \cdots & x_{k-L-1} \\ \vdots & \vdots & \vdots & & \vdots \\ \vdots & \vdots & \vdots & & \vdots \\ x_{k-L} & x_{k-L-1} & x_{k-L-2} & \cdots & x_{k-2L} \end{bmatrix} \quad 3.33$$

The partial differentiation of Eq. 3.32 with respect to the adaptive filter coefficients yields the column vector Eq. 3.34.

$$\frac{\partial [e_k]}{\partial \overline{W_k}} = - \overline{\overline{X_k}}\, \overline{C_k}^T \quad 3.34$$

Eq. 3.34 is then substituted into Eq. 3.31 to give Eq. 3.35.

$$\hat{\nabla}_k = - 2 e_k \overline{\overline{X_k}}\, \overline{C_k}^T \quad 3.35$$

This is the instantaneous gradient estimate that is used as the basis for the filtered-X LMS algorithm. Combining Eq. 3.24 (from Page 43) and Eq. 3.35 yields the filtered-X LMS algorithm Eq. 3.36.

$$\overline{W}_{k+1} = \overline{W}_k + 2\mu e_k \overline{\overline{X_k}}\, \overline{C}_k^T \quad 3.36$$

As before μ is the gain constant that regulates the speed and stability of adaption. Some derivations offer subtraction of the last term on the right hand side of Eq. 3.36, rather than addition. This is because these derivations are for systems with additive error estimation as in the case for acoustic pressure signals, rather than subtraction as in Figure 12.

3.6.3 Convergence and General Properties

Widrow states on p.291 in reference (36):

> "Convergence of the filtered-X algorithm as defined in ... has been demonstrated in a variety of situations. Although the arguments above indicate that adaption must take place very slowly, rapid adaptation has been achieved in most cases with no particular difficulty. Other derivations of the filtered-X LMS algorithm are currently being examined in an attempt to account for its robustness. Physically it appears to work as well as the LMS algorithm itself. The choice of initial conditions for the filtered-X algorithm is not important. The algorithm is stable and transients die out just as with the conventional LMS algorithm."

The filtered-X LMS algorithm is thus considered effective at controlling frequencies defined in the desired response d_k. However, more recent research shows that "passband disturbance" can be caused by delays in the forward-path

of active sound control systems for narrow-band signals (38). "Passband disturbance" is unwanted adaptive filter response at frequencies where control is not desired. This effect is stated as being caused by combination of the inherent time-variance of the adaptive filter and the dynamics of the forward-path, and is theoretically demonstrated for sinusoidal "synchronous" controllers. "Synchronous" means that the discrete-time sample frequency of the control system is a multiple of the signal frequency to be controlled, which is an important class of active sound control systems (53). With increasing forward-path delay, the passband disturbance has more ripple and high-Q peaks, this can degrade the stability of the system and require reduction of the update gain, increasing the convergence time of the control system. Laboratory work performed for this thesis has given subjective observation of these effects in real active sound control systems: high-Q peaks in the adaptive filter response close to the sinusoidal frequency under control slightly modulate the acoustic frequency during convergence. Darlington suggests that, by measuring the control system transfer function, the design of system stability can be improved by ensuring damped passband disturbance.

The general properties of the filtered-X algorithm are (p.197 (2)) as follows:

> "(i) it can converge on a timescale comparable with the delay in the error path {or forward-path}, and so can rapidly track changes in the primary signal; (ii) it is rather robust to errors in the estimate of the error path used to generate the filtered reference, which has a frequency response of $\hat{C}(e^{j\omega T})$ {here designated $\hat{C}$ }; in fact, Morgan (54) has shown that in the limit of slow adaption the algorithm will still converge with nearly 90° of phase error in $\hat{C}(e^{j\omega T})$ compared to $C(e^{j\omega T})$; (iii) it is relatively easy to implement and, compared to the LMS algorithm, it requires only the additional generation of the filtered reference signal."

A feature that makes the filtered-X LMS algorithm attractive for discrete-time implementation is that squaring, averaging, differentiation or integration are all not required. The mathematics require only additions and products.

3.6.4 Modelling Effects on Convergence

The use of the filtered-X algorithm for the active control of acoustics is complicated by the modification of the input signal $\mathbf{x}_k$ for the LMS update. It is not physically possible to pass the input signal through the forward-path in real-time. Instead a filter must be designed that models the forward-path transfer-function C; this model filter, $\hat{C}$, is shown in Figure 13 on Page 68. A common approach is to turn the adaptive control system off, feed white noise into the forward-path and use an LMS algorithm to minimise the difference between the output of the true forward-path C and an FIR model $\hat{C}$. Another approach has been established by Eriksson which allows modelling with continued adaptive control, called "on-line" modelling (47)(45).

The accuracy of this model filter affects the convergence of the filtered-X LMS algorithm. As Nelson and Elliott state in the last section, there is allowable deviation of the model response $\hat{C}$ from the true forward-path C. If there is too much deviation then the adaptive system is likely to be unstable; rather than converge towards the minimum MSE, the error will progressively increase. Boucher *et al* state that provided the phase error is within ±90° and the update gain is small enough, then the system will be stable (37); this reference provides theoretical analysis for this result. General results from this reference are:

> 1) The optimum update gain (that for the minimum time taken by the algorithm to converge to an optimum solution) was found to be approximately one-third of the value for which the system becomes unstable.
>
> 2) Investigation of extra delay in the forward-path reveals that for fixed phase error in each appropriate model, increasing delay reduces the optimum convergence coefficient, with an increase in the minimum convergence time.
>
> 3) For phase errors above 70° the convergence time of the system is greatly increased with extra delay in the forward-path, compared with lower phase error.

Boucher *et al* state that for phase errors less than ≈ 45° the effects of both the delays and phase errors are comparatively small. This then is a sensible criterion for model accuracy: the phase error of any model for filtered-X compensation should be within ± 45° for un-compromised LMS algorithm

convergence at the desired frequencies for control.

Darlington (38) further shows that (for sinusoidal "synchronous" active sound control systems, see Page 48) the influence of the filtered-X model phase error is not just confined to convergence time and update gain setting; additional passband disturbance can also occur. Darlington states:

> "Experiments with the active control of sound in a duct have indicated that the convergence time is only weakly dependent upon control loop phase (within ± 45° at a reference frequency component) whereas passband effects become significant for such control loop phase response.
>
> This leads to the surprising conclusion that the most significant motivation for *accurate* compensation for the dynamics of systems under the control of adaptive filters is the optimization of the passband, rather than stability/convergence issues."

The reference to ± 45° is similar to Boucher *et al*'s findings discussed above. However Darlington recognises that passband disturbance will occur for active control systems with delay in the forward-path, this passband disturbance is modified with phase errors of the model.

3.7 THE "FILTERED-U" RECURSIVE LMS ALGORITHM

3.7.1 Introduction

In this chapter, the LMS adaptive algorithm has so far been applied to transversal adaptive filters. Feintuch (41) describes the application of the LMS algorithm to a recursive filter structure:

> "Adaptive filters that are constrained to a transversal tapped delay structure appear in the literature. . . Such filters have a finite impulse response, i.e.:, they can produce only zeros with no poles in the filter transfer function. This limits the capability of transversal adaptive filters in many applications. To overcome this limitation, a new adaptive filter is described which is capable of producing poles in the transfer function and is easily implemented using two transversal adaptive filters."

Feintuch presents a simulation for the "Recursive LMS" (RLMS) filter which shows that the adaptive control filter can generate poles.

Widrow *et al* describe two disadvantages of recursive adaptive filters that are not found in the non-recursive adaptive linear combiner (p.154 (36)):

> "(i) they become unstable if the poles move outside the unit circle during the adaptive process.
>
> (ii) Their performance surfaces are generally non-quadratic and may even have local minima."
>
> These are serious disadvantages, and consequently the recursive adaptive filter has had very limited application."

Despite these considerations, Eriksson and his co-workers have published work on the use of recursive adaptive filters for the active attenuation of sound. The application of the IIR adaptive filter to active sound control systems requires compensation of the forward-path (as in the filtered-X LMS design), this was first discussed by Eriksson *et al* (44), and completed as the "filtered-U" algorithm in (45).

3.7.2 Development of the filtered-U algorithm

The development of the "filtered-U" RLMS algorithm by Eriksson (45) starts with the "full" RLMS algorithm as shown in Figure 14a on Page 69, which has been described in publications (36)(43)(55)(56). Eriksson states:

> "A weight update procedure may again be developed similar to that for the LMS algorithm in which the filter weights are modified by an amount that is proportional to the gradient of the instantaneous error signal. However, in this case, the gradient of the error signal, with respect to the weights, is not simply the filter input. Since the model output, y_k, is the sum of the output of the direct FIR filter with the transfer function A(z) and the recursive FIR filter with transfer function B(z) in Fig. 6 {here reproduced as Figure 14a on Page 69}, the gradient, with respect to the weights, includes terms representing the input as well as derivatives of the past output with respect to the weights and derivatives of the A and B weights with respect to each other. Although the dependence of the A(z) and B(z) weights on each other is usually ignored, the terms involving derivatives of the past outputs with respect to the weights lead to a pre-filtering of the input to the error correlators by 1/[1-B(z)], as shown in Fig.6(a) {here reproduced as Figure 14a on Page 69}. The completed algorithm is known as the recursive least-mean-square (RLMS) algorithm and has been described by Horvath (56), White (55) and Widrow and Stearns (36).
>
> A simplified version of the RLMS algorithm that does not include the derivatives of the past outputs eliminates the need for the pre-filtering

described above. The resulting algorithm is shown in Fig.6(b) {here reproduced as Figure 14b on Page 69}. Although generally associated with Feintuch (41), this simplified RLMS algorithm was also described by Horvath (56) and earlier by Salomonsson (57) and Mark and Haykin (58)."

The simplified RLMS algorithm can be implemented as two separate LMS algorithms, although Eriksson describes a single update equation that is similar to the LMS update equation Eq. 3.30 but with vector $\overline{W_k}$ that contain both sets of FIR filter weights, and vector $\overline{U_k}$ instead of $\overline{X_k}$ that contains both inputs vectors to the two FIR filters:

$$\overline{W}_{k+1} = \overline{W}_k + 2\mu\,\varepsilon_k\,\overline{U}_k \qquad 3.37$$

where:

$$y_k = \overline{W_k}^T\,\overline{U_k} \qquad 3.38$$

$$\overline{W_k} = [a_{0k}, a_{1k}, \ldots, a_{Lk}, b_{1k}, b_{2k}, \ldots, b_{Nk}]^T \qquad 3.39$$

$$\overline{U_k} = [x_k, \ldots, x_{k-L}, y_{k-1}, \ldots, y_{k-N}]^T \qquad 3.40$$

where a_{lk} and b_{nk} are the individual weights of the two FIR filters, and x_k and y_k are the input and output time samples of the IIR filter.

The addition of a forward-path (see Page 45) leads to the development of the "filtered-U" algorithm as in Figure 15 on Page 70. This follows a similar argument to the development of the filtered-X algorithm on Page 45. The forward-path transfer function is passed through the input node as in Figure 15a. The assumption of a linear control filter is made by assuming the convergence update gain μ is very small, then the transfer function C is commutable with the control filter as in Figure 15b. C is then passed through the output node of the IIR filter as in Figure 15c. This algorithm is described as the "filtered-U" algorithm because of Eriksson's use of $\overline{U}_k$ to describe both of the LMS update inputs x_k and y_k. The application of this development to the control of an electro-acoustic forward-path is illustrated in Figure 16a, the two model filters $\hat{C}$ of the true forward path C are identical. No generalized convergence proof is offered, neither are the considerations of Widrow and Stearns (on Page 51) addressed by Eriksson in (45). Other researchers have suggested the use of recursive adaptive filters for the active control of sound, for example see

reference (59).

A variation on the filtered-U algorithm based on the "full" RLMS algorithm is shown in Figure 16b, this has been derived from Hsia's simplification (43) of the "full" RLMS algorithm of White (55), and from Eriksson's development of the filtered-U algorithm. This suggestion restores the pre-filtering of the error correlator signals as in Figure 14a, with a rearrangement of the internal structure of the IIR filter such that one of the filtering operations is removed allowing easier computational implementation.

3.8 FEEDBACK PATHS AROUND ADAPTIVE FILTERS

"A more difficult problem than the effect of the error path {or forward-path} on the LMS algorithm is the effect of the feedback path.", page 197 of reference (2). If the input to the adaptive linear combiner x_k is acoustically sourced from the fluid medium under control, then there is the potential for the adaptive filter output to feedback into the input. For example see Figure 17a on Page 72, where an adaptive control system is configured to act on the sound field in a pipe. The filter output is converted to acoustic energy by loudspeaker S, the forward-path is measured by microphone B and this signal is compared with the desired signal for error estimation. The input is sourced from microphone A, this gives rise to the feedback path; note that this control system is considered feed-forward, rather than feedback (see Section 3.3 on Page 35). It is possible for this feedback path

> "to destabilise the LMS algorithm, since it is possible for the adaptive filter to pass through a state in which there is a gain of unity around the feedback-controller loop. This will cause an instability which can saturate the hardware being used to implement the adaptive filter, and prevent further convergence." (2)

The mathematics that describes the convergence of an adaptive system in the presence of feedback path become more complicated - this is later examined in Section 6.6.3 on Page 143. Visual analysis techniques have been used to study the output of such systems (60). The results show that adaptive filters in the presence of feedback can behave as chaotic systems under certain conditions, and therefore can have erratic output. The adaptive algorithm can produce

"bursting" in the error signal of a feedback active sound control system as observed later in this thesis in Section 7.6.1 on Page 219. To prevent both instability and unpredictable behaviour, effort in control system design has generally tried to cancel the effects of feedback paths (40). There are three approaches to stabilise adaptive filters with potentially unstable feedback paths: (i) the use of directional microphones and speakers to minimize transmission of sound from the control loudspeaker S to the input microphone A; (ii) the use of a separate "feedback cancellation" filter; (iii) cancel the feedback path by the use of recursive adaptive filters.

The first approach is typified in works by Swinbanks (10) and Jessel (11). The main limitation of this approach "is that directional arrays are usually highly dependent on the narrow spacing of the array elements and are only directional over a relatively narrow frequency range" (44).

The second approach has been investigated by Warnaka *et al* (61), and is depicted for a typical acoustic control problem situation in Figure 17b on Page 72. A model of the feedback path $\hat{\mathbf{F}}$ is made prior to starting the active controller (Warnaka *et al* suggest feeding white noise into the loudspeaker S, and using an separate LMS algorithm to minimise the difference between the output of the true feedback path (the signal from the detection microphone A) and a linear combiner model $\hat{\mathbf{F}}$ of the feedback path). During training the adaptive filter will be off, so the modelling process can be described as "off-line". The effects of feedback are greatly reduced with an accurate model. However, Nelson and Elliott discuss that a few problems exist (2): (i) this approach may be inefficient as **F** may have a long impulse response, thus requiring a mathematically complicated filter $\hat{\mathbf{F}}$; (ii) if $\hat{\mathbf{F}}$ does not exactly match **F** the potential for such an unstable loop still exists; (iii) **F** may be time-variant, thus repeated off-line modelling of $\hat{\mathbf{F}}$ may be necessary. On-line modelling of the feedback path $\hat{\mathbf{F}}$ might be possible if the additional modelling white noise is tolerable.

The third approach of using recursive adaptive algorithms has been considered

by Eriksson and his co-workers. The presence of a feedback path around an adaptive filter creates poles; recursive or infinite-impulse response (IIR) adaptive filter algorithms are therefore more suitable for control purposes than non-recursive or finite impulse response (FIR) adaptive linear combiners in the presence of feedback. Eriksson's filtered-U RLMS algorithm is suggested in the literature as a suitable control algorithm (40)(44)(45).

The effect of the second and third approaches on feed-forward adaptive control system stability in the presence of feedback have been discussed by Swanson in (40). The use of an additional cancellation filter to stabilise the adaptive filter in Figure 17b uses the filtered-X LMS algorithm after Warnaka *et al* (61), whereas Eriksson (45) develops the filtered-U algorithm that can model poles and zeros. Warnaka's approach offers a considerable margin of stability if the cancellation filter is accurate. The use of recursive filters by Eriksson is stable if the magnitude of **B** is less than 1, this ensures loop stability of the transfer function **1/1-B** shown in Figure 14. Swanson states that for typical control problems there will be non-unique solutions for **A** and **B** for optimum MSE convergence, and for an active sound control problem illustrates theoretical active noise cancellation with two different solutions in **A** and **B**. However, it is not possible to generalise what the transfer functions of **A** and **B** will converge to. Swanson concludes that it is not clear which method offers the best measure of stability robustness:

> "Given contamination of the reference noise by feedback from the active control source, it is not clear whether adaptive feed-forward control with feedback compensation or on-line plant estimation offers the best measure of stability robustness. The on-line pole-zero modeling (sic) system will track plant transfer function changes but does carry additional adaptive stability constraints which must be enforced."

Swanson refers here to feedback cancellation as "feedback compensation".

The second approach has been examined recently by Elliott and Sutton (52) for feed-forward and feedback controllers for the active reduction of noise. The performance of a conventional feedback controller is compromised by loop stability. However, the use of an ideal feedback cancellation filter ensures loop

stability. Elliott and Sutton identify this system as "Internal Model Control" (IMC) - a recognised technique in the control literature. The use of IMC transforms the feedback problem into a (pseudo) feed-forward problem so that techniques for describing control performance developed for feed-forward systems can be used. The performance of a true feed-forward system with feedback cancellation is shown to depend on the cross-correlation between the offending noise and the *feedback cancelled reference signal* filtered by the system under control, or "plant". Using the same analysis, the performance of the ideal IMC feedback system depends on the cross-correlation between the noise and the *noise* filtered by the plant. The performance is thus dependent of the statistics of the noise, the plant and, for feed-forward controllers, the coherence of the reference signal with the noise. If the noise is a pure tone, then either feed-forward or feedback IMC control is capable of infinite attenuation. However, if the noise is white and there is delay in the plant (or in the active controller) then the IMC feedback controller can not reduce the noise.

A problem with IMC is that the feedback cancellation filter may become inaccurate if changes occur in the plant. Consequently the feedback cancellation will not be ideal and this can affect the performance and also cause the control system to become unstable. Elliott and Sutton use the term "robustness" to describe the stability of the control system to changes in the plant. Using an uncertainty model of the plant and the complementary sensitivity function the calculation of the robustness of the system is described. Elliott and Sutton then show that a simple modification to the cost function of an adaptive controller used in the IMC feedback system increases the robustness. Other cost functions that tend to improve robustness are described.

Elliott and Sutton present illustrative simulations for the performance of feed-forward and IMC feedback controllers for the active reduction of noise in cars. By assuming that the plant is a simple delay and using noise measured in a real car, IMC feedback control is shown to be able to provide significant noise reduction with shorter plant delays. For longer plant delays feed-forward control is more successful. For this noise, the potential performance of the IMC

feedback control system was better than that of the feed-forward control system if the plant delay was smaller than 1.5 ms. Finally, Elliott and Sutton quantify the relationship of achievable noise reduction with robustness for a given plant delay. This work has increased the understanding of the performance and robustness of IMC active controllers for the active control of sound.

3.8.1 Performance analysis of a simplified Internal Model Control feedback controller

It is of interest to analyze the performance of the Internal Model Control (IMC) feedback controller described in the previous section. Elliott and Sutton have shown that the application of IMC causes the control filter to adopt a feed-forward structure, see reference (52). An analysis of the control filter with the method of least squares (see Section 2.5 of reference (2)) is presented in this section.

A schematic of the control filter in a single channel IMC feedback controller is shown in Figure 18a on Page 73. This has been reproduced from Figure 4b in reference (52) where it was assumed that the feedback cancellation was exact. The control problem can be simplified by assuming that the plant, **G** in Figure 18a, is a pure delay τ (an assumption used in simulations in (52)) and the control filter, **W** in Figure 18a, is a simple linear gain as shown in Figure 18b. The sampled value of the error signal, **e**, can then be written in terms of the excitation, **d**, as Eq. 3.41.

$$e(k) = d(k) - W.d(k-\tau) \qquad 3.41$$

The optimum value of **W** depends on the *cost function* that the control problem is to minimise. The simplest cost function, **J**, is the average or expected value of the square of the error signal as shown in Eq. 3.42.

$$J = E[e^2(k)] \qquad 3.42$$

The performance of the controller is assessed by quantifying the minimum value of the cost function for the variables **W** and **d**. Expanding Eq. 3.42 by substituting from Eq. 3.41 gives Eq. 3.43.

$$J = E[d^2(k)] - 2W.E[d(k).d(k-\tau)] + W^2.E[d^2(k-\tau)] \qquad \textbf{3.43}$$

If the disturbance is stationary then the averages of the squared value and the squared delayed value are identical. Furthermore, if the disturbance has a mean value of zero then the average squared value is simply the variance of the signal, σ_d^2 as expressed in Eq. 3.44.

$$\sigma_d^2 = E[d^2(k)] = E[d^2(k-\tau)] \qquad \textbf{3.44}$$

Equation 3.43 can then be rewritten by normalising the cost function as shown in Eq. 3.45. This operation creates the dimensionless normalised cost function Ψ.

$$\Psi = \frac{J}{\sigma_d^2} = 1 - 2W.\frac{E[d(k).d(k-\tau)]}{\sigma_d^2} + W^2 \qquad \textbf{3.45}$$

The minimum value of Ψ is found by differentiating with respect to the variable W and equating to zero as in Eq. 3.46.

$$\frac{d\Psi}{dW} = -2.\frac{E[d(k).d(k-\tau)]}{\sigma_d^2} + 2W = 0 \qquad \textbf{3.46}$$

The optimum value of W that minimises Eq. 3.45 is therefore Eq. 3.47.

$$W_{opt} = \frac{E[d(k).d(k-\tau)]}{\sigma_d^2} \qquad \textbf{3.47}$$

That this value of W minimises Ψ is confirmed by differentiating Eq. 3.46 with respect to W and noting that the result is positive. The minimum value of Ψ is found by substituting Eq. 3.47 into Eq. 3.45 as expressed in Eq. 3.48.

$$\Psi_{opt} = 1 - \left[\frac{E[d(k).d(k-\tau)]}{\sigma_d^2}\right]^2 \qquad \textbf{3.48}$$

The quantity $E[d(k).d(k-\tau)] / \sigma_d^2$ is the normalised autocorrelation coefficient $\rho_d(\tau)$ of the disturbance d for a lag of τ which is easily measured in real control problems. If the plant delay τ is zero then $\rho_d(\tau)$ is unity, the optimum control filter W_{opt} is also unity and Ψ is zero. This confirms an intuitive understanding of the control problem outlined in Figure 18a on Page 73. For positive values of plant delay τ (real plants can not have negative delay) the performance of this controller depends on the statistics of the disturbance. For example, if the disturbance is white noise, for which $\rho_d(\tau)$ is zero when τ is not zero, then Ψ is

unity and the controller performance is negligible. If the disturbance is sinusoidal with period equal to the plant delay then Ψ is zero and the controller performance is ideal; for other periods the performance can vary from negligible to ideal depending on the value of $\rho_d(\tau)$. The control filter **W** is implemented more commonly as a linear combiner and Elliott and Sutton present an analysis in (52).

3.9 SUMMARY

This chapter has reviewed control techniques that are currently used for the active control of sound. The filtered-X LMS algorithm has been discussed, with reference to its' general performance and implementation. Reference was made to the implementation problems of modelling and feedback; solutions for the feedback problem include the use of a fixed cancellation filter and recursive adaptive filters such as the filtered-U RLMS algorithm. The filtered-U RLMS algorithm offers useful benefits over the filtered-X LMS algorithm for the active control of sound, however doubts remain about the adaptive stability of control systems that use the filtered-U RLMS algorithm for general application.

3.10 CHAPTER FIGURES

The figures referred to in this chapter appear on the following pages.

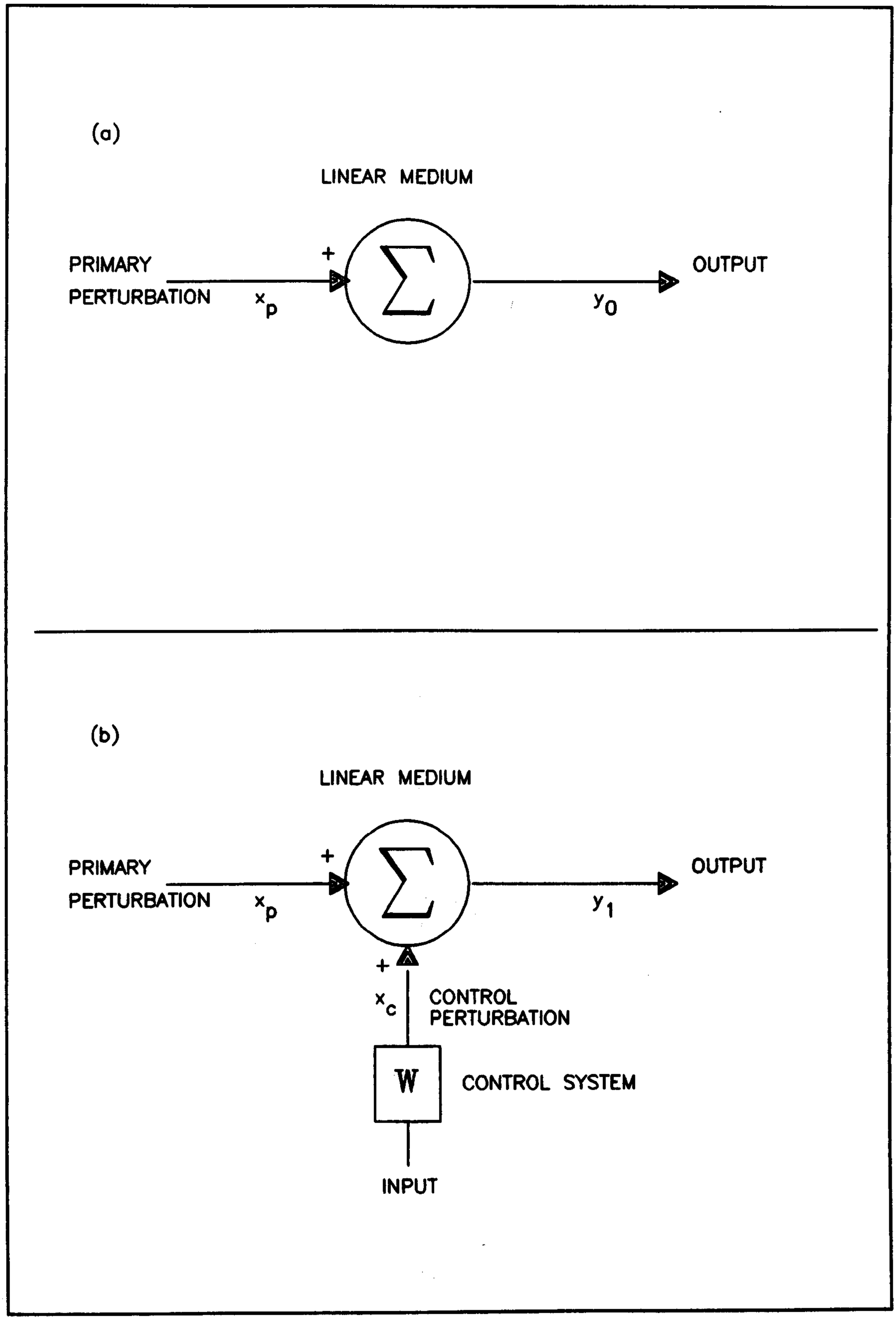

Figure 5. The modification of a primary disturbance by a secondary control disturbance in a linear medium: (a) with no control, (b) with control disturbance x_c generated by system W driven by an input.

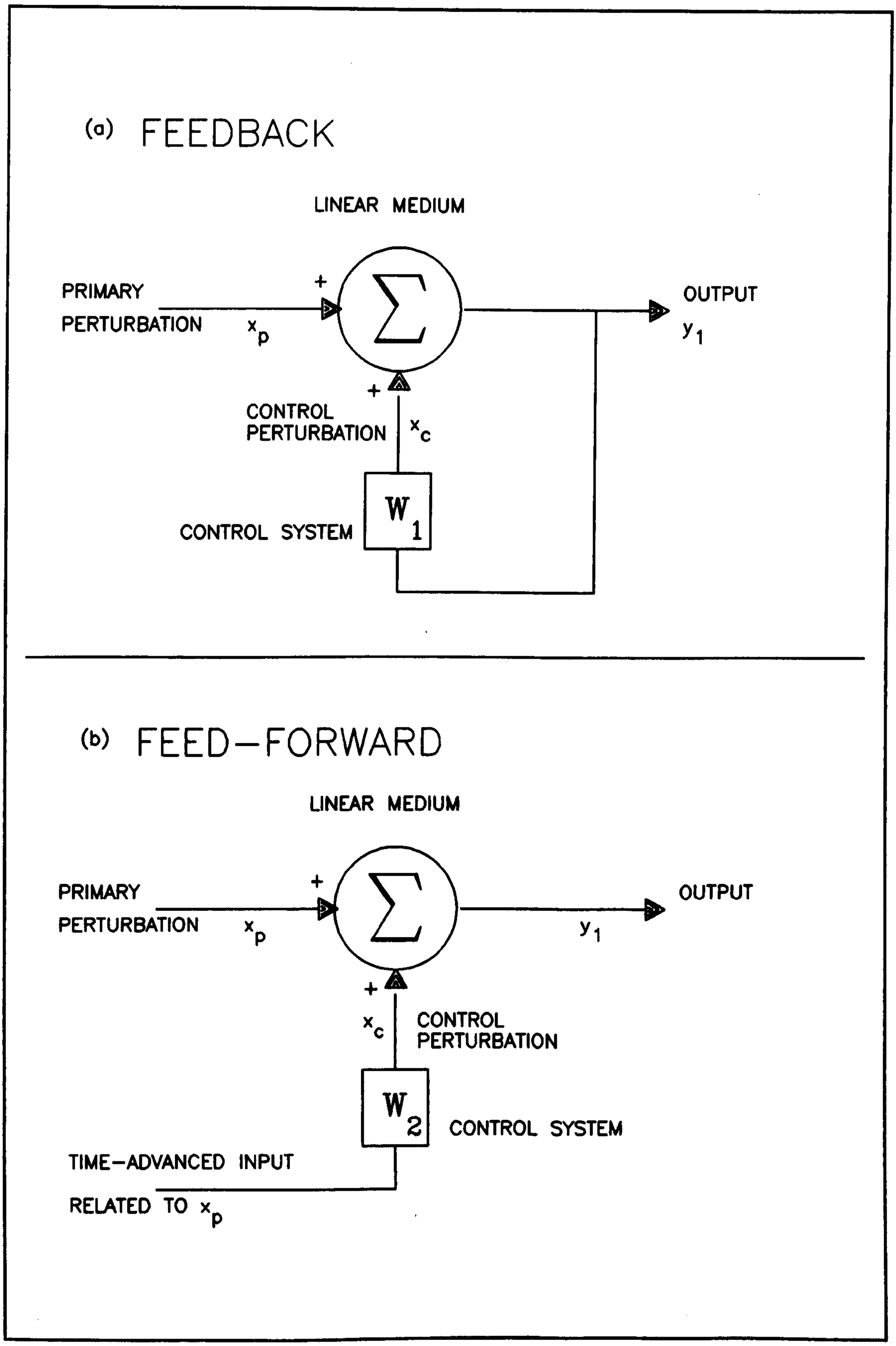

Figure 6. The configuration of the control system input: (a) feedback, (b) feed-forward.

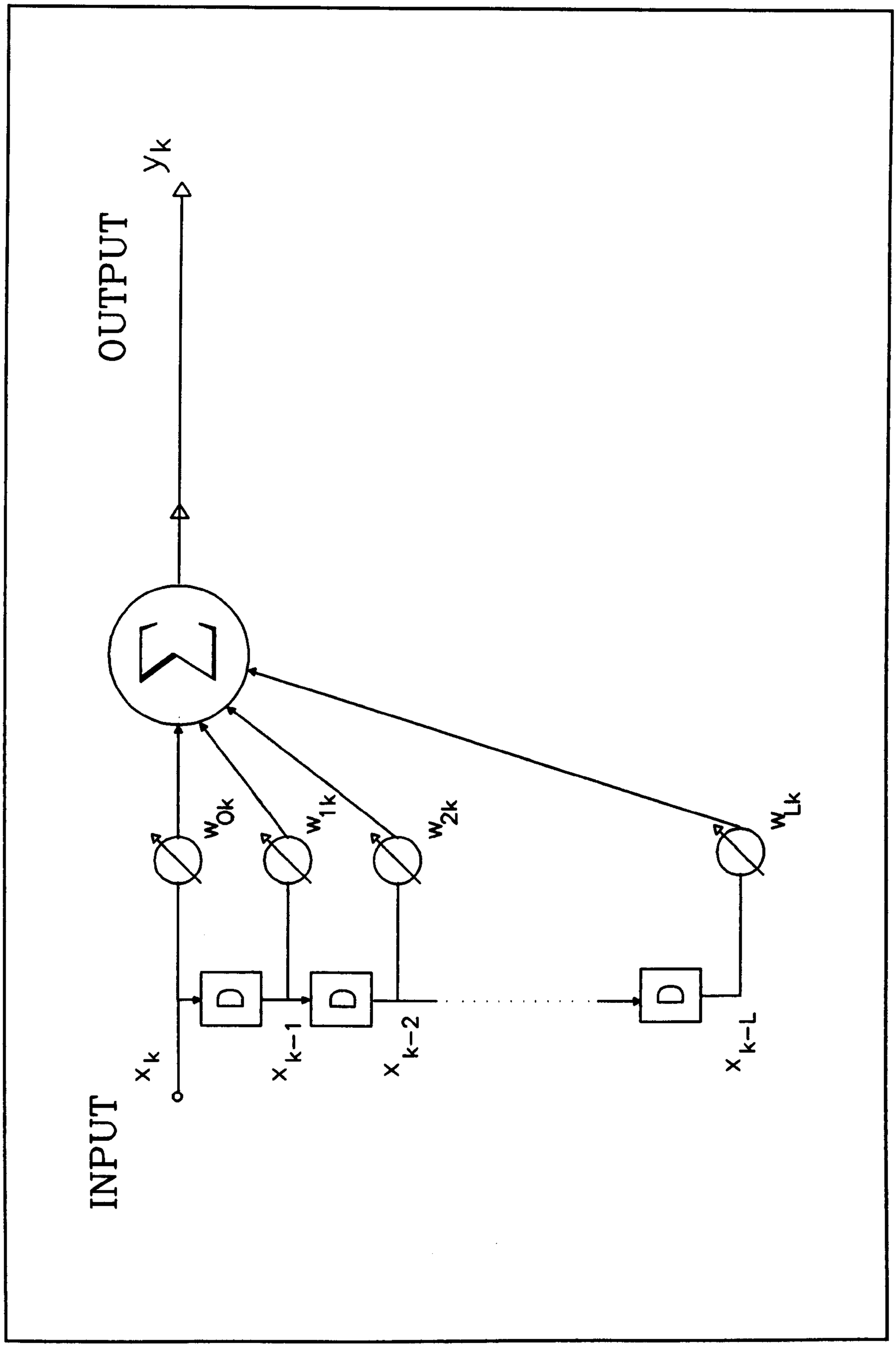

Figure 7. The adaptive linear combiner as a single-input transversal filter after Widrow et al

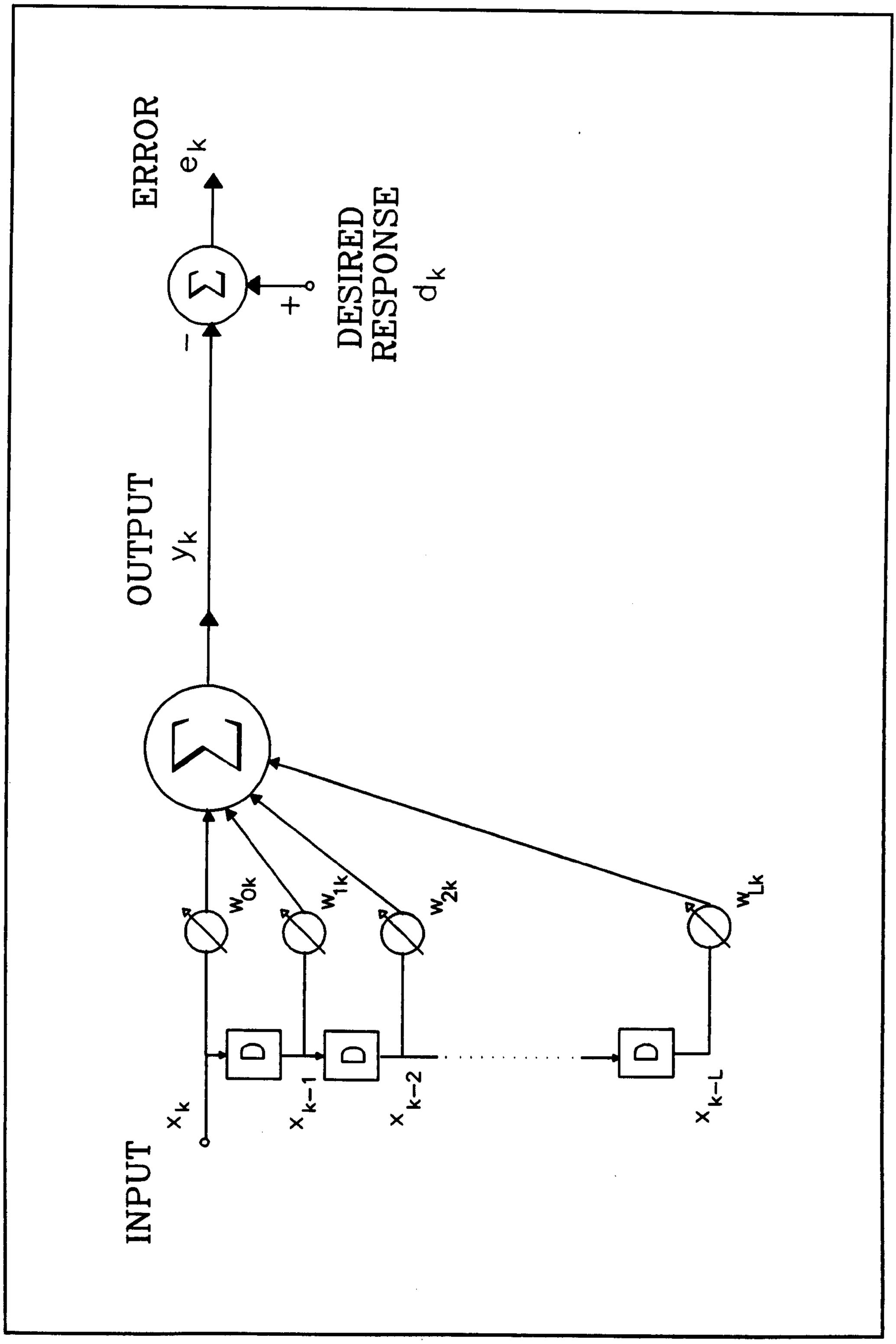

Figure 8. The adaptive linear combiner with desired response and error signals after Widrow et al.

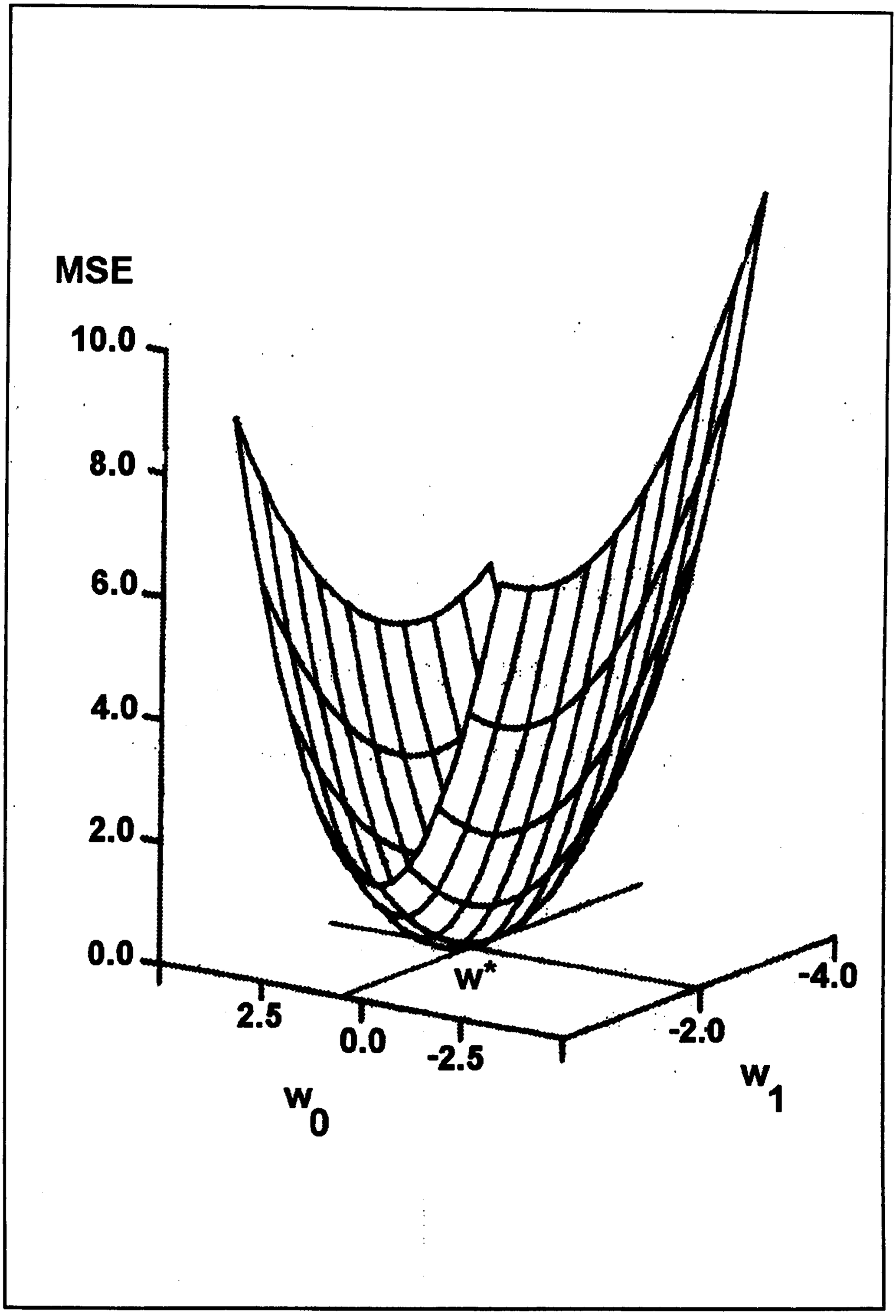

Figure 9. Portion of a two-dimensional quadratic performance surface, after Widrow & Stearns. The minimum mean-square error is 0.0 in this example, with an optimum weight vector $\mathbf{W}^* = (0.65,-2.10)$.

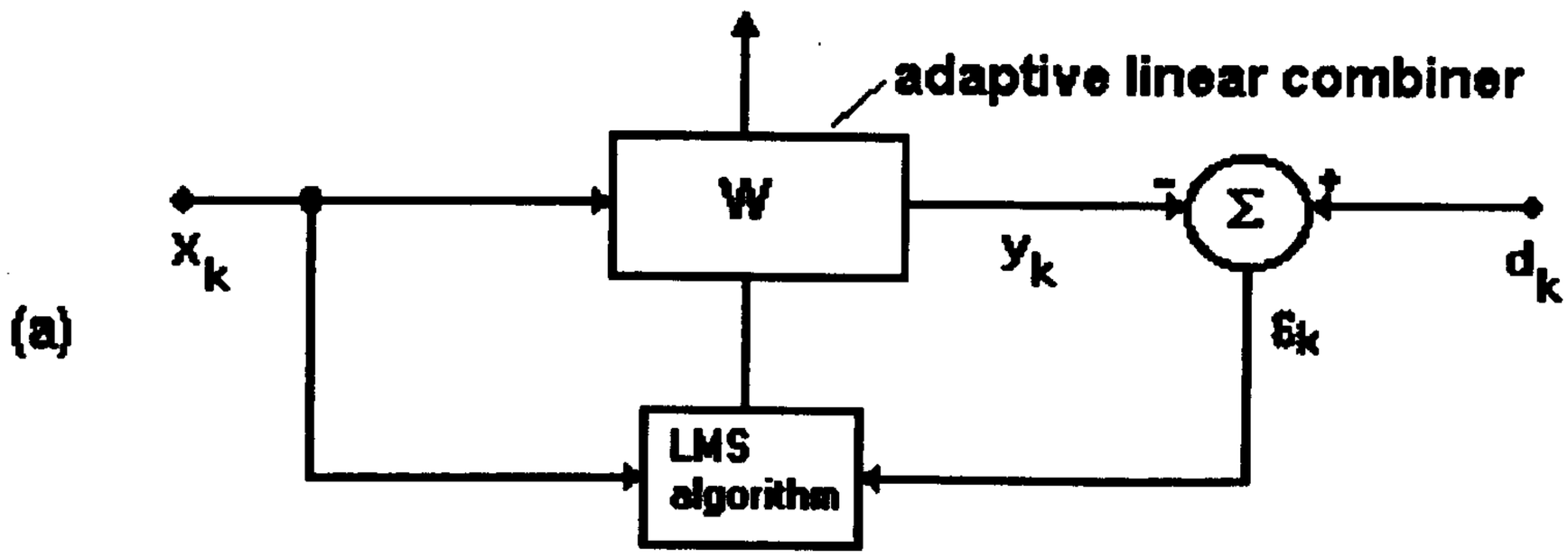

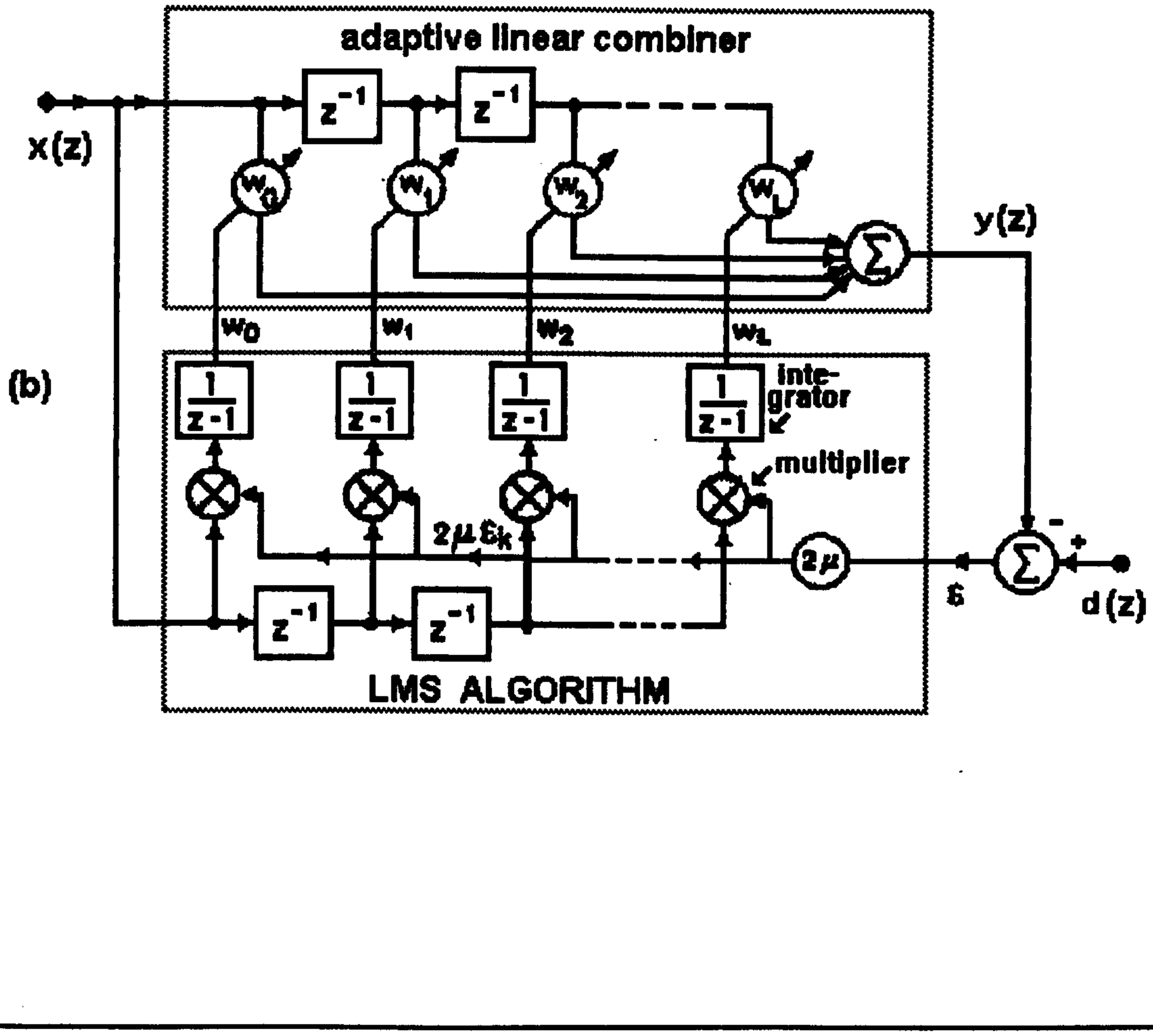

Figure 10. Block diagrams of the LMS algorithm applied to the adaptive linear combiner, (a) shows the overall form, (b) shows details of the LMS update mathematics in the z-domain.

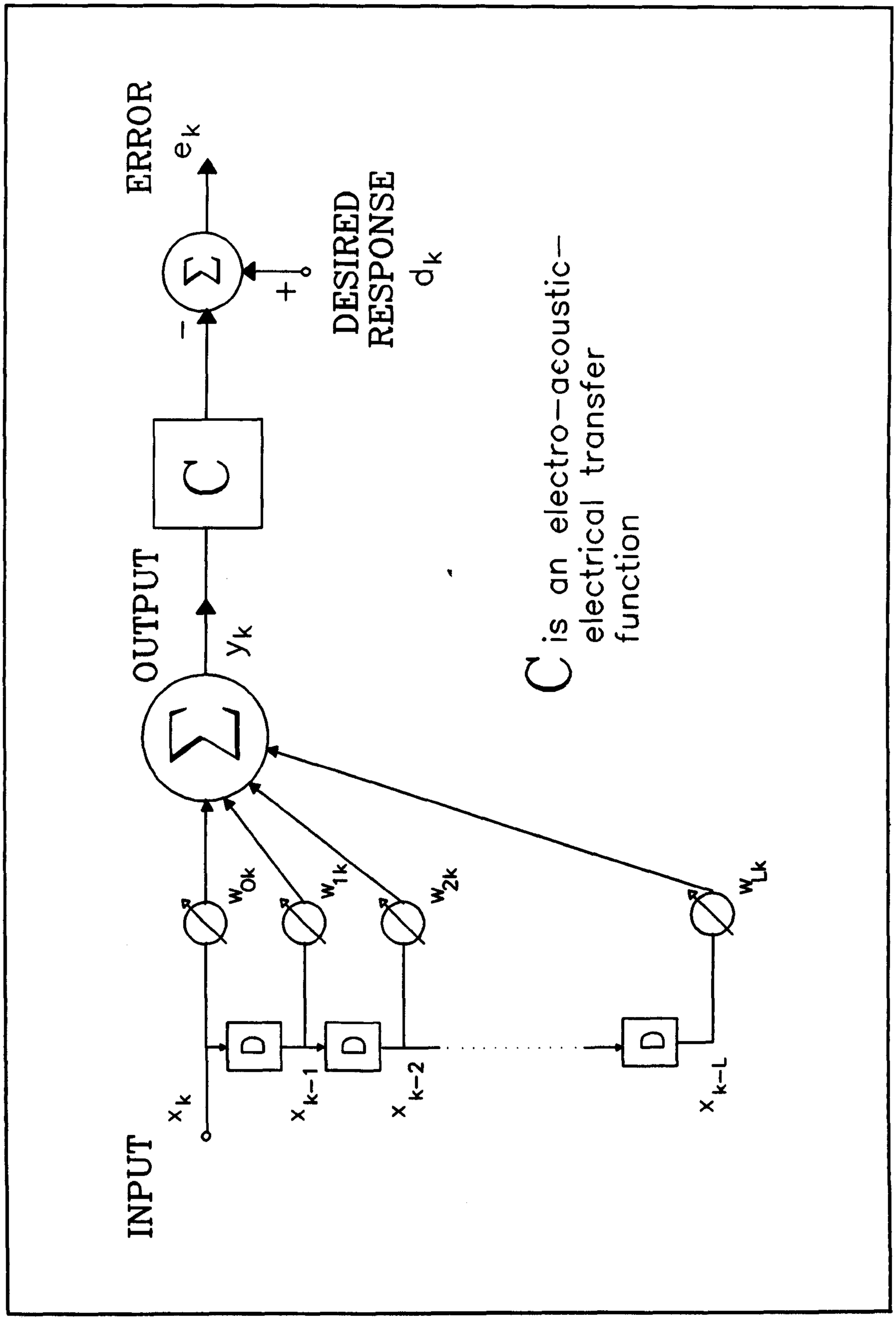

Figure 11. The adaptive linear combiner used for active acoustic control. The presence of the "forward path" C dictates modification of the LMS weight update method.

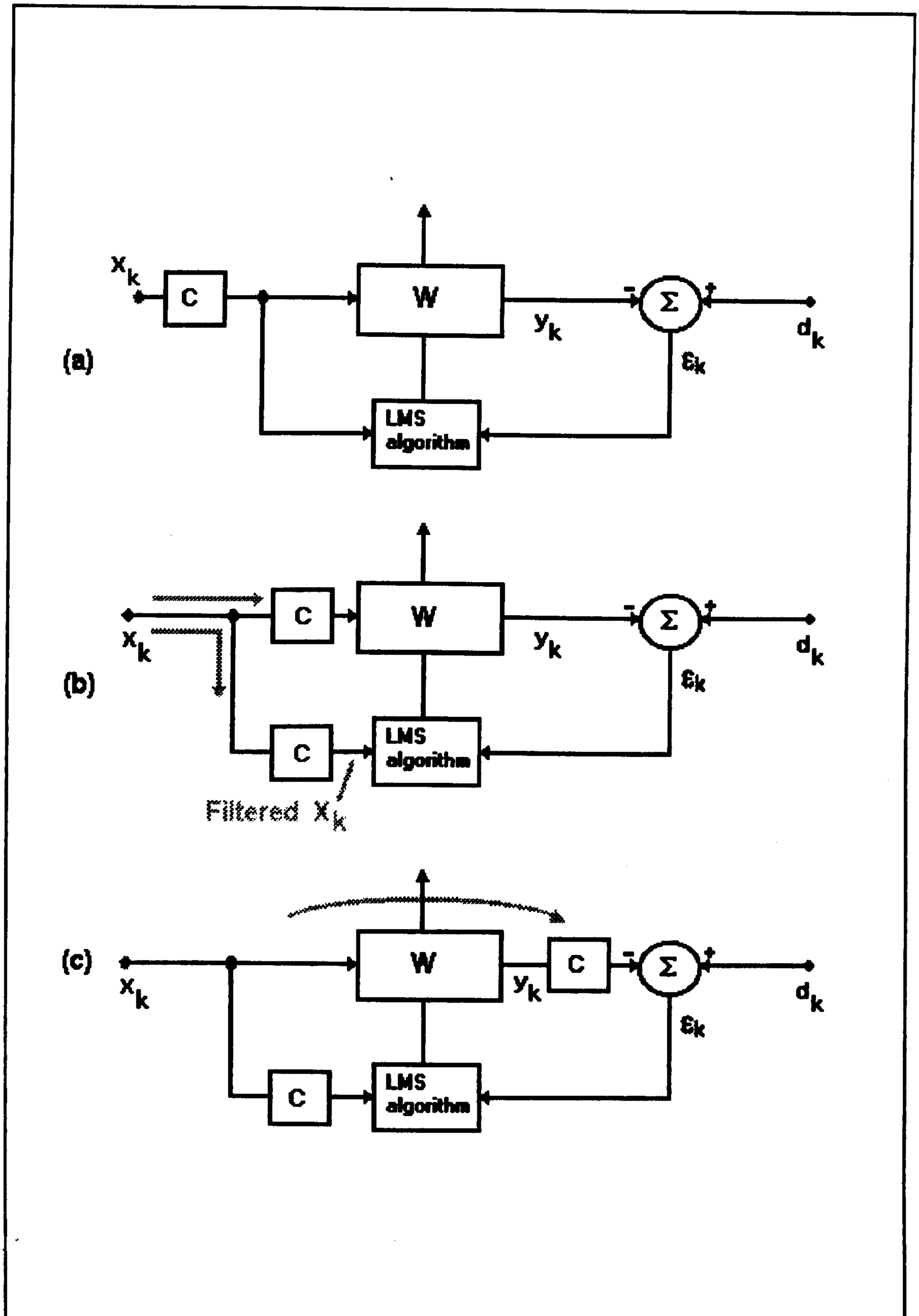

Figure 12. Development of the Filtered-X LMS algorithm, after Widrow et al. The change from (b) to (c) assumes that the adaptive filter and C(z) are linear, and therefore commutable.

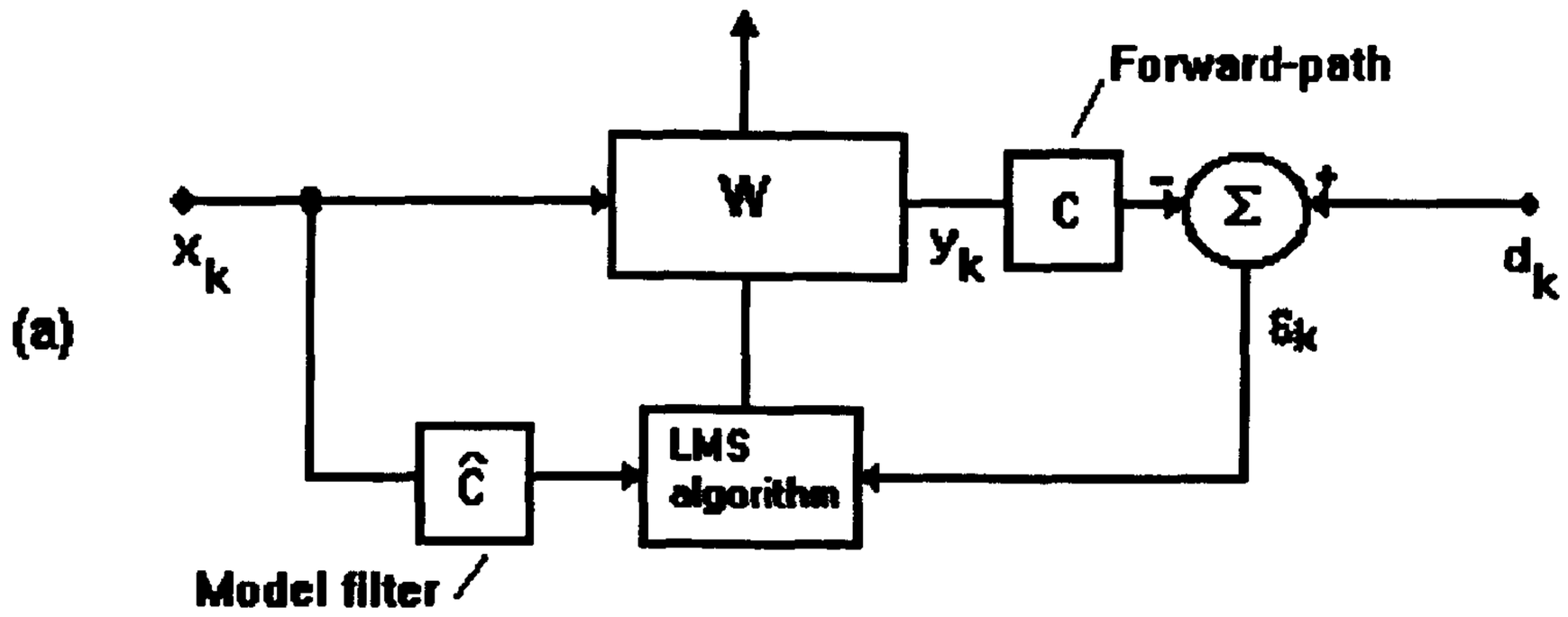

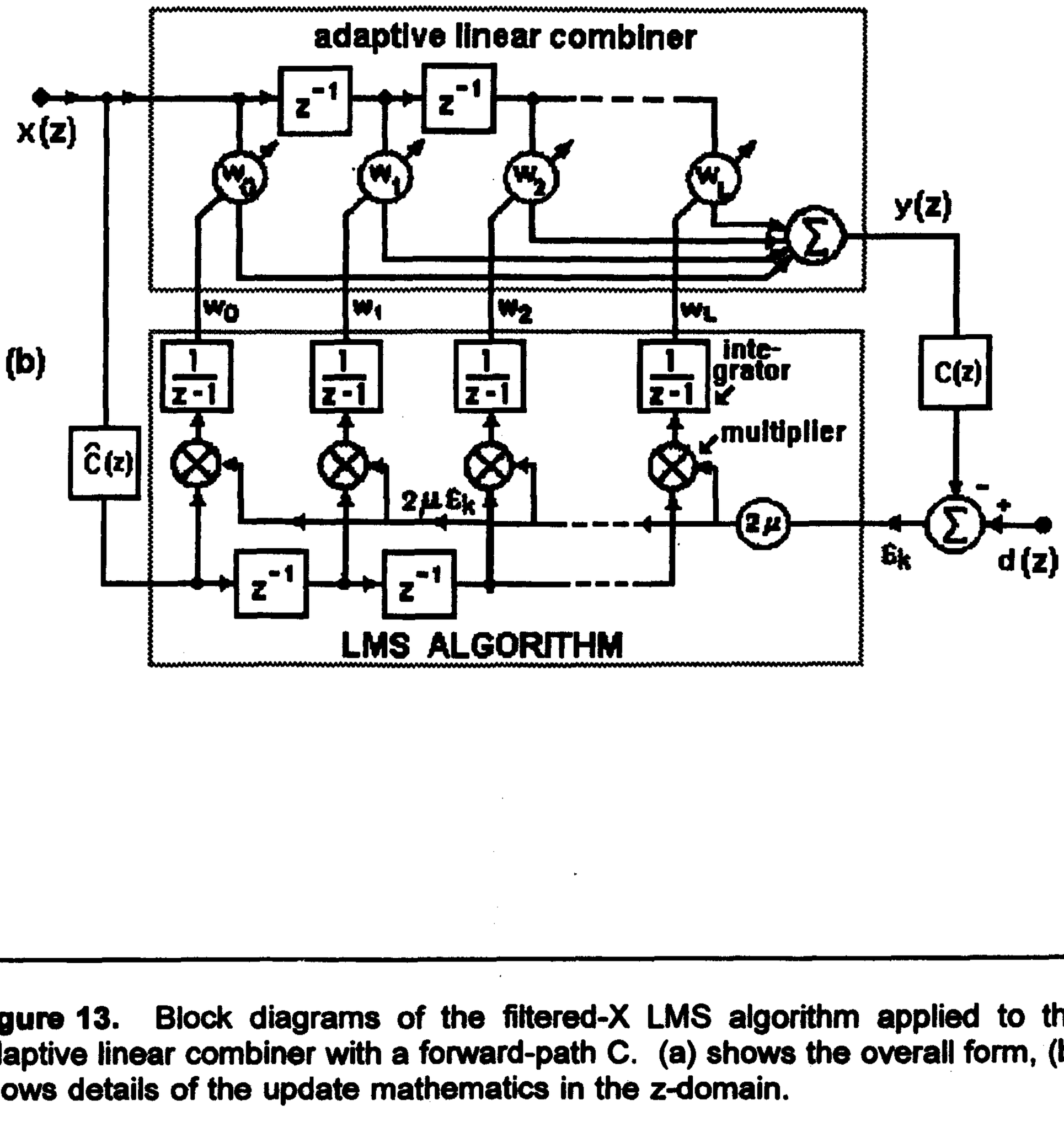

Figure 13. Block diagrams of the filtered-X LMS algorithm applied to the adaptive linear combiner with a forward-path C. (a) shows the overall form, (b) shows details of the update mathematics in the z-domain.

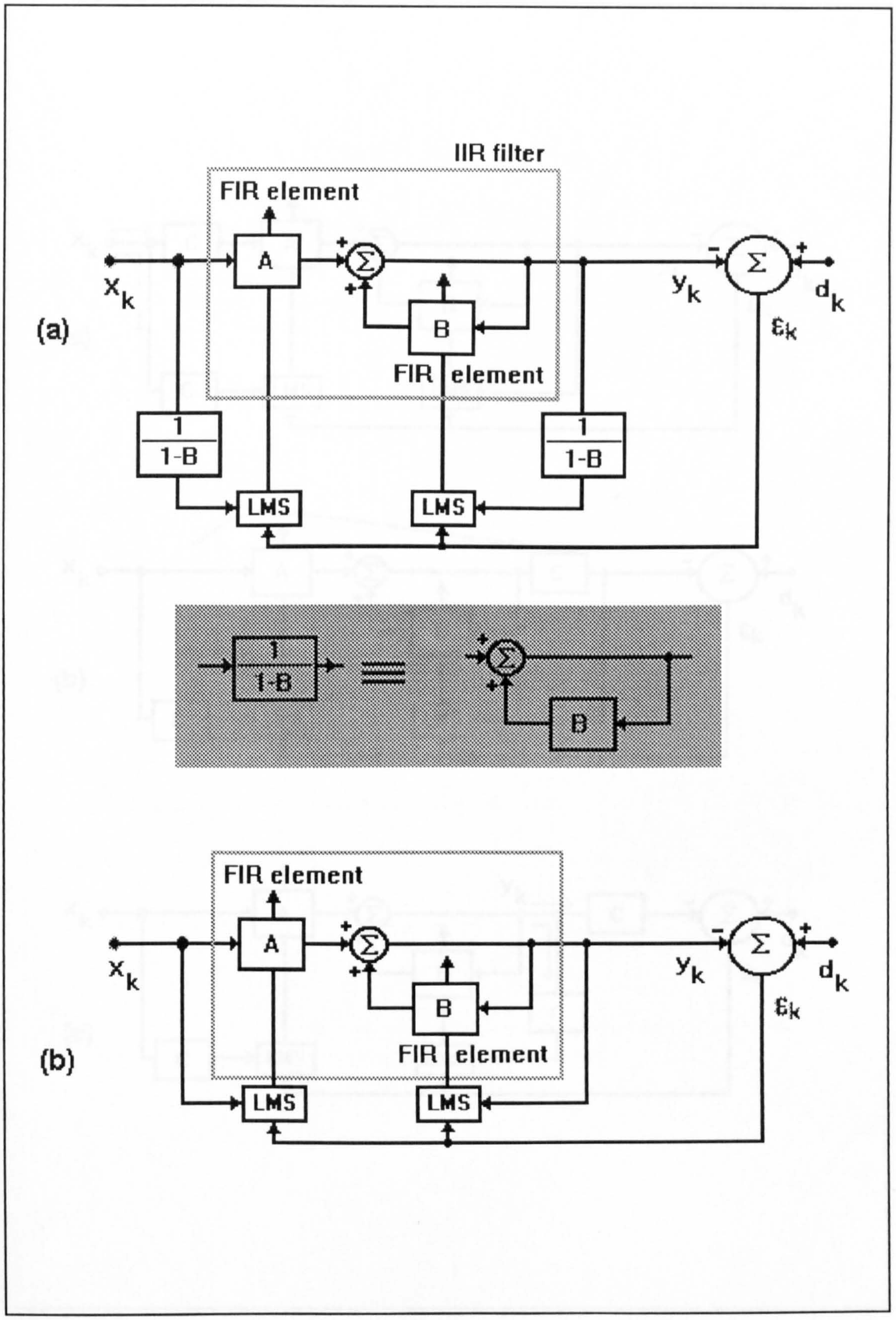

Figure 14. The full RLMS algorithm (a) uses FIR filter elements, A and B, to form a pole-zero IIR filter and requires filtering of the update inputs by 1/(1-B). The simplified RLMS algorithm does not require filtering of these inputs.

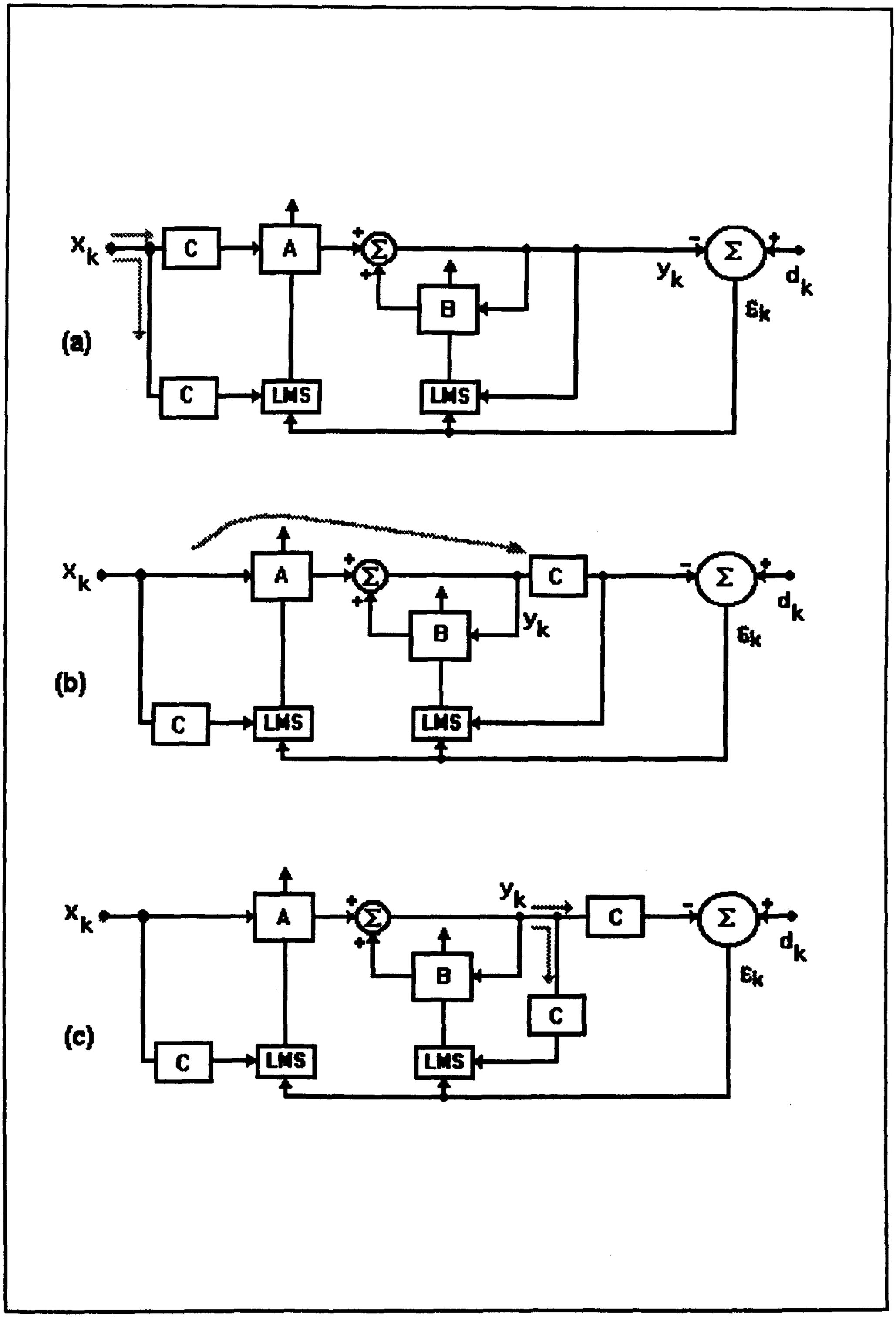

Figure 15. Development of the filtered-U RLMS algorithm, after Eriksson, 1990. The change from (a) to (b) assumes that the IIR adaptive filter and C are linear, and therefore commutable.

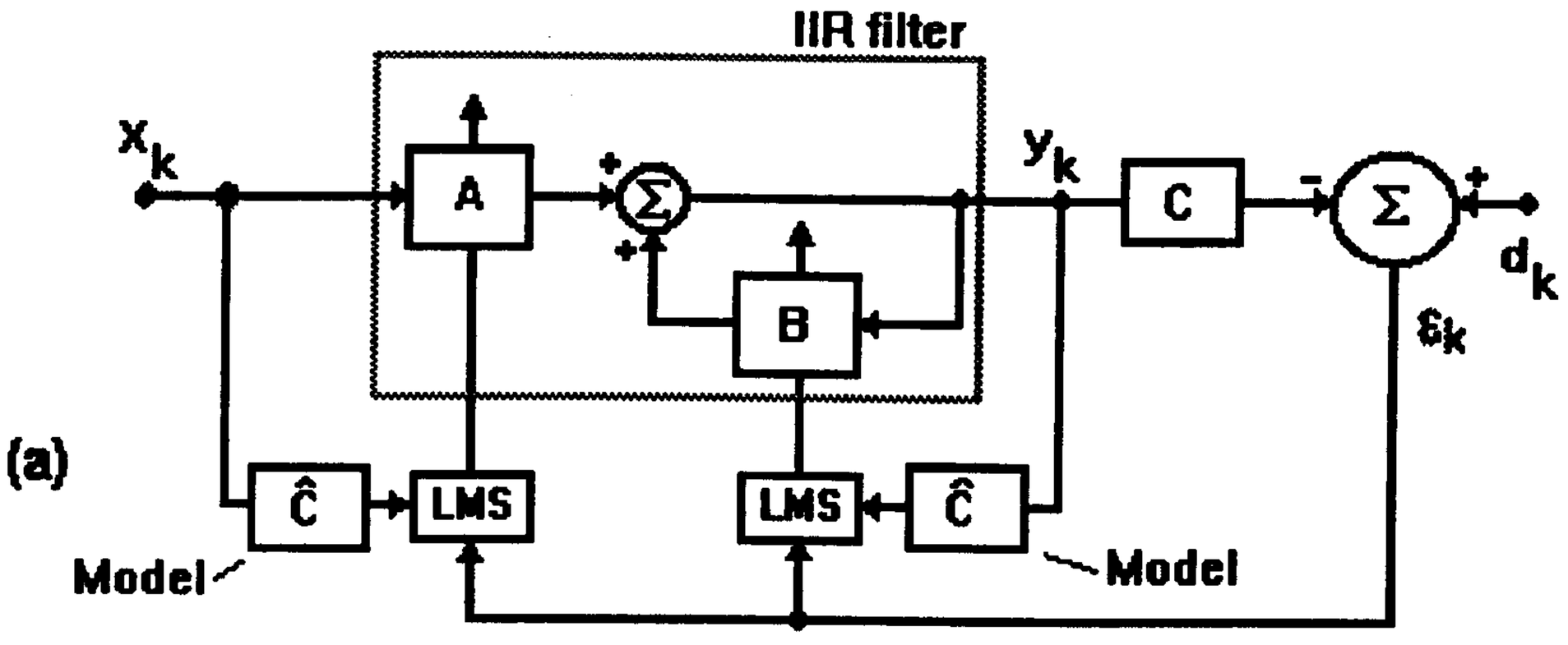

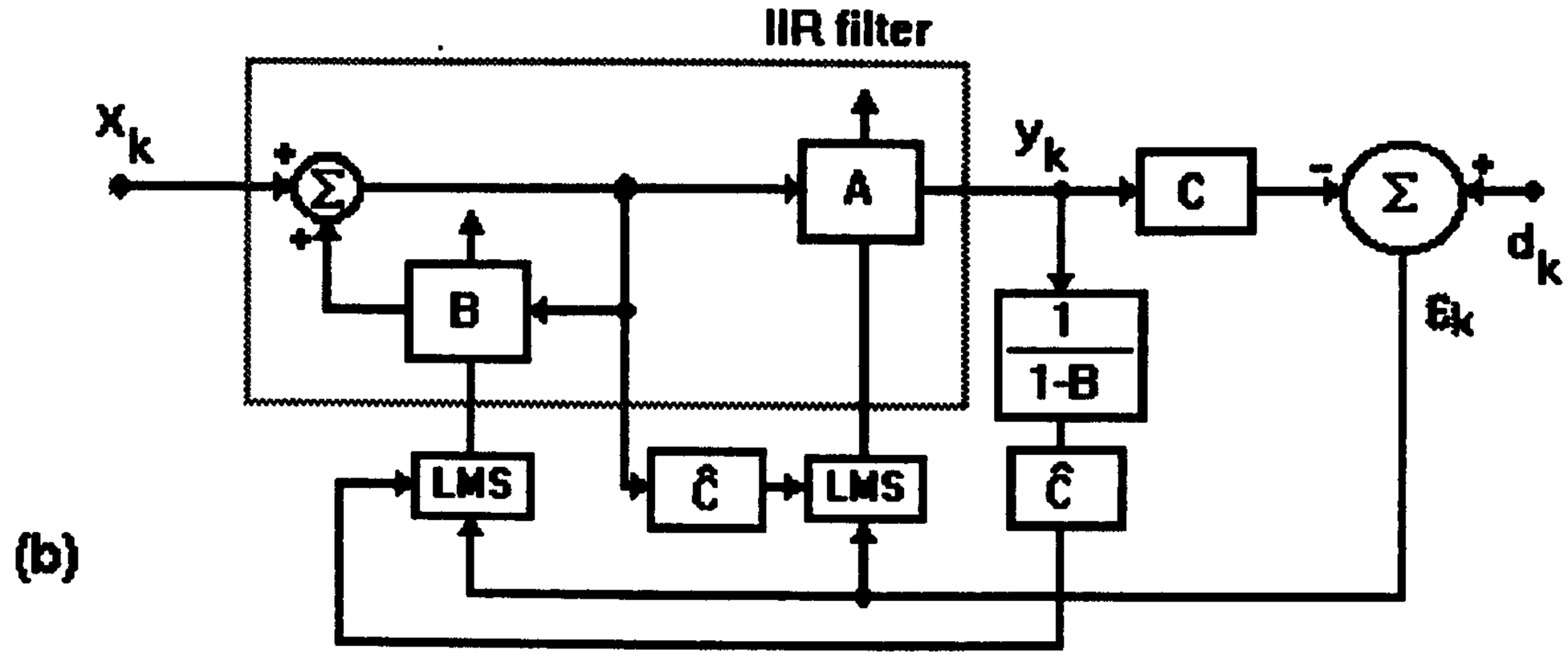

Figure 16. Block diagrams of a filtered-U RLMS algorithm implementation with an electro-acoustic forward path C. (a) shows the simplified form after Eriksson, 1990, (b) shows a possible implementation of the full filtered-U RLMS algorithm.

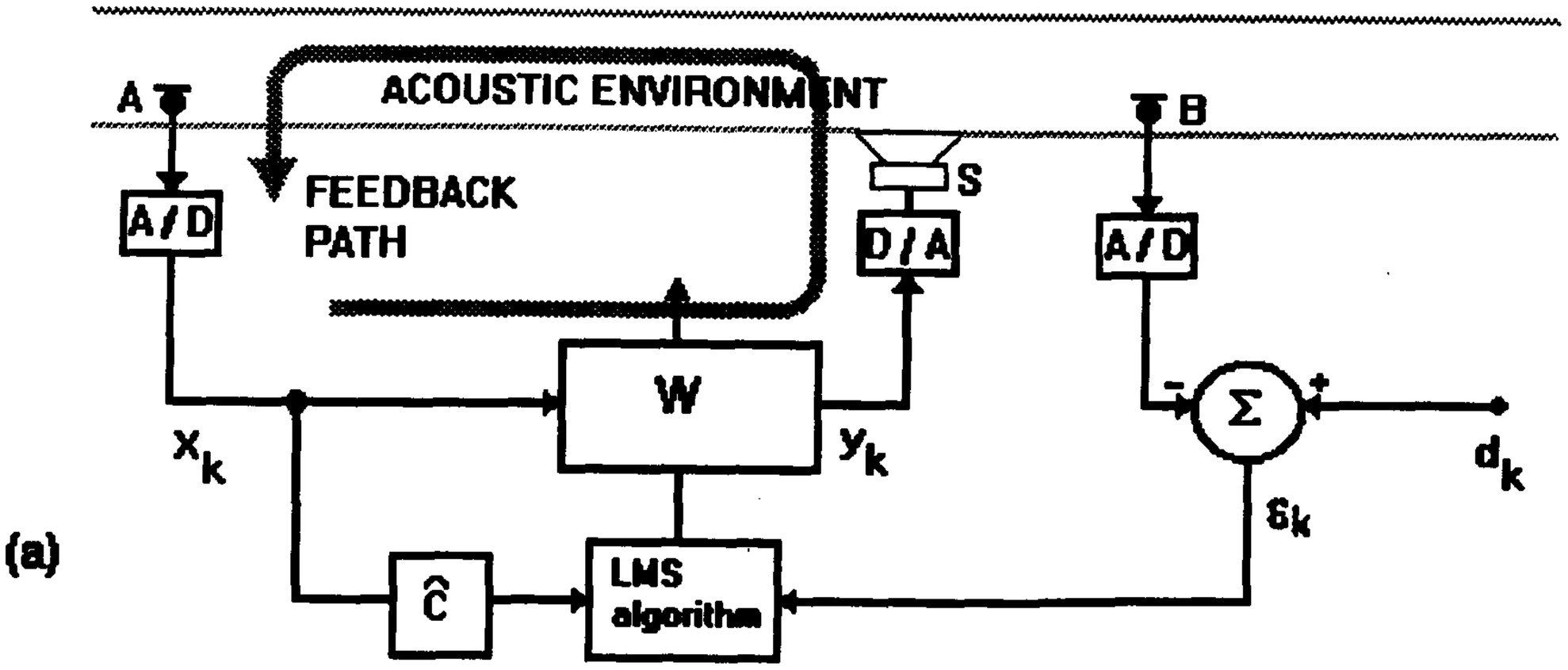

Figure 17. Feedback path in an active sound control system. (a) shows the feedback path around the system, (b) shows a feedback cancellation strategy (after Warnaka et al, 1984) where a path model subtracts feedback components from input.

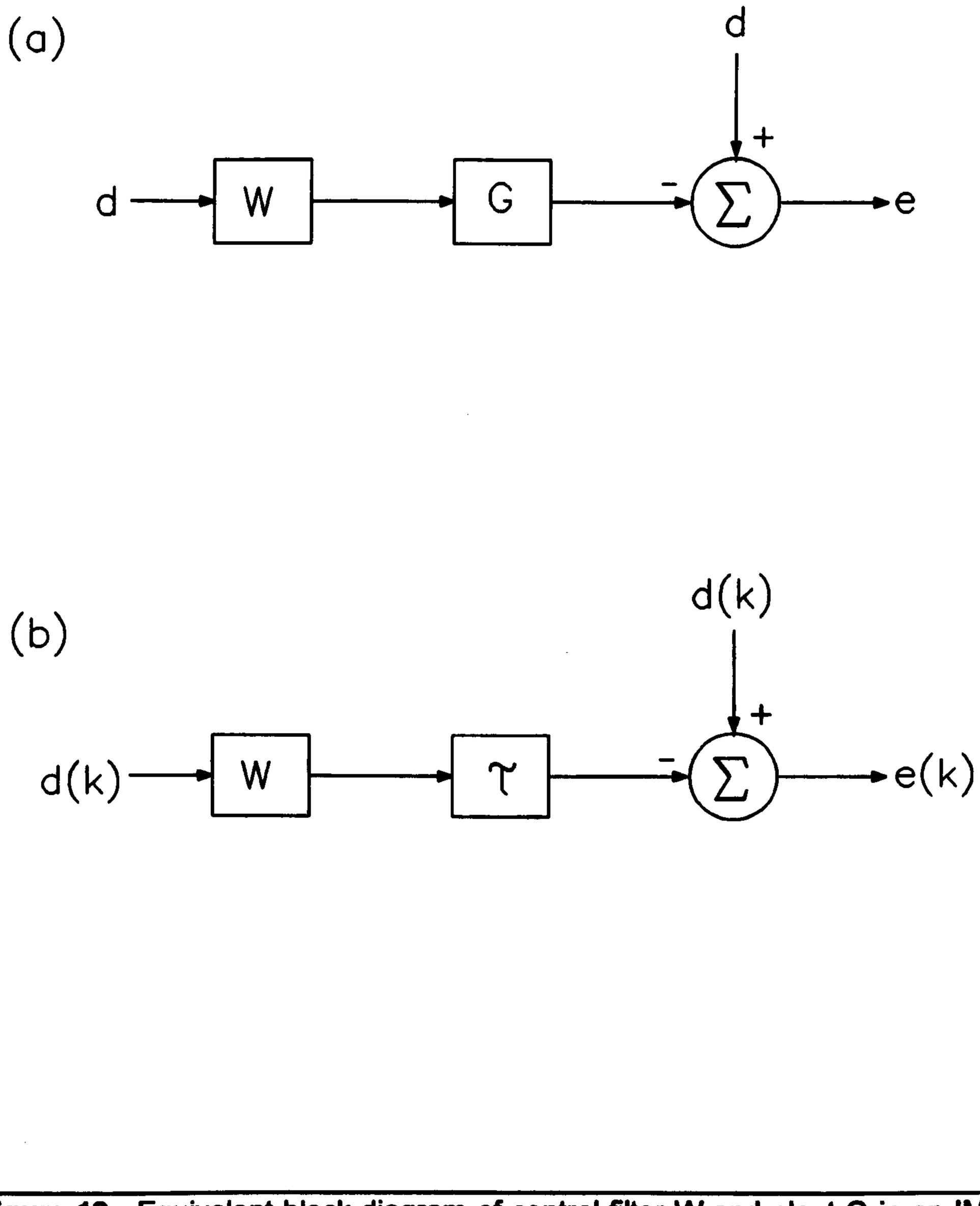

Figure 18. Equivalent block diagram of control filter W and plant G in an IMC feedback controller with ideal feedback cancellation. (a) from Fig.4 of reference [Elliott, 1994], (b) shows plant as a pure delay τ.

4 BACKGROUND THEORY AND CONSTRAINTS ON THE CONTROL OF SPECIFIC ACOUSTIC IMPEDANCE

4.1 INTRODUCTION

This thesis studies the application of active control to modify impedance. This chapter presents theory in Section 4.2 that establishes how the application of a control force can modify the impedance of a simple compliantly-suspended piston. The conventional electrodynamic loudspeaker is shown to provide a convenient means of implementing the controlled piston in Section 4.3. Physical operating limits for the controlled loudspeaker are presented in Section 4.4 for different controlled impedances. A summary of this chapter is given in Section 4.5. The theory presented in this chapter is original except in Section 4.2.1, which is adapted from reference (3).

4.2 ACTIVE CONTROL OF SPECIFIC ACOUSTIC IMPEDANCE

This thesis is based on research performed on the active control of the surface impedance of the simple compliantly-suspended piston. It is helpful to present the background theory in two parts: (i) the surface impedance of a simple compliantly-suspended piston; (ii) the influence of an additional control force on the piston.

4.2.1 The Specific Acoustic Impedance of a Compliantly-Suspended Piston

Consider a piston mounted on a simple linear suspension located as the boundary termination to a pipe. Figure 19a on Page 84 shows the mechanical components of such a system. If there are normally incident plane waves with consistent pressure over the piston surface it is possible to derive the impedance of this acoustic boundary in terms of the mechanical components (3).

The equation of motion of the piston is defined in Eq. 4.1 by considering the forces acting on the piston. The total force on the piston (represented in Figure 19a) is a sum of the forces due to the stiffness and damping of the suspension and the acoustic reaction.

$$M_m \frac{d^2x}{dt^2} = -\left(R_m \frac{dx}{dt} + K_m x \right) - Sp(t) \qquad \textbf{4.1}$$

S is the piston surface area, M_m is the mechanical mass, K_m is the mechanical stiffness of the suspension and R_m is the mechanical resistance to the motion. The total pressure at the surface due to the incident plane waves is ***p(t)***. In this case there are no other forces acting on the opposite surface of the piston. The displacement of the piston is ***x*** and the velocity of the piston is:

$$\frac{dx}{dt} = u(t) \qquad ms^{-1} \qquad \textbf{4.2}$$

The Fourier transform of Eq. 4.1 with rearrangement is :

$$u(j\omega) \cdot \left(j\omega M_m + R_m + \frac{K_m}{j\omega} \right) = -Sp(j\omega) \qquad \textbf{4.3}$$

where ω is the frequency and ***j*** is the complex operator. By rearranging Eq. 4.3 the surface mechanical impedance z_m is:

$$z_m(j\omega) = \frac{S\,p(j\omega)}{u(j\omega)} = -R_m - j\left[\omega M_m - \frac{K_m}{\omega} \right] \qquad \textbf{4.4}$$

The area transformation of mechanical impedance Eq. 4.4 allows the specific acoustic impedance at the surface of the piston to be specified in terms of the piston velocity $u(j\omega)$ and frequency ω as in Eq. 4.5.

$$z(j\omega) = \frac{p(j\omega)}{u(j\omega)} = -\left[R_m + j\left[\omega M_m - \frac{K_m}{\omega} \right] \right] S^{-1} \qquad kgm^{-2}s^{-1} \qquad \textbf{4.5}$$

4.2.2 Modifying the surface impedance of a piston with a control force

The application of control can modify the surface impedance of the piston. This is theoretically shown in this section. Active control can be introduced by applying a force input ***F(t)*** on the piston (see Figure 19b on Page 84). The equation of motion is then described by Eq. 4.6.

$$M_m \frac{d^2x}{dt^2} = -\left(R_m \frac{dx}{dt} + K_m x \right) - Sp(t) + F(t) \qquad \textbf{4.6}$$

In similar development from Eq. 4.1 to Eq. 4.5, Eq. 4.6 can be manipulated by Fourier transform and rearrangement to give the surface impedance of the

controlled boundary, Eq. 4.7.

$$z(j\omega) = \frac{p(j\omega)}{u(j\omega)} = \left[\frac{F(j\omega)}{u(j\omega)} - R_m - j\left[\omega M_m - \frac{K_m}{\omega} \right] \right] S^{-1} \quad kgm^{-2}s^{-1} \qquad \textbf{4.7}$$

Note the presence of surface velocity ***u*** on both sides of the equation. This couples ***F*** with the surface velocity and complicates the design of the required forcing function. Equation 4.7 indicates that the impedance of the piston can be altered to any value if an appropriate forcing function ***F*** is applied. This is consistent with the findings of Bobber and Beatty, see Section 2.4.1. Physical limitations on the realizable impedance are described in Section 4.4.

4.3 ACTIVE IMPEDANCE CONTROL OF A LOUDSPEAKER

The control of the impedance of a piston by a force input was described in Section 4.2. This section reveals that the controlled piston can be realized by a conventional electrodynamic loudspeaker. The control of the impedance at the loudspeaker cone is achieved by applying a voltage to the loudspeaker voice-coil. The theoretical uncontrolled impedance of a loudspeaker is numerically calculated.

A practical example of a piston is the compliantly-suspended cone of a loudspeaker. The loudspeaker is an electro-mechanical device that generates acoustic pressure from an electrical signal. The loudspeaker has an (approximately) plane impervious surface (the cone) which is linearly suspended with respect to mechanical ground (the frame) by a suspension designed to permit uniform "piston-like" displacement of the cone. The loudspeaker also has a motor system with which controlling forces can be applied to the cone.

The total force on the loudspeaker cone (represented by the forced piston in Figure 19b on Page 84) is a sum of the forces due to the motor coil system, the stiffness and damping of the suspension and the acoustic reaction. The force

due to the motor coil system is:

$$F(t) = BI(t) = \frac{BIV(t)}{Z_{EB}} - \frac{(Bl)^2 u(t)}{Z_{EB}} \qquad 4.8$$

where ***V*** is the voltage applied to the voice coil and ***i*** is the voice coil current, Z_{EB} is the blocked electrical impedance and ***Bl*** is the force factor of the drive system. The second term represents the force generated by the back-emf induced in the voice coil during motion. Substituting the frequency domain form of Eq. 4.8 into the equation of motion of the forced piston, Eq. 4.7, gives the specific acoustic impedance of the loudspeaker cone Eq. 4.9.

$$z(j\omega) = \frac{p(j\omega)}{u(j\omega)} = \frac{V(j\omega)}{u(j\omega)} \cdot \frac{Bl}{SZ_{EB}} - \left[\frac{(Bl)^2}{Z_{EB}} + R_m + j\left[\omega M_m - \frac{K_m}{\omega} \right] \right] S^{-1} \qquad 4.9$$

Equation 4.9 demonstrates that the specific acoustic impedance at the cone of a loudspeaker can be controlled by applying a control voltage function ***V(jω)*** to the voice-coil. The controlled impedance of the cone is also a function of the cone velocity and the physical parameters of the loudspeaker. Equation 4.9 also shows that the generation of a desired constant impedance demands that the voltage applied to the voice-coil is directly proportional to the cone velocity at each frequency. This has implications on the design of a control system to generate the voice-coil voltage - see Section 5.2 on Page 90.

The specific acoustic impedance of the loudspeaker can be calculated from Equation 4.9. The loudspeaker cone is loaded by the acoustical environment in which it operates. The variables in Eq. 4.9 are quantified by assuming that the loudspeaker and the acoustic environment are *lumped*. This is a common means of analysis of acoustical systems and is briefly explained here. At lower frequencies where the wavelength of sound is much greater than any dimension of an acoustic system, the acoustic system elements such as mass, stiffness and damping can be considered as *lumped*. This means that each element can be considered as a unique entity, and is mathematically separable. A relevant discussion on the lumping of elements of acoustical systems is presented on pp.73-75 of (2):

"Acoustical systems are generally defined by partial differential equations

> derived in ..., which lead to the acoustic wave equation. Wave propagation implies that the acoustic variables are delayed in their propagation from one part of an acoustical system to another. When the dimensions of an acoustical system are sufficiently small, this time delay is sufficiently small to be neglected compared to the period of the signal at the highest frequency of interest. Under these conditions the partial differential equations governing an acoustical system can be reasonably well approximated by a manageable number of ordinary differential equations, and the resulting model of the system is said to have *lumped elements*."

If the acoustical system has lumped elements then it is illustrative to model the components with an equivalent electrical circuit. The compliant elements of a lumped acoustical system can be represented in an electrical equivalent as capacitance, the mass elements as inductance and the acoustical resistances as electrical resistance. An electrical equivalent circuit that represents the lumped electrical, mechanical and acoustical components of the loudspeaker and acoustical environment is displayed in Figure 20 on Page 85. The "rear radiation load" components represent the acoustic load presented to the rear of the cone. The "loudspeaker parameters" arise from the mechanical components of cone mass, suspension stiffness and damping. The "electrical load" arises from the electrical components of the system. The surface impedance at the loudspeaker cone is seen to depend on all of these components. The circuit also illustrates that the acoustical-domain components can be combined to form a single capacitance, inductance and resistance. These combined components can be converted back from the acoustic domain to quantify the mechanical resistance, mass and stiffness variables in Equation 4.9.

A numerical example is calculated from Equation 4.9 and presented in Figure 21 on Page 86. This is for a loudspeaker manufactured by KEF Electronics Limited, Tovil, Maidstone, England designated the B200A mounted in a 25 litre sealed box (specifications for the KEF B200A are in Appendix 1). In this example there is no voltage applied to the motor coil system ($V(j\omega)=0$ in Equation 4.9) so this can be termed the *natural* specific acoustic impedance of the surface. The driver-box resonance is seen in Figure 21 with a minimum in the magnitude of impedance at 65Hz (the resonant frequency of this system is calculated in Appendix 2 on Page 310 as around 65Hz). The magnitude of impedance at

65Hz is 423 rayls which is near to the characteristic impedance of air defined as 415 Rayls in Section 1.2 on Page 3. The theoretical natural specific acoustic impedance is compared with measurements in Section 7.4 on Page 206.

4.4 CONSTRAINTS ON THE CONTROLLED IMPEDANCE OF A LOUDSPEAKER

The control of the impedance of a piston by a force input was described in Section 4.2. The conventional electrodynamic loudspeaker provides a convenient means of implementing the piston, see Section 4.3. Equation 4.7 shows that any physically realizable impedance can be created provided a suitable forcing function ***F*** can be designed. Constraints arise because it is not always possible to generate a suitable function for ***F***, either because of physical limitations of the loudspeaker, or because of limitations in the control system. Constraints on controlled impedance caused by control system limitations are described in Chapters 6 and 7. This section will describe constraints imposed by physical limitations of the loudspeaker when the impedance of the cone is controlled. These have been published in (30)(31).

An ideal loudspeaker is characterized by a linear equation of motion. Real loudspeakers depart from this ideal in two important respects; they have non-linear suspensions and motor systems, and the voice coil can handle only a finite power. Both of these non-ideal properties define edges of the physical operational envelope of actively controlled impedances built around loudspeakers, which are discussed below. These sections contain original work part of which has been published in (31).

4.4.1 Suspension Non-linearity

The suspension of a practical loudspeaker does not have a linear compliance (and damping) term, rather the compliance reduces as the cone is displaced further from equilibrium - the suspension stiffness hardens. There is, therefore, an absolute limit on the cone excursion. Well before this fracture limit is reached, the suspension will become significantly non-linear and it is appropriate

to define a limit of (approximately) linear cone excursion or displacement. This limit of linear excursion, $|X|_{max}$, defines a frequency dependant limit of maximum linear velocity, $|u|_{max}$:

$$|u|_{max} = \omega |X|_{max} \qquad \textbf{4.10}$$

Note that the transducer has a velocity zero at d.c., as a consequence of the linear cone excursion limit.

The maximum pressure that exists at the velocity-limited cone for any impedance is given by :

$$|p|_{max} = |u|_{max} |z_d| \qquad \textbf{4.11}$$

An example of this limitation on the pressure at the cone is presented in Section 4.4.3 on Page 81 for z=**415** Rayls.

4.4.2 Loudspeaker Power Handling

The motor system of an electrodynamic loudspeaker has a finite electrical power handling capacity which limits the voice coil current and resulting electrical force applied to the cone. This force limit imposes a limit on the cone velocity, when the impedance at the cone is controlled to a desired value z_d. If the maximum power handling of the voice coil is W watts, then the maximum rms voice coil current is:

$$I_{rms} = \left[\frac{W}{\Re(Z_{EB})}\right]^{\frac{1}{2}} \qquad \textbf{4.12}$$

where I_{rms} is the root mean square voice coil current, and Z_{EB} is the electrical impedance of the loudspeaker. Assuming that control of the desired impedance is successful then Eq. 4.8, Eq. 4.6 and Eq. 4.12 can be combined to yield a limit on the maximum velocity :

$$|u|_{max} = \left|\frac{Bl}{Sz + j\omega M_m + R + \frac{K}{j\omega}}\right| \cdot \left[\frac{W}{\Re(Z_{EB})}\right]^{\frac{1}{2}} \qquad \textbf{4.13}$$

The velocity limit defined by Eq. 4.13 can be used either to specify the maximum velocity and corresponding pressure permissable for a given z (see examples in Section 4.4.3 on Page 81), or minimum z for a specified maximum pressure.

4.4.3 Numerical Examples

This section presents numerical examples of the operational limits on controlled impedance of a KEF B200A loudspeaker. Three different controlled impedances are considered:

1. $z=415$ Rayls
2. $z=0$
3. $z=\infty$

The limits on cone velocity and/or surface acoustic pressure are presented for each controlled impedance. These are imposed by the maximum linear cone excursion and the voice coil power handling of the loudspeaker, see Sections 4.4.1 and 4.4.2. The experimental research rig developed for this thesis used KEF B200A drive units. The manufacturer's specifications are reported in Appendix 1 and are used for the calculation of the results presented in this section.

If the KEF B200A loudspeaker is controlled, such that the specific acoustic impedance at the cone is 415 Rayls, then the velocity limits can be calculated from Equations 4.10 and 4.13 and are shown in Figure 22 on Page 87. The actual velocity limit is defined by the smallest of Equations 4.10 and 4.13 at any frequency. The linear displacement limit dominates at low frequencies, whilst at frequencies above approximately 80Hz the velocity of the cone is limited by the power handling of the coil. As the impedance at the surface of the cone is known to be 415 Rayls, the maximum pressure which can be sustained at the cone of this active absorber can be calculated from Equation 4.11. This maximum pressure is plotted on the right hand vertical scale in Figure 22. The maximum sound pressure level (SPL) varies between approximately 135 and 150dB from 20Hz to 500Hz. This theoretical result is consistent with the practical maximum SPLs of 110-140dB noted by Guicking (21) for the control of a different loudspeaker, see Section 2.4.2 on Page 14.

The second example is for a controlled impedance of zero Rayls. This occurs when the cone pressure is zero despite motion of the cone. The theoretical velocity limits from Equations 4.10 and 4.13 are plotted for the KEF B200A

loudspeaker in Figure 23 on Page 88. The actual velocity limit is defined by the smallest of Equations 4.10 and 4.13 at any frequency. The linear displacement limit of the cone dominates at low frequencies, whilst at frequencies above approximately 110Hz the velocity of the cone is limited by the power handling of the coil. The cone velocity limit is similar to that of the first example of $z=415$. The larger Q of the power limit occurs because less control force from the motor system is needed to control the cone as there is less opposing force because of no incident acoustic pressure. This is most significant near to the driver resonance; at other frequencies the reactive components dominate the total force acting on the cone.

The third example is for ideal active reflection, which can be created by forcing the impedance to $z=\infty$. This occurs when the cone has zero velocity for some incident pressure. Substituting for F in Eq. 4.6 with Eq. 4.8, taking the Fourier transform and setting $u=0$ yields

$$p(j\omega)\Big|_{z=\infty} = \frac{Bl \,.\, V(j\omega)}{S\, Z_{EB}} \qquad 4.14$$

The control voltage for the voice coil is directly proportional to the pressure at the surface of the cone. The maximum voice coil voltage therefore dictates the maximum pressure at the cone for successful forcing of impedance to $z=\infty$. The maximum voice coil voltage depends on the programme power rating of the loudspeaker and is given by Eq. 4.15.

$$V_{max} = [\, W \,.\, \Re(Z_{EB})]^{\frac{1}{2}} \qquad 4.15$$

The magnitude of the maximum pressure is found by substituting Eq. 4.15 into Eq. 4.14 and taking the magnitude, Eq. 4.16.

$$|p(j\omega)|_{max}\Big|_{z=\infty} = \left|\frac{Bl}{S Z_{EB}}\right| [\, W \,.\, \Re(Z_{EB})\,]^{\frac{1}{2}} \qquad 4.16$$

This relationship for the KEF B200A loudspeaker is plotted in Figure 24 on Page 89. The cone has zero velocity, therefore the mechanical resonance and suspension non-linearity have no effect on the pressure limit.

Equation 4.14 describes the relationship between the cone pressure and

voice-coil voltage for a controlled loudspeaker of infinite impedance. This can be used as the transfer function in an active controller (a "control law") to force infinite impedance as discussed in Section 6.3.1 on Page 106.

4.5 SUMMARY

Theory that describes the specific acoustic impedance of a simple compliantly-suspended piston has been presented. Analysis has established the control of the piston impedance by an input force. If a control system can create an appropriate input force then the impedance of the piston can be forced to any realizable value. The conventional electrodynamic loudspeaker provides a convenient means of implementing the controlled piston. The impedance of the loudspeaker cone can be controlled by applying a voltage signal to the voice-coil. Operational constraints that limit acoustic pressure and/or surface velocity arise from the limited cone displacement and force actuation of the loudspeaker voice-coil system. The limits have been theoretically examined for different impedances. The operational constraints for a controlled impedance of 415 Rayls, that for ideal acoustic absorption, are consistent with practical observation in the literature.

4.6 CHAPTER FIGURES

The figures referred to in this chapter appear on the following pages.

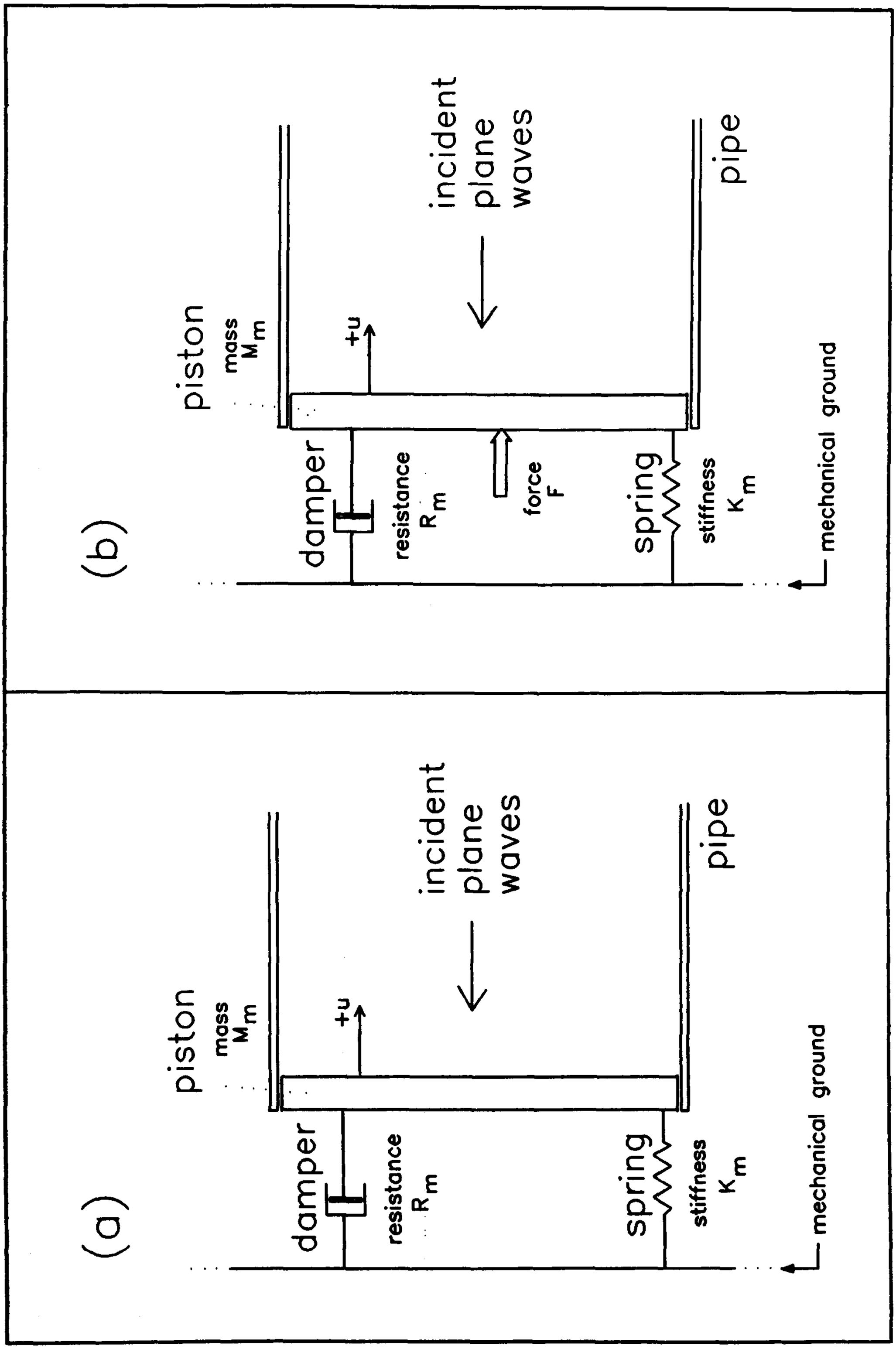

Figure 19. Compliantly suspended boundary without (a) and (b) with forced input

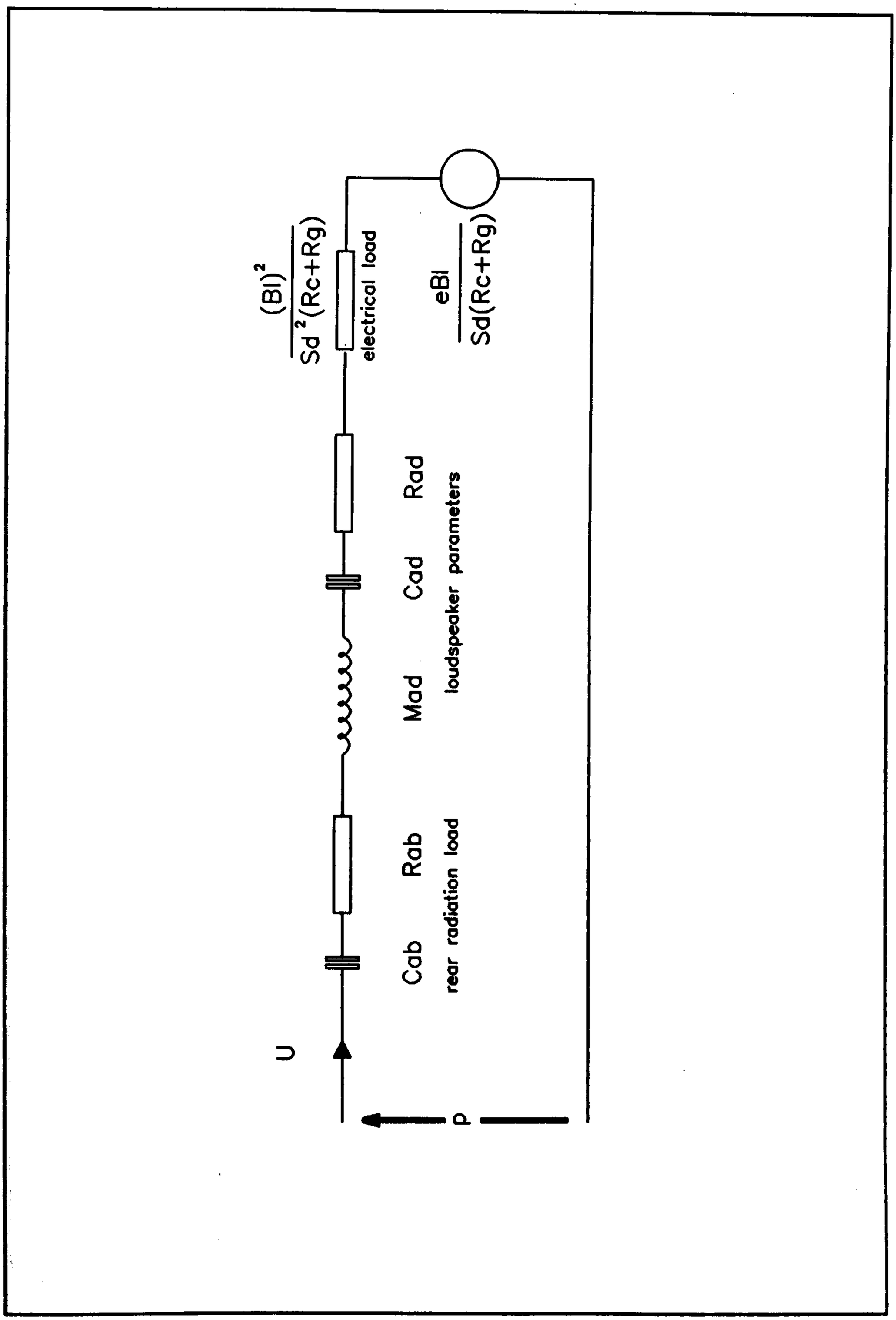

Figure 20. The specific acoustic impedance at the surface of a loudspeaker cone mounted in a sealed box seen using an electrical equivalent in the acoustic domain

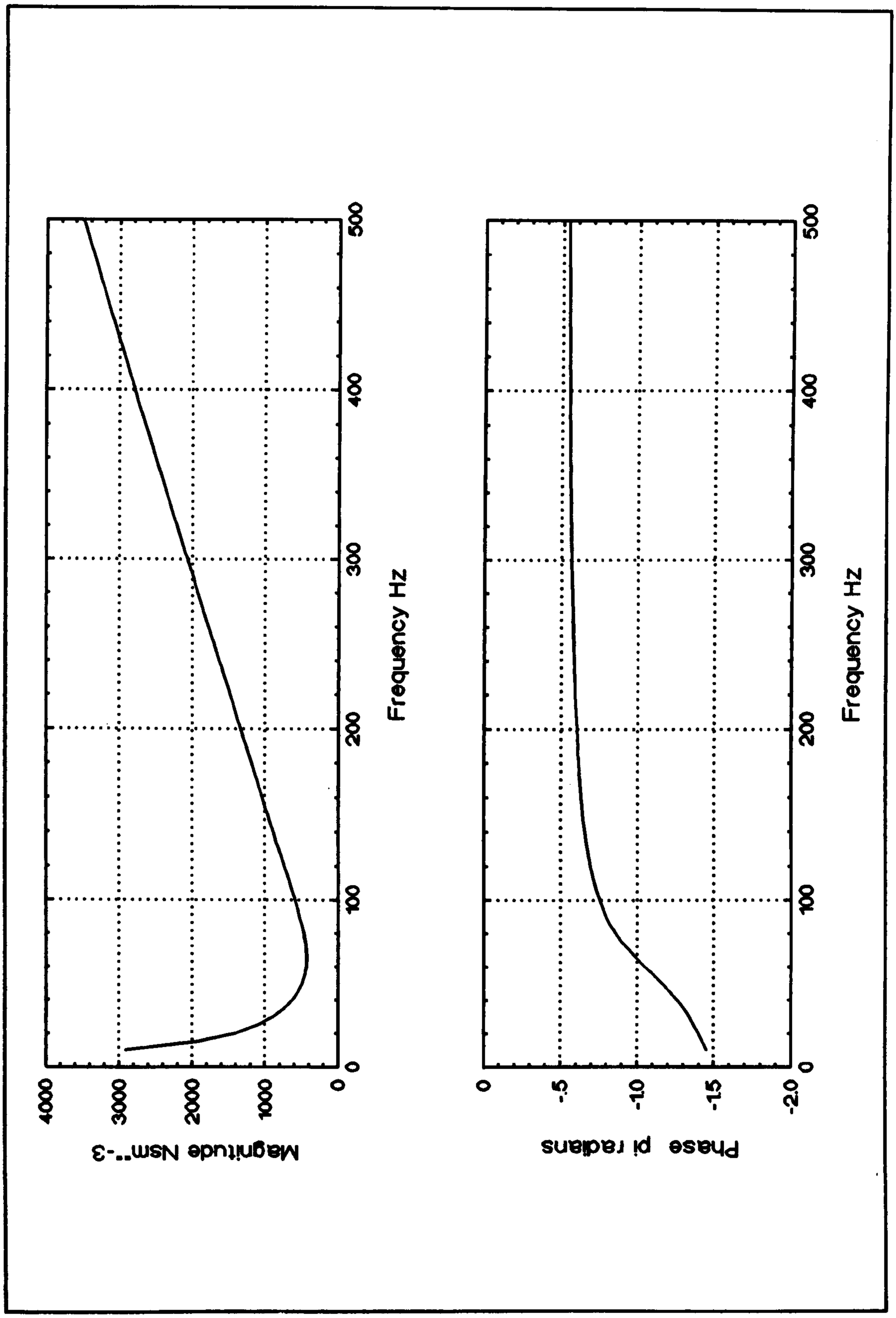

Figure 21. Theoretical specific surface acoustic impedance of a KEF B200A loudspeaker mounted in a 25 litre sealed box when connected to an electrical impedance of zero ohms

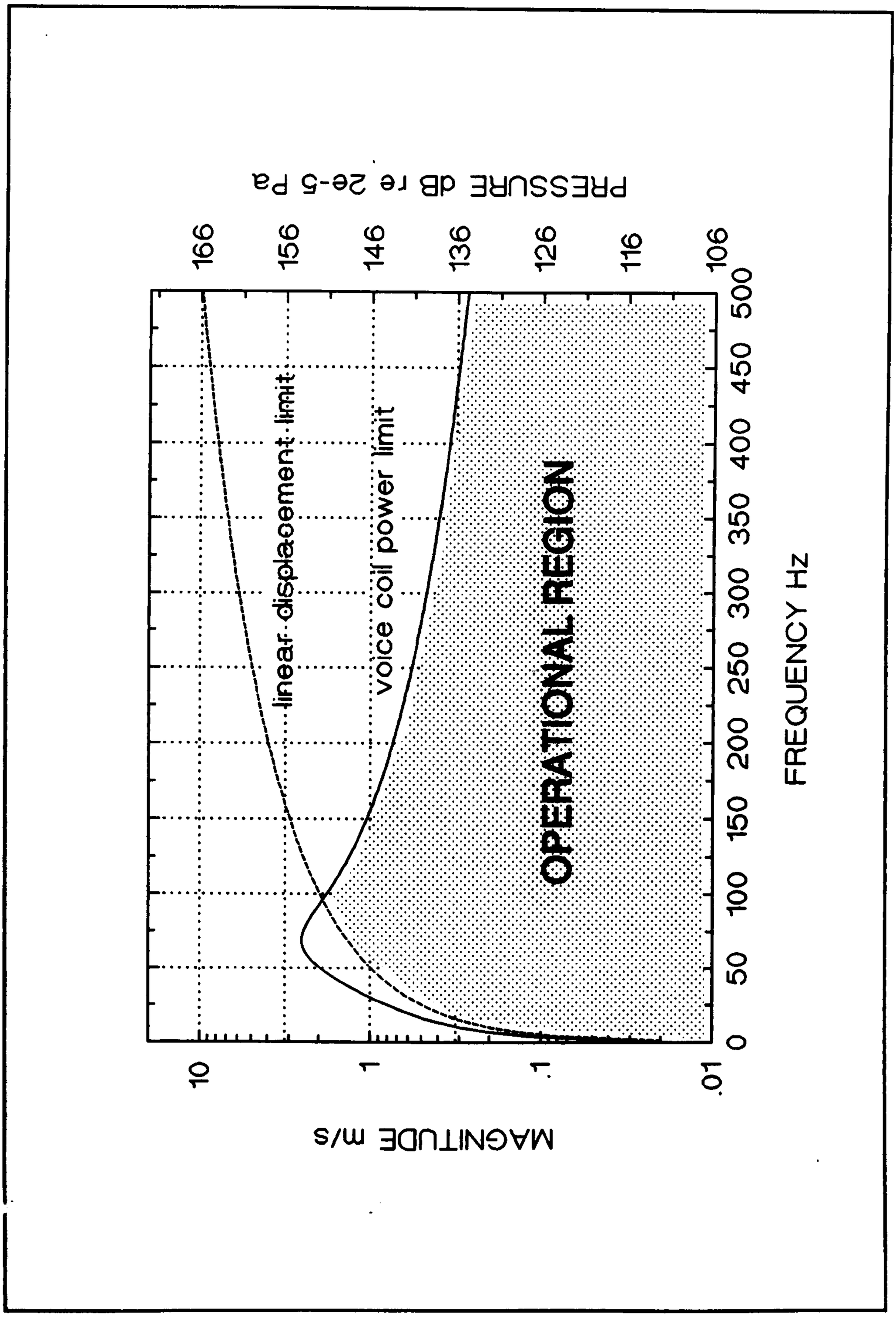

Figure 22. Theoretical cone velocity limit for an actively controlled KEF B200A loudspeaker with surface acoustic impedance of 415 Rayls. Sound pressure on right hand vertical scale.

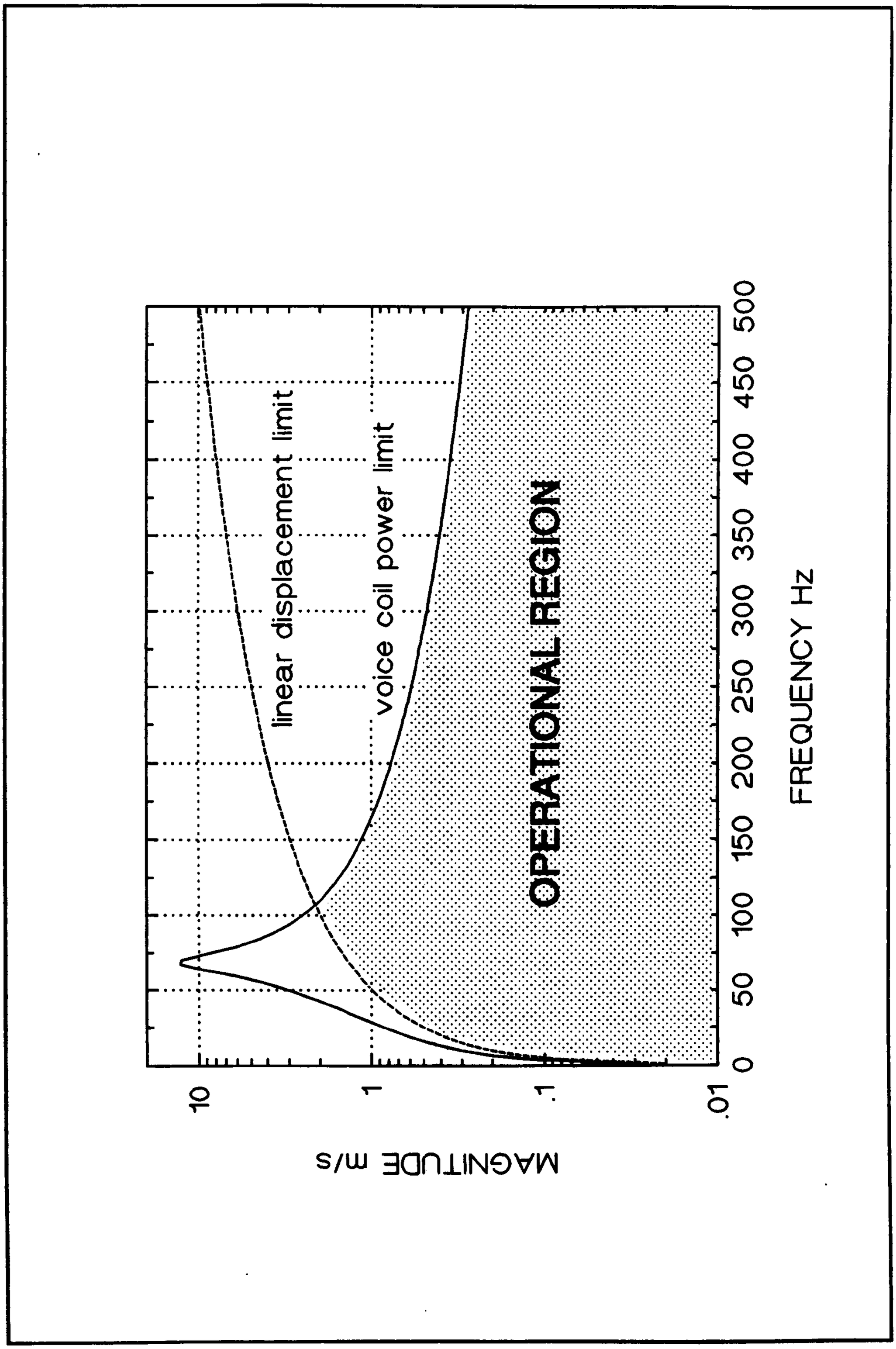

Figure 23. Theoretical cone velocity limit for an actively controlled KEF B200A loudspeaker when surface acoustic impedance is forced to zero

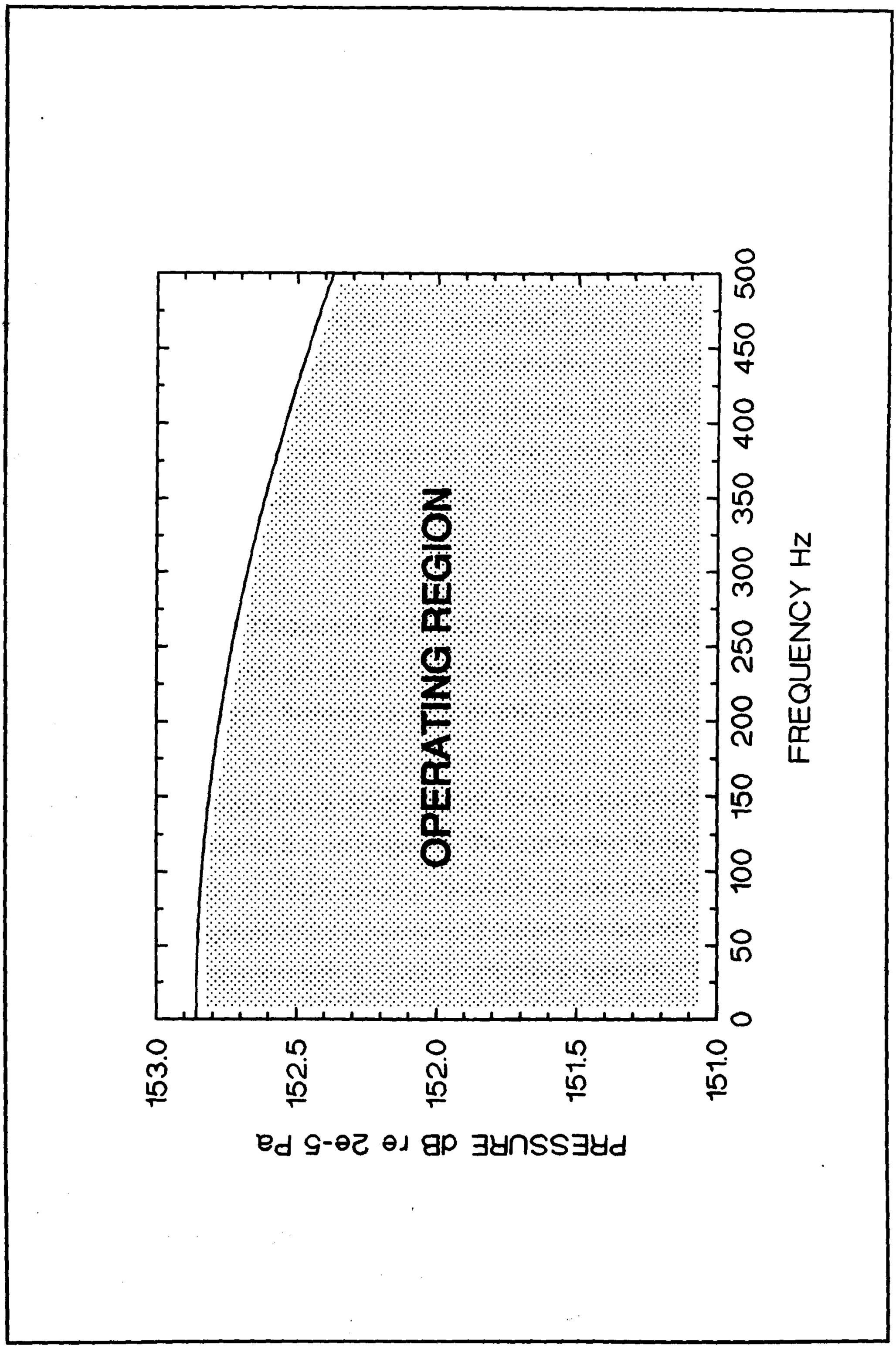

Figure 24. Theoretical cone pressure limit for an actively controlled KEF B200A loudspeaker with a surface acoustic impedance of infinity

5 METHOD FOR THE ACTIVE CONTROL OF IMPEDANCE

5.1 INTRODUCTION

This thesis concerns the modification of impedance with active control techniques. An active controller scheme for the control of impedance is described in Section 5.2. This thesis identifies an error determination method with which the active controller can be automatically designed to modify the impedance of the simple compliantly-suspended piston. This method and a variation are described in Section 5.3. An abbreviated phrase to refer to control systems that use this method has been designated "mic-accr" in Section 2.4.3 on Page 20. The digital implementation of the automatically designed active control system is described in Section 5.4. A summary of the chapter is given in Section 5.5.

5.2 AN ACTIVE CONTROLLER FOR THE CONTROL OF IMPEDANCE

This section describes an active controller scheme for the control of the impedance of a piston. Several variants of the controller are illustrated.

It has been established that a control forcing function can modify the impedance **z** of a piston in Section 4.2.2 on Page 75. The controlled impedances developed during this research are built around conventional electrodynamic loudspeaker drivers. The loudspeaker has a convenient means for applying control forces to the "piston-like" cone through the voice-coil motor system. The application of a control voltage function to the voice-coil can modify the **z** of the cone, see Section 4.3 on Page 76.

The generation of the appropriate control voltage for the desired **z** is the task of the active controller, typically implemented with a single channel linear filter. Figure 25 on Page 98 shows a schematic for the control of the impedance of a loudspeaker cone. This figure shows an electrically-driven loudspeaker acting as an acoustic source of energy at the right hand end of an acoustic waveguide. At the other end there is a loudspeaker that is driven by an active controller so that the impedance presented to the pipe is a desired value. This loudspeaker

is therefore described as a "controlled impedance termination" to the duct. Other aspects of this diagram are explained later in this section. The active controller should be regarded here as a "black box" that contains a linear filter that operates on the input to generate an output. Later sections in the thesis describe the required transfer function and implementation of the controller. The voltage **V**, see Figure 25, required to force the **z** of the cone of the "controlled impedance termination" to some pre-specified constant value must be proportional to the cone velocity $\mathbf{u}_{cone}$ as shown in Equation 4.9 on Page 77. The use of a *linear* filter as the controller therefore demands that the input is coherent with the cone velocity. The input to the controller is often called the "reference" (see Figure 25).

The one-dimensional laboratory test-rig offers four signals that are each potentially suitable (ie: coherent with the cone velocity) as the reference to the linear controller: cone pressure $\mathbf{p}_{cone}$, cone velocity $\mathbf{u}_{cone}$, the upstream pressure at some point in the duct **p** and the electronic source signal as illustrated in Figure 25 on Page 98. There are certain conditions for which the pressure or velocity measurements are zero and then the "black box" controller will not be able to produce the correct output voltage. These conditions are discussed in Section 6.3 on Page 105.

The selection of the reference can cause the controller to be a feed-forward or feedback system as defined in Section 3.3 on Page 35. The controller is a feedback system when either the cone pressure or the cone velocity is used as the reference signal. Potential feed-forward system reference signals are either a microphone in the duct positioned away from the cone, or the electrical signal that drives the far-end source. The selection of the reference signal changes the required transfer function of the controller. Therefore the selection of the reference signal distinguishes variants of the active controller. Section 6.3 on Page 105 presents theoretical analysis of the required control filter transfer function for the acoustic control of impedance. The theoretical "loop stability" of the controller is described in Section 6.4 on Page 117.

The active controller can be implemented with either analogue or digital signal processing electronics. It is often difficult to design the required transfer function for the active controller. The required transfer function may be complex and may change with the course of time. These problems can be overcome with the use of an automatically designed active controller based on "adaptive" methods (see Section 3.4 on Page 36). The next section describes a method that enables the active controller "black box" to use adaptive methods.

5.3 THE MIC-ACCR METHOD FOR ACTIVE CONTROLLER DESIGN

The specific acoustic impedance of a vibrating surface is fully described by the ratio of the acoustic pressure at the surface to the surface velocity. It is, therefore, possible to evaluate the surface impedance by direct measurement of acoustic pressure and surface velocity with transducers. A novel method for the design of active controllers to control impedance is based on "instrumenting" the surface with a microphone and an accelerometer. An abbreviated phrase to refer to control systems that use this method has been designated "mic-accr" in Section 2.4.3 on Page 20. This section describes this method for the control of the impedance of a simple compliantly-suspended piston. The piston is realized with a conventional electrodynamic loudspeaker as explained in Section 4.3. The control objective is to modify the surface impedance of the loudspeaker cone to a desired value.

The acoustic pressure and acceleration of the cone of the loudspeaker are measured by attaching conventional lightweight transducers to the cone, see Figure 26a on Page 99 reproduced from (33). The cone velocity is determined by electronically integrating the acceleration signal. The surface impedance can be directly calculated according to Equation 1.1 on Page 3 from the two measured signals.

The method relies on the specification of the *desired* surface impedance z_d with the filter H, see Figure 26a. This filter operates on the actual cone pressure signal p to produce a desired cone velocity u_d (the cone velocity which is caused by the actual cone pressure when the surface impedance has the desired value

$\mathbf{z_d}$). The filter **H** is often referred to as the "*desired filter*" throughout the rest of the thesis. The method determines the difference, or "**error**", between the desired velocity signal $\mathbf{u_d}$ and the actual cone velocity signal **u**. If an active controller operates so that, in response to an incident pressure on the cone, the error is made zero then the cone will have the desired impedance. The process of minimising an error signal between a measured and a desired signal is often used in contemporary adaptive control systems. The adaptive design of the controller is outlined later in this chapter.

The inclusion of the adjustable desired filter **H** allows easy selection of the desired impedance in the practical adaptive control system. However there are constraints on the implementable impedance imposed by this method. Since **H** must be a physically realizable filter, it must always be causally stable. In the method illustrated in Figure 26a this means that the desired impedance must be minimum phase. Also a desired impedance of zero can not be realized as **H** would necessarily have infinite gain. The specification of a desired impedance of either non-minimum phase or of zero value can be achieved by re-configuring the method, see Figure 26b.

In this configuration, the method also relies on the specification of the *desired* surface impedance $\mathbf{z_d}$ with a desired filter **H**, see Figure 26b. This filter operates on the actual cone velocity signal **u** to produce a desired cone pressure signal $\mathbf{p_d}$ (the cone pressure which would exist for the same cone velocity but when the surface impedance has the desired value $\mathbf{z_d}$). The method determines the error between the desired pressure signal $\mathbf{p_d}$ and the actual cone pressure signal **p**. If a controller operates so that, in response to an incident pressure on the cone, the error is made zero then the cone will have the desired impedance. This variation of the method can implement a desired impedance of zero. However infinite impedances can not be realized as **H** would have infinite gain.

Adjustment of the filter transfer function **H** enables a suitable controller to generate desired surface impedances of zero or infinity providing the appropriate configuration of the method is selected from Figure 26a or b. Laboratory tests

demonstrate that either configuration can be used to force characteristic impedance of a loudspeaker cone with a suitable controller. Results are presented later in Chapter 8 on Page 271. The inclusion of the filter **H** also allows frequency-dependent desired impedances to be specified. There is, however, a value of impedance that is not realizable - "negative characteristic" impedance. This is discussed in the text after Equation 6.59 on Page 119. **H** can also compensate for transducer measurement errors in the control system implementations, see Section 6.2 on Page 102. The signal processing that is required by the method can be implemented with either analogue or digital techniques. Digital techniques were found to be more suitable for laboratory work, see Section 7.5 on Page 215.

The next section outlines adaptive digital controllers that use the mic-accr method for the active control of impedance of the simple compliantly-suspended piston.

5.4 ADAPTIVE DIGITAL CONTROLLERS

The active controller described in Section 5.2 on Page 90 for the control of impedance can be based on a linear filtering operation. The controller can then be implemented with digital signal processing techniques either as a finite impulse response (FIR) or a infinite impulse response (IIR) filter. This section describes two adaptive digital mic-accr control systems based on FIR and IIR filters that use the mic-accr method described in Section 5.3.

The active controller can be implemented with a linear FIR filter. The coefficients of an FIR control filter can easily be adaptively modified by the LMS algorithm in a filtered-X configuration (described in Section 3.6 on Page 45) to minimise the error signal generated by the mic-accr method. A schematic for the adaptive control system in the laboratory test-rig is shown in Figure 27 on Page 100. This figure shows an electrically-driven loudspeaker acting as an acoustic source of energy at the right hand end of an acoustic waveguide. At the other end there is the loudspeaker that is controlled so that the impedance presented to the pipe is forced to a desired value. The control voltage is

generated from the digital to analogue conversion (D/A) of the output of the linear FIR filter. The filter input is taken from the analogue to digital conversion (A/D) of one of the four reference signals available in the test-rig - see Figure 25 on Page 98. The specification of the desired impedance with the desired filter and the error determination are performed as shown in either Figure 26a or Figure 26b; the selection depend on whether the desired filter is realizable (see Section 5.3).

The coefficients of the FIR control filter are adapted by the LMS algorithm. The LMS algorithm requires a filtered version of the reference signal for stable adaptive convergence because of the transfer function between the FIR filter output and the error determination. This is the filtered-X version of the LMS algorithm described in Section 3.6 on Page 45. The filtering of the reference signal is performed by the "stability compensation filter". This configuration of this digital FIR filter is described in Section 6.6 on Page 139. The coefficients are designed prior to starting the control system as described in Section 7.5 on Page 215. The LMS algorithm uses the filtered reference and error signals to calculate new coefficients for the FIR control filter every sample period. The D/A converted output of the filter then modifies the impedance of the loudspeaker. The implementation of this system modifies the surface impedance of the loudspeaker to desired values.

The control filter can also be implemented with two FIR filters that, together, form an IIR filter structure. The coefficients of this IIR control filter are adaptively updated in a filtered-U configuration (described in Section 3.7 on Page 50) to minimise the error generated by the mic-accr method. A schematic for the adaptive control system in the laboratory test-rig is shown in Figure 28 on Page 101. This IIR system is similar in arrangement to the previous FIR system. The controller input is also taken from the A/D conversion of one of the four reference signals available in the test-rig - see Figure 25 on Page 98. The specification of the desired impedance with the desired filter and the error determination are performed as shown in either Figure 26a or Figure 26b; the selection depend on whether the desired filter is realizable (see Section 5.3).

There are now two linear FIR filters **A** and **B**. Filter **B** is configured in a feedback loop to enable an IIR filter structure. Each filter is updated with an LMS algorithm. Both LMS algorithms use the same error signal but require different signals from the system. The LMS algorithm for **A** requires a compensated reference signal. The LMS algorithm for **B** requires a compensated controller output signal. The compensation of both signals is performed with identical "stability compensation" FIR filters designated as **C** in Figure 28. The configuration of these filters are described in Section 6.6 on Page 139. The coefficients of **C** are designed prior to starting the control system as described in Section 7.5 on Page 215.

A simple change to the IIR configuration of the control system produces the FIR configuration. If the output of filter **B** in Figure 28 is disconnected, or made zero then the control system is identical to the FIR configuration. This simple change is realized in the digital implementation of the control system created during the research - this is described in Section 3.5.2.2 on Page 326 in Appendix 3.

Practical implementations of this system allow stable control of desired impedances as discussed later in this thesis. The implementation of this system is described in Section 7.5 on Page 215. The stability aspects are described in Section 7.6 on Page 219. The constraint of causality on the control system performance with band-limited noise is described in Section 7.7 on Page 225 for different reference signals. The performance of a feedback implementation of the control system is described in Section 7.8 on Page 228. Results for a feed-forward implementation are presented in Chapter 8 on Page 271.

5.5 SUMMARY

An active controller scheme for the control of impedance of a loudspeaker cone has been described. The output of the controller must be coherent with the velocity of the cone. As the controller is a linear system then the input must also be coherent with the velocity. Several signals are available that are suitable for the controller input. The selection of the input signal complicates the controller design. Theoretical sections published later in the thesis analyze the required

controller transfer functions.

The mic-accr method has been presented. This method offers a basis for the automatic (or "adaptive") design of the active controller for pre-specified desired impedances. Extremes of desired impedance demand selection of one of two variations of the method. One of the variations is suitable for the control of frequency-dependent impedances of non-minimum phase.

The configuration of the active controller and the mic-accr method enables the use of adaptive control systems. The control systems, based on linear digital filters, have been outlined. Later sections in this thesis show that these systems successfully control the impedance of the loudspeaker cone for defined incident acoustic waves.

5.6 CHAPTER FIGURES

The figures referred to in this chapter appear on the following pages.

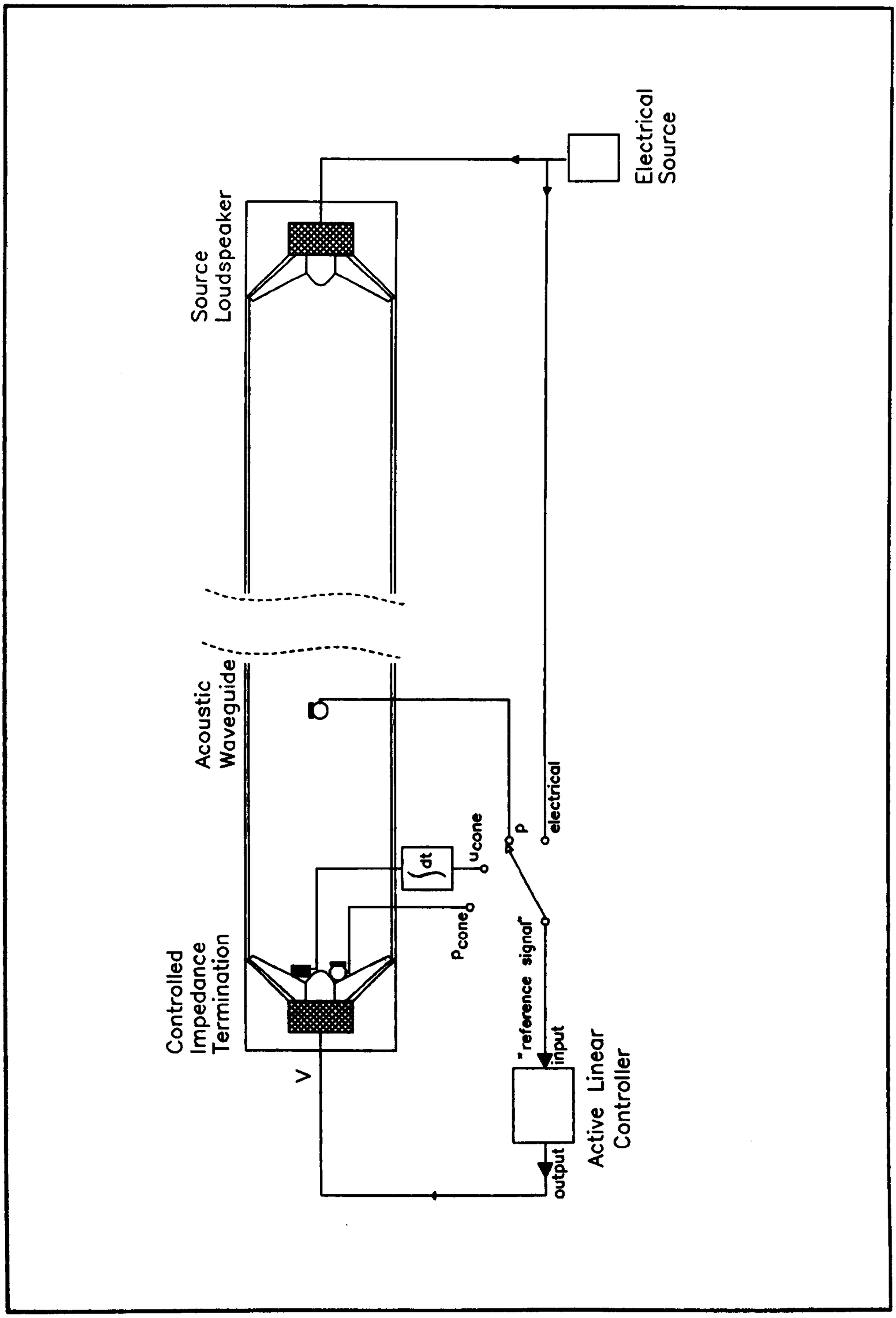

Figure 25. Active controller for the control of acoustic impedance of a loudspeaker cone in an acoustic waveguide. Four suitable input, or "reference", signals are available for the linear controller.

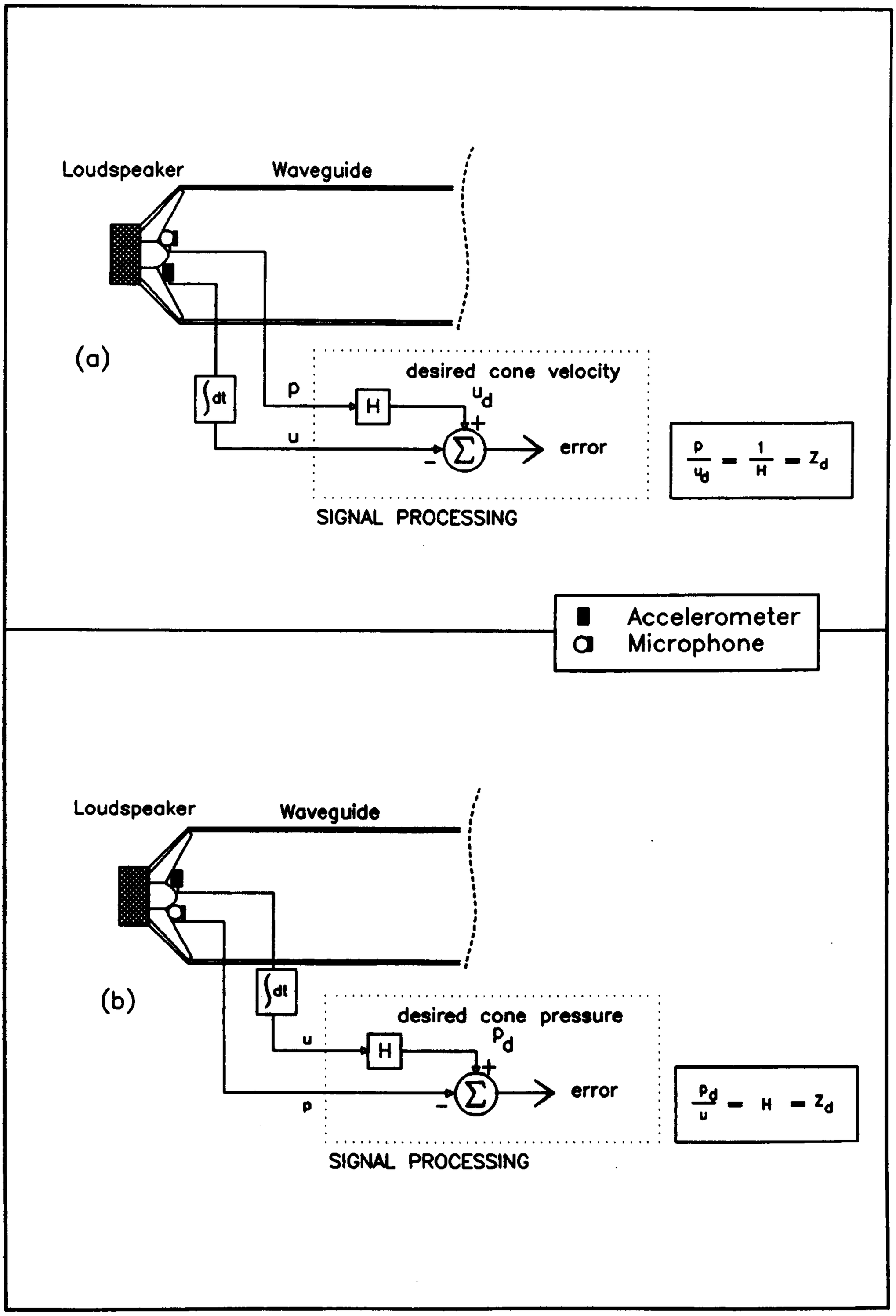

Figure 26. The mic-accr method for acoustic impedance control. The method relies on measurement of acoustic pressure and velocity. Desired z is specified with filter H. (a) and (b) show different variations.

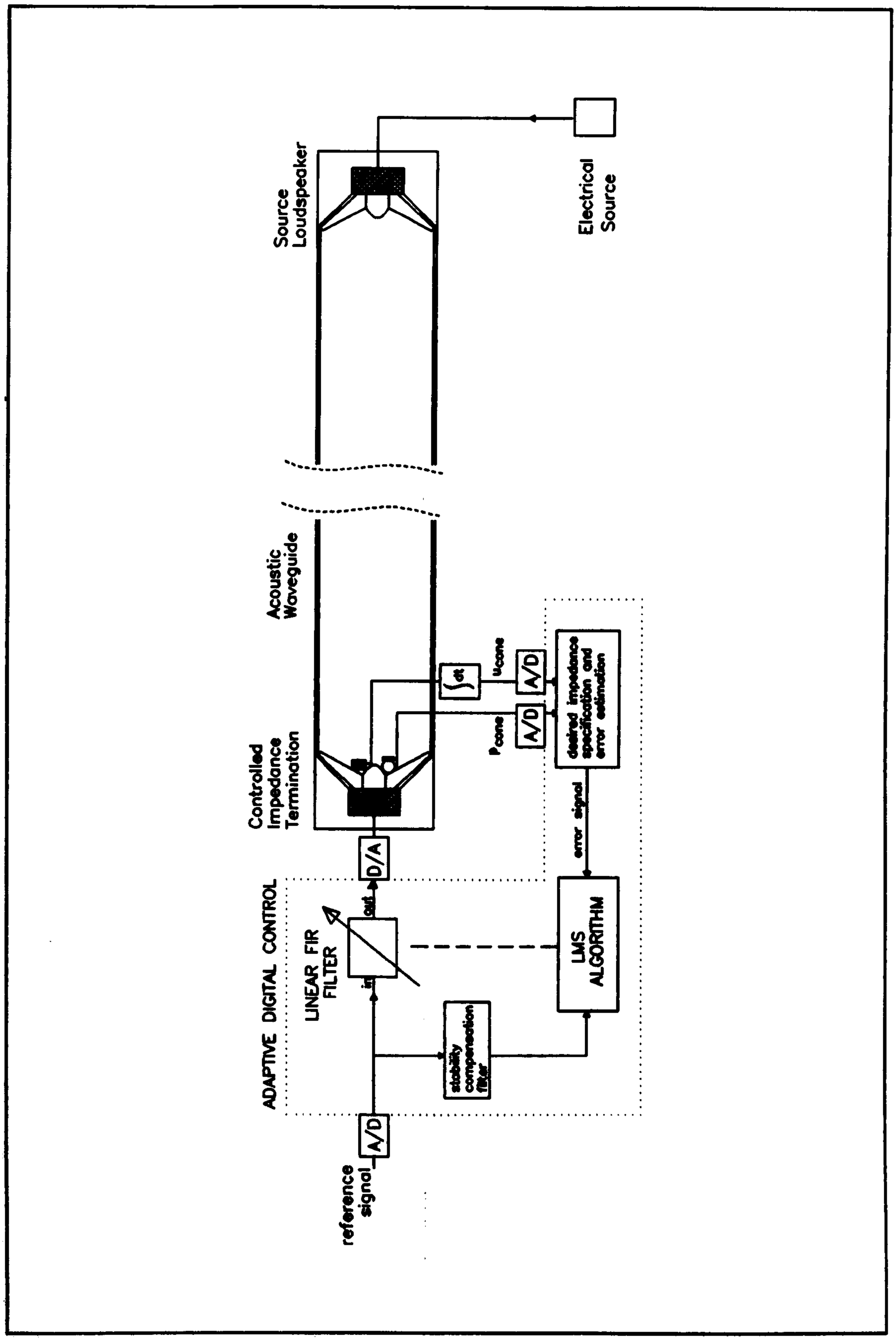

Figure 27. Adaptive digital "mic-accr" control system for the control of acoustic impedance. The selection of the reference signal affects system performance.

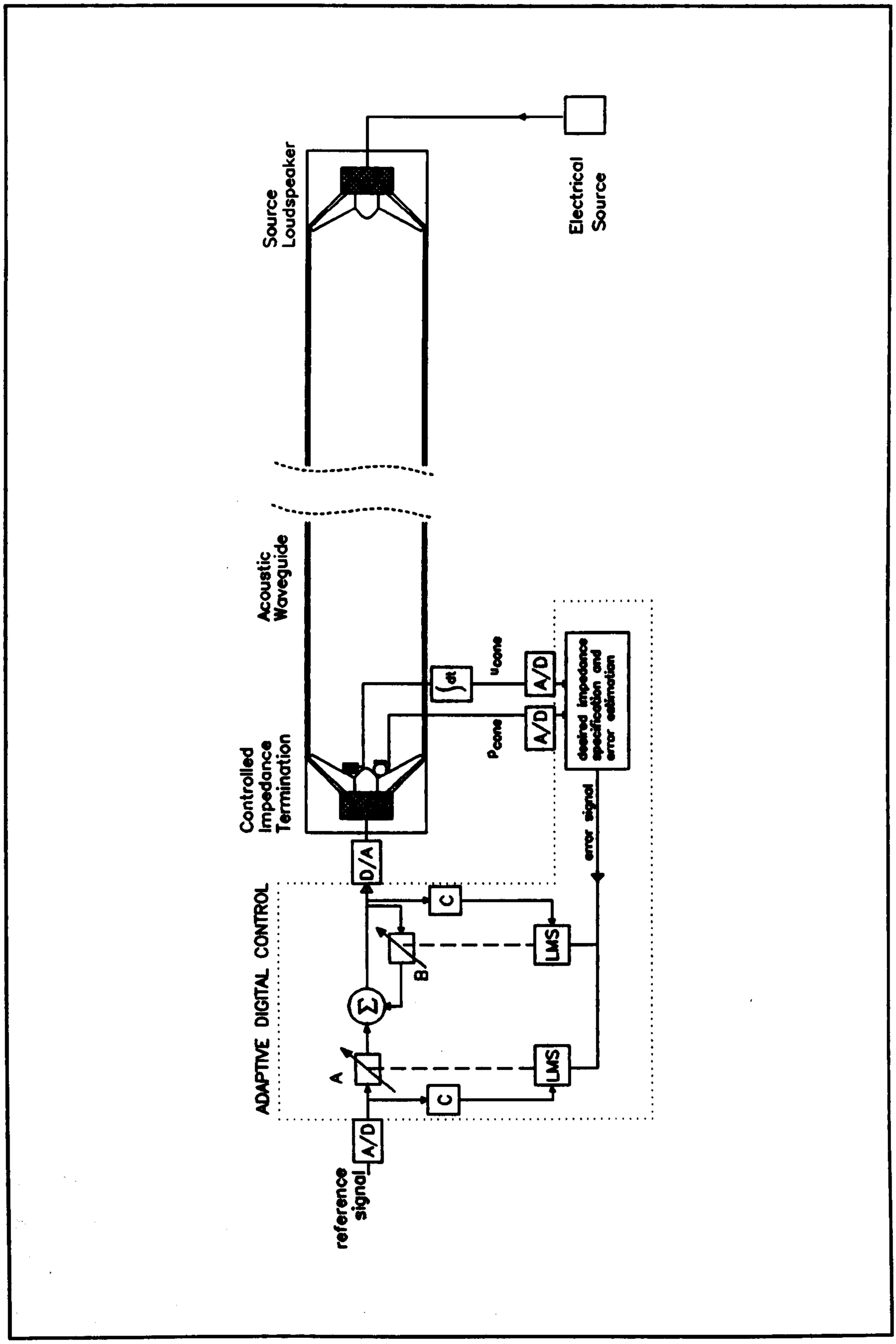

Figure 28. Adaptive digital "mic-accr" control system for the control of acoustic impedance. The selection of the reference signal affects system performance.

6 THEORETICAL CONSIDERATIONS ON THE CONTROLLED IMPEDANCE METHOD

6.1 INTRODUCTION

A method for the active control of impedance has been presented in Chapter 5. This method measures the acoustic pressure and velocity at a controlled surface. Active control systems can then be configured for the control of pre-specified desired impedance. This chapter presents original theory on the operation of active control systems for the control of impedance.

The effect on the controlled impedance of errors in the observation of impedance in mic-accr control systems is described in Section 6.2. The required active controller transfer functions for the control of impedance are presented in Section 6.3. Feedback loop stability issues are discussed in Section 6.4. A common solution that increases loop stability is the use of feedback cancellation - the optimum transfer functions for active impedance control with this technique are defined in Section 6.5. The adaptive implementation of the mic-accr control system requires compensation for stable convergence - compensation strategies are described in Section 6.6. Theoretical transfer functions for the compensation of the adaptive control of a loudspeaker in a waveguide are described in Section 6.7 and compared with measurements from the research test-rig. A feedback system for the active control of acoustic absorption has been proposed by Mazzola (34). This is examined in Section 6.8 for the control of a conventional loudspeaker. Theoretical active controller transfer functions for the mic-accr and 2-mic control systems are compared in Section 6.9. A summary of the chapter is given in Section 6.10.

6.2 IMPEDANCE OBSERVATION ERROR EFFECTS ON MIC-ACCR CONTROL SYSTEMS

The mic-accr method relies on measurements of the acoustic pressure and velocity as a basis for the adaptive design of an active controller for the control of impedance, see Chapter 5. This section describes the theoretical effects of error in the measurement and the specification of the desired impedance on the

control system performance. This is illustrated in the context of an active absorber.

The surface impedance ***z*** is described by the ratio of acoustic pressure ***p*** to velocity ***u***, Eq. 6.1.

$$z = \frac{p}{u} \quad Rayls \qquad 6.1$$

The acoustic pressure is measured with a microphone. The velocity is measured by electronically integrating the output of an accelerometer. The measurements produce two electrical signals that correspond to the acoustic pressure and velocity. The voltage V_p corresponding to the acoustic pressure ***p*** at the controlled surface is described by Eq. 6.2.

$$V_p = M.p \qquad 6.2$$

M is a frequency dependant factor describing the sensitivity of the microphone and voltage amplifier (V/Pa). The voltage V_u corresponding to the velocity of the mic-accr system's surface is Eq. 6.3.

$$V_u = A.u \qquad 6.3$$

A is a frequency dependant factor describing the combined sensitivity of the accelerometer, charge amplifier and integrator (Vs/m).

The mic-accr method is described in Section 5.3 on Page 92 and illustrated in Figure 26 on Page 99. The method uses voltages V_p and V_u and a desired filter (see Section 5.3) to calculate an error signal. In order to force the surface impedance to a desired value, an adaptive control system attempts to minimise the error signal. This process is illustrated in the schematic of Figure 29 on Page 164. This figure resembles Figure 26 but incorporates Eq. 6.2 and Eq. 6.3. ***H*** is the desired filter that specifies the desired impedance. The error signal, ***e***, of Figure 29a is described by Eq. 6.4.

$$e = M.p.H - A.u \qquad 6.4$$

If the active controller is ideal and therefore minimises ***e*** to zero then Eq. 6.4 can be rearranged to give the impedance implemented at the cone Eq. 6.5.

$$z = \frac{p}{u} = \frac{A}{M.H} \qquad \textbf{6.5}$$

The controlled impedance depends on the desired filter ***H*** *and* the transducer sensitivities. Filter ***H*** specifies the desired impedance z_d and must compensate for the transducer sensitivities with a scaling factor k_h, Eq. 6.6.

$$H = \frac{1}{k_h . z_d} \qquad \textbf{6.6}$$

Let ***k*** ($sPam^{-1}$) be a scaling term to describe for the potentially frequency dependant transducer sensitivities ***M*** and ***A***, Eq. 6.7.

$$k = \frac{M}{A} \qquad \textbf{6.7}$$

For practical transducers it is difficult to design the desired impedance filter H which adequately compensates for the transducer sensitivity scaling term Eq. 6.7 over the entire operating frequency range of the mic-accr system. If the scaling factor used in the filter k_h is not accurately specified then the impedance implemented is not z_d but Eq. 6.8.

$$z = \frac{k_h}{k} . z_d \qquad \textbf{6.8}$$

A similar analysis on the error signal of the alternative arrangement of the method seen in Figure 29b produces the same implemented impedance Eq. 6.8 when the desired filter ***H*** of Figure 29b is described by Eq. 6.9.

$$H = k_h . z_d \qquad \textbf{6.9}$$

The impedance implemented by the control system is seen in Eq. 6.8 to include the factor $k_h k^{-1}$. If the system is perfectly observed, then this "impedance observation" factor has unit value. If the actual transducer sensitivities differ from those specified by ***M*** and ***A***, or if k_h differs from k^{-1} , then the observation factor is of non-unit value and the implemented impedance will not be the desired impedance z_d.

The influence of error in the impedance observation can be illustrated by considering the reflection coefficient of the loudspeaker cone when the mic-accr

system acts to make $z_d = \rho_0 c$ - that for an ideal acoustic absorption. The reflection coefficient of the ideal acoustic absorber is zero from Equation A5.12 on Page 346. Rearranging A5.12 gives Eq. 6.10.

$$R = \frac{z - \rho_0 c}{z + \rho_0 c} \qquad 6.10$$

Substituting for z from Eq. 6.8 and noting that $z_d = \rho_0 c$, gives Eq. 6.11 where Δk is defined in Eq. 6.12.

$$R_{absorber} = \frac{\frac{\Delta k}{k}}{2 + \frac{\Delta k}{k}} \qquad 6.11$$

$$\Delta k = k_h - k \qquad 6.12$$

The relationship between the magnitude of the reflection coefficient and the magnitude and phase of the impedance observation factor, $k_h k^{-1}$ are shown in Figure 30 on Page 165. It is seen that the impedance of the surface of the absorber must be observed with less than 1dB of magnitude error and less than 5 degrees of phase error if the magnitude of the reflection coefficient is to be lower than 5%.

6.3 ACTIVE CONTROLLER FILTER SOLUTIONS

The active controller for the control of impedance is implemented with a filter, see Section 5.2 on Page 90. The selection of the input signal, or reference, for the controller filter dictates the required controller filter transfer function (or solution) for a desired impedance. This section presents original theory on the required controller filter transfer functions for the control of impedance.

The difference between active controller feedback and feed-forward structures is described in Section 3.3 on Page 35. The active controller is a feedback structure when either the cone pressure or the cone velocity is used as the reference signal. The controller is a feed-forward structure when the reference signal is either from a microphone in the duct positioned some distance from the boundary surface, or from the electrical signal that drives the far-end source.

Figure 25 on Page 98 illustrates the four reference signals for the active controller. The required active controller transfer functions for optimum control are presented in the following sections. The pressure and velocity reference signals sometimes are zero and then the controller will not function correctly. Each section discusses this potential problem.

6.3.1 Cone pressure as reference

Consider a reference signal of cone pressure for the active controller filter. The reference signal is selected as p_{cone} in Figure 25 and the active controller is a feedback structure. This section defines the optimum transfer function of the active controller for the control of a desired impedance.

For non-zero values of controlled impedance there will be acoustic pressure at the cone and so the reference may be taken from the cone microphone signal. However, at desired impedance values approaching zero then pressure at the cone must also become near zero by definition - there is then little correlated energy in the reference signal to drive the controller and consequently the controller will not function correctly. The controller, therefore, does not work for desired impedances of zero.

The output voltage of the controller V, Eq. 6.13, is the product of the cone pressure p_{cone} and the controller filter transfer function W.

$$V = p_{cone} W \qquad 6.13$$

The impedance z at the loudspeaker cone is defined in Eq. 6.14.

$$z = \frac{p_{cone}}{u_{cone}} \quad Rayls \qquad 6.14$$

It is possible to identify the relationship between the impedance z and the transfer function of controller filter, W, by solving the equation of motion at the cone. The total force on the cone, Eq. 6.15, is the sum of the forces due to the motor system, the acoustic reaction, and the stiffness and damping of the suspension

$$F = \left[\frac{BI\,V - (BI)^2\,u_{cone}}{Z_{EB}}\right] - [p_{cone}\,S] - \left[R\,u_{cone} + \frac{K\,u_{cone}}{j\omega}\right] \qquad 6.15$$

where F is the total force on the cone in (newtons), BI is the transformation factor (newtons per ampere), V is the controller output voltage applied to the voice-coil (volts), Z_{EB} is the blocked electrical impedance of the loudspeaker (ohms), S is the cone area (square metres), R is the total damping (newton-seconds per metre), K is the total compliance (metres per newton), ω is the angular frequency (radians per second).

Substituting the total force defined in Eq. 6.15 into Newtons second law for the motion of the cone yields Eq. 6.16 where M is the mass of the cone (kg).

$$M\,j\omega\,u_{cone} = \left[\frac{BI\,V - (BI)^2\,u_{cone}}{Z_{EB}}\right] - [p_{cone}\,S] - \left[R\,u_{cone} + \frac{K\,u_{cone}}{j\omega}\right] \qquad 6.16$$

Rearranging Eq. 6.16 so that terms V, p_{cone} and u_{cone} are separated yields Eq. 6.17 where Z_M, the mechanical loudspeaker impedance, is defined in Eq. 6.18.

$$\left[\frac{BI}{Z_{EB}}\right]V - [S]p_{cone} = \left[Z_M + \frac{(BI)^2}{Z_{EB}}\right]u_{cone} \qquad 6.17$$

$$Z_M = M j\omega + R + \frac{K}{j\omega} \qquad 6.18$$

Substituting for V in Eq. 6.17 from Eq. 6.13 to include the controller transfer function yields Eq. 6.19.

$$\left[\frac{BI}{Z_{EB}}\right]p_{cone}\,W - [S]p_{cone} = \left[Z_M + \frac{(BI)^2}{Z_{EB}}\right]u_{cone} \qquad 6.19$$

Substituting u_{cone} in Eq. 6.19 from Eq. 6.14 yields Eq. 6.20.

$$\left[\frac{BI}{Z_{EB}}\right]p_{cone}\,W - [S]\,p_{cone} = \left[Z_M + \frac{(BI)^2}{Z_{EB}}\right]p_{cone}\,z^{-1} \qquad 6.20$$

Eq. 6.20 is rearranged to express the controlled impedance at the cone z in terms of the active controller transfer function W as Eq. 6.21.

$$z = \left[\frac{1}{W\frac{Bl}{Z_{EB}} - S} \right] \cdot \left[Z_M + \frac{(Bl)^2}{Z_{EB}} \right] \qquad 6.21$$

The optimum controller filter solution W_{OPT}, Eq. 6.22, for a desired impedance of z_d is found by rearrangement of Eq. 6.21.

$$W_{opt} = z_d^{-1} \left[\frac{Z_M Z_{EB}}{Bl} + Bl \right] + \frac{S Z_{EB}}{Bl} \qquad 6.22$$

The optimum controller filter Eq. 6.22, with the cone pressure as the reference input to the filter, required to force the surface impedance at the cone of the loudspeaker to the desired value of z_d has two additive terms. The first term is proportional to the inverse of the desired impedance, whilst the second term, (SZ_{EB} / Bl), is independent of the required impedance. This second term is the filter required to hold the cone of the loudspeaker perfectly still, implementing an infinite impedance of $z_d = \infty$, see Eq. 6.23. This relationship has been noted in Section 4.4.3, see Equation 4.14 on Page 82.

$$W_{opt}\Big|_{z_d \to \infty} = \frac{S Z_{EB}}{Bl} \qquad 6.23$$

In order for the optimum controller filter, defined in Eq. 6.22, to be realizable, the desired surface impedance should have a causally stable inverse (as z_d^{-1} is a factor of the first term of the right hand side of Eq. 6.22). The controller filter, with a reference input of p_{cone} is therefore not stable for a desired impedance of zero (this confirms the intuitive discussion presented at the start of this section). The other potential problem in specifying the optimum controller filter W_{opt} are the singularities in the mechanical impedance of the loudspeaker, Z_M , at zero and infinite frequencies. Z_M has infinite magnitude at dc due to suspension stiffness - this would require that W_{opt} should have infinite dc gain, which is, clearly, impractical. Practical implementations of the mic-accr are band-pass limited (at low frequencies by the linear excursion of the suspension, see Section 4.4.1 on Page 79, and at higher frequencies by the practical bandwidth of the control system) so the singularities in the ideal filter solution are never encountered.

6.3.2 Cone velocity as reference

Consider a reference input signal of cone velocity for the active controller filter. The reference signal is selected as u_{cone} in Figure 25 on Page 98. The active controller is a feedback structure with this reference signal. This section defines the optimum transfer function of the active controller for the control of a desired impedance.

Equation 4.9 on Page 77 shows that a suitable control voltage for the control of a loudspeaker's surface impedance is proportional to cone velocity. The cone velocity is then an appropriate reference input for the linear control filter. For lower values of controlled impedance there is non-zero cone velocity - and so the reference may be taken from the cone velocity measurement signal. If the desired impedance approaches infinity then the cone velocity must approach zero by definition and there will be no correlated energy to drive the controller. Cone velocity is therefore suitable as the reference signal input of the active controller for non-infinite controlled impedances.

The output voltage of the controller V, Eq. 6.24, is the product of the cone pressure u_{cone} and the controller filter transfer function W.

$$V = u_{cone} W \qquad 6.24$$

In a similar process to the last section (e.g.: substitute V in Eq. 6.17 from Eq. 6.24 and rearrange), the optimum solution of the controller with a reference input of cone velocity u_{cone} for a desired impedance z_d is derived as Eq. 6.25.

$$W_{opt} = z_d \left[\frac{S Z_{EB}}{Bl}\right] + \left[\frac{Z_M Z_{EB}}{Bl} + Bl\right] \qquad 6.25$$

The optimum controller filter solution, Eq. 6.25, has two additive terms. The first term is proportional to the desired impedance, whilst the second term is independent of the required impedance. The second term describes the filter required to minimise the pressure at the vibrating cone of the loudspeaker, implementing a desired impedance of $z_d = 0$, see Eq. 6.26.

$$W_{opt}\Big|_{z_d=0} = \frac{Z_M Z_{EB}}{Bl} + Bl \qquad 6.26$$

In order for the optimum controller filter, Eq. 6.25, to be realizable, the desired surface impedance should be causally stable (as z_d is a factor of the first term of the right hand side of Eq. 6.25). The controller filter, with a reference input of u_{cone}, is therefore not stable for desired infinite impedance (this confirms the intuitive discussion presented at the start of this section). The other potential problem in specifying the optimum controller filter W_{opt} are the singularities in the mechanical impedance of the loudspeaker, Z_M , as described in the last section.

6.3.3 Duct pressure as reference

Consider a reference input signal of pressure measured at some point in the waveguide for the active controller filter. The reference signal is selected as p in Figure 25 on Page 98. If the pressure measurement is taken at a distance sufficiently far away from the controlled cone ("upstream" of the cone) then the active controller adopts a feed-forward structure (however, there is still the possibility of acoustic feedback in the system - see Section 6.4.4). The necessary distance must be such that the acoustic time delay (the delay associated with the time taken for an acoustic wave to propagate over the distance) must be larger than the overall delay in the controller filter. If the controller is based on a digital filter then delays are caused by sampling, digital processing time and the associated anti-aliasing and reconstruction filters. This section defines the optimum transfer function of the active controller with a reference input taken from a pressure measurement at some point in the duct. The optimum solution is significantly more complicated than the feedback controller solutions presented in Sections 6.3.1 and 6.3.2.

If the sound field in the duct is modal then reference pressure measurements taken at pressure nodes will not have enough energy to drive the controller. Theory in this section shows that, if the desired controlled impedance is infinite, then the controller filter is not realizable for reference measurements at these locations. The position of the reference pressure measurement in a modal sound field must be considered for real implementations of the controller filter.

The output voltage of the controller, Eq. 6.27, is the product of the pressure at some point in the duct p_{duct} and the controller filter transfer function W.

$$V = p_{duct} W \qquad 6.27$$

The impedance z at the loudspeaker cone is Eq. 6.28.

$$z = \frac{p_{cone}}{u_{cone}} \qquad 6.28$$

The relationship between the impedance z and the output voltage signal of the controller transfer function is found by solving the equation of motion as in Section 6.3.1. Substituting V in Eq. 6.17 from Eq. 6.27 yields Eq. 6.29 (where Z_M, the mechanical loudspeaker impedance, is defined in Eq. 6.18 of Section 6.3.1).

$$\left[\frac{Bl}{Z_{EB}}\right] p_{duct} W - [S] p_{cone} = \left[Z_M + \frac{(Bl)^2}{Z_{EB}}\right] u_{cone} \qquad 6.29$$

If the relationship between p_{duct} and p_{cone} is linear, which is true with plane waves propagating axially in the waveguide at frequencies below the plane wave cut-off frequency of the duct, a frequency-domain transfer function L can be defined in Eq. 6.30. This has a unique solution for the impedance termination and will be defined later.

$$L = \frac{p_{cone}}{p_{duct}} \qquad 6.30$$

Substituting for p_{duct} in Eq. 6.29 from Eq. 6.30 gives Eq. 6.31.

$$\left[\frac{Bl}{Z_{EB}}\right] W L^{-1} p_{cone} - [S] p_{cone} = \left[Z_M + \frac{(Bl)^2}{Z_{EB}}\right] u_{cone} \qquad 6.31$$

Substituting u_{cone} in Eq. 6.31 from Eq. 6.28 and rearranging to express the impedance at the cone z in terms of the active controller transfer function W gives Eq. 6.32.

$$z = \left[\frac{1}{\frac{W}{L}\cdot\frac{Bl}{Z_{EB}} - S}\right] \cdot \left[Z_M + \frac{(Bl)^2}{Z_{EB}}\right] \qquad 6.32$$

The optimum controller filter solution W_{opt}, Eq. 6.33, for a desired impedance of z_d is found by rearrangement of Eq. 6.32.

$$W_{opt} = \left[z_d^{-1} \left(\frac{Z_M Z_{EB}}{Bl} + Bl \right) + \frac{S Z_{EB}}{Bl} \right] . L \qquad 6.33$$

The optimum transfer function Eq. 6.33 of the controller includes the acoustic transfer function ***L*** Eq. 6.30 between the reference signal pressure p_{duct} and the pressure at the cone p_{cone}.

L can be defined by assuming that plane waves propagate in the duct, the waveguide is loss-less and the radiation load "seen" by the controlled impedance is characteristic. If harmonic plane waves are propagating axially in the waveguide then the acoustic pressure at a location ***r*** metres from the loudspeaker cone in the pipe can be defined as the sum of the incident and reflected propagating waves in Eq. 6.34.

$$p(r,t) = A e^{j(\omega t + kr)} + B e^{j(\omega t - kr)} \qquad 6.34$$

where ***A*** and ***B*** are determined by the impedance at the waveguide termination, ***k*** is the wavenumber and ω is the angular frequency. Equation 6.30 is the ratio of the pressure at ***r*** =0 metres to the pressure at ***r*** =***d*** metres as expressed in Eq. 6.35.

$$L = \frac{p_{inc}(0,t) + p_{refl}(0,t)}{p_{inc}(d,t) + p_{refl}(d,t)} = \frac{p(0,t)}{p(d,t)} \qquad 6.35$$

Eq. 6.30 can therefore be rewritten as Eq. 6.36 by substituting for p_{cone} and p_{duct} from Eq. 6.34 (***r*** is zero for p_{cone}).

$$L = \frac{A + B}{\frac{A}{e^{-jkd}} + B e^{-jkd}} \qquad 6.36$$

The transfer function between the component of pressure due to propagating waves *from* the controlled loudspeaker cone *to* the upstream microphone location can be described as a pure delay because the radiation load is assumed to be characteristic. Define the delay as ***F*** in Eq. 6.37.

$$F = e^{-j\omega d/c} \qquad 6.37$$

The term ***d*** in Eq. 6.37 describes the distance (metres) between the loudspeaker cone and duct microphone and ***c*** is the speed of sound. Substituting Eq. 6.37 into Eq. 6.36 and dividing through by ***A*** gives Eq. 6.38.

$$L = \frac{1 + \frac{B}{A}}{\frac{1}{F} + F\frac{B}{A}} \qquad 6.38$$

The relationship ***B / A*** is found by considering the continuity of velocity at the surface of the cone - the particle velocity ***v*** in the acoustic wave must equal the velocity of the cone u_{cone} Eq. 6.39.

$$u_{cone} = v_{inc} + v_{ref} \qquad 6.39$$

The terms v_{inc} and v_{ref} in Eq. 6.39 are the particle velocity components due to the incident and reflected waves. The velocity components are determined from the pressure at the surface (found from Eq. 6.34 with ***d*** set to zero) and the impedance of the medium, $\rho_0 c$, see Eq. 6.40 and Eq. 6.41. The positive and negative signs are consistent with the velocity sign convention used in the derivation of the controller from the equation of motion at the surface. The velocity sign convention is illustrated in Figure 31a on Page 166.

$$v_{inc} = -\frac{A.e^{j(\omega t)}}{\rho_0 c} \qquad 6.40$$

$$v_{ref} = \frac{B.e^{j(\omega t)}}{\rho_0 c} \qquad 6.41$$

The specific acoustic impedance at the cone ***z*** is the ratio of the cone pressure and cone velocity Eq. 6.42. The cone velocity is found by substituting Eq. 6.40 and Eq. 6.41 into Eq. 6.39 and the cone pressure is found from Eq. 6.34 with ***d*** set to zero.

$$z = \frac{p_{cone}}{u_{cone}} = \rho_0 c.\left(\frac{A + B}{-A + B}\right) \qquad 6.42$$

Rearranging Eq. 6.42 gives Eq. 6.43.

$$\frac{B}{A} = \frac{\frac{z}{\rho_0 c} + 1}{\frac{z}{\rho_0 c} - 1} \qquad 6.43$$

Substituting this into Eq. 6.38 gives the transfer function ***L***, Eq. 6.44.

$$L = \frac{1 + \dfrac{z/\rho_0 c + 1}{z/\rho_0 c - 1}}{\dfrac{1}{F} + F\dfrac{z/\rho_0 c + 1}{z/\rho_0 c - 1}} \qquad 6.44$$

The transfer function L depends on the acoustic delay F between the loudspeaker cone and the upstream pressure measurement in the waveguide and the impedance of the loudspeaker cone z. The optimal controller transfer function, Eq. 6.45, is found by substituting Eq. 6.44 into Eq. 6.33.

$$W_{opt} = \left[z_d^{-1}\left(\frac{Z_M Z_{EB}}{Bl} + Bl\right) + \frac{S Z_{EB}}{Bl} \right] \frac{\left[1 + \left(\dfrac{z_d/\rho_0 c+1}{z_d/\rho_0 c-1}\right)\right]}{\left[\dfrac{1}{F} + F\left(\dfrac{z_d/\rho_0 c+1}{z_d/\rho_0 c-1}\right)\right]} \qquad 6.45$$

This solution is for when plane waves propagate in the duct, the waveguide is loss-less and the radiation load "seen" by the controlled impedance is characteristic. A more general solution has been expressed in Eq. 6.33. All terms have been defined in Section 6.3.1 except for the delay term F, see Eq. 6.37. The optimum controller filter solution, Eq. 6.45, is significantly more complicated than the feedback controller solutions Eq. 6.22 and Eq. 6.25 presented on Page 108 and Page 109 in Sections 6.3.1 and 6.3.2. However if the delay d is zero, such that $F = 1$, then Eq. 6.45 reduces to Eq. 6.22. This is to be expected because when d is zero the reference input is the cone pressure for which the optimum control solution is Eq. 6.22, see Section 6.3.1.

In order for the optimum controller filter, Eq. 6.45, to be realizable, the desired surface impedance should have a causally stable inverse (as z_d^{-1} is a factor of the first term of the right hand side of Eq. 6.45). The other potential problem in specifying the optimum controller filter are the singularities in the mechanical impedance of the loudspeaker, Z_M, at zero and infinite frequencies. These singularities in the ideal filter solution are never encountered in practical implementations as discussed in Section 6.3.1.

If the desired impedance is characteristic, ie $z_d = -\rho_0 c$ (negative because of the assigned positive velocity direction), then Eq. 6.45 simplifies to Eq. 6.46.

$$W_{opt}\Big|_{z_d=-\rho_0 c} = \left[(-\rho_0 c)^{-1} \left(\frac{Z_M Z_{EB}}{Bl} + Bl \right) + \frac{S Z_{EB}}{Bl} \right] . F \qquad 6.46$$

This is the similar to Eq. 6.22 but with the additional delay term F . This corresponds to the acoustic delay between the pressure location used to take the reference input and the loudspeaker cone.

If the desired impedance z_d is zero, then the optimum controller solution Eq. 6.45 is indeterminate. Therefore this controller, with a reference input of p_{duct}, is not able to generate an appropriate control signal for a desired impedance of zero.

If the desired impedance z_d is infinite then Eq. 6.45 simplifies to Eq. 6.47.

$$W_{opt}\Big|_{z_d=\infty} = \frac{S Z_{EB}}{Bl} \cdot \frac{2}{\frac{1}{F} + F} \qquad 6.47$$

Substituting the delay term F in Eq. 6.47 from Eq. 6.37 gives Eq. 6.48.

$$W_{opt}\Big|_{z_d=\infty} = \frac{S Z_{EB}}{Bl} \cdot \frac{2}{e^{+j\omega d/c} + e^{-j\omega d/c}} \qquad 6.48$$

This is rewritten as Eq. 6.49.

$$W_{opt}\Big|_{z_d=\infty} = \frac{S Z_{EB}}{Bl} \cdot \frac{1}{\cos(\omega d/c)} \qquad 6.49$$

The cosine term is zero when $\omega d/c = (n+\frac{1}{2})\pi$ for $n=0,1,2,....$. Therefore the optimum controller filter Eq. 6.49 is not realizable at these values. The various spacings of the reference pressure measurement from the cone, d, that correspond to singularities are rewritten in Eq. 6.50 where λ is the wavelength of a propagating harmonic acoustic wave in the duct.

$$d = \frac{\lambda}{2} \cdot \left(n + \frac{1}{2} \right) \qquad \text{for } n=0,1,2... \qquad 6.50$$

As the impedance at the cone is infinite, standing-waves will occur in the duct sound field because of interference between the incident and reflected components of the propagating harmonic acoustic wave. The spacings described by Eq. 6.50, at which the optimum controller filter is not realizable, correspond to the *positions of the pressure nodes* in the sound field. In a real implementation of the controller filter for controlled impedances that cause

standing waves, the spacing of the reference pressure measurement away the controlled cone must be chosen for the wavelength of the acoustic signal so that the optimum controller filter is realizable.

6.3.4 Electrical source signal as reference

Consider the active controller filter with a reference signal taken from the electrical signal used for the source loudspeaker. The reference signal is selected as *electrical* in Figure 25 on Page 98. If the time delay taken for the electrical source signal to be converted into acoustic pressure wave and propagate along the duct to the controlled loudspeaker cone is sufficiently long then the active controller adopts a feed-forward structure. The time delay must be longer than the total inherent delay in the implementation of the controller. If the controller is based on a digital filter then inherent delays are caused by sampling, digital processing time and the associated anti-aliasing and reconstruction filters. This section defines the optimum transfer function of the active controller with a reference input taken from the electrical source signal.

The use of the electrical source as the reference signal simplifies the implementation of the active controller as there will always be sufficient energy in the reference signal and there are no potentially unstable loops around the controller as there is no acoustic feedback into the reference signal. However, the optimum controller transfer function now includes the dynamics of the source loudspeaker and duct. The derivation of the controller transfer function follows that presented in Section 6.3.3. If the relationship between electrical source signal V_s and p_{cone} is linear, a frequency-domain transfer function L can be defined Eq. 6.51.

$$L = \frac{p_{cone}}{V_e} \qquad \textbf{6.51}$$

The optimum controller transfer function Eq. 6.33 defined in Section 6.3.3 now applies for L Eq. 6.51 and is reproduced here:

$$W_{opt} = \left[z_d^{-1} \left(\frac{Z_M Z_{EB}}{Bl} + Bl \right) + \frac{S Z_{EB}}{Bl} \right] . L \qquad \textbf{6.52}$$

The transfer function L includes the electro-acoustical conversion of the source loudspeaker and the acoustics of the pipe and the far-end controlled loudspeaker. The optimum controller filter must include this in its impulse response. The practical implementation of the adaptive FIR filter must therefore have enough coefficients to model L.

6.4 ACTIVE CONTROLLER FEEDBACK LOOP STABILITY

The use of either cone pressure, cone velocity or waveguide pressure as the reference input to the active controller has been discussed in Chapter 5. Optimum controller solutions have been presented in Section 6.3. The use of these reference signals causes a signal path that returns measures of the controller output back into the controller input. Such loops (often called feedback loops because the path feeds output signals back to the input) will oscillate if the gain around the loop exceeds unity when the phase shift is zero radians or a multiple of 2π radians. The active controller is then unstable and will be unable to perform the control task. Loop instability problems and practical methods that stabilise active control systems have been discussed in Section 3.8 on Page 53.

The analysis of loop stability requires identification of the feedback loop path. This is described in Section 6.4.1. The following three sections describe the loop stability of the optimum active controllers for the three reference signals. The final section discusses loop stability when the active controller is an adaptive filter.

6.4.1 Identification of the feedback loop

This section identifies the feedback loop path by considering the continuity of velocity at the surface of the controlled cone.

Consider a surface of specific acoustic impedance z_s excited by incident acoustic plane waves as depicted in Figure 31a on Page 166. The positive velocity direction is assigned so that the following theory is consistent with the equations of motion for the controlled cone presented in Chapter 4 and in earlier sections of this chapter. This is also consistent with Mazzola (34). The total pressure at the surface of the cone is the sum of the incident and reflected pressure waves, Eq. 6.53.

$$p_{cone} = p_i + p_r \qquad 6.53$$

The surface impedance is defined as Eq. 6.54.

$$z_s = \frac{p_{cone}}{u_{cone}} \qquad 6.54$$

The numerical value of the surface impedance is negative because of the assigned velocity direction.

The surface velocity u_{cone} must be equal to the particle velocity v at the surface for the continuity of velocity. This is described in Eq. 6.55 where v_i and v_r are the particle velocity components of the incident and reflected acoustic waves.

$$u_{cone} = v_i + v_r \qquad 6.55$$

Eq. 6.55 can be rewritten as Eq. 6.56 where the impedance in air is assumed to be characteristic, $\rho_0 c$.

$$u_{cone} = -\frac{p_i}{\rho_0 c} + \frac{p_r}{\rho_0 c} \qquad 6.56$$

Rearranging Eq. 6.56 to separate the reflected pressure term gives Eq. 6.57.

$$p_r = p_i + u_{cone} \cdot \rho_0 c \qquad 6.57$$

The pressure at the cone is then deduced by substituting Eq. 6.57 into Eq. 6.53 to give Eq. 6.58.

$$p_{cone} = 2p_i + u_{cone} \cdot \rho_0 c \qquad 6.58$$

The first term of Eq. 6.58 is double the incident pressure p_i and the second term represents the pressure that is generated by the vibrating surface. This term is called p_{rad} in this thesis (Mazzola describes this term as $P_p(0,t)$ - see the section on Page 21 reproduced from reference (34)). Eq. 6.58 can be rewritten as Eq. 6.59 by substituting u_{cone} from Eq. 6.54.

$$p_{cone} = \frac{2p_i}{1 - \frac{\rho_0 c}{z_s}} \qquad 6.59$$

If the surface impedance z_s is infinite, such that u_{cone} is zero, then the pressure at the cone is $2p_i$ from Eq. 6.59. This effect is often referred to as "pressure-doubling". If the surface impedance is characteristic, such that $z_s = -\rho_0 c$ (negative because of the assigned positive velocity direction), then the pressure at the cone is p_i . If the surface impedance is zero then $p_{cone}=0$. Eq. 6.59 reveals that if the surface impedance is "negative characteristic", such that $z_s = +\rho_0 c$, then the pressure at the cone becomes infinite. For this case the velocity must also become infinite according to Eq. 6.54. This impedance is never encountered in real passive systems.

A schematic that illustrates the relationship between the cone pressure and velocity and the impedances of the surface and medium is presented in Figure 31b on Page 166. This arises from Eq. 6.54 and Eq. 6.58. The active controller is configured to modify the surface impedance z_s shown in the dotted box. If the surface impedance is that of a loudspeaker cone then the relationship in the dotted box is described by considering the equation of motion at the cone - see Section 6.3.1. For this case the schematic can be redrawn as Figure 32 on Page 167 from examination of Eq. 6.17 on Page 107. The active controller must generate a suitable control voltage V to create a desired surface impedance at the cone. If the reference input to the controller is cone pressure then the active controller W is seen in Figure 33 on Page 168. The reference input contains components due to the incident pressure and the output of the controller via the radiation impedance path $\rho_0 c$. Therefore there is a feedback loop path around the active controller. The loop stability of this and other forms

of the active controller are analyzed in the following sections. Note that a further potential feedback path exists, in which reflected pressure propagates away from the controlled cone and is again reflected, to form a component of the incident pressure p_i. In a practical duct this feedback path has magnitude gain equal to or smaller than the direct path described above via the impedance $\rho_0 c$ and we assume here that this does not significantly alter the direct path. The following sections therefore analyze the loop stability only for the direct path. The stability can be determined with the Nyquist stability criterion (see, for example, section 7.4 in reference (2)).

To reduce the complexity in later sections we define Z_{LS} in Eq. 6.60.

$$Z_{LS} = Z_M + \frac{(Bl)^2}{Z_{EB}} \qquad 6.60$$

where Z_M , the mechanical loudspeaker impedance, is defined in Eq. 6.18 on Page 107. The un-driven or "natural" specific acoustic impedance of the loudspeaker cone, z_{NAT}, that occurs when the controller is disabled (such that W =0 in Eq. 6.21 on Page 108 and the voltage applied to the voice-coil is zero) is expressed in Eq. 6.61 where S is the surface area of the cone.

$$z_{NAT} = -\frac{Z_{LS}}{S} \quad Rayls \qquad 6.61$$

6.4.2 Cone pressure as reference

The presence of a feedback path around the active controller has been established in Section 6.4.1 for when the reference input is the cone pressure. This section analyzes the loop stability of this controller.

A schematic of the active control of the impedance of a loudspeaker cone for incident acoustic plane waves is shown in Figure 34 on Page 169. The feedback path exists because the pressure at the cone p_{cone}, the input to the controller, contains a component in p_{rad} that arises from the controller output voltage V. This can be clearly seen by considering the excitations to the system. There are two input excitations - the incident pressure p_i and the voltage applied to the voice-coil V. The pressure at the cone results from these

inputs and can be considered as a sum of two components. The first component is the pressure that occurs at the cone from the incident pressure when zero voltage is applied to the voice-coil. The cone pressure is defined in Eq. 6.59 on Page 119 where z_s is the impedance of the cone. When the voltage is zero the impedance z_s is simply z_{NAT}, see Eq. 6.61. The second component is the pressure that would occur from the cone from the action of the control voltage V alone and is termed p_V. The pressure at the cone can therefore be described as Eq. 6.62.

$$p_{cone} = \frac{2p_i}{1 - \frac{\rho_0 c}{z_{NAT}}} + p_V \qquad 6.62$$

These two pressure components can not be observed separately in a real system. However, as p_V arises from the action of the control voltage, it is possible to indirectly observe p_V by observing V. Eq. 6.62 allows the schematic of Figure 34 on Page 169 to be redrawn as Figure 35 on Page 170 where the transfer function C describes the relationship between the pressure p_V and the control voltage V. The pressure at the cone can then be expressed in terms of the two input excitations p_i and V in Eq. 6.63.

$$p_{cone} = p_i \cdot \frac{2}{1 - \frac{\rho_0 c}{z_{NAT}}} + V \cdot C \qquad 6.63$$

The open loop gain G_0, of the feedback loop seen in Figure 35, is the product of the controller transfer function W and C, Eq. 6.64.

$$G_0 = W \cdot C \qquad 6.64$$

The loop stability of the feedback loop can be determined by the Nyquist stability criterion. This can be stated as "*provided the open loop system ... W(s)C(s)... is stable, the closed loop system having transfer function ... [1-W(s)C(s)]$^{-1}$ ... will be stable provided the Nyquist plot of ... W(s)C(s) ... does not encircle the point (1,j0)*", page 216 of reference (2). In order to make a Nyquist plot of the loop gain, Eq. 6.64, it is necessary to express G_0 in terms of the system variables shown in Figure 34. The transfer function C is expressed in Eq. 6.65 from examination of Figure 34 when p_i is set to zero.

$$C = \frac{\frac{\rho_0 c}{Z_{LS}} \cdot \frac{Bl}{Z_{EB}}}{1 + S.\frac{\rho_0 c}{Z_{LS}}} \qquad \textbf{6.65}$$

This can be rewritten as Eq. 6.66 where z_{NAT} is expressed in Eq. 6.61.

$$C = \frac{\frac{Bl}{S.Z_{EB}}}{-\frac{Z_{NAT}}{\rho_0 c} + 1} \qquad \textbf{6.66}$$

The optimum controller solution for a desired impedance, z_d, has been defined as Eq. 6.22 on Page 108 in Section 6.3.1. This can be rewritten as Eq. 6.67.

$$W_{opt} = \frac{S.Z_{EB}}{Bl}\left[-z_d^{-1}.z_{NAT} + 1 \right] \qquad \textbf{6.67}$$

Substituting W_{opt} from 6.67 and C from 6.66 into Eq. 6.64 yields Eq. 6.68.

$$G_0 = \frac{-\frac{Z_{NAT}}{Z_d} + 1}{-\frac{Z_{NAT}}{\rho_0 c} + 1} \qquad \textbf{6.68}$$

The open loop gain is seen to depend on the desired impedance, the radiation impedance and the natural impedance of the loudspeaker. Nyquist plots of the open loop gain as a function of desired impedance can be made by quantifying the value of z_{NAT} in Eq. 6.68 - this is performed later in this section. If z_d is zero the open loop gain has a singularity and it is not possible to test for the Nyquist stability criterion. However, this does not imply that the closed system will be unstable - indeed many feedback systems operate optimally with a theoretical open loop gain of infinity. If z_d is infinite then G_0 becomes Eq. 6.69.

$$G_0\Big|_{z_d=\infty} = \frac{1}{-\frac{Z_{NAT}}{\rho_0 c} + 1} \qquad \textbf{6.69}$$

The open loop gain, Eq. 6.68, is zero (and therefore the feedback loop is unconditionally stable) if $z_d = z_{NAT}$. However, as this is the natural impedance of the loudspeaker for which the controller W is zero, this result is of little consequence.

Some general observations can be made for certain values of z_{NAT}. The open loop gain is infinite if $z_{NAT} = \rho_0 c$. This is the negative characteristic impedance, referred to on Page 119, which is never encountered with a real loudspeaker. At zero and infinite frequencies, z_{NAT} is infinite imaginary because of singularities in the mechanical impedance of the loudspeaker. The open loop gain is then described by Eq. 6.70.

$$G_0 \Big|_{\omega=0,\infty} = \frac{\rho_0 c}{z_d} \qquad 6.70$$

At other frequencies it is necessary to quantify z_{NAT} for a specific loudspeaker driver and thereby restrict the analysis. The rest of this section will evaluate G_0 and the loop stability for the natural impedance of a KEF B200A loudspeaker.

The natural specific acoustic impedance at the surface of a loudspeaker is defined in Section 4.3 on Page 76 and results for the KEF B200A loudspeaker are displayed in Figure 21 on Page 86 when the voltage applied to the voice-coil is zero ($V(j\omega)=0$ in Eq. 4.9). At the resonant frequency, $\omega_1 = 2\pi.65$Hz, z_{NAT} is real with a value of approximately -423 Rayls. If the desired impedance is infinite then, from Eq. 6.69, the open loop gain is approximately (½,j0). At other frequencies the real value is between 0, see Eq. 6.70, and ½. Therefore, as the open loop gain never has the value ($\geq$1,j0), the controller is unconditionally stable according to the Nyquist stability criterion. Nyquist plots, calculated from Eq. 6.68 using the manufacturers data for the KEF B200A loudspeaker, are presented in Figure 36 on Page 171 for four values of desired impedance: -10000 Rayls; -415 Rayls; -200 Rayls and -50 Rayls. The plots have zero imaginary components when ω=0, ω_1 and ∞. The (1,j0) point is not enclosed by any of the plots. Therefore, all of these configurations are stable when the loop is closed. This analysis demonstrates that the optimum active controller that uses cone pressure as a reference input is stable for all values of desired impedance (except for a desired impedance of zero) when controlling a KEF B200A loudspeaker that "sees" a radiation impedance of $\rho_0 c$.

Real implementations of the active controller are not always optimum because of delays in the forward path. For a digital implementation, delays are of the

order of milliseconds in current systems (for example, Elliott and Sutton use example delays of 1 and 5ms in their simulations (52)). The effect of a simple delay on the loop stability is now described. If the active controller ***W*** includes a fixed time delay, τ, then the open loop gain can be described in the frequency domain as Eq. 6.71.

$$G_0 = e^{-j\omega\tau} \cdot \frac{-\frac{Z_{NAT}}{Z_d} + 1}{-\frac{Z_{NAT}}{\rho_0 c} + 1} \qquad 6.71$$

The delay term has no effect on the magnitude but increases the phase of the open loop gain. As an example, Nyquist plots are presented for a 1ms delay in the active controller path in Figure 37 on Page 172 for four values of desired impedance, z_d: -415 Rayls; -400 Rayls; -200 Rayls and -50 Rayls. The plots have the same real and imaginary values for ω=0 as the plots with equivalent values of z_d in Figure 36. However, at higher frequencies the delay term adds phase. At large values of impedance (z_d < -415 Rayls) the stability is not compromised as the magnitude is always less than unity. At low values of impedance (z_d > -415 Rayls) the plots enclose the (1,j0) point. Therefore, for these values, the controller configurations are unstable when the loop is closed. For the examples presented in Figure 37 the plots first cross the positive real axis at values (>1,j0) at frequencies of between 520 and 540Hz and continue to encircle the (1,j0) point at higher frequencies. At these frequencies the value of z_{NAT} approaches infinite imaginary. Therefore the value of the open loop gain approaches Eq. 6.72.

$$G_0\Big|_{\omega\to\infty} \approx e^{-j\omega\tau} \cdot \frac{\rho_0 c}{z_d} \qquad 6.72$$

The magnitude of Eq. 6.72 does not depend on the delay term and so can be expressed as Eq. 6.73 for this case.

$$\left| G_0 \right|_{\omega\to\infty} \approx \left| \frac{\rho_0 c}{z_d} \right| \qquad 6.73$$

In order for the Nyquist plot not to encircle the (1,j0) point so that the closed loop system is stable, the magnitude of open loop gain must be less than or equal to

unity. This is satisfied, therefore guaranteeing loop stability for the controller for any value of τ, if the relationship in Eq. 6.74 is observed.

$$|z_d|_{\omega=\infty} \geq \rho_0 c \qquad 6.74$$

Eq. 6.74 is an important result of this thesis. It states that an optimum active controller, with a fixed delay of the order encountered in current systems, that uses cone pressure as a reference input is only stable when the magnitude of the desired impedance of the loudspeaker cone is greater than or equal to the radiation load presented to the cone. Therefore it is possible to implement an active ideal absorber using this active controller, although the system will be "on the edge" of instability at higher frequencies. This is seen in the Nyquist plot for a desired impedance of -415 Rayls in Figure 37 on Page 172.

6.4.3 Cone velocity as reference

A schematic of the active control of the impedance of a loudspeaker cone for incident acoustic plane waves is shown in Figure 38 on Page 173. The active controller W uses cone velocity as the reference input. This section analyzes the loop stability of this controller. This section follows a similar development to the last section.

The feedback path exists because the cone velocity u_{cone}, contains a component that arises from the controller output voltage V. There are two input excitations to the system shown in Figure 38 - the incident pressure p_i and the voltage applied to the voice-coil V. The velocity of the cone results from these inputs and can be considered as a sum of two components. The first component is the cone velocity that occurs when excited by the incident pressure when zero voltage is applied to the voice-coil. The relationship between cone velocity, cone pressure and incident pressure is defined in Eq. 6.58 on Page 119. Substituting for cone pressure in 6.58 from Eq. 6.59 and rearranging gives Eq. 6.75.

$$u_{cone} = p_l . \frac{\frac{2}{z_s}}{1 - \frac{\rho_0 c}{z_s}} \qquad 6.75$$

where z_s is the impedance of the cone. When the voice-coil voltage is zero the impedance z_s is z_{NAT}, see Eq. 6.61 on Page 120. The second component is the cone velocity that occurs from the action of the control voltage V and is here termed u_V. The cone velocity can therefore be described as Eq. 6.76.

$$u_{cone} = p_l . \frac{\frac{2}{z_{NAT}}}{1 - \frac{\rho_0 c}{z_{NAT}}} + u_V \qquad 6.76$$

The two velocity components can not be observed separately in a real system (although it is possible to indirectly observe u_V from the controller voltage). Eq. 6.76 allows the schematic of Figure 38 to be redrawn as Figure 39 on Page 174 where D is a transfer function that relates u_V and V. The cone velocity can then be expressed in terms of the two excitations in Eq. 6.77.

$$u_{cone} = 2\, p_l . \frac{\frac{1}{z_{NAT}}}{1 - \frac{\rho_0 c}{z_{NAT}}} + V . D \qquad 6.77$$

The open loop gain G_0, of the feedback loop seen in Figure 39, is the product of the controller W and D, Eq. 6.78.

$$G_0 = W . D \qquad 6.78$$

As in the previous section, the loop stability can be determined by the Nyquist stability criterion. D is expressed in Eq. 6.79 from examination of Figure 39 when p_l is set to zero.

$$D = \frac{\frac{1}{Z_{LS}} . \frac{Bl}{Z_{EB}}}{1 + S . \frac{\rho_0 c}{Z_{LS}}} \qquad 6.79$$

This can be rewritten as Eq. 6.80 where z_{NAT} is expressed in 6.61.

$$D = \frac{\frac{Bl}{SZ_{EB}}}{-Z_{NAT} + \rho_0 c} \qquad 6.80$$

The optimum controller solution for a desired impedance, z_d, has been defined in Eq. 6.25 on Page 109 in Section 6.3.2. This can be rewritten as Eq. 6.81.

$$W_{opt} = \frac{SZ_{EB}}{Bl} [\ z_d - Z_{NAT}\ ] \qquad 6.81$$

Substituting W_{opt} from Eq. 6.81 and D from Eq. 6.80 into Eq. 6.78 yields Eq. 6.82.

$$G_0 = \frac{z_d - Z_{NAT}}{\rho_0 c - Z_{NAT}} \qquad 6.82$$

The open loop gain G_0 depends on the desired impedance, the radiation impedance and the natural impedance of the loudspeaker. Some general observations can be made for certain values of z_{NAT}. G_0 is infinite if $z_{NAT} = +\rho_0 c$. This is the negative characteristic impedance which is never encountered in a real loudspeaker. At zero and infinite frequencies, z_{NAT} becomes infinite imaginary. G_0 is then Eq. 6.83.

$$G_0\Big|_{\omega=0,\infty} = 1\angle 0 \qquad 6.83$$

At other frequencies it is necessary to quantify z_{NAT} to further the analysis. Some general observations also can be made for certain values of z_d. If z_d is zero G_0 is Eq. 6.84.

$$G_0\Big|_{z_d=0} = \frac{-Z_{NAT}}{\rho_0 c - Z_{NAT}} \qquad 6.84$$

If z_d is z_{NAT} then G_0 is zero. However, the desired impedance is then the same as the natural impedance of the loudspeaker for which the controller W is zero. If z_d is infinite the open loop gain has a singularity and it is not possible to apply the Nyquist stability criterion. The rest of this section will evaluate G_0 and the loop stability for the natural impedance of a KEF B200A loudspeaker.

The natural impedance at the surface of a loudspeaker is defined in Section 4.3 on Page 76 and results for the KEF B200A loudspeaker are displayed in Figure 21 on Page 86 when the voltage applied to the voice-coil is zero (

$V(j\omega)=0$ in Eq. 4.9). Nyquist plots, calculated from Eq. 6.82, are presented in Figure 40 on Page 175 for four values of desired impedance: -4000 Rayls; -1250 Rayls; -415 Rayls and -50 Rayls. The plots have zero imaginary components when $\omega=0$, ω_1 and ∞. The (1,j0) point is not encircled by any of the plots. Therefore, all of these configurations are stable when the loop is closed. This analysis demonstrates that the optimum active controller that uses cone velocity as a reference is stable for all values of desired impedance (except for a desired impedance of infinity) when controlling a KEF B200A loudspeaker that is presented with a radiation impedance of $\rho_0 c$.

It has been stated in the last section that real implementations are not always optimum because of delays in the controller path. Eq. 6.82 can also be extended to include a fixed delay in the controller path of τ seconds as expressed in Eq. 6.85.

$$G_0 = e^{-j\omega\tau} \cdot \frac{Z_d - Z_{NAT}}{\rho_0 c - Z_{NAT}} \qquad 6.85$$

As before, the delay term has no effect on the magnitude but increases the phase of G_0. Nyquist plots are presented for a 1ms delay in Figure 41 on Page 176 for four values of z_d: -4000 Rayls; -1300 Rayls; -1250 Rayls and -415 Rayls. The plots have the same real and imaginary values for $\omega=0$ as the equivalent plots in Figure 40. At higher frequencies the delay term adds phase. If the magnitude is always less than, or equal to unity then the (1,j0) point is never encircled. This is the case for lower values of desired impedance when $z_d >$ ~ -1250 Rayls. When z_d is -1250 Rayls the magnitude of G_0 is approximately unity at all frequencies. This is clearly seen by the locus of points with unity radius in Figure 40 and Figure 41. At higher values of desired impedance ($z_d <$ ~ -1250 Rayls) the (1,j0) point is encircled. Therefore, according to the Nyquist stability criterion, these configurations will be unstable when the loop is closed. For the examples of -4000 Rayls and -1300 Rayls the Nyquist plots first cross the positive real axis at values (>1,j0) at frequencies of 252Hz and 195Hz respectively. At higher frequencies crossings also occur, but with reducing positive real values as G_0 tends towards Eq. 6.83. The results are specific to this particular loudspeaker and this value of radiation impedance. For

other acoustic systems different conditions apply. However, this analysis indicates that feedback loop instabilities can occur for larger values of impedance when the active controller has a fixed delay and uses the cone velocity as a reference.

6.4.4 Duct pressure as reference

A schematic of the active control of the impedance of a loudspeaker cone when excited by incident acoustic plane waves is shown in Figure 42 on Page 177. The active controller ***W*** has a reference input of duct pressure measured at distance ***d*** metres from the cone. This section analyzes the loop stability of this controller.

The relationship between the cone pressure and the duct pressure has been defined in Section 6.3.3 as ***L*** in Eq. 6.30 on Page 111. The value of ***L*** has been shown in Eq. 6.44 on Page 114 to depend on the distance ***d*** and the impedance of the controlled surface if the following assumptions are made: (1) plane harmonic waves propagate in the duct; (2) the waveguide is loss-less; (3) the radiation load presented to the controlled surface is characteristic - this implies that the duct is infinite. The duct pressure at position **d** metres from the controlled surface can be defined as Eq. 6.86 by considering the delays associated with the "time of flight" in the duct.

$$p_{duct} = p_I e^{+jkd} + p_I e^{-jkd} + U_{cone} \cdot \rho_0 c \cdot e^{-jkd} \qquad \textbf{6.86}$$

The first and second terms are the incident and reflected components of the blocked pressure and the third term is the radiated pressure. Note that when **d=0** the right hand side of Eq. 6.86 is identical to that of Eq. 6.58 because the duct pressure must equal the cone pressure. Eq. 6.86 allows the schematic of Figure 42 to be redrawn as Figure 43 on Page 178 where **F** is the delay defined in Eq. 6.37 on Page 112. The feedback path around the active controller is illustrated with the curved line.

The velocity of the controlled surface results from two input excitations - the incident pressure p_I and the controller voltage **V**. The cone velocity can be

considered as the linear addition of the velocities that occur with each excitation, see Eq. 6.87.

$$u_{cone} = u_{p_I} + u_v \qquad 6.87$$

Eq. 6.87 can then be expressed in terms of the input excitations as Eq. 6.88 by examination of Figure 42.

$$u_{cone} = p_I . \frac{2 / z_{NAT}}{1 - \rho_0 c / z_{NAT}} + V . \frac{(Bl) / (Z_{LS} . Z_{EB})}{1 - \rho_0 c / z_{NAT}} \qquad 6.88$$

where z_{NAT} and Z_{LS} have been expressed in Section 6.4.1. Substituting Eq. 6.88 into Eq. 6.86 yields the relationship between the duct pressure, incident pressure and controller voltage, Eq. 6.89.

$$p_{duct} = p_I . \left[F + F^{-1} + F . \frac{\rho_0 c / z_{NAT}}{1 - \rho_0 c / z_{NAT}} \right] + V . \left[\frac{(\rho_0 c Bl) / (Z_{LS} . Z_{EB})}{1 - \rho_0 c / z_{NAT}} \right] . F \qquad 6.89$$

If the first bracketed term is referred to as **A**, and the second bracketed term is referred to as **C** (which is identical to Eq. 6.65 on Page 122) then the schematic of Figure 43 can be redrawn as Figure 44 on Page 179. This shows the feedback loop around the active controller. The open loop gain of the feedback loop for zero incident pressure is then described by Eq. 6.90.

$$G_0 \Big|_{p_I = 0} = W . F . C \qquad 6.90$$

The optimum solution is fully expressed in Eq. 6.45 on Page 114. Substituting W_{opt} from Eq. 6.45 and C from Eq. 6.65 into Eq. 6.90 yields Eq. 6.91.

$$G_0 \Big|_{p_I = 0} = \frac{-\frac{Z_{NAT}}{Z_d} + 1}{-\frac{Z_{NAT}}{\rho_0 c} + 1} . \frac{1 + \left(\frac{Z_d / \rho_0 c + 1}{Z_d / \rho_0 c - 1} \right)}{\frac{1}{F^2} + \left(\frac{Z_d / \rho_0 c + 1}{Z_d / \rho_0 c - 1} \right)} \qquad 6.91$$

The open loop gain is seen to depend on the desired impedance, the radiation impedance, the natural impedance of the loudspeaker and the delay between the duct microphone and the controlled surface. The open loop gain will now be considered for three different desired impedances.

If the desired impedance is characteristic, z_d equal to $-\rho_0 c$ (negative with the assigned velocity direction), then Eq. 6.91 simplifies to Eq. 6.92.

$$G_0\Big|_{p_l=0,\ z_d=-\rho_0 c} = \frac{+\dfrac{Z_{NAT}}{\rho_0 c}+1}{-\dfrac{Z_{NAT}}{\rho_0 c}+1}\cdot F^2 \qquad 6.92$$

This is similar to Eq. 6.71 on Page 124 when z_d is equal to $-\rho_0 c$, and is identical when the delay term F^2 has the same value as $e^{j\omega\tau}$. Therefore, the discussion presented from Page 124 onwards to the end of Section 6.4.2 also applies here. However, whereas the delay term arises in Eq. 6.71 because of inherent delays in active controller implementations, here the delay term can be modified by moving the duct microphone. In a real implementation the open loop gain Eq. 6.92 must also include the delay term $e^{j\omega\tau}$.

A similar controller for the control of the reflection coefficient R of a loudspeaker cone as the end of a duct after Guicking *et al* is described in the literature (20). The researchers were able to hand adjust the gain and phase of the W so that R was close to zero (hence z was close to characteristic) over the frequency range 100 to 400Hz. At higher frequencies the controller was not stable when attempting to make R close or equal to zero. This is consistent with the theory presented here: at higher frequencies the phase associated with the delay term F^2 will cause the closed loop optimum controller to be "on the edge of instability". Laboratory tests made during the research for this thesis also show that, for this controller, optimum control is stable over restricted frequency ranges for desired impedances close or equal to the characteristic impedance of air.

If the desired impedance z_d is zero then Eq. 6.91 is also zero. Therefore the feedback loop for this controller is unconditionally stable. This result originates from the fact that the optimum controller solution is zero when $z_d=0$, see Eq. 6.45 on Page 114. This controller is not able to generate an appropriate control signal for a desired impedance of zero and so this result is not useful.

If the desired impedance z_d is infinite then Eq. 6.91 becomes Eq. 6.93.

$$G_0\Big|_{p_1=0,\ z_d=\infty} = \frac{2}{\left(-\frac{Z_{NAT}}{\rho_0 c}+1\right).\left(\frac{1}{F^2}+1\right)} \qquad \textbf{6.93}$$

Eq. 6.93 has a singularity when the right hand bracket in the denominator has zero real and imaginary values. This occurs when $F^{-2} = (-1,j0)$. Recalling the value of F from Eq. 6.37 on Page 112 allows the singularity to be expressed in terms of frequency, duct microphone spacing and the speed of sound in air, Eq. 6.94.

$$2\omega.\frac{d}{c} = (2n+1).\pi \qquad \text{for } n=0,1,2... \qquad \textbf{6.94}$$

This expresses the same relationship as Eq. 6.50 on Page 115. At this singularity the open loop gain will be positive real infinite and so the feedback loop will oscillate when closed.

It has been shown that for desired characteristic impedance the stability is similar to that of the controller with fixed delays described in Section 6.4.2 - although the Nyquist stability criterion is satisfied, the feedback loop is "on the edge" of instability. For a desired infinite impedance, loop instabilities occur at frequencies defined by Eq. 6.94. At these frequencies the optimum controller is not realizable, see the discussion presented after Eq. 6.50 on Page 115. Therefore, the implementation of this controller for desired infinite impedance can only operate with restricted frequency bandwidth unless feedback cancellation techniques are used. The theory presented in this section does not describe fully the real acoustics as the radiation impedance is assumed to be characteristic and the duct can have energy losses.

6.4.5 Adaptive controllers

The use of an adaptive filter as the active controller complicates the analysis of loop stability because of the changing gain of the adaptive filter. The theoretical analysis of loop stability of the last three sections does not account for this. Instead fixed filter solutions have been used to draw conclusions about the stability for desired impedances. The changing transfer function of an adaptive

filter introduces an extra dynamical variable into the analysis of the feedback loop. This is discussed in Section 6.6.3 on Page 143.

6.5 ACTIVE CONTROLLER FILTER SOLUTIONS FOR FEEDBACK CANCELLATION

Optimum solutions for the active controller have been described in Section 6.3. However, three of the controllers have stability problems arising from feedback paths for certain values of controlled impedance, see Section 6.4. A common solution that increases stability is the use of a "feedback cancellation" filter, see Section 3.8. However, this approach alters the controller solutions. This section describes the required controller filter transfer functions. For consistency with the previous theory assume that the radiation impedance presented to the controlled loudspeaker is characteristic. The consequences of this assumption are discussed in each section.

6.5.1 Cone pressure as reference

The presence of a feedback loop around the active controller has been identified in Section 6.4.2. A schematic that illustrates the loop has been presented in Figure 34 on Page 169. The effect of the feedback loop can be reduced by the feedback cancellation strategy shown in Figure 45a on Page 180 (this technique has been described in the literature - see Section 3.8). The single controller filter $\boldsymbol{W}$ is replaced with two filters $\hat{\boldsymbol{C}}$ and $\boldsymbol{G}$. $\hat{\boldsymbol{C}}$ contains a model of the feedback path $\boldsymbol{C}$. The output of $\hat{\boldsymbol{C}}$ is subtracted from the cone pressure. If the model is accurate then the effect of this is to cancel the feedback path. The input signal to the filter $\boldsymbol{G}$ is then effectively the cone pressure arising from the incident pressure component alone, see Figure 45b. In this feedback controller arrangement Elliott and Sutton have described the filter $\boldsymbol{G}$ as a feed-forward structure because the input no longer contains the component arising from the output (52). This section defines the optimum transfer function for $\boldsymbol{G}$ for the control of a desired impedance.

The optimum controller filter solution for $\boldsymbol{W}$ is defined in Eq. 6.22 on Page 108 for a desired impedance of z_d. The required transfer function of the two filter

structure of Figure 45a is therefore expressed as Eq. 6.95 where the right hand side is a rearranged version of Eq. 6.22 (see Eq. 6.67 on Page 122) and z_{NAT} is defined in Eq. 6.61 on Page 120.

$$\frac{G_{opt}}{1 + \hat{C}_{opt} G_{opt}} = W_{opt} = \frac{Z_{EB} \cdot S}{Bl} \cdot \left[- \frac{z_{NAT}}{z_d} + 1 \right] \qquad 6.95$$

Eq. 6.95 is rearranged to give the optimum transfer function of G, Eq. 6.96.

$$G_{opt} = \frac{\frac{Z_{EB} \cdot S}{Bl} \cdot \left[- \frac{z_{NAT}}{z_d} + 1 \right]}{1 - \hat{C}_{opt} \cdot \frac{Z_{EB} \cdot S}{Bl} \cdot \left[- \frac{z_{NAT}}{z_d} + 1 \right]} \qquad 6.96$$

If the filter $\hat{C}$ is zero then G_{opt} is identical to the transfer function of W_{opt} in Eq. 6.22 as expected.

The relationship $\hat{C}$ is defined in Eq. 6.66 on Page 122. If $\hat{C}$ is assumed to be an exact model then the optimum value is defined as Eq. 6.97.

$$\hat{C}_{opt} = \frac{\frac{Bl}{S \cdot Z_{EB}}}{- \frac{z_{NAT}}{\rho_0 c} + 1} \qquad 6.97$$

Substituting for $\hat{C}$ from Eq. 6.97 in Eq. 6.96 and rearranging gives the optimum transfer function of the filter G required to force the surface impedance at the cone of the loudspeaker to the desired value of z_d, Eq. 6.98.

$$G_{opt} = \frac{\frac{Z_{EB} \cdot S}{Bl}}{\left[- \frac{z_{NAT}}{z_d} + 1 \right]^{-1} - \left[- \frac{z_{NAT}}{\rho_0 c} + 1 \right]^{-1}} \qquad 6.98$$

If the desired impedance z_d is zero such that the cone pressure is zero then Eq. 6.98 becomes Eq. 6.99.

$$G_{opt} \Big|_{z_d = 0} = - \frac{Z_{EB} \cdot S}{Bl} \cdot \left[- \frac{z_{NAT}}{\rho_0 c} + 1 \right] \qquad 6.99$$

The magnitude of the loop gain $|G_{opt} \cdot \hat{C}|$ is therefore unity and this theoretical controller acts as a controlled oscillator. If the desired impedance z_d is infinity then Eq. 6.98 becomes Eq. 6.100.

$$G_{opt}\Big|_{z_d=\infty} = \frac{\frac{Z_{EB}.S}{Bl}}{1 - \left[-\frac{Z_{NAT}}{\rho_0 c} + 1 \right]^{-1}} \qquad 6.100$$

For other real desired impedances, recalling that z_d is negative with this velocity sign convention, G_{opt} is also stable but further simplifications of Eq. 6.98 are not produced.

The optimum filters G and $\hat{C}$ both contain the radiation impedance term assumed to be $+\rho_0 c$. However if the radiation impedance presented to the controlled loudspeaker is the input impedance to a pipe then the filters required to implement the optimum solutions become more complicated - this is consistent with a discussion by Nelson and Elliott, see Page 54 in Section 3.8. The other potential problem in specifying the optimum filter G_{opt} are the singularities in the mechanical impedance of the loudspeaker, Z_{LS}, at zero and infinite frequencies. The discussion of this for Eq. 6.22 on Page 108 also applies here - the singularities are never encountered in the practical system.

6.5.2 Cone velocity as reference

The presence of a feedback loop around this active controller has been identified in Section 6.4.3. A schematic that illustrates the loop has been presented in Figure 39 on Page 174. The effect of the feedback loop can be reduced by the feedback cancellation strategy shown in Figure 46a on Page 181. The single controller filter W is replaced with two filters $\hat{D}$ and G. $\hat{D}$ contains a model of the feedback path D. The output of $\hat{D}$ is subtracted from the cone velocity. If the model is accurate then the effect of this is to cancel the feedback path. The input signal to the filter G is then effectively the cone velocity arising from the incident pressure component, see Figure 46b. This section defines the optimum transfer function for G for the control of a desired impedance.

The optimum controller filter solution for W is defined in Eq. 6.25 on Page 109 for a desired impedance of z_d. The required transfer function of the two filter structure of Figure 46a is therefore expressed as Eq. 6.101 where the right hand

side is a rearranged version of Eq. 6.25 (see Eq. 6.81 on Page 127) and z_{NAT} is defined in Eq. 6.61 on Page 120.

$$\frac{G_{opt}}{1 + \hat{D}_{opt} G_{opt}} = W_{opt} = \frac{Z_{EB} \cdot S}{Bl} \cdot [\, z_d - z_{NAT} \,] \qquad 6.101$$

Eq. 6.101 is rearranged to give the optimum transfer function of G, Eq. 6.102.

$$G_{opt} = \frac{\frac{Z_{EB} \cdot S}{Bl} \cdot [\, z_d - z_{NAT} \,]}{1 - \hat{D}_{opt} \cdot \frac{Z_{EB} \cdot S}{Bl} \cdot [\, z_d - z_{NAT} \,]} \qquad 6.102$$

If the filter $\hat{D}$ zero then G_{opt} is identical to the transfer function of W_{opt} in Eq. 6.25 as expected.

The relationship D is defined in Eq. 6.80 on Page 127. If $\hat{D}$ is assumed to be a perfect model then the optimum value is defined as Eq. 6.103.

$$\hat{D}_{opt} = \frac{\frac{Bl}{Z_{EB} \cdot S}}{-z_{NAT} + \rho_0 c} \qquad 6.103$$

Substituting for $\hat{D}$ from Eq. 6.103 in Eq. 6.102 and rearranging gives the optimum transfer function of the filter G_{opt} required to force the surface impedance at the cone of the loudspeaker to the desired value of z_d, Eq. 6.104.

$$G_{opt} = \frac{\frac{Z_{EB} \cdot S}{Bl}}{[\, z_d - z_{NAT} \,]^{-1} - [\, \rho_0 c - z_{NAT} \,]^{-1}} \qquad 6.104$$

If the desired impedance z_d is infinity such that the cone velocity is zero then Eq. 6.104 becomes Eq. 6.105.

$$G_{opt}\Big|_{z_d = \infty} = -\frac{Z_{EB} \cdot S}{Bl} \cdot [\, \rho_0 c - z_{NAT} \,] \qquad 6.105$$

The magnitude of the loop gain $|G_{opt} \cdot \hat{D}|$ is therefore unity and this theoretical controller acts as a controlled oscillator. For other real desired impedances, recalling that z_d is negative with this velocity sign convention, G_{opt} is also stable but further simplifications of Eq. 6.104 are not produced.

The optimum filters G and $\hat{D}$ both contain the radiation impedance term assumed to be $+\rho_0 c$. However if the radiation impedance presented to the

controlled loudspeaker is the input impedance to a pipe then the filters required to implement the optimum solutions become more complicated - this is similar to the discussion in the last section. Also the other potential problem in specifying the optimum filter G_{opt} are the singularities in the mechanical impedance of the loudspeaker, Z_{LS}, at zero and infinite frequencies. The discussion of this for Eq. 6.22 on Page 108 also applies here - the singularities are never encountered in the practical system.

6.5.3 Duct pressure as reference

The presence of a feedback loop around this active controller has been identified in Section 6.4.4. A schematic that illustrates the loop has been presented in Figure 44 on Page 179. The effect of the feedback loop can be reduced by the feedback cancellation strategy shown in Figure 47a on Page 182. The single controller filter W is replaced with two filters $\hat{F}$ and G. $\hat{F}$ contains a model of the feedback path. The output of $\hat{F}$ is subtracted from the duct pressure. If the model is accurate then the effect of this is to cancel the feedback path. The input signal to the filter G is then effectively the incident pressure component, see Figure 47b. This section defines the optimum transfer function for G for the control of a desired impedance.

For optimum control, the overall transfer function of the two filter structure of Figure 47a must be identical to the optimum controller filter solution for W (defined in Eq. 6.33 on Page 112 for a desired impedance of z_d). This is expressed in Eq. 6.106.

$$\frac{G_{opt}}{1 + \hat{F}_{opt} G_{opt}} = W_{opt} \qquad 6.106$$

Eq. 6.106 can be rearranged to express the optimum value of G, Eq. 6.107.

$$G_{opt} = \frac{W_{opt}}{1 - \hat{F}_{opt} W_{opt}} \qquad 6.107$$

If the feedback canceller is disabled, such that $\hat{F}_{opt}$ is zero, then G_{opt} must equal W_{opt}. However, a more useful observation is that $\hat{F}_{opt}W_{opt}$ is the open-loop gain described by Eq. 6.91 on Page 130 in Section 6.4.4. The discussion in that section revealed that, for a desired characteristic impedance, the open-loop gain

contains a delay term, see Eq. 6.92 on Page 131. As this appears on the denominator of Eq. 6.107, G_{opt} may have a non-causal solution.

The relationship $\hat{F}$ is the model of the product of Eq. 6.65 on Page 122 and the delay F. If $\hat{F}$ is assumed to be a perfect model then the optimum transfer function is Eq. 6.108.

$$\hat{F}_{opt} = F.\frac{\frac{Bl}{Z_{EB}.S}}{-\frac{Z_{NAT}}{\rho_0 c}+1} \qquad 6.108$$

where the delay term F on the right hand side has been defined in Eq. 6.37 on Page 112. Substitution of Eq. 6.107 by Eq. 6.108 and Eq. 6.33 on Page 112 and rearrangement produces the solution G_{opt} required to force the surface impedance at the cone of the loudspeaker to the desired value of z_d, Eq. 6.109.

$$G_{opt} = \frac{\frac{Z_{EB}S}{Bl}.\left[\frac{-Z_{NAT}}{z_d}+1\right].L}{1-\left[\frac{\frac{-Z_{NAT}}{z_d}+1}{-\frac{Z_{NAT}}{\rho_0 c}+1}\right].F.L} \qquad 6.109$$

If the desired impedance z_d is zero such that the cone pressure is zero then Eq. 6.109 becomes Eq. 6.110.

$$G_{opt}\Big|_{z_d=0} = -\frac{Z_{EB}.S}{Bl}.\left[-\frac{Z_{NAT}}{\rho_0 c}+1\right].F^{-1} \qquad 6.110$$

The theoretical magnitude of the loop gain $|G_{opt}.\hat{F}|$ is therefore unity and this theoretical controller acts as a controlled oscillator. However, the optimum solution can not be implemented as F^{-1} is an advance term - Eq. 6.110 is a non-causal solution.

If the desired impedance is characteristic then Eq. 6.109 becomes Eq. 6.111.

$$G_{opt}\Big|_{z_d=-\rho_0 c} = \frac{\frac{Z_{EB}S}{Bl}\cdot\left[\frac{Z_{NAT}}{\rho_0 c}+1\right].F}{1-\left[\frac{\frac{Z_{NAT}}{\rho_0 c}+1}{-\frac{Z_{NAT}}{\rho_0 c}+1}\right].F^2} \qquad \textbf{6.111}$$

A delay term appears on the denominator and this optimum solution may contain non-causal components. For other real desired impedances, recalling that z_d is negative with this velocity sign convention, there are also potential causality problems with the implementation of G_{opt} because of the *F.L* term in the denominator. This needs to be studied further. Although the optimum solution for the filter *G* may not be fully implementable, a causally constrained solution of *G* may force near-desired impedances for broad-band noise - see, for example, the discussion presented in Section 6.12 of reference (2). With adaptive implementations of *G*, experimental work undertaken for this thesis observed useful control for both periodic and restricted band-width noise.

6.6 FILTERED-X COMPENSATION FOR MIC-ACCR ADAPTIVE CONTROL SYSTEMS

The mic-accr method can be used as the basis for an adaptive control system for the control of impedance. The mic-accr method and suitable adaptive control are described in Chapter 5. The adaptive control system can use either the "filtered-X" or "filtered-U" variations of the LMS algorithm (these are described in Chapter 3). Both of these adaptive algorithms require a "stability compensation filter". This section describes how the stability compensation filter is configured for the adaptive control system based on the mic-accr method.

The position of the stability compensation filter in a filtered-X implementation of the mic-accr adaptive control system is shown in Figure 48 on Page 183. Since the filtered-U algorithm requires two compensation filters of identical transfer function to the compensation filter used in the filtered-X algorithm, the discussion in this section also applies to the filtered-U algorithm. For stable operation of the adaptive algorithm this filter must be a close approximation to the transfer

function of the "forward-path" in the control system, see Section 3.6.4 on Page 49. The forward-path ***C*** and the stability compensation filter **<*C*>** are shown in Figure 49a on Page 184 for a typical filtered-X LMS implementation and theoretical analysis is presented in Section 6.6.1. Theoretical analysis on filtered-X implementations of the mic-accr adaptive control system are presented in Section 6.6.2.

6.6.1 Typical filtered-X LMS implementation

Consider a typical implementation of the filtered-X LMS algorithm with a forward path of ***C*** shown in Figure 49a on Page 184. The error signal is described in Eq. 6.112.

$$e_k = d_k - y_k \qquad 6.112$$

Squaring Eq. 6.112 yields Eq. 6.113.

$$e_k^2 = d_k^2 - 2y_k d_k + y_k^2 \qquad 6.113$$

The output of the forward-path y_k is :

$$y_k = \overline{c_k}^T \overline{\overline{X_k}}\, \overline{W_k} \qquad 6.114$$

Where $\overline{\overline{X}}_k$ was defined in Eq. 3.33 on Page 47. Substituting Eq. 6.114 into Eq. 6.113 gives:

$$e_k^2 = d_k^2 - 2d_k \overline{c_k}^T \overline{\overline{X_k}} \overline{W_k} + \left[\overline{c_k}^T \overline{\overline{X_k}} \overline{W_k}\right].\left[\overline{c_k}^T \overline{\overline{X_k}} \overline{W_k}\right] \qquad 6.115$$

The instantaneous squared error is a quadratic in terms of the active control filter coefficients $\overline{W_k}$. In order to determine the instantaneous gradient estimate Eq. 6.116 used in the LMS algorithm (see Section 3.5.6 on Page 43) it is necessary to perform partial differentiation of Eq. 6.115 with respect to the control filter coefficients. It is assumed that d_k *has no dependence on* W.

$$\frac{\partial e_k^2}{\partial \overline{W_k}} = -2d_k \overline{\overline{X_k}}\, \overline{c_k} + 2\left[\overline{\overline{X_k}}\, \overline{c_k}\right].\left[\overline{c_k}^T \overline{\overline{X_k}} \overline{W_k}\right] \qquad 6.116$$

Substituting Eq. 6.112 and Eq. 6.114 into Eq. 6.116 yields the instantaneous gradient estimate of the filtered-X LMS update algorithm Eq. 6.117 for the typical implementation shown in Figure 49a.

$$\hat{\nabla}_k = \frac{\partial \varepsilon_k^2}{\partial \overline{W}_k} = -2\varepsilon_k \overline{\overline{X}_k}\,\overline{C}_k \qquad 6.117$$

The update equation for the adaptive control filter Eq. 6.118 is found by substituting Eq. 6.117 into Equation 3.24 on Page 43.

$$\overline{W}_{k+1} = \overline{W}_k + 2\mu\varepsilon_k \overline{\overline{X}_k}\,\overline{C}_k \qquad 6.118$$

Equation 6.118 shows that the adaptive filter weight update requires the error signal, ε_k, and the convolution of the time history of the reference signal x_k and the forward-path impulse response C. The convolution is implemented in the control system with the compensation filter <C> in Figure 49a.

6.6.2 Mic-accr filtered-X LMS implementations

The mic-accr adaptive control system is more complicated than the typical implementation described in Section 6.6.1. The specification of the desired signal, d_k in Figure 49a on Page 184, in the mic-accr system is initially considered as the output of the desired impedance filter H in Figure 49b. The desired filter is described in Section 5.3. In Figure 49b A is the transfer function between the output of the control filter W and the acoustic pressure at the cone p_{cone} and B is the transfer function between the output of the control filter W and the cone velocity signal u_{cone}. This is the mic-accr method indicated in Figure 26a on Page 99. The following theory is equally applicable to the variation shown in Figure 26b. The stability compensation filter <B> of Figure 49b models the transfer function B in similar arrangement to the typical filtered-X implementation of Figure 49a. The practical implementation of this adaptive control system was found occasionally to have unstable convergence. A theoretical analysis of this system follows. A more stable implementation of the mic-accr system is then presented.

The desired signal d_k of Figure 49b is the vector product Eq. 6.119.

$$d_k = \overline{a}_k^T \overline{\overline{X}_k}\,\overline{W}_k \qquad 6.119$$

where $\overline{\overline{X}_k}$ is defined in Eq. 3.33 on Page 47, and $\overline{a}_k$ is a discrete time-domain vector representing the convolution of the impulse responses of A and H. The

instantaneous gradient estimate of the typical filtered-X LMS system Eq. 6.116 is derived by assuming that d_k has no dependence on W . Clearly this is not true from Eq. 6.119 for the mic-accr adaptive system of Figure 49b. Substituting Eq. 6.119 into Eq. 6.115 yields the instantaneous squared error for the mic-accr control system Eq. 6.120.

$$e_k^2 = \left[\overline{G_k}^T\overline{\overline{X_k}}\,\overline{W_k}\right]^2 - 2\left[\overline{G_k}^T\overline{\overline{X_k}}\,\overline{W_k}\right].\left[\overline{B_k}^T\overline{\overline{X_k}}\,\overline{W_k}\right] + \left[\overline{B_k}^T\overline{\overline{X_k}}\,\overline{W_k}\right]^2 \quad 6.120$$

Perform partial differentiation of Eq. 6.120 with respect to the control filter to find the instantaneous gradient estimate column vector Eq. 6.121.

$$\frac{\partial e_k^2}{\partial \overline{W_k}} = 2\,\overline{\overline{X_k}}\,\overline{G_k}\left[\overline{G_k}^T\overline{\overline{X_k}}\,\overline{W_k}\right] - 4\,\overline{\overline{X_k}}\,\overline{B_k}\left[\overline{G_k}^T\overline{\overline{X_k}}\,\overline{W_k}\right] + 2\,\overline{\overline{X_k}}\,\overline{B_k}\left[\overline{B_k}^T\overline{\overline{X_k}}\,\overline{W_k}\right] \quad 6.121$$

Eq. 6.121 can be rewritten as Eq. 6.122 from Eq. 6.119.

$$\frac{\partial e_k^2}{\partial \overline{W_k}} = 2\,d_k\overline{\overline{X_k}}\,\overline{G_k} - 4\,d_k\overline{\overline{X_k}}\,\overline{B_k} + 2\,y_k\overline{\overline{X_k}}\,\overline{B_k} \quad 6.122$$

Recalling Eq. 6.112 allows the instantaneous gradient estimate Eq. 6.122 of the filtered-X LMS update algorithm for the mic-accr adaptive control system shown in Figure 49b to be rewritten as Eq. 6.123.

$$\hat{\nabla}_k = \frac{\partial e_k^2}{\partial \overline{W_k}} = 2\,d_k\overline{\overline{X_k}}\left[\overline{G_k} - \overline{B_k}\right] - 2\,e_k\overline{\overline{X_k}}\,\overline{B_k} \quad 6.123$$

The instantaneous gradient estimate Eq. 6.123 consists of two terms. The second term is the instantaneous gradient estimate of the typical filtered-X LMS implementation (see Eq. 6.117) for which the compensation filter of Figure 49b is correct. The first term arises because of the coupling between the output of adaptive control filter and the desired signal d_k (if there is no coupling, such that $G = 0$, then d_k must also be zero and therefore Eq. 6.123 becomes Eq. 6.117). The instantaneous gradient estimate is now explicitly related to the desired signal - this complicates the convergence of the adaptive algorithm in this mic-accr control system. The stability filter of Figure 49b does not compensate for this term hence the adaptive control system may be unstable for certain desired signals. However, the practical implementation of the mic-accr adaptive control system of Figure 49b has converged to make the error signal close to

zero for many signals. If the error signal goes to zero (the controller converges to an optimum solution) ***G*** must equal ***B*** and the instantaneous gradient estimate Eq. 6.123 will be zero. This indicates that stable solutions can exist for this implementation of the mic-accr system.

The mic-accr adaptive control system is more stable with the implementation shown in Figure 49c on Page 184. This implementation groups ***B*** and ***A.H*** together in the forward-path. The desired signal d_k is no longer coupled to the control filter output and is set to zero so that the desired filter ***H*** is used to set the desired impedance (see Figure 26 on Page 99). The stability filter then compensates for the entire forward-path. This arrangement is similar to that of the typical filtered-X implementation shown in Figure 49a. The forward-path is defined as ***C***, Eq. 6.124.

$$\overline{C_k} = \overline{B_k} - \overline{G_k} \qquad 6.124$$

The instantaneous gradient estimate Eq. 6.125 is found by following the derivation presented in Section 6.6.1.

$$\hat{\nabla}_k = \frac{\partial e_k^2}{\partial \overline{W_k}} = -2 e_k \overline{X_k} \overline{C_k} \qquad 6.125$$

Equation 6.125 demonstrates that the adaptive filtered-X LMS algorithm of Figure 49c is correctly compensated. Experimental testing of the practical implementation of the control system of Figure 49c reveals that is more stable than that of Figure 49b because the stability compensation filter correctly compensates for the forward-path.

6.6.3 Adaptive system with feedback

In the last section the instantaneous gradient estimate was derived for the mic-accr system. The forward-path was considered as the combination of the electro-acoustic paths between the controller output and pressure and velocity measurements, and the desired signal calculation, see Figure 49c on Page 184. This section extends the analysis of the mic-accr system by considering the effect of a feedback loop around the adaptive filter.

The reference input to the mic-accr system, $\hat{x}_k$ in Figure 50a on Page 185 now contains a component due to a feedback path ***F***. This occurs when the reference is taken from measures in the acoustic environment under control such as pressure or velocity. This creates a feedback loop around the controller and the stability of this loop must be examined. If the derivation used in the last section is followed but with respect to $\hat{x}_k$ then the instantaneous gradient estimate is Eq. 6.126.

$$\hat{\nabla}_k = \frac{\partial e_k^2}{\partial \overline{W}_k} = -2 e_k \overline{\overline{\hat{X}}}_k \overline{C}_k \qquad 6.126$$

where ***C*** has been defined in Eq. 6.124. Equation 6.126 shows that the compensation strategy is the same as the last section. The schematic is redrawn for clarity in Figure 50b on Page 185 where **<C>** is assumed to be a perfect model of ***C***.

It is not possible to measure x_k in the real system as the addition with the feedback component occurs in the acoustic environment and is not separable. However, it is illustrative to examine the relationship between the error signal and x_k. The error signal of this system is defined in Eq. 6.127.

$$e_k = -y_k \qquad 6.127$$

where

$$y_k = \frac{\overline{C}_k^T \overline{\overline{X}}_k \overline{W}_k}{1 - \overline{W}_k^T \overline{F}_k} \qquad 6.128$$

The effect of an unstable feedback loop on the error signal is clearly seen - if the magnitude of the loop gain ***W.F*** goes to unity then e_k goes to infinity and so the control system will be unstable. In this system ***W*** is adaptive and depends on the reference signal $\hat{x}_k$, the forward-path ***C***, the error signal and the adaptive update gain. As the reference and error signals depend on previous values of the input signal x_k, the adaptive filter *and the feedback path* ***F***, the relationship ***W.F*** is complicated and considered intractable. The theoretical dynamics of the error signal are therefore elusive. Observation of the dynamics of the error

signal for such a system, presented later in Section 7.6 on Page 219, reveals unusual behaviour.

In the practical control system, providing the feedback path ***F*** can be modelled, it is possible to remove the feedback components from the reference signal with the structure illustrated in Figure 50c on Page 185. This technique has been discussed for the mic-accr active controller in Section 6.5 on Page 133.

6.7 ELECTRO-ACOUSTIC PATH MODELLING

The control system requires models of the electro-acoustic paths from the controller output voltage (applied to the loudspeaker voice-coil) to the cone pressure and velocity measurements for adaptive stability, see Section 6.6. Sections 6.7.1 and 6.7.2 present theory to describe the two paths in the laboratory test-rig. The test-rig uses a uniform duct of circular cross-section terminated at either end with conventional electrodynamic loudspeakers as illustrated in Figure 51 on Page 186. Comparison is made between theoretical and real measurements from the laboratory test-rig. A discussion is presented in Section 6.7.3.

6.7.1 Relationship between cone velocity and voltage applied to voice-coil

The relationship between the cone velocity and the voltage applied to the voice-coil of a loudspeaker in the laboratory test-rig is theoretically shown in this section. Consider Figure 51 on Page 186. The lower diagram contains mechanical description of the conventional electrodynamic loudspeakers used in the laboratory test-rig. The loudspeakers are represented as simple mass-spring-damper systems that terminate a duct of length L. Each has a force applied to the cone via the motor-coil system, $F_0(t)$ and $F_1(t)$, and a force due to acoustic pressure acting on each surface, $p(0,t)$ and $p(L,t)$. Analysis using Newton's second law at the left surface (x=0) vibrating with harmonic motion and cone displacement ξ gives the equation of motion, Eq. 6.129.

$$M_m \frac{d^2\xi}{dt^2} = -R_m \frac{d\xi}{dt} - K_m\xi - Sp(0,t) + F_0(t) \qquad \textbf{6.129}$$

where M_m is the mechanical mass of the loudspeaker cone, R_m is the mechanical damping and K_m is the net mechanical stiffness associated with the cone suspension and the acoustic back-load. S is the surface area of the terminations (we assume that the radius of the pipe is identical to the radius of the loudspeaker cone), $p(0,t)$ is the acoustic pressure at the surface and $F_0(t)$ is the force acting on the surface from the voice-coil system. By Fourier transform and rearrangement Eq. 6.129 can be expressed as a ratio of the force applied to the cone and the cone velocity, Eq. 6.130.

$$\frac{F_0(j\omega)}{u(0,j\omega)} = \left[R_m + j\left(\omega M_m - \frac{K_m}{\omega}\right)\right] + \left[\frac{Sp(0,j\omega)}{u(0,j\omega)}\right] \quad kg\,s^{-1} \qquad \textbf{6.130}$$

where $u(0,j\omega)$ is the complex velocity of the cone. We define the first bracket on the right hand side of Eq. 6.130 as Z_m, the mechanical surface impedance of the loudspeaker, and the second bracket as Z_{mp}, the input mechanical impedance of the pipe. The system mechanical impedance, Eq. 6.130, therefore depends on the mechanical impedances of both the loudspeaker and the pipe as shown in Eq. 6.131.

$$\frac{F_0(j\omega)}{u(0,j\omega)} = Z_m + Z_{mp} \quad kg\,s^{-1} \qquad \textbf{6.131}$$

The force $F_0(j\omega)$, applied to the cone by the motor-coil system, is described by Eq. 6.132.

$$F_0(0,j\omega) = \frac{Bl.V(j\omega)}{Z_{EB}} - \frac{(Bl)^2.u(0,j\omega)}{Z_{EB}} \qquad \textbf{6.132}$$

where Bl is the force factor, $V(j\omega)$ is the voltage applied to the coil, Z_{EB} is the blocked electrical impedance of the coil. The second term on the right hand side is the force due to back emf generated in the coil by its motion in the field of the loudspeaker magnet. By substitution of $F_0(j\omega)$ in Eq. 6.131 from Eq. 6.132 and subsequent rearrangement the relationship between cone velocity and control voltage is given by Eq. 6.133.

$$\frac{u(0,j\omega)}{V(j\omega)} = \frac{\frac{Bl}{Z_{EB}}}{Z_{mp} + \left[Z_m + \frac{(Bl)^2}{Z_{EB}} \right]} \qquad 6.133$$

The bracketed term has been seen in earlier derivations, see Eq. 6.60 on Page 120, and the expression Eq. 6.133 has been seen in similar form for when the duct input impedance is assumed to be characteristic ($Z_{mp}/S = \rho_0 c$), see Eq. 6.80 on Page 127. Equation 6.133 is used to calculate the theoretical relationship between the cone velocity and coil voltage. First the mechanical input impedance of the pipe is calculated from Eq. 6.134 (this is derived on p200-201 of (3) and assumes that plane waves are propagating in the duct).

$$Z_{mp} = \rho_0 c S . \frac{\left(\frac{Z_{mL}}{\rho_0 c S}\right) + j \tan kL}{1 + j\left(\frac{Z_{mL}}{\rho_0 c S}\right)\tan kL} \qquad 6.134$$

where Z_{mL} is the mechanical surface impedance of the source loudspeaker positioned at x=L, see Figure 51 on Page 186. If the source loudspeaker is assumed not to have a control force acting on it, F_1=0, then Z_{mL} is the same as Z_m, the first bracket on the right hand side of Eq. 6.130. The laboratory test-rig uses a duct of length 5m terminated at either end by KEF B200A loudspeakers, parameters for this unit are contained in Appendix 1 on Page 309. The specific input impedance of the pipe is theoretically calculated for this test-rig assuming the duct to be loss-less and frequency domain results are shown in Figure 52 on Page 187. The termination impedance at x=L is seen to dominate the input impedance of the pipe near the resonant frequency, around 50Hz, of the loudspeaker-box system (also see Section 4.3 on Page 76 and Figure 21 on Page 86 for the input impedance of the un-driven loudspeaker).

The specific acoustic input impedance of the pipe is converted into mechanical input impedance by multiplying by the surface area of the boundary. The result is substituted into Eq. 6.133 to give the theoretical relationship between cone velocity and voltage applied to the coil. This has been inverse fourier-transformed to give the time domain impulse response shown in

Figure 53 on Page 188. This represents a digital response with sampling frequency of 3kHz and a corresponding bandwidth of 1.5kHz. This figure also displays the measured impulse response from the laboratory test-rig. The frequency-domain magnitude transfer functions of the responses are shown in Figure 54 on Page 189. These results are discussed in Section 6.7.3.

6.7.2 Relationship between cone pressure and voltage applied to voice-coil

The development of theory for the relationship between cone pressure and voltage applied to the voice-coil leads on from the theory of Section 6.7.1. The specific acoustic input impedance of the pipe is described by Eq. 6.135.

$$\frac{p(0,j\omega)}{u(0,j\omega)} = \frac{Z_{mp}}{S} \qquad 6.135$$

Rearranging Eq. 6.135 and dividing through by the voltage applied to the voice-coil, V, yields Eq. 6.136.

$$\frac{p(0,j\omega)}{V(j\omega)} = \frac{Z_{mp}}{S} \cdot \frac{u(0,j\omega)}{V(j\omega)} \qquad 6.136$$

Substituting Eq. 6.133 into Eq. 6.136 yields Eq. 6.137

$$\frac{p(0,j\omega)}{V(j\omega)} = \frac{\frac{Z_{mp}}{S} \cdot \frac{Bl}{Z_{EB}}}{Z_{mp} + \left[Z_m + \frac{(Bl)^2}{Z_{EB}} \right]} \qquad 6.137$$

This expression has been seen in similar form for when the duct input impedance is assumed to be characteristic ($Z_{mp}/S = \rho_0 c$), see Eq. 6.66 on Page 122. The expression Eq. 6.137 is calculated for the test-rig described in Section 6.7.1 and the time domain impulse results for the theoretical and measured cases are shown in Figure 55 on Page 190. The frequency-domain magnitude transfer functions of the responses are shown in Figure 56 on Page 191. These results are discussed in Section 6.7.3.

6.7.3 Discussion

This section discusses the theoretical and measured results presented in the last two sections.

The theory assumes that: (i) the acoustic waves in the duct are harmonic and plane; (ii) the system can be modelled in terms of lumped parameters over this frequency range; (iii) there are no pipe losses; (iv) there are no other transfer functions in the electro-acoustic paths.

The validity of the assumption that plane waves propagate depends on the dimensions of the duct. The duct diameter in the test-rig is 0.16m. The cut-off frequency of plane wave propagation (the frequency below which only plane waves can propagate) is calculated as approximately 1.25kHz from Equation 6.138 where r is the duct radius in metres (from p222 of (3)).

$$f_{cutoff} < \frac{101}{r} \quad \text{for air} \qquad 6.138$$

The lumped-parameter representation of the mechanical properties of the loudspeaker is valid if the loudspeaker cone is operating with piston motion. Anthony and Elliott were able to measure the frequency limit of piston motion of the 110mm diameter cone of a KEF B110B loudspeaker as approximately 500Hz (51). As the loudspeakers used in this research project have a larger diameter of 200mm, it is assumed that the lumped parameter model is therefore valid below some frequency limit less than 500Hz. The breakup of loudspeaker cones also depends on the rigidity of the cone material and the shape of the walls (62) so the loudspeakers used in the test-rig may operate with piston motion at higher frequencies. Sound energy losses from the duct are more difficult to quantify - no theoretical estimations are presented for this. The measured responses from the laboratory include the effects of an additional transfer function. The digital control filter output is filtered with a low-pass "reconstruction" filter that removes the digital sampling signal (3kHz) from the output. The reconstruction filter used in the laboratory has a sixth order roll-off above 1kHz as shown in Figure 57 on Page 192. These considerations place limit the validity of the theoretical results for the test-rig to below 500Hz.

The theoretical and measured relationships between cone velocity and control voltage are shown in Figure 53 on Page 188 and Figure 54 on Page 189. The effects of the reactive acoustics of the pipe are observed with reflections in the impulse responses, Figure 53. This is due to reflection of sound at the terminations of the duct. The theoretical response has similar distribution and damping of the reflections compared with the measured response. The frequency domain responses, Figure 54, show that there is more sound energy at lower frequencies than higher frequencies. Therefore, the roll-off above 1kHz in the measured plot, due to the reconstruction filter, has little effect on the comparison of the time-domain responses. Furthermore, the comparison of the time-domain responses is valid as most energy is below 500Hz. The theoretical impulse response is a good approximation to that measured in the real laboratory test-rig.

The theoretical and measured relationships between cone pressure and voltage are shown in Figure 55 on Page 190 and Figure 56 on Page 191. The time-domain impulse responses, Figure 55, are seen to have similarly placed pulses due to the reflections at the terminations of the duct. The pressure impulse responses are more dependent on acoustic reflections in the duct than the velocity impulse responses. However it is difficult to compare the theoretical and measured time-domain results because of theoretical sound energy above 500Hz seen in the frequency response, see Figure 56. Below 500Hz the theoretical result is more reactive as seen by the larger peaks and troughs than the measured result, see Figure 56. This is because the real test-rig has sound energy losses in the pipe which the theoretical model does not include. The measured response also rolls-off above 1kHz because of the reconstruction filter response. As the filter response is known, see Figure 57, this can be included in the theoretical model. The convolution of the theoretical impulse response and the measured filter impulse response is shown in Figure 58 on Page 193 and the frequency domain is shown in Figure 59 on Page 194. Whilst the frequency domain shows the filter is successfully reducing the frequencies above 1kHz in the theoretical model, little difference is seen in the impulse response, Figure 58, when compared with the un-filtered theoretical response of Figure 55.

The difference between the measured and theoretical relationships between cone pressure and voltage occur because there are sound energy losses in the duct. As an exercise of illustration a filter was designed to remove the higher frequencies from the theoretical relationship. The filter response rolls off above 500Hz (⅓ of the Nyquist frequency of 1500Hz) using two poles and two zeroes. The z-domain poles are positioned at $(0.5\ ,\ \pm\frac{1}{3}\pi)$ and zeroes at $(1\ ,\ \pi)$. The response is well-damped and is implemented digitally by Eq. 6.139.

$$y[k] = x[k] + 2x[k-1] + x[k-2] + 0.125y[k-1] - 0.0703y[k-2] \qquad 6.139$$

The magnitude and phase of this filter are shown in Figure 60 on Page 195. The application of this filter to the relationship between cone pressure and control voltage modifies the frequency-domain magnitude as shown in Figure 61 on Page 196. With this approximate "weighting" of the response the theoretical and measured impulse responses of Figure 62 on Page 197 are seen to be more similar than the un-weighted responses in Figure 55 on Page 190. The polarity of the pulses is similar; the first and second pulses have strong positive tendency, the fourth and fifth have negative tendency. More damping on the later theoretical impulse response pulses (representing larger energy losses) would further match the measured result.

It has already been shown that an adaptive implementation of the control system requires models of these electro-acoustic paths for adaptive stability, see Section 6.6. The filters **<*B*>** and **<*A*>** in Figure 49c on Page 184 must model the ***u /V*** and ***p /V*** impulse responses shown in Figure 53 and Figure 55. The required modelling accuracy for LMS algorithm adaptive stability and convergence has been discussed by other researchers, see Section 3.6.4 on Page 49. The results of the last two sections show that the electro-acoustic paths in this test-rig have complex transfer functions largely influenced by the reactive duct acoustics. Therefore the filters must have suitably long impulse responses. As the theory does not estimate the exact transfer functions, it is better to determine the filter responses from direct measurements of the paths. The real-time laboratory adaptive control system uses FIR compensation filters of up to 512 coefficients with a sampling frequency of 3kHz. Conventional fast digital signal

processors meets the required computational demands. The compensation filter design procedure in the practical system is described in Section 7.5 on Page 215.

6.8 MAZZOLA'S CONTROL SYSTEM

Mazzola describes a control system for the active control of acoustic absorption (34). This has been discussed on Page 21 in Section 2.4.3, and the application of this system for acoustic absorption with a plate is shown in Figure 4 on Page 33 (this figure reproduced from Mazzola's book). The control law of this system is defined in terms of the plate velocity, pressure and radiation impedance, see Equation M.5 on Page 22. Consequently measurements of pressure and velocity are used to configure the control system - this is a similar approach to the mic-accr system described in this thesis. It is, therefore, of interest to apply Mazzola's system to the control of a loudspeaker cone. A schematic is presented in Figure 63a on Page 198. The sign convention for velocity in this thesis is identical with Mazzola's, so the control system schematic for the loudspeaker is consistent with the plate schematic of Figure 4. For clarity, the two functions **K** and $\mathbf{G_p}$ are grouped as a single identical transfer function implemented by an active controller ***W***. For consistency with the previous work in this thesis, the velocity **V** is termed ***u*** and the control voltage **E** is termed ***V***. Also the radiation load impedance (assumed to be $+\rho c$ by Mazzola) is simply called z_{RAD} and the model filter is labelled $\hat{z}_{RAD}$. The input to the active controller ***W*** is defined as the error signal, ***e***. Section 6.8.1 defines the impedance at the surface of the loudspeaker as a function of the controller ***W*** and the optimum controller solution. Section 6.8.2 studies the loop stability of this system. This work is original.

6.8.1 Active controller solution

The input to the active controller is defined as the error signal, **e** in the schematic shown in Figure 63a on Page 198. The error signal is defined in terms of the acoustic pressure at the cone p_{cone}, the cone velocity u_{cone} and the radiation load filter $\hat{z}_{RAD}$ in Eq. 6.140.

$$e = -p_{cone} - \hat{z}_{RAD} \cdot u_{cone} \qquad 6.140$$

The control system attempts to create a control voltage signal V such that the value of e is zero. If this is achieved then Eq. 6.140 can be rearranged to describe the impedance at the surface z_s in Eq. 6.141.

$$z_s = \frac{p_{cone}}{u_{cone}} = -\hat{z}_{RAD} \qquad 6.141$$

If the model filter $\hat{z}_{RAD}$ is an accurate representation of the true radiation impedance z_{RAD} then the loudspeaker cone will completely absorb incident pressure (this assumes that the active controller function is correctly forcing e to zero). If the model filter is not an accurate representation of the radiation impedance then the performance of the active absorber is limited. The relationship between the surface impedance z_s and the active controller function W will now be defined.

The output voltage of the controller V is the product of the error signal, e and the controller filter transfer function W.

$$V = e.W \qquad 6.142$$

The error signal, Eq. 6.140, can be rewritten as Eq. 6.143.

$$e = p_{cone} \cdot \left(-1 - \frac{\hat{z}_{RAD}}{z_s} \right) \qquad 6.143$$

The analysis of the total force on the loudspeaker cone in terms of V, p_{cone} and u_{cone} has been given in Section 6.3.1, see Eq. 6.17 on Page 107. Substituting for V in Eq. 6.17 gives Eq. 6.144.

$$\left[\frac{Bl}{Z_{EB}}\right] p_{cone} . W . \left(-1 - \frac{\hat{z}_{RAD}}{z_s} \right) - [S] p_{cone} = Z_{LS} . u_{cone} \qquad 6.144$$

where Z_{LS} is defined in Eq. 6.60 on Page 120. Eq. 6.144 is easily rearranged to give the controlled impedance at the surface of the loudspeaker, Eq. 6.145 where z_{NAT} is the un-driven specific acoustic impedance of the loudspeaker defined in Eq. 6.61 on Page 120.

If the active controller W is zero so that the control is effectively off, the un-driven impedance of the loudspeaker is z_{NAT} from Eq. 6.145. This is consistent with previous theory in this thesis. Eq. 6.144 can also be rearranged

$$z_s = -\frac{W.\frac{Bl}{Z_{EB}S}.\hat{z}_{RAD} - z_{NAT}}{W.\frac{Bl}{Z_{EB}S} + 1} \qquad 6.145$$

to give the required active controller transfer function for a desired value of z_s, Eq. 6.146.

$$W = -\frac{Z_{EB}S}{Bl}.\frac{-\frac{z_{NAT}}{z_s} + 1}{\frac{\hat{z}_{RAD}}{z_s} + 1} \qquad 6.146$$

The active controller is seen to be dependent on the loudspeaker parameters, Z_{EB}, Bl, S and z_{NAT}, the model filter $\hat{z}_{RAD}$ and the desired impedance z_s. If the desired impedance is $-\hat{z}_{RAD}$, that for ideal sound absorption (see Eq. 6.141), then the required gain of the optimum controller is infinity from Eq. 6.146. This is not realizable. However examination of Eq. 6.145 indicates that the controlled impedance of the KEF B200A loudspeaker can be close to $-\hat{z}_{RAD}$ when W is set to the typical gains that can be implemented with conventional analogue techniques. A complete study of Mazzola's system must also include an analysis of loop stability: this is presented in the next section.

6.8.2 Loop stability

The presence of a loop associated with the radiation impedance that couples the cone velocity to the cone pressure has been established in Section 6.4.1 on Page 118. This causes a feedback loop that affects the stability of the controlled impedance. The loop stability of Mazzola's controller is examined in this section.

An analysis based on the continuity of velocity in Section 6.4.1 has established a model of the electro-acoustics of a controlled loudspeaker shown in Figure 32 on Page 167. A schematic for the control of a loudspeaker by Mazzola's system, based on Figure 32, is given in Figure 63b on Page 198. The output of the controller W affects the cone pressure and cone velocity which are both used to form the input to the controller. Therefore there is the potential for a feedback loop around the controller. This is analyzed by considering the relationships between the cone pressure and cone velocity and the controller

output. Sections 6.4.2 and 6.4.3 have presented schematics that separate controller output and incident pressure components for cone pressure and cone velocity reference signals, see Figure 35 on Page 170 and Figure 39 on Page 174. Therefore Figure 63b can be redrawn as Figure 64 on Page 199 with all notation defined in Sections 6.4.2 and 6.4.3. C and D have been defined in Eq. 6.66 on Page 122 and Eq. 6.80 on Page 127. These equations are reproduced here in Eq. 6.147 and Eq. 6.148 where z_{RAD} represents the radiation load impedance, assumed to be $+\rho_0 c$ in the derivation of these relationships - this is consistent with Mazzola's work.

$$C = \frac{\frac{Bl}{Z_{EB}S}}{-\frac{z_{NAT}}{z_{RAD}} + 1} \qquad 6.147$$

$$D = \frac{\frac{Bl}{Z_{EB}S}}{-z_{NAT} + z_{RAD}} \qquad 6.148$$

If there is no incident pressure, such that $p_i = 0$, then the electro-acoustic model of Figure 64 can be redrawn as Figure 65a on Page 200 and the feedback loop is illustrated clearly by redrawing Figure 65a as Figure 65b - the loop is shown with the curved line. The stability of the feedback loop can be assessed by applying the Nyquist stability criterion. The open loop gain G_0 is expressed in Eq. 6.149.

$$G_0 = W.[-C - z_{RAD}.D] \qquad 6.149$$

Substituting C and D in Eq. 6.149 from Eq. 6.147 and Eq. 6.148 and rearranging gives Eq. 6.150.

$$G_0 = W.\frac{Bl}{Z_{EB}S}.\left(\frac{-z_{RAD} - z_{RAD}}{z_{RAD} - z_{NAT}}\right) \qquad 6.150$$

The term W in Eq. 6.150 can be substituted from Eq. 6.146 and rearranged to give Eq. 6.151.

$$G_0 = -\left(\frac{z_S - z_{NAT}}{z_S + \hat{z}_{RAD}}\right).\left(\frac{-z_{RAD} - \hat{z}_{RAD}}{z_{RAD} - z_{NAT}}\right) \qquad 6.151$$

At zero and infinite frequencies the value of z_{NAT} for any loudspeaker is infinite and imaginary and G_0 is then Eq. 6.152 from examination of Eq. 6.151.

$$G_0\Big|_{\omega=0,\infty} = \frac{z_{RAD} + \hat{z}_{RAD}}{z_s + \hat{z}_{RAD}} \qquad 6.152$$

In order to examine the stability of the feedback loop it is necessary to make a Nyquist plot of Eq. 6.151. This restricts the analysis to particular values of z_s, z_{NAT}, z_{RAD} and $\hat{z}_{RAD}$. It is assumed here that the radiation impedance is $z_{RAD} = +\rho_0 c$ and that $\hat{z}_{RAD} = z_{RAD}$. The optimum value of G_0 is infinite for exact acoustic absorption (the denominator of the left hand bracket is zero because $z_s = -z_{RAD}$ from Eq. 6.141) for which it is not possible to apply the Nyquist stability criterion. However, real implementations of this are not possible because the required gain of W is infinity. Controlled values of z_s that are close to $-z_{RAD}$ will also provide good sound absorption and the loop stability for some typical cases will now be analyzed. Theoretical values of z_{NAT} of the KEF B200A loudspeaker will be used to further this analysis for consistency with Sections 6.4.2 and 6.4.3.

The natural specific acoustic impedance at the surface of a loudspeaker is defined in Section 4.3 on Page 76 and results for the KEF B200A loudspeaker are displayed in Figure 21 on Page 86 when the voltage applied to the voice-coil is zero ($V(j\omega)=0$ in Eq. 4.9). At the resonant frequency, $\omega_1 = 2\pi.65$Hz, z_{NAT} is real with a value of approximately -423 Rayls. Nyquist plots, calculated from Eq. 6.151 using the data for the KEF B200A loudspeaker in Figure 21, are presented in Figure 66 on Page 201 for two values of controlled impedance: -423 Rayls and -406 Rayls. These two values both correspond to an acoustic absorption coefficient, alpha, of approximately 0.99. The plots have zero imaginary components when $\omega=0$, ω_1 and ∞. The (1,j0) point is not enclosed by either the plots. Therefore, according to the Nyquist stability criterion, these configurations are stable when the loop is closed. This analysis demonstrates that Mazzola's active controller is stable for near-exact sound absorption when controlling a KEF B200A loudspeaker that is presented with a radiation impedance of $+\rho_0 c$. The 1,j0 point is only encircled when the desired impedance is greater than +415

Rayls which is deduced by quantifying Eq. 6.152. However, as this is negative impedance because of the assigned velocity direction, this instability is not of importance in the implementation of active sound absorption.

Mazzola's system is suitable for analogue implementation. Typical analogue implementations do not have the inherent time delays of conventional digital implementations. Therefore the development of the analysis of open loop gain in Sections 6.4.2 and 6.4.3 to include a time delay τ (see, for example, Eq. 6.71 on Page 124) does not apply here. Analogue feedback systems often have phase shift associated with the gain roll-off of electronic amplification which can cause loop instabilities. Apart from this potential problem, the analysis presented in this section indicates that Mazzola's system is stable for the control of near-exact sound absorption with defined radiation loads.

6.9 COMPARISON OF ADAPTIVE FILTERS FOR MIC-ACCR AND 2-MIC CONTROL

The mic-accr control system, introduced in Section 2.4.3 on Page 20 and described in Chapter 5, and the 2-mic control system discussed in Section 2.4.2 on Page 14 are current methods for the active control of impedance. Publications on the 2-mic system indicate that it has been used to create absorbing terminations - see references (24) (29). It is of interest to compare theoretically the optimal filter solutions of the two adaptive control systems.

The mic-accr and 2-mic control systems have similar forward-path layouts when the mic-accr method is arranged as shown in Figure 26b on Page 99 and thus can be compared. Schematics for the two systems are presented in Figure 67 on Page 202. In this section each system is assumed to have the same reference input $x(k)$, and each system operates in an acoustic environment described by B_k. In both cases the desired signal $d(k)$ is set to zero. Both systems specify the desired impedance with a "desired filter" (see Section 5.3) - H for the mic-accr system and Δ for the 2-mic system. The adaptive systems are configured to minimise the difference between the desired filter output and

the cone pressure p_c. Analysis of each system is presented separately in the next two sections. Conclusions are made in Section 6.9.3 on Page 160.

6.9.1 Mic-accr system

This section presents a mathematical description of the mic-accr system shown in Figure 67a on Page 202. The derivation follows similar patterns to theory presented in Sections 3.5 and 3.6. The system is implementing a real impedance such that the desired impedance filter H is a single multiplication with no time delay. The error signal is described by Eq. 6.153.

$$e(k) = -\overline{B_k}^T \overline{\overline{X_k}}\,\overline{W_k} + u_c(k).H \qquad 6.153$$

Where $\overline{\overline{X_k}}$ was defined in Eq. 3.33 on Page 47. Squaring Eq. 6.153 yields Eq. 6.154.

$$e^2(k) = \left[\overline{B_k}^T \overline{\overline{X_k}}\,\overline{W_k}\right]^2 - 2.u_c(k).H.\left[\overline{B_k}^T \overline{\overline{X_k}}\,\overline{W_k}\right] + u_c^2(k)H^2 \qquad 6.154$$

The LMS adaptive algorithm uses an instantaneous gradient estimate (see Section 3.5.6). This is found by partial differentiation of the squared error Eq. 6.154 to give Eq. 6.155 which is re-arranged to give Eq. 6.156. The partial differentiation is performed assuming that u_c(k) is not dependent on the change of the adaptive filter coefficients, which is only true if the weights are adapted very slowly.

$$\frac{\delta e^2(k)}{\delta \overline{W_k}} = 2\overline{\overline{X_k}}\,\overline{B_k}.\left[\overline{B_k}^T \overline{\overline{X_k}}\,\overline{W_k}\right] - 2u_c(k).H.\overline{\overline{X_k}}\,\overline{B_k} \qquad 6.155$$

$$= -2\overline{\overline{X_k}}\,\overline{B_k}.\left[-\overline{B_k}^T \overline{\overline{X_k}}\,\overline{W_k} + u_c(k).H\right] \qquad 6.156$$

The bracketed portion of Eq. 6.156 is the instantaneous error **e(k)**; the instantaneous gradient estimate for the adaptive update is then Eq. 6.157.

$$\frac{\delta e^2(k)}{\delta \overline{W_k}} = -2\,e(k).\overline{\overline{X_k}}\,\overline{B_k} \qquad 6.157$$

The optimum filter solution occurs when Eq. 6.155 (or Eq. 6.156) is reduced to zero. The optimum control filter Eq. 6.158 is obtained by setting Eq. 6.156 to zero.

$$\overline{W}^{*} = u_c(k) . H \left[\overline{\overline{X}_k} \, \overline{B_k} \right]^{-1} \qquad \textbf{6.158}$$

With optimum control the cone pressure will equal the product of the cone velocity and the desired impedance filter ***H***, so Eq. 6.158 can be rewritten as Eq. 6.159.

$$\overline{W}^{*} = p_o(k) \left[\overline{\overline{X}_k} \, \overline{B_k} \right]^{-1} \qquad \textbf{6.159}$$

6.9.2 2-mic system

This section contains a mathematical description of the 2-mic control system schematic shown in Figure 67b on Page 202. The desired signal filter **Δ** is a time delay (see (29)). The error signal is described by Eq. 6.160.

$$e(k) = \Delta p_u(k) - \overline{B_k}^T \overline{\overline{X}_k} \, \overline{W_k} \qquad \textbf{6.160}$$

Squaring Eq. 6.160 yields Eq. 6.161.

$$e^2(k) = \left[\overline{B_k}^T \overline{\overline{X}_k} \, \overline{W_k} \right]^2 - 2\Delta p_u(k) \overline{B_k}^T \overline{\overline{X}_k} \, \overline{W_k} + \Delta^2 p_u^2(k) \qquad \textbf{6.161}$$

The LMS adaptive algorithm uses an instantaneous gradient estimate (see Section 3.5.6). This is found by partial differentiation of the squared error Eq. 6.161 to give Eq. 6.162 which is re-arranged to give Eq. 6.163. The partial differentiation is performed assuming that $p_u(k)$ is not dependent on the change of the adaptive filter coefficients, which is only true if the weights are adapted very slowly.

$$\frac{\delta e^2(k)}{\delta \overline{W_k}} = 2 \overline{\overline{X}_k} \, \overline{B_k} \left[\overline{B_k}^T \overline{\overline{X}_k} \, \overline{W_k} \right] - 2\Delta p_u(k) \, \overline{\overline{X}_k} \, \overline{B_k} \qquad \textbf{6.162}$$

$$= -2 \overline{\overline{X}_k} \, \overline{B_k} . \left[- \overline{B_k}^T \overline{\overline{X}_k} \, \overline{W_k} + \Delta p_u(k) \right] \qquad \textbf{6.163}$$

The bracketed portion of Eq. 6.163 is the instantaneous error $e(k)$; the instantaneous gradient estimate for the adaptive update is thus Eq. 6.164.

$$\frac{\delta e^2(k)}{\delta \overline{W_k}} = -2 e(k) . \overline{\overline{X}_k} \, \overline{B_k} \qquad \textbf{6.164}$$

The optimum filter solution occurs when Eq. 6.162 (or Eq. 6.163) is reduced to zero. The optimum control filter Eq. 6.165 is obtained by setting Eq. 6.163 to zero.

$$\overline{\boldsymbol{W}}^{*} = \Delta\, p_u(k) \left[\overline{\overline{\boldsymbol{X}_k}\, \boldsymbol{B}_k} \right]^{-1} \qquad 6.165$$

With optimum control the cone pressure $p_c(k)$ will equal the product of the pressure $p_u(k)$ and the desired filter Δ, so Eq. 6.165 can be rewritten as Eq. 6.166.

$$\overline{\boldsymbol{W}}^{*} = p_c(k) \left[\overline{\overline{\boldsymbol{X}_k}\, \boldsymbol{B}_k} \right]^{-1} \qquad 6.166$$

6.9.3 Conclusions

The optimum control filter solutions for the mic-accr and 2-mic control systems have been shown by Equations 6.159 and 6.166 to be identical. This confirms that both control methods have the same control target - to create a defined surface impedance. The gradient estimate equations for each control method, Equations 6.157 and 6.164, are identical so the *performance surfaces*, see Section 3.5.3, are also identical. Therefore the convergent properties (such as stability and speed) of the two adaptive algorithms can be assumed as identical for the same reference input and acoustic environment.

6.10 SUMMARY

Theory has been presented to describe the operation of active control systems for the control of impedance. This section reviews the material presented in this chapter.

The effect of errors in the observation of impedance on controlled impedances has been presented in Section 6.2. Assuming that the active controller is ideal, the implemented impedance with a mic-accr control system depends on the desired impedance, the accuracy of the acoustic pressure and velocity measurements and the desired filter accuracy. The desired filter can compensate for inaccuracy in the pressure and velocity measurements. The effect of error from these combined factors has been illustrated with a description of the reflection coefficient of an active acoustic absorber.

Section 6.3 presented theoretical optimum filter solutions for the active controller for four variations of reference signal. The use of cone pressure as a reference

was discussed in Section 6.3.1. The optimum controller is not realizable for desired zero impedances. The use of cone velocity was discussed in Section 6.3.2. The optimum controller is not realizable for a desired controlled impedance of infinity. In both cases the optimum control transfer functions can be implemented for other desired impedances assuming that the controller filter has no inherent delay. The use of acoustic pressure measured at some point in the duct was discussed in Section 6.3.3. The optimum control filter solution is significantly more complicated than that for a reference input of cone pressure. However the optimum filter solutions are similar for a desired characteristic impedance. The optimum controller is not realizable when the desired impedance is zero. The position of the acoustic pressure measurement must be considered carefully if the sound field is modal. Finally the use of the electrical source signal was discussed in Section 6.3.4. The optimum controller filter has the most complicated transfer function. This reference signal will always have sufficient energy to drive the active controller. There are no potentially unstable loops around the controller as there is no acoustic feedback. The other three reference signals cause the controller to be potentially instable as there are acoustic feedback loops.

The theoretical optimum control filter solutions, presented in this chapter, indicate that the active controller filter is realizable for definable desired impedances. A complete description of the implementation problems of the mic-accr system must also include consideration of the controller stability in the presence of feedback loop paths. This was discussed in Section 6.4. The stability of the active controller that uses cone pressure as a reference was defined in Section 6.4.2. The optimum implementation of this controller was shown to be stable for all desired impedances when a defined radiation load is presented to the cone of a particular loudspeaker. However, it was shown that practical implementations with inherent delays of the typical order of current digital systems are only stable when the desired impedance is equal to or greater than the characteristic impedance of air. The loop stability of the active controller that uses cone velocity as a reference was defined in Section 6.4.3. The optimum controller is also stable for all desired impedances for the same

set of conditions. As in the previous case, implementation delays can cause loop instability. The value of desired impedance at the onset of instability is dictated by the radiation load and loudspeaker parameters. These important results show that instabilities can exist with either of these active controllers for certain conditions. This original work has established operating envelopes of stable controlled impedance for these controller configurations.

The loop stability of the active controller that uses duct pressure as a reference was defined in Section 6.4.4. The implementation of the ideal controller for three values of impedance was discussed. The controller can not force zero impedance. For near characteristic impedances the controller is only stable over broader frequency bandwidths when the impedance is greater or equal to characteristic impedance; when the controlled impedance is characteristic the control system is "on the edge" of instability. For desired infinite impedance the controller is unstable at certain combinations of frequency and spacing of the duct pressure measurement for the reference input. It was concluded that feedback cancellation techniques are necessary for stable control. The effects of the feedback path are reduced with feedback cancellation. The optimum transfer functions for active controllers based on this technique have been described in Section 6.5. If the radiation impedance presented to the controlled impedance is complicated, such as the input impedance to a pipe, then the impulse responses of the optimum transfer functions are also complicated - this is consistent with the literature. The optimum active controller based on feedback cancellation with a reference input of duct pressure may have non-causal components and therefore might not be fully implementable for broad-band signals.

Two compensation configurations for the adaptive LMS implementation of the mic-accr control system have been presented in Section 6.6. One of the configurations has stability problems but can converge for certain solutions. The other configuration is more stable. Analysis of adaptive controllers in the presence of feedback was considered in Section 6.6.3. The definition of a general description of the dynamics of the system is not considered possible.

Theoretical transfer functions for electro-acoustic paths in the test-rig have been described in Section 6.7. These are similar to measured transfer functions but are not identical because sound energy losses are not included in the theory. The results have implications on the impulse response length of the compensation filters required for the stability and convergence of adaptive control systems.

Mazzola's control system for the active control of acoustic absorption has been examined in Section 6.8 for the control of a loudspeaker. The optimum controller solution indicates that a practical implementation of the system can force the cone to have near-characteristic impedance and therefore absorb incident sound. An analysis of the feedback loop indicates that this system is stable for a defined radiation load and loudspeaker.

Theoretical active controller transfer functions for a mic-accr and a 2-mic control system have been compared in Section 6.9. The optimum solutions are identical. This confirms that the active controllers perform the same control task. The theory suggests that the convergent behaviour of the two adaptive algorithms is identical for the same acoustic noise environment.

6.11 CHAPTER FIGURES

The figures referred to in this chapter appear on the following pages.

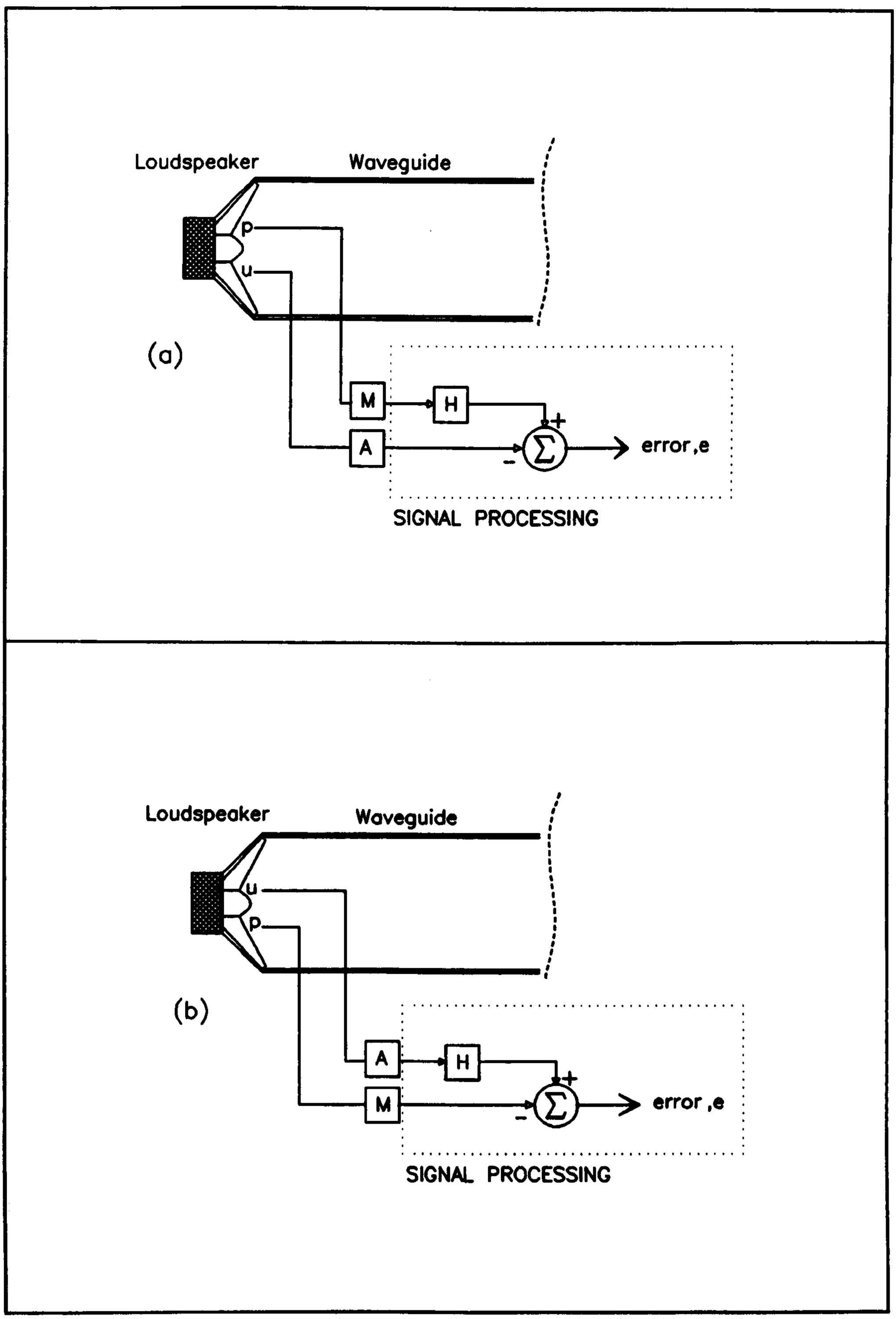

Figure 29. A schematic of the mic-accr method. M and A are factors associated with the measurement of pressure p and velocity u. (a) and (b) show different variations.

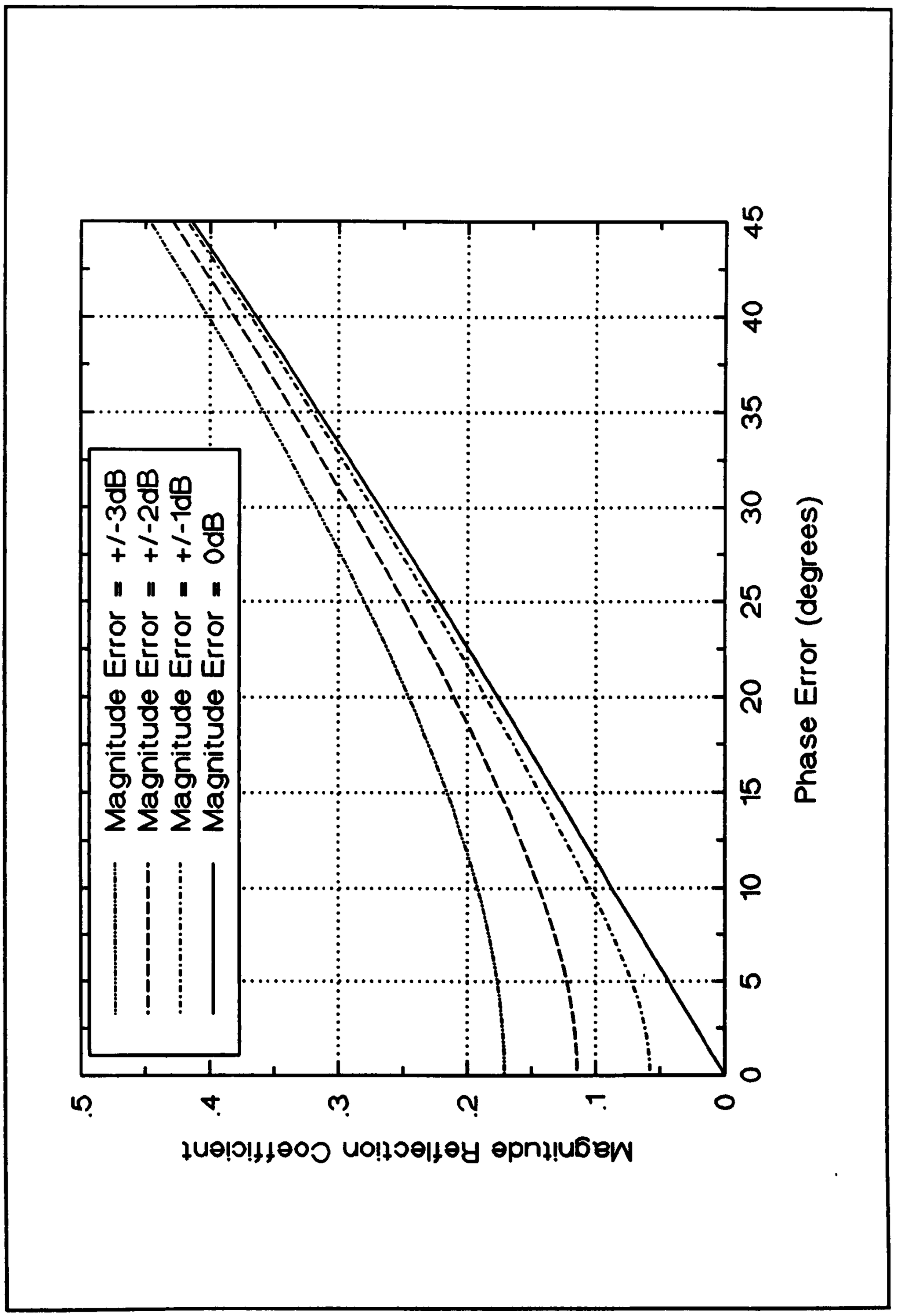

Figure 30. The effect of error in the impedance observation on the magnitude of reflection coefficient of an active acoustic absorber controlled by a mic-accr system.

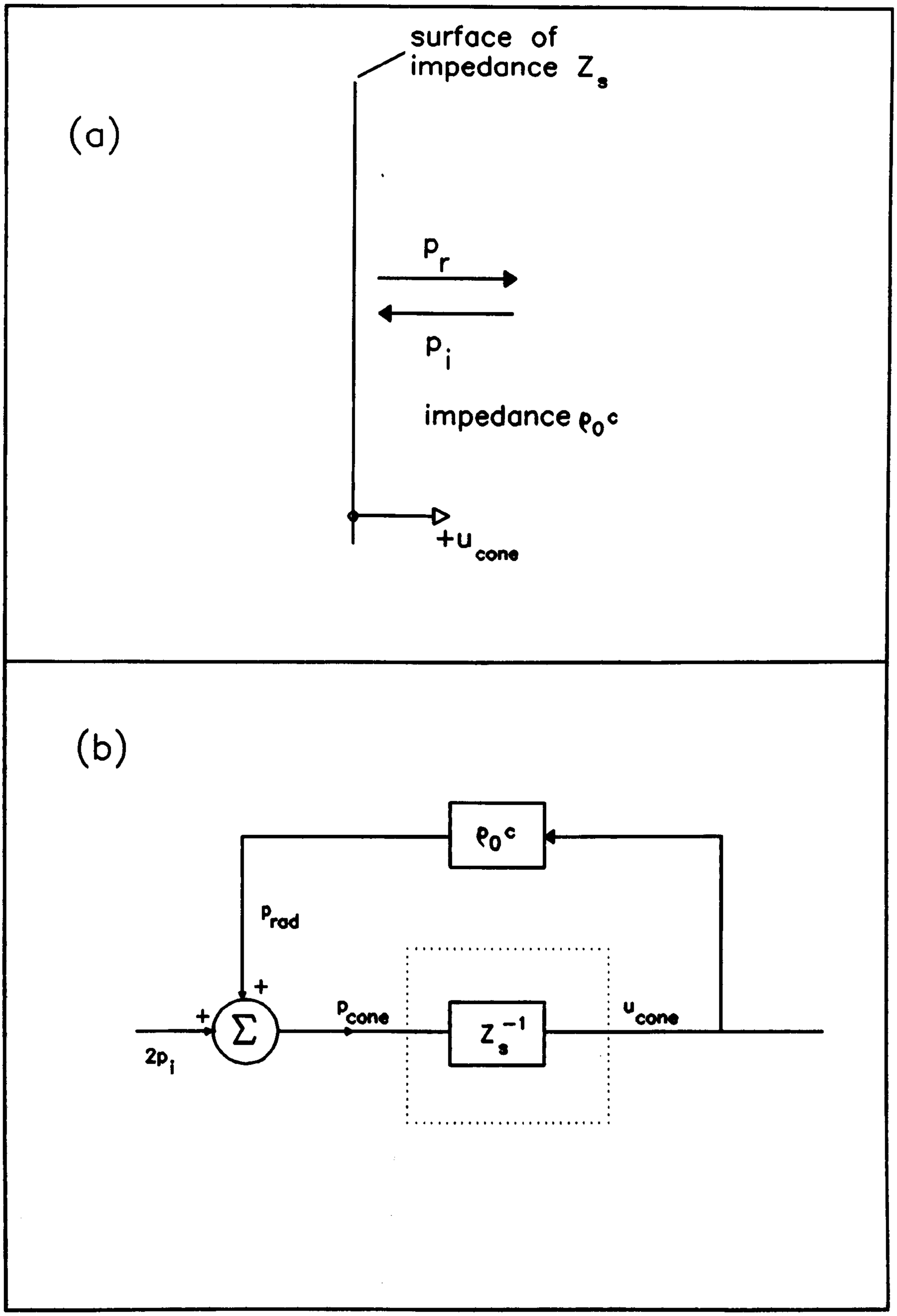

Figure 31. (a) shows the surface of a boundary of specific acoustic impedance z_s excited by normally incident acoustic plane waves. (b) illustrates the acoustics at the surface. This arises from the continuity of velocity.

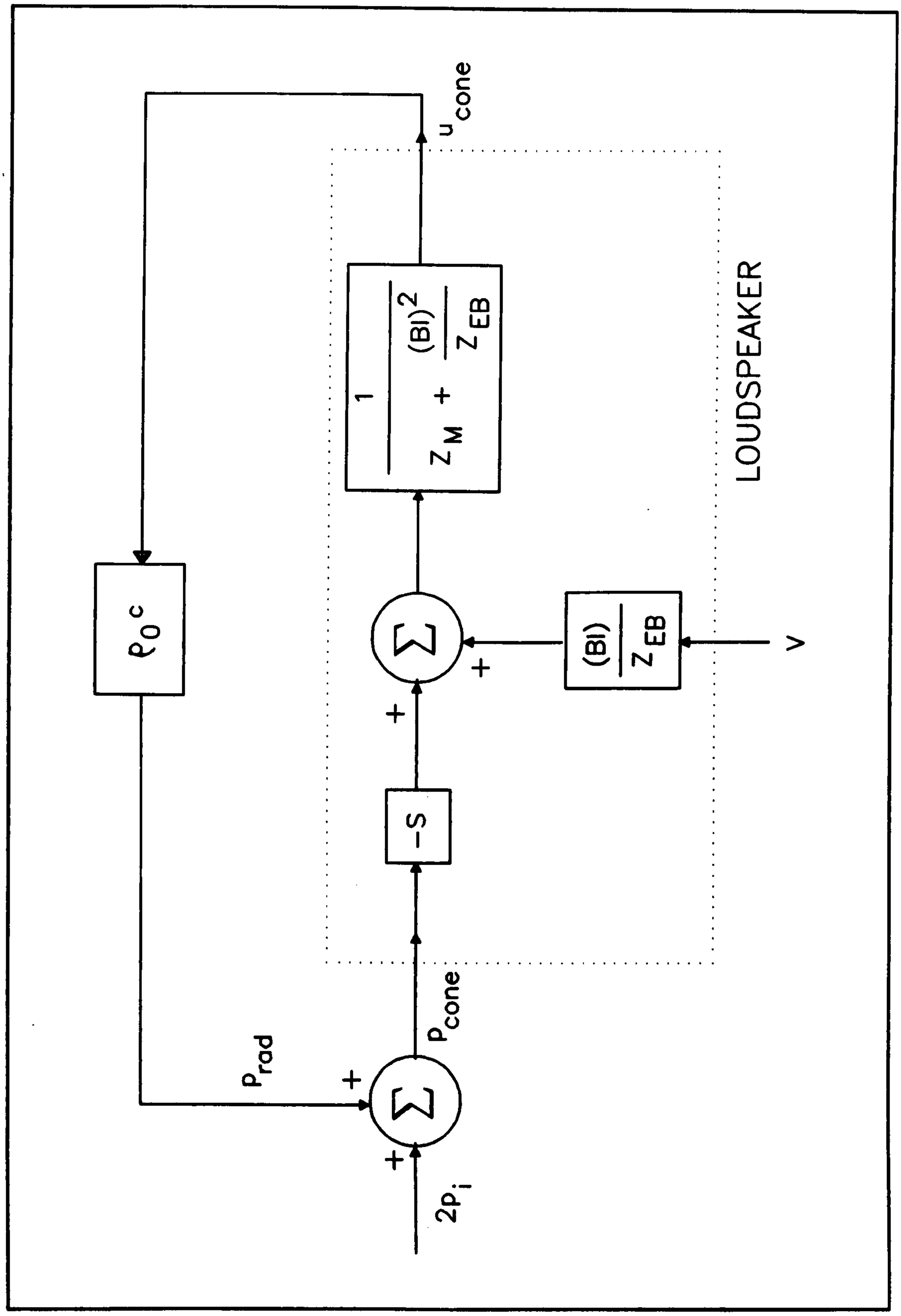

Figure 32. Schematic of the pressure & velocity relationship at the surface of a loudspeaker cone excited by incident acoustic wave p_i and electrically driven by voice-coil voltage V.

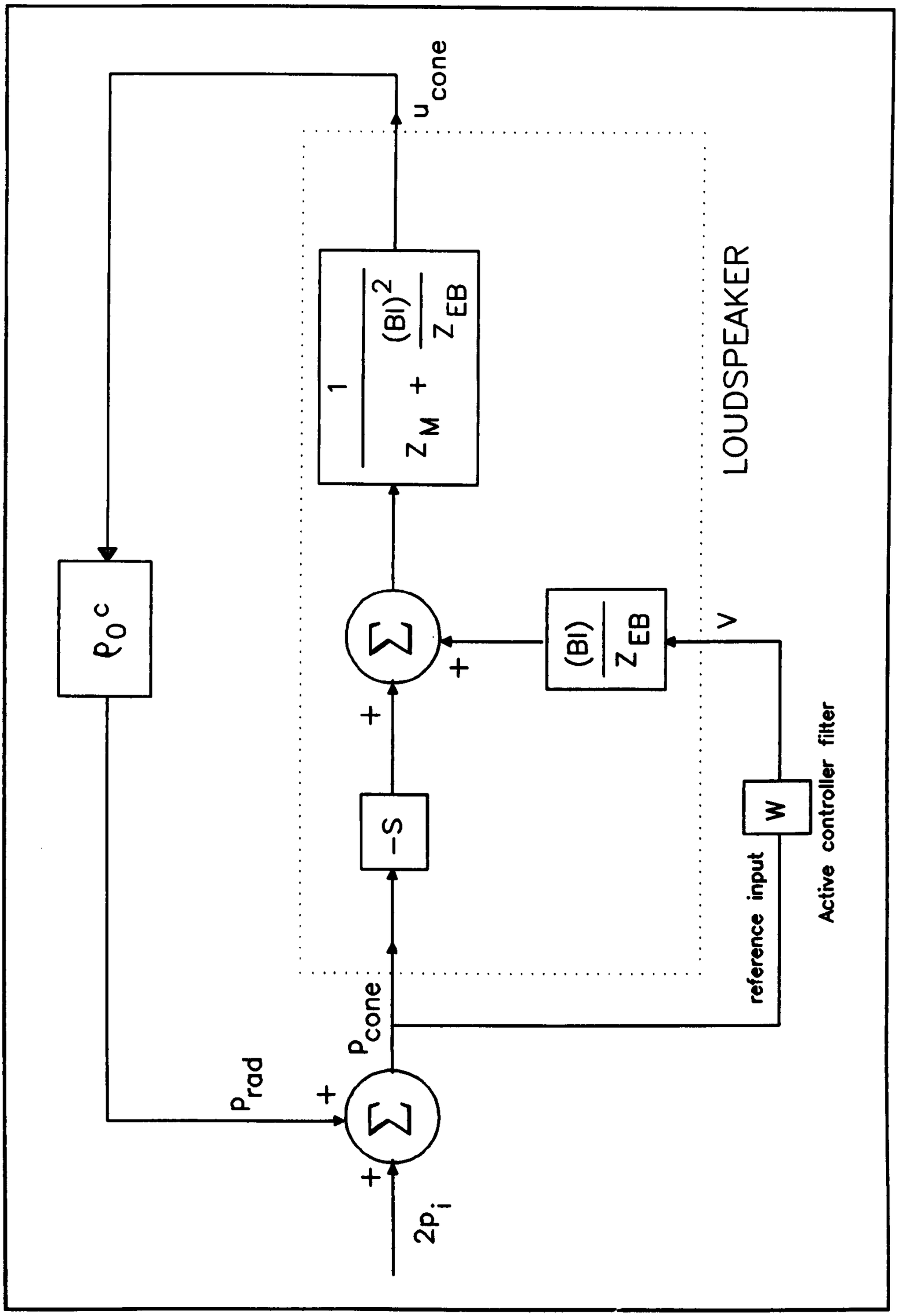

Figure 33. Schematic of the pressure & velocity relationship at the surface of a loudspeaker cone excited by incident acoustic wave p_i. A feedback path exists around controller W.

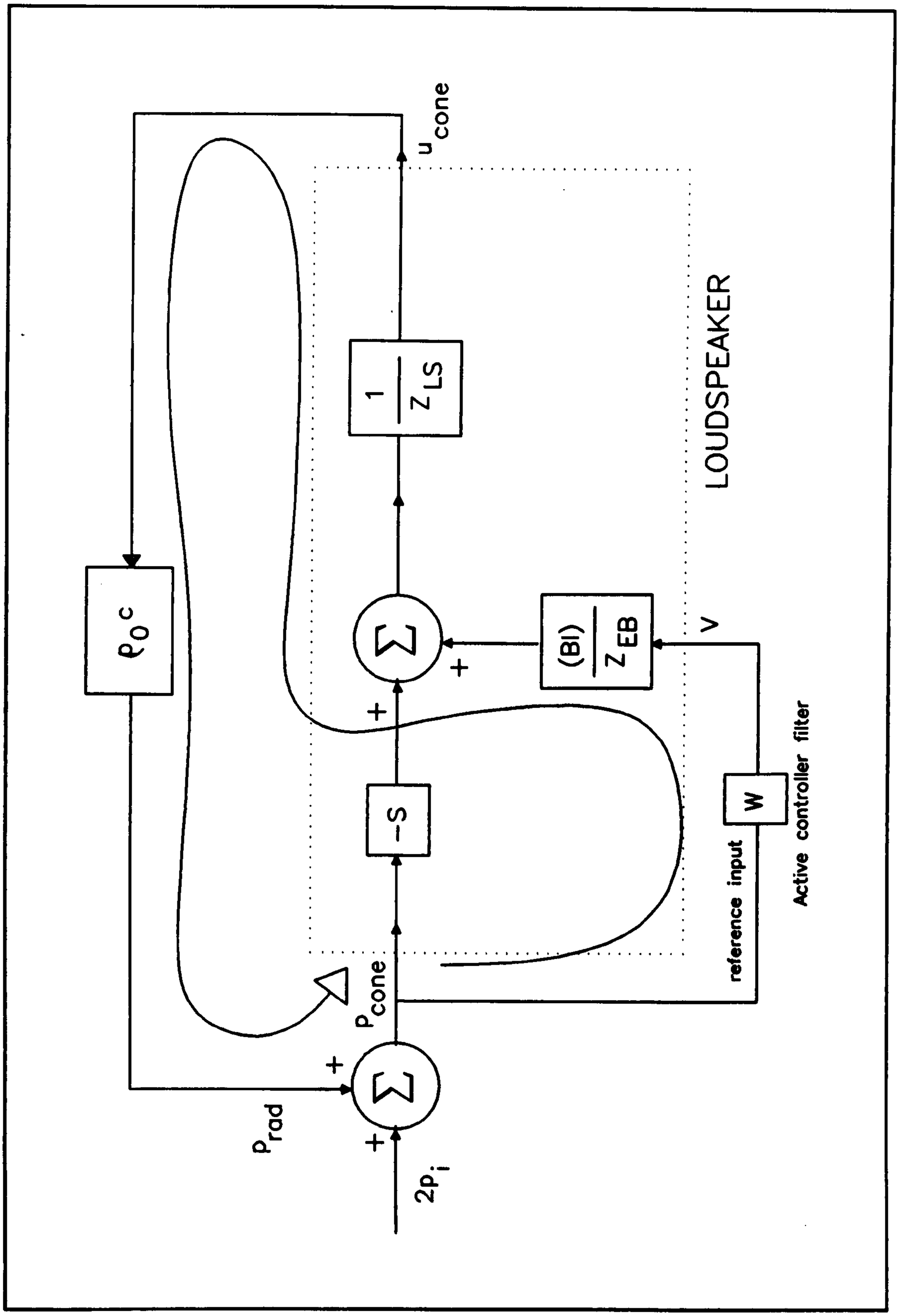

Figure 34. The pressure & velocity relationship at the surface of a loudspeaker cone excited by incident acoustic wave p_i. A feedback path exists around W shown by the curved line.

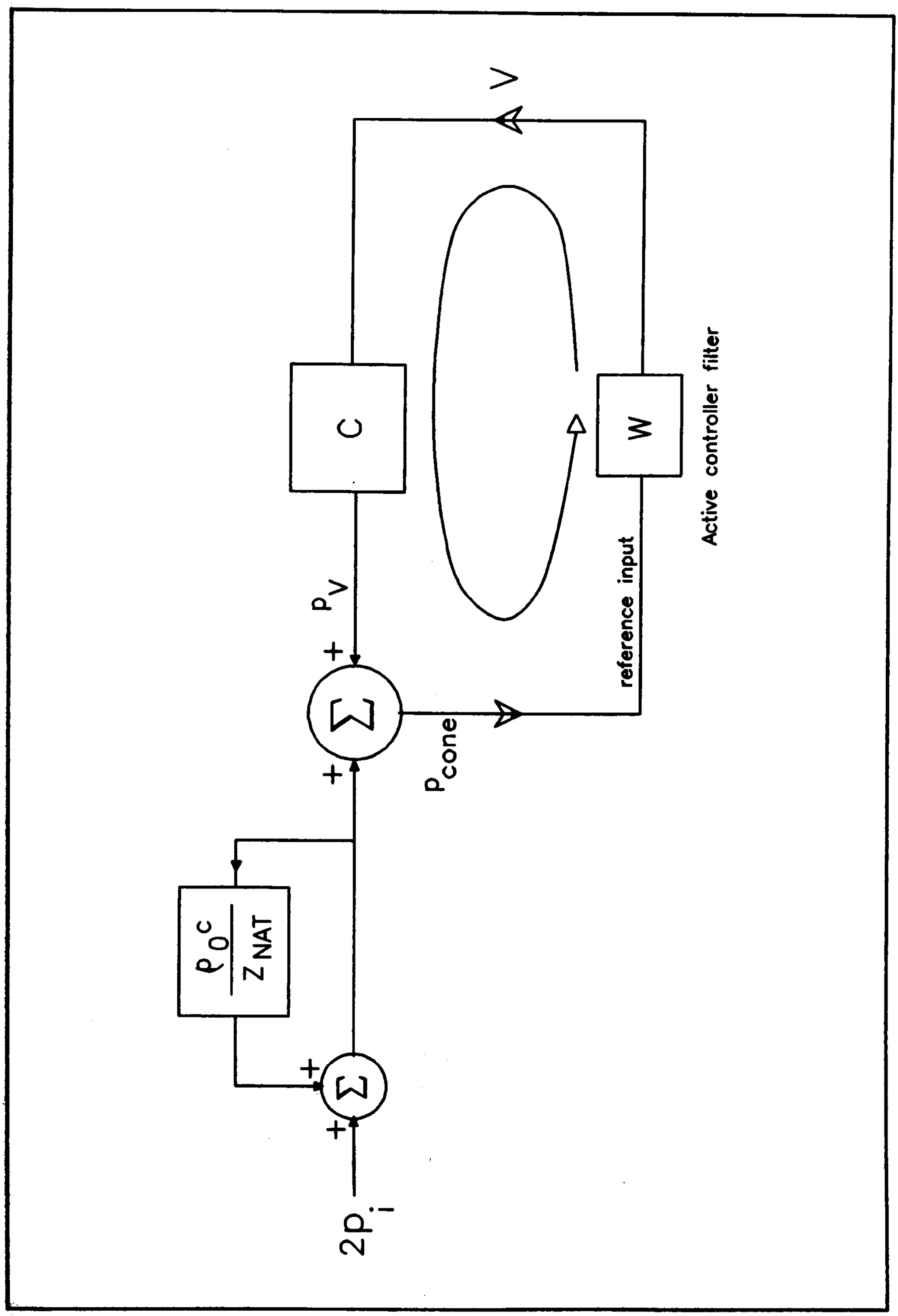

Figure 35. Schematic of the cone pressure at the surface of a loudspeaker cone excited by incident pressure p_i and controller voltage V. Feedback loop around W is shown by curved line.

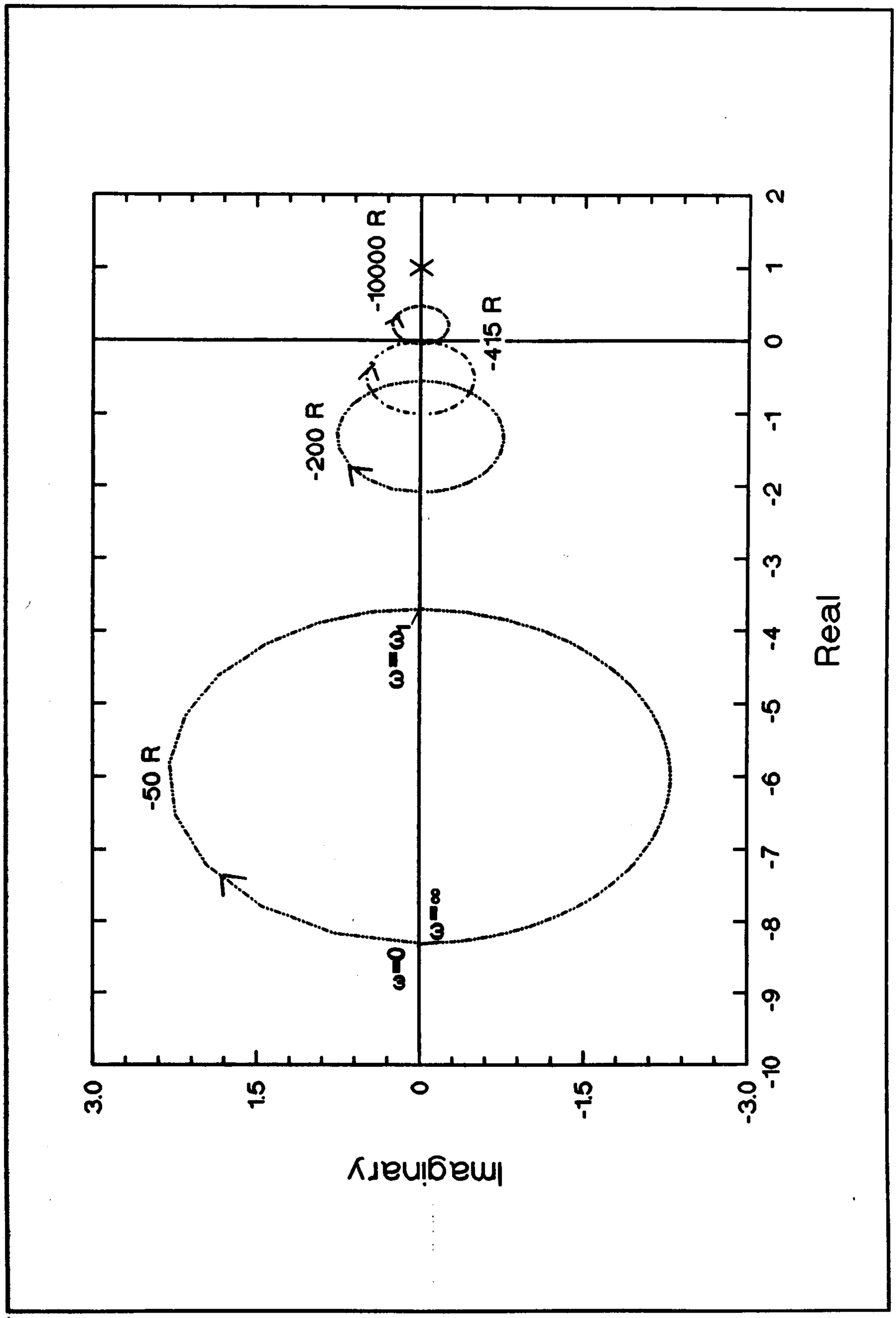

Figure 36. Nyquist plot of W(jw).C(jw) for optimum controller with reference p_{cone} and a KEF B200A loudspeaker for four values of z. Values of ω from 0 to $+\infty$. 1 j0 is not enclosed: all systems are stable when loop is closed.

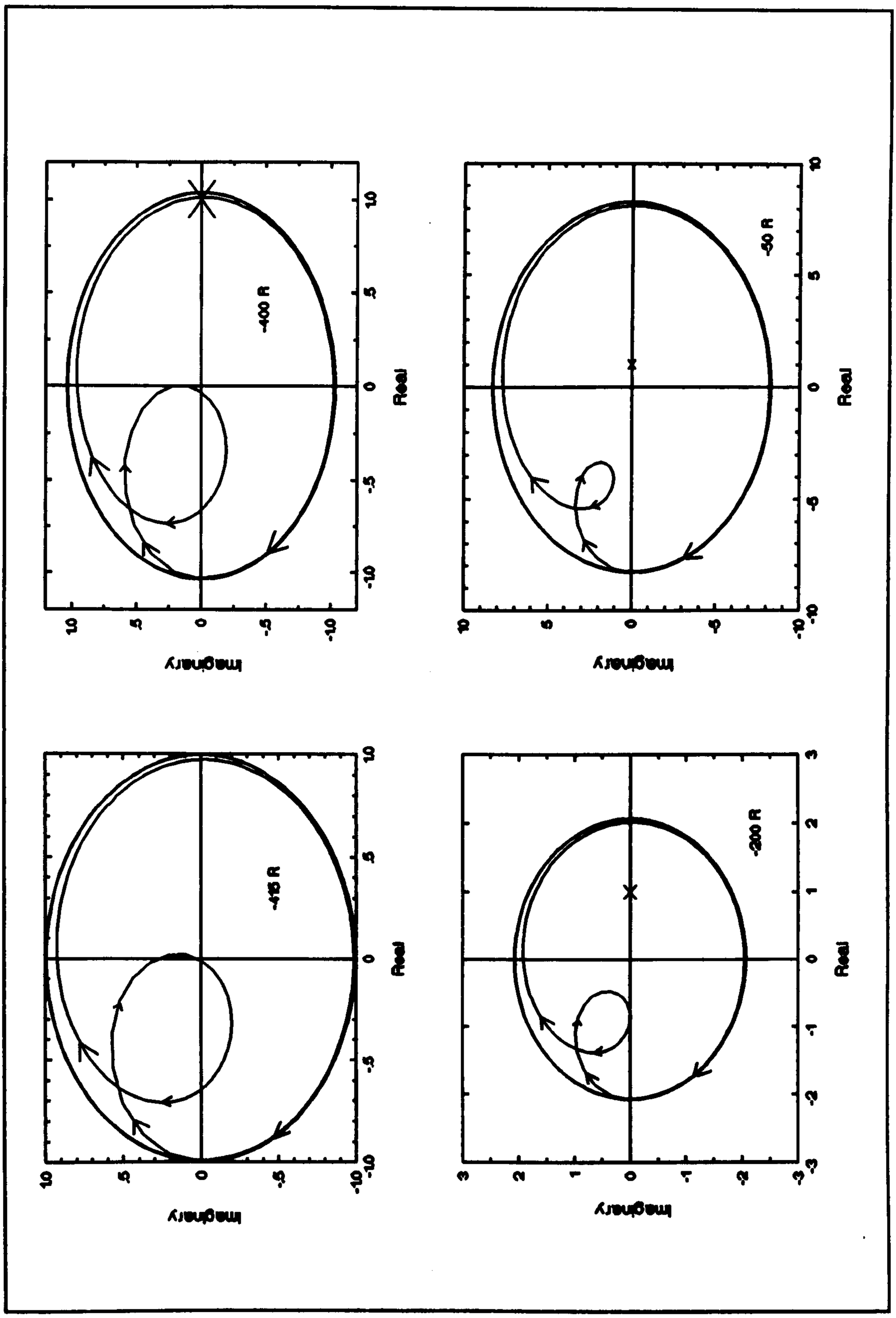

Figure 37. Nyquist plot of W(jw).C(jw) for controller with 1ms delay with reference p_{cone} and a KEF B200A loudspeaker for four values of z. Values of ω from 0 to $+\infty$. 1,j0 is enclosed for z > -415 Rayls.

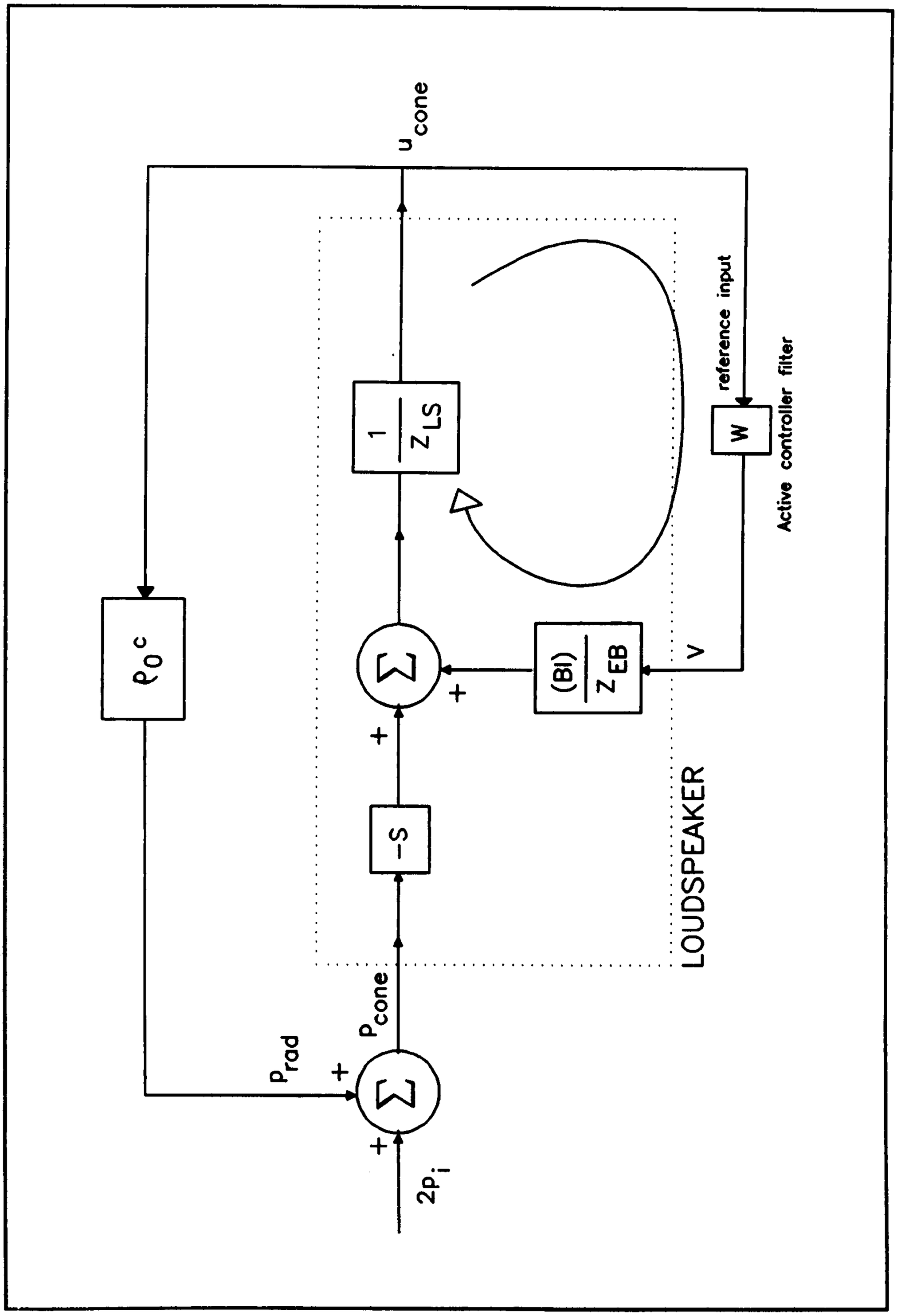

Figure 38. The pressure & velocity relationship at the surface of a loudspeaker cone excited by incident acoustic wave p_i. A feedback path exists around W shown by the curved line.

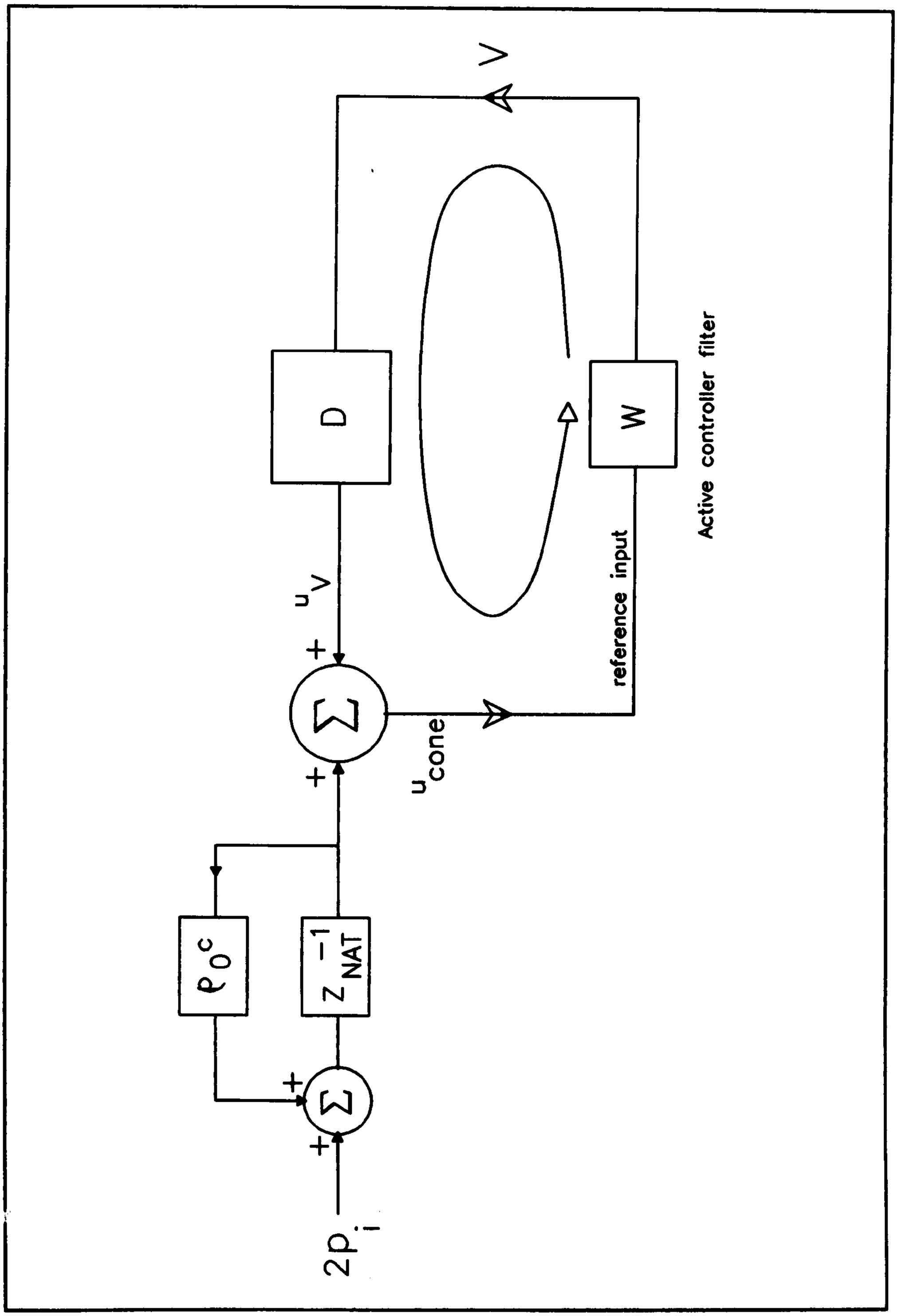

Figure 39. Schematic of the cone velocity at the surface of a loudspeaker cone excited by incident pressure p_i and controller voltage **V**. Feedback loop around **W** is shown by curved line.

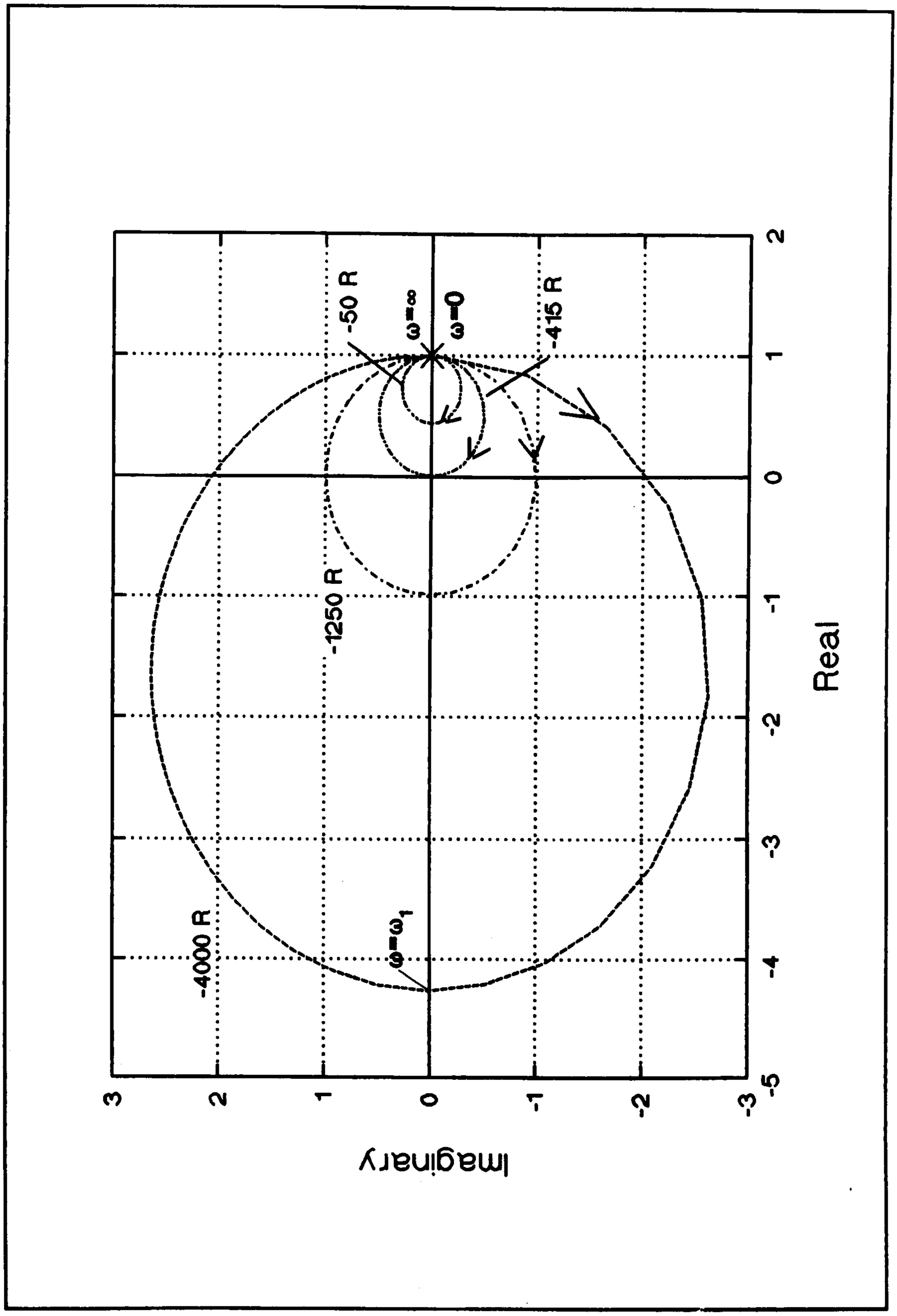

Figure 40. Nyquist plot of W(jw).D(jw) for optimum controller with reference u_{cone} and a KEF B200A loudspeaker for four values of z. Values of ω from 0 to $+\infty$. 1,j0 is not encircled: all systems are stable when loop is closed.

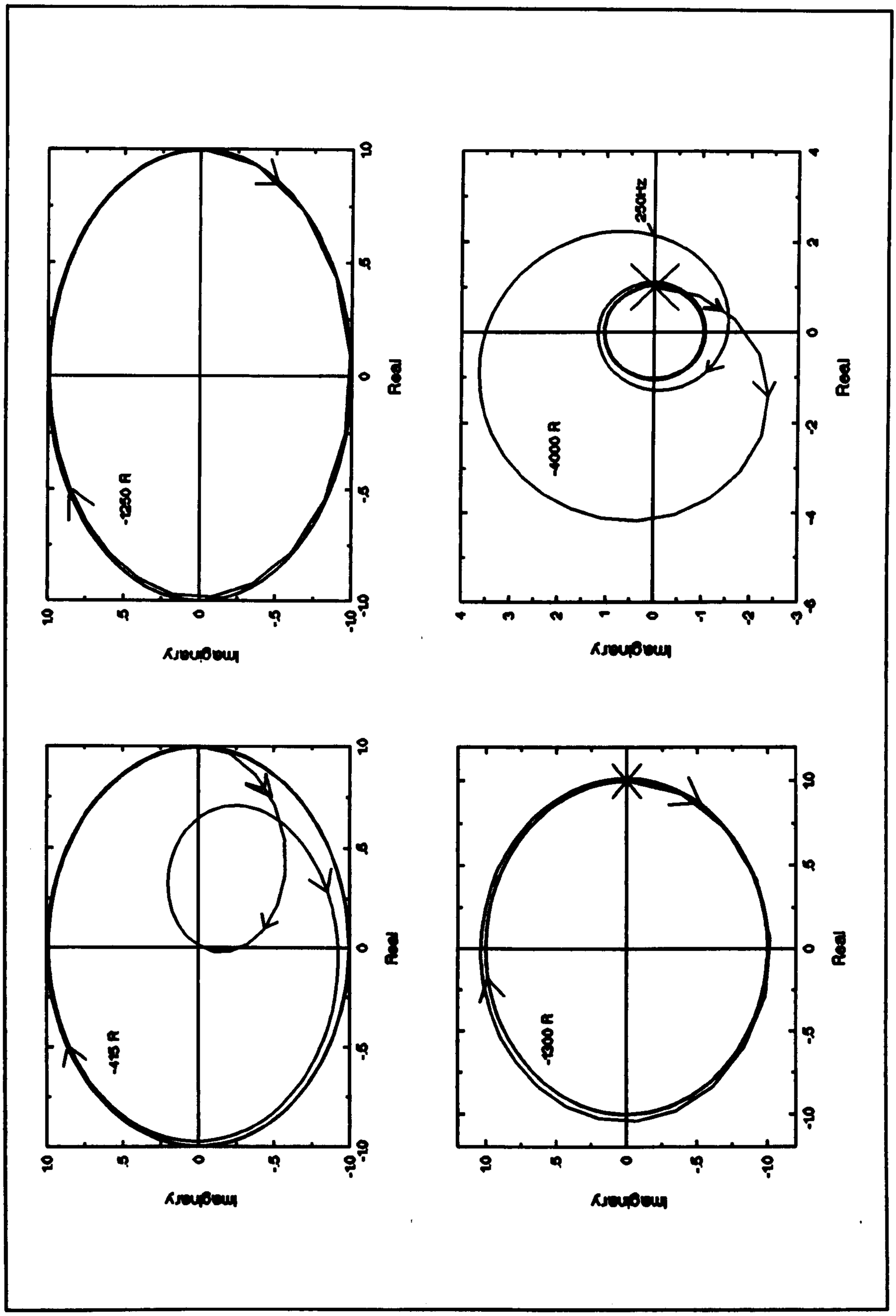

Figure 41. Nyquist plot of W(jw).D(jw) for controller with 1ms delay with reference u_{cone} and a KEF B200A loudspeaker for four values of z. Values of ω from 0 to $+\infty$. 1,j0 is enclosed for z < -1250 Rayls.

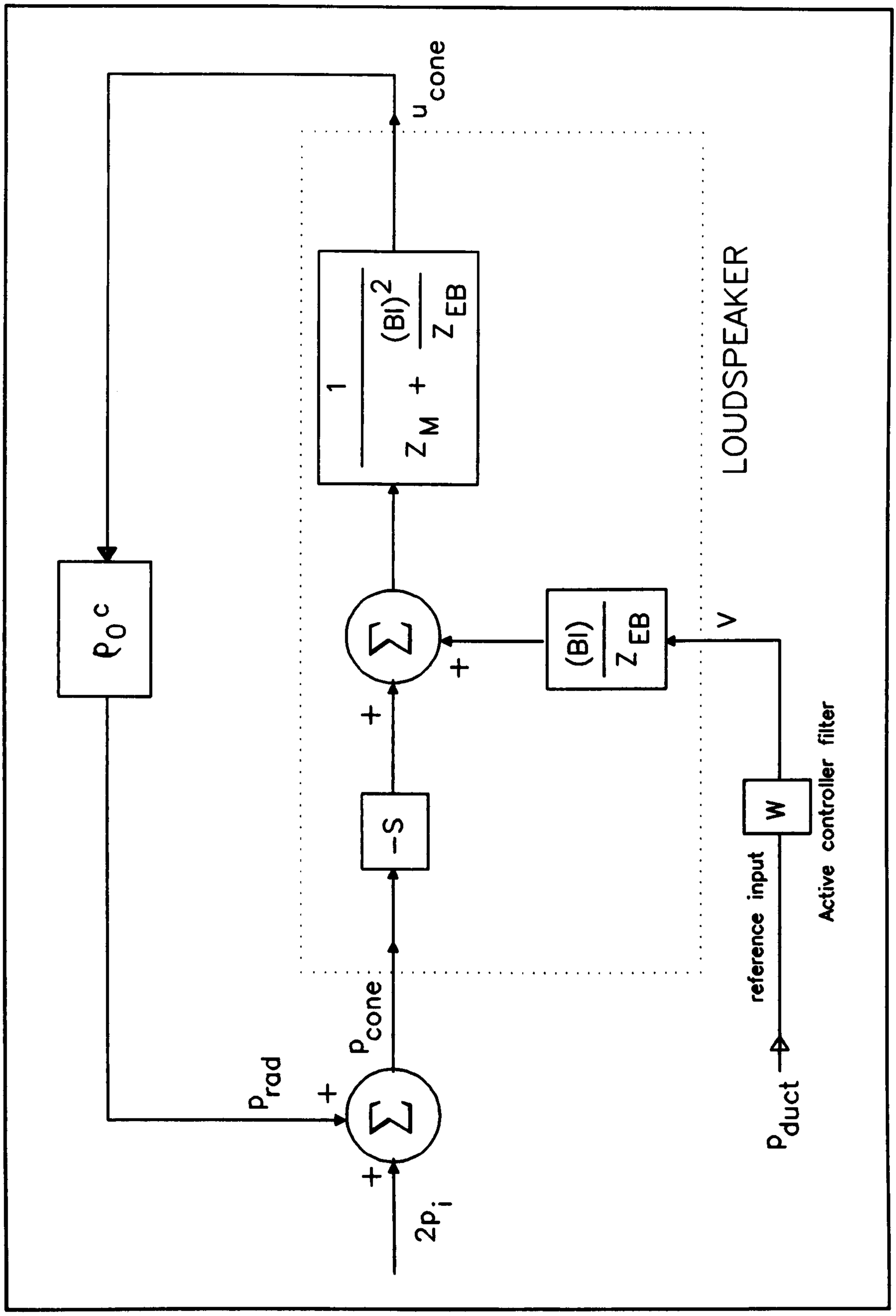

Figure 42. The pressure & velocity relationship at the surface of a loudspeaker cone excited by incident acoustic wave p_i. The reference signal is the pressure in the duct at d metres from the cone

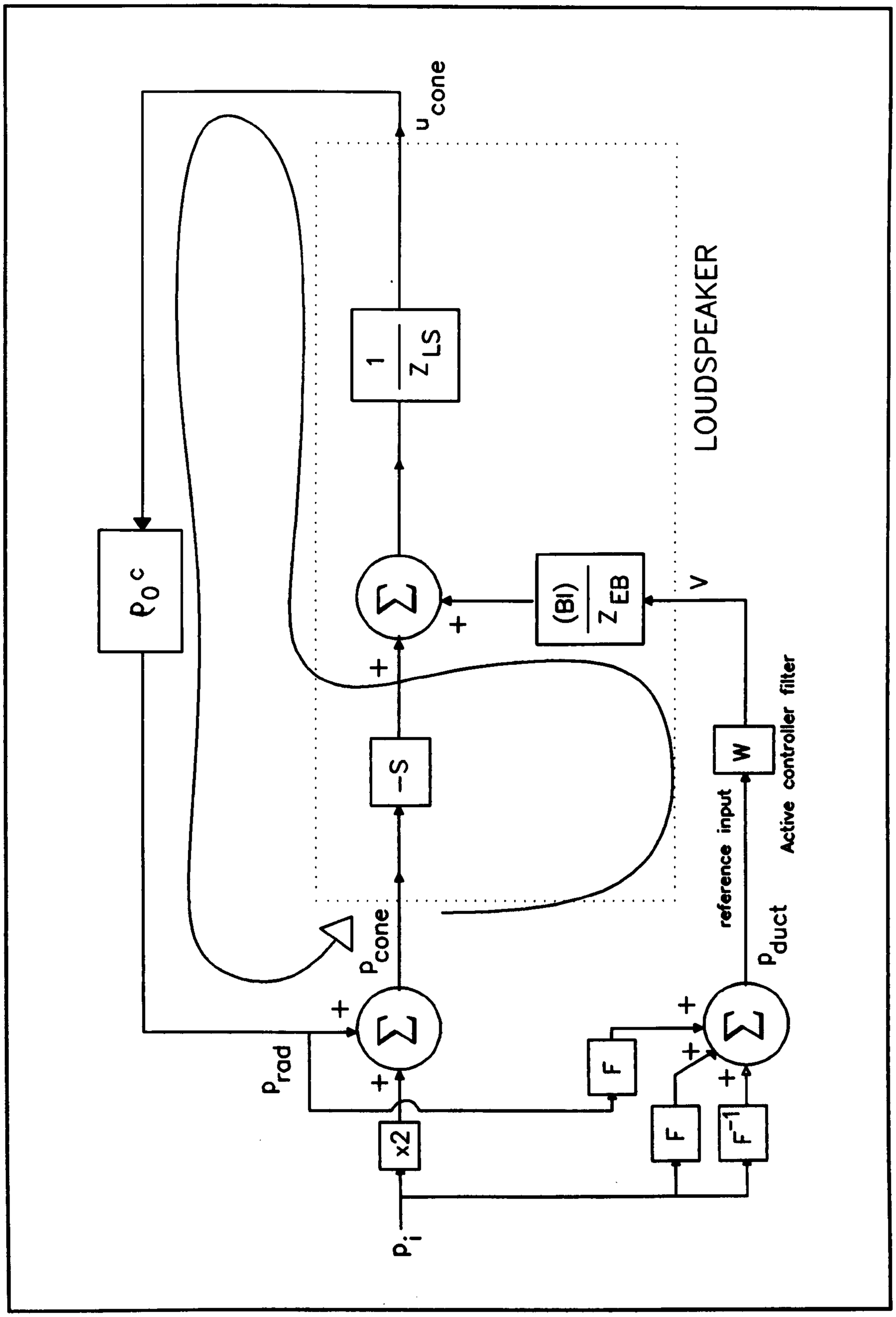

Figure 43. The pressure & velocity relationship at the surface of a loudspeaker cone excited by incident acoustic wave p_i. A feedback path exists around W shown by the curved line.

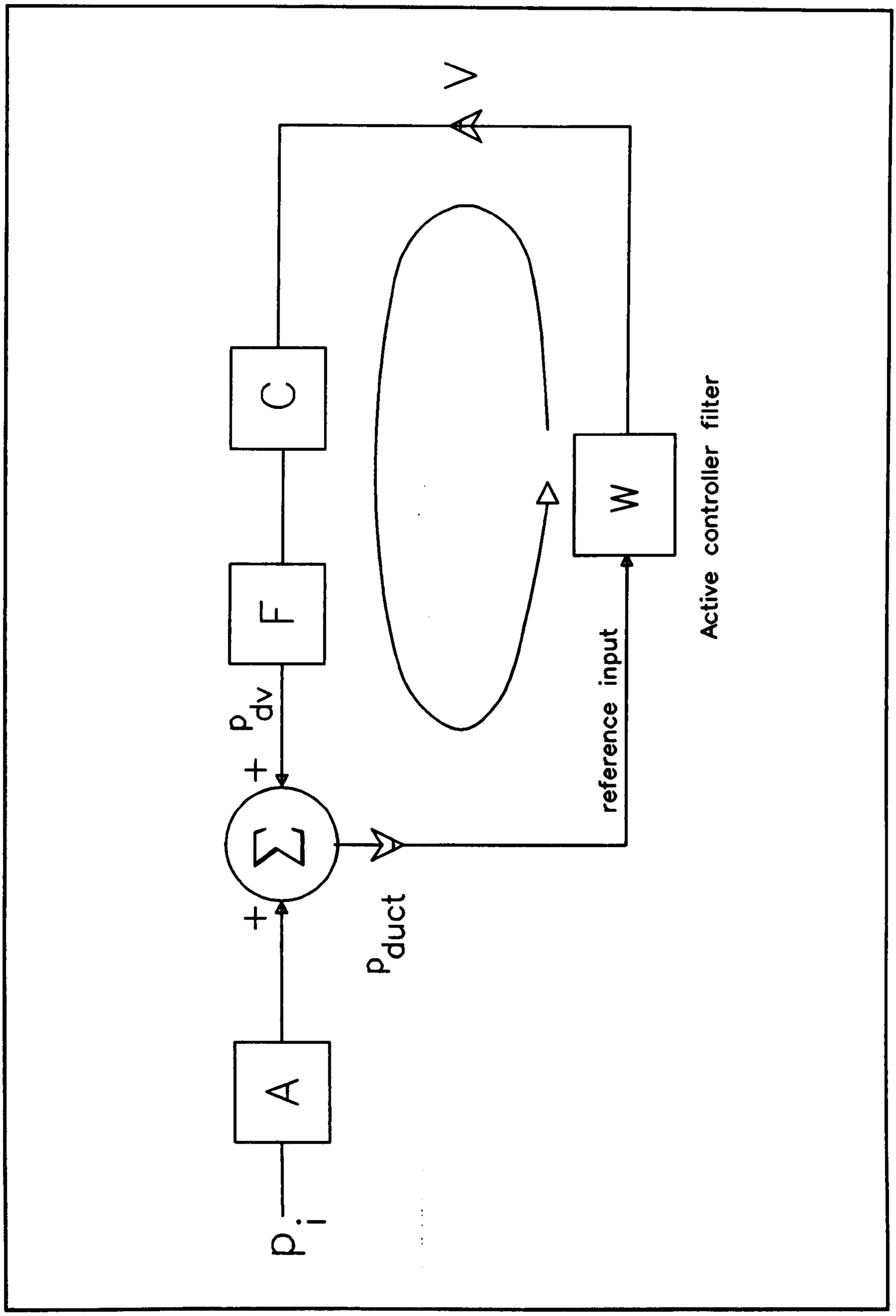

Figure 44. Schematic of the cone pressure at the surface of a loudspeaker cone excited by incident pressure $\mathbf{p_i}$ and controller voltage **V**. Feedback loop around **W** is shown by curved line.

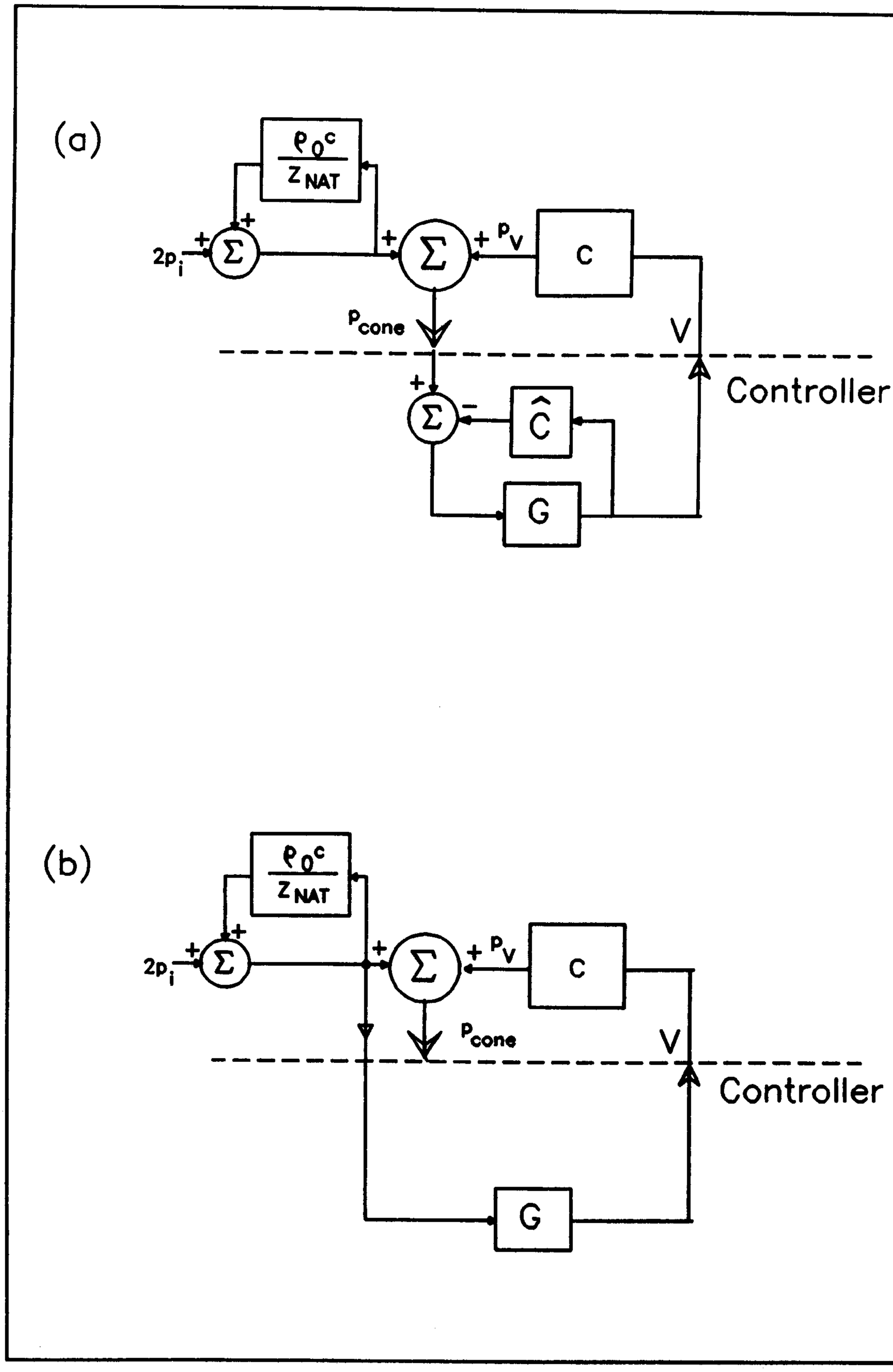

Figure 45. Active controller with cone pressure as reference with feedback cancellation filter $\hat{C}$ (a). If cancellation is exact then effective input to G is shown in (b).

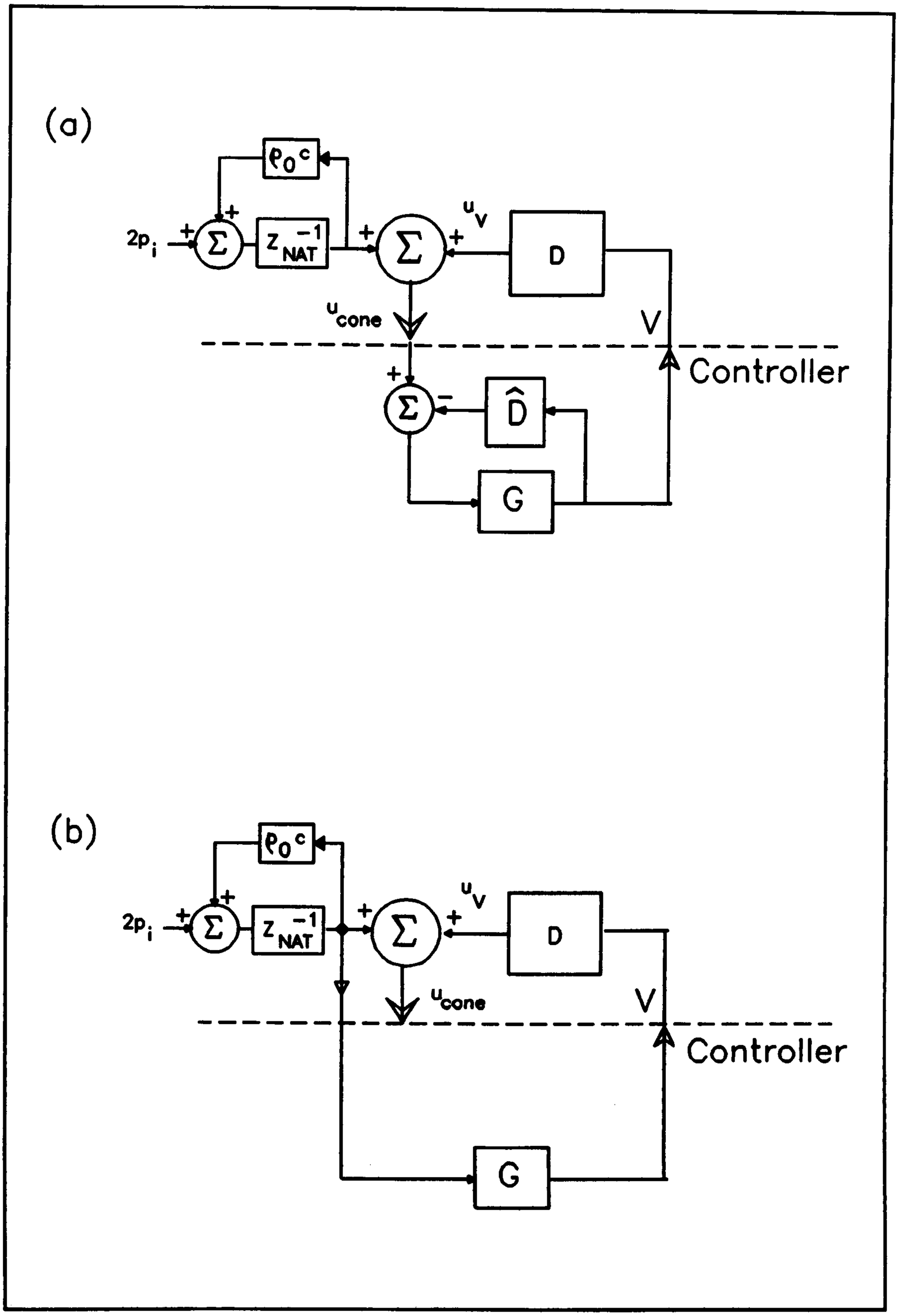

Figure 46. Active controller with cone velocity as reference with feedback cancellation filter $\hat{D}$ (a). If cancellation is exact then effective input to G is shown in (b).

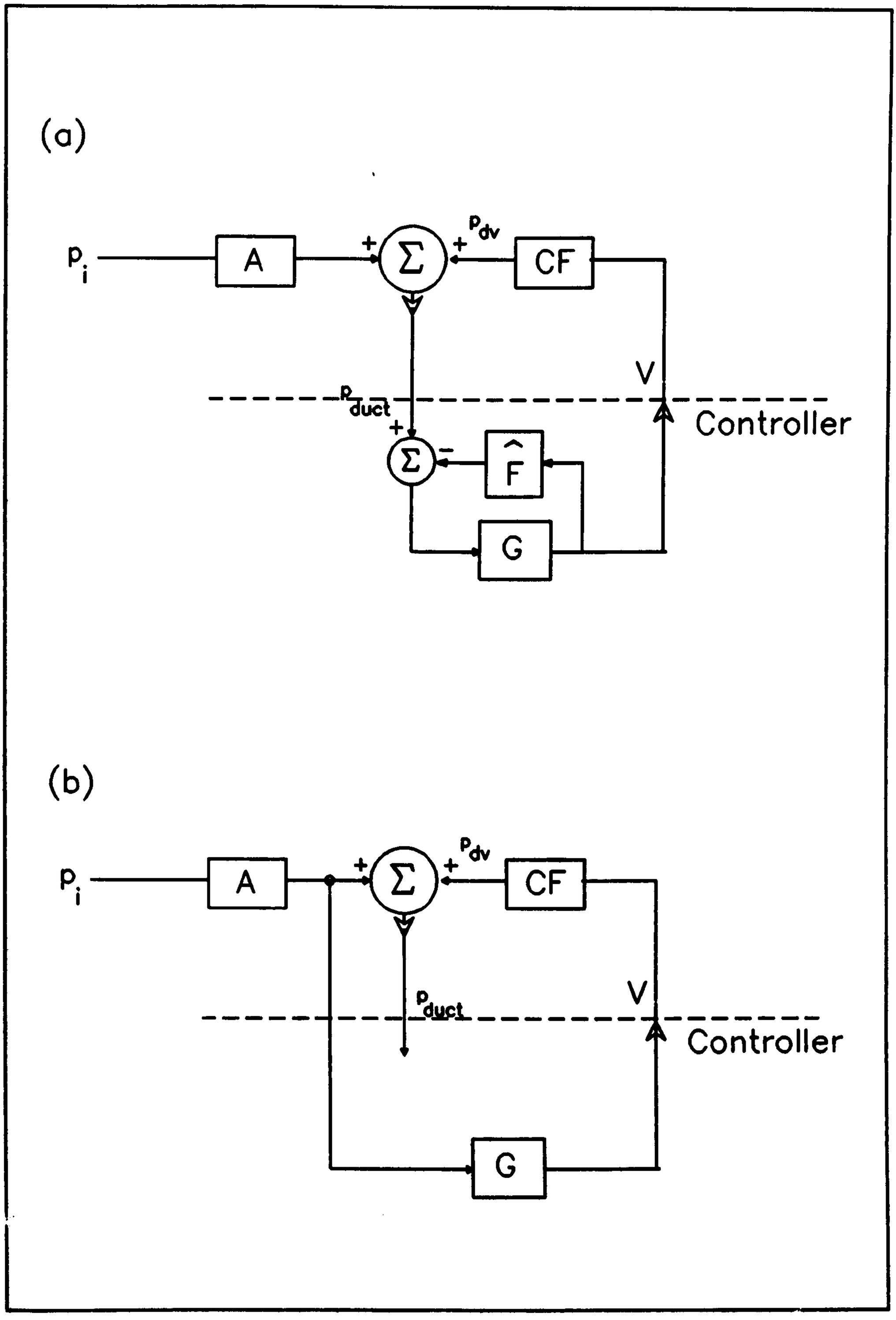

Figure 47. Active controller for duct pressure as reference with feedback cancellation filter $\hat{F}$ (a). If cancellation is exact then effective input to G is shown in (b).

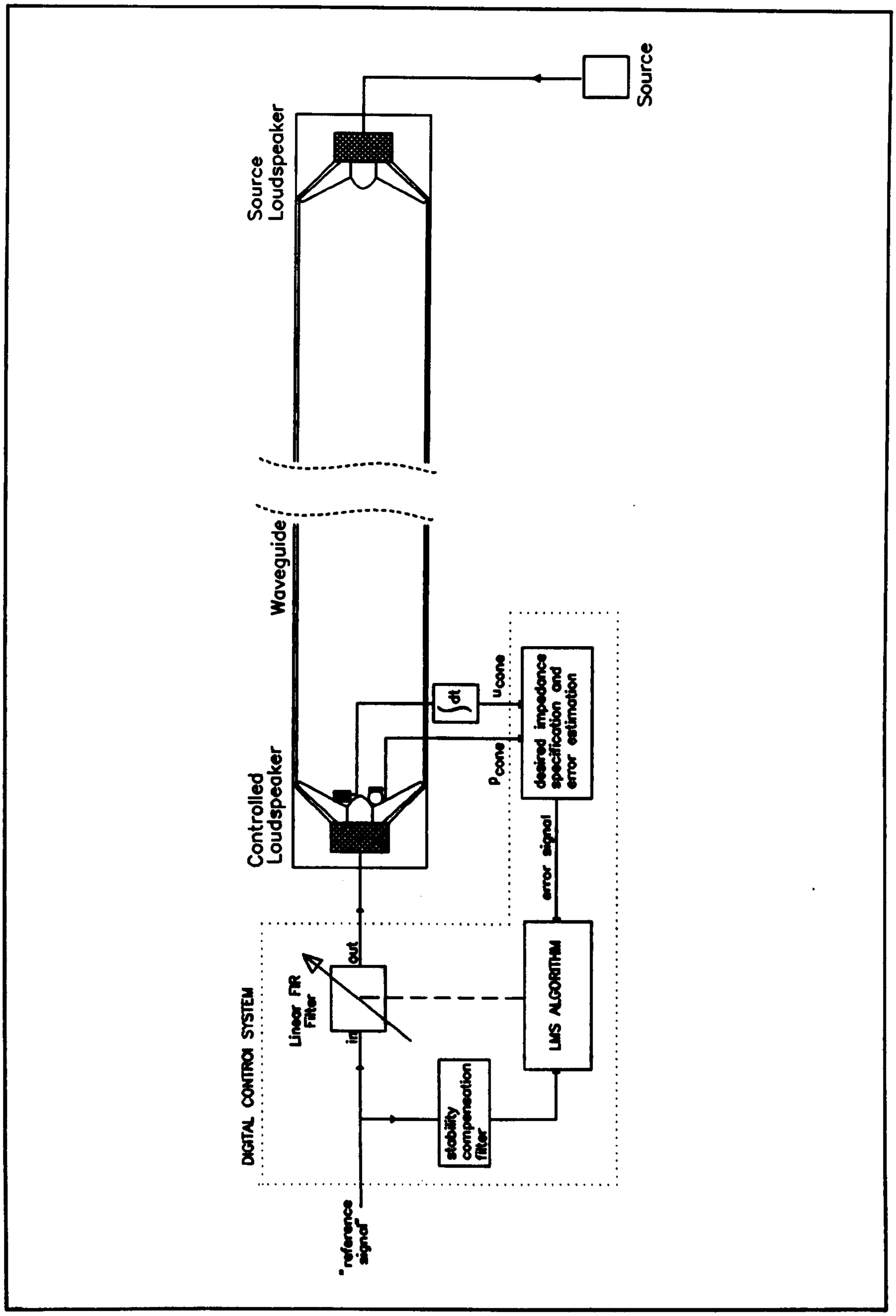

Figure 48. Mic-accr acoustic impedance control system based on the filtered-X LMS adaptive algorithm. The selection of the reference signal affects system performance.

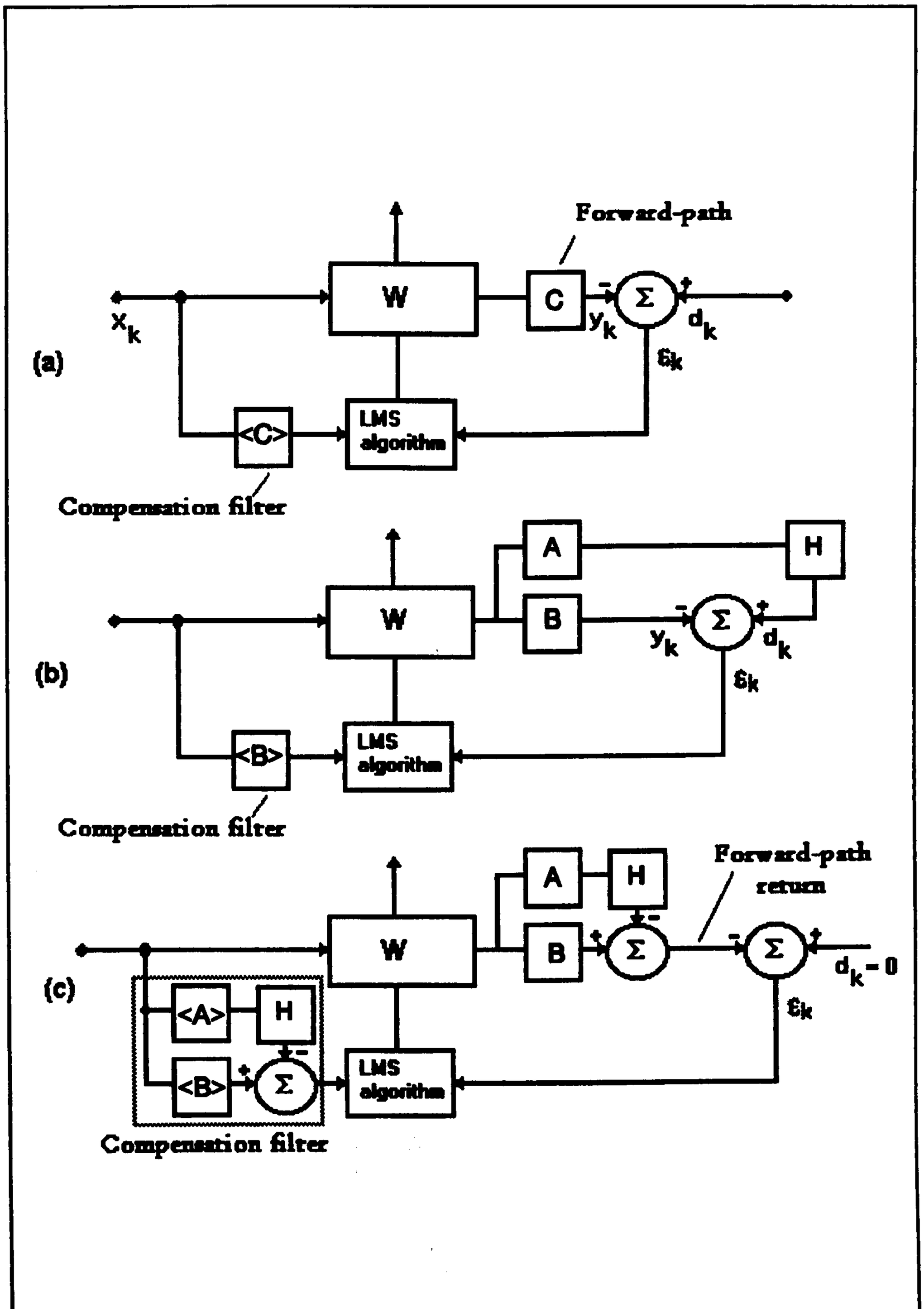

Figure 49. Development of the compensation filter for the mic-accr control system. (a) shows a typical filtered-X LMS implementation. Mic-accr control system (c) has more stable adaptive convergence than (b).

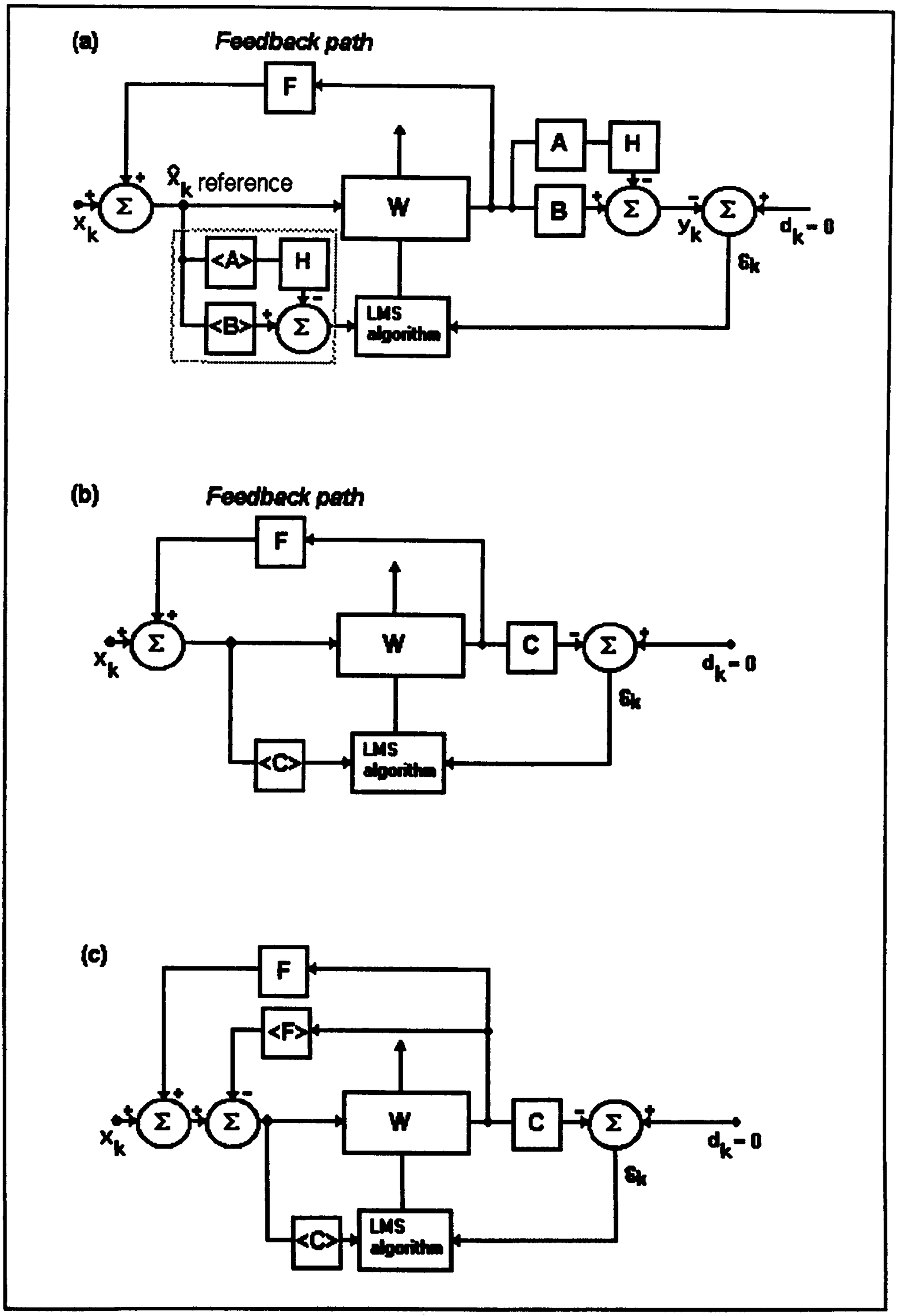

Figure 50. Feedback path around the mic-accr control system. (a) shows full mic-accr filtered-X LMS implementation, (b) is simplified. (c) shows feedback cancellation filter <F>.

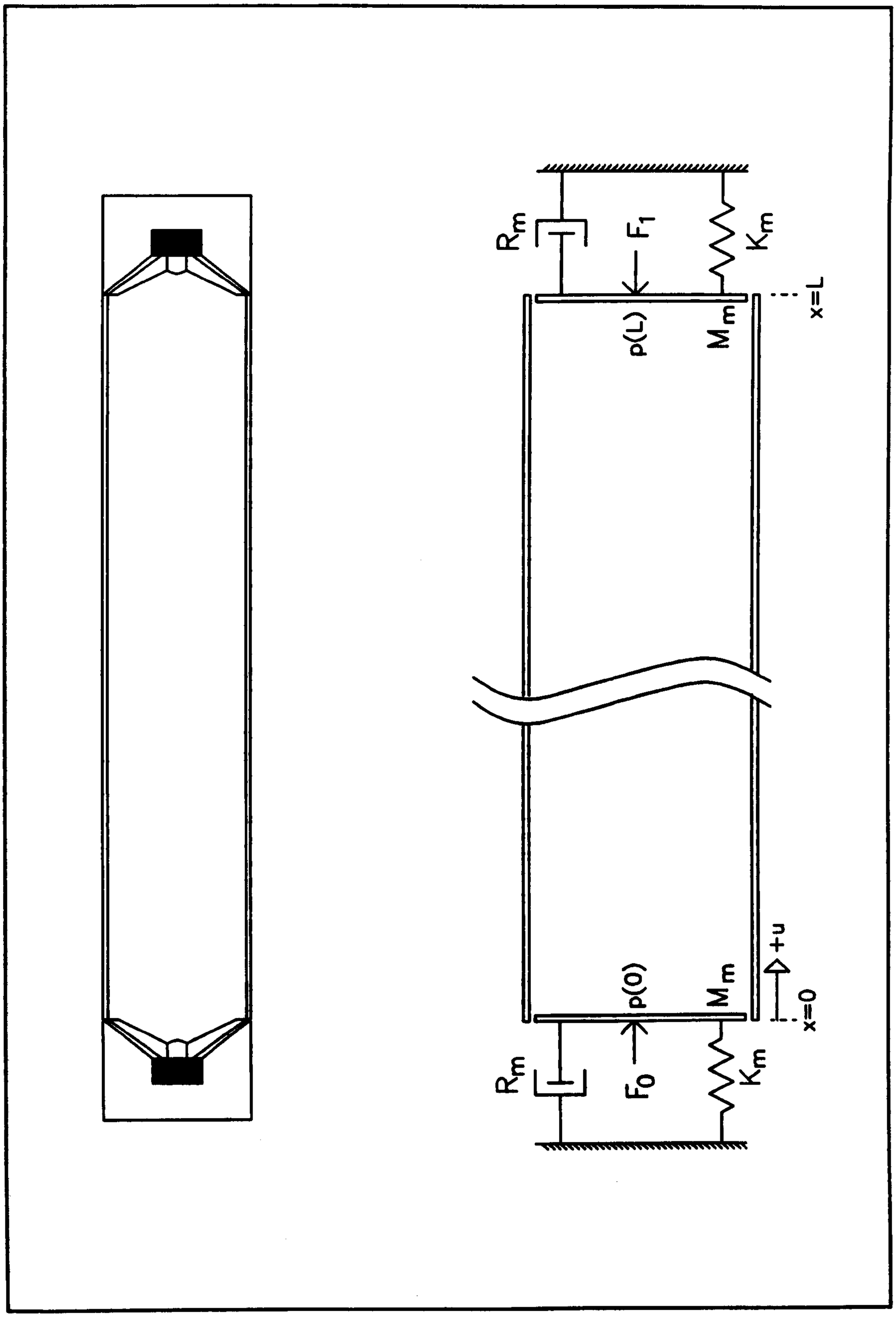

Figure 51. Schematic of the laboratory test-rig. Consists of a duct terminated at either end by a loudspeaker. Lower diagram shows the mechanical components of the terminations.

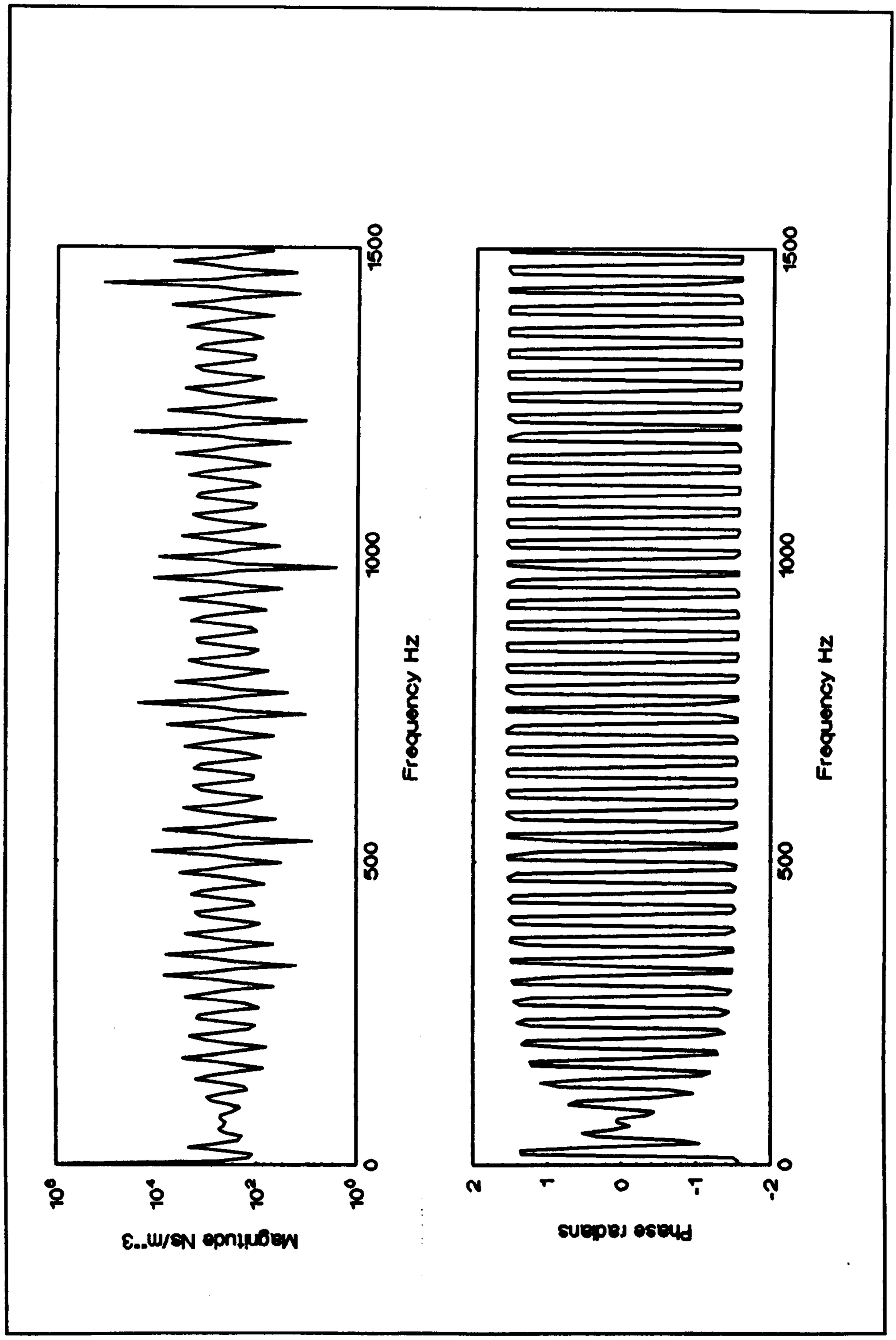

Figure 52. Frequency-domain theoretical specific acoustic input impedance of a 5 metre loss-less duct terminated by a KEF B200A loudspeaker.

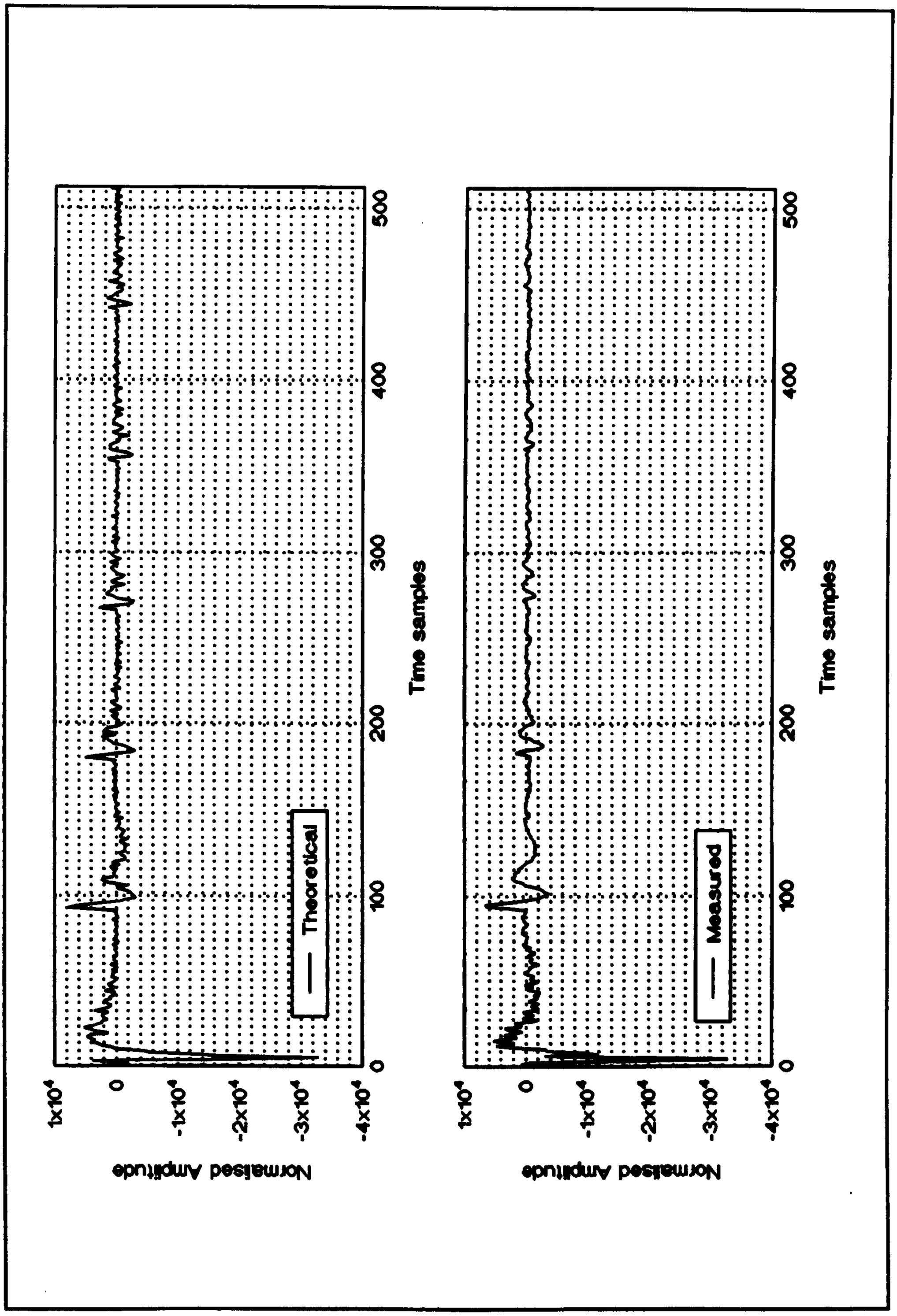

Figure 53. Impulse responses between cone velocity and voltage applied to voice-coil. Upper graph shows theoretical, lower shows measured response from laboratory test-rig.

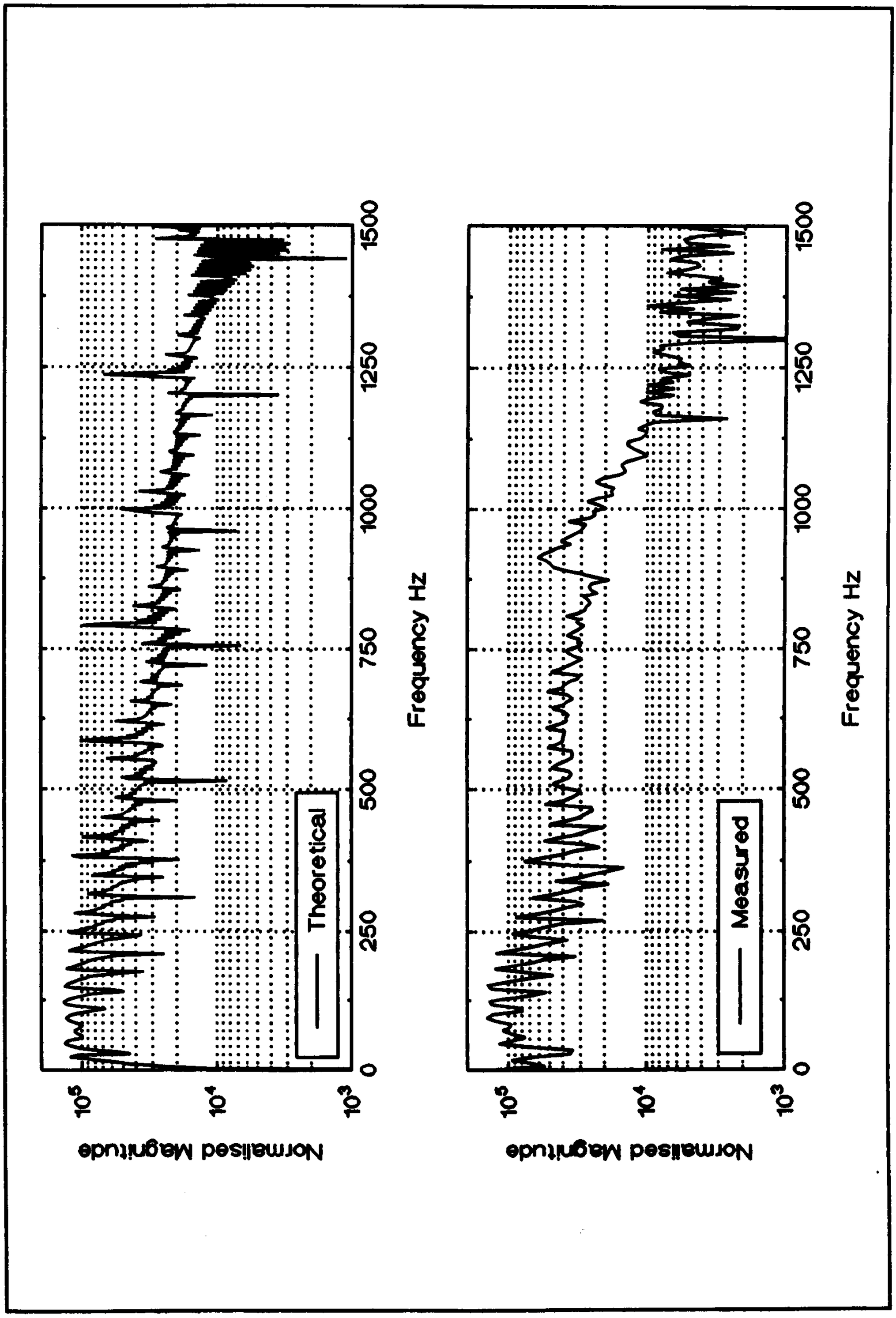

Figure 54. Frequency domain magnitude transfer function of the relationship between cone velocity and voltage applied to voice-coil. Upper graph shows theoretical and lower shows measured response.

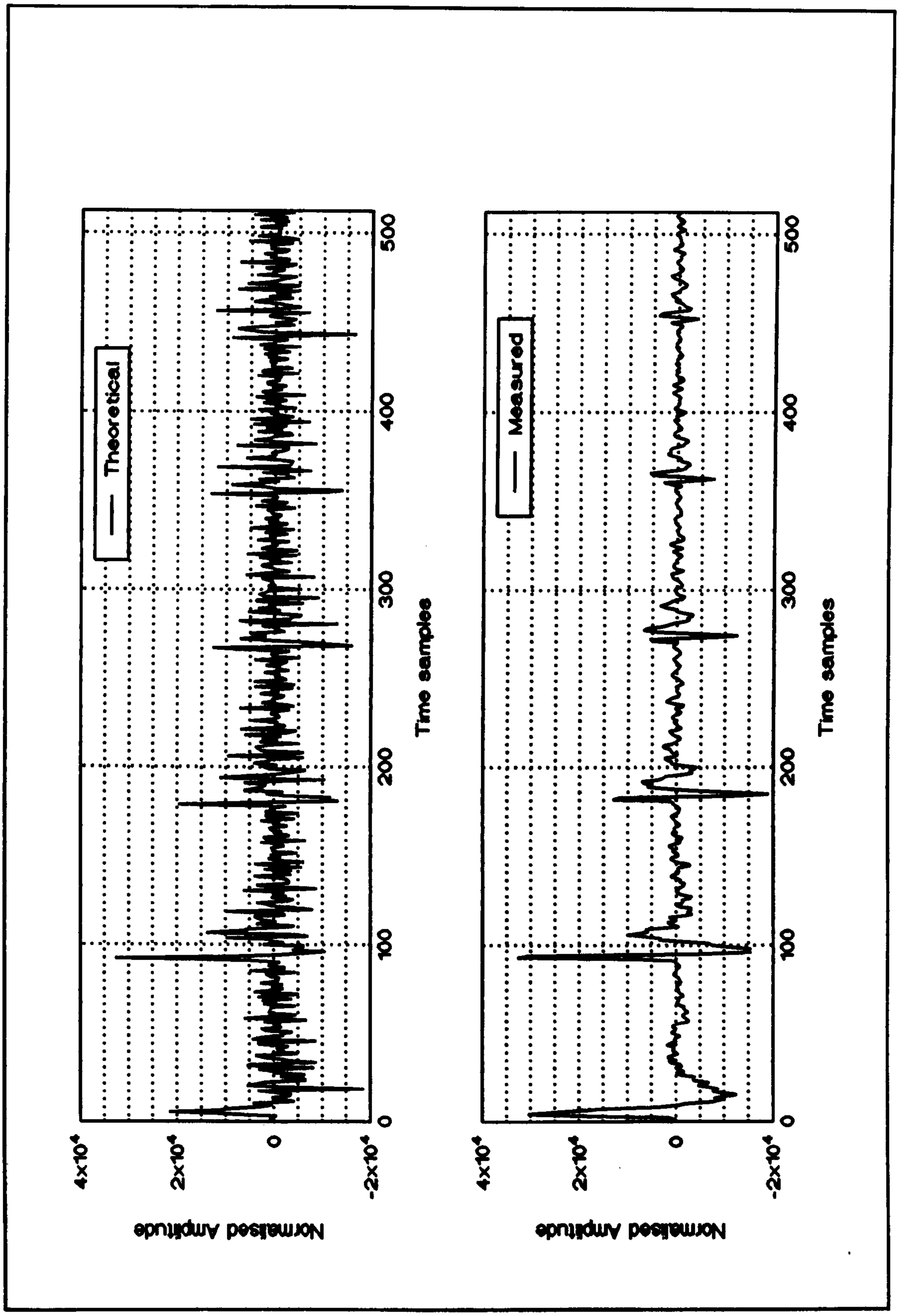

Figure 55. Time domain impulse responses for the relationship between cone pressure and voltage applied to voice-coil. Upper graph shows theoretical response, lower graph shows measured result from laboratory test-rig.

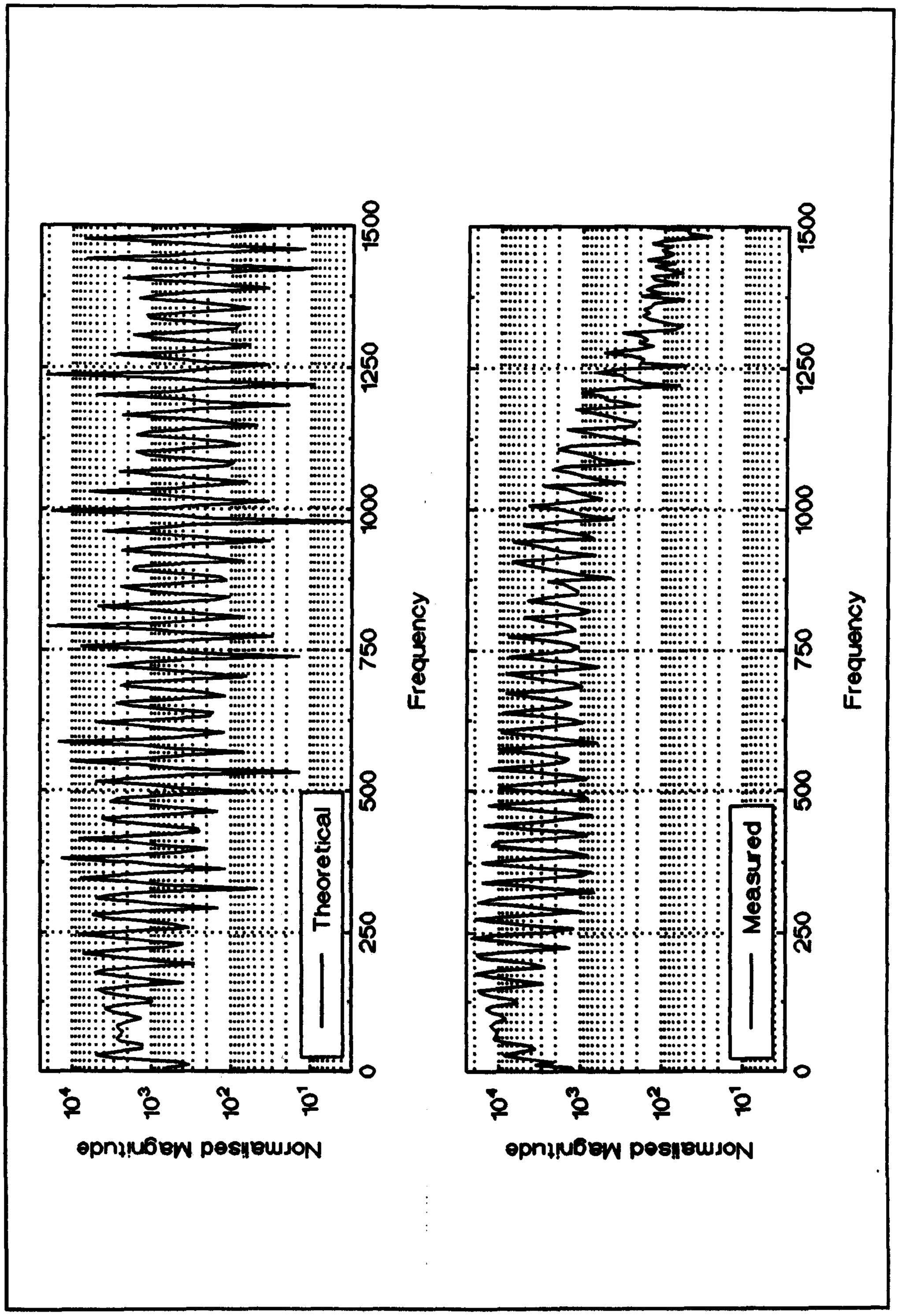

Figure 56. Frequency domain magnitude transfer function of the relationship between cone pressure and voltage applied to voice-coil. Upper graph shows theoretical and lower shows measured response.

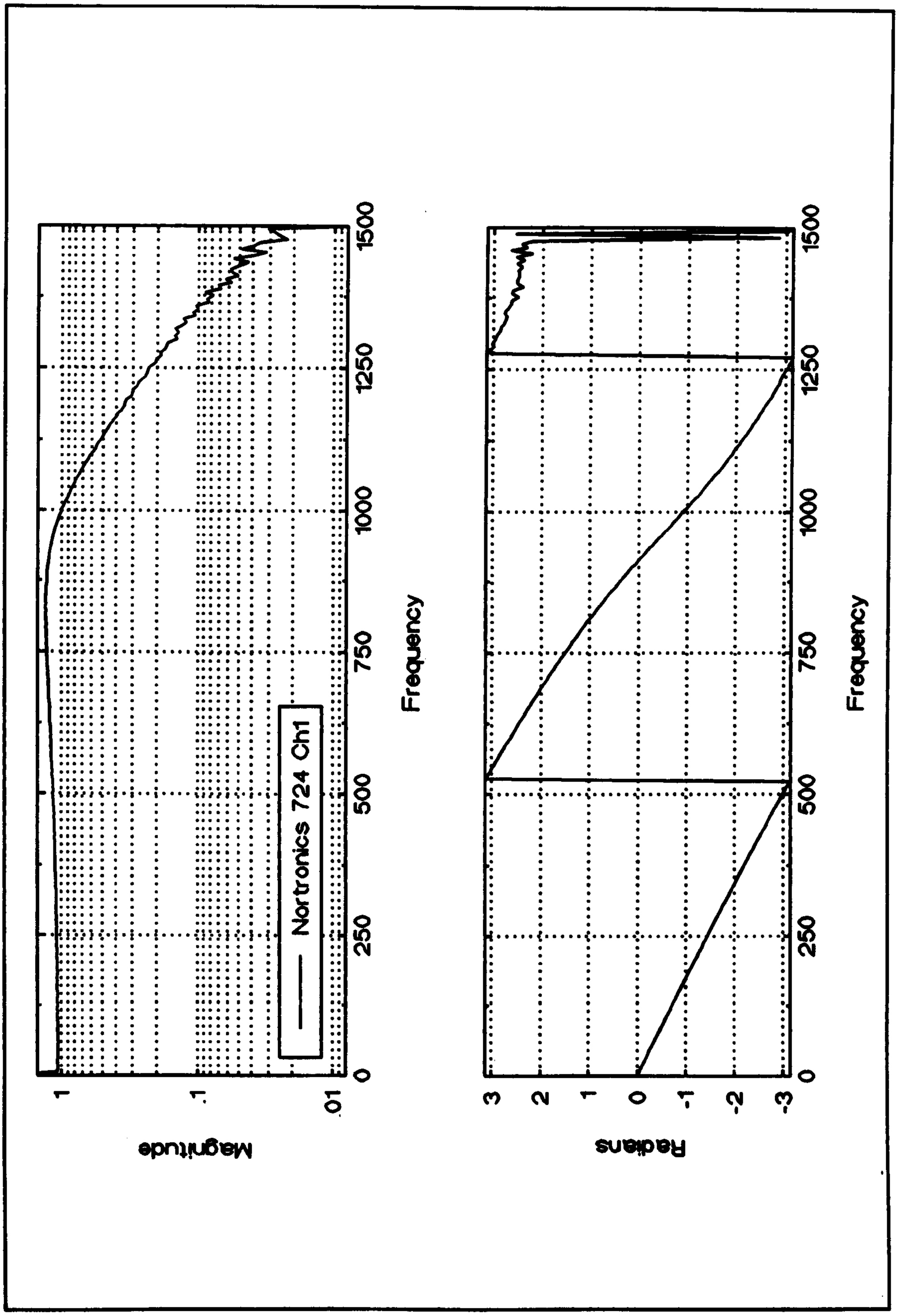

Figure 57. Reconstruction filter transfer function used in the laboratory test-rig. This measured with MLSSA measurement system. The filter is implemented by a digital filter set Nortronics 724, low pass bandwidth 1000Hz.

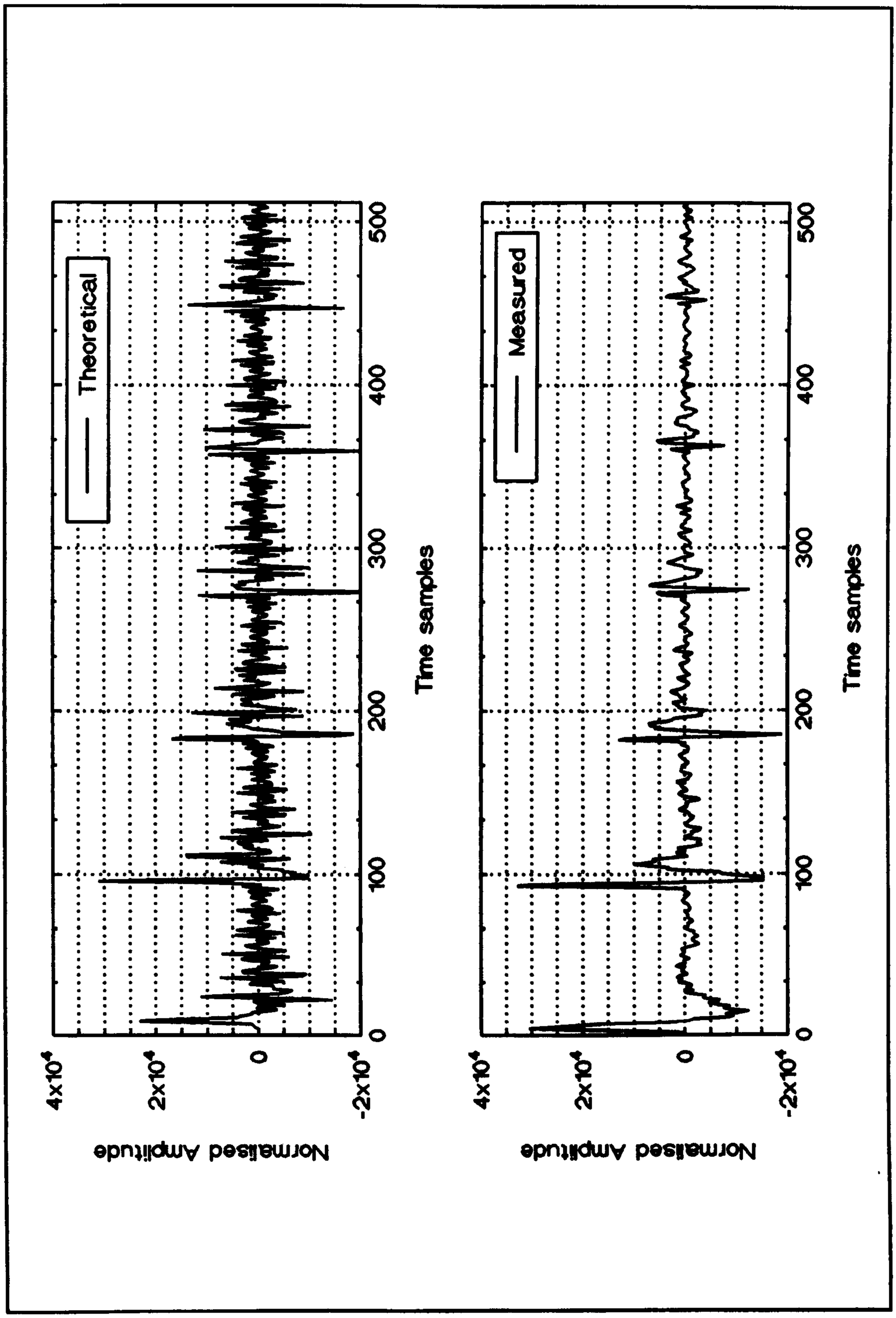

Figure 58. Impulse responses between cone pressure and voltage applied to voice-coil. Upper is theoretical response convoluted with measured reconstruction filter response, lower is measured result from laboratory test-rig.

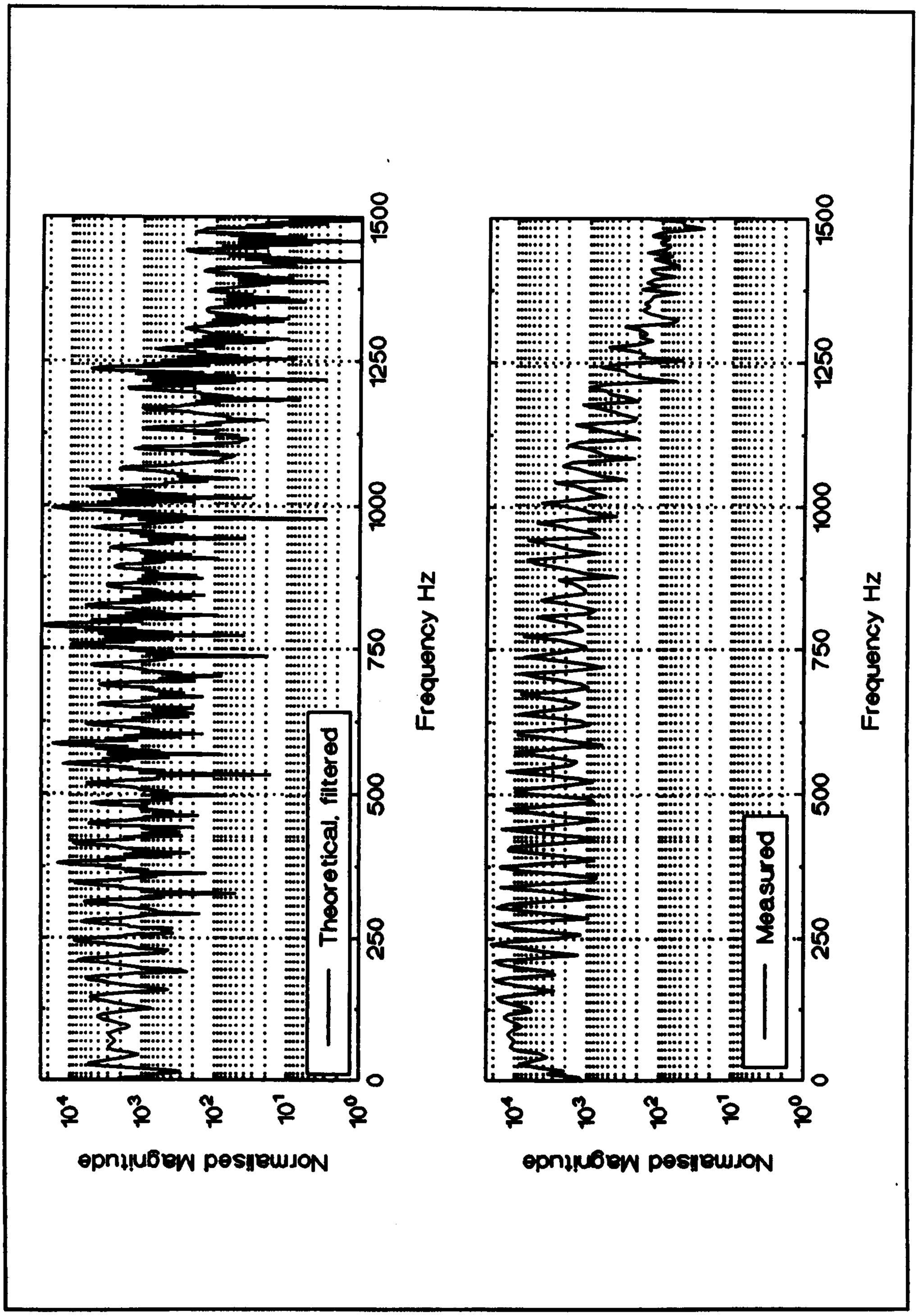

Figure 59. Frequency domain magnitude of the transfer function between cone pressure and voltage applied to voice-coil. Upper graph shows theoretical function filtered by measured reconstruction filter, lower shows measured response.

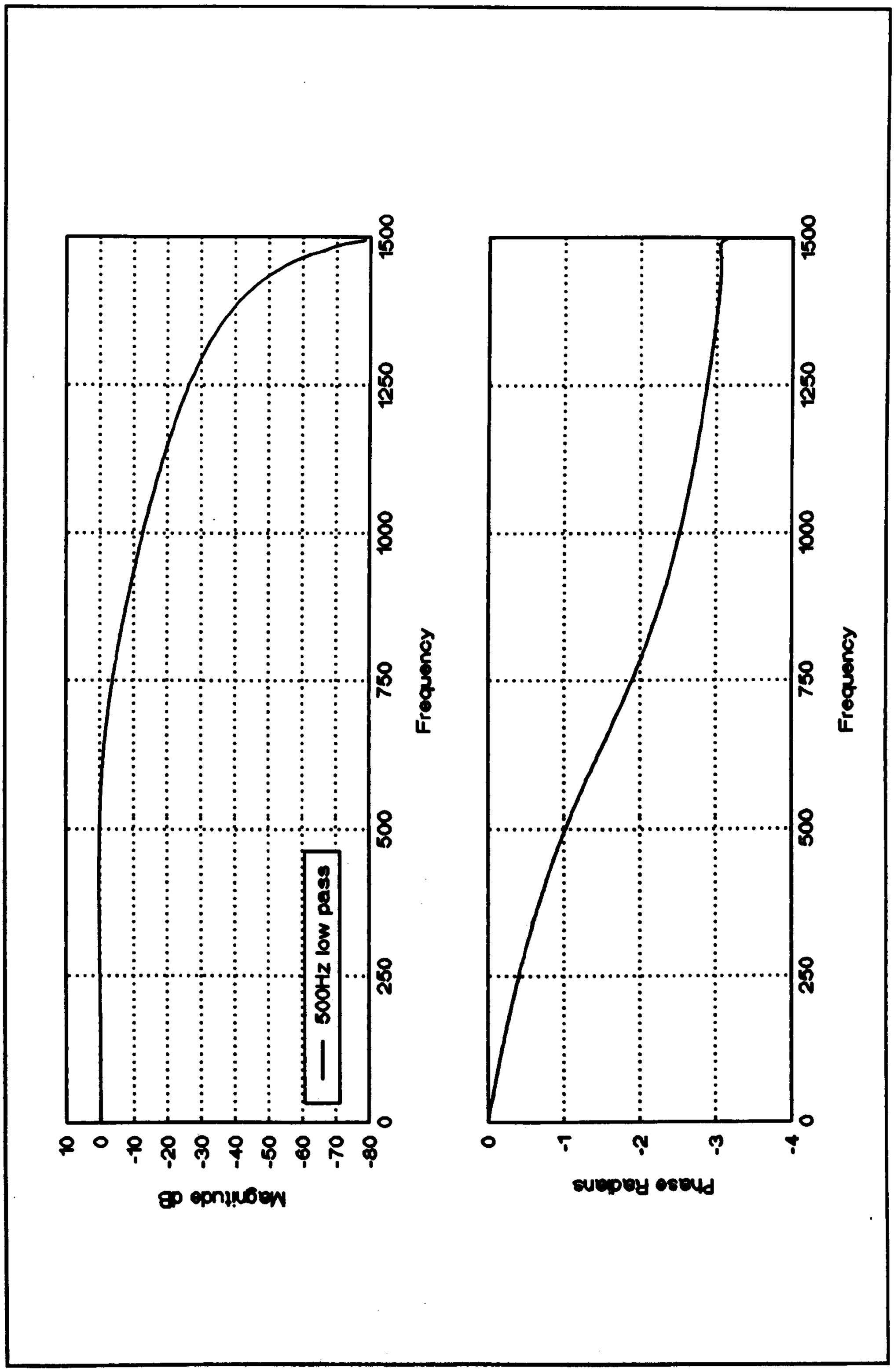

Figure 60. Magnitude and phase of low pass filter response.

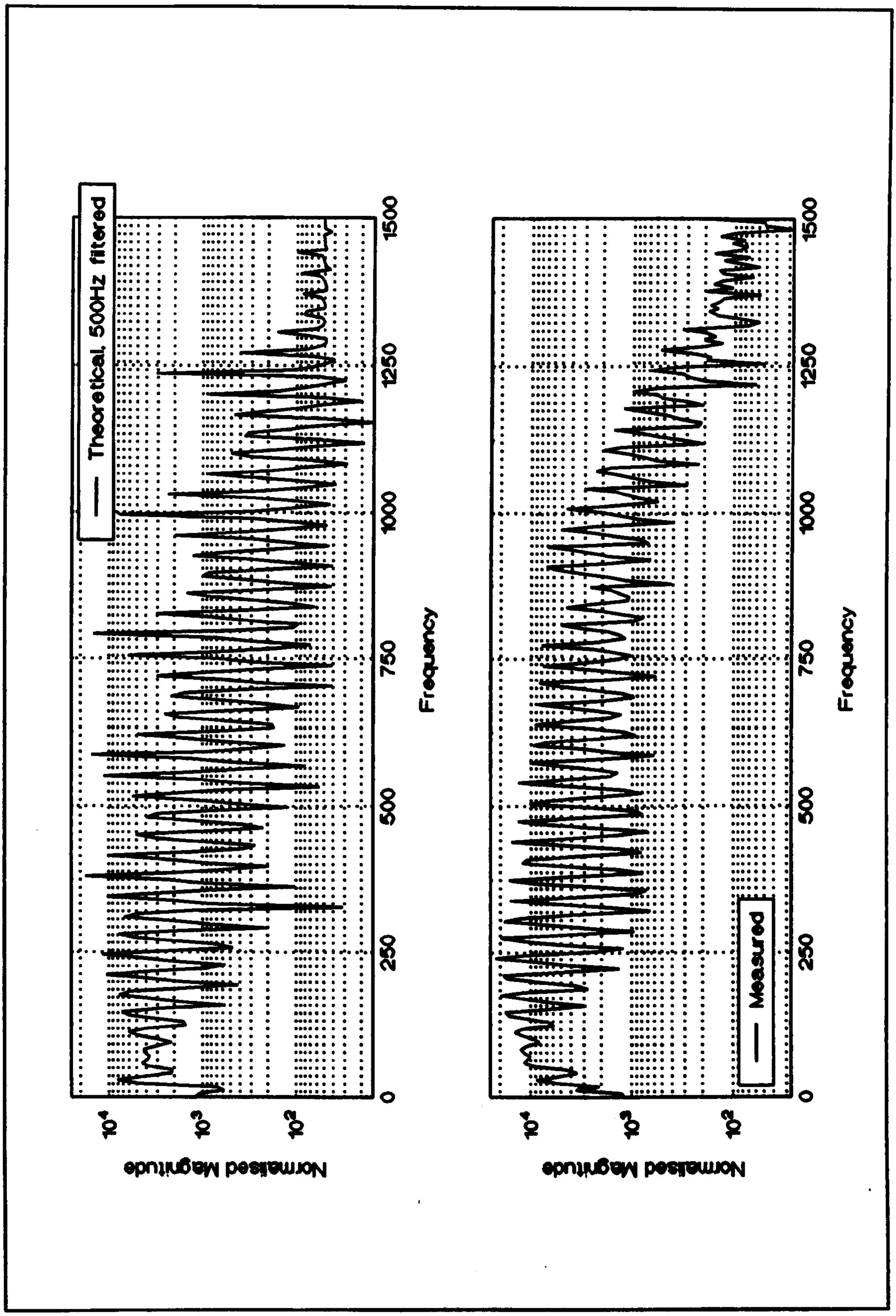

Figure 61. Frequency-domain magnitude of relationship between cone pressure and control voltage. Upper graph shows theoretical result with approximate weighting to reduce higher frequencies, lower graph shows measured result.

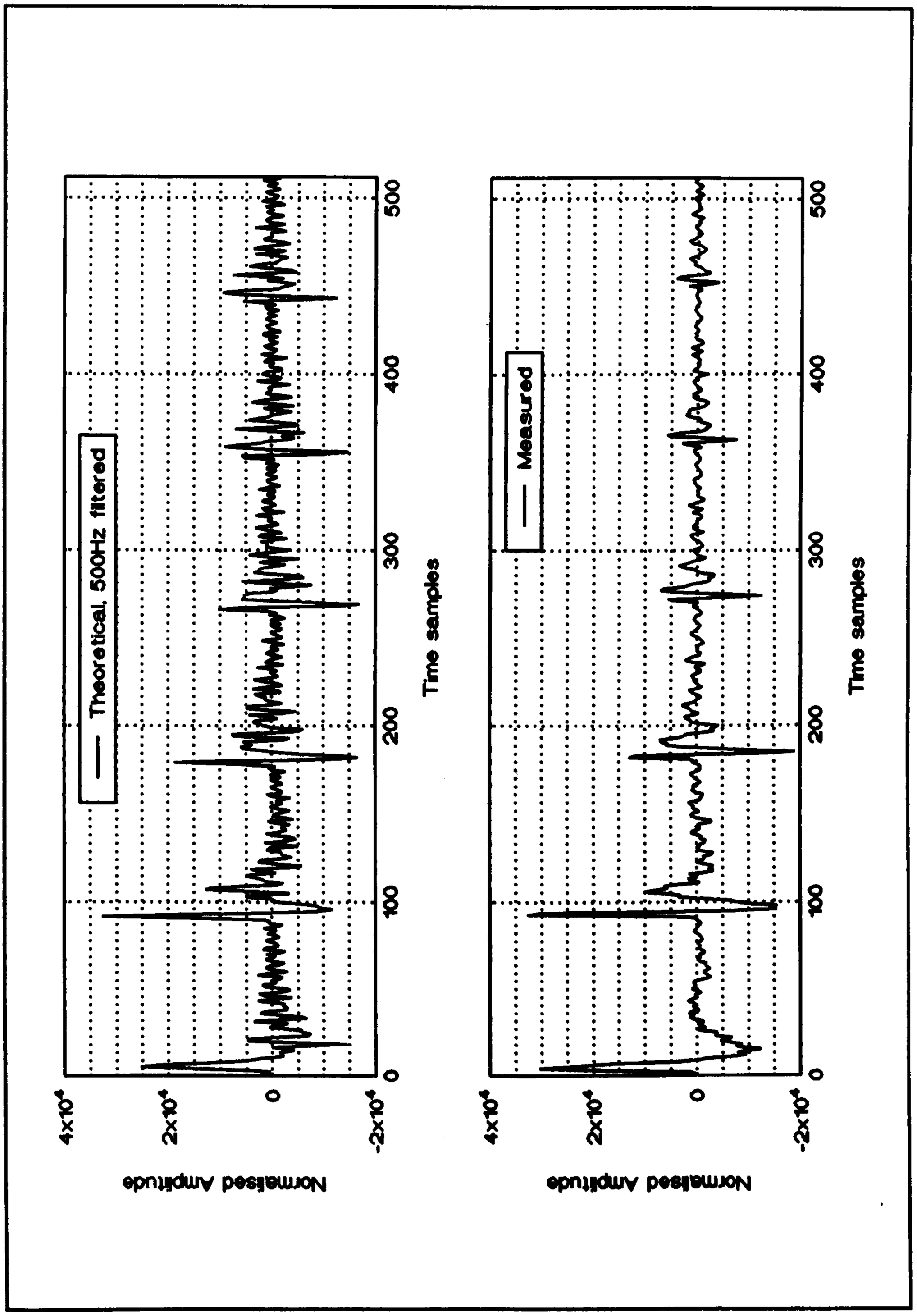

Figure 62. Time-domain impulse responses of the relationship between cone pressure and control voltage. Upper graph shows theoretical response with approximate weighting to reduce higher frequencies, lower graph shows measured response.

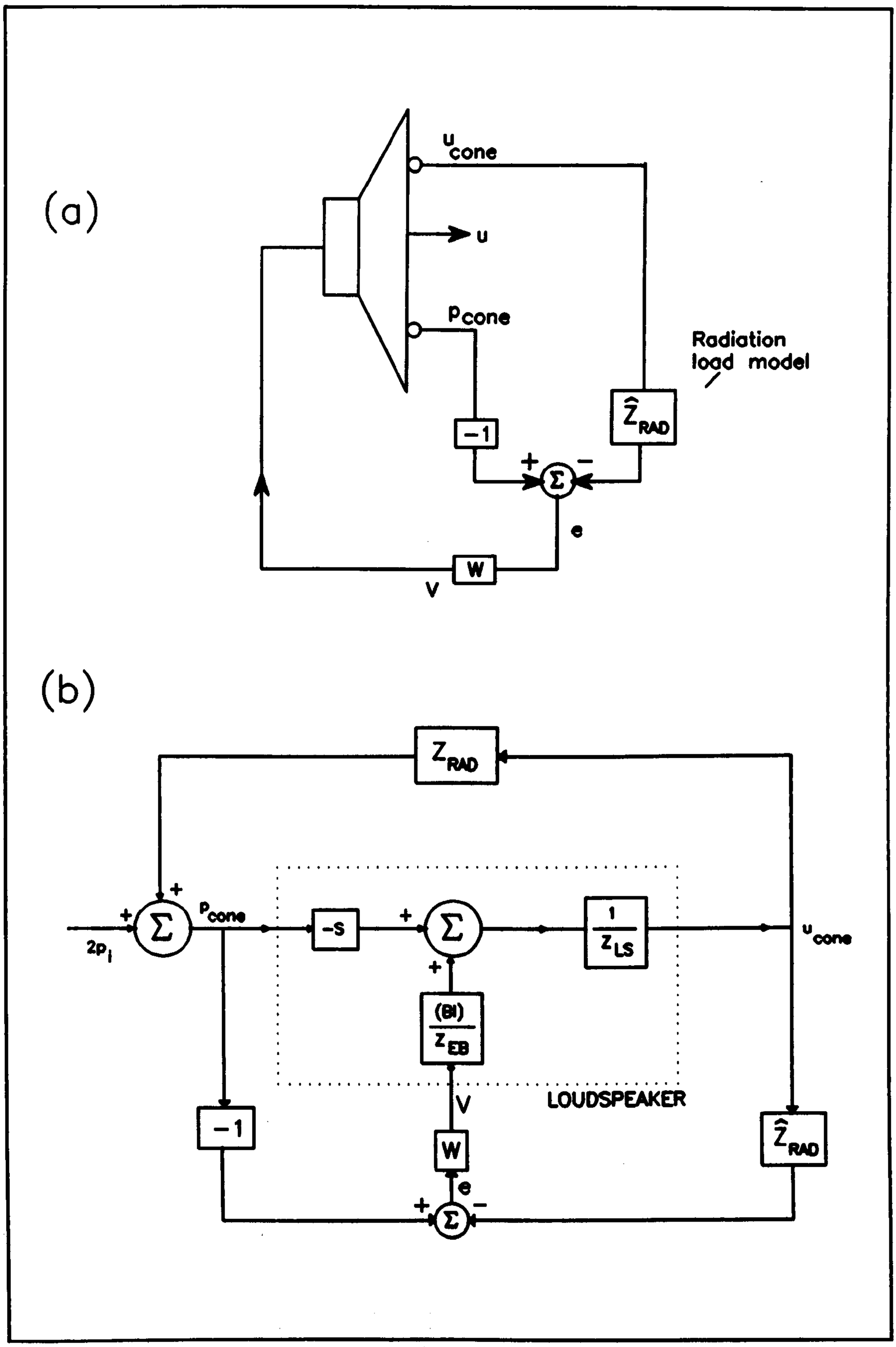

Figure 63. Acoustic absorption control system after Mazzola applied to conventional loudspeaker - schematic in (a), electro-acoustic model in (b).

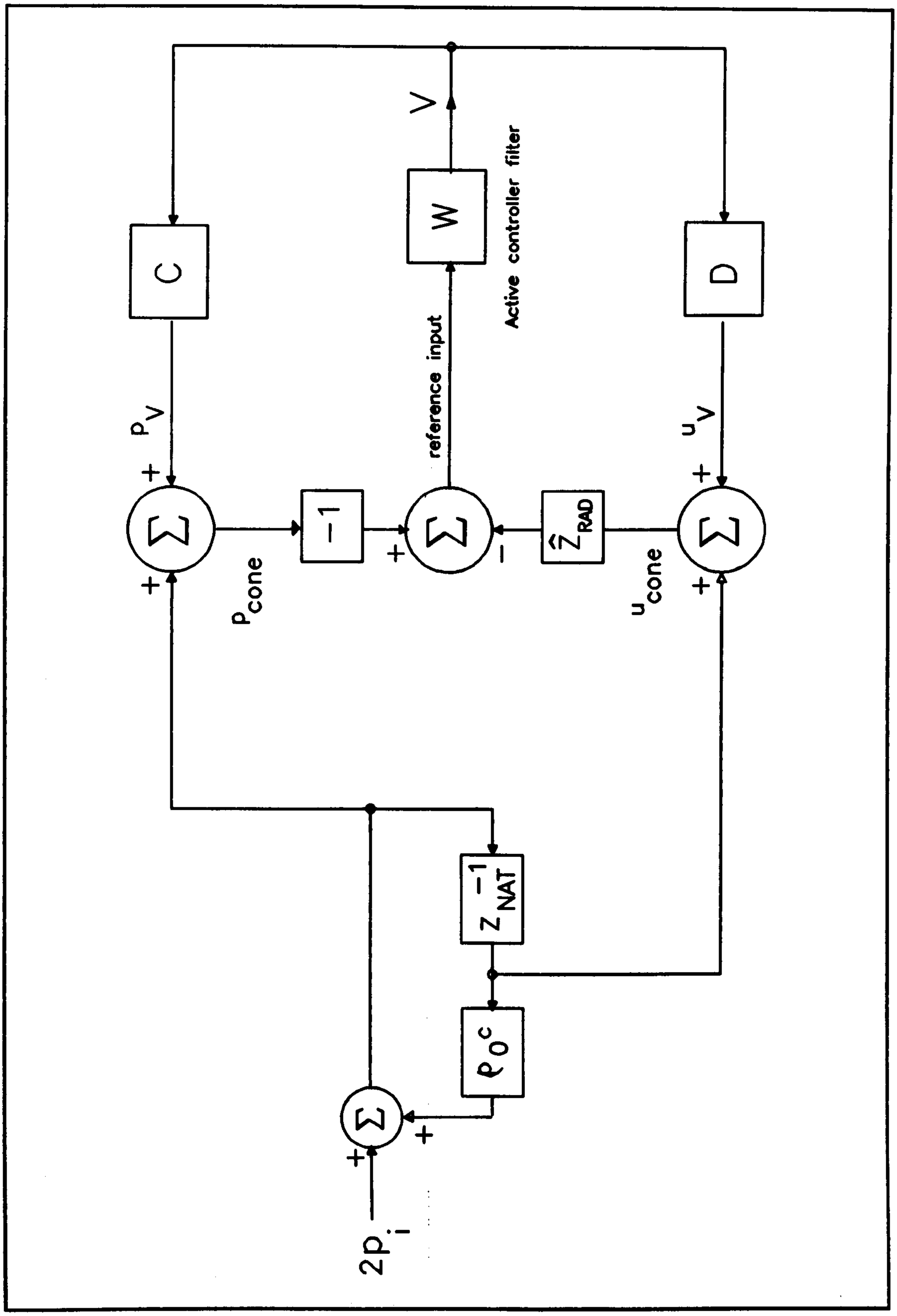

Figure 64. Schematic of the pressure and velocity at the surface of a loudspeaker cone excited by incident pressure p_i and controller voltage V for Mazzola's control system.

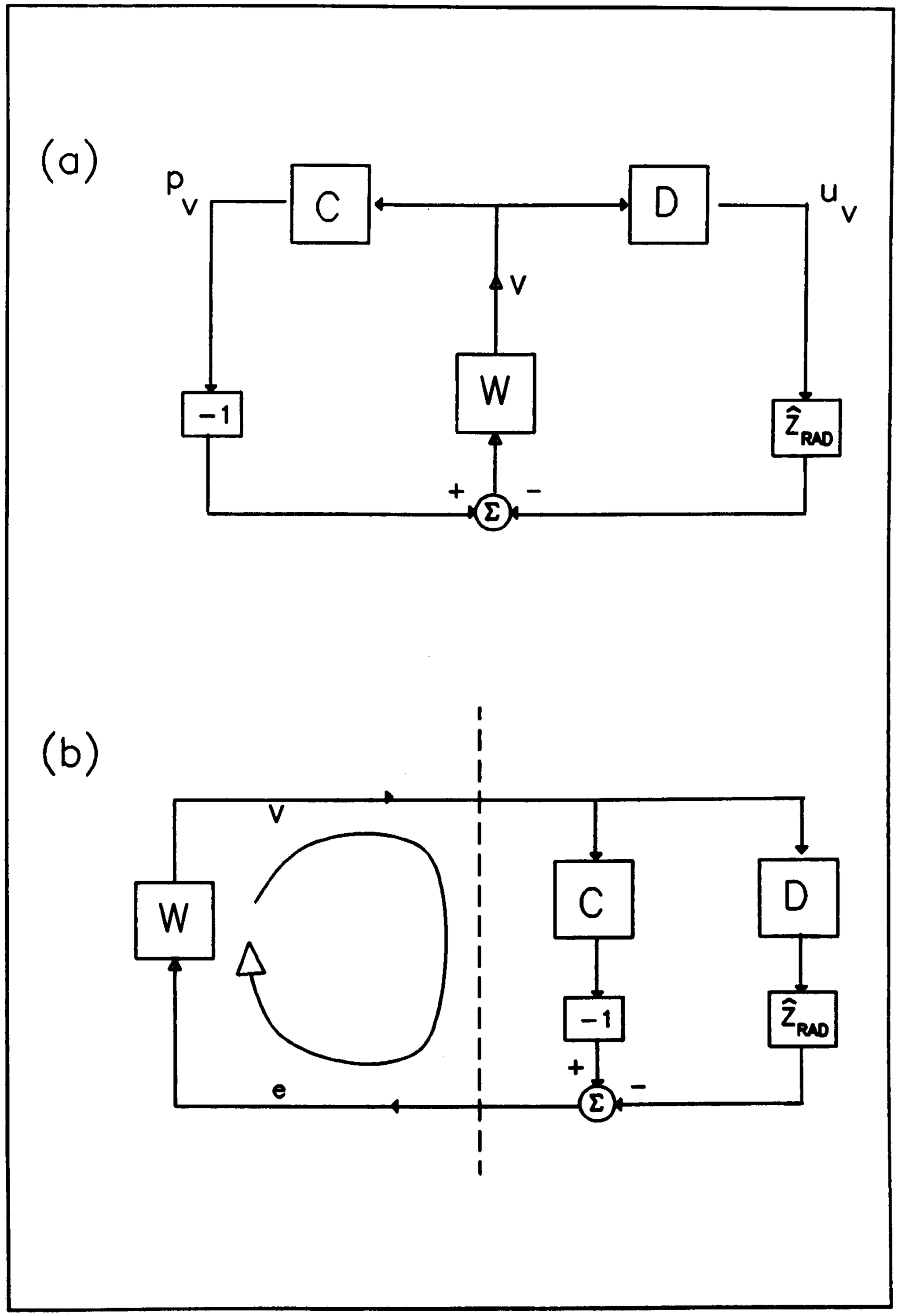

Figure 65. Identification of feedback path in Mazzola's control system applied to conventional loudspeaker - electro-acoustic model with zero incident pressure (a), redrawn in (b).

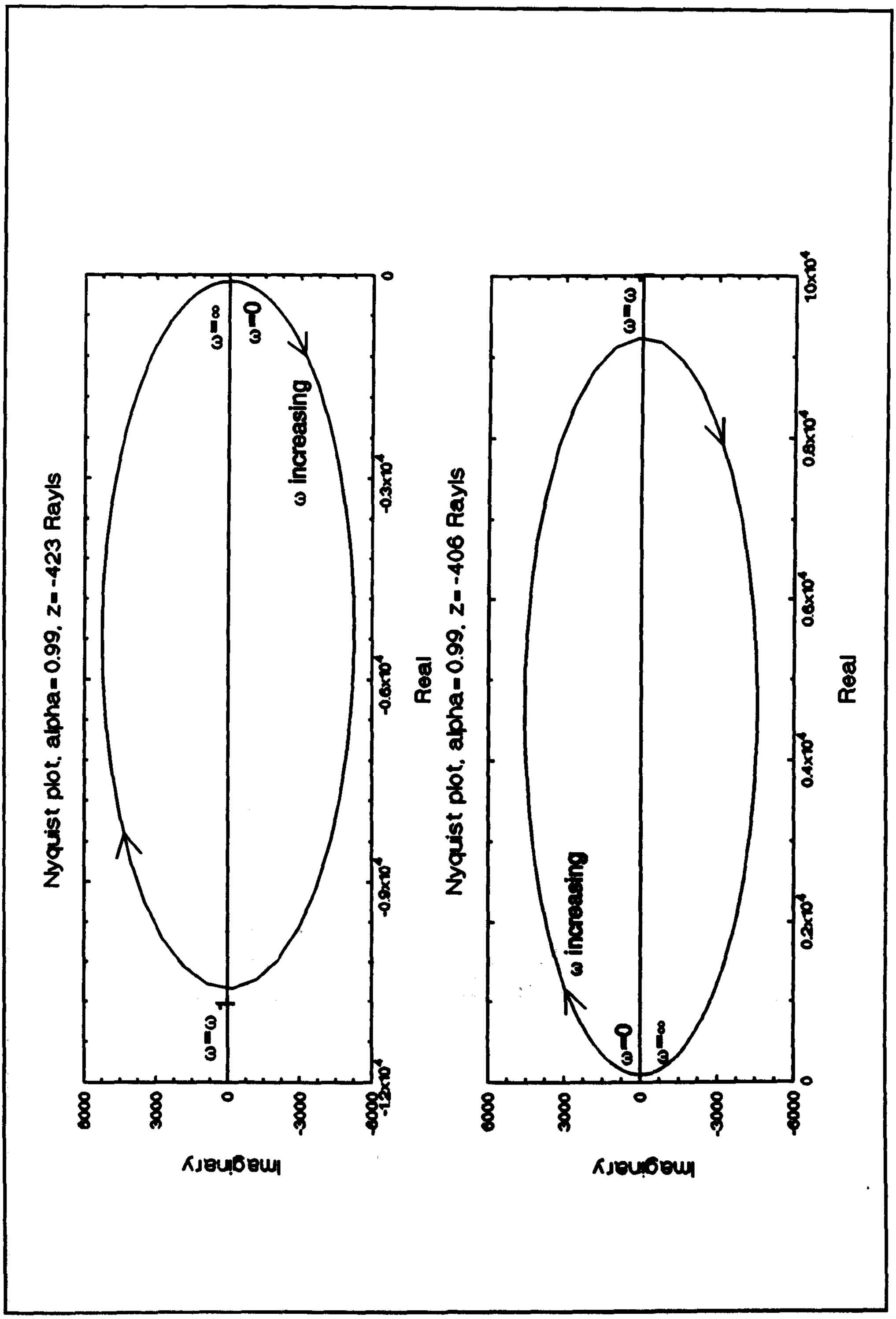

Figure 66. Nyquist plot for Mazzola's controller acting on a KEF B200A loudspeaker for two values of z. Values of ω from 0 to $+\infty$. 1,j0 is not encircled: both systems are stable when loop is closed.

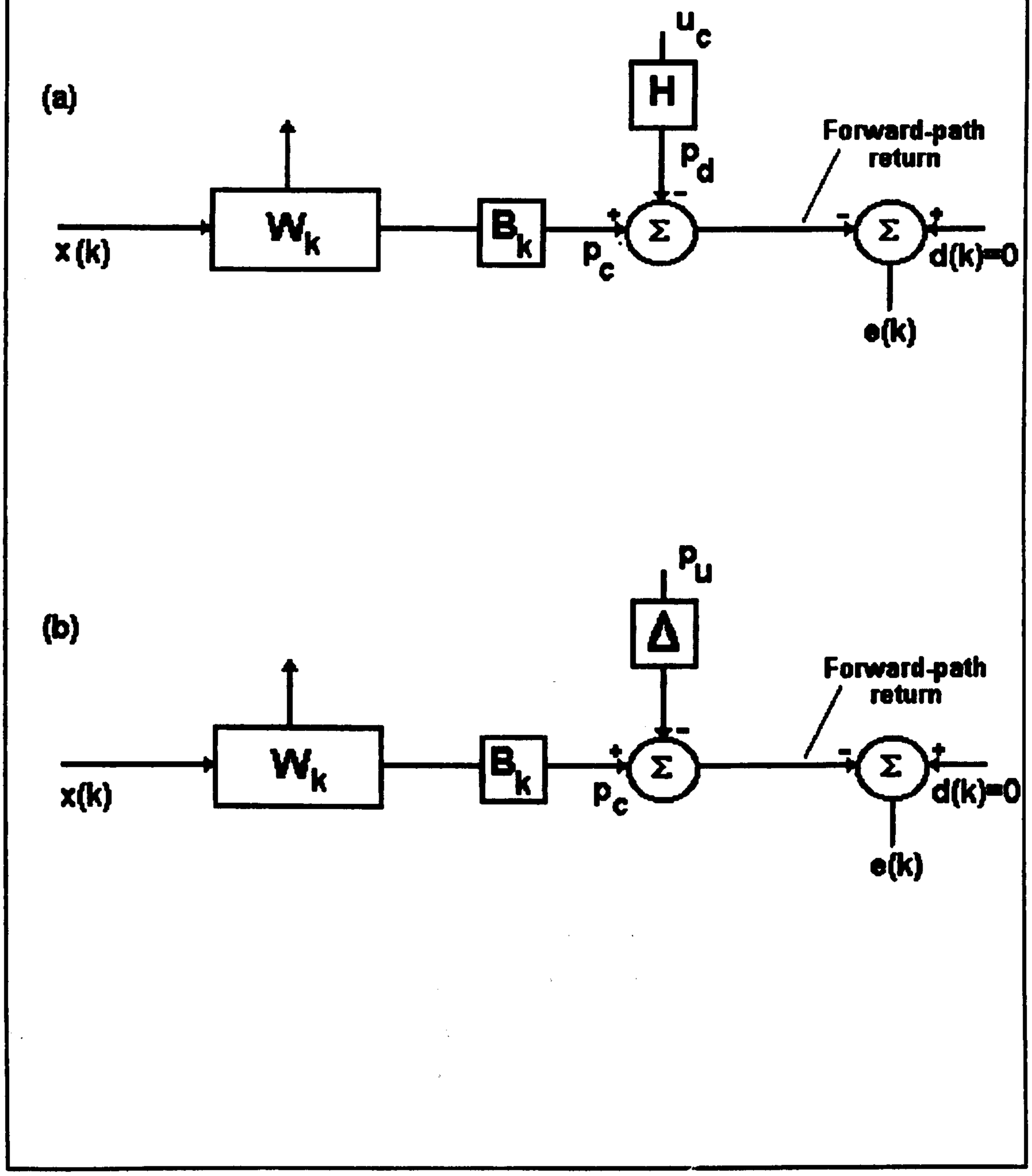

Figure 67. Simplified schematics of the mic-accr (a) and 2-mic (b) control systems. The mic-accr system is configured so that the forward-paths of the two systems are identical.

7 EXPERIMENTAL IMPLEMENTATION

7.1 INTRODUCTION

An active control system for the modification of impedance has been described in Chapter 5 and analyzed in Chapter 6. This chapter describes the implementation of this control system in the experimental test-rig used in this research.

The acoustic experimentation was performed on an acoustic waveguide at frequencies below the plane wave cut-off frequency so that the propagation of sound could be considered as one-dimensional. Both ends of the waveguide were terminated with a conventional electrodynamic loudspeaker; at one end the loudspeaker was used as an acoustic source and at the other end the specific acoustic impedance of the loudspeaker was controlled. The digital adaptive control system was implemented on a real-time digital signal processing board. Schematics for the laboratory control system are shown in Figure 25 on Page 98 and Figure 48 on Page 183. The components of the test-rig are described in the following sections.

Descriptions of the acoustic waveguide and source are given in Sections 7.2 and 7.3. The electro-acoustic components of the controlled impedance are described in Section 7.4 and limitations of the transducer measurements are discussed. The implementation of the digital control system is described in Section 7.5. The stability of the feedback control system is described in Section 7.6. Causal constraints that affect the performance of the system for broadband signals are described in Section 7.7. The performance of the digital feedback implementation of the mic-accr system is discussed in Section 7.8. The effect of impedance observation errors on the controlled impedance of the mic-accr system is described in Section 7.9.

7.2 ACOUSTIC WAVEGUIDE

The acoustic experimentation was performed on an acoustic waveguide so as to limit the sound propagation to one-dimension. The waveguide was

implemented with a circular PVC pipe of internal diameter 0.16m. The plane wave cut-off frequency is calculated as approximately 1.25kHz from Equation 6.138 on Page 149. Below this frequency one-dimensional plane waves propagate along the length of the duct. The laboratory duct was made of three sections of pipe; two 1m length sections and one section of length 3m. The pipe was supported by a wood construction (see Figure 68a on Page 237) and the three sections bolt together using bolts and wing nuts allowing a total duct length of 5m.

The measurement of the controlled impedance was performed with standing wave ratio (SWR) measurements in the duct (theory for SWR measurements is described in Appendix 5 on Page 344). SWR measurements are performed on harmonic waves and require measurement of: (i) the position of the first sound pressure minimum from the surface under test; (ii) the rms sound pressure ratio of the minimum and first subsequent maximum sound pressure points on the standing wave acoustic field in the duct; (iii) the second maximum sound pressure if compensation for duct leakage is required. To facilitate this a microphone was mounted on a movable trolley inside the 3m duct section allowing pressure measurement in the acoustic field. The trolley was made of wood and was moved in the duct with nylon line to find the maximum and minimum sound pressure locations along the 3m section. The 3m length of the section imposed a lower frequency limit of around 57Hz above which SWR measurements could be made for any termination impedance. Between 28.5Hz and 57Hz the SWR of termination impedances could be measured if the first minimum occurred before the first maximum when moving away from the surface. Duct sound leakage could be compensated above 114Hz. Between 57 and 114Hz duct sound leakage could be compensated for certain termination impedances. Below 57Hz duct sound leakage could not be compensated.

The laboratory test-rig SWR measurement was compared with an existing test-rig facility at the Department of Applied Acoustics, University of Salford. The length of the new waveguide was 5m whereas the existing waveguide was 0.8m in length - the shorter length of the existing facility restricted comparison to

frequencies above 160Hz. The existing waveguide was square in cross-section and constructed with 6mm steel walls. Lead-fronted plywood was used as the acoustic termination to both waveguides. The thickness of the lead was 1.5mm and the backing plywood thickness was 8mm thick. Care was taken to ensure that the samples were terminating the waveguides without air gaps. The magnitude of the reflection coefficient is calculated from the SWR measurement and is shown in Figure 69 on Page 238. The average difference in the magnitude of the reflection coefficient between the two test-rigs is 0.8% from 160Hz to 400Hz.

A later attempt was made to measure active sound absorption in the waveguide by measuring sound intensity with a Nortronics intensity probe. This probe uses ultrasonic frequencies to measure sound energy flow. The results were erratic and confusing. This was likely to be because of ultrasonic interference created in the confined duct space. The use of this intensity probe for test-rig measurements was abandoned.

7.3 ACOUSTIC SOURCE

The acoustic source, situated at one end of the duct, was implemented with a conventional electrodynamic loudspeaker made by KEF Electronics and designated the B200A. This unit is a 200mm plastic-cone loudspeaker which has an effective surface area of 0.022m^2 which is similar to the cross-sectional area of the duct 0.020m^2. Matching the radiating area to the duct area prevents compression effects and presents an (approximately) uniform surface impedance across the termination when the cone vibrates with piston-like motion.

This loudspeaker was mounted in a sealed box as shown in Figure 68b on Page 237. The design of the sealed box affects the performance of the loudspeaker system - for example the internal box volume affects the Q of the system resonance. Closed loudspeaker box design techniques are presented in (63)(64). The internal box volume used for the acoustic source was 25 litres and the Q of the system resonance is calculated as 1.0 in Appendix 2 on Page 310. The theoretical resonant frequency is 65Hz. The lower 3dB roll-off

frequency is calculated as 52Hz. A theoretical peak of 1.3dB occurs at 92Hz in the magnitude frequency response. The reference efficiency of the acoustic source is 0.3%. Parameters for the KEF B200A are presented in Appendix 1 and equations and solutions for the closed box design are presented in Appendix 2.

The sealed box internal dimension ratio was 1.6 : 1 : 0.6, this minimised the possibility of overlapping standing wave frequencies in the three dimensions (62). All panels were constructed from 20mm thick chipboard. The loudspeaker box was bolted to the pipe mounts as seen in Figure 68a on Page 237 so as to create an airtight seal.

7.4 CONTROLLED IMPEDANCE TERMINATION

The controlled impedance was implemented with a conventional electrodynamic loudspeaker as discussed in Section 5.3 on Page 92. The loudspeaker and box design are discussed in Section 7.4.1. In the control system the velocity and pressure at the cone were measured with an accelerometer and a microphone. The selection and testing of these transducers is described in Sections 7.4.2 and 7.4.3. The mass-loading of the loudspeaker cone by the accelerometer is described in Section 7.4.2.1. The influence of impedance observation error with these transducers on controlled impedance is discussed later in Section 7.9.

7.4.1 Loudspeaker and Box Design

The loudspeaker used as the controlled impedance termination in the laboratory test-rig was made by KEF Electronics and designated the B200A. This was selected for use because: (i) the surface area is similar to the duct cross-sectional area thus, when the cone vibrates with piston-like motion, an (approximately) uniform surface impedance is presented over the duct termination and compression effects are reduced; (ii) the B200A is an inexpensive, well known and established design. Parameters of the KEF B200A are in Appendix 1. Another KEF B200A loudspeaker was also used as the source, see previous Section 7.3. At the end of the research a different 8 inch

loudspeaker, Peerless model 831483, was used as the impedance termination for comparative purposes. This also has a similar surface area to the duct.

The KEF B200A was mounted in a 25 litre closed box - theoretical acoustic specifications for the system are presented in Appendix 2. The box affects the total system compliance and damping (see C_{ab} and R_{ab} in Figure 20 on Page 85) hence the specific acoustic impedance at the cone of the un-driven system. This impedance is defined and calculated for this system (assuming the box contained only air) in Section 4.3 on Page 76. The initial system had a packed box filling of glass fibre to reduce internal standing waves. The box filling was found to affect the impedance. The theoretical and measured reflection coefficients for the system are shown in Figure 70 on Page 239, and corresponding specific acoustic impedance values are in Figure 71 on Page 240. The deviation around 125Hz and 160Hz between theoretical and measured values were checked and found to due to the box filling. The results for the same system without box filling are shown in Figure 72 and Figure 73. The theoretical results have different damping from the measured results, adjusting the damping in the theoretical model improves the fit but does not provide any benefit to this discussion. The box filling affected the natural resonant frequency of the system. The results for the system without box filling are preferred because of less deviation in the smoothness of the curves. The system was subsequently used without box filling. Below the upper test frequency limit of 500Hz used in this work there was only one internal box mode, calculated at 357Hz. Effects of this single standing wave on the impedance of the system were not considered.

7.4.2 Accelerometer

The acceleration of the controlled impedance surface was transduced with an inexpensive accelerometer manufactured by Knowles Electronics of Burgess Hill, UK designated the BU-1771. The active sensor is a ceramic vibration transducer, connected to an internal FET amplifier circuit. The manufacturer's specification indicates a flat frequency response to 2kHz. The low weight of this transducer (0.28g) was the original selection consideration as mass-loading of

the cone was considered likely. The acceleration measurement of the cone was later found to be inaccurate due to mass-loading, see Section 7.4.2.1 on Page 210.

Knowles electronics provide three connection variations with which the signal from the BU-1771 is buffered and the internal FET correctly biased: two types for higher sensitivity measurements (accelerations of less than 10g) that use two- and three-wires; a lower sensitivity three-wire connection for larger accelerations. The three connection types were considered for test-rig use. The typical accelerations on the KEF B200A cone at lower frequencies (below 150-200Hz) resulted in distortion in the output signals of the two high sensitivity types. The maximum acceleration of the B200A cone is calculated as approximately 100g from the force factor **Bl** and cone mass and the peak coil current of 3.8A. The low-sensitivity connection output was less distorted: 2nd order harmonic distortion observed in the output of the three-wire high sensitivity connection was 20dB more than that of the low sensitivity connection type. The three-wire low sensitivity connection was used in the test-rig - here this is called the "Type 1" circuit and is shown in Figure 74 on Page 243. The maximum acceleration that can be measured by the accelerometer with this circuit is calculated as 1500g at 1kHz. This calculation is based on the accelerometer sensitivity quoted by Knowles Electronics, 5.6mV/g, and an 8v2 biasing voltage. A fourth wiring method called "Type 2", also shown in Figure 74, was found during the research that gave 20dB gain more than the Type 1 connection, thus reducing noise, with low harmonic distortion. Additional circuitry based on standard OP-amp techniques designed during this research to integrate the accelerometer signal, remove dc and provide gain is detailed in Figure 74. The phase shift of the integration circuit was measured as within 2.5° of -90° above 40Hz - see Table 2 in Appendix 4. The effect of this (small) error is discussed later. The circuitry was designed for broadband performance so as to prevent additional phase.

The dust cap of the loudspeaker was initially considered as a suitable place to mount the accelerometer - however the dust cap material was too soft. Instead

the accelerometer was mounted with epoxy resin on the KEF B200A cone at a point where the circular dust cap meets the cone (shown in Figure 76 on Page 245, this figure discussed later). This position causes possible electro-magnetic coupling between the current applied to the voice-coil and the accelerometer output voltage. In order to reduce any electrical pick-up the hook-up wires were placed at right angles to the voice-coil, and the metal accelerometer case was earthed. The metal chassis of the KEF B200A was also earthed. After taking these precautions components due to electrical pick-up were measured as more than 47dB below the total signal output over the frequency range 40-1000Hz. Investigation of the effect of the transducer output signal from moving in the field of the loudspeaker's fixed magnet found that the transducer response was within ±0.1dB and ±1° of the response outside of the magnetic field - this was probably equal to or less than the resolution of the measuring equipment. The conclusion from these measurements is that there was negligible electro-magnetic pick-up by the accelerometer when mounted on the KEF B200A loudspeaker cone.

The velocity measurement from the BU-1771 accelerometer and associated electronics was tested by comparison with a Brüel and Kjær (B&K) 4374 accelerometer and 2635 charge amplifier. The 4374 was secured with double-sided tape on top of the BU-1771 mounted on the KEF B200A cone. The 2635 charge amplifier was set to velocity measurement with a band-width of 1Hz to 30kHz. The loudspeaker was driven with a maximum length sequence from the MLSSA measurement system and radiated into the laboratory space. The velocity transfer function between the Knowles/Op-amp circuitry and the B&K setup is shown for Types 1 and 2 in Figure 75 on Page 244. The results have not been normalised, the Type 1 and 2 magnitude responses are within 1dB over most of the range 50-500Hz. Type 1 is seen to have better phase matching with the B&K setup than Type 2 - within ±10° whereas Type 2 has a maximum 22° difference from the B&K setup near 50Hz. The phase error caused by the test-rig integration circuitry (< 2.5°, see earlier in this section) is a small component of the phase deviation from the B&K velocity measurement. The velocity measurement differences affect the mic-accr system impedance

control performance - this is discussed later in Section 7.9. Figure 30 on Page 165 shows that when implementing an ideal active absorber (for which magnitude of reflection coefficient |R| = 0) differences in measurement similar to the differences between the Type 1 and Type 2 Knowles setups and the B&K setup could cause the actual |R| to be up to 0.18. If the B&K setup is assumed to be accurate then Type 1 is more accurate than Type 2; however the choice of which connection type to use in the mic-accr system is later made by observation of the performance of the controlled impedance.

The accelerometer was found to mass-load the cone. This is described in the following section.

7.4.2.1 Mass-loading

The moving mass of the KEF B200A loudspeaker cone is quoted by the manufacturer as 24.0g. The relatively low weight of the Knowles BU-1771 accelerometer, 0.28g, might intuitively be assumed to have little effect on the cone vibration. However, the weight of the cone material in contact with the small mounting area taken by the accelerometer, about 0.5% of the total cone surface area, is about 0.1g. The transducer significantly changes the mass at this location. The effect of this 'mass-loading' is that the vibration at this location may be modified. Therefore the velocity may not be the same as at other locations on the previously piston-like cone and then the measurement will not fully describe the cone velocity. This section presents a description of the 'effective mass' at a location on an infinite panel after Smith (65). However, the effect of the mass loading on vibration at other parts of the cone can not be deduced from this analysis. Measurements from the test-rig are used to show that the accelerometer alters the vibration of the cone.

The force/velocity response seen at an excitation point on a large plate varies with frequency when vibrated transversely and can be calculated by assuming an infinite plate of thickness **h**, modulus **E**, density ρ and Poisson's ratio γ. At the driving point the force/velocity response is given in Equation 7.1 reproduced from (65).

$$\frac{F}{v} = 8\left[\frac{E}{(1-\gamma^2)} \cdot \frac{h^3}{12} \cdot \rho h\right]^{\frac{1}{2}} \qquad 7.1$$

Since acceleration is the product of velocity and frequency, the 'effective mass' seen at this point M_e is given by $F = M_e \omega v$, and so the effective mass is described by Eq. 7.2.

$$M_e = \frac{8h^2}{\omega}\left[\frac{E\rho}{12(1-\gamma^2)}\right]^{\frac{1}{2}} \qquad 7.2$$

Ideally the mass of the transducer should not be more than about 5% of the effective mass to prevent mass-loading (65).

Calculation of the effective mass of an infinite panel made of KEF B200A cone material is made from Eq. 7.2. The cone has $h = 0.65$mm and $\rho = 1640$ kg/m^3. As the values of E and γ are not known, estimates are used here. The typical value of γ of many materials is around 0.3, and E is typically between 1×10^{10} and 1×10^{7}Pa for most materials. It is illustrative to assume that Poisson's ratio for the material is 0.3 and the Young's modulus is the highest possible value ($E = 1\times10^{10}$) - this reveals the highest value of M_e. For these values Eq. 7.2 gives $M_e = 4.1 / \omega$. The BU-1771 is 0.28g in weight, additional accelerometer securing material (such as blutack, epoxy resin) can be 0.5g. This simple calculation shows that below 81Hz the mass of the accelerometer is less than 5% of the effective mass. Above this frequency mass-loading occurs. This calculation is based on a optimistic value for E, so mass-loading of the cone material by the Knowles BU-1771 is clearly likely over all frequencies used in the experimental test-rig (40-500Hz). This conclusion assumes that the panel has infinite dimensions and has no other loading.

The accelerometer mounting location and the KEF B200A cone can not be considered to be the same as in the previous analysis. The cone material is also stiffer at this specific position because of the cone shape, see Figure 76 on Page 245. The effects of mass-loading are harder to analyze. However, simple measurements can be used to determine if mass-loading occurs.

An experimental attempt to observe mass-loading was made. With one BU-1771 secured at a position on the join between the dust cap and cone, a second BU-1771 was attached using blutack at various locations around the cone and the velocity responses were compared. The second accelerometer and securing blutack weighed 0.8g. The second accelerometer locations are shown in Figure 76 on Page 245 by the * symbols and codes An, Bn and Cn. Velocity transfer functions were made between the fixed accelerometer and the second accelerometer at these locations, these are shown in Figure 77, Figure 78 and Figure 79 on Page 246-Page 248.

The first of these figures, Figure 77 on Page 246, shows measured velocity transfer functions between the second and first accelerometers, here called the reference, for the second accelerometer positioned: (i) on top of the first accelerometer - this was a "control" test to verify later measurements; (ii) at two other locations A2 and A3 depicted in Figure 76 on Page 245. The first transfer function (the solid line) exhibits some deviations above 300Hz that may be due to the use of blutack to attach the second accelerometer. Below 300Hz the magnitude and phase are within ±0.5dB and ±3° - therefore the two accelerometers produced similar velocity measurements at this single location. The results are discussed hereafter only for frequencies below 300Hz. At the two other locations the transfer functions are different between 230 and 280Hz. At frequencies such as these the cone, without transducers, is considered to have piston-like motion. However, the velocity measurements were different, this is believed to be due to mass-loading of the cone by the accelerometers. Below 200Hz the velocity measurements were similar. Figure 78 shows the velocity transfer functions for the second accelerometer locations B1 to B4. A damped resonance is seen at around 200Hz. Figure 79 shows results for when the second accelerometer locations were at the edge of the cone C1 to C4, the resonance is seen to have dropped to 150Hz and the mass-loading affected the magnitude and phase from 50Hz upwards. If the KEF B200A cone (without accelerometers) is assumed to vibrate as a uniform piston below 300Hz, then these results show that the accelerometers mass-load the KEF B200A cone.

It is therefore likely that there will be errors in the observation of surface velocity with the reference accelerometer. The similarity of the responses below 200Hz in Figure 77 suggests that there is less mass-loading at lower frequencies when the accelerometers are positioned where the dust cap meets the cone than at other cone positions - this may be because of the extra stiffness of the cone shape. It is not possible to quantify the absolute measurement error of a single accelerometer from these results unless gross assumptions are made. For example, if one signal is assumed to be an accurate representation of the velocity of the *un-loaded* cone then the other signal quantifies the velocity measurement error. Clearly, this will produce dubious conclusions on the real behaviour. In the absence of a better method of measuring velocity at discrete points over the cone, such as laser velocimetry (51), it is only possible to conclude that mass-loading occurs with the Knowles BU-1771 mounted on the KEF B200A cone, the vibration at some locations on the cone may be less affected.

7.4.3 Microphone

A low-cost lightweight microphone manufactured by Sennheiser was selected for use in the test-rig. The microphone model number is KE4-211. This microphone is a low noise omnidirectional design with an integral FET amplifier. The microphone capsule is cylindrical with a diameter of 4.7mm and length of 4.2mm. The capsule weighs 0.31g. The capsule has a single hole for acoustic energy to reach the diaphragm. In the test-rig the microphone FET was biased and the output signal buffered by circuitry shown in Figure 80 on Page 249.

Two locations for instrumenting the acoustic pressure at the surface of the cone were considered: (i) position the microphone capsule close to the cone surface - a "rigidly mounted mic"; (ii) secure the microphone capsule on the cone - a "cone mounted mic". The first location was achieved by rigidly mounting the microphone at the centre of a spider of four stiff metal wires in a 'mate panel' shown in Figure 68 on Page 237. The mic diaphragm faced the loudspeaker dust cap. The capsule face was at a distance of 5mm from the stationary cone position. This did not affect normal cone excursions - the linear peak excursion

of the KEF B200A cone is 3mm. The mic spacing from the cone corresponded to a 2.6° phase shift at 500Hz - for an ideal active absorber this pressure measurement error corresponds to a small error in |**R**| of around 0.02 (from Figure 30 on Page 165). The second location reduced the distance from the cone to the microphone by mounting the capsule on the cone. However, the motion of the cone then moved the capsule body with the possibility of exciting the diaphragm. The output signal would then have contained a component corresponding to the capsule acceleration. To reduce this component the capsule was mounted side-on to the cone in the circular groove between the dust cap and cone with double-sided tape. There was also the possibility of inductive coupling from the voice-coil and electro-magnetic effects from moving the capsule in the field of the loudspeaker magnet. The effect of these components was quantified by sealing the capsule acoustic hole with blutack so that the microphone output signal contained little or no pressure component and then applying harmonic signals to the loudspeaker voice-coil. The microphone output signals were often below the noise floor of the microphone/buffer circuitry and those that could be observed were typically 38-50dB below the signals measured with the mic capsule acoustic hole uncovered. These tests showed that this mounting method caused little microphone response to any of these mechanisms.

The measurement of pressure of the Sennheiser microphones and OP-amp circuitry was checked by comparison with a Brüel and Kjær model 4135 ¼" microphone and a B&K measurement amplifier. For each of the tests the 4135 was positioned within 5mm of the Sennheiser microphone under test in front of the B200A cone. The loudspeaker was driven with a maximum length sequence from the MLSSA measurement system and radiated into the laboratory space. Transfer functions between the rigidly mounted and cone mounted Sennheiser KE4-211 microphones and the B&K microphone are shown in Figure 81 on Page 250. The rigid mic (positioned in the mate panel) has a poorer response than the cone mic used on the surface of the cone - the cone mic has a 'flatter' magnitude response. With normalised magnitude the rigidly mounted microphone is within ±1.5dB and the cone mounted microphone is within ±1dB

of the B&K microphone. Both microphones have sloping phase responses of around ±15° compared with the B&K mic. The Sennheiser microphone responses are within 2dB and 10° of each other over most of the frequency range 50 to 500Hz.

The transfer function between the surface microphones was measured to show differences in the response at the two positions - on the mate panel, and on the cone surface. Figure 82 on Page 251 shows two transfer functions between the rigid mic and the cone mic. The 'uncorrected' measurement shows differences of up to 2dB and 10° between the two pressure measurement locations. The 'corrected' version which compensates for the two microphones different responses (the difference between the two curves in Figure 81) reveals that the two positions produce pressure measurements that are within ±1db and ±10°.

The responses of the two Sennheiser microphones are within ±1.5dB and ±15° of the B&K microphone pressure measurement. The pressure measurement differences affect the mic-accr system impedance control performance - this is discussed later in Section 7.9. Figure 30 on Page 165 shows that when implementing an ideal active absorber (for which magnitude of reflection coefficient $|R| = 0$) differences in measurement similar to the maximum differences between the rigidly and cone mounted Sennheiser setups and the B&K setup could cause the real $|R|$ to be up to 0.15. The choice of which connection type to use in the mic-accr system is later made by observation of the performance of the controlled impedance.

7.5 MIC-ACCR DIGITAL ADAPTIVE CONTROL SYSTEM

This section describes the implementation of the mic-accr digital control system for the laboratory test-rig. A fundamental description of the system has been given in Chapter 5 on Page 90 where schematics of the adaptive control (shown in Figure 27 on Page 100 and Figure 28 on Page 101) are described.

The real-time digital adaptive control system was programmed with assembly code and run on a floating point digital signal processor made by AT&T and designated the DSP32C. Loughborough Sound Images Ltd., Loughborough, UK manufacture a development board for the IBM PC that uses the DSP32C processor and provides analogue to digital (A/D) and digital to analogue (D/A) conversion. The use of this development board, named "LSI DSP32C System board", is described in Appendix 3 on Page 314. Extra A/D convertors were provided on an additional board named "PC/Stereo board". A schematic for the control implementation is shown in Figure 124 on Page 325. This schematic shows the mic-accr control system with the reference A/D converter, **DSP32C INA**, sourced from upstream pressure in the duct (changing the signal to **DSP32C INA** allowed the system to be configured either as feedback or feed-forward, see Section 6.3 on Page 105). The two adaptive filters **W** and **R** were updated by LMS algorithms with update gains of α and β respectively. For a non-recursive filtered-X LMS implementation β was set to zero - the output of filter **R** was then always zero. The control signal was converted by D/A converter **DSP32C OUTB** and then filtered by a reconstruction filter, see Section 7.5.1, and amplified by an audio power amplifier before being fed to the loudspeaker. The error signal, **e(k)** was calculated by filtering the signal from **PC/Stereo INA** through the desired filter **H** and subtracting the signal from **PC/Stereo INB**.

The design of the two compensation filters, **C** in Figure 124, that improved the stability and convergence of the adaptive system has been described in Section 6.6 on Page 139 with reference to Figure 49c on Page 184 . Typical transfer functions in the test-rig have been presented in Section 6.7. When designing the filter coefficients the practical implementation measured impulse responses with the control system turned off - this is known as "off-line" modelling. Pulses were injected into the control signal output and the two electro-acoustic path impulse responses of **A** and **B** in Figure 49c were measured and averaged separately to give impulse responses **<A>** and **<B>** (digital pulses were sent to **DSP32C OUTB** in Figure 124 and signals from **PC/Stereo INA** and **PC/Stereo INB** were measured and averaged). The impulse response of **<A>** was convoluted with

the desired impedance filter response **H** and then subtracted from the response **<B>** to create a single impulse response. The coefficients for the two FIR compensation filters **C** were directly programmed from this response.

Figure 124 also shows the user selected feedback cancelation filter **F** used to improve loop stability in the control system when the reference signal was taken from measures of pressure or velocity (loop stability problems have been described in Section 6.4 on Page 117). This FIR filter was designed before the adaptive controller was started (designed "off-line") by measuring the impulse response of the feedback path from **DSP32C OUTB** to **DSP32C INA**, and directly programming the filter coefficients from the response.

The processes for feedback cancellation and compensation filter design were software driven in the practical control system and were observed to produce filters of sufficient accuracy for the stability and convergence of the adaptive system. The analogue signals that are sampled by the digital system must have sufficient voltage so that the analogue to digital conversion provides sufficient resolution. The analogue signals in the test-rig were adjusted to provide sufficient level and the desired impedance filter (**H** in Figure 124) then set with the correct coefficients for the desired impedance.

The digital implementation of the mic-accr method on a digital signal processor had significant advantages over analogue implementation for the laboratory work performed for this thesis:

(i) Software control of the desired filter **H** was more flexible than implementation of a corresponding analogue filter in hardware, especially when frequency-dependent impedances were desired.

(ii) The desired filter for ideal acoustic absorption ($z_d = \rho_0 c$) was a simple implementation of a single multiplication. This was very easy and efficient to implement with the digital signal processor.

(iii) The selection of the two mic-accr method variations (see Figure 26a and Figure 26b) can be software controlled.

(iv) The control system used adaptive digital control processes based on the mic-accr method (see Chapter 5) that automatically designed the control filter coefficients.

7.5.1 Anti-aliasing and Reconstruction Filters

'Aliasing' occurs when sampling data that contains components that are higher in frequency than half the sampling frequency. When sampled these higher frequency signals are modulated to frequencies below the sampling frequency. Aliasing can be prevented by removing the higher frequency components with filters before sampling. Anti-aliasing filters are generally set to remove signals higher than half the sampling frequency, and are of high order to maximise frequency band-width. The phase imposed on the sampled data was not desirable in the test-rig as this would have constituted observation error of the transduced pressure and velocity of the controlled surface. The DSP32C System board and PC/Stereo board had fourth-order anti-aliasing analogue filters and these were set to 10KHz with Butterworth characteristic to minimise phase shift over the intended control frequencies of below 500Hz. The possibility of aliasing distortions occurred for frequencies between 1.5kHz and 10kHz - however efforts were made to ensure that the laboratory test-rig signals did not contain these frequencies.

'Reconstruction' filters are used to remove the "digital steps" from output produced by D/A conversion. The control system produced a control signal output that contains such steps. These were removed by a linear low-pass filter as the additional frequencies were undesirable. The control signal was reconstructed with a seventh order digital low-pass filter that rolls off above 1kHz as shown in the measured transfer function Figure 57 on Page 192. Over the test frequencies this had an approximately linear phase shift with π radians near 500Hz. The compensation filters included this phase shift thus allowing convergence of the adaptive control system.

7.6 STABILITY OF MIC-ACCR FEEDBACK DIGITAL CONTROL SYSTEMS

The loop stability of the fixed active controller has been examined in Section 6.4 on Page 117. The complicated dynamics of the adaptive system in the presence of feedback have been discussed in Section 6.6.3 on Page 143. This section discusses the stability of adaptive feedback control with measurements from the experimental laboratory test-rig. Loop instability was observed with the two feedback control strategies for different desired impedances (these strategies are distinguished by choice of reference signal as discussed in Section 5.2 on Page 90). The experimental work shows that it is necessary to stabilise the feedback loop for certain desired impedances.

7.6.1 Observation of Loop Instability

The feedback control systems can be unstable because of feedback loop paths around the controller - see Section 6.4 on Page 117. Experimentation near the onset of instability observed "bursting" and erratic output. This section describes an experiment that illustrates these problems.

The laboratory test-rig was set up for active impedance control with a digital feedback adaptive control system based on the mic-accr technique - a schematic is given in Figure 83 on Page 252. The control system modified the impedance of the loudspeaker at the left hand termination of the 5 metre waveguide (the "controlled loudspeaker"). Acoustic signals were generated by the loudspeaker at the right hand termination (the "source"). The source was electrically driven by a 250Hz sinusoid. The control system measured the pressure at the cone ("p_{cone}") and cone velocity ("u_{cone}") and calculated the real-time error signal by comparing the measured velocity with the cone velocity that would have occurred with a desired impedance set by filter H. The adaptive filtered-X LMS algorithm attempted to minimise this error by adjusting the weights of the linear FIR filter (a linear combiner) that generated the control signal to modify the dynamics of the cone. The FIR filter contained 16 taps with a control system sampling frequency set to 3000Hz. The control system reference signal was the pressure at the surface of the cone ("p_{cone}") in the waveguide. The adaptive controller had no feedback cancellation in this experiment. The filter H was set

for a desired impedance of near-$\rho_o c$ and the control system was on the verge of instability. The adaptive update speed of the controller was set by the update gain value "alpha". This experiment studied the convergence of the adaptive control system by observing the error signal for different values of alpha.

The upper graph of Figure 84 on Page 253 shows a plot of the adaptive control system error for alpha set to 0.05. The x-axis shows time in milliseconds and the y-axis is the sampled amplitude of the error measured with an ONO-SOKKI CF-360 data analyzer. After the start of the adaptive controller, the system converged in approximately 100msec to the minimum error observed over the rest of the plot. A stable adaptive control system would hold this value of minimum error, however "bursting" in the error amplitude started to occur. The delay between each distinct burst increased as the bursting level decreased and the error settled on an approximately steady non-zero error value between 3000 and 5500msecs. The adaptive control then went unstable at 5800msecs.

The next observation was for alpha set to 0.0005 and is displayed in the lower graph of Figure 84 on Page 253. Reducing the update gain slowed the adaptive convergence. As for the previous gain, the controller initially converged to the minimum error but took approximately 300msec to do so. Bursting in the error amplitude then started to occur until the error settled on an approximately steady non-zero error value at 3500msecs. At 4500msec bursting of the error recommenced but with a different burst period. The adaptive control system eventually went unstable.

The next observation was for alpha set to 0.0001 and is displayed in the upper graph of Figure 85 on Page 254. Reducing alpha further slowed the controller convergence; initial convergence to the minimum error occurred over approximately 1200msec. Bursting in the error amplitude then started to occur. The adaptive control system eventually went unstable.

The final observation was performed for alpha set to 0.00005 and is displayed in the lower graph of Figure 85 on Page 254. The initial convergence then took

approximately 1700msec. Bursting in the error amplitude then started to occur. The adaptive control system eventually went unstable.

Reducing the adaptive update gain of the feedback control system slowed the adaptive convergence as to be expected. This indicated that the adaptive algorithm was attempting to converge correctly. However, as the controlled impedance became close to the desired impedance the feedback of the output to the input of the adaptive control system caused loop instability. This behaviour was practically observed with the bursting in the adaptive control system error; when the feedback loop went unstable the error level went up, so the adaptive control system converged to reduce the error level. This became a periodic process with the convergent speed of the adaptive algorithm affecting the period of bursting. The system went unstable when the adaptive algorithm could not converge. This behaviour illustrates the implementation problem of stability of the adaptive feedback mic-accr control system: for this desired impedance the feedback around the adaptive system causes instability and the adaptive system is not able to converge to a solution that allows overall system stability. In order to stabilise the convergence when controlling near-characteristic impedances the gain of the feedback loop must be reduced.

In this experiment the adaptive algorithm adapted the weights of a *linear* 16-tap FIR filter. However, these observations show that the adaptive feedback system can actually behave *non-linearly*; the system was excited with a single frequency harmonic signal and in response generated other frequencies during bursting. This indicates that a correct mathematical description of the dynamics of the error signal may contain non-linear components of the input excitation.

The observations presented in this section were from a feedback control system that used the cone pressure as reference input. Similar laboratory observations were made when using the cone velocity as the reference for different values of desired impedance.

7.6.2 Feedback Loop Stabilisation

Section 7.6.1 demonstrated that the mic-accr feedback control system had loop stability problems when forcing desired near-characteristic impedances. Techniques for the reduction of the effects of the feedback path are described in Section 3.8 on Page 53. This section describes the observation of increased stability of the adaptive system using these techniques.

7.6.2.1 Recursive filtered-U adaptive algorithm

The first attempt at stabilising the feedback loop was performed by replacing the non-recursive filtered-X algorithm with the recursive filtered-U algorithm described in Section 3.7 on Page 50. The filtered-U algorithm can generate poles in addition to zeros and this feature has been suggested by other researchers to help in the control of feedback loops in active acoustic control systems - see Section 3.8 on Page 53. An experiment which illustrated the increased stability of the control system when using the recursive filtered-U algorithm is described in this section.

A measurement was made of a "bursting" instability and is shown in the upper plot of Figure 86 on Page 255. This case was for a mic-accr filtered-X LMS control system with a reference input of cone pressure forcing a one-dimensional impedance of near characteristic impedance for a 100Hz normally-incident harmonic plane wave. A schematic of the laboratory test-rig is presented in Figure 83 on Page 252 and has been described in Section 7.6.1. The adaptive FIR filter had 14 taps and the update gain was set to 0.00001. Figure 86 shows the mean-square-error of the control system against time. The adaptive system reduced the error to a stable level after about 30 seconds but during the convergence the error was seen to "burst". Without any stabilisation for the feedback loop the control system was close to instability. The bursting was reduced by replacing the non-recursive filtered-X algorithm with the recursive filtered-U algorithm for the same laboratory conditions. Stability was enforced for this case as shown in the lower plot in Figure 86 on Page 255. Careful adjustment of the control system was made to observe these results. For stable convergence the number of poles and zeros in the recursive control filter were

adjusted and the update gains of the 14 tap non-recursive and 8 tap recursive adaptive sections (α and β in Figure 124 on Page 325) were given different values of 0.00001 and 0.001 respectively.

These observations required careful setting of the filter coefficients and update gains. It is, therefore, concluded that these results provide no basis to suggest that the algorithm would be stable for other desired impedances with other noise signals in different acoustic environments.

7.6.2.2 Feedback cancellation

A more general solution is achieved by using the filtered-X LMS algorithm with Feedback cancellation.

Feedback cancellation has been successfully used by other researchers for the stabilisation of active acoustic control systems, see Section 3.8. The mic-accr feedback control systems (using either cone pressure or cone velocity as reference input) were successfully stabilised with a fixed "off-line" modelled feedback cancellation filter in conjunction with an LMS adaptive controller filter. The required filter solutions for optimum control have been described in Section 6.5 on Page 133. The digital implementation is described in Section 7.5 on Page 215. The feedback cancellation was user selected in the control system by a software-controlled switch. This allowed quick assessment of uncontrolled loop stability with the cancellation turned off and the stability with the fixed feedback cancellation turned on.

An experimental measurement was made of the mic-accr control system forcing a desired characteristic impedance at the termination of the 5m waveguide. The reference input was cone pressure. The incident wave was a 250Hz sinusoid. The filtered-X LMS algorithm adapted an 8 coefficient linear combiner sampling at 3kHz with an update coefficient, α, of 0.01. The measured error signal of the controller without and with feedback cancellation is presented in Figure 87 on Page 256. In each case the control system was started at 1 sec. Without feedback cancellation the controller was not able to converge; the error signal

was seen to burst because of the instability of the feedback loop for this desired impedance - see the upper plot of Figure 87 (bursting has already been described in Section 7.6.1). With a feedback cancellation filter of 512 taps, the controller converged and the error became small - see the lower plot of Figure 87. SWR measurements were made for the converged controller with feedback cancellation. The magnitude of the controlled impedance was 407 Rayls with phase 0.06 radians. This corresponds to a sound absorption coefficient of 0.97 - the uncontrolled value was 0.2. The use of feedback cancellation therefore allowed a high degree of active sound absorption of the acoustical signal.

The problems of fixed feedback cancellation, described in reference (2), are reproduced here from Section 3.8 on Page 53: (i) this approach may be inefficient as feedback path may have a long impulse response, thus requiring a mathematically complicated cancellation filter; (ii) if the filter does not exactly match the feedback path the potential for an unstable loop still exists; (iii) the feedback path may be time-variant, thus repeated off-line modelling of the path may be necessary. These problems are now discussed for the mic-accr laboratory test-rig system : (i) the control system was implemented on a digital signal processing chip. The digital control system had adjustable sampling frequency - sampling at 3kHz was suitable for the plane wave bandwidth of the waveguide used in the test-rig. The impulse response of the feedback path in the waveguide was less than 0.2 seconds - the cancellation filter was found to be easily implementable with an FIR coefficient length of not more than 512 taps for a sampling frequency of 3kHz; (ii) the modelling of the feedback path in the test-rig was usually of sufficient accuracy to be experimentally successful at stabilising unstable loops; (iii) the modelling of the feedback path in the test-rig waveguide with a single off-line measurement was of sufficient accuracy to allow successful control system convergence for nearly all cases. Generally, these problems were not found to affect the implementation of the mic-accr control system in the laboratory system. However, occasionally the controller would be unstable with feedback cancellation for certain spot frequencies - an example is mentioned in Section 7.8. This problem was compounded by the highly reactive

nature of the feedback path caused by the duct radiation load in the experiments. The application of the mic-accr feedback control system to non-laboratory acoustic situations may require further consideration of these potential problems.

7.7 CAUSAL CONSTRAINTS ON DIGITAL IMPLEMENTATION OF THE MIC-ACCR SYSTEM

The active controller filter, shown in Figure 25 on Page 98, can either be implemented with analogue or digital signal processing techniques. The use of a digital filter introduces delay in the control system response because of the finite instruction rate of the processing element, sampling delays in the data convertor systems and large group delays through high order anti-aliasing and reconstruction filters. This section discusses the effect of this delay on the control system with reference to results from the laboratory test-rig (31).

The effect of the overall delay in the control path on the controlled performance is different for the feedback and feed-forward implementations that occur with selection of the control filter reference signal. Selection of the reference signal is discussed in Section 5.2 on Page 91. If the reference signal is selected so that the system is feedback then the control filter must act as both a filter and *predictor* for correct control of broad-band noise. In order for the controlling filter to be realizable, it must have an impulse response which is causal - it is not able to compensate for the delays by introducing an equal advance component. The presence of pure delays in the control loop of the feedback system therefore causes a causal constraint on the controlled performance. Experimental results are presented which illustrate the causal constraint and further illustrate a practically useful relationship between an easily measured property of the incident pressure's autocorrelation function and the expected performance of the actively controlled impedance.

Although it is not possible to introduce an advance into the response of a physical filter, it is possible to derive the input signal to the controller from a point in the duct d metres upstream of the active termination. The incident

pressure component of this upstream pressure is advanced by d/c seconds (the controller has adopted a partially feed-forward structure). If the delay inherent in the control loop is T seconds then the total equivalent delay in the system with upstream pressure sensing is (T-d/c) seconds - it is possible to eliminate all of the delay if the upstream microphone is far enough away from the cone. This has been experimentally examined and results to support this are presented here.

A schematic that details the laboratory control system is shown in Figure 88 on Page 257. The control system modified the impedance of the loudspeaker at the left hand termination of the 5 metre waveguide (the "controlled loudspeaker"). Acoustic signals were generated by the loudspeaker at the right hand termination (the "source"). Both loudspeakers were B200A models from KEF electronics. The source was electrically driven by a one octave band of pink noise, centred on 200Hz, which generated 110dB SPL at the controlled cone. The control system instrumented the pressure at the cone ("p_{cone}") and cone velocity ("u_{cone}") and calculated the real-time error in cone velocity by comparing the measured velocity with the cone velocity that would have occurred with a desired impedance of $\rho_0 c$ set by filter H. The adaptive LMS algorithm attempted to minimise this error by adjusting the weights of the linear FIR filter that generated the control signal used to modify the dynamics of the cone. The FIR filter contained 128 taps with a control system sampling frequency set at 3000Hz. The maximum possible delay in the impulse response of the FIR filter was 42 msec (corresponding to the time taken for an acoustic signal to propagate across a distance of approximately 14 metres).

The control system used a microphone to measure pressure ("p_{ref}") in the waveguide for the reference signal. This "reference microphone" was positioned at increasing distances away from the cone and the performance of the adaptive control system was measured by observing the mean square of the velocity error. At each reported position, the average mean square velocity was taken from thirty two, 45 seconds evolutions of the adaptive controller. The adaptive controller needed the feedback cancellation filter for adaptive stability. The filter

was re-designed at each position of the reference microphone by measuring the feedback path before the adaptive controller was started. The experiment also observed the autocorrelation of the pressure at the cone.

Figure 89 on Page 258 shows a plot of the normalized averaged mean square velocity error for this control system, as a function of the spacing from the cone to the reference microphone. The velocity error in implementing the $z=\rho_0 c$ termination is seen to hold roughly constant value until the reference microphone distance increases to approximately 25cm, after which point the error decreases. The delay in the control path was measured as 1.3 msec (corresponding to the time taken for an acoustic signal to propagate across a distance of approximately 45cm). Also shown is the maximum absolute value of the incident pressure's autocorrelation function for lag greater than the effective delay (T-d/c). Experience has shown this parameter to be reasonable well correlated with the norm of the optimum controller's impulse response vector and, consequently, with the coherence between the actual and predicted cone velocities. According to this empirically observed relationship, the optimum mean squared velocity error in the implementation of a desired impedance is described in Eq. 7.3.

$$E[e^2] \propto 1 - \left(Max(|r_{xx}(\tau)|) \right)^2_{\tau > (T-d/c)} \qquad 7.3$$

Equation 7.3 shows that the causal constraint can effectively be removed by increasing d, when the system becomes a pure feed-forward controller. Equation 7.3 also reveals that a pure feedback system (d=0) can estimate a desired impedance to an accuracy which can be predicted if the autocorrelation function of the incident pressure signal is known.

The laboratory experiment was not able to directly measure the controlled impedance at the cone because of the use of noise as the incident pressure. SWR measurement works with sinusoidal signals for which there is no causal constraint on the controller (Eq. 7.3 reveals that the optimum mean squared error of the controller has no causal restriction with sinusoidal signals). It is possible to calculate the theoretical magnitude of the reflection coefficient from

the real and imaginary parts of the velocity error as in Section 6.2 on Page 102. However the experiment observed the mean squared velocity error and not the real and imaginary parts, so theoretical calculation of the reflection coefficient can not be made.

7.8 PERFORMANCE OF MIC-ACCR FEEDBACK CONTROL SYSTEM

The previous two sections have described the stability and causal constraints of the digital feedback mic-accr adaptive control system. This section discusses the controlled impedance performance - the ability of the system to correctly force a desired impedance.

The laboratory implementation of the digital feedback mic-accr control system has been observed to force real impedances for normally-incident sinusoidal plane waves from 50Hz to 500Hz. Impedances that were much larger than 415 Rayls required cone pressure as the reference signal. Impedances that were much less than 415 Rayls required cone velocity as the reference signal. Both methods forced characteristic impedance when the feedback loop was stabilized with feedback cancellation. The adaptive convergence for these conditions was stable. Without feedback cancellation the feedback control systems were unstable when attempting to force certain values of desired impedance because of feedback loop instability. Theory for the controller stability has been presented in Sections 6.4.2 and 6.4.3 - if there is a delay in the controller then, in both cases, the stability depends on the radiation load, the natural specific acoustic impedance of the loudspeaker under control and the desired impedance. The experimental stability of the controller, outlined in Figure 83 on Page 252, was observed for sinusoidal incident waves as a function of controlled impedance. The filtered-X LMS algorithm adapted an 8 tap linear combiner with a sampling frequency of 3kHz and an update coefficient, α, of 0.001. The controller filter had a fixed delay of 1.3ms. The cone pressure was used as the reference input to the adaptive combiner. The adaptive compensation filter had 512 taps and the optional feedback cancellation filter also had 512 taps. The first observations were made without feedback cancellation. The value of the desired filter H was adjusted at spot frequencies to find the *minimum* stable

value of controlled impedance below which the loop would go unstable. These values are marked with circles in Figure 90 on Page 259. These values are of the same order as those suggested by the theory - see Section 6.4.2 - although differences occur because the radiation load is not purely characteristic. Above 200Hz the minimum values were all greater then 500 Rayls and these circles are marked with arrows to illustrate this. For desired impedances that were less than the marked values the controller was unstable without feedback cancellation - this is illustrated with the shaded area in Figure 90. The second observations were made with feedback cancellation. The desired filter **H** was set so that the impedance at 160Hz was close to 415 Rayls. Then the controlled impedance at other spot frequencies was measured with SWR measurements when the adaptive controller had minimised the error signal for this unique value of **H**. These values are marked as crosses in Figure 90. The controlled impedance deviated by up to ±20% from the desired value of 415 Rayls - this is explained in Section 7.9 on Page 230. Above 160Hz the controller was stable because of the feedback cancellation. However, at 315Hz the controller was still not stable. This is believed to have been due to errors in the model filter of the feedback path. These observations indicate that exact feedback cancellation can stabilise the feedback loop so that the mic-accr controller can force near-characteristic impedance for sinusoidal incident waves.

The digital control system was also observed to force desired impedances for plane wave normally-incident noise of sufficiently limited bandwidth. The delay in the forward path placed causal constraints on the control system performance, see Section 7.7 on Page 225. This research has demonstrated that the control system performance is related to the autocorrelation function of the noise and the delay in the system under control. The feedback control system with feedback cancellation was stable but could not completely converge when attempting to force a characteristic impedance for an octave band of noise centred on 200Hz.

The performance and also the stability of feedback control with feedback cancellation is related to the statistics of the noise and the dynamics of the

system under control. This is the subject of recent research by Elliott and Sutton (52). Observations of the mic-accr system show stable converged solutions for pure tone signals. However, for other noise signals there remains ambiguity about the performance of the feedback control system. An investigation of the controlled impedance performance for noise signals is recommended as further work.

7.9 IMPEDANCE OBSERVATION ERROR WITH THE MIC-ACCR METHOD

A theoretical treatment of the effects of impedance observation error on the mic-accr control system performance is given in Section 6.2 on Page 102. This section presents results from the laboratory test-rig that illustrate impedance observation error and the effect on the controlled impedance. Section 7.9.1 describes an experimental investigation of the accuracy of controlled impedance and concludes that there was impedance observation error in the laboratory test-rig. Section 7.9.2 calculates the impedance observation factor defined in Section 6.2 from measurements of the pressure and velocity transducer accuracy described in Sections 7.4.2 and 7.4.3.

7.9.1 An experimental investigation of controlled impedance

The laboratory experiment ran two different digital active impedance control systems based on the filtered-X LMS algorithm set for desired characteristic impedance: (i) a mic-accr adaptive feed-forward system; (ii) a 2-mic adaptive feed-forward system originated from (29). Theoretical analysis in Section 6.9 on Page 157 shows that the optimum solutions of the adaptive filters are the same for these two control systems. The purpose of the experiment was to measure and compare the controlled impedance of the two systems. The two systems are detailed in schematics shown in Figure 91 on Page 260, and Figure 92 on Page 261.

Each system controlled the impedance of a KEF B200A loudspeaker at the left hand termination of a 5 metre waveguide. At the right hand termination is the source KEF B200A loudspeaker which was driven with electrical sinusoidal waves. Both control systems had: (i) the reference signal taken from the

electrical source signal; (ii) a sampling frequency of 7.16kHz; (iii) 48 taps in the linear FIR control filter; (iv) an update gain of 0.001; (v) 512 taps in the stability compensation FIR filter; (vi) sound pressure level of around 105dB at 100Hz at controlled cone surface. These measures were taken to allow comparison of the controlled impedance of the two systems. The use of the electrical source signal as reference input prevented feedback around the adaptive control systems. Feedback cancellation was therefore not required.

The mic-accr system detailed in Figure 91 was configured so that the desired impedance filter **H** is directly proportional to the desired impedance. This results from connecting the pressure and cone velocity signals as shown in Figure 26b on Page 99. The desired characteristic impedance was set by observing the standing wave ratio of the controlled KEF B200A for a source frequency of 160Hz. The single tap of **H** was manually adjusted to make a controlled impedance of 415 Rayls. The system was later tested without further adjustment of **H**. The mic-accr system instrumented the cone pressure with a microphone that was rigidly mounted in front of the cone - see Section 7.4.3 on Page 213. The cone velocity was taken from the cone-mounted accelerometer by connection method "Type 1" described in Section 7.4.2 on Page 207.

The 2-mic system detailed in Figure 92 forces the loudspeaker cone to have characteristic impedance. The desired filter was a single delay **Δ** which corresponded to the time delay of the spacing of the two microphones M1 and M2. This was 5cm in the experiment and set the digital sampling frequency of the system at 6.8kHz. However, experimentation revealed that a sampling frequency of 7.16kHz produced a controlled impedance that was closer to the desired characteristic impedance. Microphone M1 was positioned 4cm away from the controlled cone. The system used matched B&K microphones from a B&K intensity probe. The outputs of the two microphones were adjusted to be within ±0.2dB in magnitude over the experimental frequency range using the MLSSA measurement system.

Both systems were allowed to adapt with sinusoidal waves over a range of 50-500Hz. SWR tests were made after complete convergence at single frequencies. The magnitude and phase of the impedance are calculated from the SWR results. Observation of the 2-mic system performance included measurement of the pressure and cone velocity signals.

The controlled impedances of the two systems were different despite having the same adaptive filter. Figure 93 on Page 262 displays the results. The solid lines show the measured magnitude and phase of the controlled impedance of the mic-accr system. The system is described as #1 to distinguish the connection of Figure 26b on Page 99 from that of Figure 26a which is described later with #2. The controlled impedance at 160Hz had magnitude 414 Rayls and phase 0.0069 radians. At other frequencies the controlled impedance deviated from the desired characteristic impedance by up to 80 Rayls and 0.93 radians of phase. The dashed lines shows the magnitude and phase of the controlled impedance of the 2-mic system. This system was closer to the desired characteristic impedance over the frequency range with maximum deviation of 38 Rayls and 0.094 radians.

The poorer performance of the mic-accr was studied by experimental investigation. The first test re-configured the connection system to that of Figure 26a (here designated #2) and set **H** to the inverse of **H** used in #1. The controlled impedance for the two configurations are shown in Figure 94 on Page 263. The two configurations had similar controlled impedances. There were different values of magnitude at 63Hz and 250Hz, however the results do not explain the difference between the 2-mic and mic-accr system. The next test adjusted the magnitude of the desired filter **H** by $\pm$1dB for the configuration #1. The controlled impedance magnitude was changed by around $\pm$1dB as shown in Figure 95 on Page 264 but with little difference in the controlled phase. This indicates that the magnitude of **H** in #1 was set correctly.

Observation of the cone pressure and cone velocity whilst the 2-mic system controlled the impedance revealed the reason for the poorer performance of the

mic-accr system: the cone pressure and cone velocity measurements did not observe the true values. Results are shown in Figure 96 on Page 265. The solid lines shows the magnitude and phase of the controlled impedance of the mic-accr system taken from Figure 93. The dashed lines shows the magnitude and phase of the observed impedance calculated from pressure and cone velocity measurements during control with the 2-mic system. The deviation in the controlled impedance of the mic-accr system is seen to be due to measurement error with the mic-accr method on the KEF B200A loudspeaker. This is examined in Section 7.9.2.

Later implementations of the mic-accr control system performed better. Using a cone mounted microphone and changing the accelerometer connections to "Type 2" (see Section 7.4.2 on Page 207) reduced the error in the observation of impedance phase over the 63-250Hz frequency range, see dashed line in the lower plot in Figure 97 on Page 266. The reduction in the phase of the controlled impedance significantly reduced the reflection coefficient of the controlled loudspeaker. See Section 8.1 on Page 271 for final results.

7.9.2 Impedance observation factor

The accuracy of velocity and pressure measurements with the BU-1771 accelerometer and KE4-211 microphone transducers has been described in Sections 7.4.2 and 7.4.3. This section describes the effect on the controlled impedance of the mic-accr control system. This is facilitated by the calculation of the "impedance observation factor" (described on Page 104 in Section 6.2) from the accuracy measurements. The controlled impedance is directly proportional to this factor and the desired impedance, see Equation 6.8 on Page 104.

The impedance observation factor contains two scaling terms. The first term, **k** in Equation 6.8, describes the sensitivity and accuracy of pressure and velocity measurements and the second, $\mathbf{k}_h$ in Equation 6.8, is a scaling term in the desired filter **H**. This is included to allow compensation for **k**. It is easy to compensate for **k** when the magnitude is frequency-independent: this is a simple

adjustment of the gain of the desired filter. However, it is more difficult to accurately specify k_h for frequency-dependent values of **k**. During practical experiments k_h was set as a simple gain with no phase component. Typically, the controlled impedance was measured at a single frequency with SWR techniques and the gain of k_h set manually so that the impedance would be as close to the desired value as possible. The residual difference between the controlled and desired impedance was then due to frequency-dependent inaccuracies in the pressure and velocity measurements. The transducers have been compared with Brüel and Kjær transducers and the results are presented in Sections 7.4.2 and 7.4.3. The impedance observation factor will now be calculated from these results, assuming that the magnitude is corrected as would be the case in the practical experiments with the gain adjustment of k_h. This is called the "calculated factor" in the subsequent text. The impedance observation factor measured in the test-rig, the transfer function between the controlled and desired impedance - the "measured factor", will be compared with the calculated factor. Also, the phrase "impedance observation factor" is abbreviated to z_f in the subsequent text.

The calculated and measured z_f are compared for the four configurations of transducer connection. The microphone is either mounted in a rigid spider or on the surface of the cone - the comparison of pressure measurement with a B&K microphone is shown in Figure 81 on Page 250. The accelerometer is wired with one of two methods - the comparison of velocity measurement with a B&K accelerometer is shown in Figure 75 on Page 244. The calculated z_f is determined by calculating the transfer function between the velocity comparison and pressure comparison, assuming that the B&K measurements are accurate, and normalising the result so that the magnitude of z_f is close to unity below 200Hz. The measured z_f was taken from a filtered-X LMS mic-accr control system sampling at 3kHz forcing a desired characteristic impedance for sinusoidal plane waves with the desired filter adjusted to make the magnitude of z_f unity at 160Hz.

The calculated and measured values of z_f with rigid mounting of the microphone are shown in Figure 98 on Page 267 for Type 1 wiring of the accelerometer, Figure 99 on Page 268 for Type 2 wiring (the pressure minima locations in the duct at 50Hz and 65Hz were outside of the physical range of the trolley mic, therefore results are not available at these frequencies). The values of z_f for the cone mounted microphone are shown in Figure 100 on Page 269 for Type 1 wiring and Figure 101 on Page 270 for Type 2 wiring. Also, the magnitude of the reflection coefficient is shown for each configuration. The "calculated" reflection coefficient was directly calculated from the calculated values of z_f. The "measured" reflection coefficient was determined with SWR measurements on the laboratory test-rig.

The four configurations have different calculated values of z_f - this is because of different observation of pressure and velocity by each configuration. Typically, the calculated z_f magnitude is less than 2dB from unity and the phase is less than 20°. The maximum calculated magnitude of reflection coefficient is around 0.2. The calculated z_f results are best for the configuration of cone microphone and Type 1 wired accelerometer. The calculated z_f of the other configurations have more phase. The measured z_f magnitude is within 1.5dB of the calculated z_f magnitude below 250Hz for all of the configurations, and the phase is within 20°. The measured z_f results are best for the configuration of cone microphone and Type 2 wired accelerometer. Although the trend of the plots are not closely matched, the differences between calculated and measured values of z_f and the ideal value of z_f (unity magnitude and 0° phase) are of the same order below 250Hz. However, a more important observation is that there are significant differences between the calculated and measured values of z_f above 250Hz. Therefore, the accuracy of the transducers does not fully describe the measured value of z_f at these frequencies. The calculated values of z_f were determined from the comparison of the transducers with B&K transducers. Other potential components that were not included are: (i) mass-loading of the cone by the transducers; (ii) near-field effects on pressure measurements; (iii) data acquisition and filtering errors in the control system; (iv) the accuracy of the B&K transducers and measurements.

Mass-loading of the KEF B200A cone has been observed, see Section 7.4.2.1 on Page 210. However the results do not provide an accurate description of the effects on the cone velocity measurement. Techniques that measure point velocity such as "laser velocimetry" would be useful in further studies of this problem. Near-field effects have not been considered because theory in the literature (such as Section 8.8 of (3)) suggests that there is no near-field for a piston of the KEF B200A cone size with incident plane waves of the frequencies (up to 500Hz) encountered in the test-rig. The data sampling convertors and anti-aliasing filters have been reversed with little change in the controlled impedance, see Figure 94 on Page 263, therefore these processes are considered near-identical. Therefore the value of **k** (which accounts for the difference in the pressure and velocity observation, see Equation 6.7 on Page 104) is not affected and consequently the effect on z_f is negligible. The B&K transducers and MLSSA measurement system were the most accurate devices available to the author and are assumed to be correct.

The value of controlled impedance is directly proportional to the value of the impedance observation factor z_f. For the KEF B200A, the measured values of z_f below 250Hz are similar to values of z_f calculated from the difference in cone pressure and velocity measurement of the transducers with B&K transducers. Above 250Hz the mass-loading of the KEF B200A cone by the transducers is considered as the cause of deviation in the measured value of z_f. It has been suggested that techniques such as laser velocimetry could help to understand this problem further.

7.10 CHAPTER FIGURES

The figures referred to in this chapter appear on the following pages.

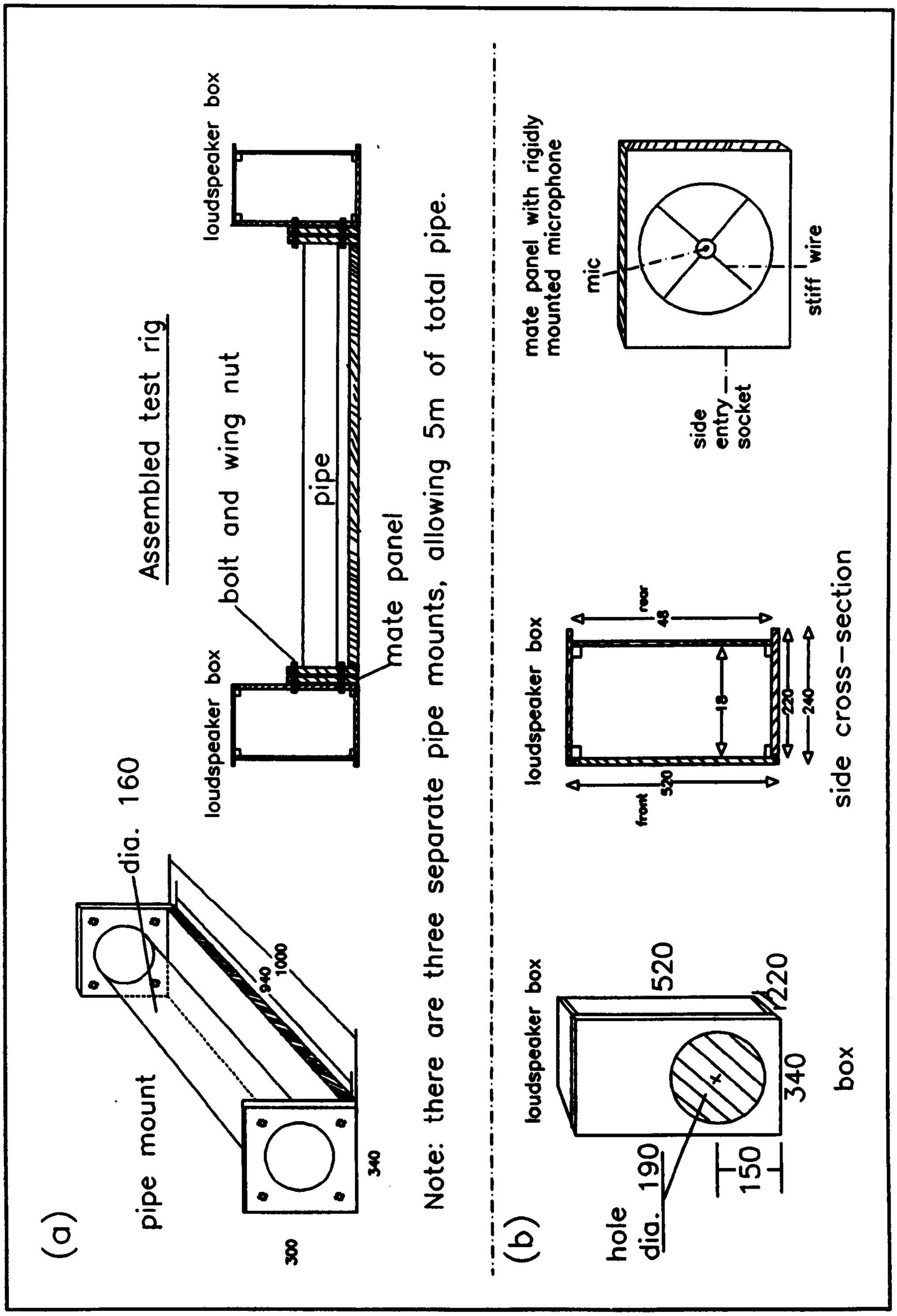

Figure 68. Test rig dimensions. Upper diagram (a) shows the supported duct and the assembled test-rig. Lower diagram (b) shows loudspeaker dimensions and the mate panel that is placed between duct and loudspeaker box.

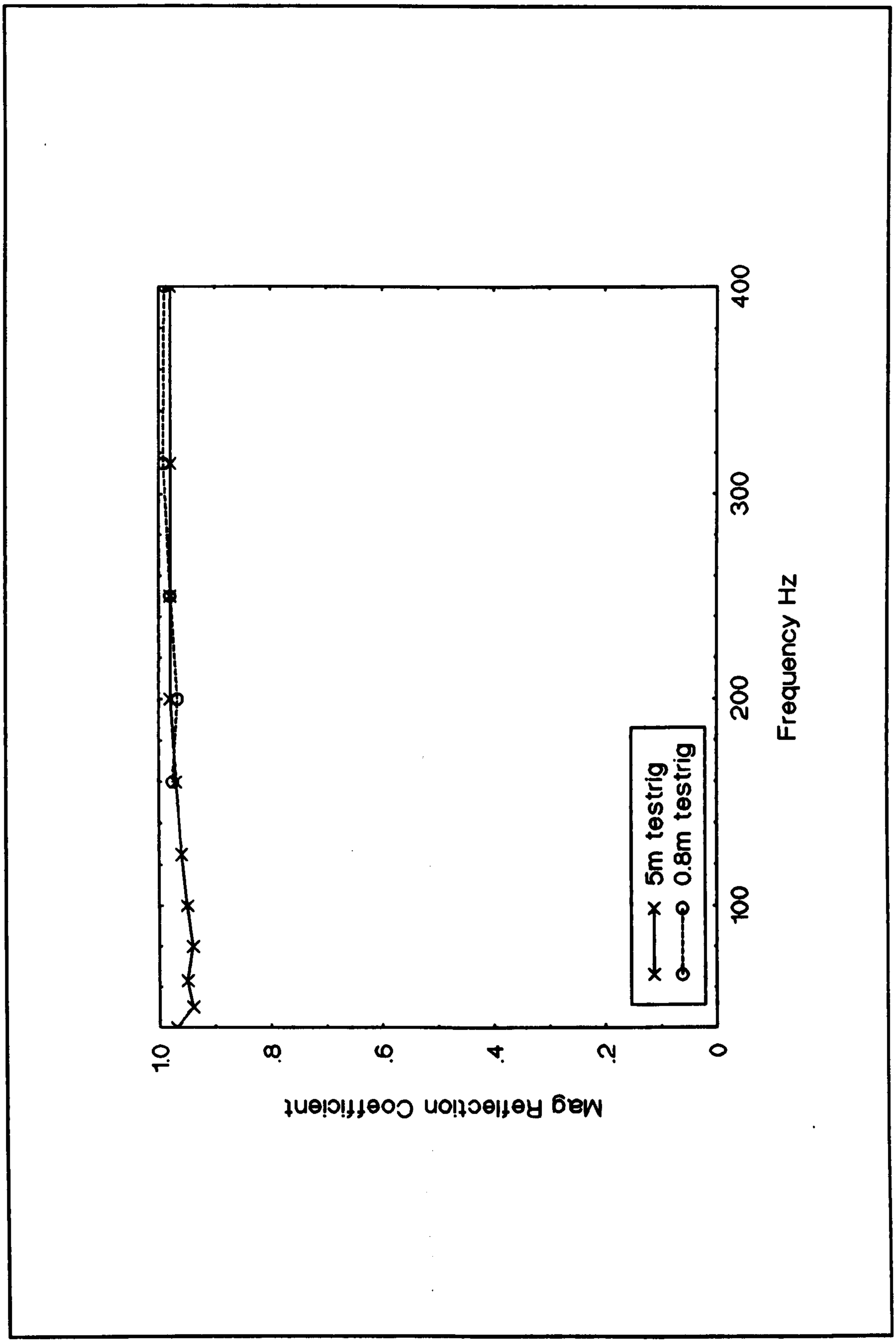

Figure 69. Measurement comparison of magnitude of reflection coefficient of lead-fronted plywood between two different acoustic waveguides.

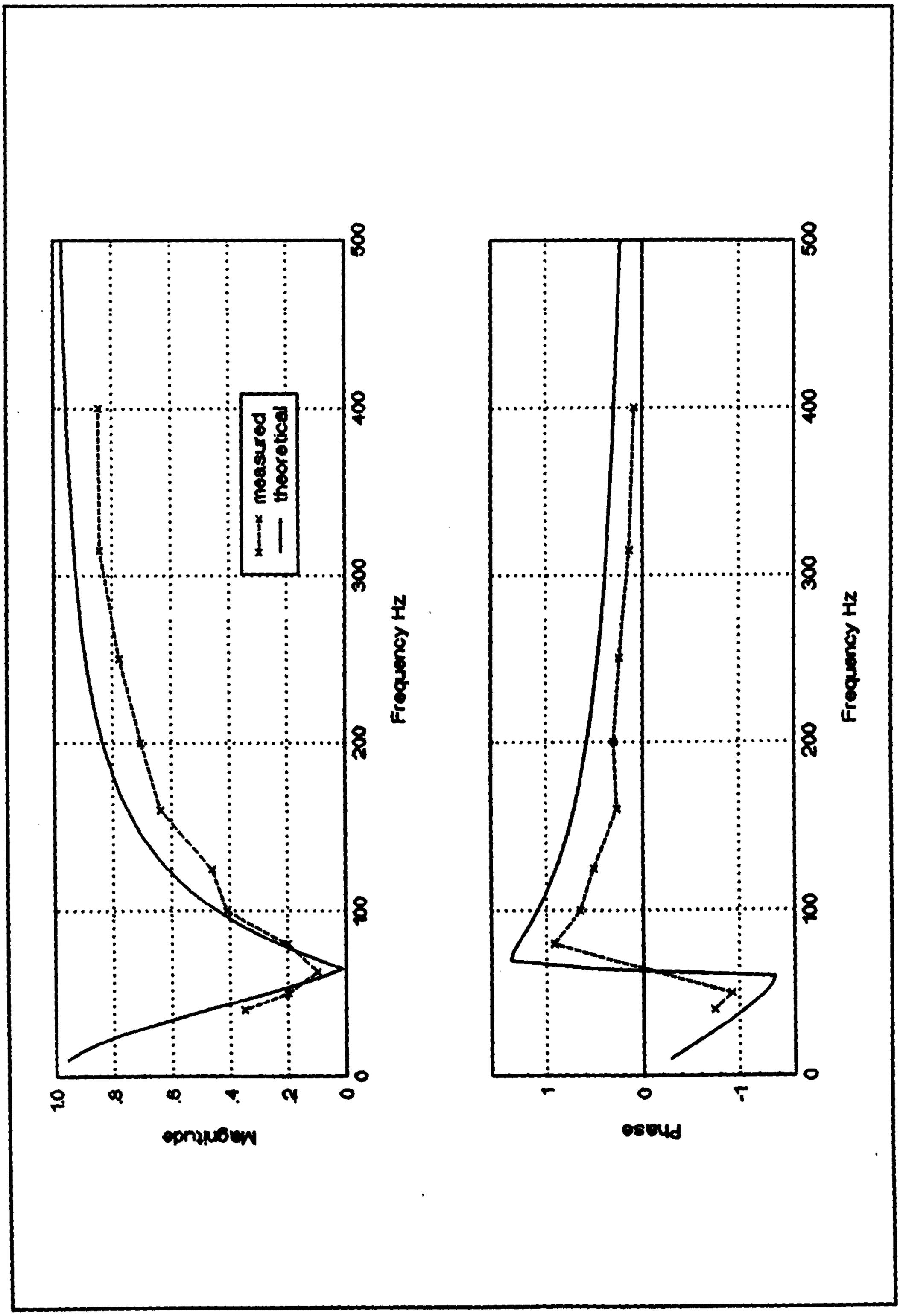

Figure 70. Theoretical and measured magnitude and phase of reflection coefficient for KEF B200A loudspeaker in a 25 litre box with packed glass-fibre filling.

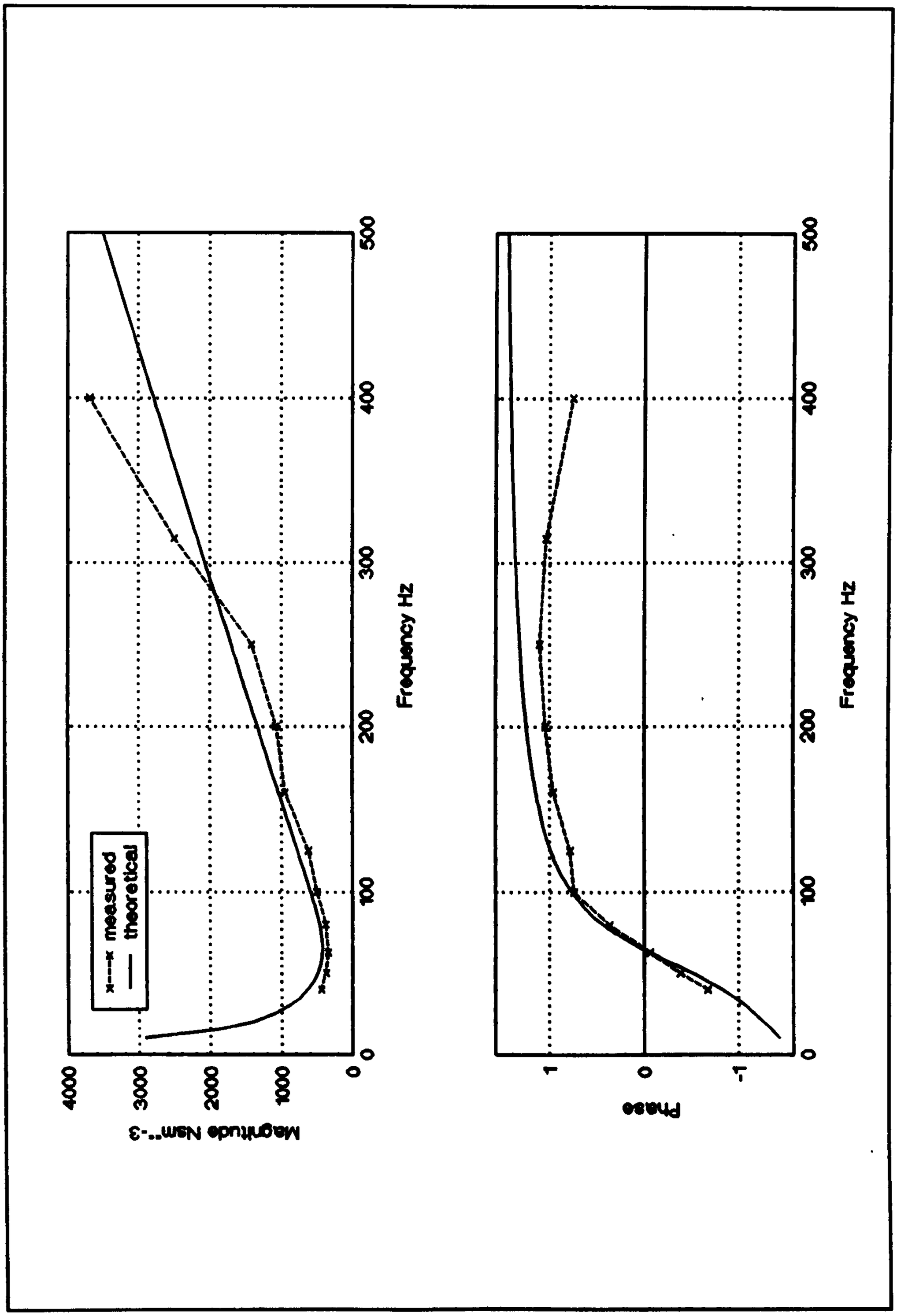

Figure 71. Theoretical and measured magnitude and phase of the input impedance of the KEF B200A mounted in a 25 litre cabinet with packed glass-fibre filling.

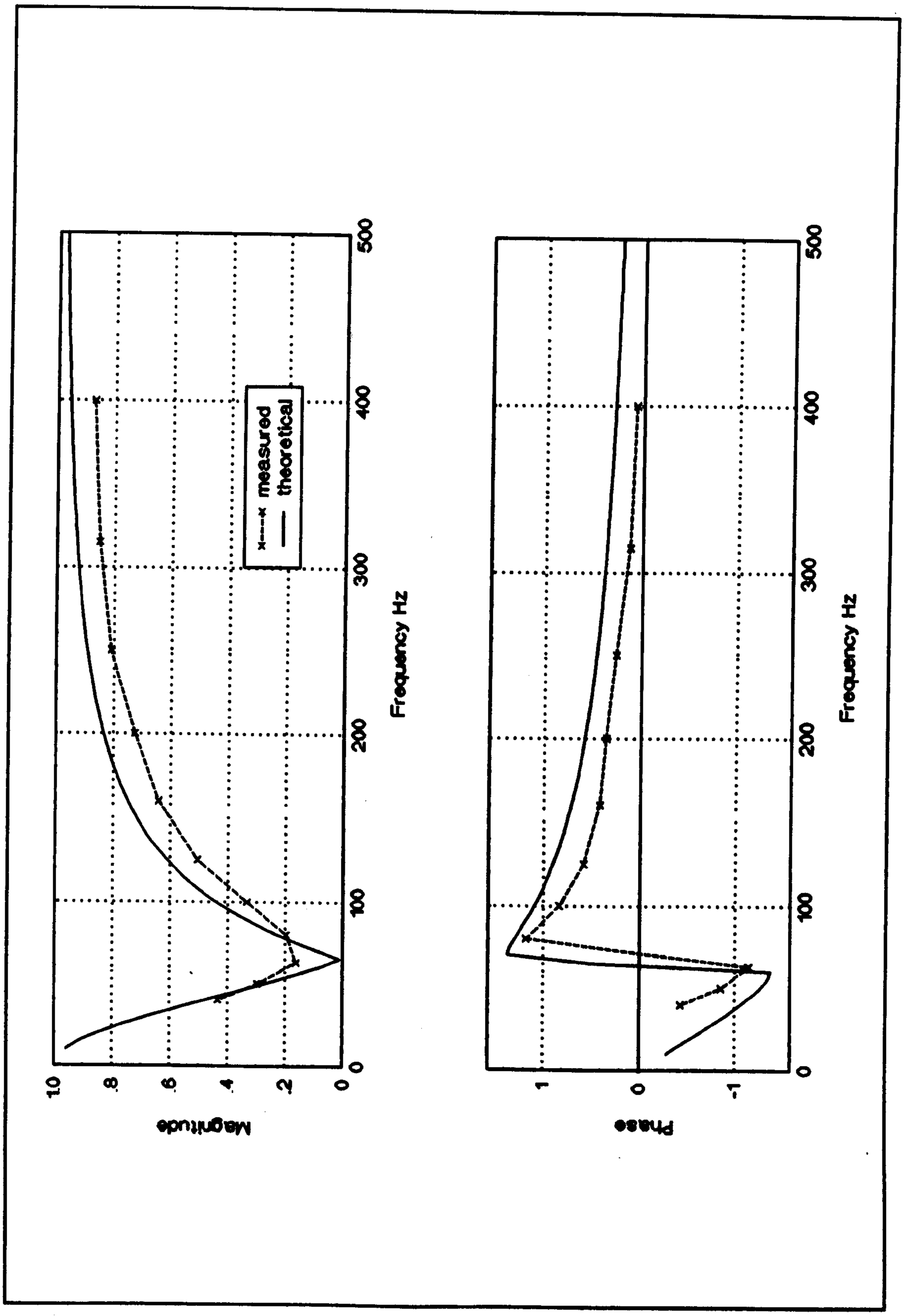

Figure 72. Theoretical and measured magnitude and phase of the reflection coefficient of the KEF B200A loudspeaker mounted in a 25 litre sealed box with no internal filling.

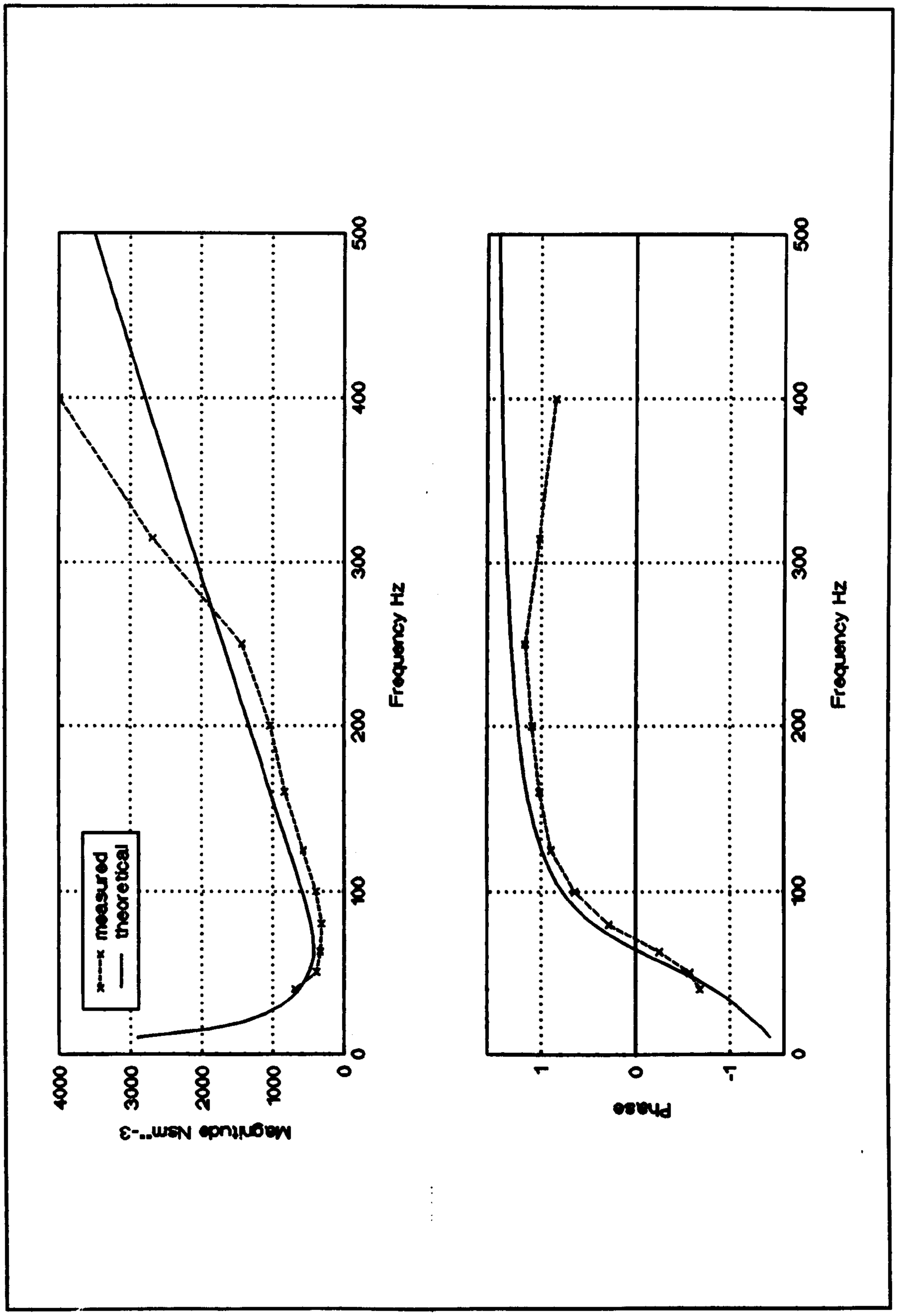

Figure 73. Theoretical and measured magnitude and phase of the input impedance of the KEF B200A mounted in a 25 litre cabinet with no internal filling.

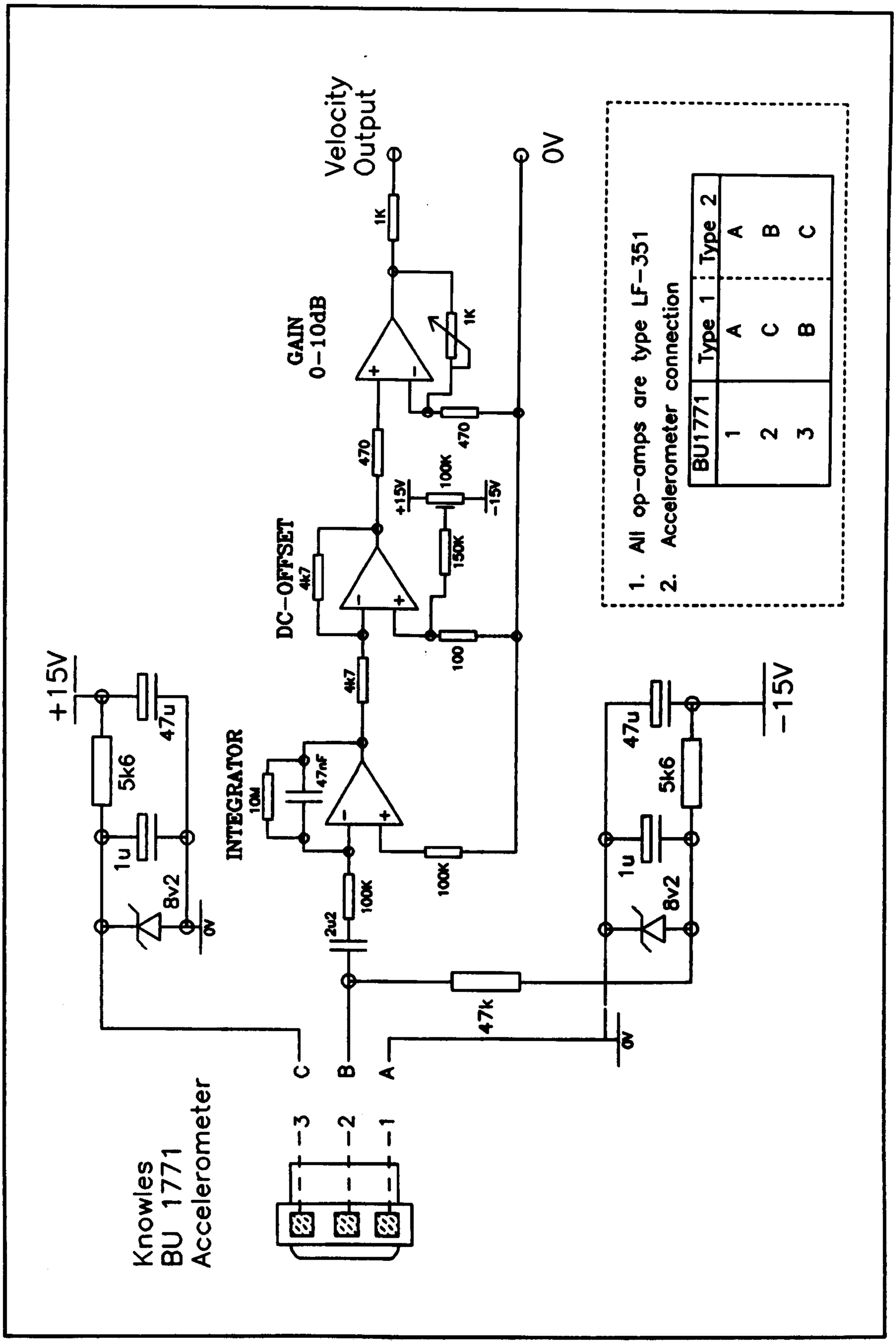

Figure 74. **Connection schematic and circuitry for the Knowles BU-1771 accelerometer. Connection Types 1 & 2 are explained in the text.**

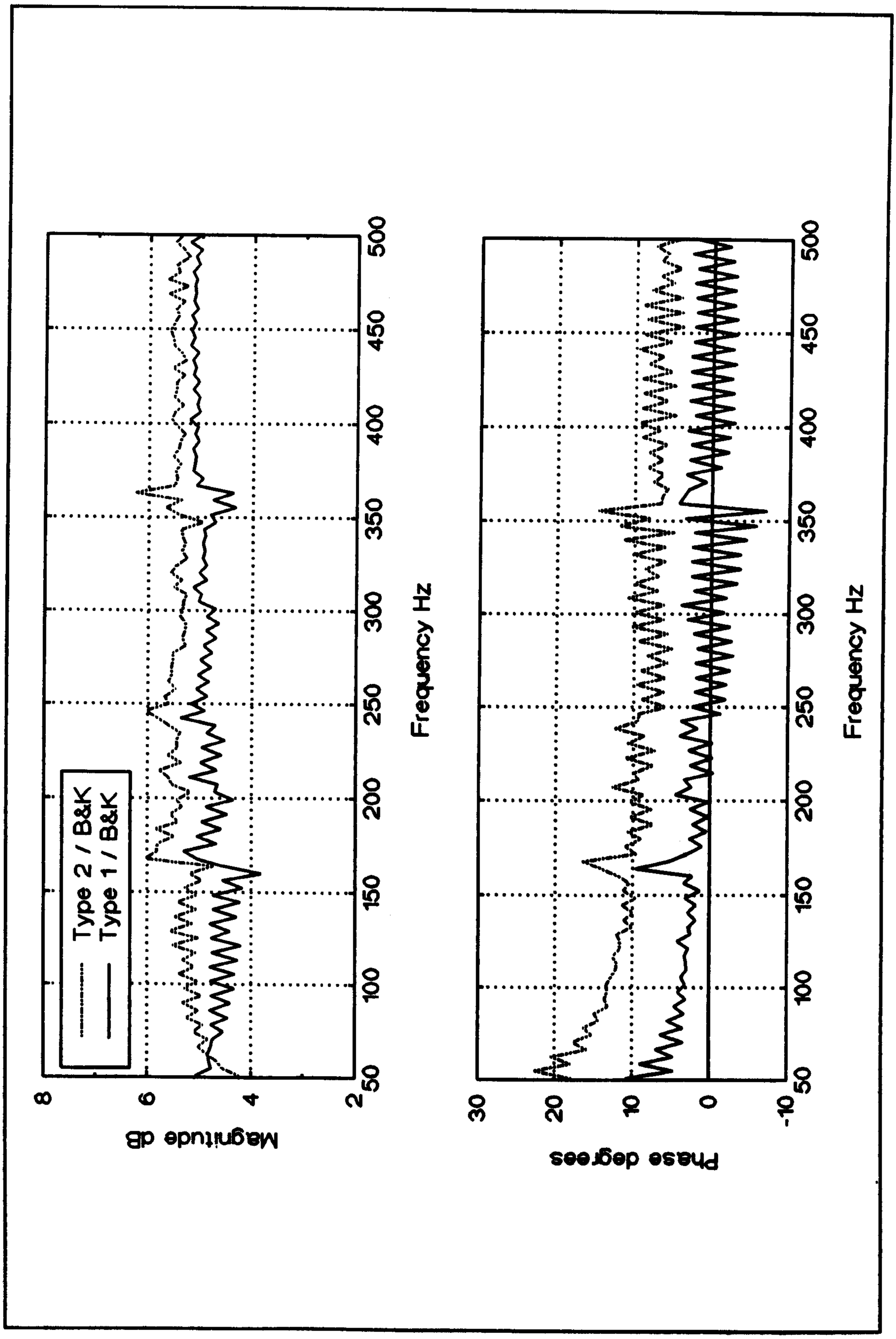

Figure 75. Magnitude and phase of velocity transfer function between Knowles BU-1771 with OP-amp circuitry and Brüel and Kjær accelerometer/charge amp.

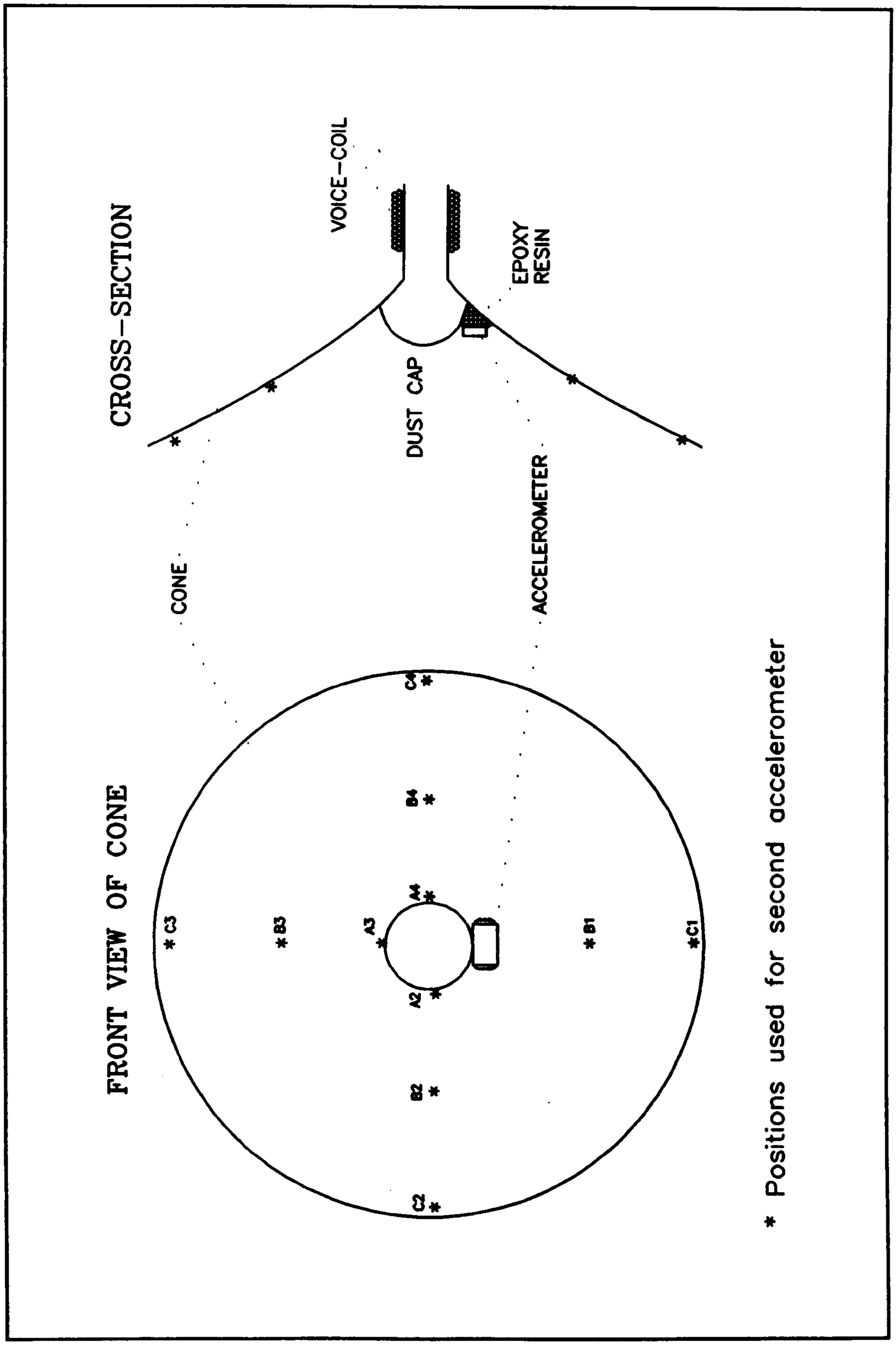

Figure 76. Accelerometer attachment locations used in the mic-accr system. Second accelerometer locations are shown by *.

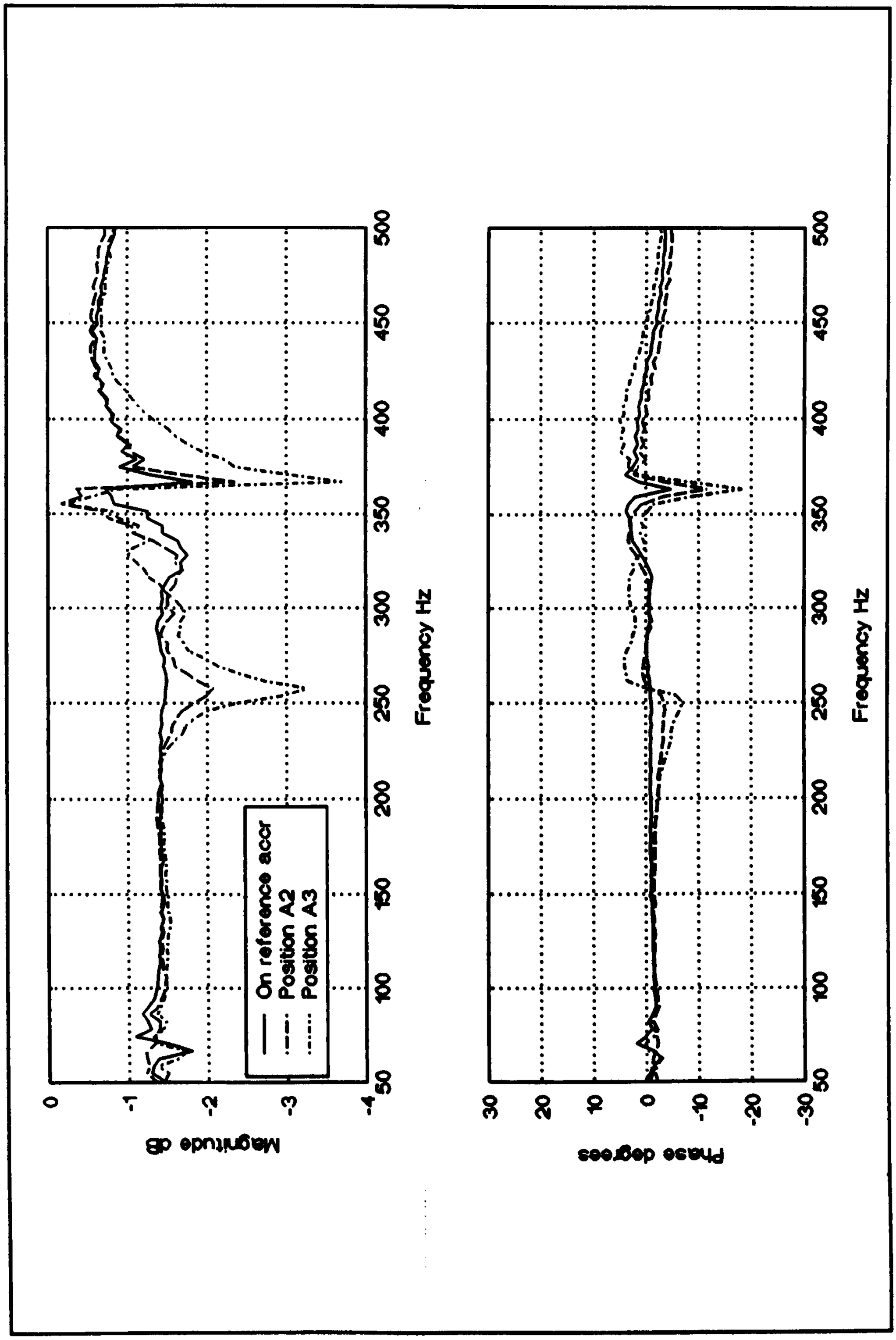

Figure 77. Transfer function between outputs of two BU-1771 accelerometers mounted at different positions on KEF B200A cone.

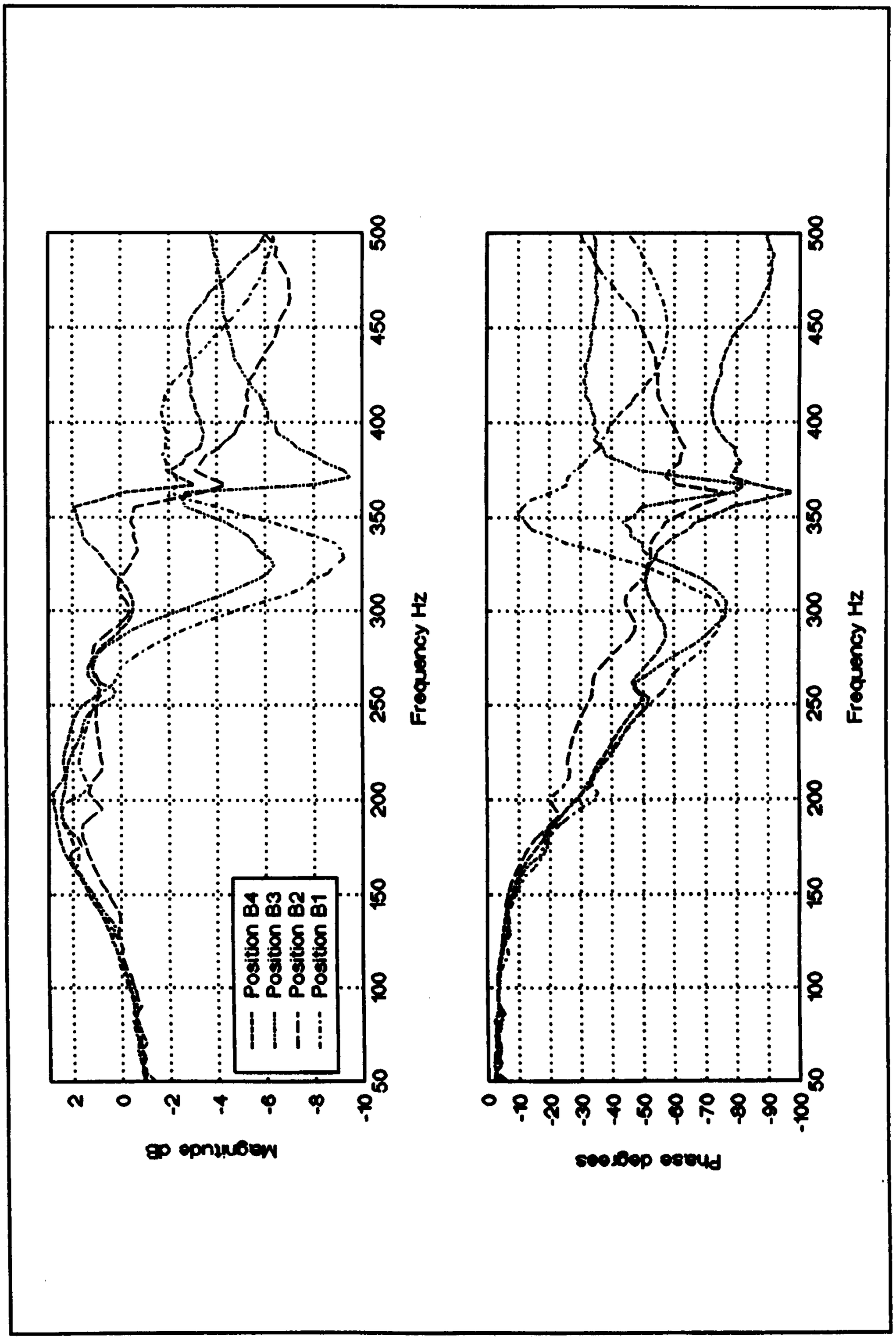

Figure 78. Transfer function between fixed accelerometer on KEF B200A loudspeaker cone and second accelerometer at other locations.

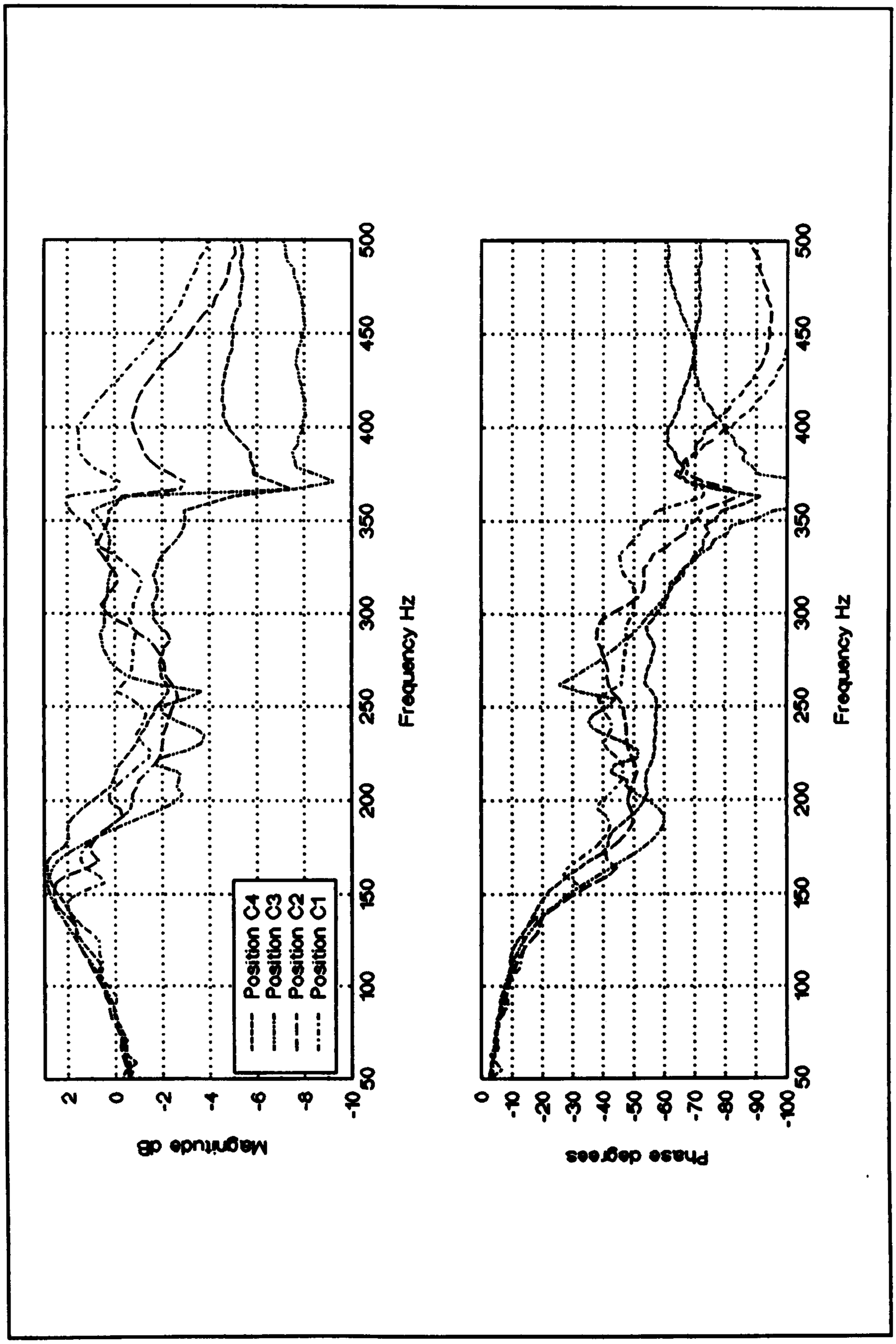

Figure 79. Transfer function between fixed accelerometer on KEF B200A loudspeaker cone and second accelerometer at other locations.

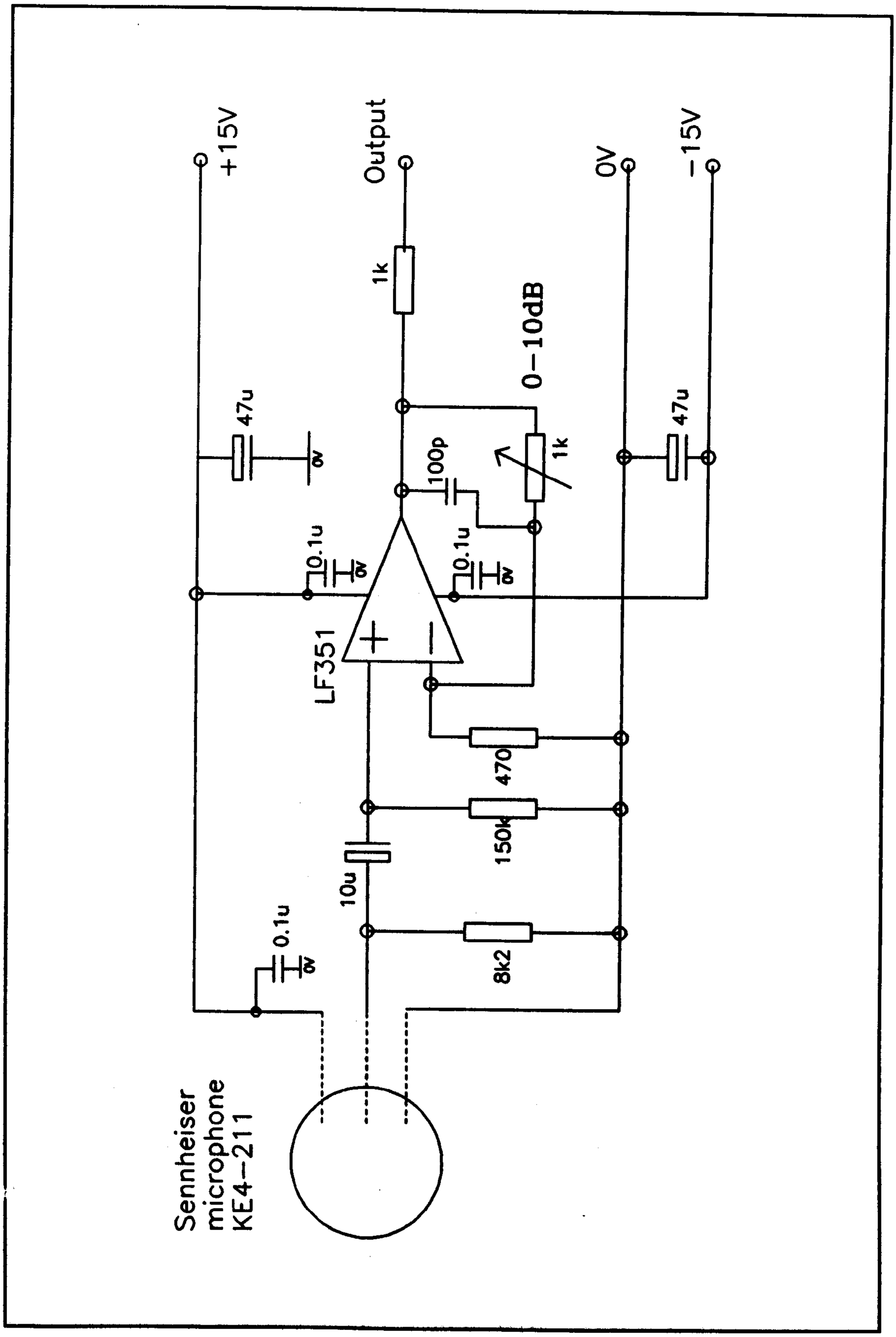

Figure 80. FET-biasing and buffering OP-amp circuitry for the Sennheiser KE4-211 microphone.

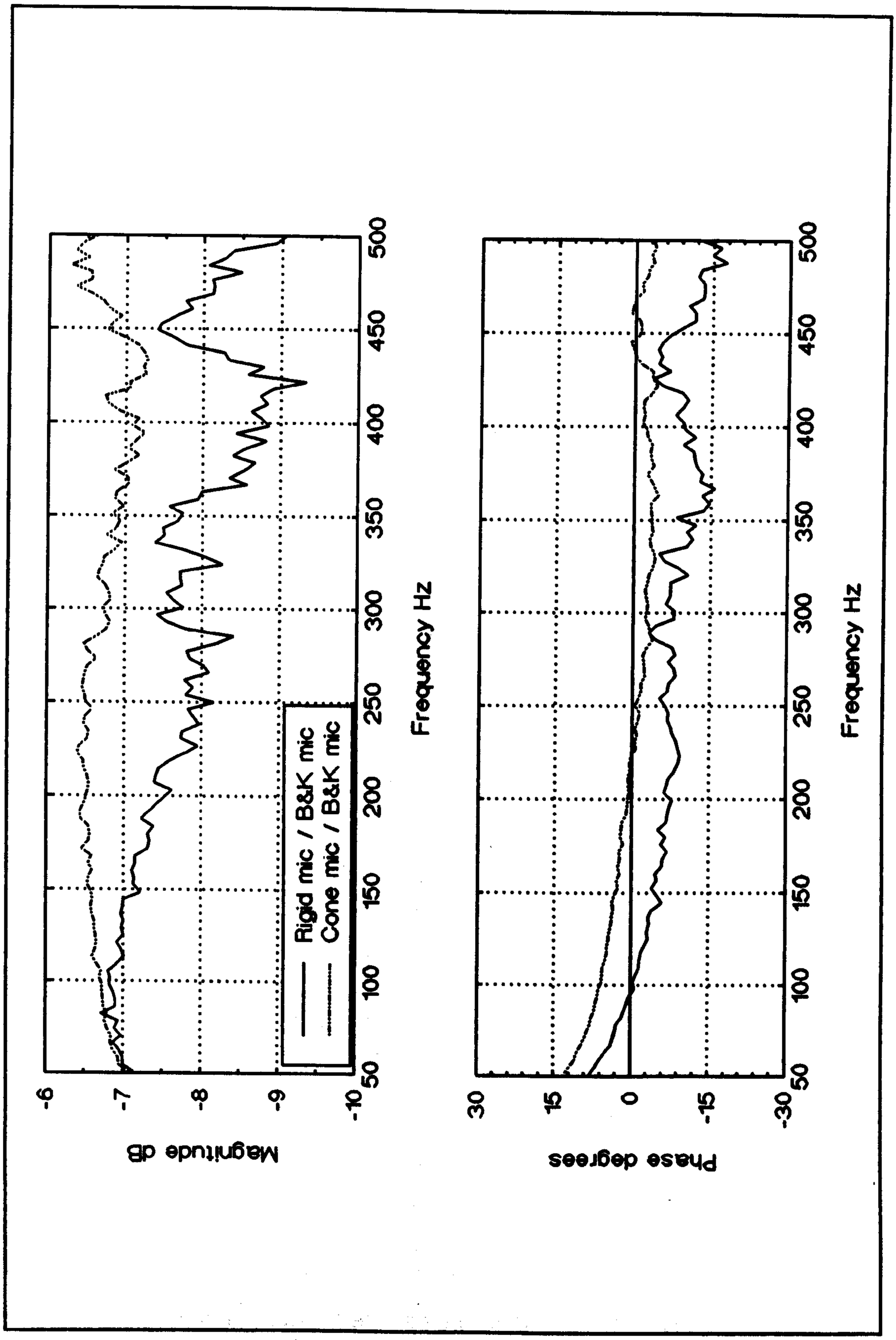

Figure 81. Un-normalised transfer functions between two Sennheiser KE4-211 microphones and a Brüel and Kjær 4135 microphone.

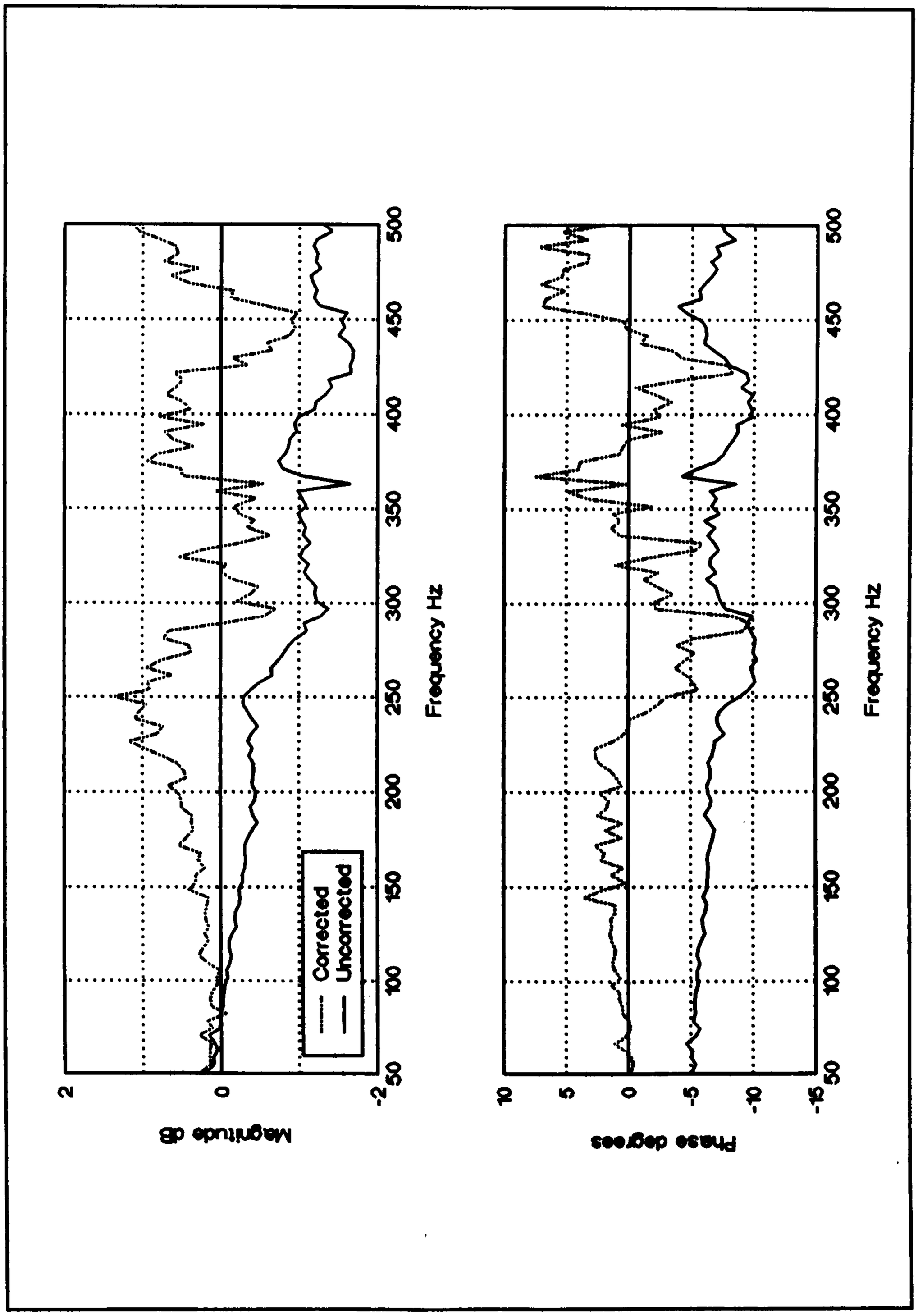

Figure 82. Transfer function between the Sennheiser microphone mounted on the mate panel and the Sennheiser cone microphone. The dotted line has a correction applied from the comparison of each mic with a Brüel & Kjær model 4135 microphone.

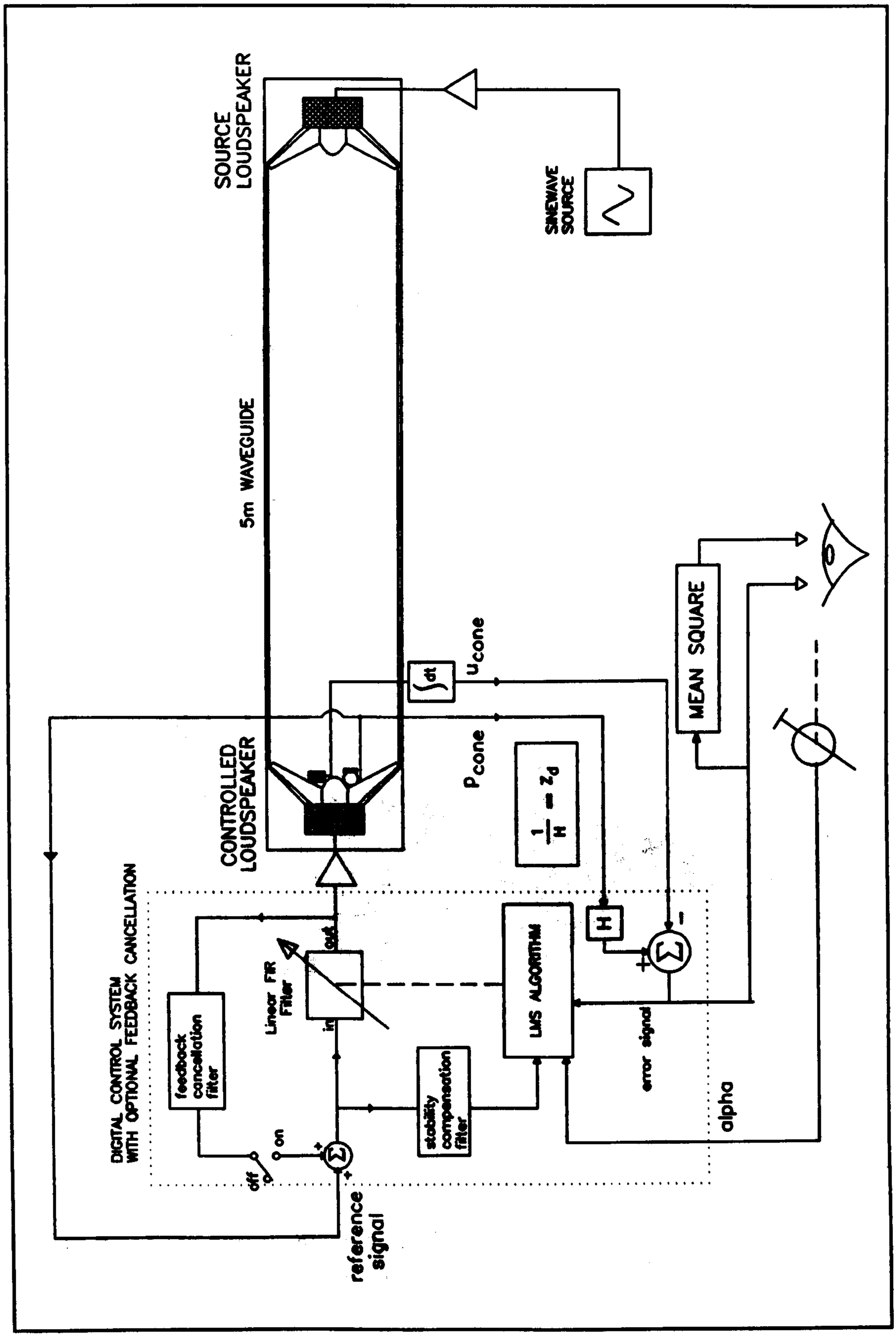

Figure 83. Mic-accr feedback adaptive control system based on the filtered-X LMS algorithm with selectable fixed feedback cancellation FIR filter.

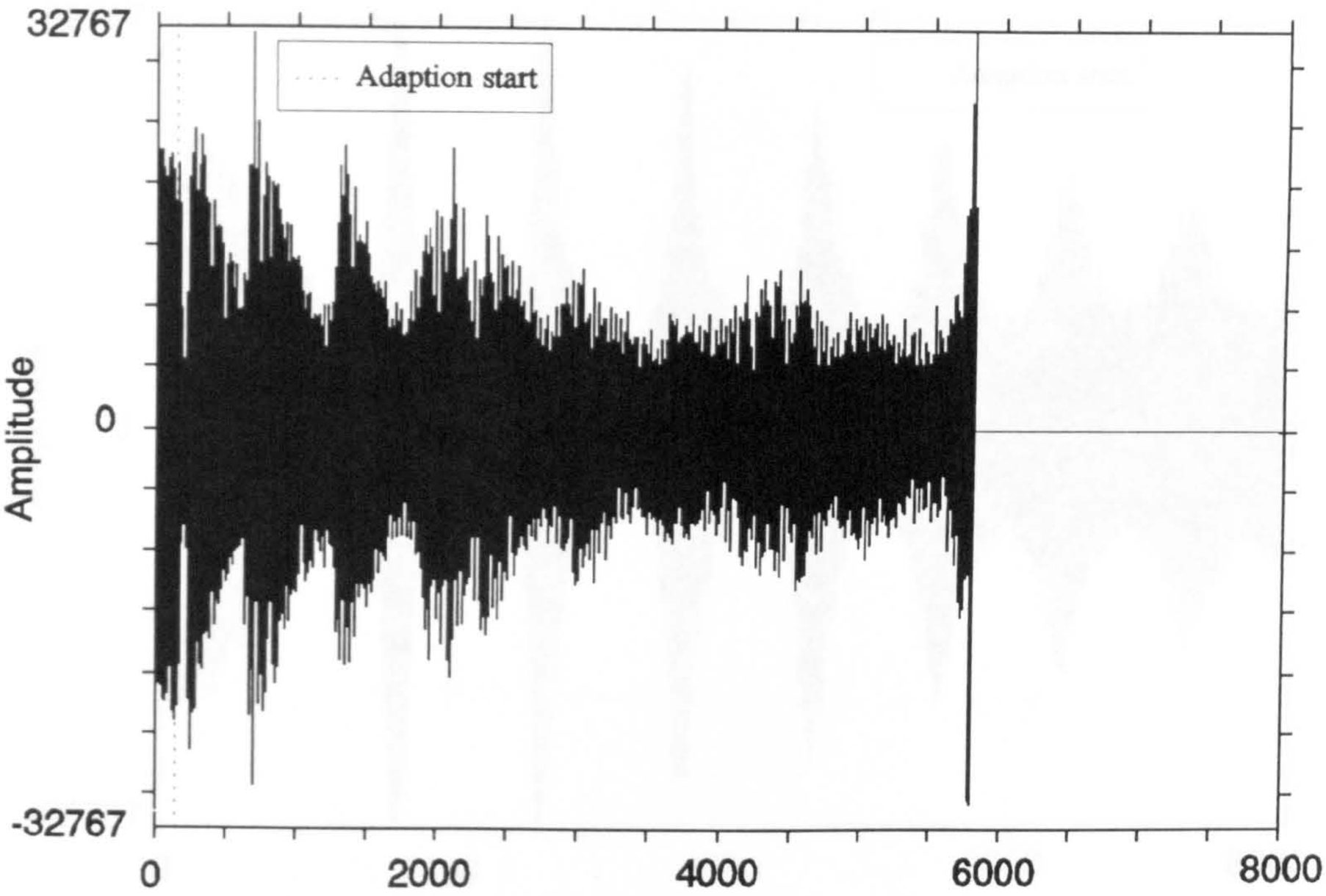

Figure 84. Time domain sampled plots of control system "bursting" error. Mic-accr system configured as a feedback system. Top plot for α=0.05, bottom for α=0.005.

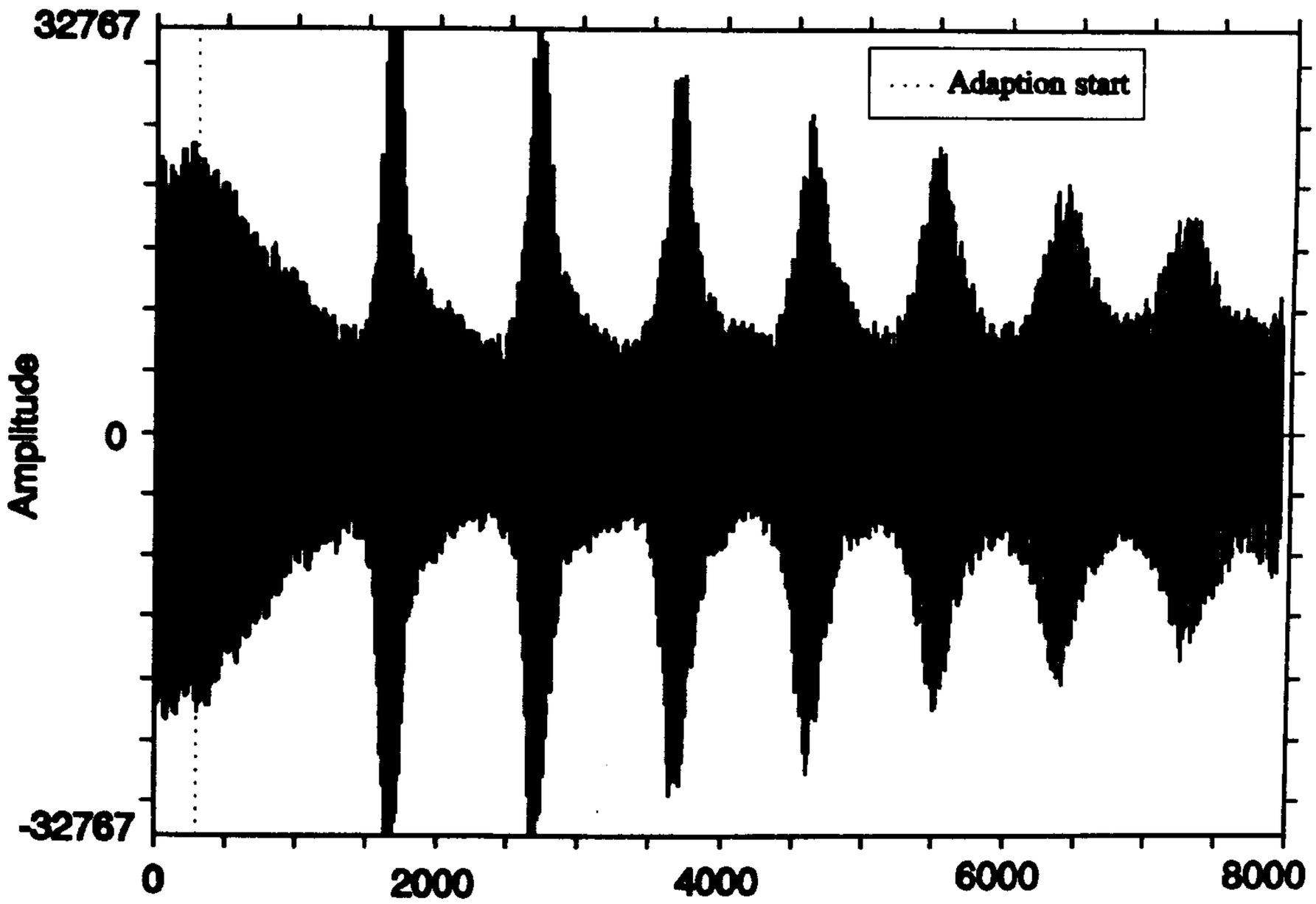

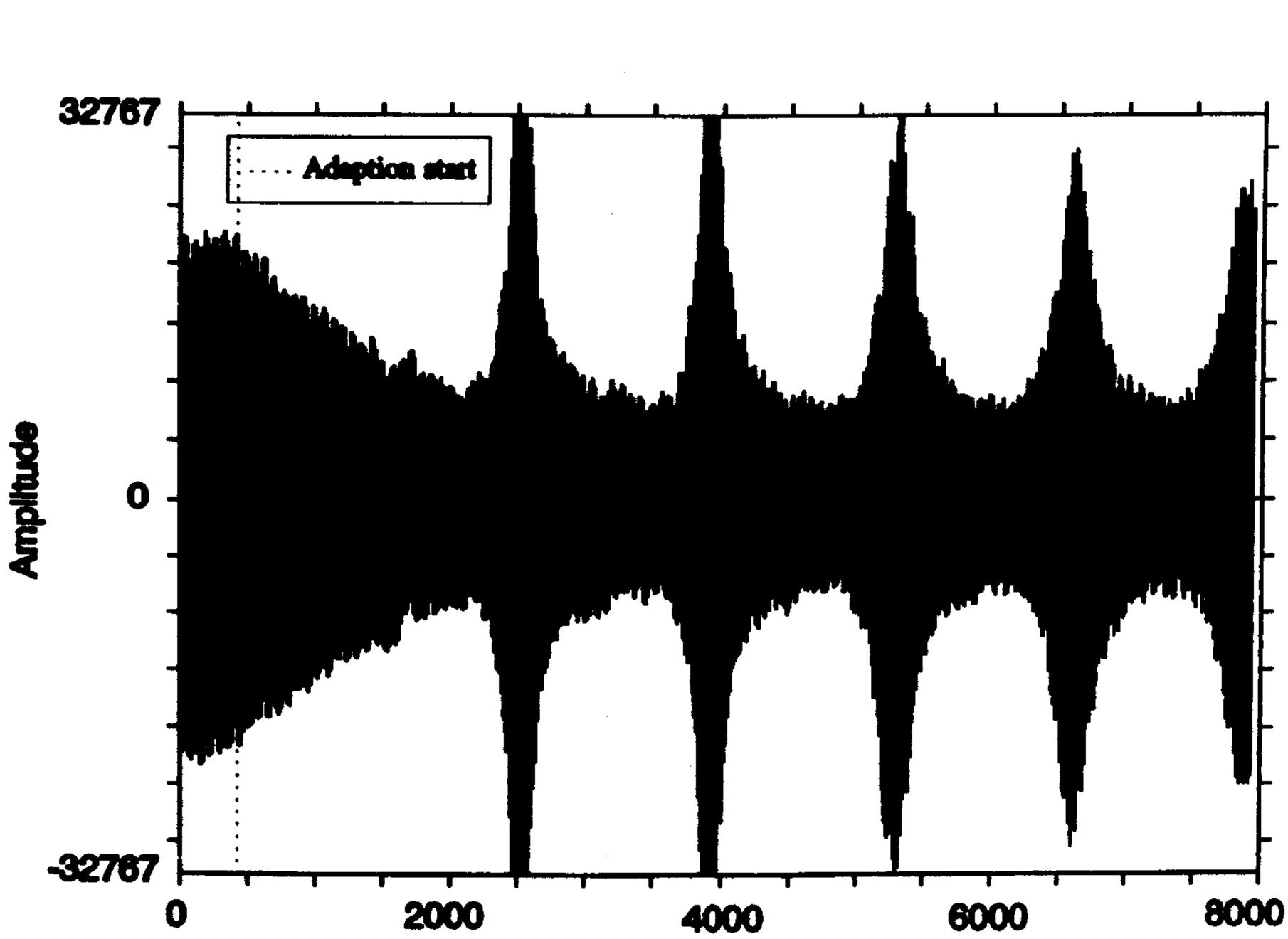

Figure 85. Time domain sampled plots of control system "bursting" error. Micaccr system configured as a feedback system. Top plot for α=0.001, bottom for α=0.0005.

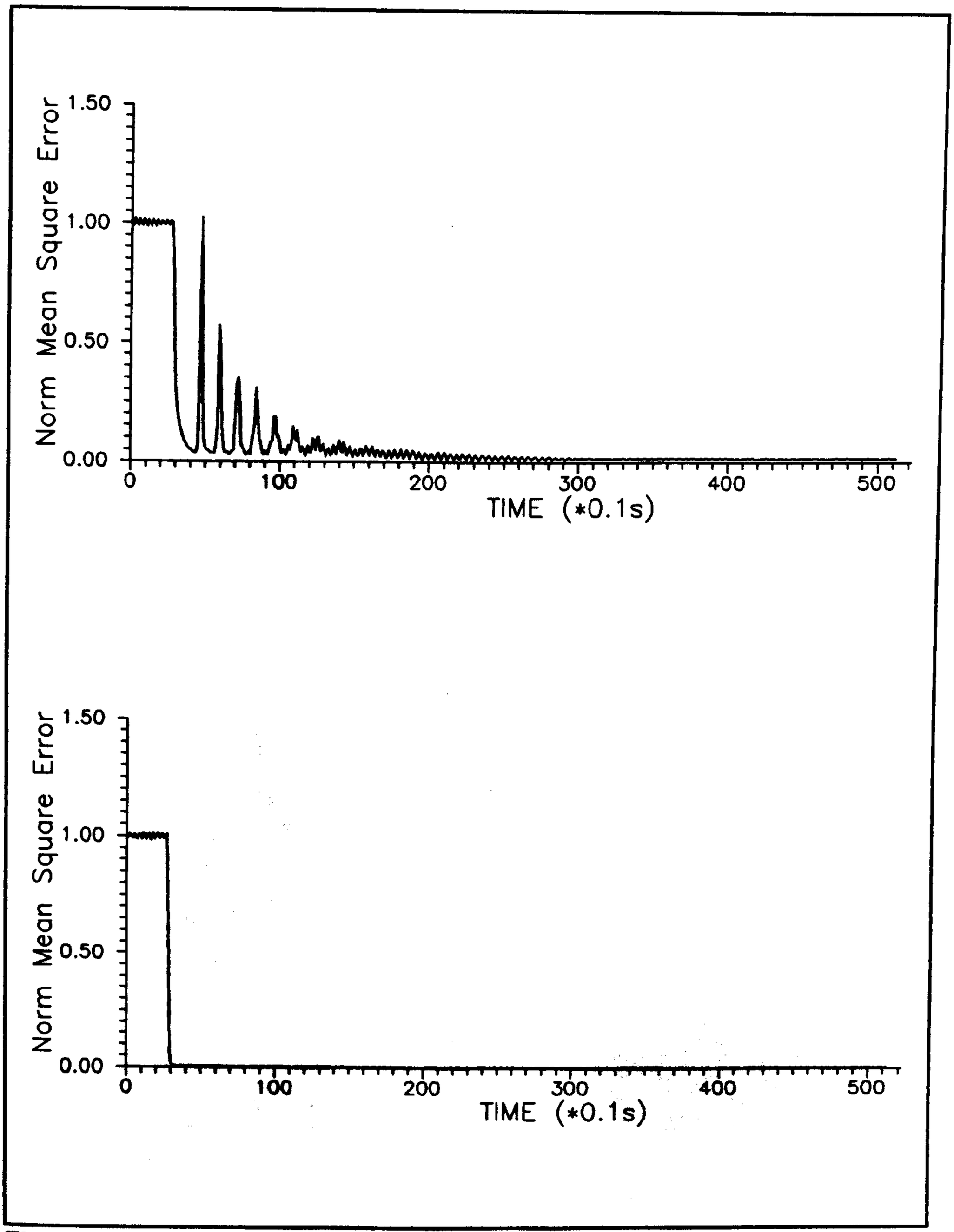

Figure 86. Normalised MS error of adaptive control system with cone pressure as reference, z_d = 1200 Rayls. Top figure for non-recursive filtered-X LMS algorithm. Bottom figure for recursive filtered-U algorithm.

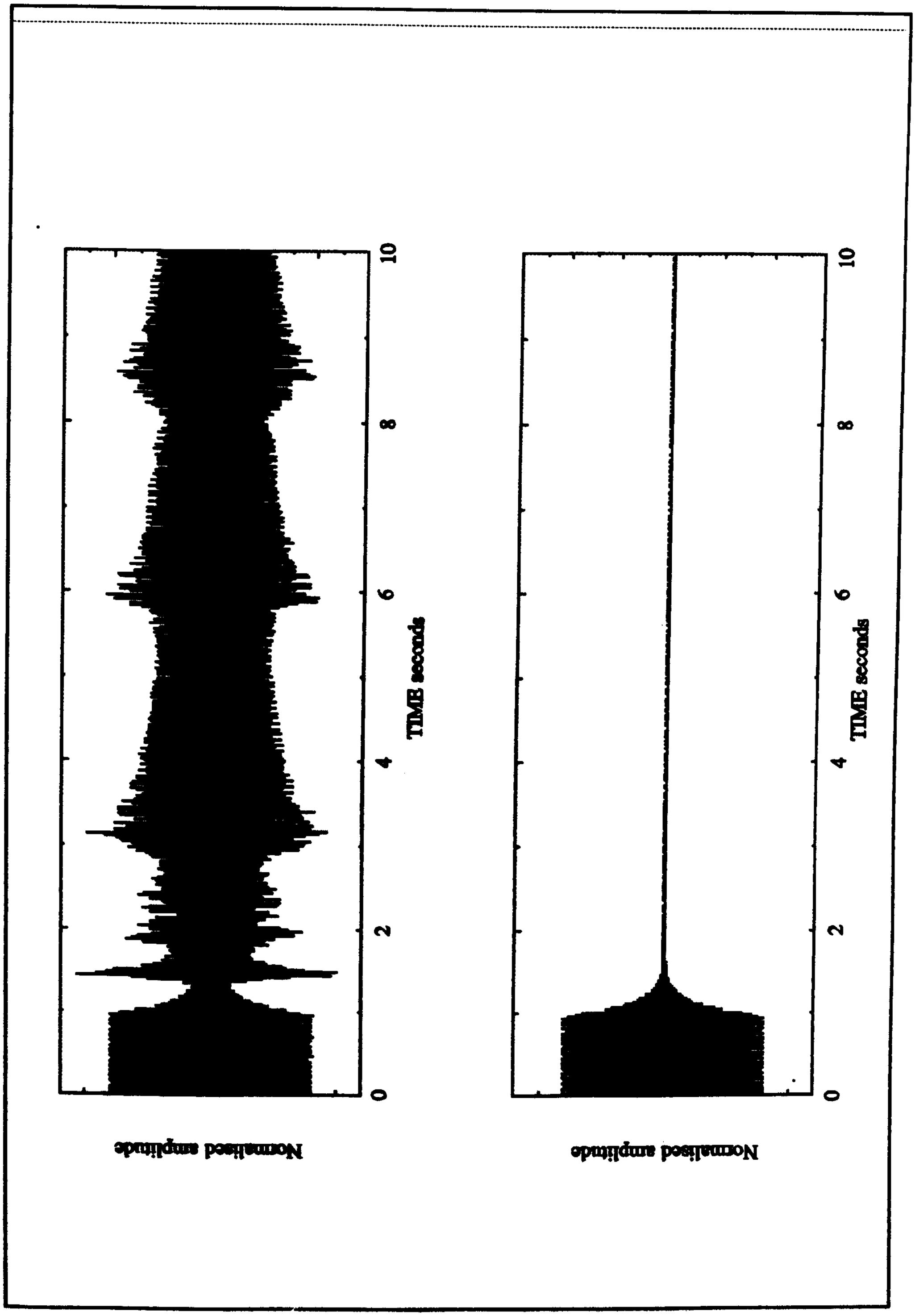

Figure 87. Normalised error of adaptive 8 tap filtered-X LMS mic-accr control system with cone pressure as reference, z_d=415 Rayls for 250Hz sine-wave. Upper plot without and lower plot with feedback cancellation.

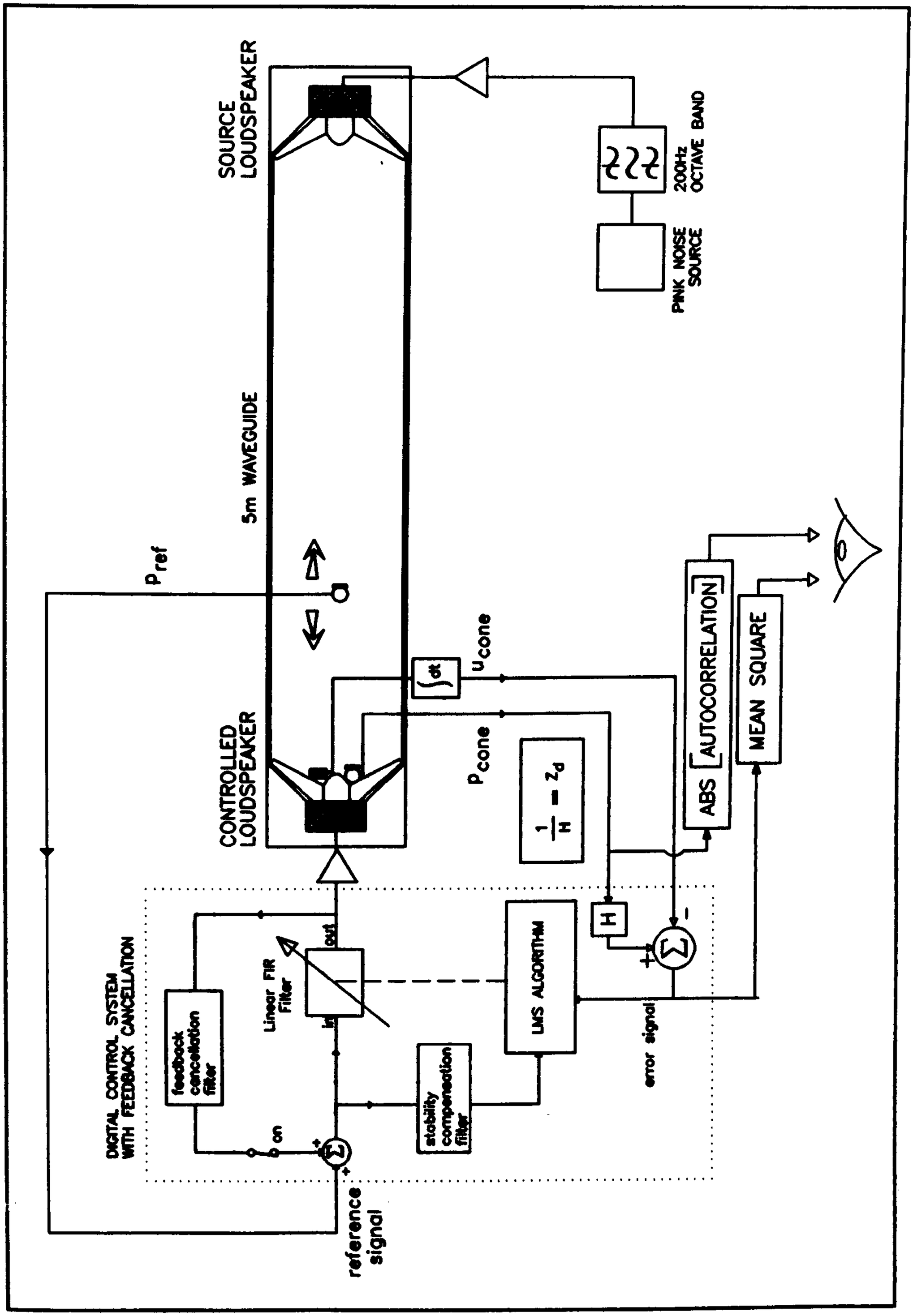

Figure 88. Laboratory test-rig of mic-accr adaptive control system configured for characteristic impedance $Z_d = \rho_0 c$. Acoustic pressure at different locations in the waveguide is used as reference signal.

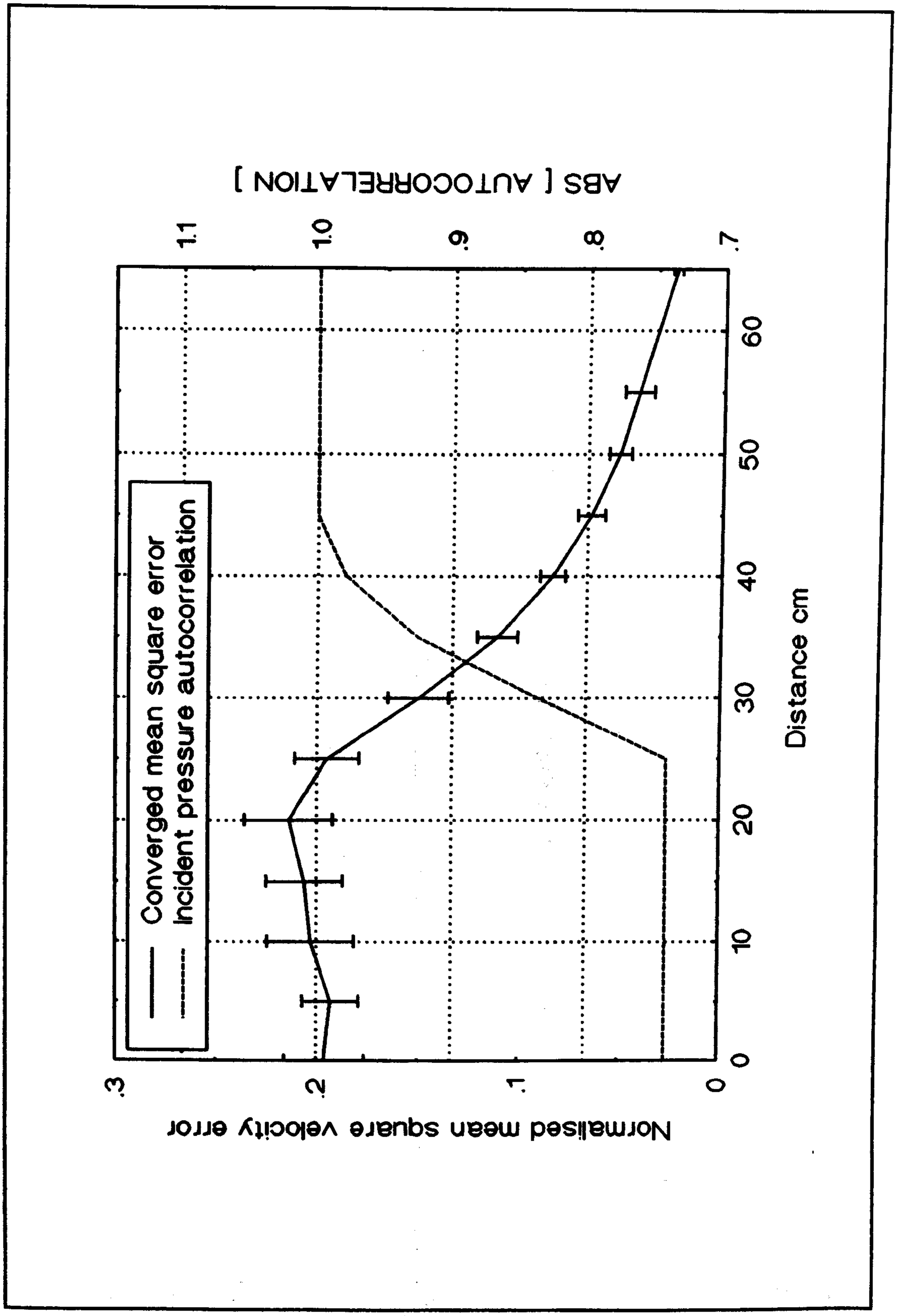

Figure 89. Converged MS velocity error and Max $\{|r_{xx}(\tau)|\}_{(\tau > (T-d/c))}$ for adaptive digital control (z_d=415) with upstream pressure detection (error bars show $\pm\sigma$).

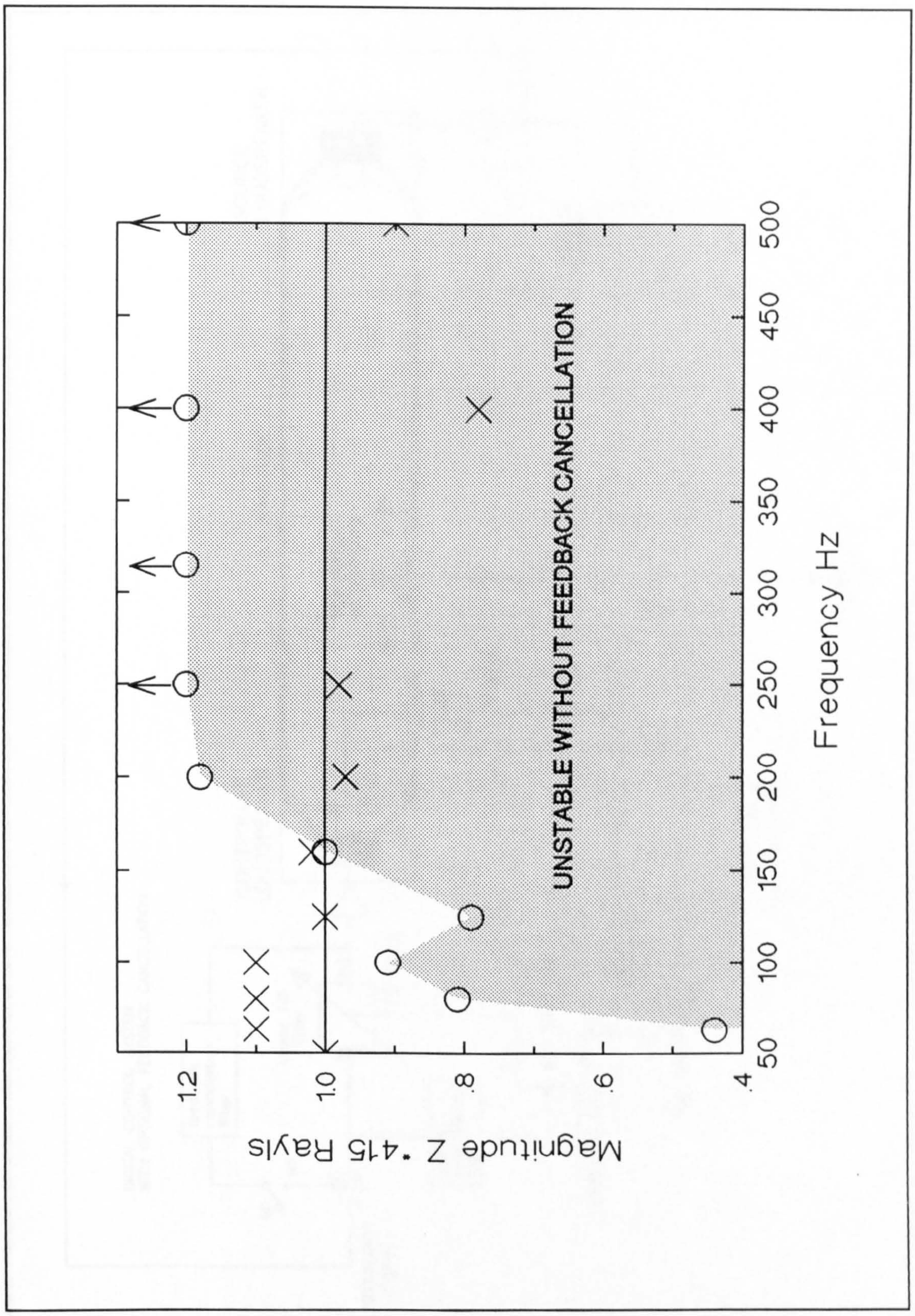

Figure 90. Controlled impedance magnitude for mic-accr control system with cone pressure as reference for spot sinusoidal waves. Circles show stability limits that exist without feedback cancellation, crosses show stable values with feedback cancellation.

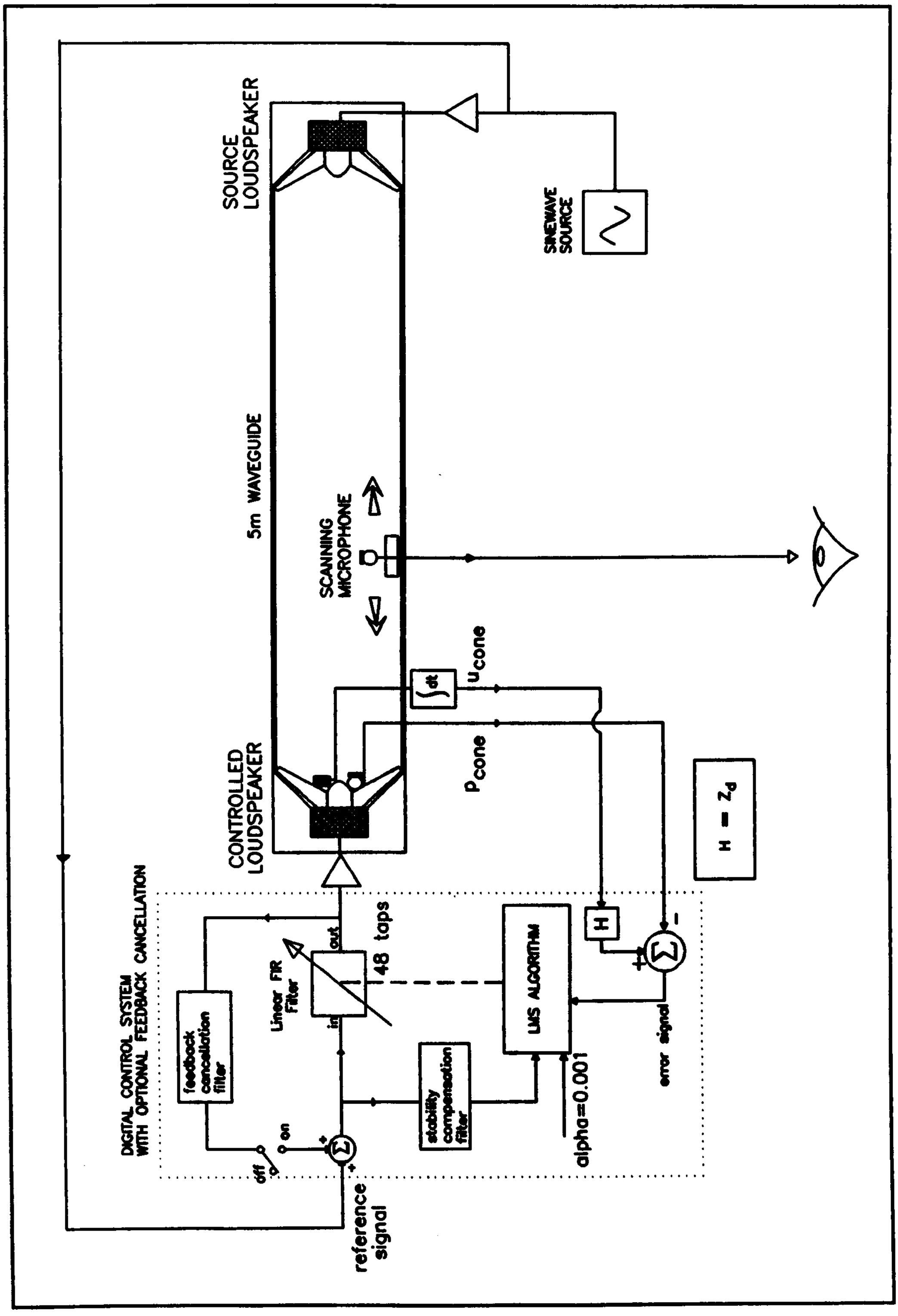

Figure 91. Schematic of laboratory test-rig. Mic-accr feed-forward control system for the active control of acoustic impedance. Sinusoidal signals used as source energy.

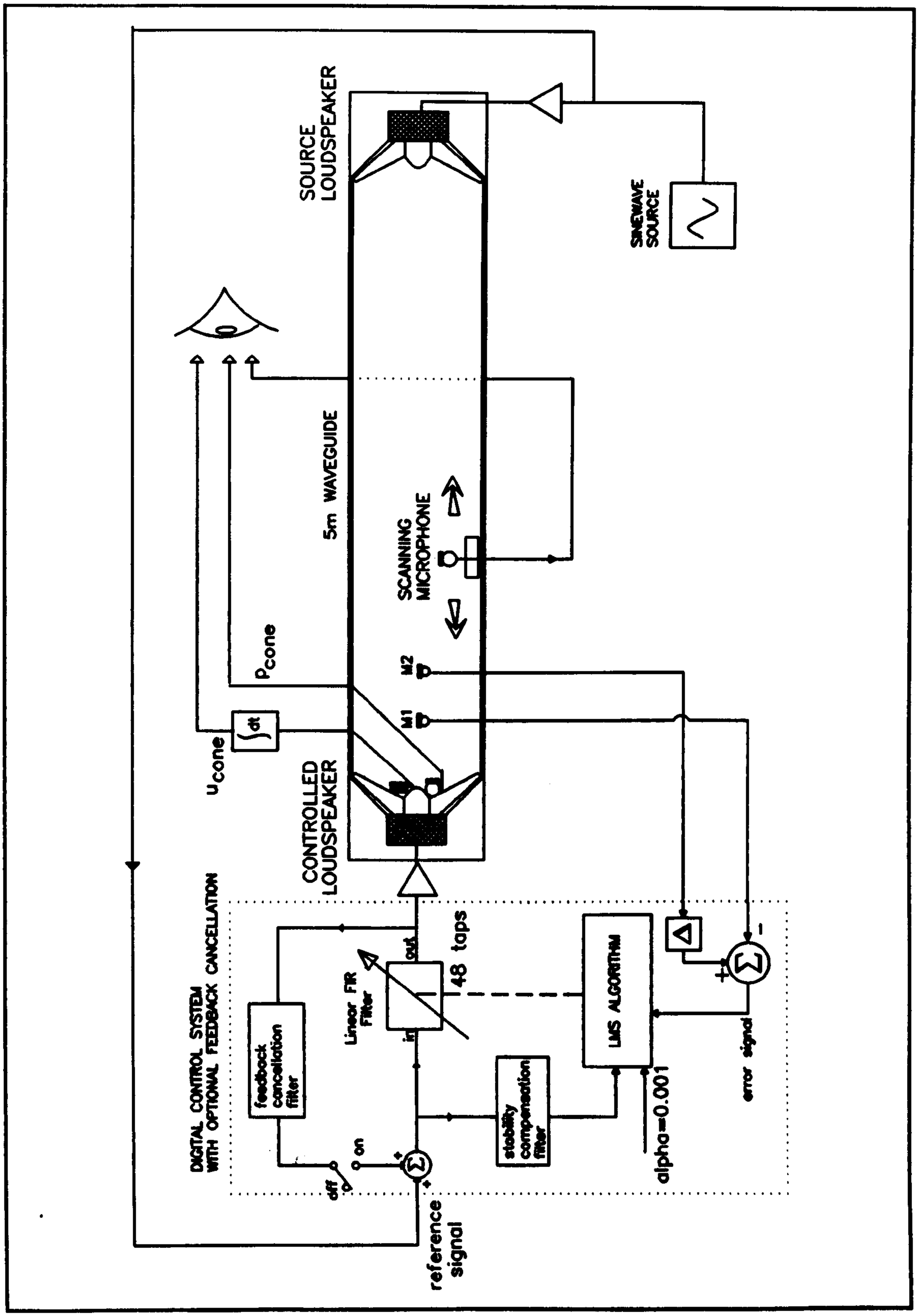

Figure 92. Schematic of laboratory test-rig. 2-mic feed-forward control system for active acoustic absorption. The experiment made SWR measurements and also observed impedance of the controlled cone with pressure and velocity measurement.

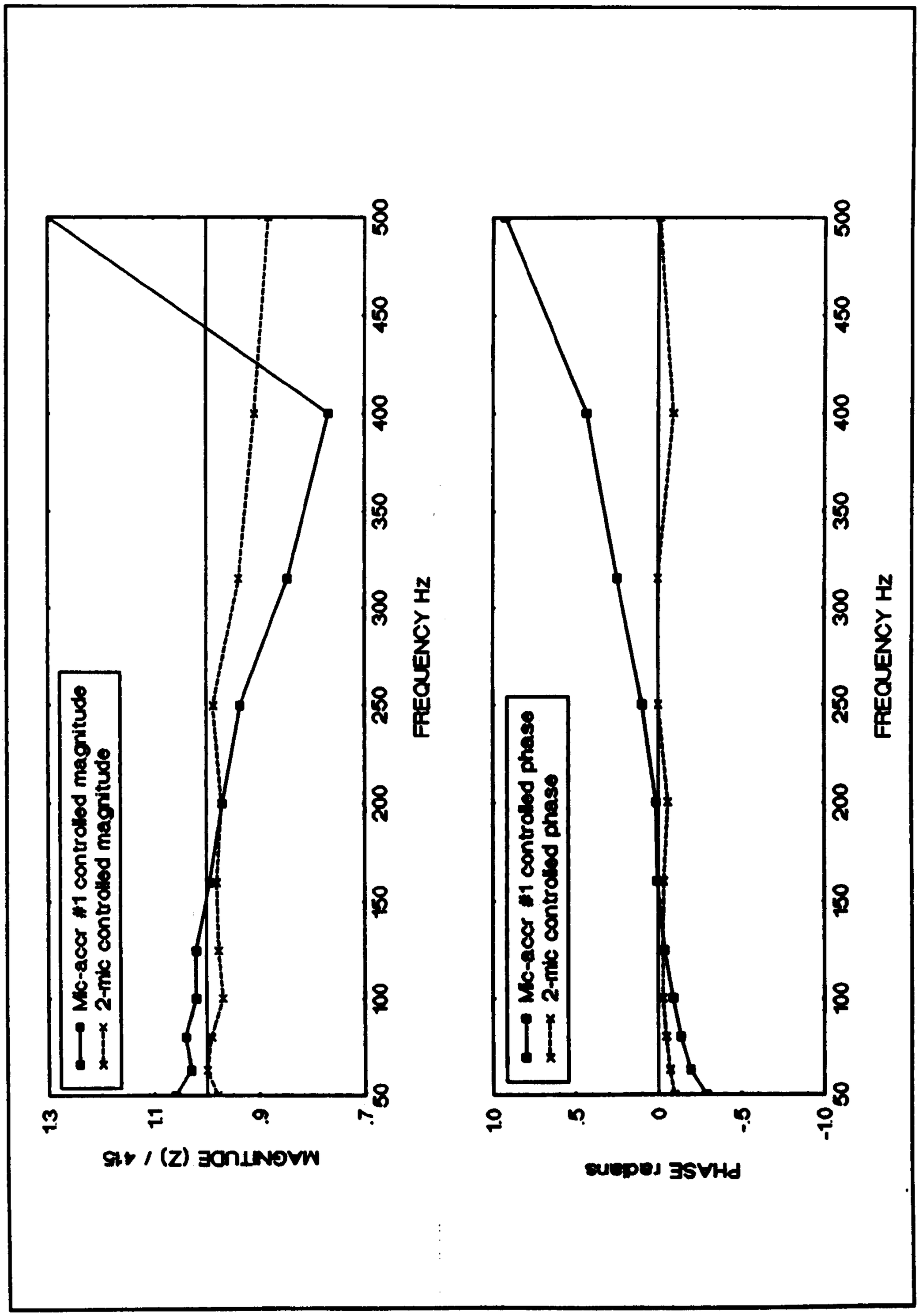

Figure 93. Magnitude and phase of controlled acoustic impedance of a KEF B200A by mic-accr and 2-mic adaptive feed-forward control systems for sinusoidal normally-incident plane waves. Both systems configured for desired real z=415 rayls.

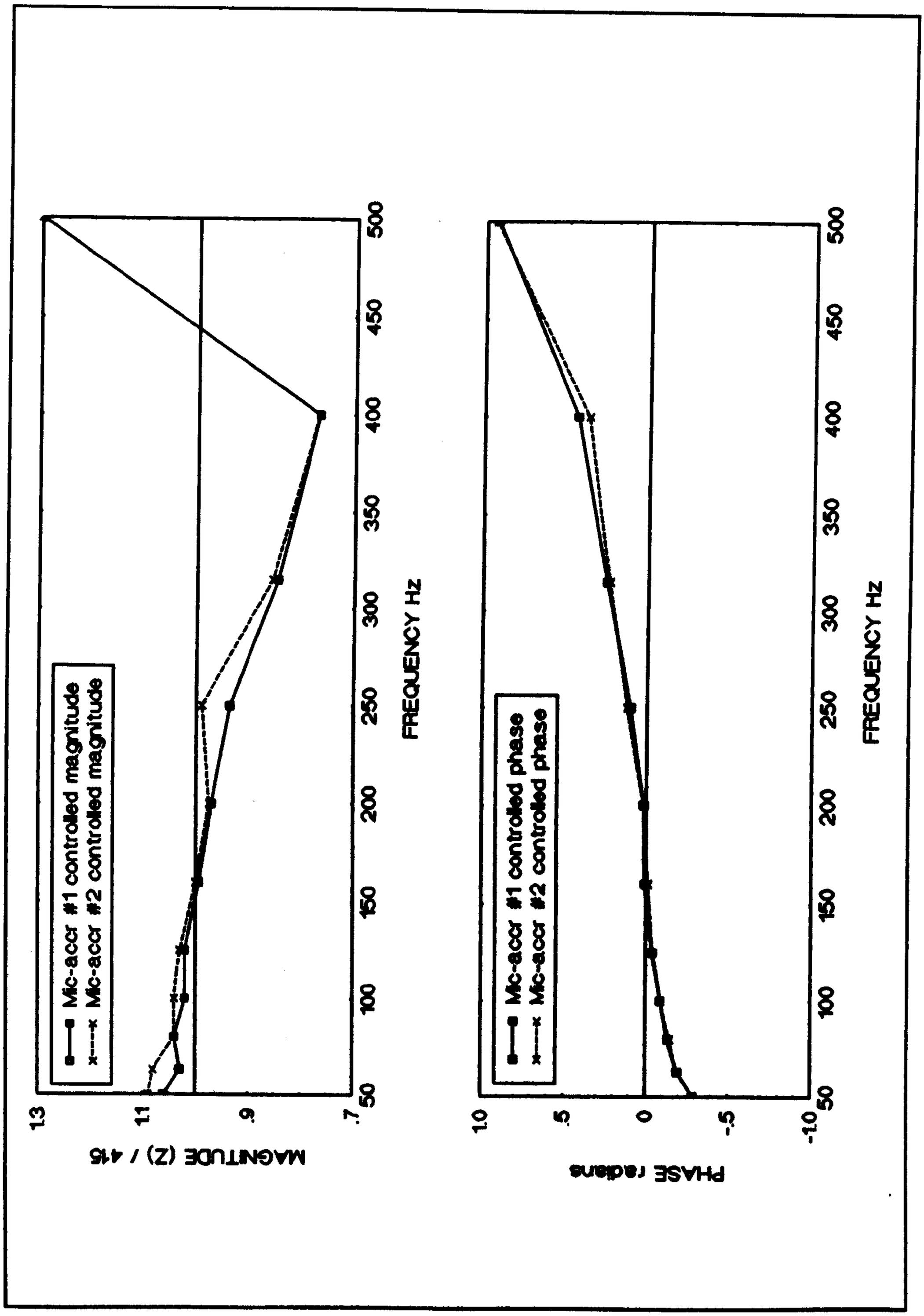

Figure 94. Magnitude and phase of controlled acoustic impedance of a KEF B200A loudspeaker with a mic-accr adaptive digital feed-forward control system. Plots show the two different connection methods of the cone pressure and velocity.

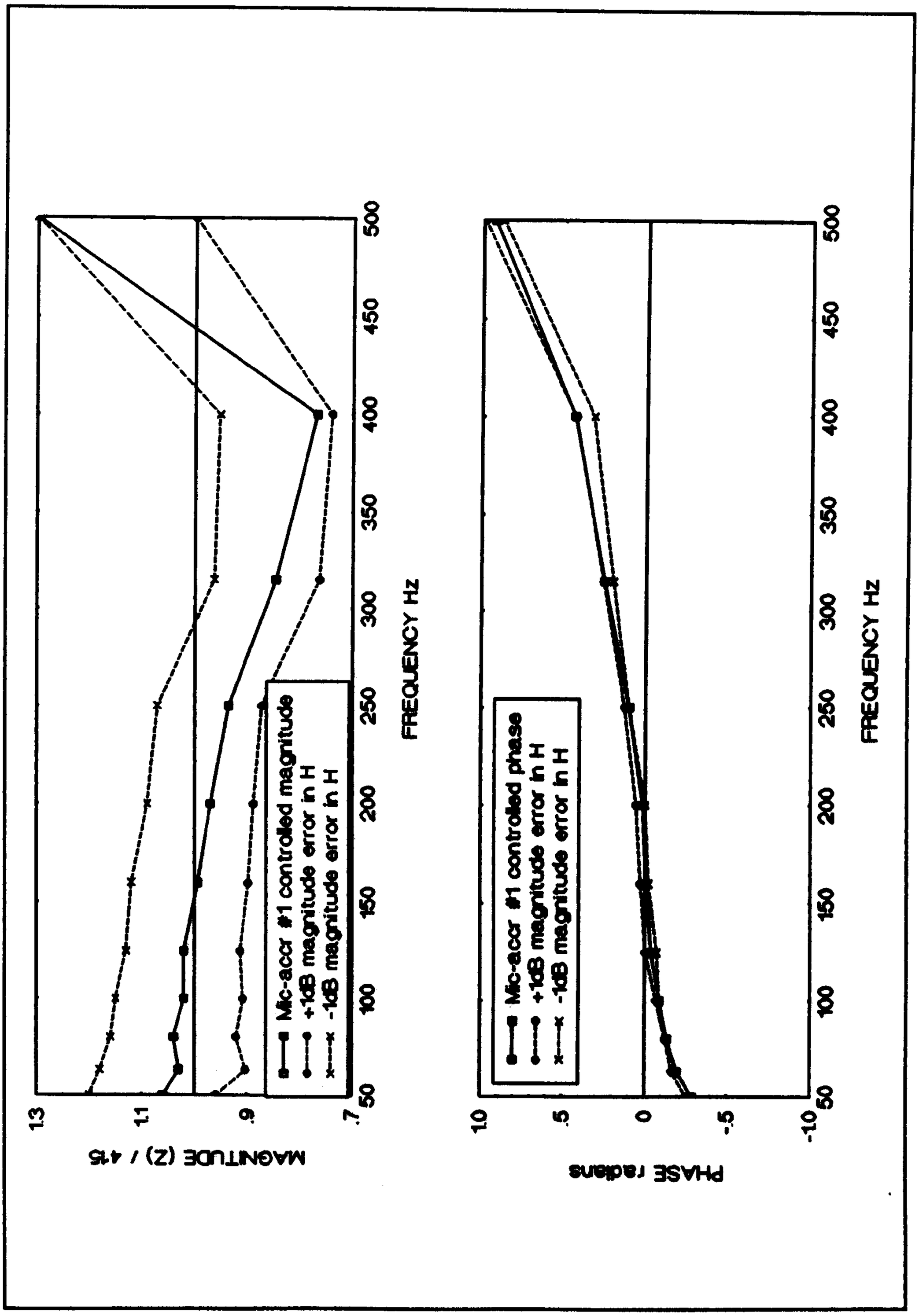

Figure 95. Magnitude and phase of controlled impedance of a KEF B200A loudspeaker controlled by the mic-accr adaptive digital feed-forward control system. The plots show a magnitude change ("error") of ±1dB in the desired impedance filter H.

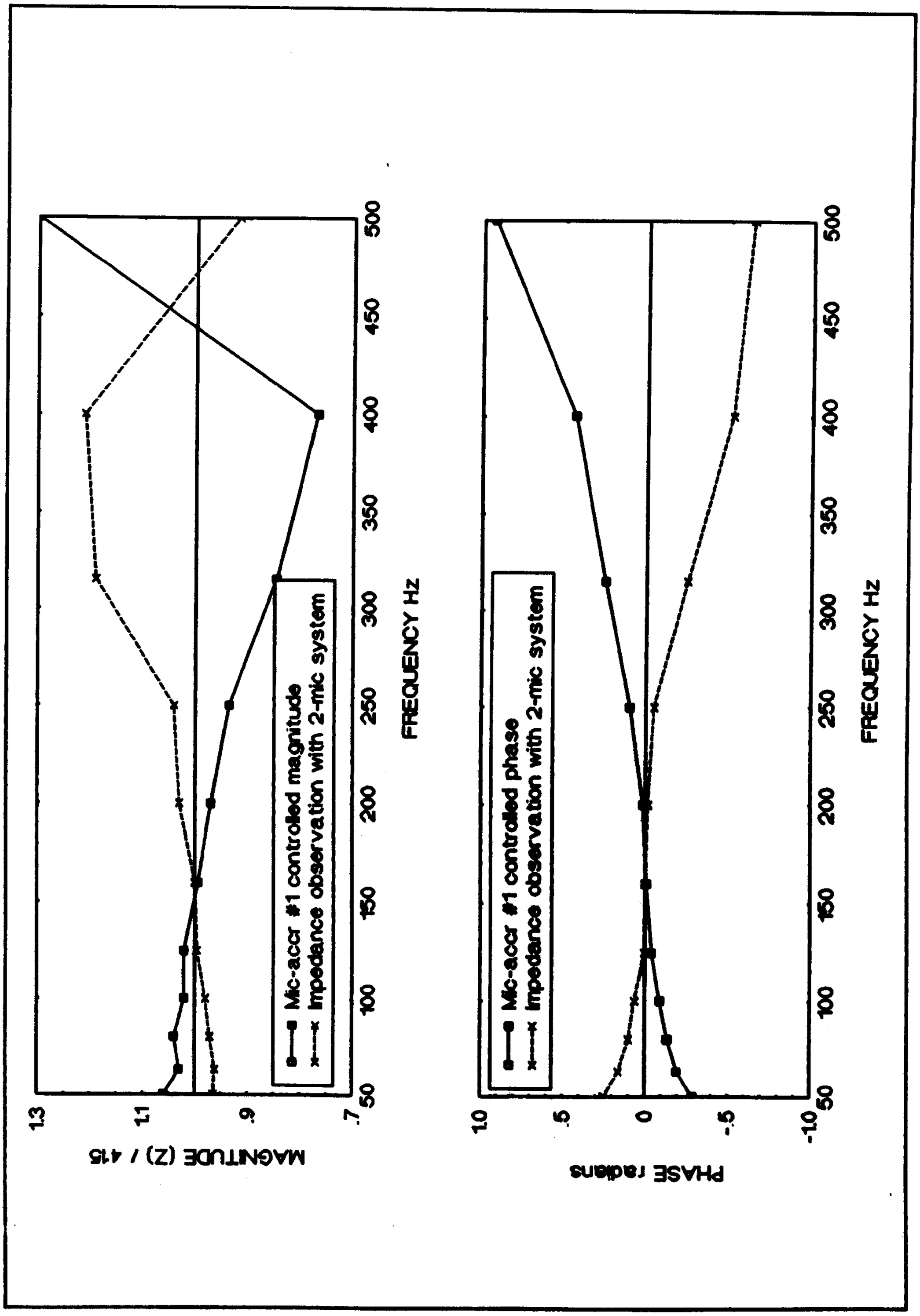

Figure 96. Solid line shows measured impedance z for mic-accr control of a KEF B200A set for a desired z=415. Dashed line shows the measured z observation of the mic-accr method for 2-mic control creating a near characteristic z.

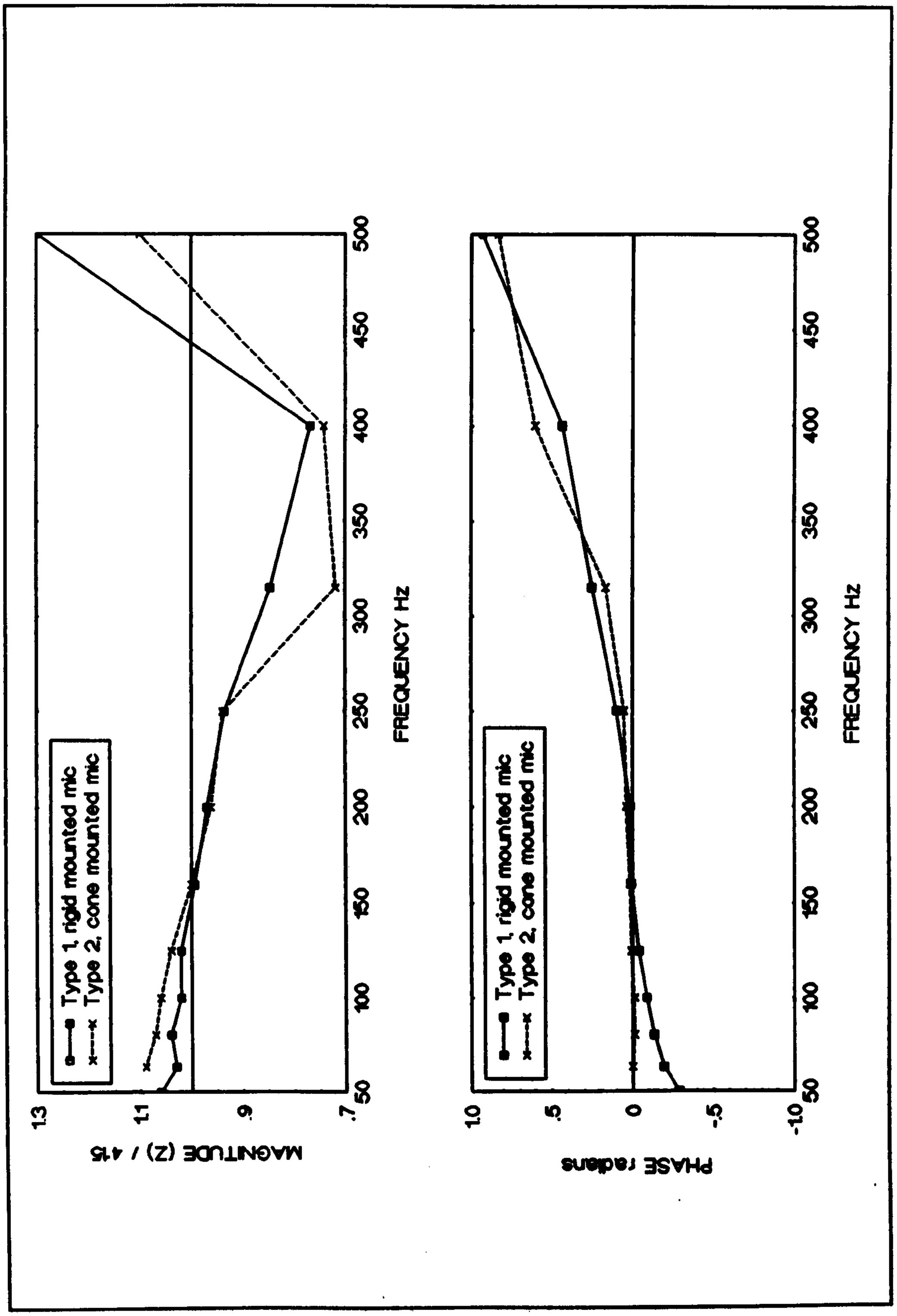

Figure 97. Magnitude and phase of controlled acoustic impedance for different impedance observation of a KEF B200A loudspeaker with mic-accr control system.

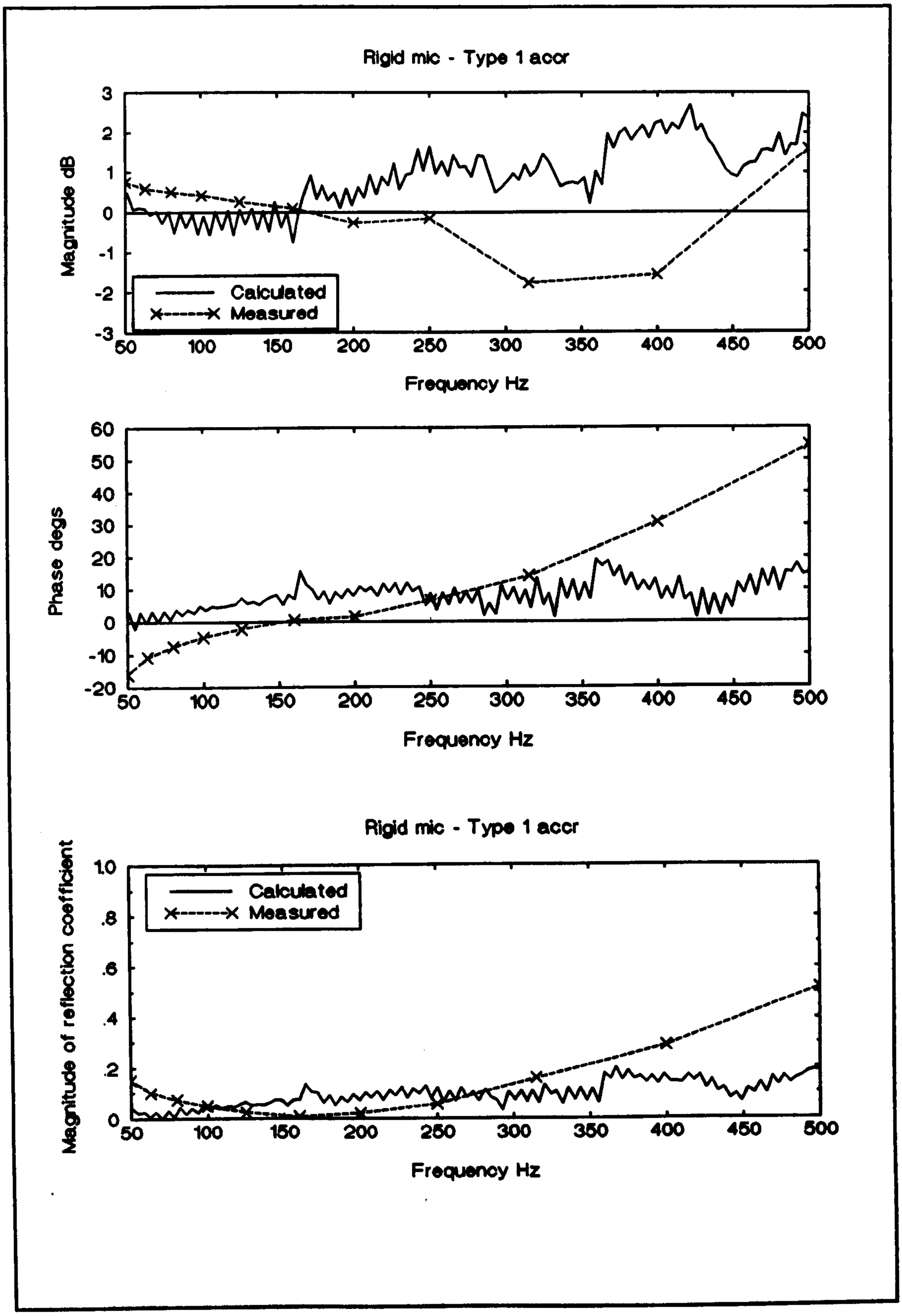

Figure 98. Calculated and measured z observation factors for rigidly mounted mic and type 1 wired accelerometer. Upper and middle plots are magnitude and phase, lower plot is |R|

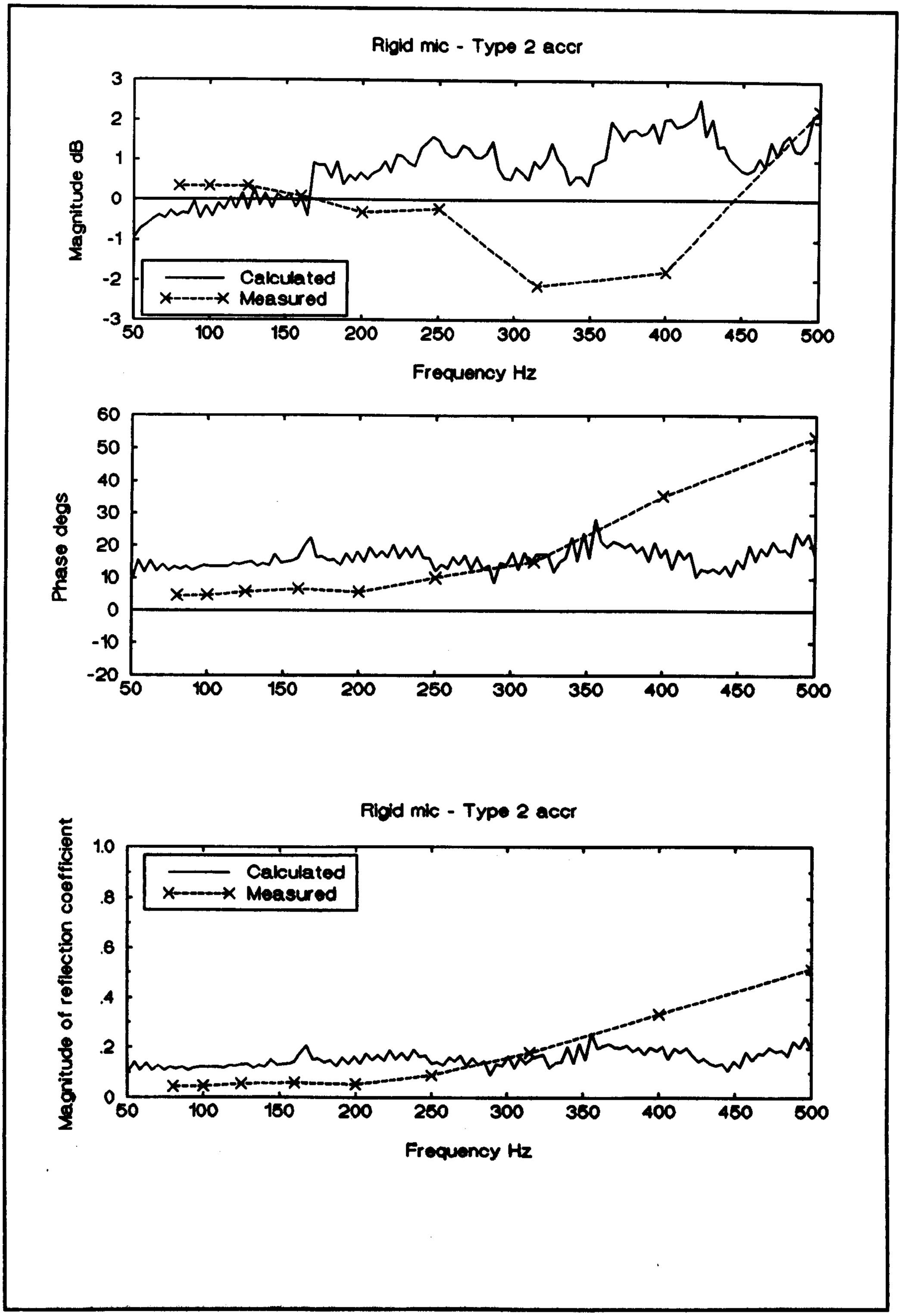

Figure 99. Calculated and measured z observation factors for rigidly mounted mic and type 2 wired accelerometer. Upper and middle plots are magnitude and phase, lower plot is |R|

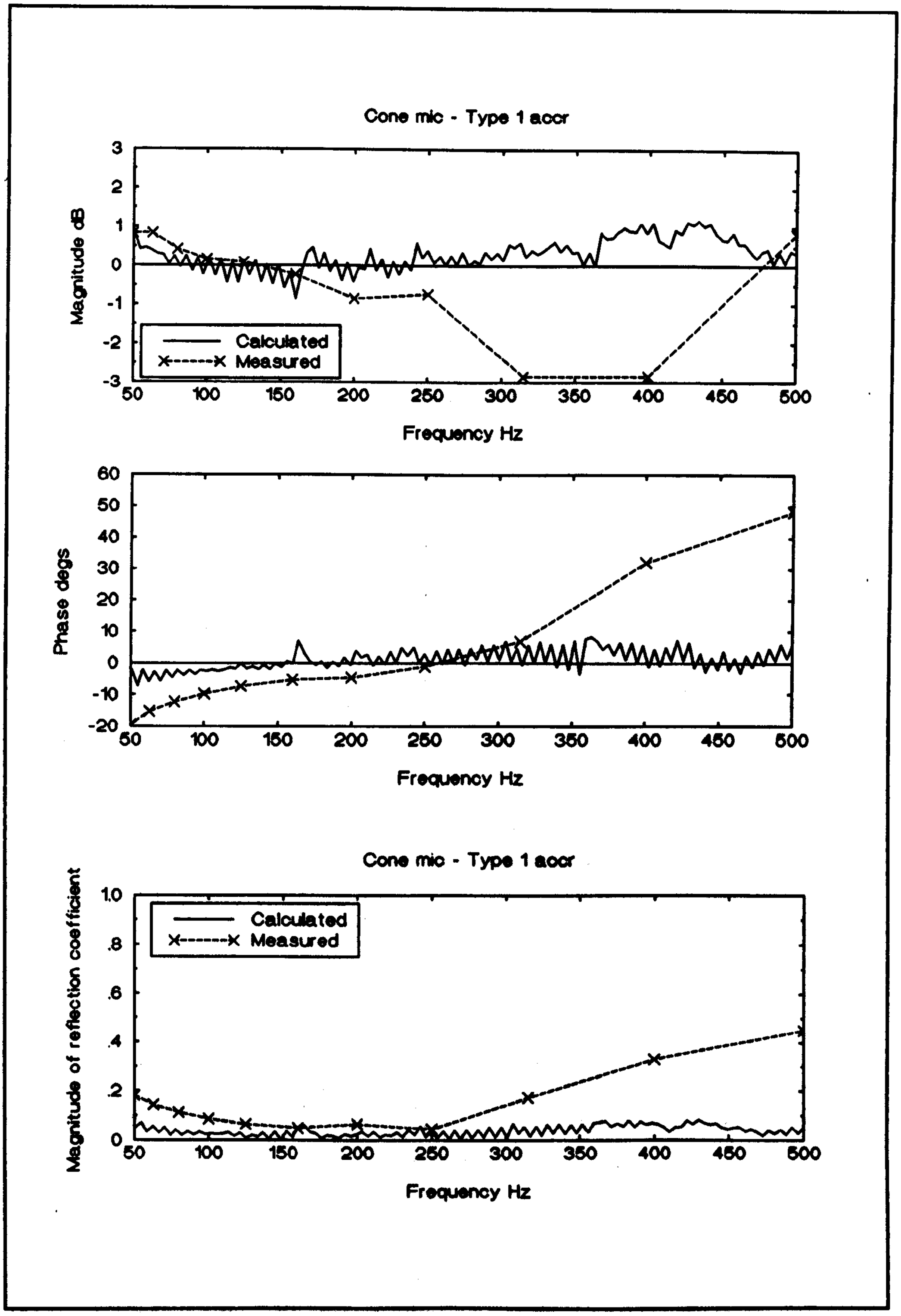

Figure 100. Calculated and measured z observation factors for cone mounted mic and type 1 wired accelerometer. Upper and middle plots are magnitude and phase, lower plot is |R|

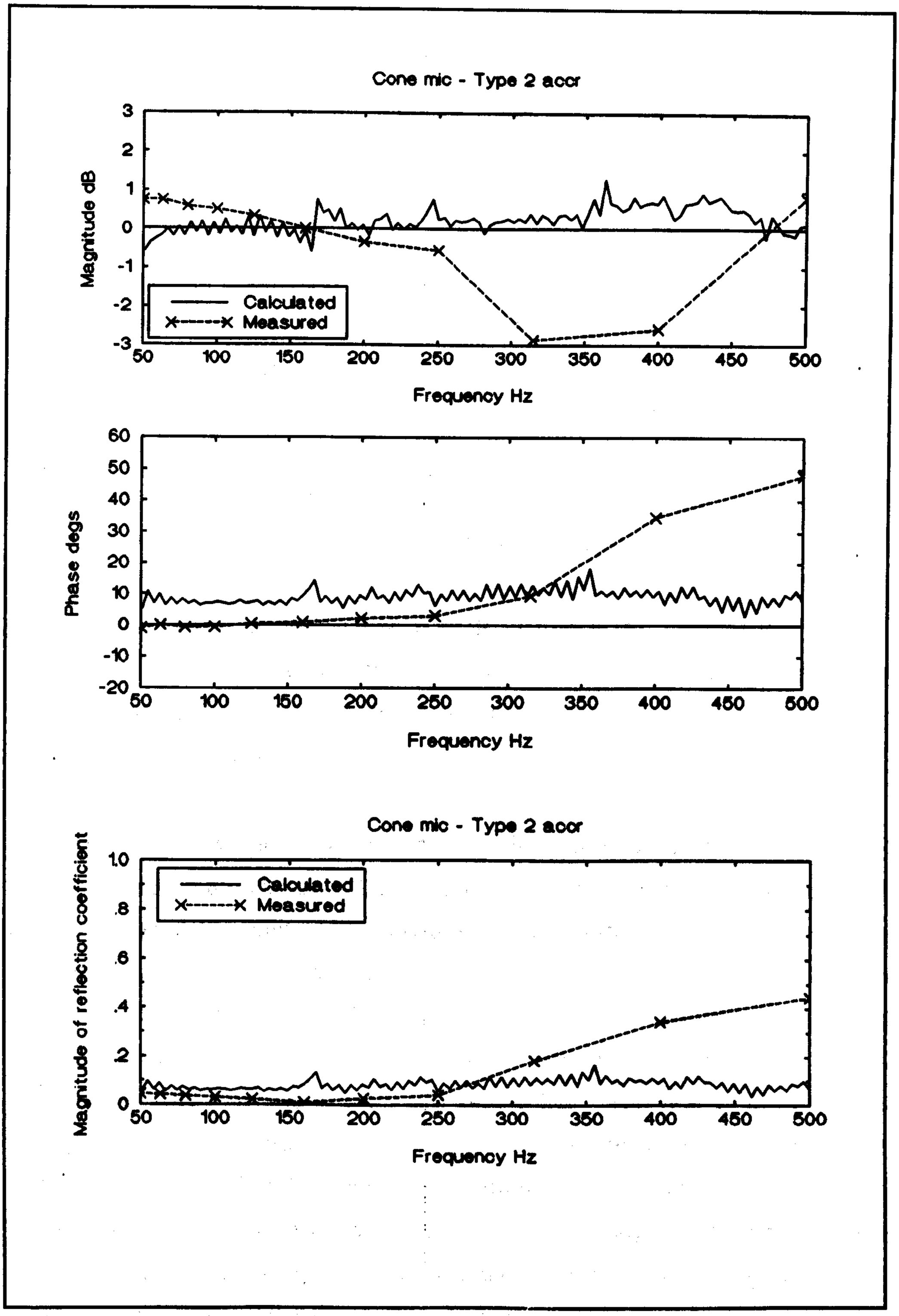

Figure 101. Calculated and measured z observation factors for cone mounted mic and type 2 wired accelerometer. Upper and middle plots are magnitude and phase, lower plot is |R|

8 EXPERIMENTAL RESULTS ON IMPEDANCE CONTROL

This chapter describes experimental results on the active control of impedance of a loudspeaker cone with an adaptive digital feed-forward implementation of the mic-accr method.

The generation of characteristic impedance is described for sinusoidal and random signals in Sections 8.1 and 8.2 respectively. The effectiveness of the controlled impedance is illustrated with observation of acoustic absorption of transient signals. Results measured from a digital feed-forward adaptive implementation of the 2-mic method are also presented. The generation of desired infinite impedance is described for sinusoidal and random signals in Section 8.3. The generation of a desired frequency-dependent impedance for sinusoidal and random signals is demonstrated in Section 8.4.

8.1 CHARACTERISTIC IMPEDANCE FOR SINUSOIDAL SIGNALS

This section presents results from the laboratory test-rig for the mic-accr feed-forward system forcing a characteristic impedance for normally-incident sinusoidal plane waves.

The laboratory experiment ran a mic-accr feed-forward active impedance control system based on the filtered-X LMS algorithm. The purpose of the experiment was to measure the controlled impedance of the system. A schematic of the system is shown in Figure 102 on Page 282. The system controlled the impedance of either a KEF B200A or a Peerless 831483 loudspeaker situated at the left hand termination of a 5 metre waveguide. The KEF B200A loudspeaker was mounted in a 25 litre sealed box. The rear of the Peerless loudspeaker radiated into the laboratory space. At the right hand termination was the source KEF B200A loudspeaker mounted in a 25 litre sealed box which was electrically driven with sinusoidal signals. The waveguide has a plane wave bandwidth of approximately 1.25kHz as noted in Section 7.2 on Page 203. The reference signal was taken from the electrical source signal - this prevented feedback around the adaptive control system. The sampling frequency was 2999Hz. The adaptive linear FIR control filter had 200 taps and the update gain

was set at 0.001. The stability compensation FIR filter had 512 taps. The maximum sound pressure level in the duct at 100Hz measured with the travelling microphone was around 110dB. The mic-accr system was configured so that the desired impedance filter **H** was directly proportional to the desired impedance. This results from connecting the pressure and cone velocity signals as shown in Figure 26b on Page 99. The desired characteristic impedance was set by observing the standing wave ratio for a source frequency of 160Hz. The single tap of **H** was manually adjusted to make a controlled impedance of 415 Rayls. The system was tested without further adjustment of **H**. The adaptive system converged with sinusoidal signals over a frequency range of 50Hz to 500Hz. SWR measurements were made after maximum convergence at selected frequencies for each loudspeaker.

The mic-accr system instrumented the cone pressure of the KEF B200A with a microphone that was mounted on the cone - see Section 7.4.3 on Page 213. The cone velocity of the KEF B200A was taken from the cone-mounted accelerometer by connection method "Type 2" described in Section 7.4.2 on Page 207. The combination of the cone microphone and Type 2 wired accelerometer produced the best controlled impedance performance from 50 to 250Hz when compared with other combinations on this loudspeaker. The magnitude and phase of the impedance are calculated from the SWR measurements and are shown in Figure 103 on Page 283 and the corresponding magnitude and phase of the reflection coefficient are shown in Figure 104 on Page 284. The controlled impedance at 160Hz had magnitude 415 Rayls and phase 0.0153 radians. The phase of the controlled impedance was within ± 0.1 radians over 50 to 250Hz. The controlled reflection coefficient was less than 0.05 over 50 to 250Hz. At frequencies greater than 250Hz the controlled impedance is less close to characteristic. An investigation described in Section 7.9 shows that this is because of impedance observation error and it is likely that the transducers mass-load the cone.

The mic-accr system instrumented the cone pressure of the Peerless 831483 with a microphone that was mounted near to the cone - see Section 7.4.3 on

Page 213. The cone velocity was taken from the cone-mounted accelerometer by connection method "Type 2" described in Section 7.4.2 on Page 207. The instrumentation combination of the off-cone microphone and Type 2 wired accelerometer produced the best controlled impedance performance when compared with other combinations on this loudspeaker. The magnitude and phase of the impedance are calculated from the SWR measurements and are shown in Figure 105 on Page 285 and the corresponding magnitude and phase of the reflection coefficient are shown in Figure 106 on Page 286. The controlled impedance at 160Hz had magnitude 423 Rayls and phase 0.028 radians. The phase of the controlled impedance was within ± 0.2 radians over the whole range of tested frequencies. The controlled reflection coefficient was less than 0.05 over 80Hz to 250Hz.

The results show that the controlled impedances of the two loudspeakers were different when driven by the same control system - see Figure 107 on Page 287. The magnitude and phase of the equivalent reflection coefficients are shown in Figure 108 on Page 288. The controlled impedance of the Peerless loudspeaker was closer to characteristic over the measured frequency range than the KEF B200A. It is suggested that this is because of lower impedance observation error. The results for the Peerless loudspeaker controlled by the mic-accr system are also plotted against results from the 2-mic system control of the KEF B200A (described in Section 7.9 on Page 230) in Figure 109 and Figure 110 on Page 289 and Page 290. The two systems have similar performance - further adjustment of the digital filter H in the mic-accr system would have produced closer results.

8.2 CHARACTERISTIC IMPEDANCE FOR BAND-LIMITED RANDOM AND TRANSIENT SIGNALS

This section presents results from the laboratory test-rig for the mic-accr system forcing a characteristic impedance for normally-incident band-limited random plane waves. The adaptive impedance control system was trained with noise, and the controlled impedance was then assessed with SWR measurements.

The controlled impedance was also evaluated with transient signals of restricted band-width.

The laboratory experiment ran a mic-accr feed-forward active impedance control system based on the filtered-X LMS algorithm. The purpose of the experiment was to measure the controlled impedance of the system when trained with random signals. A schematic of the system is shown in Figure 111 on Page 291. The system controlled the impedance of a KEF B200A situated at the left hand termination of a 5 metre waveguide. The KEF B200A loudspeaker was mounted in a 25 litre sealed box. At the right hand termination was a source KEF B200A loudspeaker also mounted in a 25 litre sealed box. This was electrically driven with either band-limited pink noise or pulses, or a sinusoidal signal. The reference signal was taken from microphone $\mathbf{M_R}$ situated 2 metres away from the cone. There was, therefore, the potential for feedback around the control system. The sampling frequency was set to 2999Hz. The adaptive linear FIR control filter had 200 taps and the update gain was set at 0.01. The stability compensation FIR filter had 512 taps. The mic-accr system was configured so that the desired impedance filter **H** was inversely proportional to the desired impedance. The pressure and cone velocity signals and the desired filter **H** were connected as shown in Figure 26a on Page 99. The desired impedance was set by observing the standing wave ratio for a source frequency of 160Hz. The single tap of **H** was manually adjusted to make a controlled impedance of 415 Rayls. The system was tested without further adjustment of **H**. The mic-accr system instrumented the cone pressure of the KEF B200A with a microphone that was mounted near to the cone - see Section 7.4.3 on Page 213. The cone velocity of the KEF B200A was taken from the cone-mounted accelerometer by connection method "Type 1" described in Section 7.4.2 on Page 207. The waveguide had a plane wave bandwidth of approximately 1.25kHz (see Section 7.2 on Page 203). The acoustic noise used in the test was restricted to a band-width of 500Hz. The implementation of the control system allowed the user to halt the adaptation during convergence to fix the weights of the linear FIR filter. The control system was allowed to converge

for approximately 30 seconds with band-limited noise then the update was halted. The control system was stable without feedback cancellation.

An SWR measurement test was made of the fixed controlled impedance with sinusoidal acoustic plane waves from 50Hz to 315Hz. The adaptive control was fixed to prevent further control adaptation with the SWR measurement sinusoidal signals, so that the test measured standing-wave ratios of the noise-trained adaptive control system. The magnitude and phase of the impedance are calculated from the SWR measurements and are shown in Figure 112 on Page 292 and the corresponding magnitude and phase of the reflection coefficient are shown in Figure 113 on Page 293. The controlled impedance at 160Hz had magnitude 415 Rayls and phase -0.046 radians. The phase of the controlled impedance was within ± 0.4 radians over 50Hz to 315Hz. The controlled reflection coefficient was less than 0.18 over 50Hz to 250Hz. This instrumentation combination on the KEF B200A does not have the best controlled impedance performance and therefore the reflection coefficients were not the lowest - see Section 8.1 on Page 271 for lower results with better instrumentation. However these results show that the mic-accr feed-forward system converged successfully to force near-characteristic impedance for band-limited random noise.

The fixed controlled impedance was also effective for transient signals. Pressure responses for band-limited input pulses of acoustic energy in the waveguide are shown in Figure 114 on Page 294. The two graphs in this figure show the averaged response of 50 sampled pressure measurements taken from a microphone positioned 1 metre from the controlled surface. The sampling frequency was 1.5kHz, and 500 samples are plotted in each graph. The source loudspeaker was electrically driven with pulses which were band-width limited to approximately 300Hz with a low-pass electronic filter. The upper plot was for the KEF B200A termination without control and reflected pulses are seen. The duration of the pulse is similar to the acoustic delay from the measurement position to the controlled surface and back. Therefore each incident and reflected pulse are difficult to distinguish. The lower plot shows the reduction in

the reflected components caused by the introduction of the fixed active control on the KEF B200A, so producing a termination of near-characteristic impedance. The plots show that the initial direct pulse was not modified by the controlled termination. Modification of the direct pulse would indicate that the controlled termination was generating energy prior to the arrival of the pulse at the termination.

The frequency-domain pressure response in the waveguide is examined by performing a Fast Fourier Transform (FFT) on the transient data shown in Figure 114. Frequency magnitude results are shown in Figure 115 on Page 295 from a 512 point FFT on the non-windowed data. The plot is restricted to the test frequency band-width of 500Hz - frequency components above 500Hz have negligible level. The dashed line is the frequency magnitude response of the pressure with the *uncontrolled* KEF B200A termination (the time data is shown in upper plot of Figure 114). The solid line is the response with the *controlled* KEF B200A termination (time data is shown in lower plot of Figure 114). The transient signal contained energy mostly between 40Hz and 300Hz. The lower frequency limit is due to the natural response of the loudspeaker with this radiation load. The 3dB-down frequency is calculated as 50Hz in Appendix 2. The upper frequency limit is due to the band-width of the 300Hz low-pass electronic filter. Between 50 and 280Hz the pressure response varied by up to 6dB which may have been due to: (i) damped resonance in the source loudspeaker system; (ii) the response of the measurement microphone - a low cost omni-directional design; (iii) the source filter and power-amplifier response. Further study of these effects does not enhance the evaluation of the controlled impedance.

The pressure magnitude response with the uncontrolled loudspeaker (dashed line in Figure 115) shows that the sound field was modal - this was caused by interference between incident and reflected waves from the uncontrolled surface. At higher frequencies the uncontrolled KEF B200A was more reflective (see Figure 113) and the acoustic resonances were more pronounced. Over the frequency range 40Hz to 300Hz the solid line shows that a considerable

reduction in the modal nature of the sound field was caused by terminating the waveguide with the near-characteristic controlled impedance. Outside of the 40Hz to 300Hz frequency range the controlled termination also reduced resonances in the sound field. These results indicate that the near-characteristic controlled impedance absorbed transient pressure waves effectively.

8.3 INFINITE IMPEDANCE FOR BAND-LIMITED RANDOM AND TRANSIENT SIGNALS

This section presents results from the laboratory test-rig for the mic-accr system forcing an infinite impedance termination for normally-incident band-limited random plane waves. The controlled termination was initially assessed with SWR measurements using sinusoidal plane waves. The adaptive control system was then trained with noise, and evaluated with transient signals of restricted band-width. The results are compared with results from equivalent tests on a lead termination.

The laboratory tests were performed on the test-rig setup described in Section 8.2 on Page 273. A schematic of the system is shown in Figure 111 on Page 291, refer to Section 8.2 for a general description. The control system configuration is described in the rest of this section. The reference signal for the control filter was taken from the duct microphone $\mathbf{M_R}$. There was, therefore, a potentially unstable feedback loop around the controller. The desired infinite impedance was established by setting the single tap of H (shown in Figure 111) to zero so that the control system attempted to reduce the measured cone velocity to zero.

An SWR measurement test was made of the controlled impedance with sinusoidal acoustic plane waves from 50Hz to 400Hz. The duct microphone $\mathbf{M_R}$ was positioned 1m from the cone and so the frequencies at which pressure nodes occur at this position for infinite controlled impedance are calculated as approximately 85Hz, 255Hz and 425Hz (see Section 6.3.3 on Page 115). Therefore the theoretical solution of the optimum controller without feedback cancellation, Equation 6.49 on Page 115, is not implementable at these

frequencies. Also the analysis on loop stability, see Section 6.4.4, indicates that there are potentially unstable loops. This was consistent with observation in the laboratory. However, the controller was stable when feedback cancellation was used. In order to correctly model the measured feedback path, the feedback cancellation filter used 512 taps. The compensation filter had 500 taps and all of the remaining processing time was used to allocate 100 taps for the adaptive FIR filter. In this configuration the adaptive filter successfully converged. The magnitude and phase of the reflection coefficients are calculated from the SWR measurements and are shown in Figure 116 on Page 296. The solid plotted lines show the reflection coefficient results of the uncontrolled and controlled KEF B200A termination. The dashed lines show the reflection coefficient results of 1.5mm lead sheet backed by plywood measured in the same waveguide (these have been described in Section 7.2 on Page 203). From 50Hz to 250Hz the control system forced a reflection coefficient of near-unity magnitude and near-zero phase, thus demonstrating high values of controlled impedance. The magnitude of the reflection coefficient of the controlled KEF B200A was greater than 0.9 over 50Hz to 200Hz, and the magnitude and phase were similar to the lead-faced plywood results. The magnitude of the reflection coefficient of the controlled KEF B200A dropped above 200Hz because of the chosen instrumentation of cone velocity. The control system forced the infinite impedance by minimising the cone velocity measured with an accelerometer mounted on the cone. The accelerometer mass-loaded the cone, see Section 7.4.2.1 on Page 210. Therefore the control system minimised cone velocity at the accelerometer position but not necessarily over the whole cone. Other loudspeakers such as the Peerless model 831483 appear to be less susceptible to mass-loading by the accelerometer.

The control system was allowed to converge for approximately 30 seconds with band-limited noise then the update was halted. The fixed controlled impedance was tested with transient signals as described in Section 8.2. Pressure responses in the waveguide are shown in Figure 117 on Page 297. The two graphs in this figure show the averaged response of 50 sampled pressure measurements taken from the duct microphone positioned 1 metre from the

termination. The sampling frequency was 1kHz and 500 samples are plotted in each graph. The upper graph is for the termination of 1.5mm lead sheet backed by plywood and acoustic reflections of the pulse are seen. The lower graph shows reflected pulses of similar level with the controlled KEF B200A terminating the waveguide (the response for the uncontrolled KEF B200A, shown in the upper plot of Figure 114 on Page 294 with a different time scale, had reflected components that were lower in magnitude and decayed more quickly because of higher acoustic absorption). Towards the end of the impulse response low-level "ringing" occurred, see lower plot of Figure 117. A 256 point FFT on the *last* 256 samples of this response reveals that the ringing is mainly composed of two frequencies - 32Hz and 137Hz which are principal frequency components over the *first* 256 samples. The adaptive filter had 100 taps and at a sampling frequency of 2999Hz the maximum filter delay was around 0.033 seconds. The filter impulse response alone was not long enough to cause the observed ringing. Two possible mechanisms could have caused the ringing: (i) the impulse response of the *combined* adaptive filter and feedback cancellation filter was long enough; (ii) the feedback path model may not have been accurate and therefore the feedback loop may have been near to instability. As the controller was stable this was not investigated further.

The frequency-domain pressure response in the waveguide for transient signals is examined by performing a Fast Fourier Transform (FFT) on the sampled data shown in the upper and lower graphs of Figure 117 on Page 297. Frequency results are shown in Figure 118 on Page 298 from 512 point FFTs of the non-windowed sampled data. The dashed line is the pressure response with the lead-faced plywood termination and is plotted in both graphs. The solid lines are the pressure responses with the KEF B200A termination with the upper graph describing the uncontrolled case, and the lower graph describing the controlled case. The uncontrolled case is taken from Figure 115 on Page 295. A discussion of the band-width of the transient signal is given in Section 8.2. The lower plot of Figure 118 shows that for termination loads of infinite impedance the transient signal had more energy below 50Hz than the characteristic

impedance load described in the previous section. This may have due to higher source efficiency with this radiation load at these frequencies.

All of the plotted lines in Figure 118 show modal behaviour of the waveguide sound field caused by sound reflection at the terminations. With the lead-faced plywood termination minima occurred in the pressure response at frequencies of approximately 86Hz and 256Hz - these frequencies are consistent with the theory of Section 6.3.3 on Page 115. The uncontrolled KEF B200A was more reflective at higher frequencies (as seen in the SWR results of Figure 116). At frequencies above 200Hz the upper graph of Figure 118 confirms that the pressure response was similar to that of the lead-faced plywood. However, at frequencies below 200Hz the reduced reflection of the uncontrolled KEF B200A created a less modal sound field in the pipe compared to the lead-faced plywood. The action of the mic-accr control system on the KEF B200A termination increased reflection at these frequencies, generating a similar modal sound field to the lead-faced plywood. The controlled termination created a pressure response with an approximate minimum near 80Hz. These results show that the mic-accr feed-forward control system can create large impedances for band-limited transient signals with similar acoustic reflection to that encountered with highly-reflective passive materials.

8.4 FREQUENCY-DEPENDENT IMPEDANCE

This section presents an example from the laboratory test-rig of the mic-accr system forcing a frequency-dependent impedance for normally-incident plane waves of band-limited random signals. The adaptive impedance control system was trained with noise, and the controlled impedance was then evaluated with SWR measurements. These results have been described in (33).

The laboratory test-rig is described with the schematic shown in Figure 102 on Page 282. The control filter reference signal was taken from the electrical source signal so that feedback cancellation was not required. The digital system had a sampling frequency of 2999Hz. The adaptive filter had 200 taps with an update gain set at 0.0001. Constraints on the implementable impedance with

the mic-accr method have been discussed in Section 5.3 on Page 92. The desired impedance example in this section had minimum phase and was absorptive at low frequencies, becoming more reflective at higher frequency. The desired impedance was specified with discrete time equation 8.1 which was implemented in the desired filter **H**. This was designed from an analogue bilinear prototype.

$$y(k) = k_h . [\ a0 . x(k) + a1 . x(k-1) + b1 . y(k-1)\ ] \qquad 8.1$$

where

$$a0 = +0.03845593$$
$$a1 = -0.02884055$$
$$b1 = -a1$$

and k_h is the scaling term described in Section 6.2 on Page 102. The value of k_h was set so that the controlled impedance was near-characteristic at 50Hz.

The control system was trained for about 30 seconds using pink noise, band-limited to 450Hz. The adaption was then halted and SWR measurements were made with sinusoidal signals at frequencies from 50Hz to 315Hz. The magnitude and phase of the impedance and the reflection coefficient are calculated from the SWR measurements and are shown in Figure 119 on Page 299 and Figure 120 on Page 300. The theoretical controlled impedance and reflection coefficient, calculated from knowledge of the desired filter are also plotted. The measured results track the theoretical data indicating that the controlled loudspeaker successfully created the desired impedance.

8.5 CHAPTER FIGURES

The figures referred to in this chapter appear on the following pages.

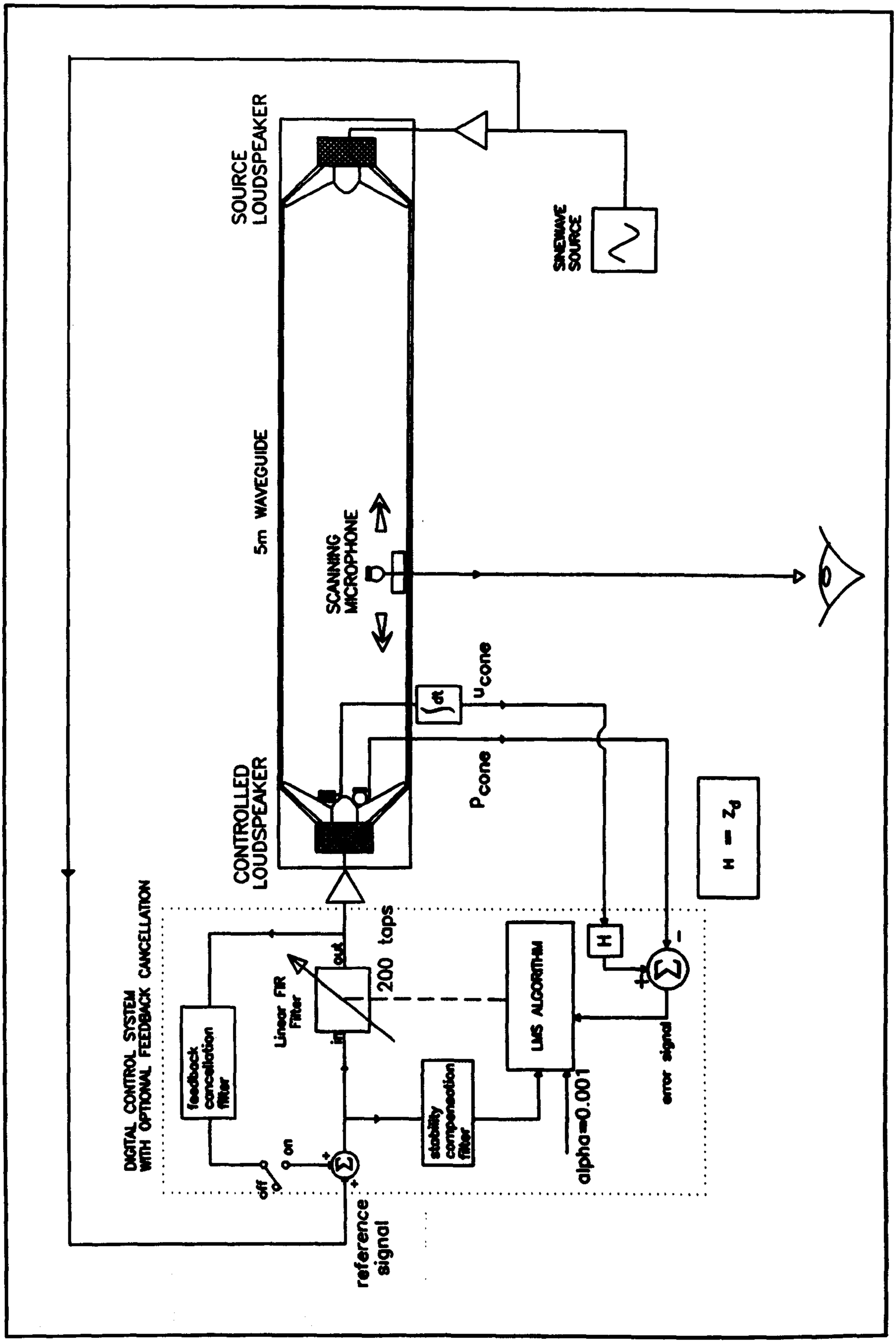

Figure 102. Schematic of mic-accr feed-forward digital control system for the active control of acoustic impedance.

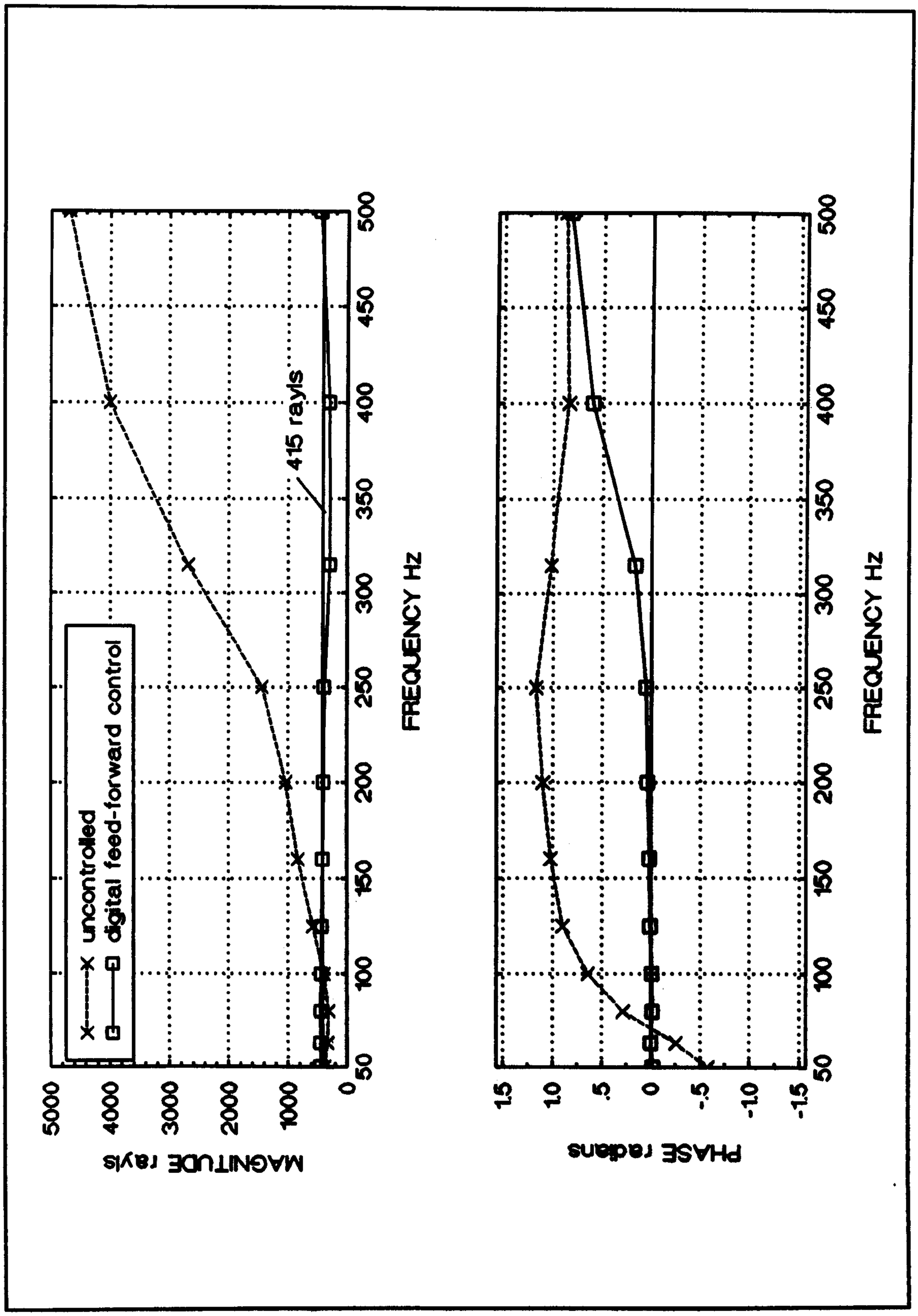

Figure 103. Magnitude and phase of acoustic impedance of KEF B200A loudspeaker for normally-incident sinusoidal plane-waves. Controlled result achieved with mic-accr feed-forward digital adaptive control system, set for a desired characteristic impedance.

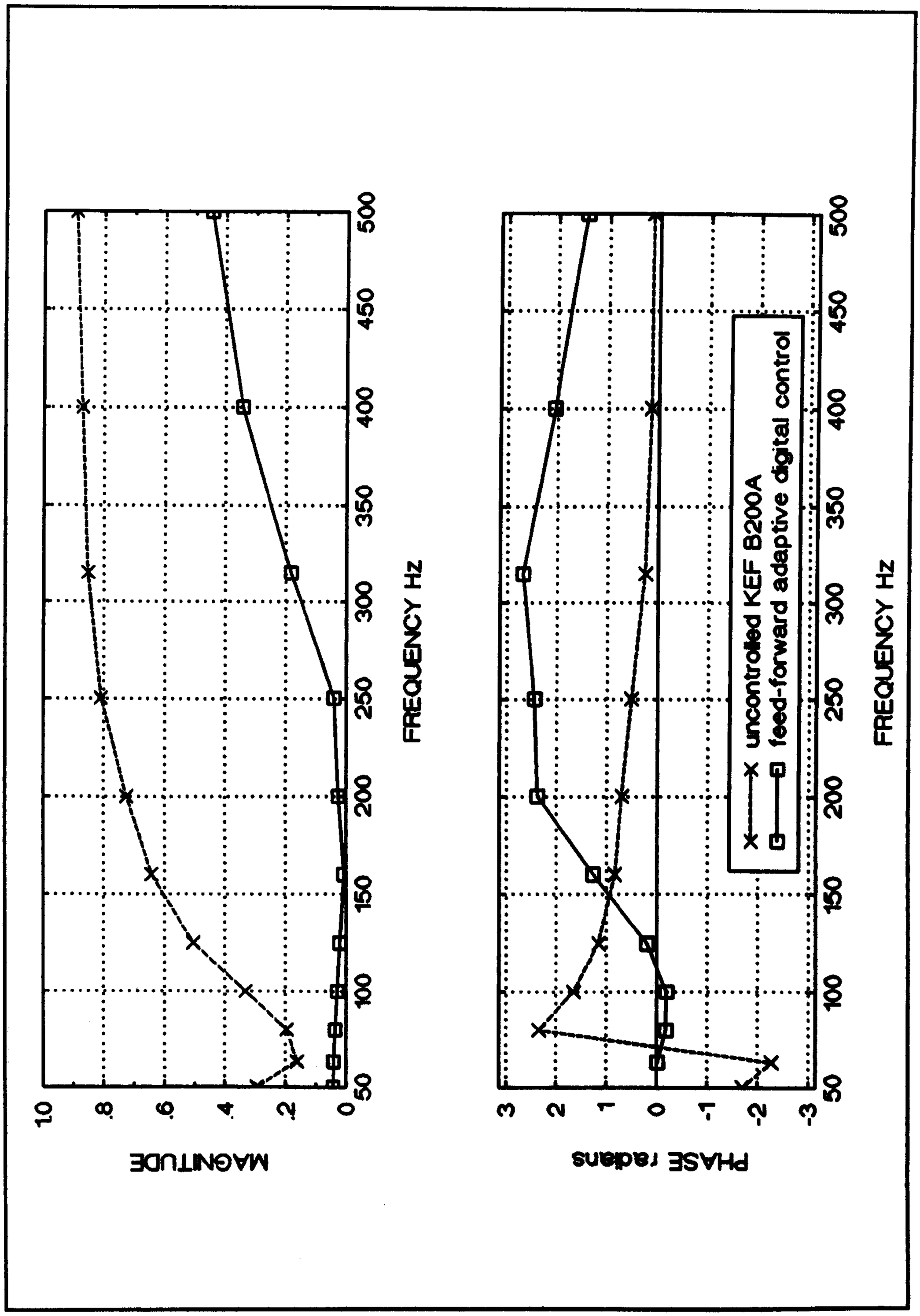

Figure 104. Magnitude and phase of reflection coefficient of KEF B200A loudspeaker for normally-incident sinusoidal plane waves. Controlled result achieved with mic-accr feed-forward digital adaptive system, set for desired characteristic impedance.

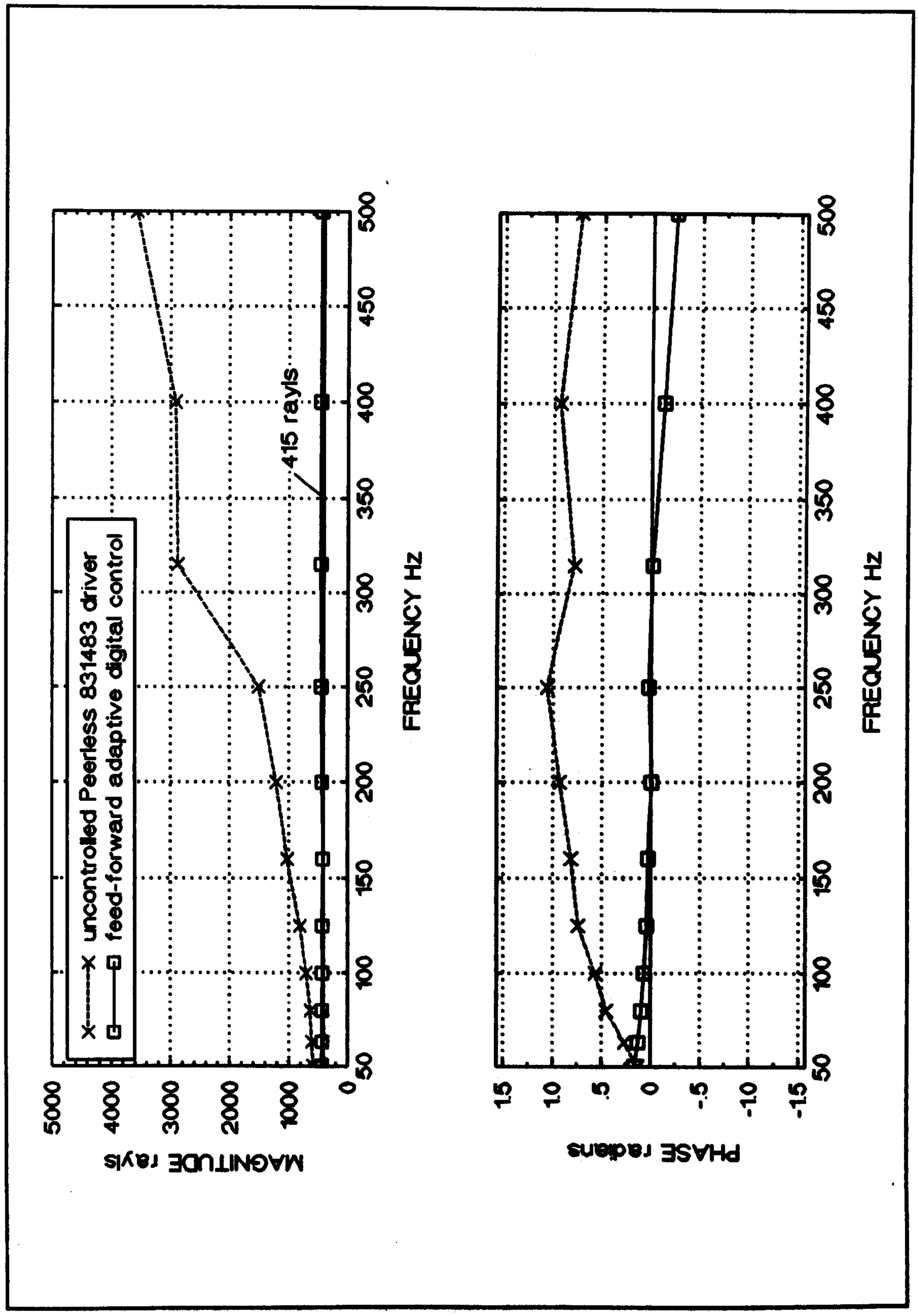

Figure 105. Magnitude and phase of acoustic impedance of Peerless 831483 loudspeaker for normally-incident sinusoidal plane-waves. Controlled result achieved with mic-accr feed-forward digital adaptive system, set for desired characteristic impedance.

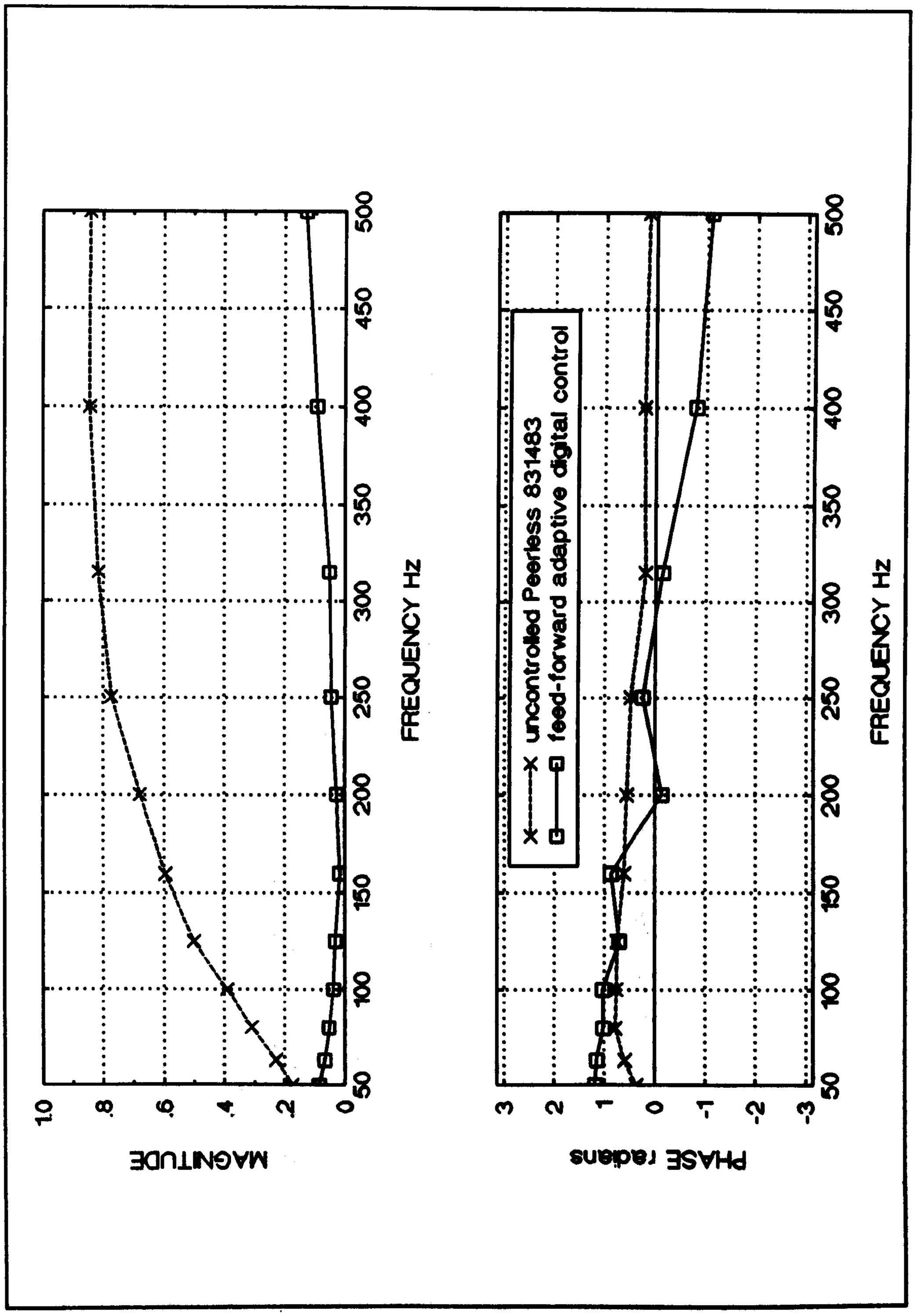

Figure 106. Magnitude and phase of reflection coefficient of Peerless 831483 loudspeaker for normally-incident sinusoidal plane-waves. Controlled result achieved with mic-accr feed-forward digital adaptive system, set for desired characteristic impedance.

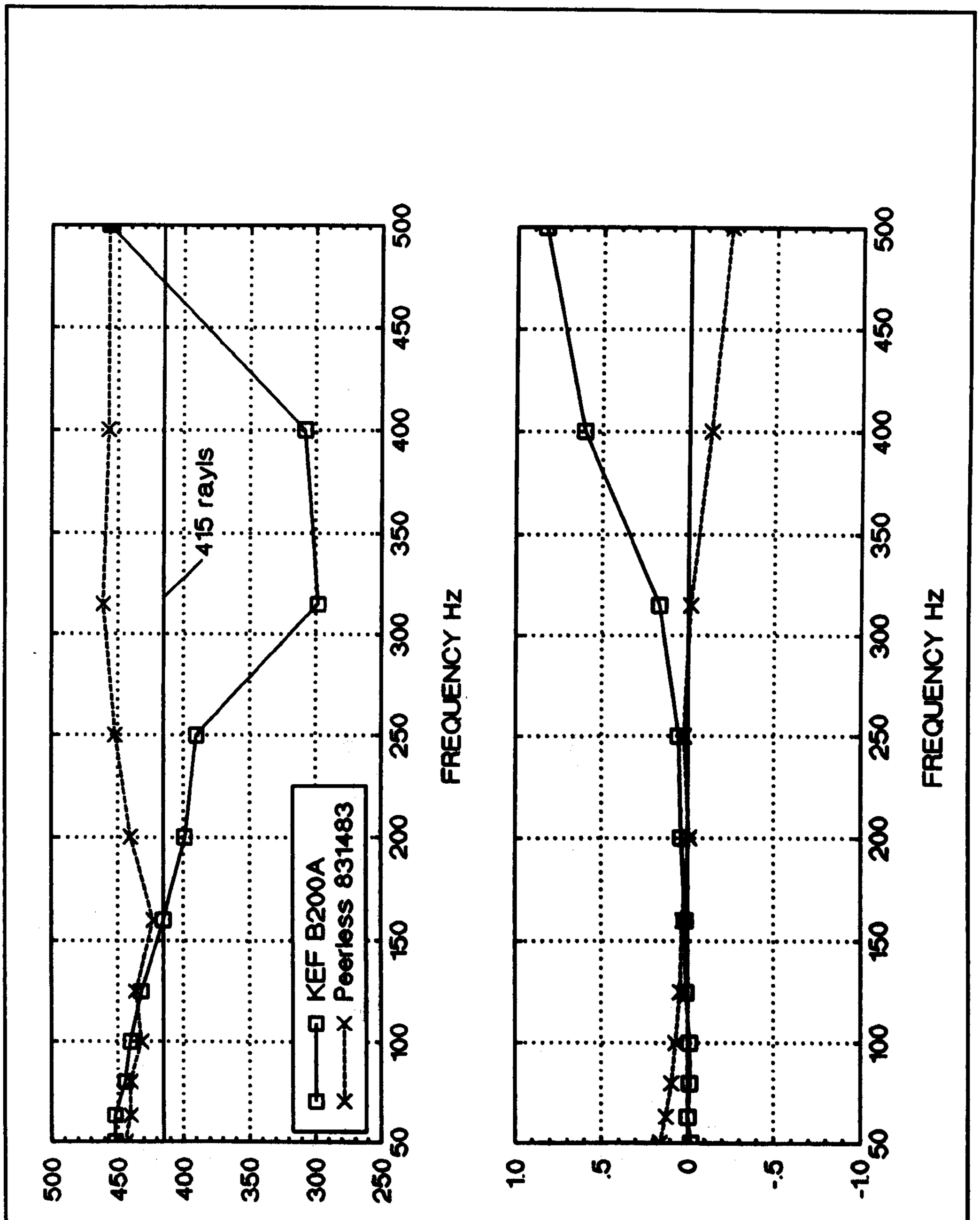

Figure 107. Magnitude and phase of controlled acoustic impedance of KEF B200A and Peerless 831483 loudspeakers for normally-incident sinusoidal plane-waves. Mic-accr feed-forward adaptive digital control system set for characteristic impedance.

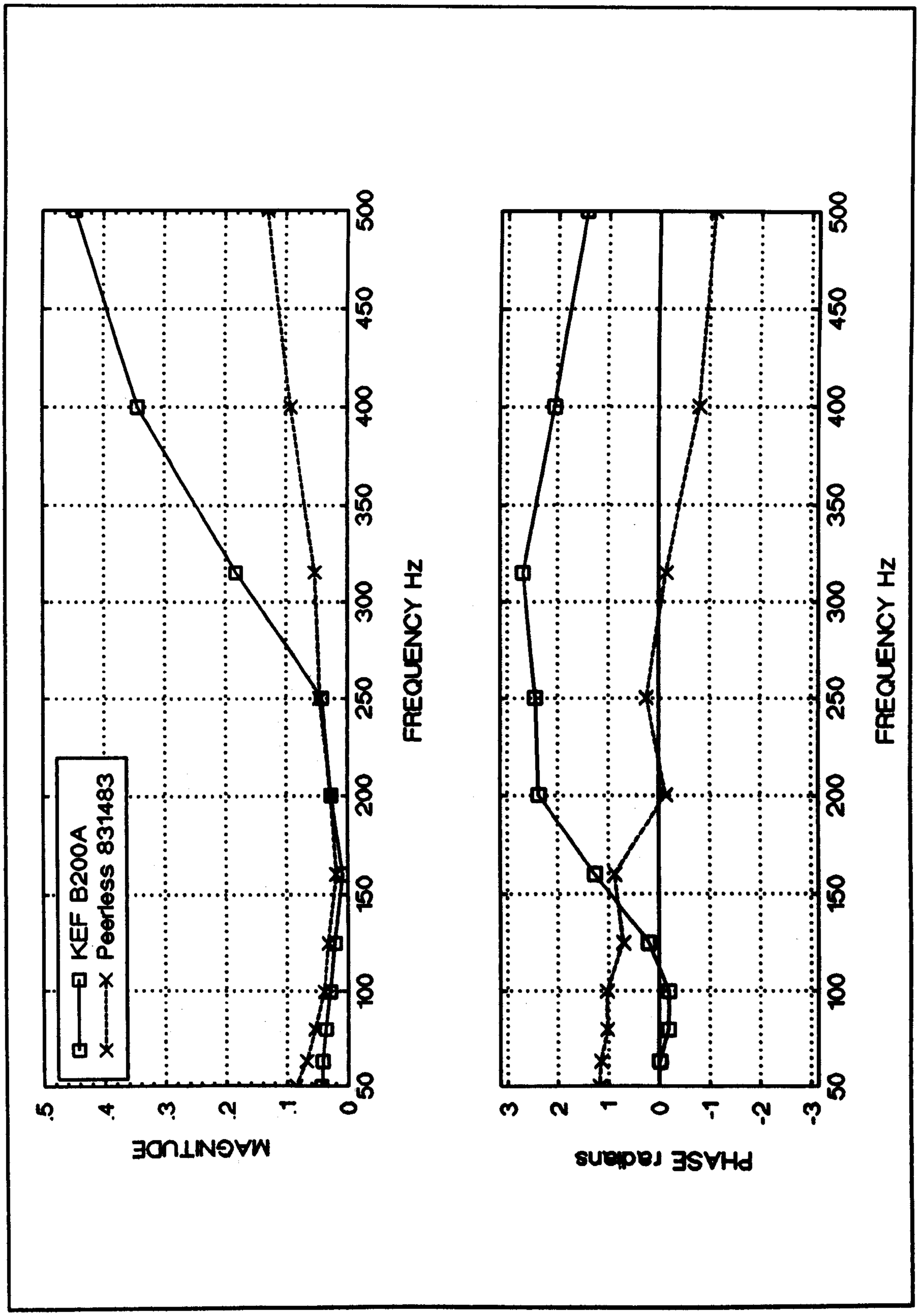

Figure 108. Magnitude and phase of controlled reflection coefficient of KEF B200A and Peerless 831483 loudspeakers for normally-incident sinusoidal plane-waves. Mic-accr feed-forward adaptive digital control system set for characteristic impedance.

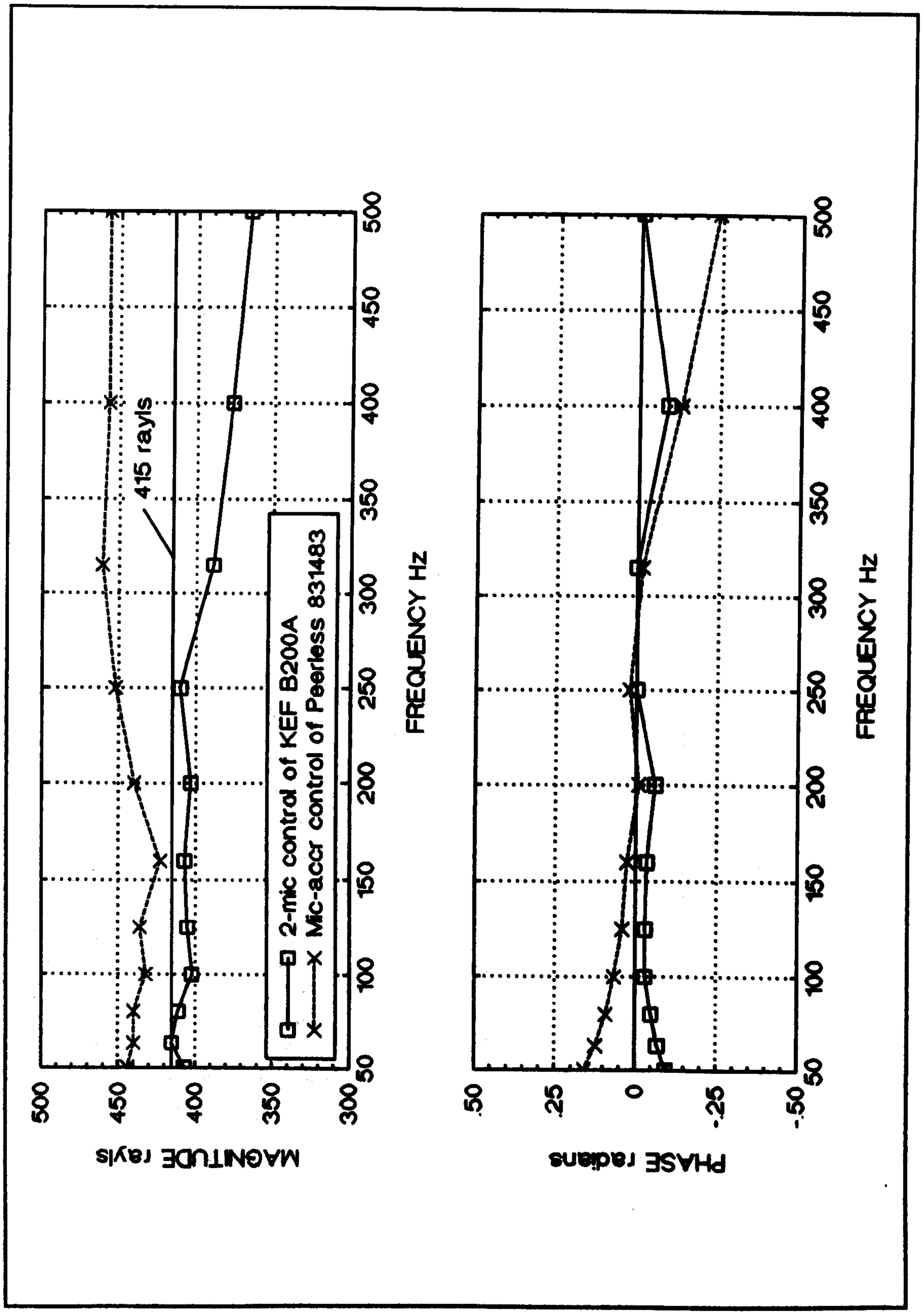

Figure 109. Magnitude and phase of acoustic impedance for 2-mic control of KEF B200A and mic-accr control of Peerless 831483 loudspeakers for normally-incident sinusoidal plane-waves. Control systems both set for characteristic impedance.

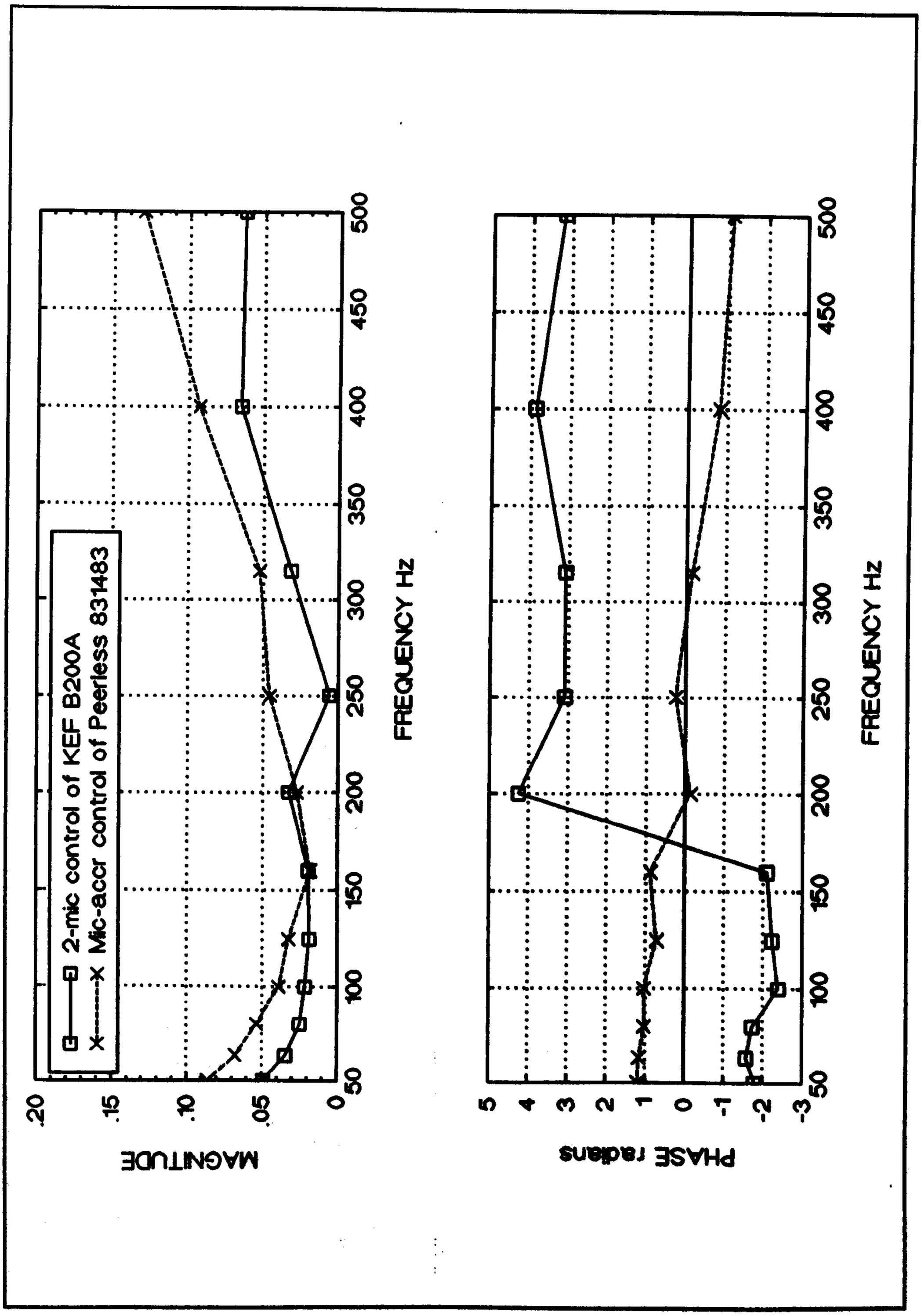

Figure 110. Magnitude and phase of reflection coefficient for 2-mic control of KEF B200A and mic-accr control of Peerless 831483 loudspeakers for normally-incident sinusoidal plane-waves. Control systems both set for characteristic impedance.

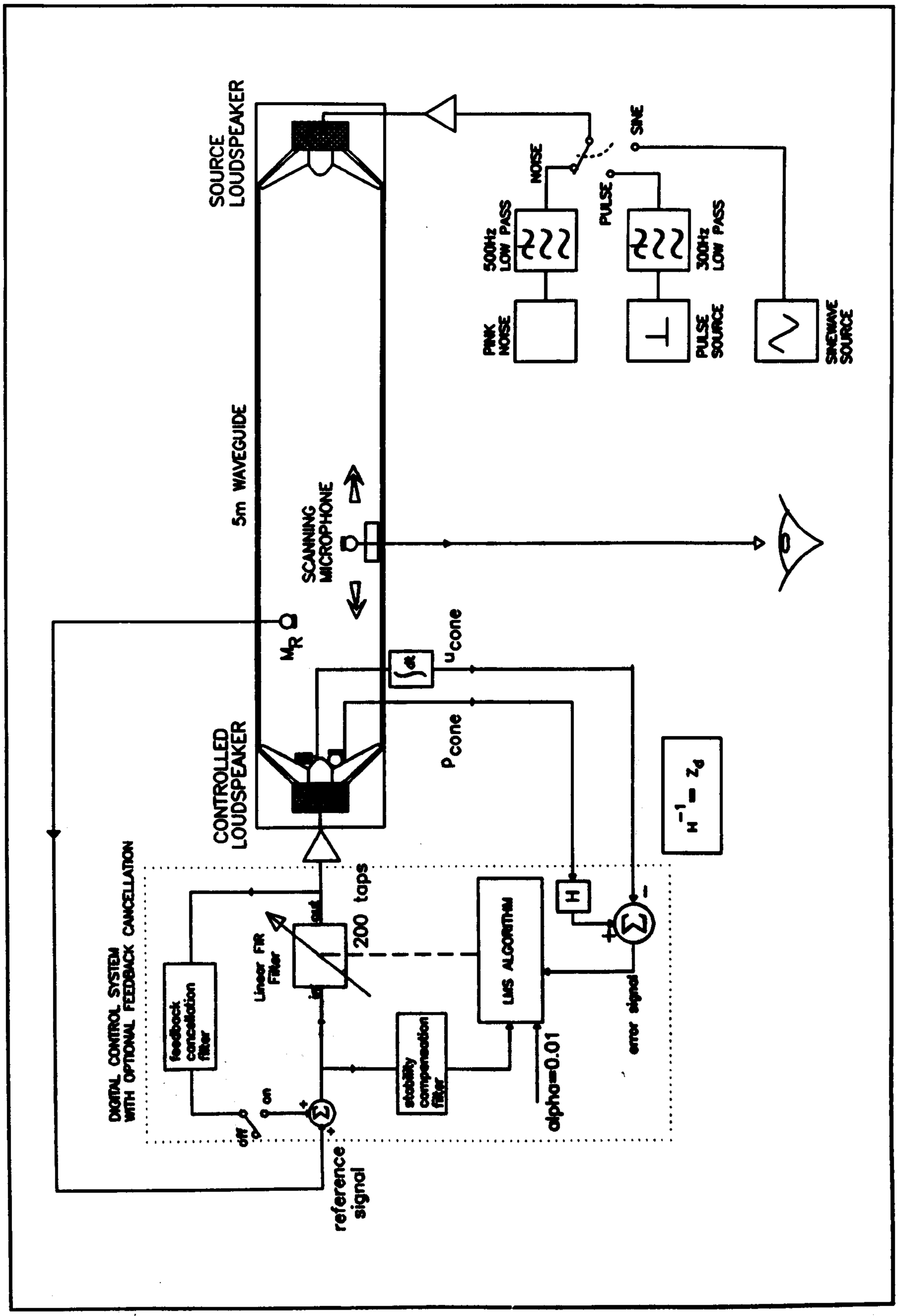

Figure 111. Schematic of laboratory test-rig of mic-accr active impedance control system. Reference input is taken from microphone M_R. Mic-accr forces desired acoustic impedance with noise, transient and sinusoidal sources.

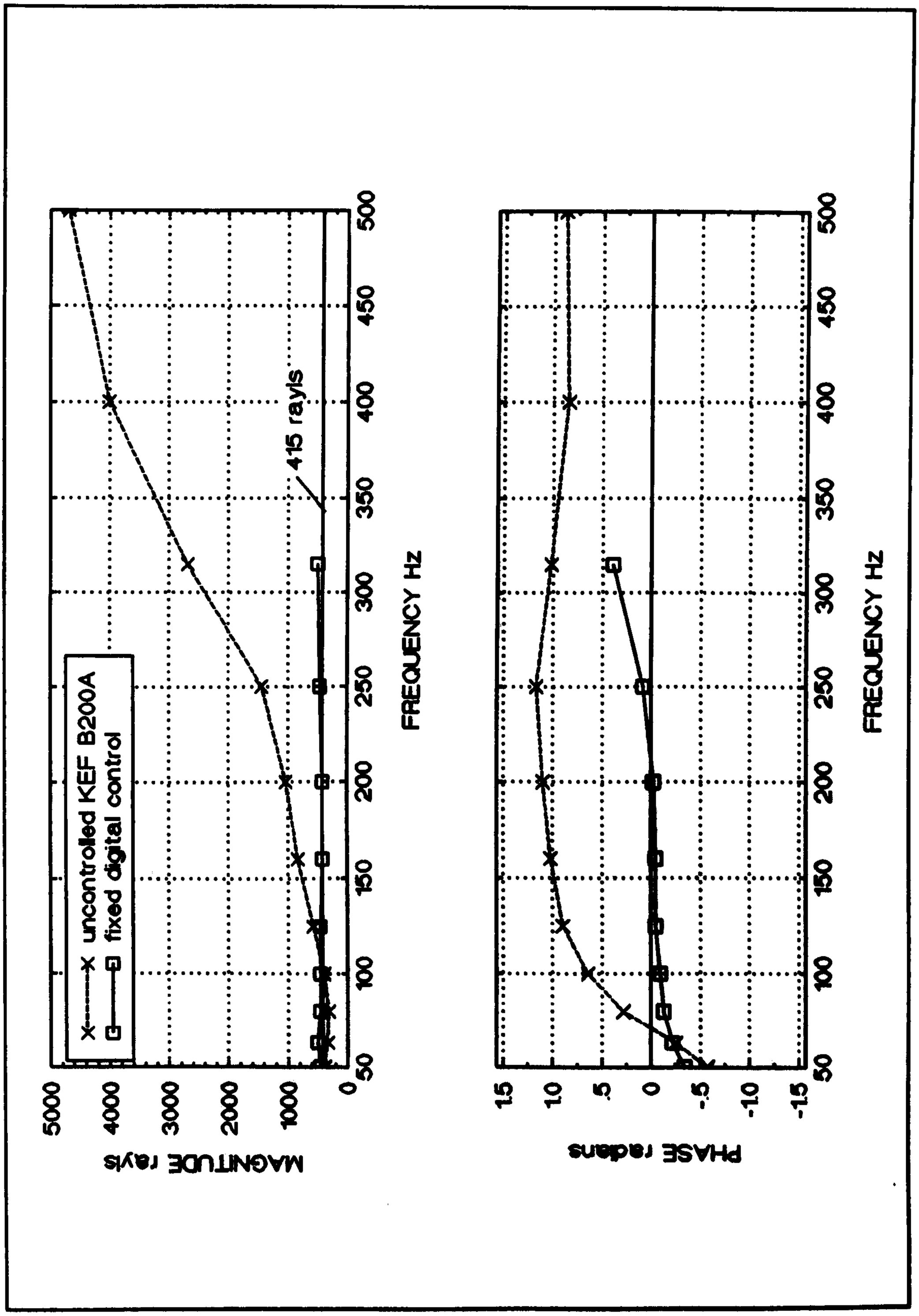

Figure 112. The measured magnitude and phase of the surface acoustic impedance presented by a KEF B200A loudspeaker to normally-incident sinusoidal plane waves when uncontrolled, and when controlled by a mic-accr feed-forward fixed digital control system.

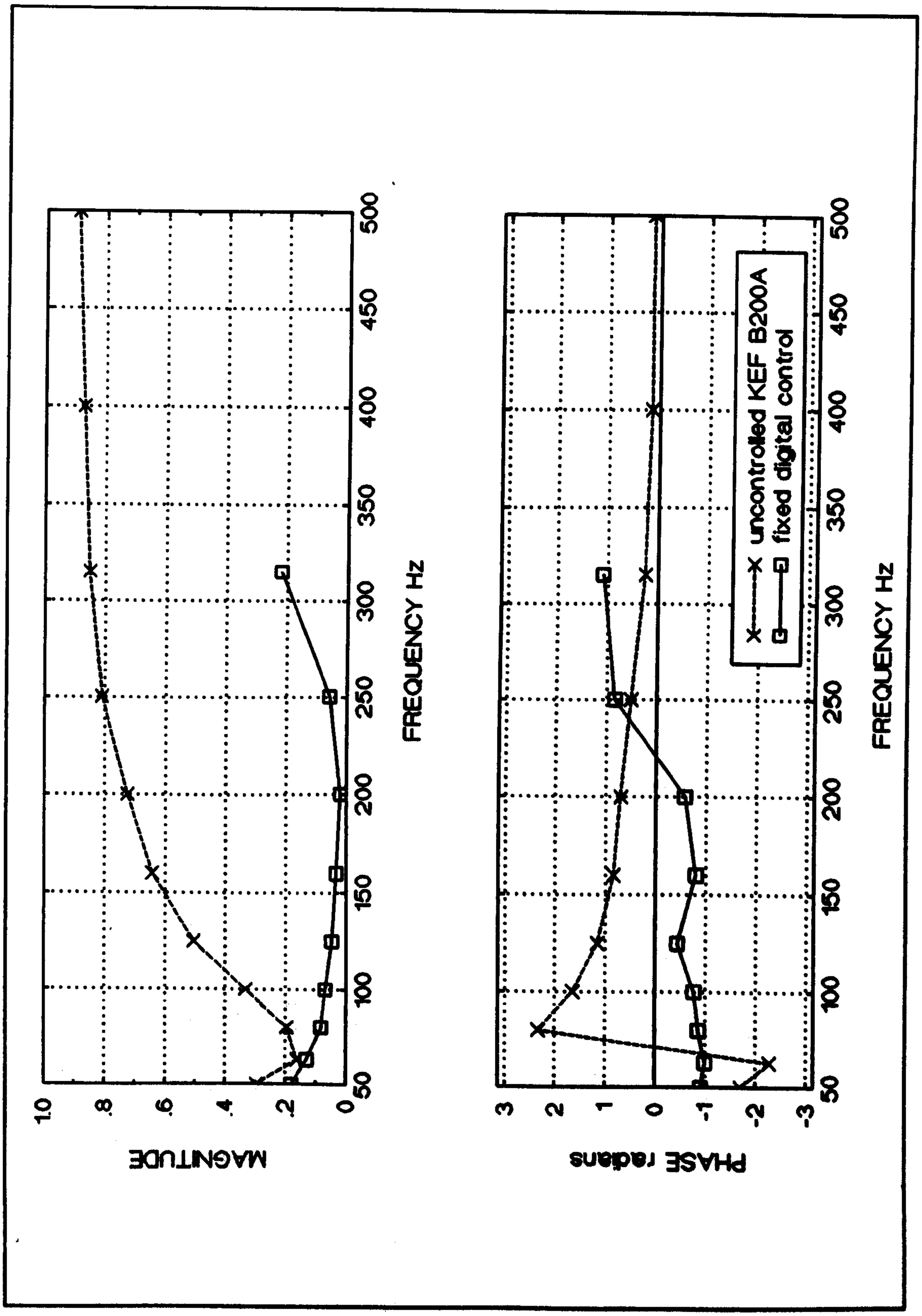

Figure 113. The measured magnitude and phase of the reflection coefficient presented by a KEF B200A loudspeaker to normally-incident sinusoidal plane waves when uncontrolled, and when controlled by a mic-accr feed-forward fixed digital control system.

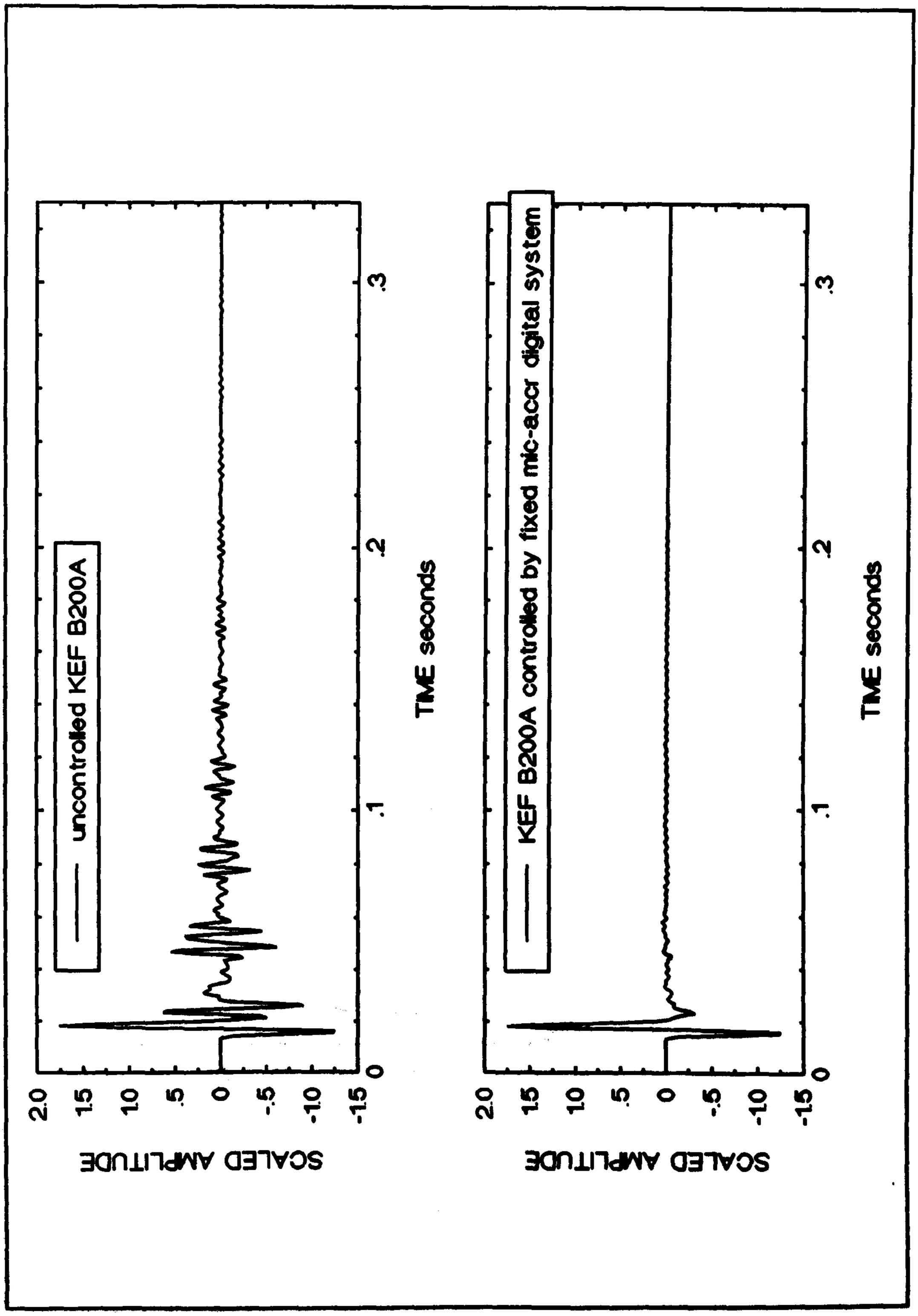

Figure 114. Averaged pressure response in the waveguide at 1 metre from the termination for a band-limited input pulse. Upper plot for the uncontrolled KEF B200A, lower plot for the controlled KEF B200A with mic-accr feed-forward fixed digital system.

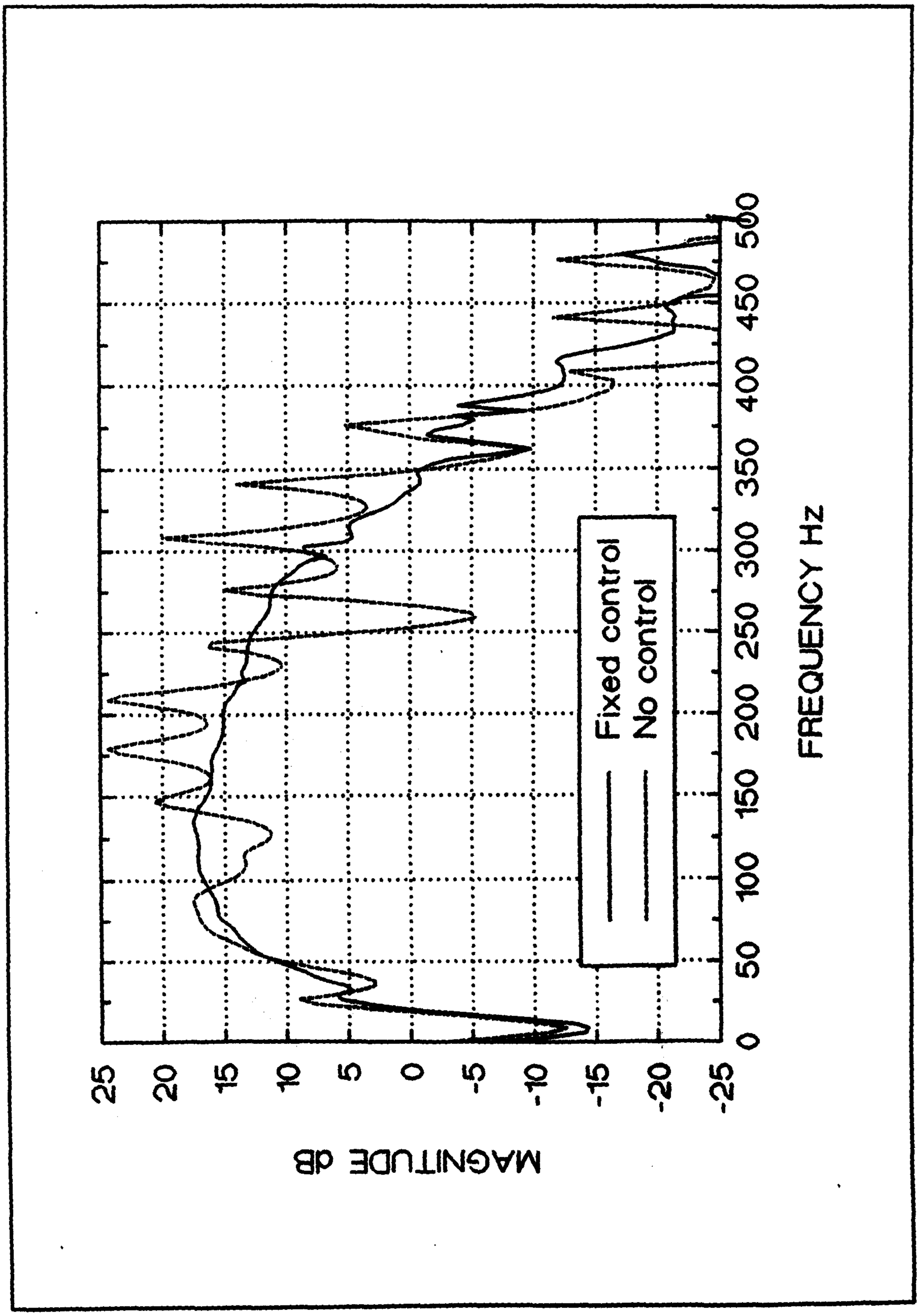

Figure 115. Frequency domain pressure response in the waveguide at 1m from the termination for a band-limited input pulse. Dashed line for the uncontrolled KEF B200A, solid line for the KEF B200A controlled by mic-accr feed-forward fixed digital system.

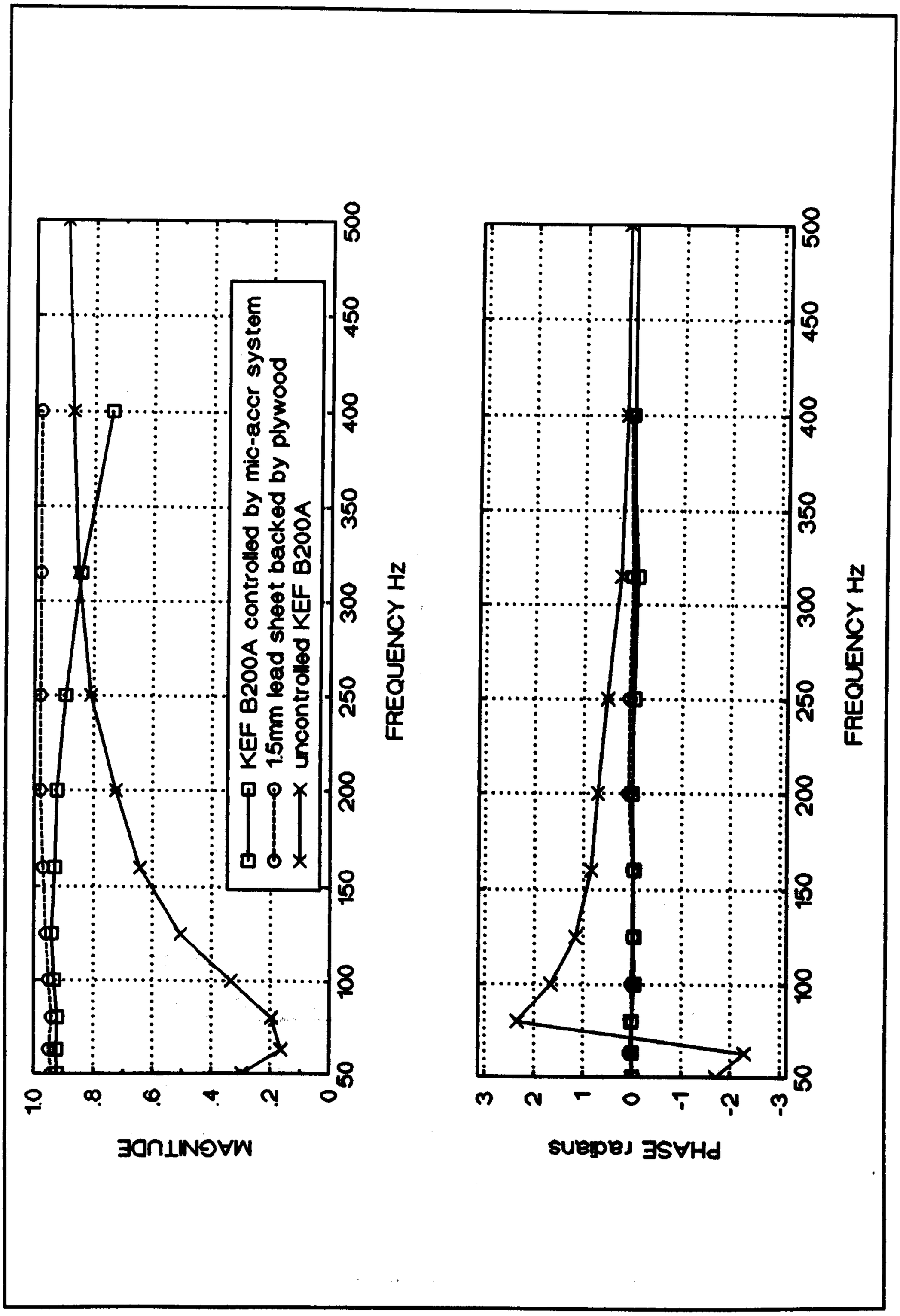

Figure 116. The measured magnitude and phase of the reflection coefficient presented by three terminations to normally-incident sinusoidal plane waves. KEF B200A controlled by mic-accr digital system set for desired infinite Z.

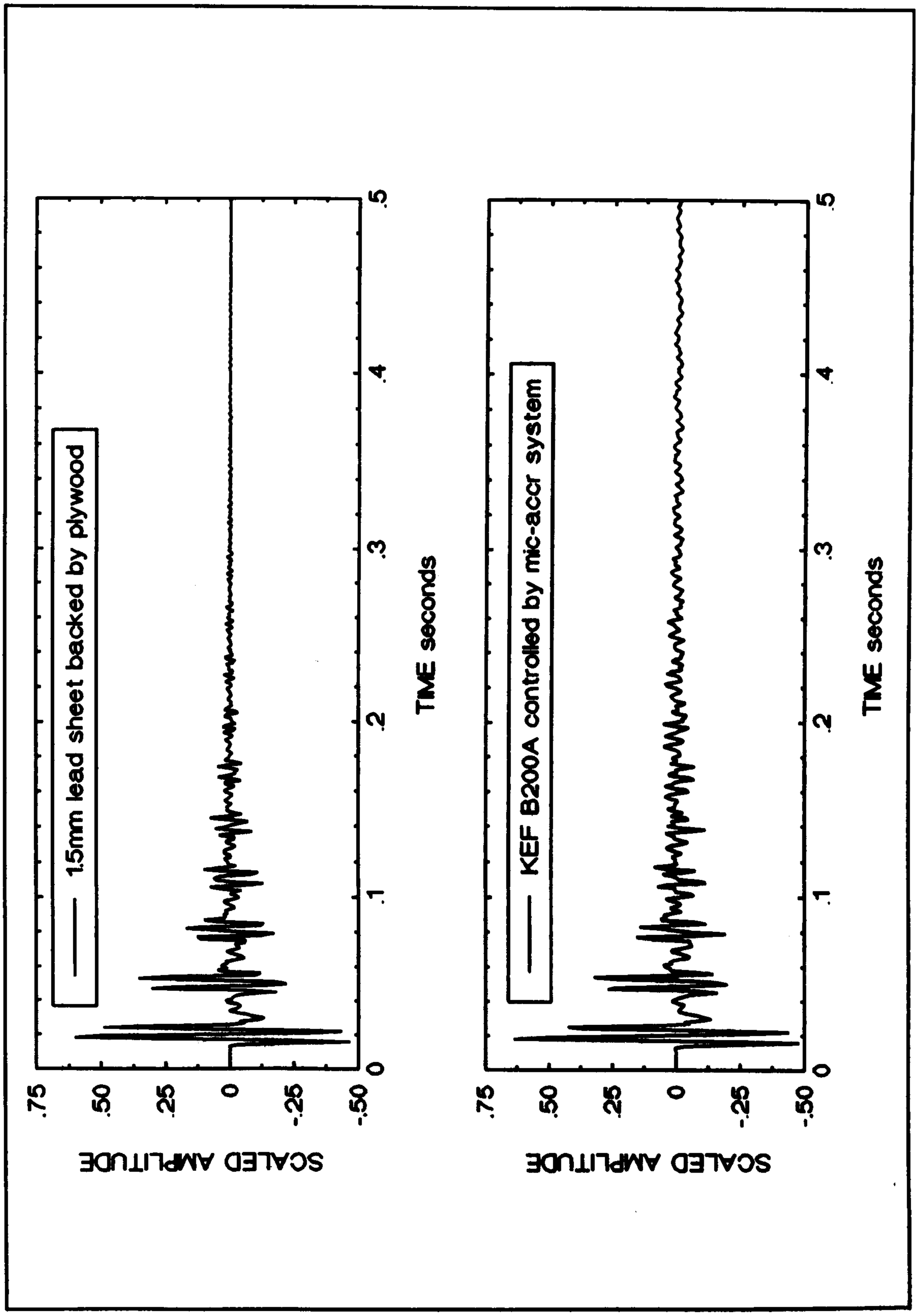

Figure 117. Averaged pressure response in the waveguide at 1 metre from the termination for a band-limited input pulse. Upper plot for 1.5mm lead sheet, lower plot for the controlled KEF B200A with mic-accr fixed digital system set for infinite Z.

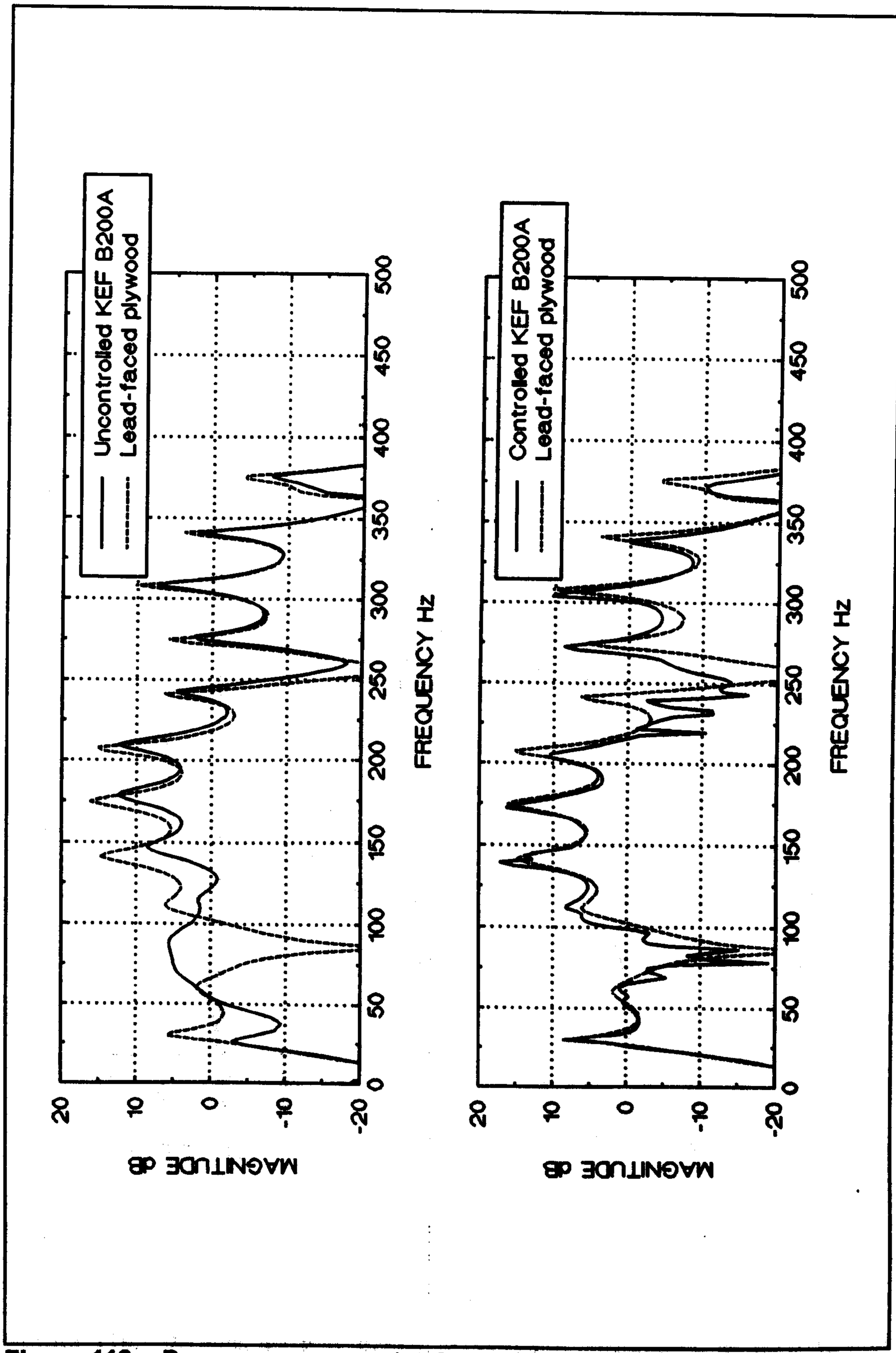

Figure 118. Pressure response 1m from termination for band-limited pulse. Dashed line for 1.5mm lead sheet. Solid line for KEF B200A with upper plot uncontrolled, lower plot controlled by fixed system set for infinite z

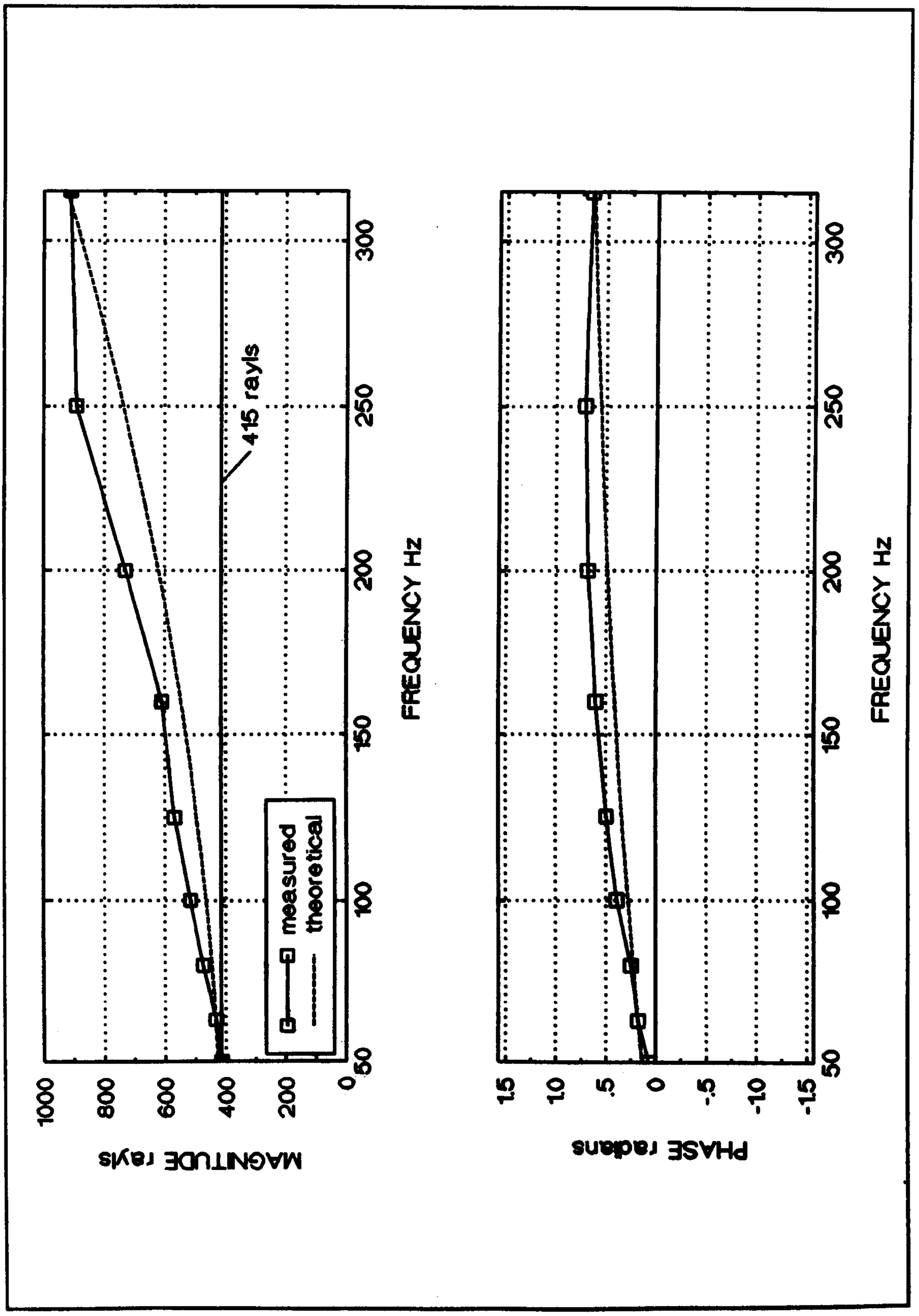

Figure 119. Magnitude and phase of acoustic impedance of KEF B200A loudspeaker for normally-incident sinusoidal plane waves. Controlled result achieved with mic-accr system, set for desired frequency-dependent impedance and trained with noise.

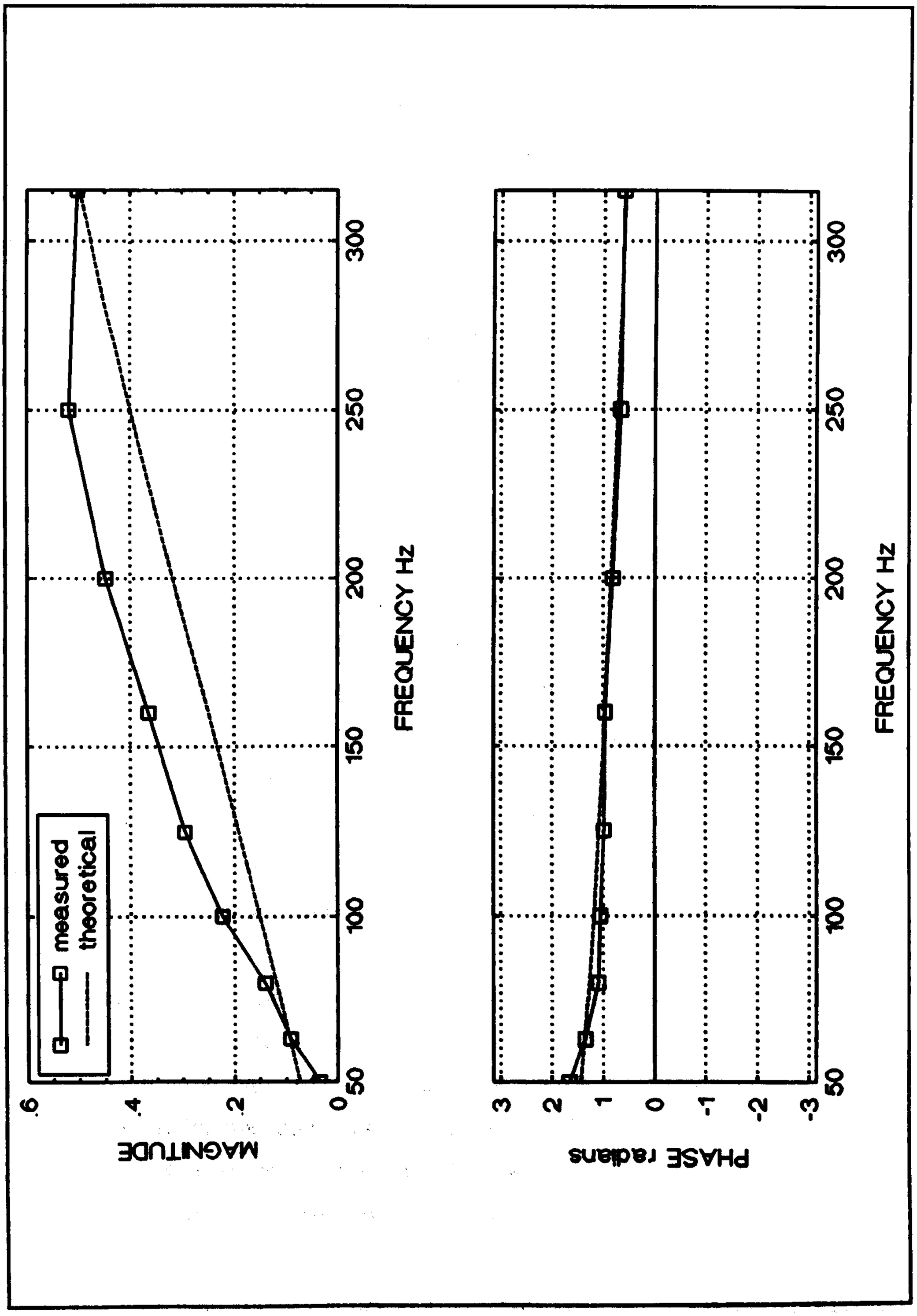

Figure 120. Magnitude and phase of reflection coefficient of KEF B200A loudspeaker for normally-incident sinusoidal plane waves. Controlled result achieved with mic-accr system, set for frequency-dependent desired Z and trained with noise.

9 DISCUSSION

The principal subject of this thesis has been the operation of active systems for the control of specific acoustic impedance. A new active controller strategy has been described and analyzed. Variations of the control strategy need to be selected to control extremes of desired impedance. As the strategy enables the use of conventional adaptive filter procedures such as the filtered-X LMS algorithm, desired impedances can be pre-specified. Successful control of the impedance at the surface of a loudspeaker cone with an experimental implementation of this strategy has been demonstrated.

The adaptive algorithm adjusts the weights of the digital controller filter according to an instantaneous gradient estimate calculated from an error signal. The determination of the error signal is a standard procedure that involves comparison of a measured signal with a desired signal. Coupling between the controller filter output and the desired signal complicated the convergence of the filtered-X algorithm, see Section 6.6. The error determination had to be re-designed to allow stable convergence. Description of such coupling problems has not been seen in the literature. This is an important issue for implementations of the filtered-X algorithm where coupling exists between the adaptive filter output and the desired signal.

The optimum active controller solutions, identified in Chapter 6, are independent of cone pressure and velocity. Practical observation of the controlled impedance, trained with random signals, with *transient signals* indicated that the adaptive controller had converged to stable and stationary solutions that were independent of pressure and velocity. This was an important verification of the performance of the controlled impedance termination.

Analysis of the loop stability of active impedance controllers has been presented in Section 6.4. This shows that when either cone pressure or cone velocity is used as an input signal, feedback loops around the controller are unstable for certain desired impedances if there is delay in the controller. This has been

observed in practical implementations. There is also a similar theoretical conclusion for when duct pressure is used as the controller input. However, practical implementations that force characteristic impedance have been stable over restricted bandwidths. Simplifications in the theory for a controller input of duct pressure may affect the theoretical conclusion. For example, sound energy losses are not included. Two conventional procedures for increasing feedback loop stability have been identified and implemented: feedback cancellation and the use of recursive filters. Experimental observations of the convergence of a filtered-U recursive filter were more stable than the filtered-X non-recursive filter. However, the recursive filter required careful adjustment. Feedback cancellation also allowed adaptive convergence but required less adjustment. Analysis of the optimum controller filter solutions without and with feedback cancellation has been presented in Chapter 6. With feedback cancellation, the filter solutions must model the radiation impedance "seen" by the controlled cone. With the reactive acoustics of the waveguide used in the practical implementation, the controller filter required more weights for convergence with broader-band signals than with sinusoidal signals. This is consistent with the literature. The analysis of the controller solution without feedback cancellation when the input is duct pressure demonstrates that the filter solution can be unstable if the pressure is measured at nodes in a modal sound field. This is consistent with an intuitive understanding of the controller. The analysis of the controller with feedback cancellation reveals a non-causal component in the filter solution. Despite this, the controller converged to a useful solution with the band-limited noise used in tests and the controlled impedance was effective for transient signals.

After ensuring feedback loop stability, the various adaptive configurations of the control strategy converged for sinusoidal signals to force desired impedances from zero to infinity. The convergence for noise signals was more complicated. An experiment indicated that the ability of the feedback controller to reduce the error signal to zero was a function of the delay in the controller loop and the statistics of the noise, see Section 7.7. The feedback controller did not converge with broad-band noise signals. This was due to the delays imposed in the practical implementation of the digital control system. A study of the

performance of the feedback control system is a principal recommendation for further work, see Section 10.1. A feed-forward implementation of the control strategy had better convergence. Feed-forward controllers that used duct pressure or the electrical source signal as an input converged to force near-desired impedances with all the noise signals used in the tests.

The control of the impedance of a piston was established in Chapter 4. The maximum sound pressure levels (SPLs) were calculated as between 135dB to 150dB for zero, characteristic and infinite controlled impedances of the KEF B200A loudspeaker cone. The practical work operated with maximum SPLs of around 120dB without any observed operational problems of the controlled impedance.

The feed-forward controllers converged with the test noise signals. Possible factors that affected the practical performance of the controlled impedances (the closeness of the controlled impedance to the desired impedance) were the adaptive controller filter solution, the linearity between the applied force from the motor-system and the voltage applied to the voice-coil, and the impedance observation error. The impedance observation error has been described in Section 6.2. If the test signals were sinusoidal then the adaptive filter converged to a solution that made the error signal effectively zero. Experimental work revealed that the controlled impedance of the KEF B200A loudspeaker by the 2-mic system had better performance than the mic-accr system. Therefore, the performance of the controlled impedance with the mic-accr system mainly depended on the impedance observation error. An effort was made to quantify this for the KEF B200A loudspeaker, see Section 7.9. At lower frequencies below 250Hz the order of the observation error was consistent with the measurement accuracy of the pressure and velocity transducers. However, at higher frequencies the observation error was larger. It is suggested that this was due to mass-loading of the cone by the transducers - this has not been verified; an accurate measurement method of the velocity over the cone surface was not available. At a later stage in the research a different loudspeaker, Peerless model 831483, was used and had much better performance at higher

frequencies. An investigation into reducing the effects of impedance observation error is suggested for further work, see Section 10.1.

It is of interest to compare the ability of the controlled (near-) characteristic impedance to absorb incident pulses with the control system described by Orduña-Bustamente *et al* in (29). Both systems have been demonstrated to absorb one-dimensional incident transient pressure but with different control systems, loudspeakers and in ducts of different dimension. Despite these differences the motivation behind the two research efforts is identical - the absorption of incident sound. The published results in Figure 10 of (29) show that this system effectively prevented reflections from the surface of the controlled loudspeaker. However, an additional effect is seen. The initial direct travelling pulse was modified before arrival at the controlled surface - therefore the surface was not acting as an ideal absorber of sound. The results from the control system presented in this thesis, see Figure 114 on Page 294, show that the initial pulse was not modified. This is the correct behaviour for an absorber of incident sound. Orduña-Bustamente's system used the electrical source signal as the controller input. This work has examined and demonstrated the mic-accr control strategy for a wider variety of inputs. This is more relevant for a "real" implementation where coherent electrical signals may not be available. The results in Figure 114 were for when the duct pressure was used as the controller filter input. The controlled impedance can therefore be considered as a "stand-alone" system which is more desirable for general application.

It is also of interest to discuss differences of the mic-accr control system with the active system for sound absorption proposed by Mazzola. An original analysis of Mazzola's control system for the control of a loudspeaker has been presented in Section 6.8. This analysis suggests that a real implementation would be stable with a defined radiation load and loudspeaker. Mazzola's system is configured to force a characteristic impedance. The control systems described in this thesis allow the desired impedance to be arbitrarily assigned and have different inputs to Mazzola's system and therefore have different optimum

solutions. Another difference is that this work demonstrates practical control of surface impedance.

The practical work performed for this thesis has tested the mic-accr control strategy with band-limited random noise and transient signals. Effort was made to use reference signals that were sourced from the acoustic environment. The principal operational simplifications used were that the system was operated for one-dimensional normally-incident plane waves and the system was operated at frequencies where the controlled surface was assumed to have piston-like motion. These simplifications were essential to establish the operation of the system. For example, the control of infinite impedance for band-limited noise and transient sound, see Section 8.3, has not been seen before in the literature. Extending the system application to more complicated acoustic environments is the final recommendation for further work.

10 CONCLUSIONS

A new strategy for the active control of specific acoustic impedance has been presented. With simple adjustment, the strategy can create desired impedances from zero to infinity for sinusoidal, band-limited random and transient signals. A study of the literature has revealed other research efforts in this field. Whilst similarities exist, this work is original. Useful results that expand the understanding of the principle of active absorption have been presented. The control of infinite impedance for transient signals has not been published before.

Analysis has established that a conventional digital implementation of an active controller with a reference input of cone pressure or cone velocity, without feedback cancellation, is unstable for certain desired impedances. Observation of a practical implementation of the controller confirms this result. Standard feedback cancellation techniques allow stable controller implementations. Feed-forward implementations of the control strategy are more effective in controlling impedance for band-limited noise and transient signals than feedback implementations. Inherent fixed delays in the feedback controller limit the performance.

The principal problem that affected the performance of the controller implementation was the observation of impedance. The correct observation of factors under control is a performance issue with any control scenario. Recommendations have been made for further work.

10.1 RECOMMENDATIONS FOR FURTHER WORK

1. The observation of impedance has a significant effect on the value of the controlled impedance with this control strategy. Problems were encountered with impedance observation error in this research. This was believed to be due to mass-loading of the surface under control. It is recommended that further work should be directed into improving the observation of impedance. Pressure

and velocity measurements of the type used in this research appear to be more accurate on some cones than others. An investigation of this would be useful to establish the best performance of the controlled impedance. Alternatively a different method for measuring velocity could be used - two other methods exist in the literature: (i) the use of laser velocimetry; (ii) the use of a second acoustically-coupled loudspeaker. Both methods have been featured in the work of Anthony and Elliott (51). The first (expensive) method allows the observation of velocity at discrete points over the surface of the cone. The second (cheaper) method could also have useful application in this work.

2. Feedback implementations of the controller had more limits on performance for noise signals than the feed-forward controller. This was due to inherent fixed delays and the general observation is consistent with the work of other researchers. Elliott and Sutton have studied feedback controllers with feedback cancellation in (52). They proposed theoretical methods for the calculation of the performance and robustness as a function of the plant under control - fixed delays affected the performance of their feedback controller. A similar investigation could be made of the feedback controllers described in this thesis. The theoretical results could be calculated from measurements of the plant and the noise (and the reference input signal for feed-forward controllers) and compared with measurements of the controlled impedance values. By incorporating some robustness without too much performance degradation, the control system could be more useful for general application. The effect of delays could be reduced by placing an analogue control filter in parallel with the digital controller. The analogue filter would not have the inherent delay of the digital controller. Such a system might produce better performance for noise signals. A potential problem is the stability of the analogue filter for characteristic impedances. For infinite impedances the analogue filter could be a complete solution, see the discussion of the optimum control solution Equation 6.22 on Page 108.

3. The controller could be applied to three-dimensional acoustic problems by creating an array of individual controlled impedances. This has been investigated by Guicking *et al* with a different control system (24).

APPENDIX 1 : KEF B200A Loudspeaker parameters

All parameters are taken from the manufacturers data sheet.

DRIVE UNIT DATA

Model		B200A
Type		SP1014
Nominal Impedance		8Ω
Frequency Response		30 - 3500 Hz
Sensitivity		88dB SPL
Net Weight		1.47Kg
Closed Box Volume		20-30 litres
Power Handling Continuous		21.9Vrms
Power Handling Programme		50W
Flux Density		1.1T
Voice Coil Diameter		26mm
Voice coil resistance	R_c	6.8Ω
Voice coil inductance	L_e	0.69mH
Effective diaphragm area	S_d	222cm^2
Linear excursion (pk-pk)		6.3mm
Damage Limited excursion		12mm
Effective Moving Mass	M_M	24.0g
Suspension Mech. Resistance	R_M	1.56 mech.Ω
Suspension Compliance	C_M	7.32x10^{-4} m/N
Compliance Equivalent Vol.	V_{AS}	51 litres
Free Air res. frequency	f_s	38Hz
Force Factor	Bl	7.3 N/A
Damping Factors Mechanical	Q_M	3.67
Electrical	Q_E	0.73
Total	Q_T	0.61

APPENDIX 2 : Loudspeaker closed box design equations (63)(64)

Equation A2.1 shows the ratio of closed box system resonance Q_{TC} to driver resonance Q_T, as a function of the system compliance ratio α.

$$\alpha = \frac{Q_{TC}}{Q_T} + 1 = \frac{V_{AS}}{V_B} \qquad \text{A2.1}$$

where V_{AS} is the equivalent closed-air volume of the driver compliance C_{MS} and V_B is the volume of air inside the closed box. If Q_{TC} is selected as 1.0 then for the KEF B200A loudspeaker (parameters in Appendix 1) α is 2.7 and V_B is 25l.

The transfer function of the sealed box system is a 2nd order high-pass filter of characteristic described by Eq. A2.2.

$$|E(j\omega)|^2 = \frac{1}{1 + \left(\frac{1}{Q_{TC}^2} - 2\right).\left(\frac{\omega_0}{\omega}\right)^2 + \left(\frac{\omega_0}{\omega}\right)^4} \qquad \text{A2.2}$$

where ω is the angular frequency and ω_0 is the system resonant frequency. The 3dB down frequency ω_3 is found by setting $|E(j\omega)|^2=0.5$ and solving for ω. For the KEF B200A mounted in a sealed box loudspeaker of internal volume 25l the 3dB down frequency is $\omega_3 = 0.79\omega_0$.

The frequency of a resonant peak in the response is found by partial differentiation of the denominator of Eq. A2.2 as in Eq. A2.3.

$$\frac{\delta\left[1 + \left(\frac{1}{Q_{TC}^2} - 2\right)\left(\frac{\omega_0}{\omega}\right)^2 + \left(\frac{\omega_0}{\omega}\right)^4\right]}{\delta\left(\frac{\omega_0}{\omega}\right)^2} = \left(\frac{1}{Q_{TC}^2} - 2\right) + 2\left(\frac{\omega_0}{\omega}\right)^2 \qquad \text{A2.3}$$

The peak frequency is found by setting Eq. A2.3 to zero and solving for ω, the magnitude at this peak can be found from Eq. A2.2. The Kef B200A loudspeaker mounted in a 25l sealed box has a peak of 1.25dB at $\omega = 1.4\omega_0$.

The system resonant frequency ω_0 for the loudspeaker cone mounted in an infinite baffle with a sealed box as a rear-radiation load is found by considering an equivalent electrical circuit for the loudspeaker closed box system shown in Figure 121 on Page 313. The resonant frequency is due to the combined inductance and capacitance in the electrical equivalent circuit Eq. A2.4.

$$\omega_0 = \frac{1}{\sqrt{M_{AT} C_{AT}}} \qquad \textbf{A2.4}$$

where the inductance is:

$$M_{AT} = M_{AD} + M_{AF} = \frac{M_M}{S_D^2} + \frac{8\rho}{3\pi^2 r} \qquad \textbf{A2.5}$$

The first term arises from the cone mass and the second term is the added mass of air that "attaches itself" to, and so moves with the cone (r is the radius of the loudspeaker cone, other values are quantified in Appendix 1). The capacitance is described by:

$$C_{AT} = \left(\frac{1}{C_{AD}} + \frac{1}{C_{AB}} \right)^{-1} = \left(\frac{1}{C_{MD} S_D^2} + \frac{\gamma P_0}{V_B} \right)^{-1} \qquad \textbf{A2.6}$$

where S_D is the surface area of the cone, $\gamma P_0 = 1.4 \times 10^5$. From Eq. A2.4, Eq. A2.5 and Eq. A2.6 the system resonant frequency of the KEF B200A loudspeaker mounted in a 25l closed box is calculated as $f_0 = 66$Hz.

The reference efficiency is described by Eq. A2.7.

$$\eta_{ref} = \left(\frac{Bl}{S_D R_e M_{AT}} \right)^2 R_e \frac{\rho}{2\pi c} \qquad \textbf{A2.7}$$

The reference efficiency for the KEF B200A loudspeaker mounted in a 25l closed box is 3.0×10^{-3}.

The loudspeaker system specifications for the KEF B200A loudspeaker mounted in a closed box are shown in Table 1.

Table 1. Specifications for KEF B200A loudspeaker in 25 litre sealed box.

V_B (litres)	25
Q_{TC}	1.0
f_0 (Hz)	65
f_3 (Hz)	52
f_{peak} (Hz)	92
η_{ref} %	0.3

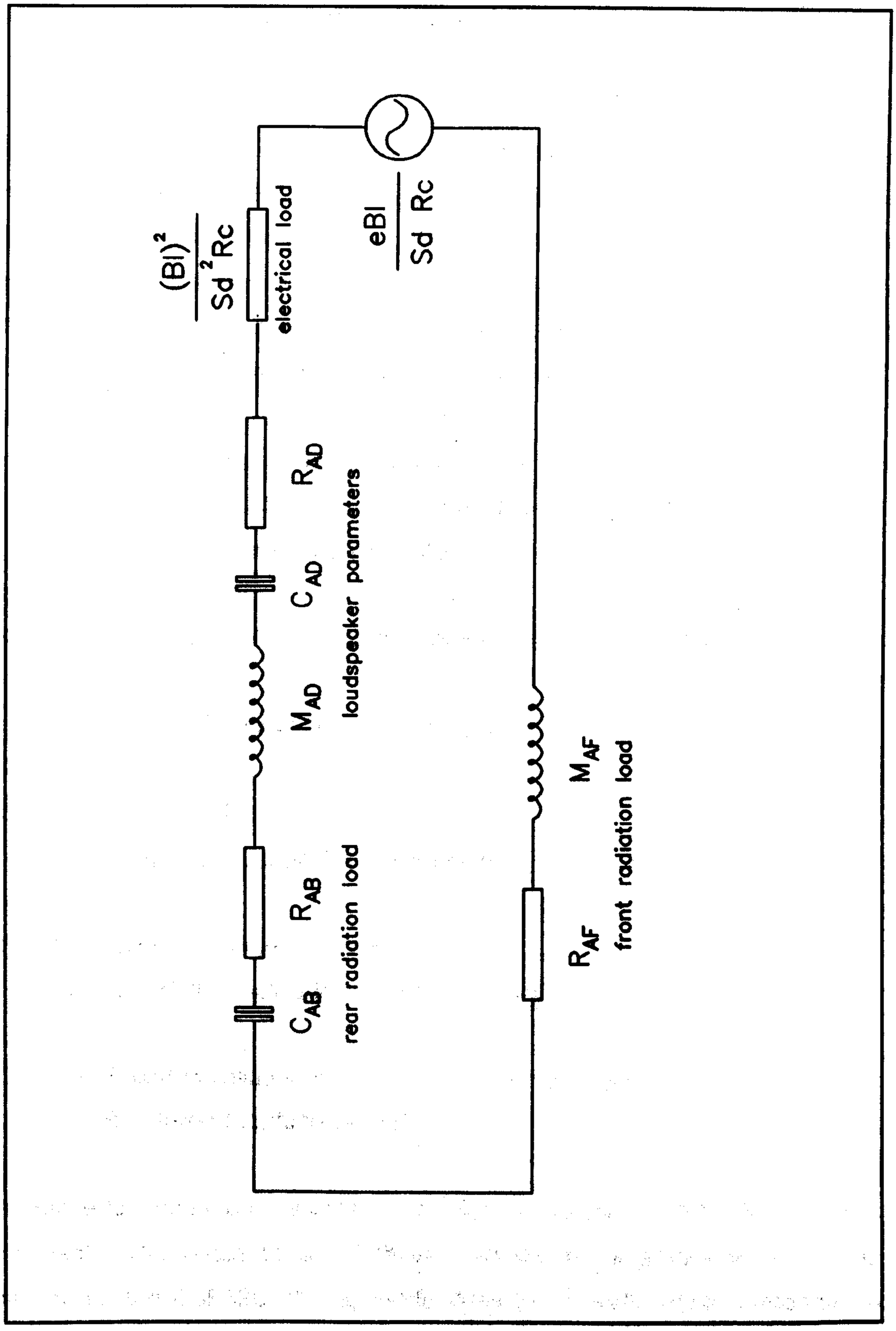

Figure 121. Electrical equivalent of the closed box loudspeaker system mounted in an infinite baffle radiating into free space.

APPENDIX 3 : The Loughborough Sound Images DSP32C System Board

3.1 Introduction

The digital adaptive mic-accr control system devised during this research is implemented on an AT&T DSP32C signal processor. This appendix describes the Loughborough Sound Images (LSI) DSP32C digital signal processing board and application software written by the thesis author. This is described in (66). The user of the board should make further reference to the manuals supplied with the DSP board. These can be categorized as follows:

Board description, installation, hardware, introduction to programming and interfacing the DSP32C board through the PC bus

"DSP32C System Board User Manual"

Complete description of the chip and programming the DSP32C in assembly language

"WE-DSP32C Digital Signal Processor"

DSP compiler and linker

"WE DSP32C Support Software Library"

DSP32C Assembly Language Routines

"WE DSP32C Application Software Library"

PC/Stereo Board installation and description of hardware

"16 Bit Stereo Interface Board"

Reference to these manuals will be necessary to supplement information in this document. Reference to all of these manuals is necessary when writing software for the DSP32C; this appendix does not provide detailed information about the programming of the DSP32C. All references to the DSP32C System Board User Manual refer to Issue 2.0 dated November 1989. All references to

the PC/Stereo board manual "16 Bit Stereo Interface Board" refer to Issue 3.0 dated July 1991. Later editions may be different.

3.2 DSP32C Board description

The Loughborough Sound Images (LSI) DSP32C digital signal processing board, when installed in an IBM PC compatible, provides powerful real time signal processing. The system allows sampling and processing of analogue signals; digital signals can also be converted to analogue signals. The board achieves this with a very high speed floating-point digital processor designated the DSP32C, two A/D-D/A convertor channels and on-board RAM. An additional pair of convertors is available on the Loughborough Sound Images PC/Stereo board. Dedicated software has been written in the Department of Applied Acoustics to accomplish a variety of tasks such as active control systems for acoustics and data acquisition.

Refer to the DSP32C System Board User Manual. The board implements an AT&T DSP32C digital proceesor. This chip is designed to perform very fast floating-point calculations (12.5 million instructions per second). The board provides two pairs of high speed 16-bit A/D and D/A convertors (max sampling frequency 200kHz) to allow interfacing to analogue signals. The board also contains RAM to allow DSP32C programs to run, and data to be stored. 6KB is provided in three banks on the DSP32C chip, 32KB is provided of external "fast" RAM chips and 256KB of external "slow" RAM chips. "Fast" RAM is accessed without delay by the DSP32C processor however "slow" RAM is accessed with time penalties (two wait-states). The A/D convertors have max input of about ± 3 volts, exceed this and input OP-amps may be destroyed. D/A convertors have max output of ± 3 volts. DSP32C board A/D convertors invert signals and D/A convertors do not. THIS IS NOT DOCUMENTED IN THE LSI MANUALS. Fourth-order anti-aliasing and reconstruction filters are available on the DSP32C system board. The roll-off frequencies are NOT software programmable. The filters are implemented with standard circuits that use resistors, capacitors and OP-amps. The default factory setting is 18.5 Khz,

which may not be suitable for your application. To change these filters refer to page 94 of the DSP32C System Board User Manual. The A/D and D/A convertors are all DC-coupled. DC offsets from external circuitry often cause problems when using the boards. The DSP32C system board provides DC offset adjustment with on-board variable pre-set potentiometers.

3.3 PC/Stereo Board description

Refer to the PC/Stereo System Board User Manual. The board implements two pairs of 16-bit A/D and D/A convertors. The board is controlled by the DSP32C board and can not work "standalone". Connection between the two boards is by a flat ribbon 50 way connector cable supplied with the PC/Stereo board. A/D convertors have max input of about ± 3 volts, exceed this and input OP-amps may be destroyed. D/A convertors have max output of ± 3 volts. PC/Stereo A/D and D/A convertors do not invert signals. Fourth-order anti-aliasing and reconstruction filters are available on the PC/Stereo board. The roll-off frequencies are NOT software programmable. The filters are implemented with standard circuits that use resistors, capacitors and OP-amps. The default factory setting is 18.5 Khz, which may not be suitable for your application. To change these filters refer to page 23 of the PC/Stereo "16-bit stereo interface board" manual. The A/D and D/A convertors are all DC-coupled. DC offsets from external circuitry often cause problems when using the boards. The PC/Stereo board provides DC offset adjustment with on-board variable pre-set potentiometers.

3.4 DSP32C and PC/Stereo Board Installation

Refer to DSP32C System Board User Manual. The DSP32C system board requires a full-length 16-bit expansion slot on an ISA bus and the PC/Stereo card requires a half length slot. A suitable computer has a large desktop or tower case with more than two spare expansion slots. Ensure that the computer power supply can supply enough current for the DSP boards - see DSP32C System Board User Manual page 15.

It is necessary to describe the board's base address memory location in the computer with an environment variable. The software will then be able to "find" the board. For a single DSP32C system board supplied by LSI with factory default settings (base address of 290 hex) add the following line to the DOS environment table.

set MON32=290

If multiple expansion boards are installed in the computer then different addresses must be used to avoid memory addressing conflicts. If the DSP32C board base address needs to be changed (see Section 2.2 of the DSP32C System Board User Manual) then change the environment variable MON32 to the new board base address. Current DSP32C software will only support a single DSP32C board (and a single PC/Stereo board if required) in a single computer.

The remainder of this section discusses the installation of PC/Stereo boards. Some pieces of software require extra A/D and D/A convertors. Extra convertors are available on the PC/Stereo board. The installation of a PC/Stereo board is described in the "16 Bit Stereo Interface Board" manual. The two boards connect together: (i) to allow the DSP32C board to control the PC/Stereo board; (ii) to clock the PC/Stereo converters at the same rate.

The DSP32C board controls the PC/Stereo board via the DSPLINK interface system using a 50-way ribbon cable supplied with the PC/Stereo board. The two boards connect together as described on page 5 of the PC/Stereo board manual.

The Department of Applied Acoustics DSP32C active control system software requires that the DSP32C and PC/Stereo board convertors are clocked at the same rate by connecting system board clock from pin 14 of the analogue interface 15-way connector on the system board (see page 85 of "DSP32C System Board User Manual") to pins 2 and 3 of the PC/Stereo board control 15-way connector (CON3, Lower - see page 4 of "16 Bit Stereo Interface Board"). Figure 122 shows the connections. Change Link 12 on the DSP32C system board so that all three pins short together (locate Link 12 with board

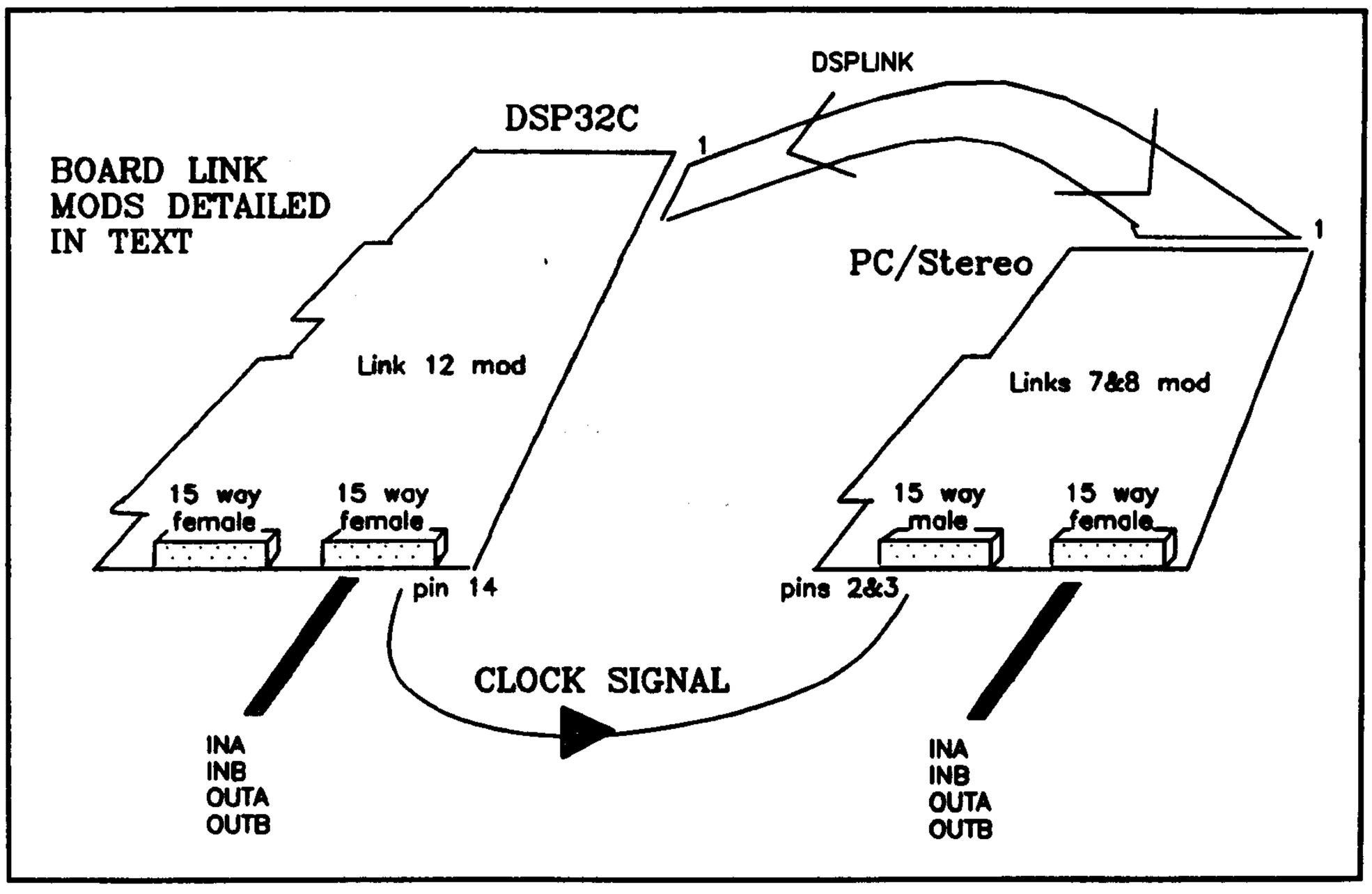

Figure 122. Connection schematic for clocking the PC/Stereo board convertors from the DSP32C timer.

lay-out diagram on page 20 of DSP32C System Board User Manual). Change links 7 and 8 on the PC/Stereo board to position C (PC/Stereo board manual page 6).

The link changes do not affect the operation of software that only use the DSP32C board. These changes have been implemented in the DSP32C installations on computers used for active control of impedance.

3.5 Applications Software

This section describes PC and DSP32C software written by Guy Nicholson between 1990 and 1993. Each section describes "standalone" executable code. The program files, although having similar names, are NOT interchangeable between the applications.

Expect to spend time setting up the connections from analogue signals to A/D convertors and D/A convertors to external devices. The multiplicity of similar

BNC connectors from the flying leads connected to the boards 15-way connectors often causes confusion. Always check to see if DC is present and potentially causing problems on the A/D inputs.

The DOS software loads the DSP32C executable software through the PC bus to the DSP32C board and transparently controls the DSP software. The user only has to load one DOS executable program at the command line to run each piece of software. The loading of a new DSP32C program over-writes the previous DSP32C program.

3.5.1 DC testing of A/D convertors

Purpose:

Test program for monitoring presence of DC offsets on DSP32C and PC/Stereo board A/D convertors.

Files: Two:

DCSET.EXE	DOS executable
DC32.OUT	DSP32C executable

Set-up and command line:

Requires DSP32C board, PC/Stereo board optional. Check board address environment variable is installed in autoexec.bat, see Page 317. The PC program DCSET.EXE needs access to DC32.OUT, so copy both files to a suitable directory. Start DCSET by typing "DCSET" on the command line.

Notes: Two screens: Title and diagnostic.

Run this program with all external equipment powered-up and connected to the A/D convertors. Diagnostic screen contains a depiction of the DSP32C and PC/Stereo boards, black boxes show averaged digital A/D signals (max of ± 32767). * symbols show locations of pre-set potentiometers on the board. Adjust either the external DC source or the board pre-sets until the black boxes have near zero values. Excessive noise will prevent near-zero DC levels however this is often satisfactory for the active impedance control programs.

If there is a run time problem (such as DSP32C board not available) then the program writes a message to the white box on the bottom right of the diagnostic screen.

If any operational difficulty occurs:

(i) Check availability of DC32.OUT.

(ii) Check base address environment variable, see Page 317.

(iii) Check board installation, see Section 3.4 of Appendix 3 on Page 316.

(iv) Turn power off then back on to reset DSP32C board.

(v) Software or hardware fault. Try another program or DSP32C board.

3.5.2 Mic-accr adaptive impedance control system

Implements an active control system based on the Least Mean Squares (LMS) adaptive algorithm for the control of impedance. This section refers to version 2.2 of the system. This control strategy is described in Chapter 5 on Page 90. The experimental implementation is described in Section 7.5 on Page 215. The LMS compensation filter is configured as shown in Figure 49c on Page 184.

Consists of five program files:

GO.EXE	DOS executable
DEF.INI	Initialisation defaults file - ASCII
TMSRB.FON	Fonts file for graphics
SAM2.OUT	DSP32C executable code
32CRLP.OUT	DSP32C executable code

Set-up and command line:

Requires DSP32C board and PC/Stereo board. Check board address environment variable is set, see Page 317. The PC program GO.EXE needs access to all of the other four files, so copy all files to a suitable directory and run the controller from there.

Start the controller from the DOS command line by typing:

GO

Disable reference sampling by typing:

GO /n

This saves start up time when the controller does not need feedback cancellation. Do NOT start the controller with "GO /n" if feedback cancellation is needed. Exit the program at any time by pressing CTRL-BREAK.

Notes:

Before running GO.EXE check for DC on the A/D convertors with the DCSET program, see Page 320. Connections to the converters are as follows:

DSP32C board

INA	reference signal for LMS algorithm
INB	not used
OUTA	diagnostic signal
OUTB	control signal

PC/Stereo board

INA	desired signal, pre-filtered
INB	forward-path return signal
OUTA	not used
OUTB	not used

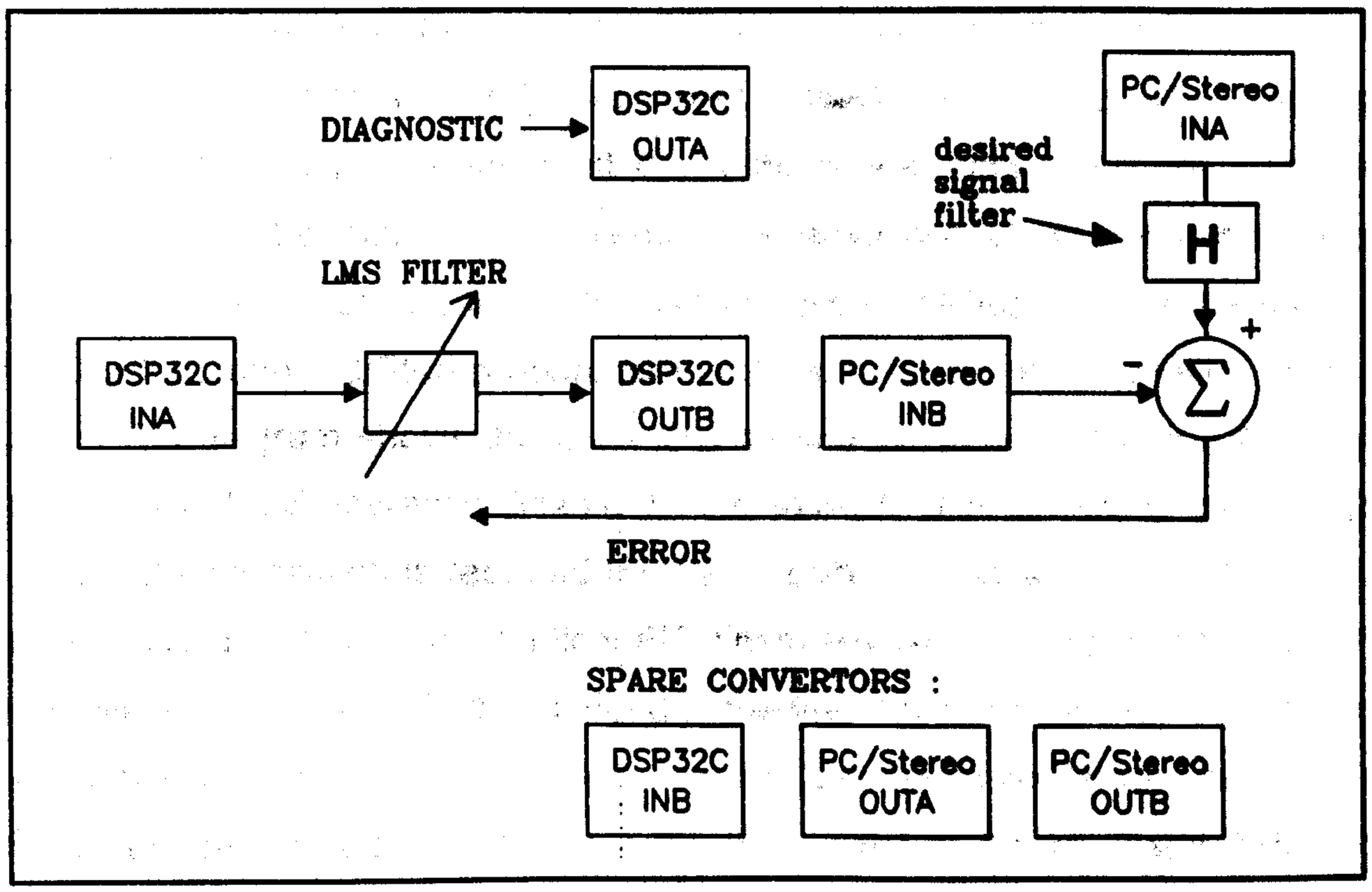

Figure 123 Connection schematic for LMS active impedance controllers v2.2 & v2.1 implemented on the DSP32C system and PC/Stereo boards.

Figure 123 shows a connection schematic for the controller. **H** is the desired filter transfer function - this sets the desired active surface impedance. Connect the analogue I/O cables supplied with the boards to the correct connectors. For location of analogue I/O 15-way connectors: see DSP32C System Board User Manual page 20 and PC/Stereo board manual Figure 2 page 4. This is often confusing because of 180 degree rotation of the boards when compared with the diagram. If in doubt take the case off and locate the bus edged-connector - this allows physical orientation with the diagram. Connect a clock signal to the PC/Stereo board as described on Page 317 of this document.

3.5.2.1 Control system and equipment connection

This section details equipment connection and control system schematic for the active control of impedance. This typifies the test-rig connections used to control the surface impedance of a conventional loudspeaker for ideal active absorption in a one-dimensional sound field. Figure 124 on Page 325 contains a diagram of the typical equipment connections and control system. These connections can be changed to implement feedback control, different reference inputs etc. The acoustic parts of the test-rig are in the top right of the figure. The DSP32C and PC/Stereo board are in a dashed box at the bottom of the figure. The diagram shows the LMS filter **W** and recursive LMS filter **R**. For non-recursive LMS operation disable the recursive filter **R** by setting the gain β to zero. Compensation is required for the stability of both adaptive LMS filters and is realised with the two identical FIR filters labelled **C**. The coefficients of these filters are calculated as described in Section 7.5 on Page 215. Feedback cancellation is enabled by FIR filter **F** that can be turned on or off. Additional information on the implementation is given in Section 7.5 on Page 215. A complete derivation and description of the LMS algorithm is in Section 3.5 on Page 37. The recursive filtered-U adaptive filter implementation of the LMS algorithm is described in Section 3.7 on Page 50.

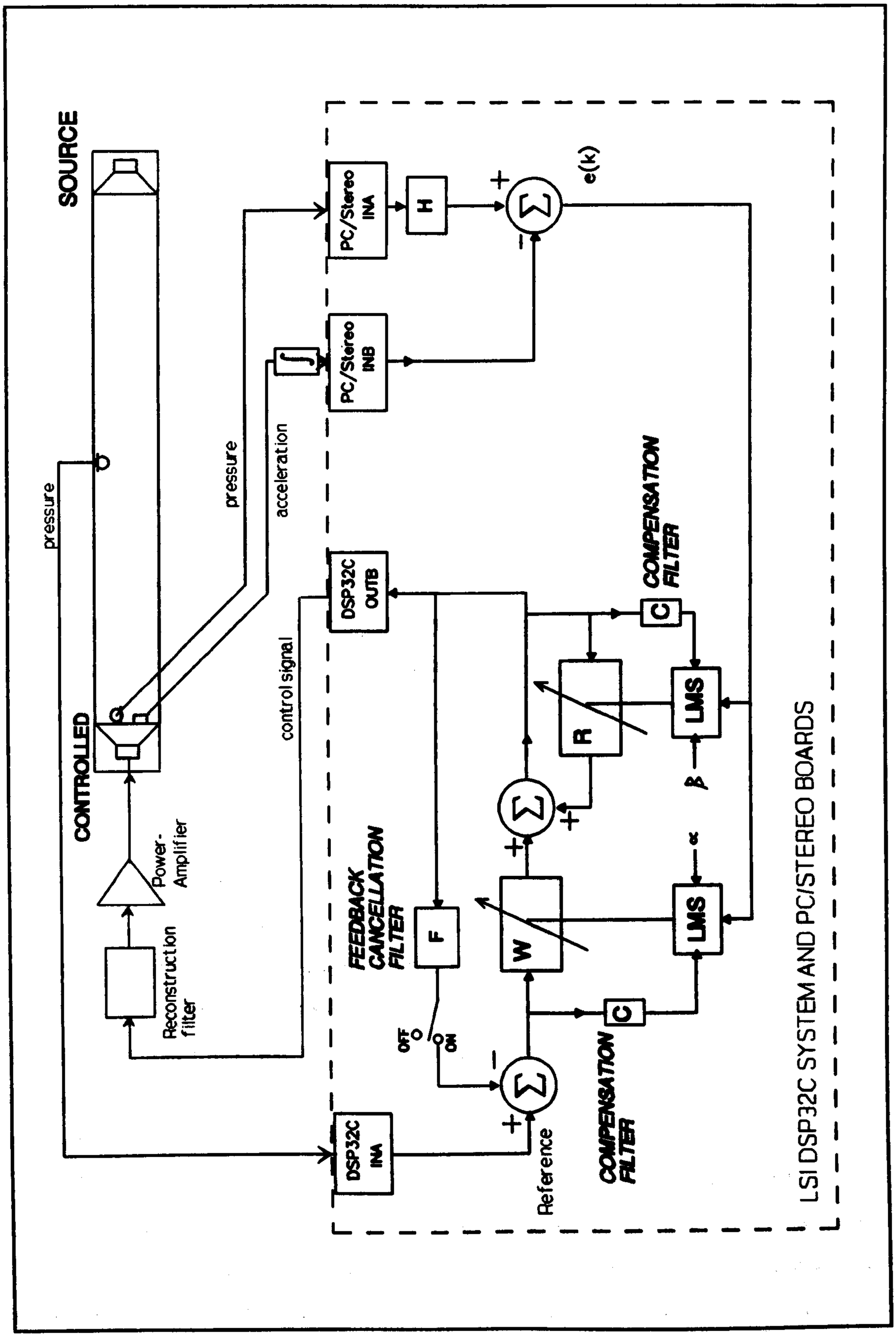

Figure 124 Typical equipment connection for one-dimensional active control of acoustic impedance of a loudspeaker.

3.5.2.2 Running the control system

The active impedance control program consists of five phases: (i) title screen; (ii) connection information screen; (iii) impulse response measurement of electro-acoustic paths; (iv) design of compensation filter screens; (v) active impedance control run-time screen. This section uses screen shots from GO.EXE (Figure 125 to Figure 130 on Page 330 to Page 332) to explain these phases. Run GO.EXE when reading this section.

The first screen seen after typing "GO" or "GO /n" on the command line is the title screen. Press any key to continue to the connection screen. Figure 125 is a screen shot of the connection screen. This details the function of the DSP32C and PC/Stereo board convertors. Connect the external electro-acoustic equipment at this stage. Press any key to continue to the measurement of the impulse responses of external electro-acoustic paths. If the board base address is not set as an environment variable (see Page 317) then a warning message appears and the program assumes that the board base address is 0x290. If a DSP32C board is not found then the program will advise the user and exit. If the program finds a DSP32C board it continues to the impulse response measurement screen.

Figure 126 shows a screen shot of the impulse response measurement screen. This allows the user to set the system sampling frequency (defaults to 3kHz) and start the impulse response measurement. The impulse response measurement consists of sending pulses from DSP32C OUTB and averaging the electro-acoustic path responses received by the A/D convertors. The number of averages can be set on this screen. All external equipment must be connected and powered. Start the impulse response measurement by pressing 'R' on the keyboard. If the DSP32C OUTB is feeding a loudspeaker then expect to hear audible clicks at a rate of a few per second - if clicks are not heard then check the connections and ancillary electronic equipment. If the A/D convertors are driven to clipping then a message appears on the PC screen - the user must reduce the signal levels before re-measuring the impulse responses. When the measurement has completed the impulse response measurement screen asks

the user either to repeat the measurement (press 'R') or continue (any key) to the filter design screens.

Screen shots of the filter design screens are shown in Figure 127 to Figure 129. These screens use the impulse response measurement results to design suitable digital filters for stability of the control system. The user has to select a suitable coefficient length for the digital filters. These screens let the user decide suitable coefficient lengths for the filters. An individual description of each screen follows.

Figure 127 shows a screen shot of the first filter design screen. This is for the design of the Feedback cancellation filter. This screen will not appear if the control system was started by typing "GO /n" on the DOS command line (see Page 322). The top left graph shows the impulse response of the path from DSP32C OUTB to DSP32C INA. Expect to see a "clean" impulse response - if not then adjust external equipment and measure the impulse response again by pressing 'R'. The bottom left and right graphs show the magnitude and phase of the Fourier Transform of the impulse response. The cancellation filter coefficients are loaded from the impulse response measurement result. Set the length of the filter by pressing 'N' on the keyboard - include all of the transient information in the impulse response measurement. A yellow vertical dashed line on the impulse response graph (top left) shows the position of the selected length on the plot. At a sampling rate of 3kHz with the active impedance rig based on a 5 metre pipe the coefficient filter length should be up to 512 samples in length. After selecting a suitable length exit the first filter design screen by pressing 'E' on the keyboard. The impulse response measurement data can then be saved before continuing to the second filter design screen.

Figure 128 is a screen shot of the second filter design screen. This is for the part design of the compensation filters. The third filter design screen (Figure 129) completes the design of the compensation filters. The top left graph shows the impulse response of the path from DSP32C OUTB to PC/Stereo INA. Expect to see a "clean" impulse response - if not then adjust

external equipment and measure the impulse response again by pressing 'R'. The bottom left and right graphs show the magnitude and phase of the Fourier Transform of the impulse response. The compensation filter coefficients are loaded from the impulse response measurement result. Set the length of the compensation filter by pressing 'N' on the keyboard - include all of the transient information in the impulse response measurement. A yellow vertical dashed line on the impulse response graph (top left) shows the position of the selected length on the plot. At a sampling rate of 3kHz with the active impedance rig based on a 5 metre pipe the coefficient filter length should be up to 512 samples in length. After selecting a suitable length exit the second filter design screen by pressing 'E' on the keyboard. The impulse response measurement data can then be saved before continuing to the third filter design screen.

Figure 129 is a screen shot of the third and final filter design screen. This completes the part design of the compensation filter. The top left graph shows the impulse response of the path from DSP32C OUTB to PC/Stereo INB. The description for this screen is the same as that for the second filter design screen

On exiting the last filter design screen the feedback cancellation and compensation filters are permanently designed. The PC program loads the DSP32C program 32CRLP.OUT and compensation filters to the LSI DSP32C system board and runs the active control system. Figure 130 is a screen shot of the control run-time screen. Halt and reset the control system by pressing the space bar. Alpha and Beta set the adaptive update speeds of the control filters. For a non-recursive filtered-X LMS implementation set Beta (β in Figure 124) equal to zero - the output of filter R is then always zero. Alpha and Beta can be instantaneously increased or decreased by a factor of ten by pressing 'Y' or 'S'. N-FWD and N-F/B show the coefficient lengths of the compensation filters. NCNR and NCR show coefficient lengths of the non-recursive and recursive adaptive filters. For an LMS implementation NCNR sets the non-recursive adaptive control filter coefficient length and NCR is of no consequence (set to 3 taps). Set the inverse gain of the digital desired filter H (shown in Figure 123) by pressing 'I' - this sets the desired active surface impedance. Adjust the

magnitude and phase of the desired filter **H** with the displayed filter coefficients. Spare DSP code lines show the code overhead for the DSP; if this goes to zero then the DSP can no longer run the current control configuration in real-time - reduce filter coefficient lengths or lower the sampling frequency. Select the diagnostic output signal from DSP32C OUTA by pressing numbers on the keyboard (not on the numeric keypad). The real-time plot on the bottom left of the screen shows the Mean Square Error (MSE) of the adaptive control filter solution. Expect this to reduce to low values as the control filter converges to a solution. The presence of DC on the input convertors will affect this plot. Suggest you monitor the control filter error from DSP32C OUTA with an oscilloscope. Iteration hold sets the delay between starting the real-time plot in the bottom left of the graph and turning the control system on. If the A/D convertors are clipped by the input signals then a warning message appears on the screen - the user must then reduce the signal levels.

The bottom right menu of Figure 130 shows other options. A DOS shell can be activated by pressing 'D'. The compensation filter coefficients are displayed by pressing 'C'. The adaptive control filter coefficients are displayed by pressing 'F' (note: this may crash the program if the weights are all zero). If the reference signal is acoustic then toggle feedback cancellation on with 'G'. The adaptive control filter update is temporarily held (but not reset) by pressing 'H'. The elapsed adaption time since the last reset of the control is shown at the bottom of the screen. Instantaneously turn the control system on and off by pressing 'O'. Exit the control system by pressing the Escape key.

The ASCII file DEF.INI sets some control system start-up values for GO.EXE: edit DEF.INI with a text file editor such as EDIT in DOS 5.0 to change control start-up values.

```
CAUSAL RECURSIVE LMS   FOR DUC / ANALOGUE INTEGRATED VELOCITY

                                                Version 2.2  Jan-On 1993


LSI DSP32C System board analogue connections:

     INA     reference mic signal.
     INB     (not used.)
     OUTA    (control diagnostic signal.)
     OUTB    anti noise control signal.

LSI PC/Stereo board analogue connections:

     INA     desired signal (pre-filtered).
     INB     forward-path return.


The controller requires transfer function estimation of
electroacoustic paths for stability.

Press any key to prepare DSP board for impulse measurement.
```

Figure 125 Connection information screen

```
IMPULSE RESPONSE MEASUREMENT                    Version 1.0 Sept 1991


Sampling system parameters:

     Sampling frequency = 2.999400 kHz
     Length of impulse response capture =    512 samples
     Number of averages = 10

Type 'S'    to change sampling frequency
Type 'N'    to change number of averages
     'Esc'  to quit
Type 'R'    to start the sampling routine
```

Figure 126 Impulse response measurement

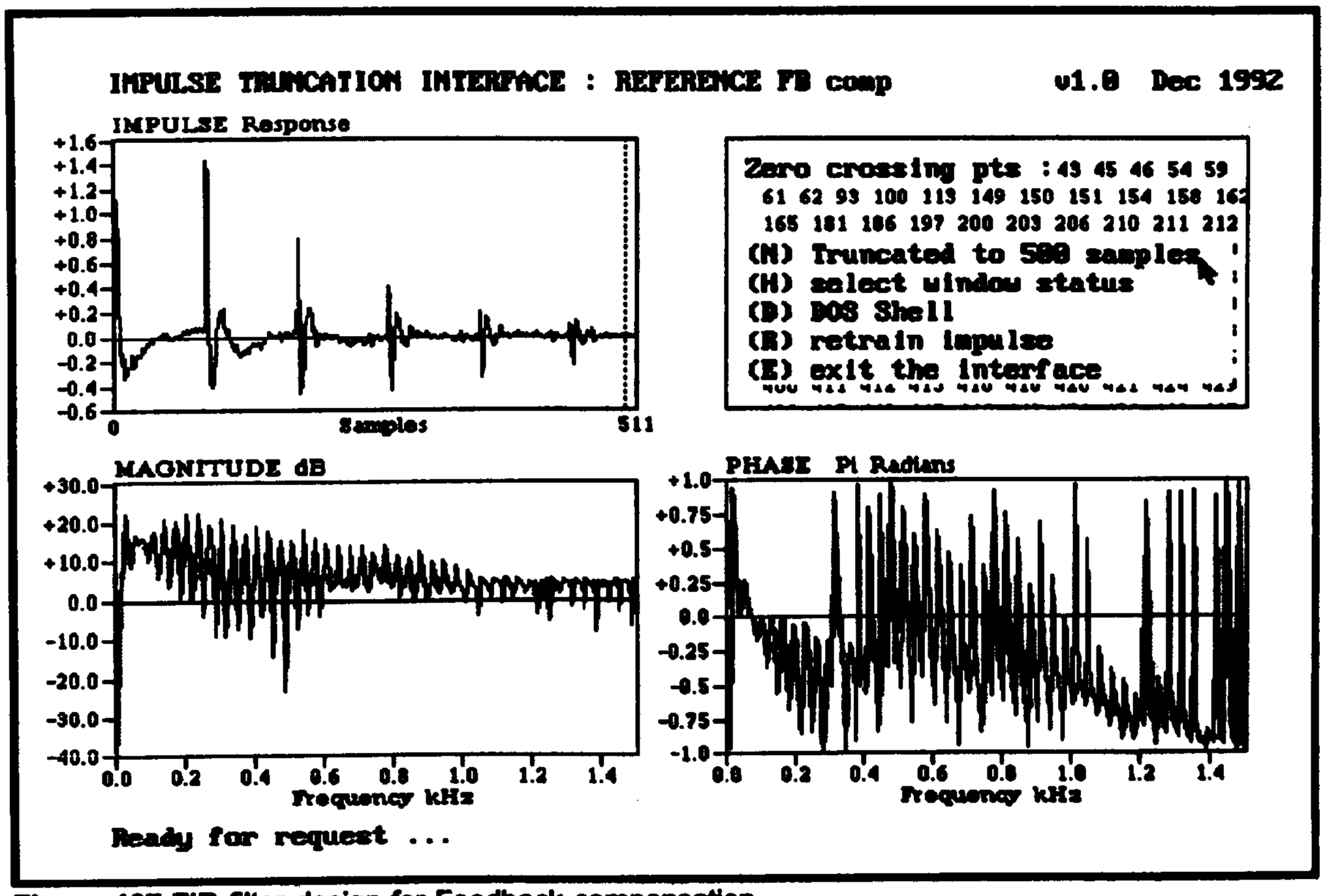

Figure 127 FIR filter design for Feedback compensation

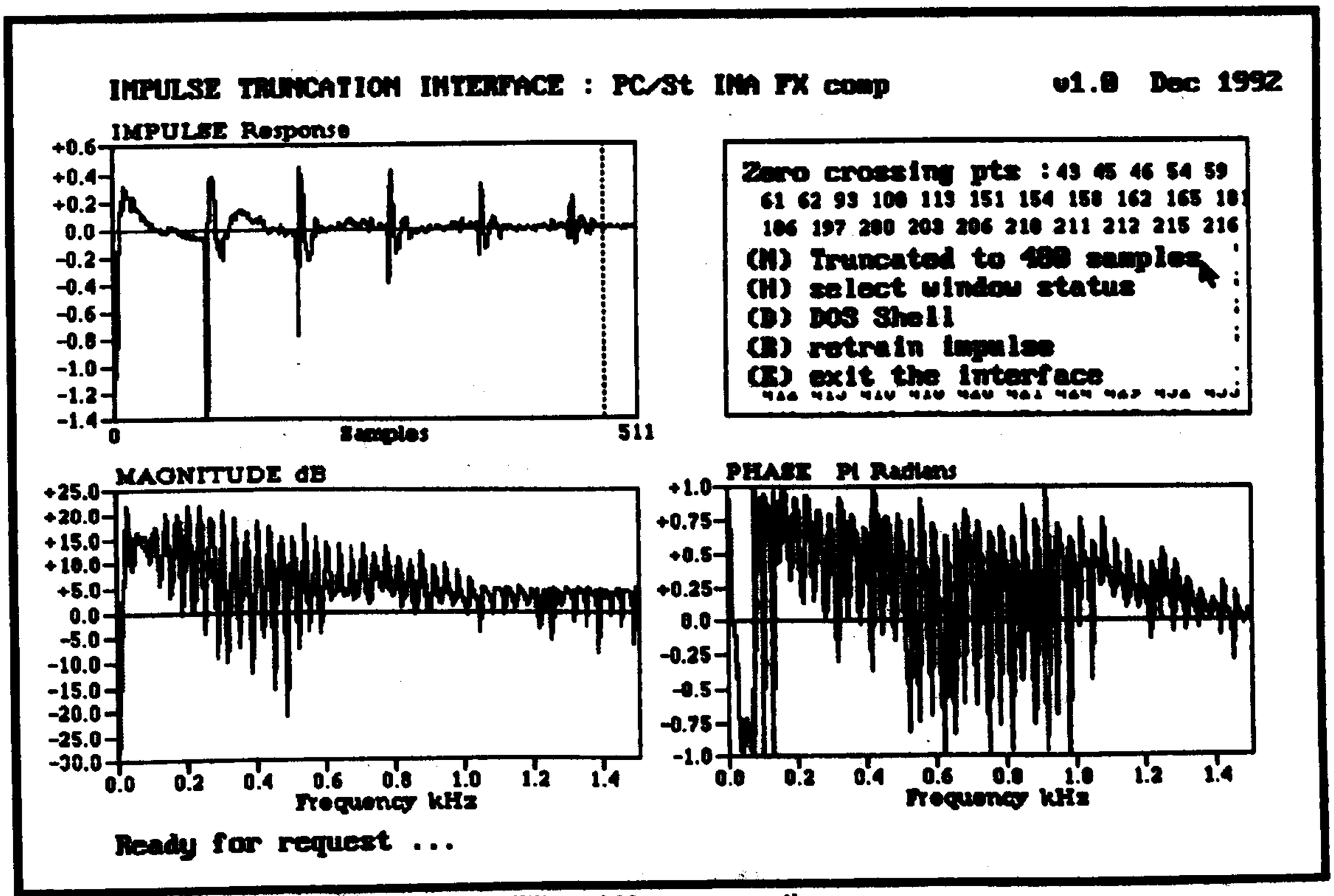

Figure 128 FIR filter part design for Filtered-X compensation

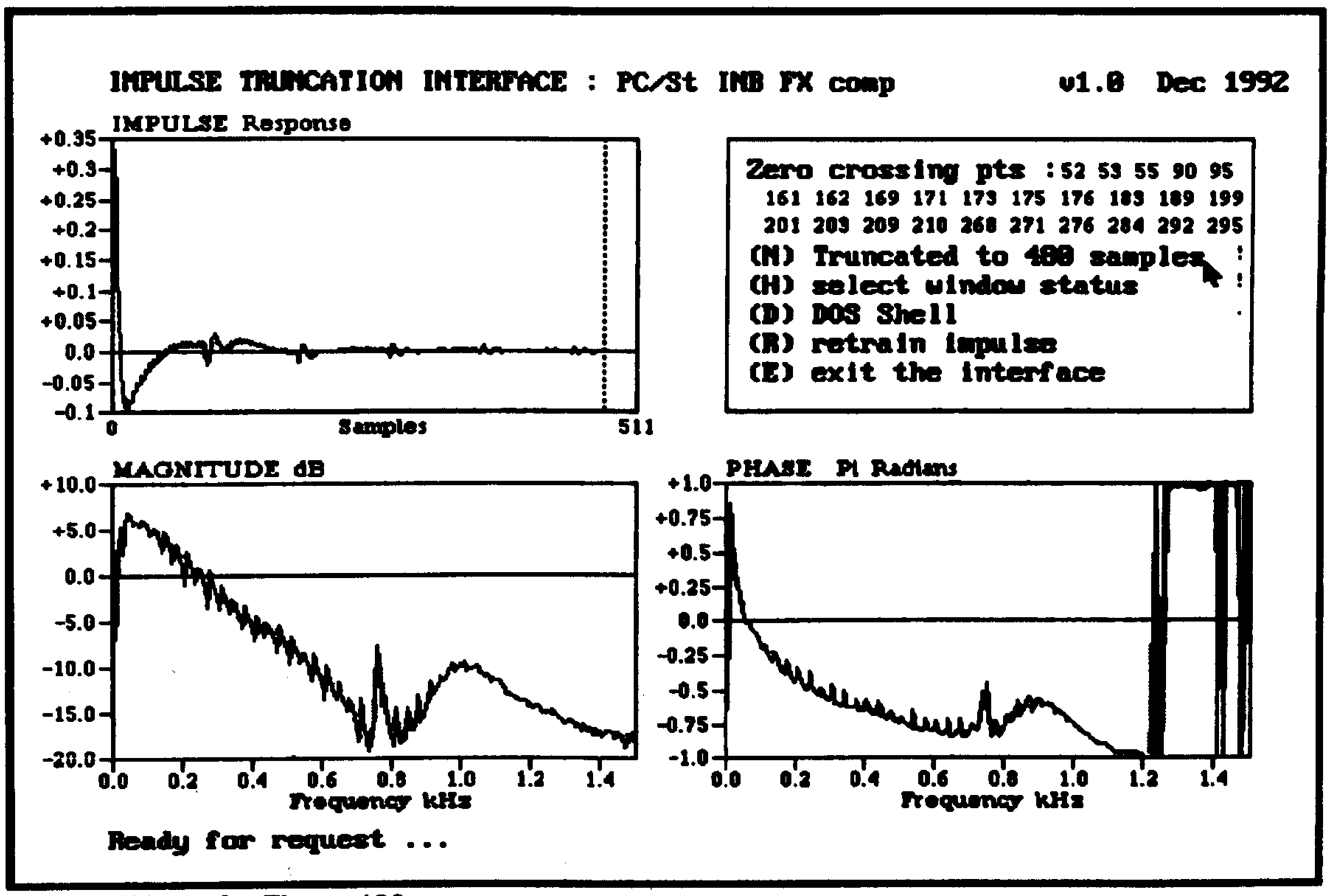

Figure 129 as for Figure 128

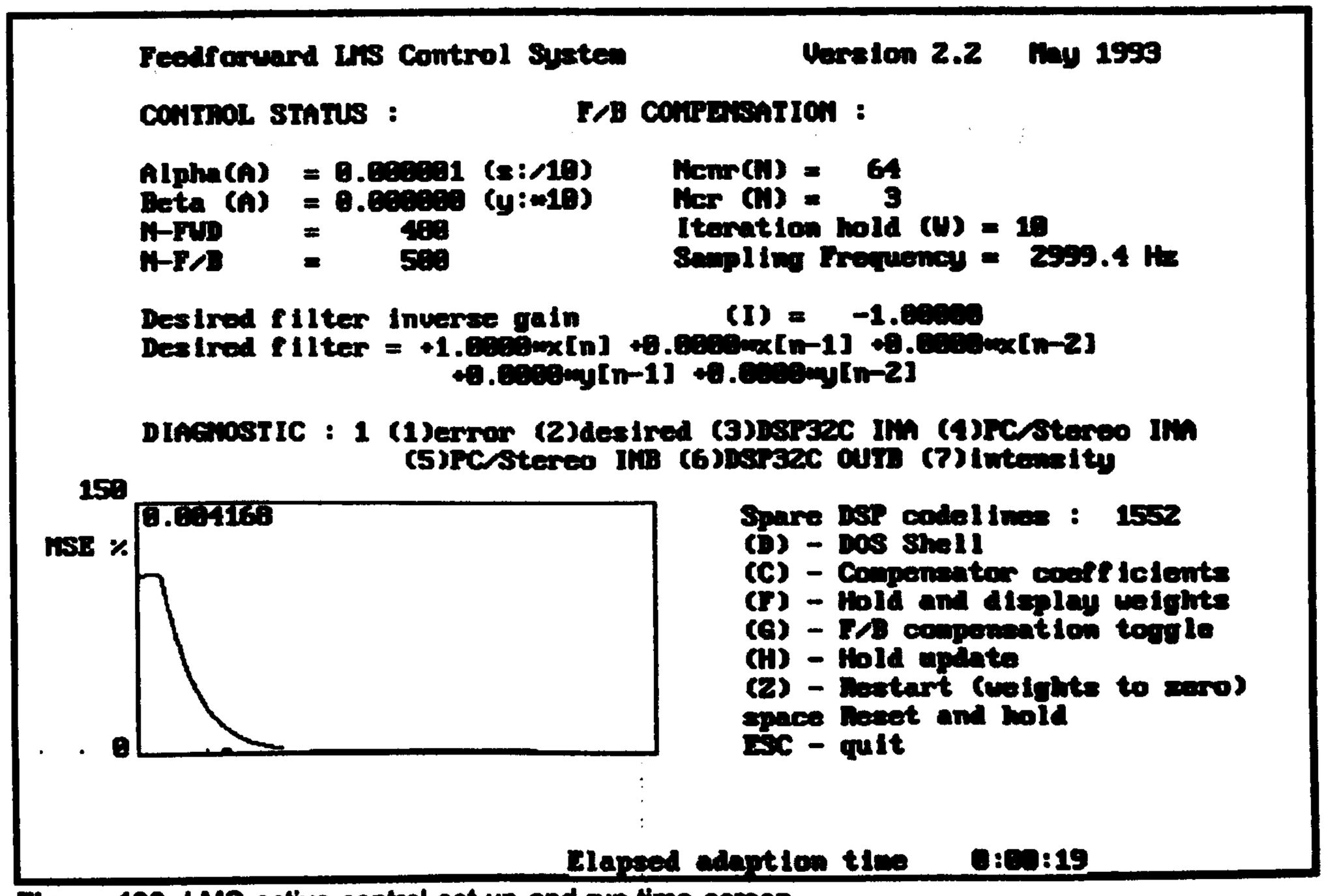

Figure 130 LMS active control set-up and run-time screen

3.5.2.3 Operational Problems

If the control is not stable:

(i) Reduce adaptive update gains.

(ii) Check polarity and value of desired filter inverse gain 'I'.

(iii) Correct for DC on the A/D convertors (DCSET.EXE).

(iv) Connect diagnostic signal from OUTA of DSP32C system board to an oscilloscope and trace around system with numbers 1-7 on the keyboard checking that external signals exist, see screen for more information.

(v) Try different acoustic frequency or type of noise.

(vi) Try version 2.1 instead of version 2.2. Version 2.1 has a different compensation strategy.

If an operational difficulty occurs:

(i) Check availability of all programs.

(ii) Check base address environment variable, see Page 317.

(iii) Check board installation, see Section 3.4 of Appendix 3 on Page 316.

(iv) Turn power off and back on to reset DSP32C board.

(v) Software or hardware fault. Try another program or DSP32C board.

3.5.3 Active absorption with 2-mic control system

Purpose:

Active control system based on the Least Mean Squares (LMS) 2-mic adaptive algorithm. Designed for active absorption using two spaced matched microphones. Control strategy based on Guicking and Nelson's work - see Section 2.4.2 on Page 14.

Files: Five:

GO.EXE	DOS executable
DEF.INI	Initialisation defaults file - ASCII
TMSRB.FON	Fonts file for graphics
SAM2MIC.OUT	DSP32C executable code
2MIC.OUT	DSP32C executable code

Set-up and command line:

Requires DSP32C board and PC/Stereo board. Check board address environment variable is installed in autoexec.bat, see Page 317. The PC program GO.EXE needs access to all of the other four files, so copy all files to a suitable directory and run the controller from there.

Start the controller from the DOS command line by typing:

GO

Disable reference sampling by typing:

GO /n

This saves start up time when the controller does not need feedback cancellation. Do NOT start the controller with "GO /n" if feedback cancellation is needed.

Notes:

Before running GO.EXE check for DC on the A/D convertors with the DCSET program, see Page 320. Connections to the convertors are as follows:

DSP32C board

INA	upstream pressure input
INB	downstream pressure input
OUTA	incident pressure
OUTB	reflected pressure

PC/Stereo board

INA	reference signal for LMS algorithm
INB	not used
OUTA	diagnostic signal
OUTB	control signal

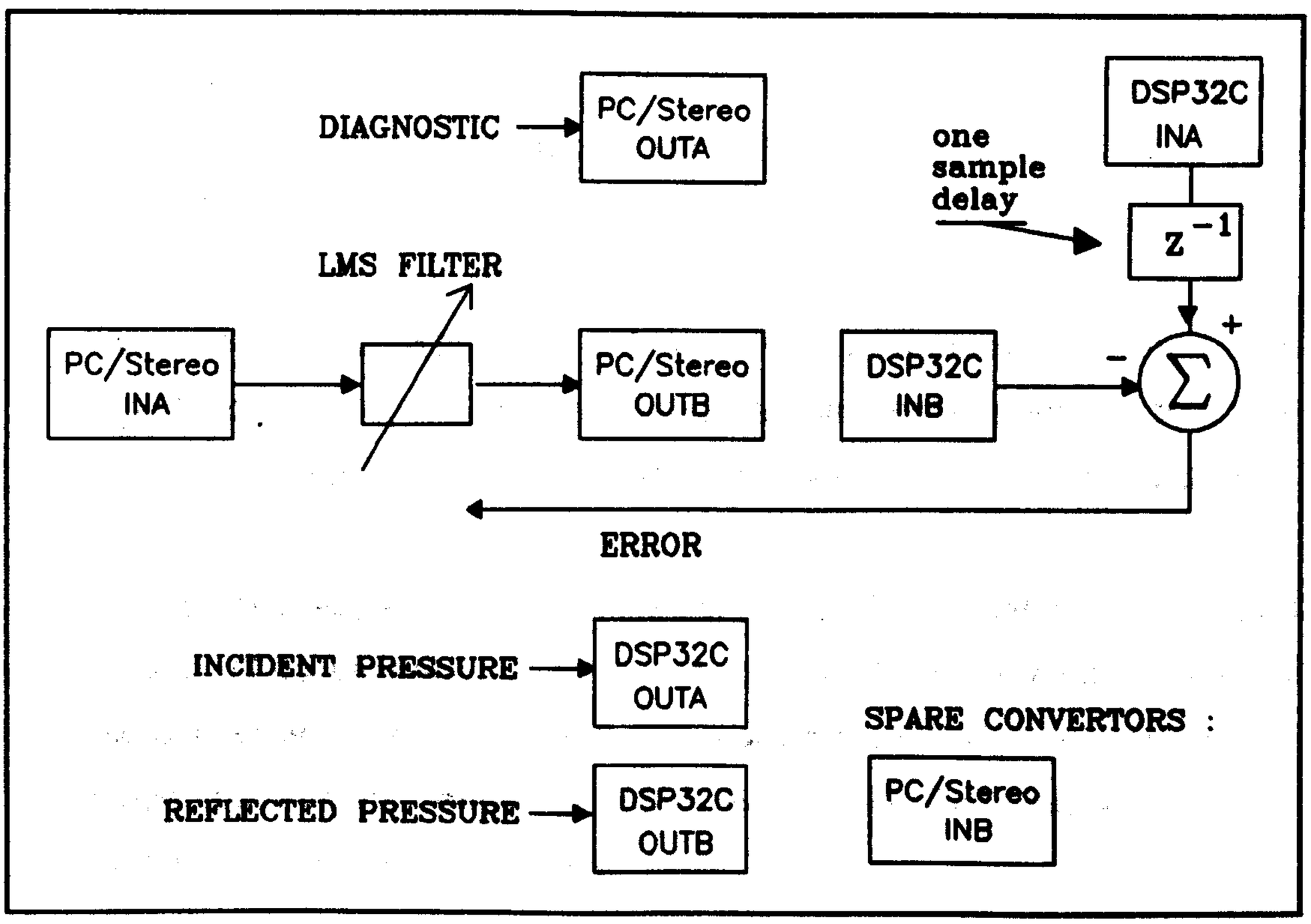

Figure 131 Schematic for the active absorber based on the "two mic method" implemented on the DSP32C system and PC/Stereo boards.

Figure 131 shows the connection schematic. Connect the analogue I/O cables supplied with the boards to the correct connectors. For location of analogue I/O 15-way connectors: see DSP32C System Board User Manual figure page 20 and PC/Stereo board manual Figure 2 page 4.

This is often confusing because of 180 degree rotation of the board when compared with the diagram. If in doubt take the case off and locate the bus edged-connector for physical orientation with the diagram. Connect a clock signal to the PC/Stereo board as described on Page 317 of this document.

The control method relies on the acoustic delay between the two spaced microphones to be equal to the sampling period. The desired filter is fixed to one sample delay with unity gain. I used the B&K intensity probe microphones spaced at 5cm with sampling frequency of 6800Hz. Close matching of the microphones is needed: ±0.5dB offers good absorption. I used MLSSA to calibrate the two microphone levels.

The ASCII file DEF.INI sets some control system start-up values for GO.EXE. To alter these values edit DEF.INI with a text file editor such as EDIT in DOS 5.0.

Five program phases that follow a similar process as the active impedance control application: title screen, information screen, real time sampling screen, compensation filter analysis, control run-time screen.

During active absorption control the control can be instantaneously turned on and off by pressing 'O' on the keyboard. Halt the adaptive control mid-convergence with 'H'. Halt and reset the controller by pressing the space bar. If the reference signal is acoustic then toggle feedback cancellation on with the 'G' key.

If control not stable:

(i) Reduce adaptive update gains.

(ii) Correct for DC on the A/D convertors (DCSET.EXE).

(iii) Connect diagnostic signal from OUTA of DSP32C system board to an oscilloscope and trace around system with numbers 1-7 on the keyboard checking that external signals exist, see screen for more information.

(iv) Try different acoustic frequency or type of noise.

If any operational difficulty occurs:

(i) Check availability of all programs.

(ii) Check base address environment variable, see Page 317.

(iii) Check board installation, see Section 3.4 of Appendix 3 on Page 316.

(iv) Turn power off and back on to reset the DSP32C board.

(v) Software or hardware fault. Try another program or DSP32C board.

3.6 Introduction on Programming the DSP32C

DSP32C software consists of two parts: the PC code and the DSP32C code.

Programming the PC requires knowledge of the 'C' programming language. You will need to buy a PC 'C' compiler as the LSI package does not include one. I use Microsoft Quick C v2.5, which is a good cheap choice for the beginner (£50 with manuals). If you choose the Borland 'C' compiler you may have to rewrite the LSI PC-DSP32C interface library (see Chapter 9 of the DSP32C System Board User Manual). If you are learning 'C' then get hold of as many source listings of programs as you can.

Programming the digital signal processor requires knowledge of DSP32C operation; when writing optimised real-time code you must be able to program in the DSP32C assembly language. AT&T do provide a DSP32C 'C' compiler to reduce the amount of assembly coding however £600 has not been available to buy this. The DSP32C System Board User Manual states that some knowledge of DSP32C assembly language is necessary when using the 'C' compiler. All of my DSP32C software has been written in the DSP32C assembly language. A precise description of the DSP32C assembly language is available in the WE-DSP32C Digital Signal Processor manual. The DSP32C compiler and linker are documented in the WE DSP32C Support Software Library manual. The applications described in this document are compiled with WE DSP32C Support Software Library v1.5. Descriptions of useful DSP32C Assembly Language Routines are in WE DSP32C Application Software Library. Despite all of this documentation there are no beginner's tutorials on assembly code basics such as registers, flags, code pipe-lining, etc. The Electrical Engineering Department provided a beginner's guide to assembly language for the BBC microcomputer that I found useful in describing things like indirect addressing.

Perform the interfacing between the PC and DSP32C code through the PC bus with the public domain interface library provided by Loughborough Sound Images, see Chapter 9 of the DSP32C System Board User Manual. I did not

use the LSI library files. Instead I slightly modified the 'C' source code of the interface library and incorporated it into the genf library for most of the applications. Ask Loughborough Sound Images for code examples of DSP32C applications.

3.6.1 Sampling Frequency and Real-time Coding

Nyquist's theorem implies that a sampling system that uses a sample and hold configuration (such as the LSI board) must have a sampling frequency that is at least twice that of the maximum data frequency. The maximum test frequency used in this work was around 500Hz so the minimum sampling frequency was 1kHz. The sampling frequency selected was 3kHz.

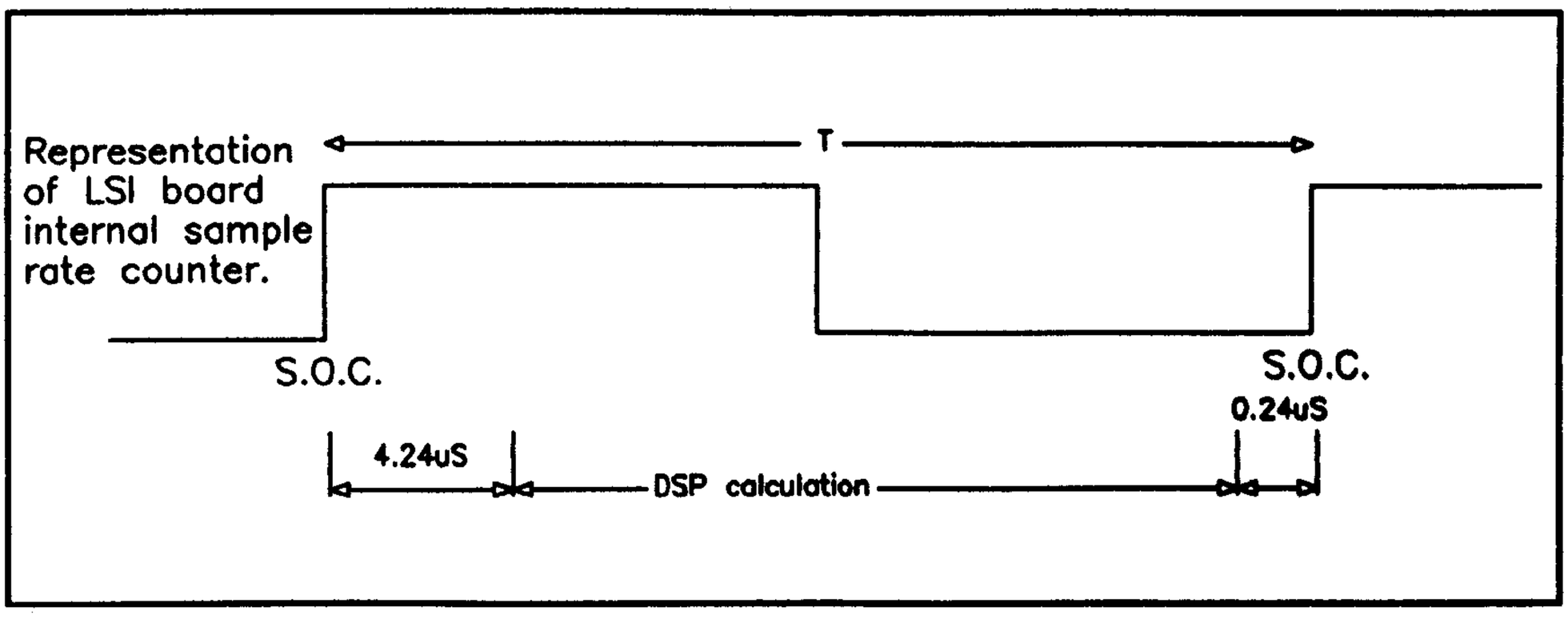

Figure 132 Real-time operation timing for the DSP32C processor on the LSI system board. T is the period of the A/D and D/A sample rate.

The LSI board data-handling causes a 4.24μS delay (see Figure 132) between the sampling of an analogue data value or start of conversion (S.O.C.), and the availability of this value to the DSP32C program. Digital signals that are to be converted into analogue signals must be ready 0.24μS before the next S.O.C. occurs. The sampling frequency of 3kHz has a period of 1000/3μS. For 'real-time' operation (so that new sample output is made in response to input from the previous sample conversion) the program must then execute all instructions in 328.8μS (this from 1000/3 - 4.24 - 0.24). The DSP32C instruction

time of 80nS allows execution of 4110 real-time instructions for a sample frequency of 3kHz.

APPENDIX 4 : Design of electronic integrator

The integration of a harmonic signal causes a phase shift of -90°. The integration of real electronic signals can be made with an electronic filter (see Figure 133) based on OP-amp techniques that places a zero at infinity in the frequency domain. With suitable selection of resistor R2 and capacitor C this filter theoretically produces a broadband phase shift of near to -270°. A subsequent inversion creates a theoretical phase shift of near to -90° that corresponds to integration. The resistor R2 is necessary to keep dc stability. Analysis of the circuit in the s-domain reveals the filter transfer function, Eq. A4.1.

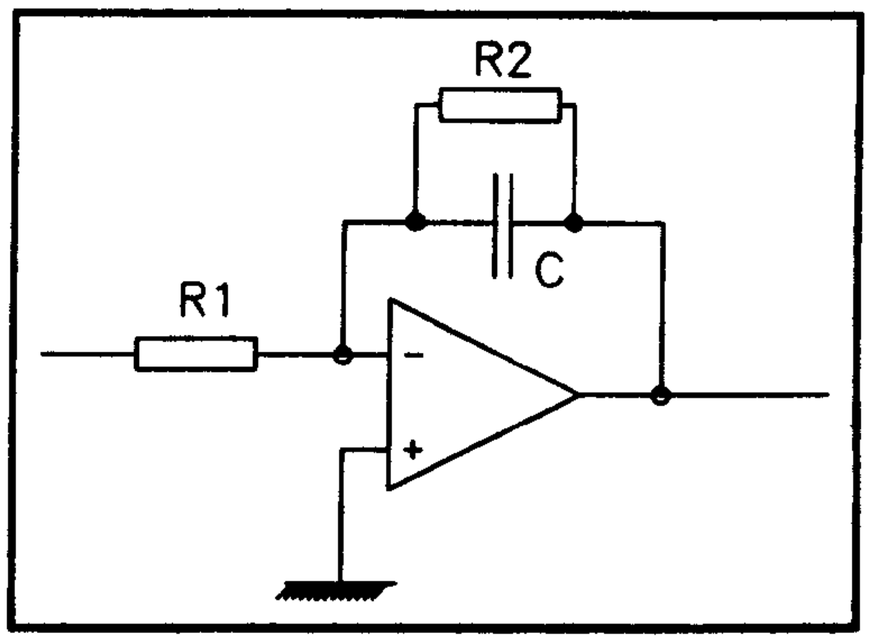

Figure 133. OP-amp integrator circuit

$$F(s) = -\frac{R2}{R1}\left[\frac{1}{1+sCR2}\right] \qquad \text{A4.1}$$

Substituting s=jω gives Eq. A4.2.

$$F(J\omega) = -\frac{R2}{R1}\left[\frac{1}{1+J\omega CR2}\right] \qquad \text{A4.2}$$

The phase of this filter circuit with subsequent 180° inversion is given by Eq. A4.3 and is dependent on the values of C and R2 and the harmonic frequency of the filter input signal.

$$\Phi = -\tan^{-1}(-\omega CR2) \qquad \text{A4.3}$$

The selection of C and R2 for desired phase is complicated by the ability of the OP-amp output to charge the capacitor C. Slew rate limiting will occur if there is insufficient current to charge the capacitor. The output current I required to charge the capacitor is the ratio of the voltage across the capacitor V to the impedance, this gives Eq. A4.4.

$$I = V \omega C \qquad \text{A4.4}$$

The maximum output current of the OP-amp is quoted in manufacturer's specification sheets so from Eq. A4.4 the maximum frequency of correct charging of the capacitor can be calculated. The test-rig circuit uses OP-amp type LF-351 with a typical maximum output current of 1mA. With a desired ±3V swing across the capacitor and a desired maximum frequency in the test-rig of 500Hz the capacitor value is calculated as 53nF from Eq. A4.4. A suitable real capacitor value is C=47nF. For a phase shift of -89° at 20Hz R2 is calculated as 9.7MΩ from Eq. A4.3. A suitable real resistor value is R2=10MΩ. R1 is selected for dc gain. The test-rig value is R1=100kΩ so that dc gain is 40dB.

The filter circuit theoretically offers at least -89° of phase shift from 20Hz with no slew-rate limiting below 500Hz for an output voltage swing of ±3V if R1=100kΩ, R2=10MΩ, C=47nF with an OP-amp type LF351.

The filter circuit is practically implemented for the test-rig as shown in Figure 134. The input capacitor 2μ2 removes dc inputs but affects the lower frequency phase performance. The second OP-amp provides dc-offset compensation for dc offsets caused by the first OP-amp and signal inversion to give a circuit integration phase shift of near -90°. This was tested before use in the test-rig and the phase and magnitude results are shown below in Table 2. The input capacitor (value 2μ2) reduces the measured phase shift at 19.25Hz from -89.1° (without input capacitor) to -85.0° with input capacitor.

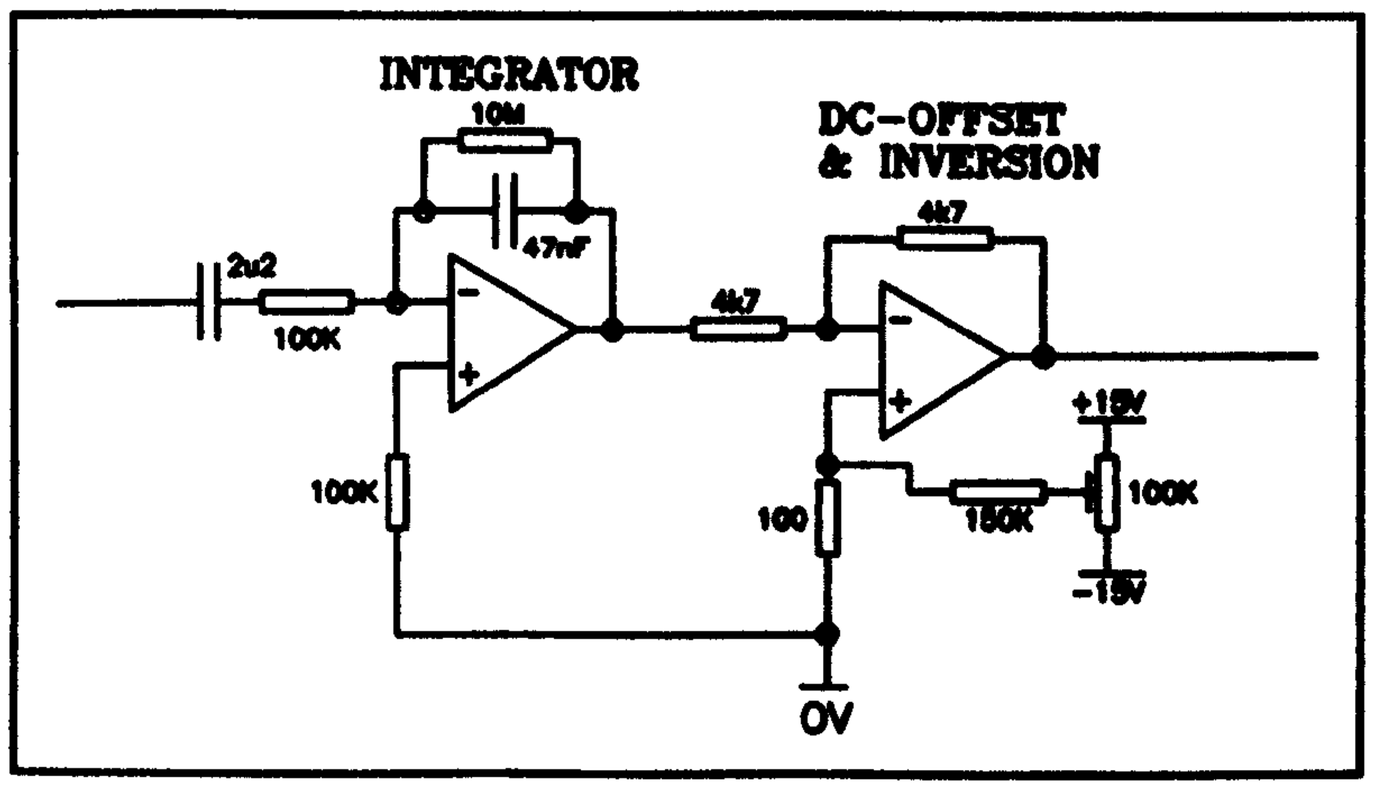

Figure 134. Test-rig integration circuitry

Table 2. Measured magnitude and phase of analogue integrator circuit

Frequency Hz	gain dB	phase °
19.25	4.63	-85.0
39.25	-1.47	-87.5
50.5	-3.63	-88.2
85.75	-8.28	-89.0
100	-9.55	-88.7

APPENDIX 5 : Standing Wave Ratio (SWR) Measurements

The measurement of one-dimensional surface impedance for plane harmonic waves can be made with standing wave ratio (SWR) measurements in a waveguide. This Appendix describes classical theory for SWR measurements. The complex amplitude reflection coefficient is defined.

Consider a surface that is excited by a normally-incident harmonic plane wave of pressure p_i, see Figure 135.

There is a reflected plane wave p_r and the surface is at position x=0. The incident and reflected plane waves are described by Eq. A5.1 and Eq. A5.2.

$$p_I = A.e^{j(\omega t - kx)} = A.e^{j\omega t}.e^{-jkx} \qquad \text{A5.1}$$

$$p_r = B.e^{j(\omega t + kx)} = B.e^{j\omega t}.e^{jkx} \qquad \text{A5.2}$$

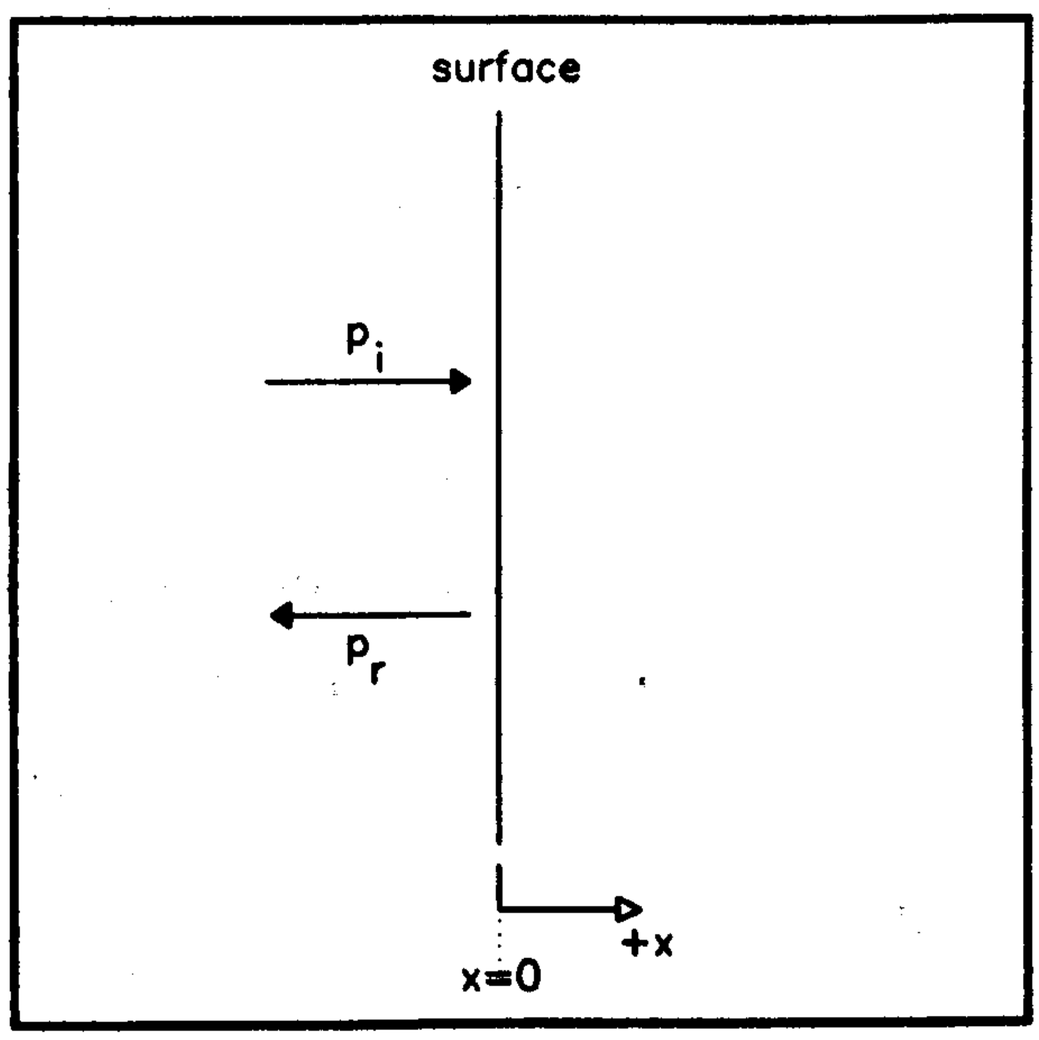

Figure 135. Boundary excited by incident acoustic pressure p_i , positioned at x=0.

A and B are both complex pressure amplitudes. The amplitude at a pressure node in the duct is |A| + |B| and the amplitude at a pressure antinode is |A| - |B|. In a waveguide the amplitude of the node and antinode can be simply measured with a microphone. The SWR is defined by the ratio of the amplitude at the antinode to that at the node Eq. A5.3.

$$SWR = \frac{|A| + |B|}{|A| - |B|} \qquad \text{A5.3}$$

Rearranging Eq. A5.3 yields Eq. A5.4.

$$\frac{|B|}{|A|} = \frac{SWR - 1}{SWR + 1} \qquad \text{A5.4}$$

The complex amplitude reflection coefficient R is defined by Eq. A5.5. Note that it includes a phase shift on reflection term Φ.

$$R = |R| . e^{j\Phi} = \frac{B}{A} \qquad \text{A5.5}$$

The phase shift can be calculated from Eq. A5.6 by measuring the distance from the surface to the first node x_{min}.

$$\Phi = \pi \left[\frac{4 x_{min} f}{c} - 1 \right] \qquad \text{A5.6}$$

Equation A5.5 combined with Eq. A5.4 gives Eq. A5.7.

$$|R| = \frac{SWR - 1}{SWR + 1} \qquad \text{A5.7}$$

Equation A5.7 shows that the magnitude of the reflection coefficient at a surface can be calculated from measurement of the pressure amplitude at the node and antinode of a standing wave field.

The complex amplitude reflection coefficient is related to the complex surface impedance by considering the pressure and velocity components at the surface. The complex specific acoustic impedance z is the ratio of total pressure to surface velocity at the surface, Eq. A5.8.

$$z = \frac{p}{u} \qquad \text{A5.8}$$

where

$$p \Big|_{x=0} = (A + B) . e^{j\omega t} \qquad \text{A5.9}$$

$$u \Big|_{x=0} = \left(\frac{A - B}{\rho_0 c} \right) . e^{j\omega t} \qquad \text{A5.10}$$

so that Eq. A5.8 becomes Eq. A5.11.

$$z \Big|_{x=0} = \rho_0 c . \left[\frac{A + B}{A - B} \right] \qquad \text{A5.11}$$

By dividing through top and bottom of Eq. A5.11 by A and substituting from Eq. A5.5 the surface impedance is related to the complex amplitude reflection coefficient as shown in Eq. A5.12.

$$z\Big|_{x=0} = \rho_0 c \left[\frac{1+R}{1-R} \right] \qquad \textbf{A5.12}$$

Equation A5.12 shows that the surface impedance can be calculated by measuring the amplitude of standing wave pressure node and antinode in the waveguide and the position of the first minima and calculating the complex amplitude reflection coefficient. Two special cases are for **R = 0** and **R = 1**. The first case is for ideal acoustic absorption when $z = \rho_0 c$, the second is for perfect acoustic reflection when $z = \infty$. Equation A5.12 can be rearranged to give Eq. A5.13.

$$R = \left[\frac{\frac{z|_{x=0}}{\rho_0 c} - 1}{\frac{z|_{x=0}}{\rho_0 c} + 1} \right] \qquad \textbf{A5.13}$$

A numerical example of the relationship between impedance and reflection coefficient is for the KEF B200A loudspeaker mounted in a 25 litre box. The parameters for the B200A loudspeaker are in Appendix 1 on Page 309. The theoretical magnitude and phase of the acoustic input impedance of the system are shown in Figure 21 on Page 86. From Eq. A5.13 the theoretical magnitude and phase of the reflection coefficient is calculated and shown here in Figure 136. The resonant frequency (calculated as 65Hz in Appendix 2 on Page 310) is seen to have zero reflection coefficient - a perfectly absorptive termination. At this frequency the acoustic input impedance is real and close to $\rho_0 c$ as shown in Figure 21.

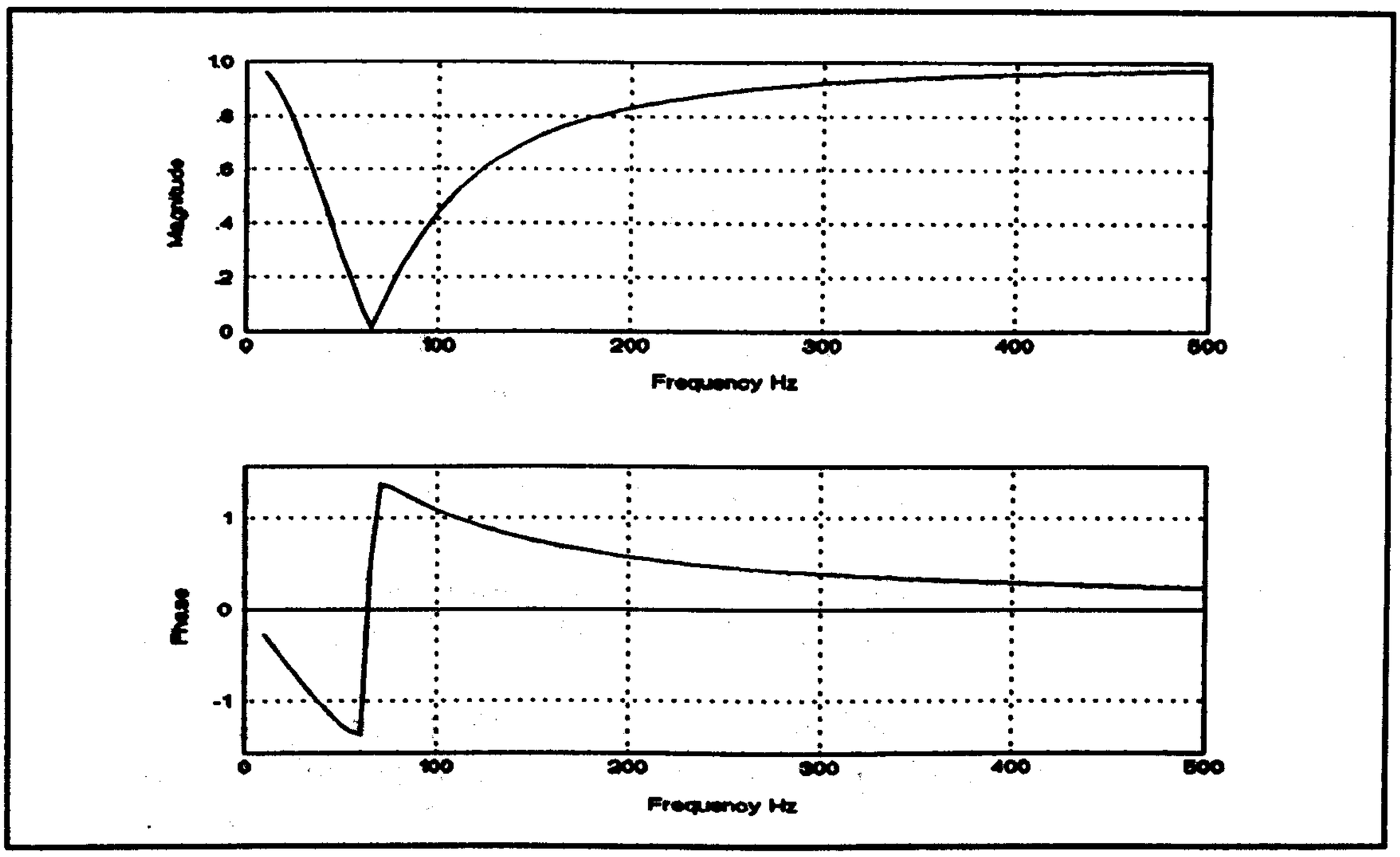

Figure 136. Theoretical magnitude and phase of the amplitude reflection coefficient for the cone of a KEF B200A loudspeaker mounted in a 25 litre sealed enclosure. The cone is assumed to vibrate as an ideal piston over this frequency range.

REFERENCES

(1) P. Lueg. "Process of silencing sound oscillations" U.S. Patent No. 2,043,416 1936. Application: 8 March 1934, Patented: 9 June 1936.

(2) P.A. Nelson and S.J. Elliott. "Active Control of Sound" 1992, Academic Press.

(3) L.E. Kinsler, A.R. Frey, A.B. Coppins and J.V. Sanders. "Fundamentals of Acoustics" 1982, John Wiley & Sons.

(4) D. Guicking. "Recent Advances in Active Noise Control" 1992, Second International Congress on Recent Developments in Air- and Structure-Borne Sound and Vibration, Auburn Univ, Alabama, USA. Mech Eng Dept Publication. Vol.1 : pp.313-320.

(5) D. Guicking. "Active Noise and Vibration Control" Drittes Physikalisches Institut, University of Gottingen, Germany. 1988. 3rd ed 1988, 1st supplement 1991.

(6) A.R.D. Curtis, P.A. Nelson and S.J. Elliott. "Active Reduction of a one-dimensional enclosed sound field: An experimental investigation of three control strategies" JASA **86(5)**: pp.2265-2268, 1990.

(7) S.D. Sommerfeldt and P.J. Nashif. "Energy Based Control of the Sound Field in Enclosures" 1992, Second International Congress on Recent Developments in Air- and Structure-Borne Sound and Vibration, Auburn University, Alabama, USA. Mech Eng Dept Publication. Vol.1 : pp.361-368.

(8) D. Guicking. "On the invention of active noise by Paul Lueg" JASA **87(5)**: pp.2251-2254, 1990.

(9) H.F. Olson and E.G. May. "Electronic Sound Absorber" JASA **25(6)**: pp.1130-1136, 1953.

(10) M.A. Swinbanks. "The Active Control of Sound Propogation in Long Ducts" J.Sound Vib. **27(3)**: pp.411-436, 1973.

(11) M.J.M. Jessel and G.A. Mangiante. "Active Sound Absorbers in an Air Duct" J.Sound and Vib **23(3)**: pp.383-390, 1972.

(12) M. Jessel. "Traduction du principede Huygens en acoustique lineaire" C.R.Acad.Sci. Paris **262**: pp.1321-1324, 1966.

(13) G. Canevet. "Active Sound Absorption in an Air Conditioning Duct" J.Sound Vib. **59(3)**: pp.333-345, 1978.

(14) G.A. Mangiante. "Active sound absorption" JASA **61(6)**: pp.1516-1523, 1977.

(15) J.H.B. Poole and H.G. Leventhall. "An Experimental Study of Swinbanks' Method of Active Attenuation of Sound in Ducts" J.Sound Vib. **49(2):** pp.257-266, 1976.

(16) R.J. Bobber and L.G. Beatty. "Impedance Tube for Underwater Sound Transducer Evaluation" JASA **31:** pp.832-833(A), 1959. Abstract

(17) R.J. Bobber. "Active Load Impedance" JASA **34(3):** pp.282-288, 1962.

(18) L.G. Beatty. "Acoustic Impedance in a Rigid-Walled Cylindrical Sound Channel Terminated at Both Ends with Active Transducers" JASA **36(6):** pp.1081-1089, 1964.

(19) K. Karcher. "Active Modification of the Acoustic Wall Impedance for Normal Incidence" PhD Thesis. Drittes Physikalisches Institut, University of Gottingen, Germany. 1982.

(20) D. Guicking and K. Karcher. "Active Impedance Control for One-dimensional Sound" J.Vib.,Acs.,Stress.and Reliability in Design **106:** pp.393-396, 1984.

(21) D. Guicking and E. Lorenz. "An Active Sound Absorber with Porous Plate" J.Vib.,Acs,Stress and Reliability in Design **106:** pp.389-392, 1984.

(22) M.R. Schroeder. "System for Determining Acoustic Reflection Coefficients" U.S. Patent No. 3,346,067 1967.

(23) M. Rollwage. "Free Field Investigation on Coherent Active Control of the Acoustic Wall Impedance" PhD Thesis. Drittes Physikalisches Institut, University of Gottingen, Germany. 1984.

(24) D. Guicking, K. Karcher and M. Rollwage. "Coherent active methods for applications in room acoustics" JASA **78(4):** pp.1426-1434, 1985.

(25) D. Guicking and M. Wenzel. "Adaptive Filter Concept for Active Control of Acoustic Wall Impedance" 1986, Winter Annual meeting of The American Society of Mechanical Engineers Dec 7-12, Anaheim, California. Vol.1

(26) D. Guicking, J. Melcher and R. Wimmel. "Active Impedance Control in Mechanical Structures" ACUSTICA **69:** pp.39-52, 1989.

(27) M. Wenzel and D. Guicking. "Simulationen und Experimente zur Adaption einer aktiven Schallwand auf eine breitbandig vorgegebene Wandimpedanz" 1990, Fotschritte der Akustik DAGA'90, Germany. : pp.899-902.

(28) D. Guicking. "Personal communication" 1992.

(29) F. Orduna-Bustamente and P.A. Nelson. "An adaptive controller for the active absorption of sound" JASA 91(5): pp.2740-2747, 1992.

(30) G.C. Nicholson and P. Darlington. "Smart Surfaces for Building Acoustics" 1991, "Noise in the Nineties", Autumn Conference, Windermere, UK. Institute of Acoustics. Vol.13(8) : pp.155-164.

(31) P. Darlington and G.C. Nicholson. "Theoretical and Practical Constraints on the Implementation of Active Acoustic Boundary Elements" 1992, Second International Congress on Recent Developments in Air- and Structure-Borne Sound and Vibration, Auburn University, Alabama, USA. Mech Eng Dept Publication. Vol.2 : pp.1011-1018.

(32) P. Darlington, K.P. Roungkvist, M.S. Nielsen and G.C. Nicholson. "A Loudspeaker System with Active Transmission Line Loading" 1992, Reproduced Sound, Windermere, UK. Institute of Acoustics Publication.

(33) G.C. Nicholson and P. Darlington. "Active Control of Acoustic Absorption, Reflection and Transmission" 1993, ACOUSTICS '93, Southampton, UK. Institute of Acoustics Publication. Vol.15(3) : pp.403-409.

(34) C.J. Mazzola. "Active Sound Absorption" 1993, Namlak, P.O.Box 804, Mamaroneck, New York 10543.

(35) P.A. Swartz and U.S.Philips-Corporation. "Electro-acoustic system having a variable reflection/absorption characteristic" U.S. Patent No. 4,712,247 1987. Found in JASA 84(2) p.799, Filed: 3 April 1984, Patented: 8 Dec 1987.

(36) B. Widrow and S.D. Stearns. "Adaptive Signal Processing" 1985, Englewood Cliffs, N.J. 07632, Prentice-Hall Signal Processing Series.

(37) C.C. Boucher, S.J. Elliott and P.A. Nelson. "The Effects of Modelling Errors on the Performance and Stability of Active Noise Control Systems" 1991, Recent Advances in Active Control of Sound and Vibration, Virginia State University, Virginia, USA. Technomic Publishing. Vol.1 : pp.291-301.

(38) P. Darlington. "Passband Disturbance in Active Sound Control Systems" 1991, Recent Advances in Active Sound and Vibration Control, Virginia State University, Virginia, USA. Technomic Publishing. Vol.1 : pp.731-741.

(39) S.D. Snyder and C.H. Hansen. "The Influence of Transducer Transfer Functions and Acoustic Time Delays on the Implementation of the LMS Algorithm in Active Noise Control Systems" J. Sound Vib. 141(3): pp.409-424, 1990.

(40) D.C. Swanson. "A Stability Robustness Comparison of Adaptive Feedforward and Feedback Control Algorithms" 1991, Recent Advances in Active Control of Sound and Vibration, Virginia State University, Virginia, USA. Technomic Publishing. Vol.1 : pp.755-767.

(41) P.L. Feintuch. "An Adaptive Recursive LMS Filter" Proc.IEEE **64:** pp.1622-1624, 1976.

(42) M.G. Larimore, J.R. Treichler and J.R. Johnson. "SHARF: An Algorithm for Adapting IIR Digital Filters" IEEE Trans. Acoust., Speech, Signal Processing **ASSP-28(4):** pp.428-440, 1980.

(43) T.C. Hsia. "A Simplified Adaptive Recursive Filter Design" Proc.IEEE **69(9):** pp.1153-1155, 1981.

(44) L.J. Eriksson, M.C. Allie and R.A. Greiner. "The Selection and Application of an IIR adaptive Filter for Use in Active Sound Attenuation" IEEE Trans. Acoust. Speech Signal Process. **ASSP-35(4):** pp.433-437, 1987.

(45) L.J. Eriksson. "Development of the filtered-U algorithm for active noise control" JASA **89(1):** pp.257-265, 1990.

(46) S.D. Sommerfeldt and J. Tichy. "Adaptive control of a two-stage vibration isolation mount" JASA **88(2):** pp.938-944, 1990.

(47) L.J. Eriksson and M.C. Allie. "Use of random noise for on-line transducer modeling in an adaptive active attenuation system" JASA **85(2):** pp.797-802, 1989.

(48) W. Ren and P.R. Kumar. "Adaptive Active Noise Control: Structures, Algorithms and Convergence Analysis" 1989, Proc of Inter-Noise 89, Newport Beach, CA, USA. Vol.1 : pp.435-440.

(49) M.W.R.M.v. Overbeek. "A method to identify the secondary path in active noise control systems" 1991, Recent Advances in Active Control of Sound and Vibration, University of Auburn, Virginia, USA. Vol.1 : pp.742-753.

(50) C.R. Fuller, C.H. Hansen and s.D. Synder. "Active Control of Sound Radiation from a Vibrating Rectangular Panel by Sound Sources and Vibration inputs: An experimental comparison" Journal and Sound and Vibration **145(2):** pp.195-215, 1991.

(51) D.K. Anthony and S.J. Elliott. "A Comparison of Three Methods of Measuring the Volume Velocity of an Acoustic Source" J.Audio Eng. Soc. **39(5):** pp.355-366, 1991.

(52) S.J. Elliott and T.J. Sutton. "Feedforward and Feedback Methods for Active Control" 1994, Spring Conference, University of Salford, UK. Institute of Acoustics. Vol.16(2) : pp.255-276.

(53) P. Darlington. "Applications of Adaptive Filters in Active Noise Control" PhD Thesis. Institute of Sound and Vibration Research, University of Southampton, UK. 1987.

(54) D.R. Morgan. "An analysis of multiple correlation cancellation loops with a filter in the auxiliary path." IEEE Trans. Acoust., Speech, Signal Processing **ASSP-28(4):** pp.454-467, 1980.

(55) S.A. White. "An Adaptive Recursive Filter" 1975, 9th Asilomar Conference on Circuits, Systems and Computers, Pacific Grove, CA, USA. IEEE, New York 1976.

(56) S. Horvath. "Comparative Performance of Linear Equalizers using a Recursive Sample-Data Filter" 1974, International Zurich Seminar on Digital Communications, Zurich, Switzerland. IEEE, New York 1974.

(57) G. Salomonsson. "An Equalizer with Feedback Filter" Ericsson Technics **28(2):** pp.57-101, 1972.

(58) J.W. Mark and S.S. Haykin. "Adaptive Equalisation for Digital Communications" Proc. IEE **118(12): pp.1711-1720, 1971.**

(59) P.A. Nelson. "Active Control of Acoustic Fields and the Reproduction of Sound" 1993, ACOUSTICS,93, ISVR, Southampton University, UK. Institite of Acoustics. Vol.15:Part 3 : pp.43-92.

(60) P. Darlington. "Subharmonic Generation and Chaos in Adaptive Filters" 1992, Signal Processing VI, EUSIPCO-92, Elsevier. : pp.199-202.

(61) G.E. Warnaka, L.A. Poole and J. Tichy. "Active Acoustic Attenuator" U.S. Patent No. 4473906 1984.

(62) M. Colloms. "High Performance Loudspeakers" 1980, Pentech Press.

(63) R.H. Small. "Closed-box loudspeaker systems Part 1 Analysis" JAES **20(10):** 1972.

(64) R.H. Small. "Closed-box loudspeaker systems Part 2 Synthesis" JAES **21(1):** 1973.

(65) J.D. Smith. "Vibration Measurement and Analysis" 1989, Butterworths.

(66) G.C. Nicholson. "User Manual for Loughborough Sound Images DSP32C Application Software" Dept. of Applied Acoustics, University of Salford, M5 4WT, UK. 1993.